

Bahman Zohuri

Neutronic Analysis For Nuclear Reactor Systems

Second Edition

EXTRAS ONLINE



Springer

Neutronic Analysis For Nuclear Reactor Systems



Bahman Zohuri

Neutronic Analysis For Nuclear Reactor Systems

Second Edition



Springer

Bahman Zohuri
Galaxy Advanced Engineering, Inc.
University of New Mexico
Albuquerque, NM, USA

Additional material to this book can be downloaded from <http://extras.springer.com>.

ISBN 978-3-030-04905-8 ISBN 978-3-030-04906-5 (eBook)
<https://doi.org/10.1007/978-3-030-04906-5>

Library of Congress Control Number: 2018963831

© Springer Nature Switzerland AG 2017, 2019

This work is subject to copyright. All rights are reserved by the Publisher, whether the whole or part of the material is concerned, specifically the rights of translation, reprinting, reuse of illustrations, recitation, broadcasting, reproduction on microfilms or in any other physical way, and transmission or information storage and retrieval, electronic adaptation, computer software, or by similar or dissimilar methodology now known or hereafter developed.

The use of general descriptive names, registered names, trademarks, service marks, etc. in this publication does not imply, even in the absence of a specific statement, that such names are exempt from the relevant protective laws and regulations and therefore free for general use.

The publisher, the authors, and the editors are safe to assume that the advice and information in this book are believed to be true and accurate at the date of publication. Neither the publisher nor the authors or the editors give a warranty, express or implied, with respect to the material contained herein or for any errors or omissions that may have been made. The publisher remains neutral with regard to jurisdictional claims in published maps and institutional affiliations.

This Springer imprint is published by the registered company Springer Nature Switzerland AG
The registered company address is: Gewerbestrasse 11, 6330 Cham, Switzerland

*This book is dedicated to Children, Natasha,
Natalie, Sasha, and Darrius*

Preface

This text develops the theory of nuclear reactors from the fundamentals of fission to the operating characteristics of modern reactors. It is aimed at senior undergraduate or first year graduate student level. It is designed as a two-semester text with the first half emphasizing reactor criticality analysis and all of the physics that goes into modern calculations. It will start with simplified one-group diffusion theory models and extend into sophisticated multi-group transport theory models. Each chapter will have at least one example covering the issues discussed. Desktop calculations will be discussed and demonstrated in examples. A small one-dimensional computer code will be provided to demonstrate the models discussed. Resonance theory, thermal scattering, and heterogeneous effects will be discussed and characterized. Detailed data sets will be provided that will allow two, three, and four groups of desktop calculations. Additional multi-group data sets will be provided with the computer disk.

The second half of the book will deal with the two main topics of interest to operating reactors – reactor kinetics/dynamics and in-core fuel management. Based on the fundamental physics discussed in the first half of the book, reactivity models will be developed using realistic reactor cross-section data and modern analytic tools. Adjoint methods will be explained in detail. Perturbation theory will be used extensively to quantify reactivity effects. Both linear and nonlinear reactor kinetic feedback models are included. Control system models will be mainly based on linearization techniques. Fuel management analysis will be based on a linear reactivity model. Code modeling will be discussed and example problems included that can be addressed with desktop methods. The theory for extending fuel management calculations to modern large-scale computers will be discussed.

Some sections and chapters of the book reflect inputs and lecture notes from Professor Emeritus William J. Garland, Department of Engineering Physics, McMaster University, Professor Hiroshi Sekimoto of Tokyo Institute of Technology, and Professor H. Van Dam of Delft University of Technology as well as some of my own lectures and notes while consulting with the Department of Energy. Some of my lecture notes from my class notes at the University of Illinois and

University of New Mexico were used as well while taking related course as graduate student.

My many thanks also go to Dr. Stanley Thompson of Oregon State University and his rich notes on the topics of “Unstable Nuclear Power,” which were available on the Internet.

It is anticipated that the first half of the book will be useful to many professionals in the nuclear industry. The second half of the book should be of use to nuclear engineering professionals concerned with operating nuclear reactors.

Albuquerque, NM, USA

Bahman Zohuri

Acknowledgment

I would like to give my heartfelt thanks to Professor Patrick McDaniel for his lecture notes given at the University of New Mexico, Nuclear Engineering Department, Professor Hiroshi Sekimoto of Tokyo Institute of Technology for his *Nuclear Reactor Theory* book, Professor H. Van Dam of Delft University of Technology for his nuclear reactor physics lecture notes AP3341, and Professor Emeritus William J. Garland, Department of Engineering Physics, McMaster University, who provided me some of his lectures and class notes and graciously gave me permission to use them in sections or chapters throughout this book where I saw it fit.

I also like to take this opportunity to thank Professor Emeritus Sydney Yip of Massachusetts Institute of Technology for his generous and rich class lectures that he provided me after participating in some of his lecture classes when he was actively teaching in the Nuclear Engineering Department of MIT.

Contents

1	Neutron Physics Background	1
1.1	Nuclei: Sizes, Composition, and Binding Energies	1
1.2	Decay of a Nucleus	7
1.3	Distribution of Nuclides and Nuclear Fission/Nuclear Fusion	10
1.4	Neutron-Nucleus Interaction	13
1.4.1	Nuclear Reactions Rates and Neutron Cross Sections	13
1.4.2	Effects of Temperature on Cross Section	19
1.4.3	Nuclear Cross-Sectional Processing Codes	19
1.4.4	Energy Dependence of Neutron Cross Sections	24
1.4.5	Types of Interactions	27
1.5	Mean Free Path	29
1.6	Nuclear Cross Section and Neutron Flux Summary	30
1.7	Fission	31
1.8	Fission Spectra	32
1.9	The Nuclear Fuel	42
1.9.1	Fertile Material	45
1.10	Liquid Drop Model of a Nucleus	46
1.11	Summary of Fission Process	47
1.12	Reactor Power Calculation	48
1.13	Relationship Between Neutron Flux and Reactor Power	49
Problems		49
References		51
2	Modeling Neutron Transport and Interactions	53
2.1	Transport Equations	53
2.2	Reaction Rates	54
2.3	Reactor Power Calculation	54
2.4	Relationship Between Neutron Flux and Reactor Power	55

2.5	Neutron Slowing Down and Thermalization	56
2.6	Macroscopic Slowing Down Power	58
2.7	Moderate Ratio	58
2.8	Integrodifferential Equation (Maxwell-Boltzmann Equation)	59
2.9	Integral Equation	62
2.10	Multi-group Diffusion Theory	64
2.11	The Multi-group Equations	67
2.12	Generating the Coefficients	72
2.13	Simplifications	75
2.14	Nuclear Criticality Concepts	76
2.15	Criticality Calculation	77
2.16	The Multiplication Factor and a Formal Calculation of Criticality	79
2.17	Fast Fission Factor ϵ Definition	85
2.18	Resonance Escape Probability p	87
2.19	Group Collapsing	89
2.19.1	Multi-group Collapsing to One Group	89
2.19.2	Multi-group Collapsing to Two Group	90
2.19.3	Two-Group Criticality	93
2.20	The Infinite Reactor	94
2.21	Finite Reactor	95
2.22	Time Dependence	96
2.23	Thermal Utilization Factor f	98
	Problems	99
	References	100
3	Spatial Effects in Modeling Neutron Diffusion:	
	One-Group Models	101
3.1	Nuclear Reactor Calculations	101
3.1.1	Neutron Spectrum	104
3.2	Control Rods in Reactors	106
3.2.1	Lattice Calculation Analysis	111
3.3	An Introduction to Neutron Transport Equation	113
3.4	Neutron Current Density Concept in General	119
3.5	Neutron Current Density and Fick's Law	120
3.6	Problem Classification and Neutron Distribution	124
3.7	Neutron Slowing Down	128
3.8	Neutron Diffusion Concept	134
3.9	The One-Group Model and One-Dimensional Analysis	135
3.9.1	Boundary Conditions for the Steady-State Diffusion Equation	138
3.9.2	Boundary Conditions: Consistent and Approximate	143

3.9.3	An Approximate Method for Solving the Diffusion Equation	147
3.9.4	The P_1 Approximate Methods in Transport Theory	150
3.10	Further Analysis Methods for One Group	152
3.10.1	Slab Geometry	155
3.10.2	Cylindrical Geometry	155
3.10.3	Spherical Geometry	157
3.11	Eigenfunction Expansion Methods and Eigenvalue Equations	158
3.11.1	Eigenvalues and Eigenfunctions Problems	163
3.12	Multidimensional Models and Boundary Conditions	169
3.12.1	The Unreflected Reactor Parallelepiped Core	173
3.12.2	The Minimum Volume of the Critical Parallelepiped	176
3.12.3	The Peak-to-Average Flux Ratio	178
3.12.4	The Finite Height Cylindrical Core	179
3.13	Relating k to the Criticality Condition	184
3.14	Analytical Solution for the Transient Case for Reactor	185
3.15	Criticality	187
3.16	Bare Critical Reactor One-Group Model	188
3.17	Bare Critical Reactor One-Group Model: Finite Geometries	191
3.18	Reflected Critical Reactors: One-Group Model	193
3.19	Infinite Reflector Case	194
3.20	Criticality for General Bare Geometries	196
3.21	Reflected Reactor Geometries	198
3.22	Reactor Criticality Calculations	201
	Problems	203
	References	212
4	Energy Effects in Modeling Neutron Diffusion: Two-Group Models	213
4.1	One-Group Diffusion Theory	213
4.2	Two-Group Diffusion Theory	214
4.3	Few-Group Analysis	218
4.3.1	Two-Group Thermal Reactor Equations	219
4.3.2	Two-Group Fast Reactor Equations	225
4.4	Transverse Buckling Approximation	227
4.5	Consistent Diffusion Theory Boundary Conditions	227
4.6	Derivation of the One-Dimensional Multi-group P_N Equations	229
4.7	Multi-group Diffusion Equations: Solution Approach	240
4.7.1	Infinite Medium for Group Collapse	241
4.7.2	Zero-Dimensional Spectrum for Group Collapse	241

4.7.3	Group Collapsing	242
4.7.4	Group Collapse	248
Problems		248
References		252
5	Numerical Methods in Modeling Neutron Diffusion	253
5.1	Introduction	253
5.2	Problem(s) Solved	253
5.2.1	Transport Equation	254
5.2.2	Angle Discretization	255
5.2.3	Energy Discretization	257
5.2.4	Spatial Discretization	259
5.2.5	Matrix Formulation	260
5.3	Solution Strategy	261
5.3.1	Types of Outer Iterations	262
5.3.2	Inhomogeneous Source (No Fission)	262
5.3.3	Inhomogeneous Source (with Fission)	263
5.3.4	Fission Eigenvalue Calculation	263
5.3.5	Eigenvalue Search Calculation	264
5.4	Middle Iterations	265
5.5	Inner Iterations	265
5.6	Upscatter Iterations	265
5.7	Inhomogeneous Sources	265
5.8	Background Concepts	266
5.8.1	Mixing Tables	266
5.8.2	Cross-Sectional Collapsing	268
5.9	Input Description	268
5.10	Output Description	283
Reference		283
6	Slowing Down Theory	285
6.1	Neutron Elastic and Inelastic Scattering for Slowing Down	285
6.2	Derivation of the Energy and Transfer Cross Section	286
6.2.1	Elastic Scattering	286
6.2.2	Inelastic Scattering	291
6.3	Derivation of the Isotropic Flux in an Infinite Hydrogen Moderator	292
6.4	Derivation of the Isotropic Flux in a Moderator Other than Hydrogen $A > 1$	296
6.5	Summary of Slowing Down Equations	298
Problems		299
Reference		302

7	Resonance Processing	303
7.1	Difficulties Presented by Resonance Cross Sections	303
7.2	What Is Nuclear Resonance: Compound Nucleus	306
7.2.1	Breit-Wigner Resonance Reaction Cross Sections	308
7.2.2	Resonance and Neutron Cross Section	311
7.3	Doppler Effect and Doppler Broadening of Resonance	314
7.4	Doppler Coefficient in Power Reactors	318
7.5	Infinite Resonance Integrals and Group Cross Section	320
7.5.1	The Flux Calculator Method	321
7.5.2	The Bondarenko Method: The Bondarenko Factor	322
7.5.3	The CENTRM Method	325
7.6	Infinite Resonance Integrals and Group Cross Sections	325
7.7	Dilution Cross Section: Dilution Factor	327
7.8	Resonance Effects	330
7.9	Homogeneous Narrow Resonance Approximation	336
7.10	Homogeneous Wide Resonance Approximation	338
7.11	Heterogeneous Narrow Resonance Approximation	340
7.12	Heterogeneous Wide Resonance Approximation	342
	Problems	345
	References	348
8	Heterogeneous Reactors and Wigner-Seitz Cells	349
8.1	Homogeneous and Heterogeneous Reactors	349
8.2	Spectrum Calculation in Heterogeneous Reactors	352
8.3	Cross-Sectional Self-Shielding and Wigner-Seitz Cells	354
	Problems	357
	References	360
9	Thermal Spectra and Thermal Cross Sections	361
9.1	Coupling to Higher-Energy Sources	361
9.2	Chemical Binding and Scattering Kernels	367
9.2.1	Scattering Materials	369
9.2.2	Thermal Cross Sectional Average	372
9.3	Derivation of the Maxwell-Boltzmann Spectrum	376
	Problems	382
	References	385
10	Perturbation Theory for Reactor Neutronics	387
10.1	Perturbation Theory	387
10.2	Zero-Dimensional Methods	388
10.2.1	Spatial Method (1 Group)	392
	Problems	398
11	Reactor Kinetics and Point Kinetics	401
11.1	Time-Dependent Diffusion Equation	401
11.2	Derivation of Exact Point Kinetics Equations (EPKE)	405

11.3	The Point Kinetics Equations	413
11.4	Dynamic Versus Static Reactivity	416
11.5	Calculating the Time-Dependent Shape Function	417
11.6	Point Kinetics Approximations	419
11.6.1	Level of Approximation to the Point Kinetics Equations	419
11.7	Adiabatic Approximation	419
11.8	Adiabatic Approximation with Pre-computed Shape Functions	420
11.9	Quasi-Static Approximation	420
11.10	Zero-Dimensional Reactors	420
	Problems	423
	References	426
12	Reactor Dynamics	427
12.1	Background on Nuclear Reactor	427
12.2	Neutron Multiplication	430
12.3	Simple Feedbacks	432
12.4	Multiple Time Constant Feedbacks	439
12.5	Fuchs-Nordheim Model	440
12.6	Fuchs-Hansen Model	443
	Problems	445
	References	448
13	Reactor Stability	451
13.1	Frequency Response	451
13.2	Linearity	453
13.3	Time Invariance	454
13.4	Nyquist Plots	456
13.5	Nonlinear Stability	462
	Problems	464
	References	465
14	Numerical Modeling for Time-Dependent Problems	467
14.1	Fast-Breeder Reactor History and Status	467
14.2	The Concept of Stiffness	474
14.3	The Quasi-Static Method	476
14.4	Bethe-Tait Models	477
	References	481
15	Fission Product Buildup and Decay	483
15.1	Background Introduction	483
15.2	Nuclear Fission and the Fission Process	486
15.3	Radioactivity and Decay of Fission Product	489
15.4	Poisons Produced by Fission	493
	Problems	495
	References	499

16 Fuel Burnup and Fuel Management	501
16.1 The World's Energy Resources	501
16.2 Today's Global Energy Market	502
16.3 Fuel Utilization and Fuel Burnup	503
16.4 Fuel Reprocessing	504
16.4.1 PUREX Process	506
16.4.2 Transuranium Elements	506
16.4.3 Vitrification	507
16.5 Fuel Management for Nuclear Reactors	508
16.6 Nuclear Fuel Cycle	511
16.7 Store and Transport High Burnup Fuel	513
16.8 Nuclear Reactors for Power Production	514
16.9 Future Nuclear Power Plant Systems	516
16.10 Next Generation of Nuclear Power Reactors for Power Production	517
Problems	519
References	521
17 Why Nuclear Power Plant Energy	523
17.1 Introduction	523
17.2 Innovative Approach	529
17.3 Methodology of Combined Cycle	531
17.4 Why We Still Need Nuclear Power	532
17.5 Is Nuclear Energy Renewable Source of Energy	532
17.6 Argument for Nuclear Power as Renewable Energy Source	534
17.7 Argument Against Nuclear Power as a Renewable Energy Source	534
17.8 Safety	535
17.9 Fuel Cycle	538
17.10 Nuclear Power Economics	542
17.11 A Nuclear Revival or Decline	549
17.12 Spent Fuel and High-Level Waste Management	551
17.13 Proliferation and Nonproliferation	555
17.14 Society Attitude and Public Understanding of Nuclear Power	556
17.15 Conclusion	558
References	559
18 Small Modular Reactors and Innovative Efficient Enhancement Design	561
18.1 Introduction	561
18.2 Generation IV Drive New Nuclear Reactor Concepts	563
18.3 Technological State- of- the-Art and Anticipated Developments	566

18.4	Next Generation Nuclear Plant (NGNP)	569
18.5	Generation IV Systems	570
18.5.1	Very High-Temperature Reactor (VHTR)	571
18.5.2	Molten Salt Reactor (MSR)	573
18.5.3	Sodium-Cooled Fast Reactor (SFR)	575
18.5.4	Supercritical Water-Cooled Reactor (SCWR)	577
18.5.5	Gas-Cooled Fast Reactor (GFR)	580
18.5.6	Lead-Cooled Fast Reactor (LFR)	582
18.6	Next Generation of Nuclear Power Reactors for Power Production	584
18.7	Goals for Generation IV Nuclear Energy Systems	584
18.8	Why We Need to Consider the Future Role of Nuclear Power Now	585
18.9	The Generation IV Roadmap Project	588
18.10	Licensing Strategy Components	591
18.11	Market and Industry Status and Potentials	592
18.12	Barriers	593
18.13	Needs	594
18.14	Synergies with Other Sectors	595
18.15	Combined Cycles for Efficiency of New Generation Nuclear Power Plants	596
18.16	Advanced Modular Reactors (AdvSMRs)	599
18.17	Advantages of Small Modular Reactors (SMRs)	602
18.18	Conclusions	605
	References	606
19	Design and Analysis of Core Design for Small Modular Reactors	609
19.1	Introduction	609
19.2	Heat Pipe Micro Reactor	617
19.3	High-Temperature Gas-Cooled Reactors/Advanced Small Modular Reactor	620
19.4	Core Design and Analysis	625
19.5	Small Modular Reactors General Concepts	628
19.5.1	Modularity and Flexibility	630
19.6	Safety Features and Licensing of Small Modular Reactors (SMRs)	630
19.6.1	Safety Features of Small Modular Reactors	631
19.6.2	Licensing of Small Modular Reactors	632
19.6.3	Nonproliferation Resistant and Security	632
19.7	Small Reactor Designs in Market	635
19.8	Conclusions	636
	References	637

Contents	xix
Appendix A Laplace Transforms	641
Appendix B Transfer Functions and Bode Plots	647
Index	659

About the Author

Bahman Zohuri is currently at the Galaxy Advanced Engineering, Inc., a consulting company that he started himself in 1991 when he left both semiconductor and defense industries after many years working as a chief scientist. After graduating from the University of Illinois in field of Physics and Applied Mathematics, as well as the University of New Mexico from Nuclear Engineering Department, he joined Westinghouse Electric Corporation where he performed thermal hydraulic analysis and natural circulation for inherent shutdown heat removal system (ISHRS). The study was performed for the core of a liquid-metal fast-breeder reactor (LMFBR) as a secondary fully inherent shutdown system for secondary loop heat exchange. All these designs were used for nuclear safety and reliability engineering for self-actuated shutdown system. He designed the mercury heat pipe and electromagnetic pumps for large pool concepts of LMFBR for heat rejection purpose for this reactor around 1978 where he received a patent for it. He later on was transferred to the defense division of Westinghouse where he was responsible for the dynamic analysis and method of launching and handling of MX missile out of the canister. The results are applied to MX launch seal performance and muzzle blast phenomena analysis (i.e., missile vibration and hydrodynamic shock formation). He also was involved in analytical calculation and computation in the study of nonlinear ion wave in rarefying plasma. The results are applied to the propagation of “soliton wave” and the resulting charge collector traces in the rarefaction characteristic of the corona of the laser-irradiated target pellet. As part of his graduate research work at Argonne National Laboratory, he performed computation and programming of multi-exchange integral in surface physics and solid-state physics. He holds different patents in areas such as diffusion processes and design of diffusion furnace while he was senior process engineer working for different semiconductor industries, such as Intel Corporation, Varian Medical Systems, and National Semiconductor Corporation. Later on, he joined Lockheed Missile and Aerospace Corporation as senior chief scientist and was responsible for the research and development (R&D) and the study of vulnerability, survivability, and both radiation and laser hardening of different components of the Strategic Defense Initiative known as Star Wars. This included payload (i.e., IR sensor) for the Defense Support Program (DSP),

Boost Surveillance and Tracking System (BSTS), and Space Surveillance and Tracking Satellite (SSTS) against laser or nuclear threat. While in there, he also studied and performed the analysis of characteristics of laser beam and nuclear radiation interaction with materials, transient radiation effects in electronics (TREE), electromagnetic pulse (EMP), system-generated electromagnetic pulse (SGEMP), single-event upset (SEU), blast, and thermomechanical, hardness assurance, maintenance, and device technology.

He did few years of consulting under his company Galaxy Advanced Engineering with Sandia National Laboratories (SNL), where he was supporting the development of operational hazard assessments for the Air Force Safety Center (AFSC) in connection with other interested parties. The intended use of the results was their eventual inclusion in Air Force Instructions (AFIs) specifically issued for directed-energy weapon (DEW) operational safety. He completed the first version of a comprehensive library of detailed laser tools for Airborne Laser (ABL), Advanced Tactical Laser (ATL), Tactical High-Energy Laser (THEL), Mobile/Tactical High-Energy Laser (M-THEL), etc.

He also was responsible on SDI computer programs involved with Battle Management C³ and artificial Intelligent and autonomous system. He is author of few publications and holds various patents such as laser-activated radioactive decay and results of thru-bulkhead initiation.

He has published many text books and other papers with different publisher that can be found on Amazon.com or the Internet on different subjects related to nuclear energy, physics, and other scientific fields.

Chapter 1

Neutron Physics Background



This chapter introduces fundamental properties of the neutron. It covers reactions induced by neutrons, nuclear fission, slowing down of neutrons in infinite media, diffusion theory, the few-group approximation, point kinetics, and fission-product poisoning. It emphasizes the nuclear physics bases of reactor design and its relationship to reactor engineering problems.

1.1 Nuclei: Sizes, Composition, and Binding Energies

The diameters of atoms and molecules are of the order of 10^{-10} – 10^{-9} m. On the other hand, the diameters of nuclei are small, of the order of 10^{-15} – 10^{-14} m. The size of molecules is often measured in Å (angstrom, $1 \text{ \AA} = 10^{-10} \text{ m}$) and nm ($1 \text{ nm} = 10^{-9} \text{ m}$). On the other hand, the size of nuclei is often measured in fm (femtometer, $1 \text{ fm} = 10^{-15} \text{ m}$). That is, the diameters of atoms and molecules are approximately 0.1–1 nm, and the diameters of nuclei are approximately 1^{-10} fm.

Because of the uncertainty principle, a much higher energy is associated with a nucleus than with an atom or a molecule, as it is much smaller. Chemical reactions are measured in the unit of eV (where 1 eV is the energy acquired when a particle with one elementary electric charge is accelerated by a potential difference of 1 V in a vacuum). In contrast, the unit of MeV ($1 \text{ MeV} = 10^6 \text{ eV}$) is usually used for nuclear reactions.

An approximate but rather more concrete explanation is given by the following. The n -th energy eigenvalue for a particle with mass m trapped inside a potential well of size L is given by the following equation:

$$E_n = N_n \frac{1}{2m} \left(\frac{\pi \hbar}{L} \right)^2 \quad (1.1)$$

Table 1.1 Masses of proton, neutron, and electron

Particle	Mass (kg)	Mass (amu)	MeV/c ²
1 atomic mass unit	1.660540×10^{-27}	1.000	931.5016
Proton	1.672623×10^{-27}	1.007276	938.280
Neutron	1.674929×10^{-27}	1.008665	939.573
Electron	9.109390×10^{-31}	0.000549	0.511

Here N_n is a constant determined by the quantum number n , and $\hbar = 6.582 \times 10^{-16}$ eVsec is the value obtained by dividing Planck's constant by 2π . We let $n = 1$ and use the mass of a nucleon and the mass of an electron shown in Table 1.1. For an electron, $(1/2 m)(\pi \hbar L)^2 = 3.8 \times 10^{-15}$ eV if $L = 1$ cm, giving a very small value. For an atom of size 0.1–1 nm, the energy is 38–0.38 eV. In the case of a proton, the energy is 200–2 MeV for a nucleus of size 1^{-10} fm.

The mass of a proton is approximately the same as that of a neutron, whereas the mass of an electron is much smaller than that of a proton or neutron. As a unit for measuring the mass of an atom (the atomic weight), the value obtained by dividing the mass of an atom with its mass number is convenient (this is called the “atomic mass unit” with symbol “amu” or “u”). However, the sum of the masses of a proton and an electron is different from the mass of a neutron.

In addition, when nucleons are bound, the mass will generally decrease from the sum of the masses of the original nucleons (this will be explained later). Thus, it is necessary to use a specific standard nuclide to determine the atomic mass unit. Various nuclides have been proposed for this standard, but from 1962, international consensus has been to use the atomic weight of ^{12}C divided by 12 to obtain the standard 1 amu. The masses of the proton, neutron, and electron using this atomic mass unit are shown in Table 1.1. They are also shown in the unit of MeV/c², which will be explained later.

In a nucleus, nucleons are attracted to each other by the nuclear force. Nucleons in such a field try to take as low an energy state as possible. That is, when separate nucleons are combined together, the lowest energy state is taken and the excess energy is released. This energy is called the binding energy. The relationship between the energy E and mass M is the following, derived from Einstein's famous relativity theory with c being speed of light:

$$E = mc^2 \quad (1.2)$$

Equation 1.2 can be used to prove that a mass of 1 amu is equivalent to an energy of 931.5016 MeV.

Something should strike you as strange about the Table 1.1 above. The carbon-12 atom has a mass of 12.000 u, and yet it contains 12 objects (6 protons and 6 neutrons) that each have a mass greater than 1.000 u, not to mention a small contribution from the 6 electrons.

This is true for all nuclei, that the mass of the nucleus is a little less than the mass of the individual neutrons, protons, and electrons. This missing mass is known as the mass defect and represents the binding energy of the nucleus.

The binding energy is the energy you would need to put in to split the nucleus into individual protons and neutrons. To find the binding energy, add the masses of the individual protons, neutrons, and electrons, subtract the mass of the atom, and convert that mass difference to energy. For carbon-12 this gives:

$$\begin{aligned}\text{Mass defect} = \Delta m &= 6^* 1.008664 \text{ u} + 6^* 1.007276 \text{ u} + 6^* 0.00054858 \text{ u} \\ &\quad - 12.000 \text{ u} = 0.098931 \text{ u}\end{aligned}$$

The binding energy in the carbon-12 atom is therefore $0.098931 \text{ u} * 931.5 \text{ MeV/u} = 92.15 \text{ MeV}$.

In a typical nucleus the binding energy is measured in MeV, considerably larger than the few eV associated with the binding energy of electrons in the atom. Nuclear reactions involve changes in the nuclear binding energy, which is why nuclear reactions give you much more energy than chemical reactions; those involve changes in electron binding energies.

However, the mass of the atom is smaller than the sum of the masses of nucleons and electrons that constitute the atom. This difference in mass is called the mass defect, $D(Z, N)$ for a nuclide with atomic number Z and neutron number N . For the mass of a hydrogen atom m_H and the mass of a neutron m_N , the mass of a neutral atom is expressed as follows:

The binding energy can be expressed as follows using Eq. 1.1 as:

$$B(Z, N) = D(Z, N)c^2 \quad (1.3)$$

The binding energy is equivalent to the mass defect, with the binding energy used when energy is being considered and the mass defect used when mass is being considered. The unit MeV is often used for the energy of nuclear reactions, with mass and energy converted according to the following relationship:

$$1 \text{ amu} = 931.5016 \text{ MeV/c}^2 \quad (1.4)$$

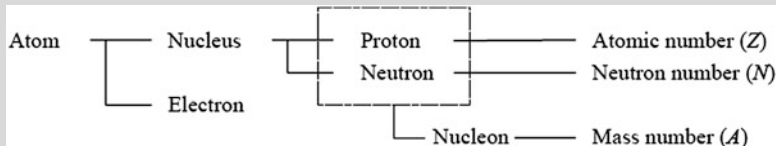
A term similar to the mass defect is the mass deviation (or mass excess), defined as the difference $M - A$, for M the mass in atomic mass units and A the mass number, which is an integer. It is important to clearly distinguish these terms. Different nuclei have different mass defects. Accordingly, energy is absorbed or released during a nuclear reaction. In addition, it is possible to determine the possibility of a certain reaction occurring by the size of the mass defect. Thus, it is very important to know the mass defect of a nuclide. In this section we are concerned with the state with the lowest internal energy of the nucleus. This state is called the ground state. States with higher internal energy are called excited states.

Bear in mind that in general, species of atoms and nuclei are called elements and nuclides, respectively. An element is determined by its proton number (the number of protons). The proton number is generally called the atomic number and is denoted by Z . A nuclide is determined by both the proton number and the neutron number (the number of neutrons denoted by N). The sum of the proton number and neutron number, namely, the nucleon number, is called the mass number and is denoted by A ($A = Z + N$). Obviously, a nuclide can also be determined by the atomic number and mass number.

In order to identify a nuclide, A and Z are usually added on the left side of the atomic symbol as superscript and subscript, respectively. For example, there are two representative nuclides for uranium, described as $^{235}_{92}\text{U}$ and $^{238}_{92}\text{U}$. If the atomic symbol is given, the atomic number can be uniquely determined; thus Z is often omitted like ^{235}U and ^{238}U .

The chemical properties of an atom are determined by the atomic number, so even if the mass numbers of nuclei are different, if the atomic numbers are the same, their chemical properties are the same. These nuclides are called isotopic elements or isotopes. If the mass numbers are the same and the atomic numbers are different, they are called isobars. If the neutron numbers are the same, they are called isotones. The above examples for uranium are isotopes.

Summarizing these and rewriting the constitution of an atom, we obtain the following figure.



Constitution of an atom

The most important force in the nucleus is the nuclear force. The nuclear force is a strong interaction, generated by the exchange of pions. The distance of interaction is very short, approximately 2 fm, and thus only neighboring nucleons interact with each other. Therefore, the contribution of the nuclear force to the mass defect is proportional to the mass number. For a_v , a suitable proportionality constant, the contribution is expressed as $a_v A$. If all the nucleons are surrounded by other nucleons, this expression is satisfactory. However, there are no nucleons outside the surface nucleons, and thus the binding energy is smaller to that extent. This is the so-called surface tension and is expressed as $a_s A^{2/3}$. The second important force in a nucleus is the Coulomb force.

Pion

In particle physics, a pion (short for **pi meson**, denoted with the Greek letter pi: p) is any of three subatomic particles: π^0 , π^+ , and π^- . Each pion consists of a quark and an antiquark and is therefore a meson. Pions are the lightest mesons and are unstable, with the charged pions π^+ and π^- decaying with a mean lifetime of 26 nanoseconds (2.6×10^{-8} s), and the neutral pion π^0 decaying with a much shorter lifetime of 8.4×10^{-17} s. Charged pions usually decay into **muons** and **muon** neutrinos and neutral pions into gamma rays.

Note that muon (μ) is an elementary particle similar to the electron, with unitary negative electric charge of -1 and a spin of $1/2$, but with a much greater mass ($105.7 \text{ MeV}/c^2$), and the three neutrinos.

As is the case with other leptons, the muon is not believed to have any sub-structure – that is, it is not thought to be composed of any simpler particles.

Inside a nucleus, there are positive charges due to protons, but there are no negative charges. Therefore, a repulsive Coulomb force operates. This force exists among the protons. Its energy is obtained by dividing the product of the electric charges by the distance between them. In this case, the distance may be considered proportional to the size of the nucleus. If the volume of the nucleus is proportional to the mass number, the contribution of the Coulomb force to the mass defect is expressed as $a_c Z^2 A^{-1/3}$. If these were the only forces existing among nucleons, a nucleus containing only neutrons would have strong binding because of the absence of the Coulomb force. However, this is not consistent with experimental results. In reality, in a strongly bound nucleus, the proton number and the neutron number are similar. Thus, there is symmetry between protons and neutrons, and the closer the proton and neutron numbers, the more stable the nucleus is. Thus, the expression $-a_l(N - Z)^2 A^{-1}$ is added to the mass defect. In addition to the above important terms, pairs of protons or of neutrons have a stabilizing property. Thus, when the proton number or the neutron number is even, the nucleus is more stable. This effect is expressed as $a_e \delta(Z, N) A^{-1/2}$, with the following function introduced:

$$\delta(Z, N) = \begin{cases} 1 & \rightarrow \text{If both } Z \text{ and } N \text{ are even} \\ 0 & \rightarrow \text{If both } A \text{ is odd} \\ -1 & \rightarrow \text{If both } Z \text{ and } N \text{ are odd} \end{cases} \quad (1.5)$$

Weiszacker and Bethe have proposed the following empirical mass formula by adding these terms together:

$$B(Z, N) = a_v A - a_s A^{1/3} - a_c Z^2 A^{-1/3} - a_l (N - Z)^2 A^{-1} + a_e \delta(Z, N) A^{-1/2} \quad (1.6)$$

The terms on the right side are, from the left, the volume term, surface term, Coulomb term, symmetry term, and even-odd term. The coefficients are determined so that the mass defect is consistent with the experimentally determined masses. An example set of coefficients determined by P. E. Hodgson, et al. [13] in 1997 is shown below:

$$a_v = 15.835 \text{ MeV}$$

$$a_s = 18.33 \text{ MeV}$$

$$a_c = 0.714 \text{ MeV}$$

$$a_I = 23.20 \text{ MeV}$$

$$a_e = 11.2 \text{ MeV}$$

This equation is simple, but it nicely reproduces the experimental data, with the errors for heavy nuclei less than 1%. However, for a detailed analysis of nuclear reactions, more accurate values are often necessary. In that case, please consult reference in footnote [14]. The binding energy per nucleon and contribution of each term will be shown later in Fig. 1.5.

In the derivation of the mass formula, we notice that for suitable values of A and N there may be a nuclide with the greatest binding energy per nucleon, that is, the most stable nuclide. In fact, ^{56}Fe has the largest binding energy per nucleon of 8.55 MeV. When A and Z depart from the suitable values, the binding energy decreases, and the nuclide becomes unstable. When the binding energy is negative, the nucleus cannot exist. However, even when the binding energy is positive, not all nuclides can exist. There are numerous cases where a nuclide will decay to another nuclide with a larger binding energy. However, the number of such decays is limited, and there are numerous nuclides in nature besides the most stable nuclides. This will be explained in a later section.

Nuclei with a neutron number N or proton number Z of 2, 8, 20, 28, 50, 82, or 126 are especially stable compared with nuclei with numbers in the vicinity. These numbers are called magic numbers. They will be shown on the chart of nuclides in Fig. 1.3.

Atom Density

One important property of a material is the atom density. The *atom density* is the number of atoms of a given type per unit volume of the material. To calculate the atom density of a substance, use the following equation:

$$N = \frac{\rho N_A}{M}$$

where:

N = atom density (atoms/cm³)

ρ = density (g/cm³)

N_A = Avogadro's number (6.022×10^{23} atoms/mole)

M = gram atomic weight

1.2 Decay of a Nucleus

Before we start talking about decay of a nucleus, we have to define a value known as Q -value, which in nuclear physics and chemistry counts for a reaction that is the amount of energy released by that reaction. The value relates to the enthalpy of a chemical reaction or the energy of radioactive decay products. It can be determined from the masses of reactants and products. Q -value affects reaction rates. By definition the energy conservation of the simple reaction enables the general definition of Q based on mass-energy equivalence as:

$$Q = (m_{Initial} - m_{Final})c^2$$

A reaction with a positive Q -value is exothermic, i.e., it has a net release of energy, since the kinetic energy of the final state is greater than the kinetic energy of the initial state. A reaction with a negative Q -value is endothermic, i.e., it requires a net energy input, since the kinetic energy of the final state is less than the kinetic energy of the initial state.

Example 1.1 If in case of particle physics the Q -value is the kinetic energy released in the decay at rest. Calculate this value for neutron decay.

Solution For neutron decay, some mass disappears as neutrons convert to a proton, electron, and neutrino:

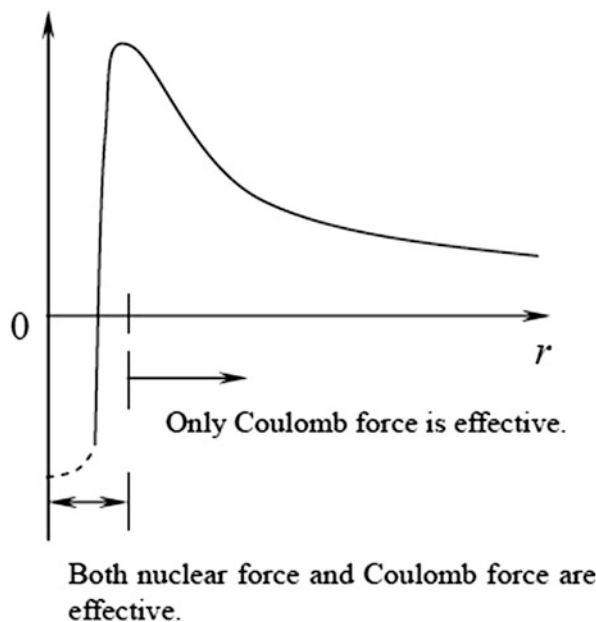
$$Q = (m_n - m_p - m_{\bar{\nu}} - m_e)c^2 = 0.782 \text{ MeV}$$

In this example m_n is the mass of the neutron, m_p is the mass of the proton, $m_{\bar{\nu}}$ is the mass of the electron antineutron, and m_e is the mass of the electron. In beta decay a typical Q -value is around 1 MeV.

Now getting back to discussion of this section on the decay of a nucleus, we can briefly explain as follows. Typical decays are α -decay, β -decay, and γ -decay, which emit α -rays, β -rays, and γ -rays, respectively. An α -ray is a nucleus of ${}^4\text{He}$, a β -ray is an electron, and a γ -ray is a high-energy photon. In β -decay, a positron may be emitted, which is called β^+ -decay. In order to distinguish the two cases, the ordinary decay in which an electron is emitted is sometimes called β^- -decay. As a competitive process for β^+ -decay, orbital electron capture occurs when a nucleus takes in an orbital electron. As a competitive process for γ -decay, internal conversion occurs, when an orbital electron is ejected, rather than a γ -ray being emitted. By α decay, Z and N both decrease by 2. By β^- -decay, Z increases by 1 and N decreases by 1. By β^+ -decay and orbital electron capture, Z decreases by 1 and N increases by 1. By γ -decay and the internal conversion, neither Z nor N change.

Some decays take place readily, while other decays rarely occur. The conservation laws for angular momentum, parity, etc. play a great role in this difference.

Fig. 1.1 Potential of the Coulomb repulsive force in nuclear decay



However, we will omit a detailed explanation of this and will instead describe other important matters.

When a positively charged particle is emitted from a nucleus, the particle should normally have to overcome the potential of the Coulomb repulsive force, shown in Fig. 1.1, since the nucleus also has a positive charge. In reality however, it is not necessary to overcome the potential peak, and a particle with an energy smaller than the peak energy can be emitted by the tunnel effect. However, the probability of this occurring rapidly decreases when the mass of the emitted particle becomes large or the height and thickness of the potential wall increase.

Therefore, the emission of a heavy particle and reactions with low Q -value occur with difficulty. As a result, the α -particle is the only positively charged particle that is regularly emitted and is generally emitted only from nuclei with large atomic numbers Z . However, α -particles can occasionally be emitted from light nuclei, and a nucleus of proton or carbon may occasionally be emitted.

In γ -decay, there is no Coulomb barrier since the emitted particle is a photon. In internal conversion, which competes with γ -decay, there is no barrier since the emitted particle is an electron, which is attracted by the nucleus. In β -decay, there is no barrier for neutrinos, since the interaction of a neutrino with other material can be ignored. When the other emitted particle is an electron, it is attracted by the nucleus, and thus there is also no barrier. In the case of a positron, there is a Coulomb barrier. Nevertheless, the mass of a positron is smaller than that of an α -particle, and

thus it can easily pass through the barrier. However, in nuclides with large atomic numbers, β^+ -decay with low decay energy rarely takes place since orbital electron capture, which is a competitive process, dominates. Since β -decay is a weak interaction and γ -decay is an electromagnetic interaction, γ -decay takes place more easily than β -decay. Spontaneous fission is another important decay for heavy nuclei. In this case, a Coulomb repulsive force even stronger than for α -decay applies, and the masses of the emitted particles are large; therefore the parent nucleus must have a sufficiently high energy. Since the neutron has no Coulomb barrier, a neutron can easily jump out of a nucleus if energy permits. Although it is not appropriate to call this a decay, it is important in relation to the later-described delayed neutron, which accompanies nuclear fission. The rate of decay is naturally proportional to the number of nuclides N under consideration and is expressed by the following equation:

$$\frac{dN}{dT} = -\lambda N \quad (1.7)$$

Here, the proportionality constant λ is unique to the particular nuclide and is called the decay constant, and the reciprocal of it is called the *mean life of the radioactive species known as $T_m = 1/\lambda$* . If we let the number of nuclides at $t = 0$ be N_0 , the following solution is obtained for Eq. 1.7:

$$N = N_0 \exp(-\lambda t) \quad (1.8)$$

The time necessary for N to become half of N_0 is called the half-life, and from Eq. 1.8, the half-life $T_{1/2}$ can be expressed using λ in the following way:

$$T_{1/2} = \frac{\ln 2}{\lambda} = T_m \cdot \ln 2 = (0.69315)T_m = \frac{0.69315}{\lambda} \quad (1.9)$$

The mean life of a nucleus τ is expressed by the following equation:

$$\tau = \frac{1}{N_0} \int_0^{\infty} t \lambda N dt = \frac{1}{\lambda} \quad (1.10)$$

The capability to emit radiation is called radioactivity. Radioactive strength is expressed by the unit Becquerel (B_q), an SI unit. One decay per second is $1 B_q$. However, the traditionally used unit, the curie (C_i), is still frequently used. The two units are converted according to the following:

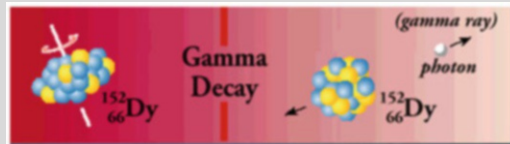
$$1 C_i = 3.7 \times 10^{10} B_q \quad (1.11)$$

1.3 Distribution of Nuclides and Nuclear Fission/Nuclear Fusion

In the previous section, it is explained that three kinds of decays can easily take place. The decays are α -decay, β -decay, and γ -decay, but their order of likelihood is γ -decay, β -decay, α -decay. In γ -decay, the nucleus does not change; see the explanation of this statement in the following box.

Gamma Decay

In gamma decay, depicted using the figure below, a nucleus changes from a higher energy state to a lower energy state through the emission of electromagnetic radiation (photons). The number of protons (and neutrons) in the nucleus does not change in this process, so the parent and daughter atoms are the same chemical element. In the gamma decay of a nucleus, the emitted photon and recoiling nucleus each have a well-defined energy after the decay. The characteristic energy is divided between only two particles.



In β -decay, the next most likely decay, the mass number A does not change, but the atomic number Z changes. Plotting neutron number Z against atomic number Z following β -decay gives a slope of 45° . On this line, the binding energy (mass defect) changes as shown in Fig. 1.2 (see Eq. 1.6). When A is odd, the last term of Eq. 1.6 becomes zero, and the points representing the binding energy for the respective nuclei stay on a parabolic curve. The nuclide at the highest point is a stable nuclide and is generally uniquely determined; nuclides with a higher Z than this decay by β^+ -decay and nuclides with the lower Z decay by β^- -decay. When A is even, the last term of Eq. 1.6 is positive if Z is even and odd if Z is negative. Therefore, the points representing the binding energy of respective nuclei are alternately on either of two parabolic curves. Thus, there is a possibility that multiple stable nuclides exist, and these stable nuclides are alternately located between unstable nuclides. Nuclides may also undergo a change in A , which is likely to take place through α -decay; however, A should be very large in this case. As a result of these decays, the only naturally occurring nuclides are those shown in Fig. 1.3.

In Fig. 1.3, we can see that the curve along the stable nuclides is convex, curving downward at high A , because of the balance of the Coulomb and symmetry terms. Therefore, when heavy nuclide fission into two nuclides of approximately equal mass, the resulting nuclides are unstable, having too many neutrons. In reality, two

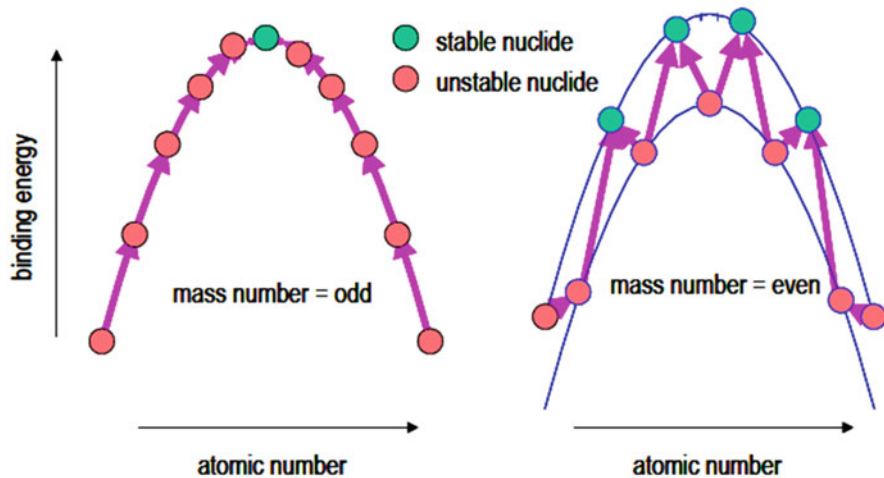


Fig. 1.2 Binding energy change in β -decay and the direction of the decay

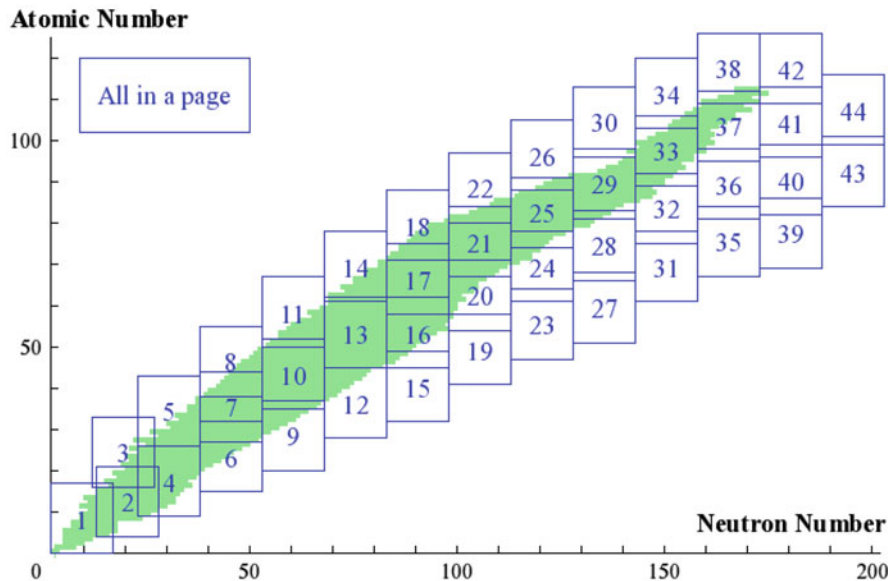


Fig. 1.3 Chart of the nuclides [15]

or three neutrons are emitted during fission, and most fission products will decay by β -decay.

If the mass number A of naturally occurring nuclides is plotted as the abscissa and the binding energy is plotted as the ordinate, Figure 1.4a is obtained. Where A is small, the surface term is large, and where A is large, the Coulomb term is large.

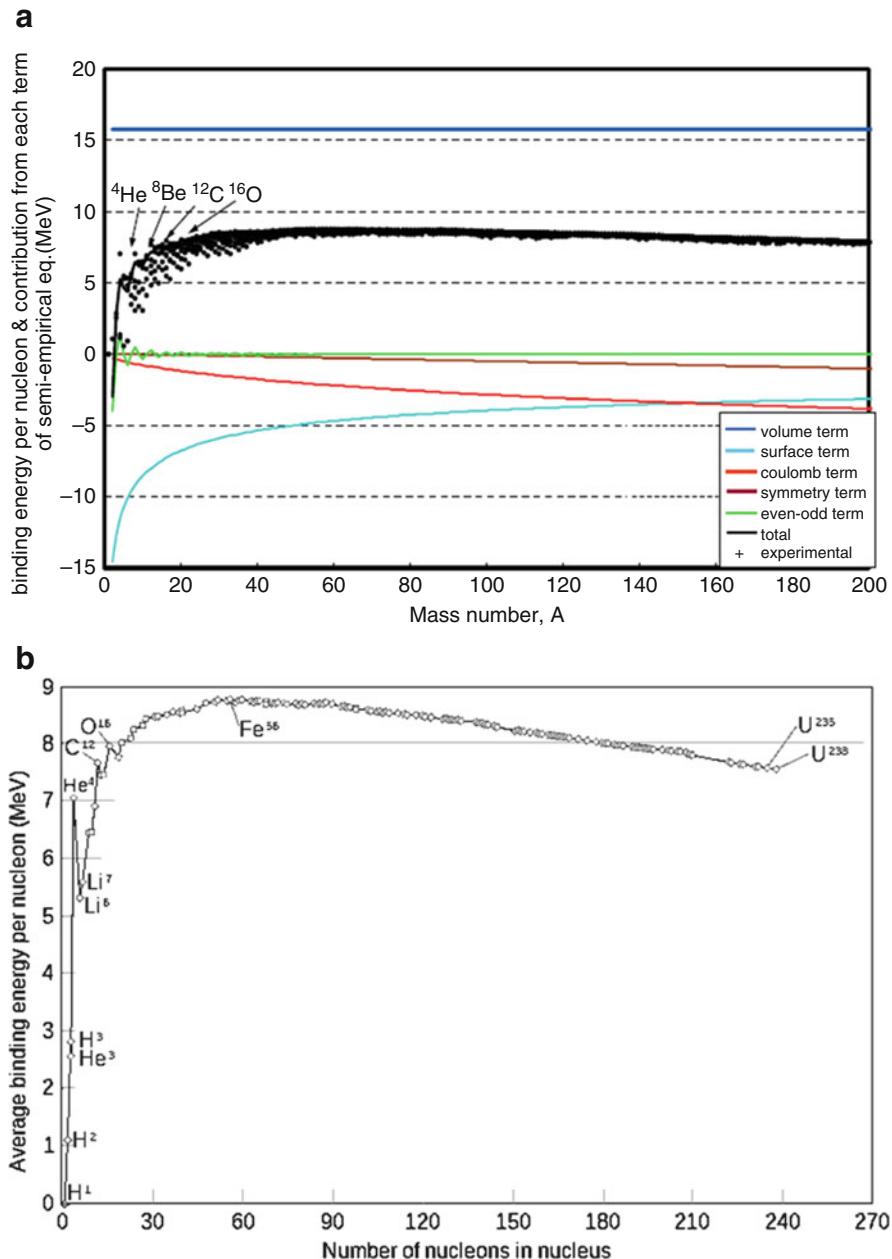


Fig. 1.4 (a) Binding energy per nucleon and contribution of each term [16]. (b) Variation of binding energy per nucleon with mass number. (From Wikimedia Commons)

According to this figure, we can see that a nuclide with small A can fuse to a nuclide with a large binding energy and release energy. Similarly, a nuclide with large A can fission into nuclides with large binding energies, releasing energy. By nuclear fission, two fission products of approximately equal mass are generated.

One of most the most interesting aspect of the nature can be shown in Figure 1.4b, which shows that the binding energy per nucleon in nuclei of various atoms differ from each other (see Problem 1.3 at the end of this chapter). Sometimes this diagram is referred to as the “most important diagram in the Universe.” And in fact, it is difficult to overestimate the importance of that curve. Assume that one uranium nucleus breaks up into two lighter nuclei. For the time being, it assumed that this is possible (this process is called nuclear fission, and later on it will be discussed how it can be done).

The total binding energy can be calculated, using Eq. 1.6. This equation is very useful since it approximates the binding energy for over 300 stable and non-stable nuclei, but it is applicable for nuclei with large mass numbers only.

1.4 Neutron-Nucleus Interaction

The central problem in nuclear reactor kinetics is to predict the evolution in time of the neutron population in a multiplying medium point reactor kinetics (This will be explained in later chapter, but for time being consider that the reactor is viewed as a point, hence the terminology of point reactor kinetics. In this regard, a distinction must be made between the behaviors of the prompt and delayed neutrons. The point kinetics model can be obtained directly from the space- and time-dependent transport equations) allows the study of the global behavior of the neutron population from the average properties of the medium. Before tackling, the equations governing the time variation of the reactor power (proportional to the total neutron population), we shall discuss briefly the properties of a neutron-multiplying medium after recalling a number of definitions; we shall give a qualitative description of the principal nuclear reactions at play in a self-sustaining chain reaction and dwell on the source of fission neutrons. Since delayed neutrons play a crucial role in reactor kinetics, we shall describe in detail their production in a reactor.

1.4.1 Nuclear Reactions Rates and Neutron Cross Sections

A neutron is an elementary particle. It is stable when bound to a nucleus by the nuclear force. In its free state, a neutron decays, with a time constant of 12 min, to a proton, accompanied by the emission of a β -particle and an antineutrino. In view of the fact, that free neutrons in a reactor either are absorbed in matter or escape, on a time scale of less than 10^{-3} s, it is clear, that neutron instability is completely negligible in reactor physics.

The power generated in a reactor comes from neutron-induced fissions. It results from the interaction between the neutrons and the nuclei of the physical medium. It is generally possible to neglect neutron-neutron interactions, because the density of neutrons is much smaller than that of nuclei. Free neutrons have a certain speed relative to nuclei. If one neglects the energy of thermal motion of the nuclei, then the kinetic energy E of a neutron represents the energy available to a nuclear reaction in a nucleus. If we denote the relative speed of a neutron by V and its mass by m [17], then:

$$E = \frac{1}{2}mv^2 \quad (1.12)$$

The energy is generally given in units of electron volts ($1 \text{ eV} = 1.6021 \times 10^{-19} \text{ J}$).

Interactions of neutrons with matter are described in terms of quantities called cross sections, which can be defined in the following fashion. Imagine a unidirectional neutron beam with a density of n neutrons per cm^3 , of speed V , impinging perpendicularly on a thin slice of a target with a density of N identical nuclei per cm^3 . Define the neutron flux ϕ by:

$$\phi = nv \quad (1.13)$$

Thus, ϕ measures the number of neutrons crossing a unit surface area (1 cm^2) per second. Experiments show that the rate R of interactions of neutrons per cm^2 of target area is proportional to the neutron flux, the density of nuclei, and the target thickness:

$$R = \sigma\phi NV \quad (1.14)$$

where the constant of proportionality σ is called the microscopic cross section. V is the volume of the target per cm^2 (i.e., the target thickness).

The microscopic cross section is a function of the speed of the neutrons relative to the nuclei of the target. It is therefore a function of the kinetic energy available to the reaction. One writes:

$$\sigma = \sigma(E) \quad (1.15)$$

Since NV is equal to the total number of nuclei per cm^2 of target area, σ is a measure of the probability that a neutron in the beam will have an interaction, per target nucleus. It is to be noted that σ has the dimensions of an area. Microscopic cross sections are usually measured in barns (b), where $1 \text{ b} = 10^{-24} \text{ cm}^2$.

Neutrons can interact with nuclei in different ways; each type of interaction will be described in terms of a specific “partial” cross section. Since the probabilities are additive, the sum of the partial cross sections (the total cross section) is a measure of the probability of an interaction of any type when a neutron hits the target.

Let us now consider a physical medium with N nuclei per cm^3 . Let us imagine that there exists, within the medium, a density n of free neutrons per cm^3 , propagating at a speed V in all directions. The rate of interactions per cm^3 will then be:

$$\begin{aligned}\frac{R}{V} &= N\sigma nv \\ &= \sum \phi\end{aligned}\tag{1.16a}$$

The constant of proportionality \sum between the rate of interactions and the scalar flux ϕ is called the macroscopic cross section.

In summary, If the total path length of all the neutrons in a cubic centimeter in a second is known (neutron flux (ϕ)), and if the probability of having an interaction per centimeter path length is also known (macroscopic cross section (\sum)), multiply them together to get the number of interactions taking place in that cubic centimeter in 1 s. This value is known as the reaction rate and is denoted by the symbol R , as we mentioned above. The reaction rate can be calculated by the equation shown below.

$$R = \phi \sum\tag{1.16b}$$

Where:

R = Reaction rate (reactions/sec)

ϕ = Neutron flux (neutron/ $\text{cm}^2\text{-sec}$)

\sum = Macroscopic cross section (cm^{-1})

Substituting the fact that $\sum N\sigma$ into Eq. 1.16b yields the equation below:

$$R = \phi N\sigma\tag{1.16c}$$

where:

σ = Microscopic cross section (cm^2)

N = atom density (atoms/ cm^3)

The reaction rate calculated will depend on which macroscopic cross section is used in the calculation. Normally, the reaction rate of greatest interest is the fission reaction rate.

Note that the microscopic cross section σ is a property of each type of nucleus for each type of interaction. If the physical medium contains many types of nuclei, it will be necessary to sum over all types in order to obtain the total macroscopic cross section:

$$\begin{aligned}\sum &= \sum (E) \\ &= \sum_i N_i \sigma_i (E)\end{aligned}\tag{1.17}$$

The macroscopic cross-sectional measures the probability of an interaction for a neutron traveling over a unit distance in the medium under consideration. The units of Σ are therefore cm^{-1} .

Each type of interaction has its own particular cross section. The total cross section, σ_t , is the sum of the cross sections for scattering, σ_s , and for absorption, σ_a ; thus, we can write:

$$\sigma_t = \sigma_s + \sigma_a \quad (1.18)$$

The scattering cross section includes those for elastic scattering, σ_e , and for inelastic scattering, σ_i . In elastic scattering, the kinetic energy of the incident neutron is shared between the target nucleus and the neutron emerging from the collision. In an inelastic scattering, the kinetic energy is not conserved, the target nucleus being left in an excited state. One has:

$$\sigma_s = \sigma_e + \sigma_i \quad (1.19)$$

On the other hand, the absorption cross section includes those for fission, σ_f , for radiative capture, σ_γ , and for reactions of the type $(n, 2n)$, $(n, 3n)$, etc.:

$$\sigma_a = \sigma_f + \sigma_\gamma + \sigma_{n,2n} + \sigma_{n,3n} + \dots \quad (1.20)$$

In summary, for neutron-nucleus reactions, the following division as shown in Fig. 1.5 is used:

Thus, the concept of the microscopic cross section is introduced to represent the probability of a neutron-nucleus reaction. The cross sections depend on the energy of the incident neutron, and this dependence is very complex. It results from the structure of the target nuclei and the type of interaction. Suppose that a uniform beam of neutrons with intensity $I \text{ cm}^{-2} \text{ s}^{-1}$ strikes a thin “film” of atoms (one atomic layer thick) with N_a atoms/cm². Then the number of interactions C per cm² per second will be proportional to the intensity I and the atom density N_a . We define the proportionality factor as the microscopic cross section (or just cross section) σ :

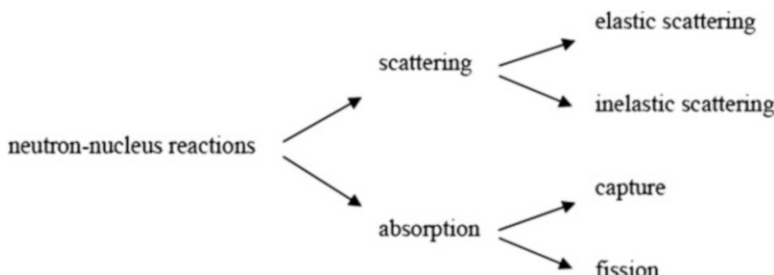
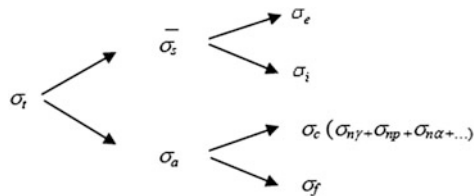
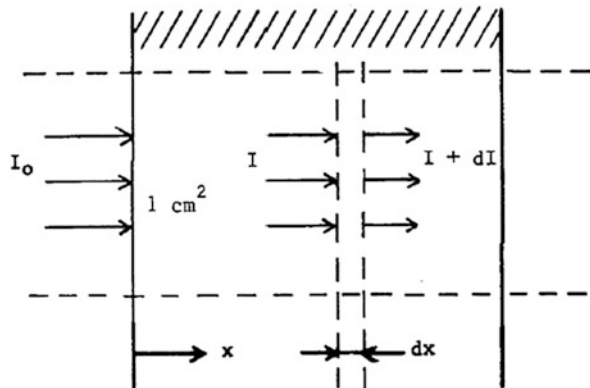


Fig. 1.5 Neutron-nucleus reactions

Fig. 1.6 Forgoing schema**Fig. 1.7** Neutron transmission through a plate

$$C = \sigma N_a I \quad (1.21)$$

The microscopic cross section is often expressed in “barns” ($1 \text{ b} = 10^{-24} \text{ cm}^2$); from this definition it follows that one can consider σ as the effective “target area” that a nucleus presents to the neutron. The microscopic cross section in general is dependent on the neutron energy and the type of reaction. In accordance with the foregoing scheme one distinguishes, see Fig. 1.6 below:

In order to be able to define the concept of the “microscopic cross section,” in the foregoing our starting point was a thin film of atoms. In order to be able to determine the microscopic cross section, transmission measurements are performed on plates of materials. Starting from the presumption that no fission or scattering occurs, the neutron attenuation by a plate with thickness x will be calculated (see Fig. 1.7).

Assume that I_0 neutrons per cm^2 and per second perpendicularly strike a plate, the atomic number density of which is N (nuclei per cm^3). Of a layer dx in the plate, the nucleus density per unit area $N_a = Ndx$. Then, according to the definition of the microscopic cross section, the reaction rate per unit area is $N\sigma I(x)dx$. This is equal to the decrease of the beam intensity, so that:

$$-dI = N\sigma I dx \quad (1.22)$$

Integration gives:

$$I(x) = I_0 e^{-N\sigma x} \quad (1.23)$$

Then the microscopic cross section σ refers to one nucleus. The product:

$$\sum = N\sigma \quad (1.24)$$

refers to one cm^3 of material and is called the macroscopic cross section, which in fact is an incorrect name, because it is not a cross section (dimension L^{-1}). From Eq. 1.23 it follows that the probability $P(x)$ that a neutron will travel a distance x in the material concerned without becoming involved in a reaction is:

$$P(x) = e^{-\sum x} \quad (1.25)$$

The probability that a neutron will be involved in a reaction between x and $x+dx$ is equal to $\sum dx$, so that for the mean free path λ of the neutrons it follows that:

$$\lambda = \int_0^\infty x e^{-\sum x} \sum dx = \frac{1}{\sum} \quad (1.26)$$

whereby one can distinguish λ_s, λ_a , etc. This quantity is also referred to as the *relaxation length*, because it is the distance in which the intensity of the neutrons that have not caused a reaction has decreased with a factor e .

If ρ represents the density of material with mass number A , then the following holds:

$$N = \frac{\rho}{A} N_A \quad (1.27)$$

In which N_A is Avogadro's number $= 6.022 \times 10^{23} \text{ mol}^{-1}$. When one has a mixture of nuclei, it holds that:

$$\sum_{mixture} = \sum_i N_i \sigma_i \quad (1.28)$$

which is proof of Eq. 1.16a as before and N_i represents the number of nuclei of the i -th type per cm^3 in the mixture concerned.

The study of cross sections has been the concern of experimental and of theoretical nuclear physics for many years. Databases of standardized data have been created jointly by several national laboratories. These files Evaluated Nuclear Data Formats (ENDF) contain an evaluation of all nuclear reactions for each nuclide and include experimental analysis combined with the prediction of theoretical models, in a format allowing electronic processing of the data. Specialized computer programs,

such as NJOY of MacFarlane, 1978, allow the preparation of data for neutronics calculations in the form of cross sections as functions of neutron energy. In this monograph, as in most treatises on neutronics, it is assumed that all cross sections $\sigma(E)$ are available.

1.4.2 Effects of Temperature on Cross Section

As discussed, the microscopic absorption cross section varies significantly as neutron energy varies. The microscopic cross sections provided on most charts and tables are measured for a standard neutron velocity of 2200 meters/second, which corresponds to an ambient temperature of 68 °F. Therefore, if our material is at a higher temperature, the absorption cross section will be lower than the value for 68 °F, and any cross sections which involve absorption (e.g., σ_a , σ_c , σ_f) must be corrected for the existing temperature.

The following formula is used to correct microscopic cross sections for temperature. Although the example illustrates absorption cross section, the same formula may be used to correct capture and fission cross sections.

$$\sigma = \sigma_0 \left(\frac{T_0}{T} \right)^{1/2} \quad (1.29)$$

Where:

σ = Microscopic cross section corrected for temperature

σ_0 = Microscopic cross section at reference temperature (68 °F or 20 °C)

T_0 = Reference temperature (68 °F) in degrees Rankine (°R) or Kelvin (°K)

T = Temperature for which corrected value is being calculated

Note: When using this formula, all temperatures must be converted to °R or °K per following relationships:

$$^{\circ}\text{R} = ^{\circ}\text{F} + 460$$

$$^{\circ}\text{K} = ^{\circ}\text{C} + 273$$

1.4.3 Nuclear Cross-Sectional Processing Codes

Neutron, gamma ray, and electron interaction cross sections determine the interactions of each these entities with the atoms and nuclei in the media that they move through. The most complicated interaction cross sections are probably the neutron

cross sections. Since these are very important in nuclear reactor design, a great deal of effort has been spent on representing experimental and theoretical data in the most accurate manner possible for neutron transport calculations.

These cross sections are so complicated that it is impossible to go to original publications to obtain data for a design calculation. So the DOE has organized the accumulated data on neutron cross sections into a library called the Evaluated Nuclear Data File. This file is divided into two parts. Part A contains all of the original publications and the raw data. Part B contains the evaluated data and recommended parameters. The data is evaluated by an organization called CSWEG, for Cross Section Evaluation Working Group. CSWEG is an almost informal volunteer group with members from a number of DOE labs. It is led by Brookhaven National Laboratory. Typically, one member of the group will be responsible for a particular nuclide and will follow it for their entire career. Updates to most of the data are not as frequent today as they were in the 1950s and 1960s.

The evaluated data is stored in Evaluated Nuclear Data Formats B (ENDF/B) on an energy grid that represents the best data as accurately as possible, with the fewest number of energy ranges as possible. The overall energy range has always been 10^{-5} eV to 20 MeV. With ENDF/B, release Number VII.1 (or 7), some nuclides have data to much higher energies. There are several interpolation formulas allowed for representing the data over a given energy range in the ENDF rulebook (ENDF-102). The basic idea is to give the energies and values at the ends of an interval, and the rule for interpolation as a compact way of representing the data. For a nucleus like H-1, broad ranges can be covered with one interpolation scheme, because the cross section does not vary very rapidly. For a nucleus like U-238, many ranges are required because the cross section does vary quite rapidly.

In fact in the resolved resonance region, from a few eV to several keV, neutron cross sections change so rapidly that it is always impossible to break the data down into a fine enough energy grids to accurately represent the rapidly changing cross section. So some generic formulas are used to represent the resonance cross sections with discrete parameters. The Breit-Wigner formula is an example.

Therefore, to perform a neutron transport calculation with multiple nuclides in a given set of materials, the first processing step that must be taken is to represent all of the cross-sectional data on a grid common to all of the nuclides in the problem. It is easiest to think of this in terms of a multi-group calculation, the approach of breaking the energy range of interest down into a finite set of energy intervals, called groups, over which the cross sections are assumed constant at some average value.

Three major DOE laboratories have developed codes, or code systems, to perform this step of representing the Evaluated Nuclear Data Formats B (ENDF/B) data on a common energy grid. The LANL code system is called NJOY, the Oak Ridge National Laboratory (ORNL) code system is called the Standardized Computer Analyses for Licensing Evaluation (SCALE), and the Argonne National Laboratory (ANL) code system is called MC2. They are not all parallel. SCALE does not actually start with ENDF but uses NJOY to preprocess some of the data to a common energy grid. At one time SCALE did it all, but it became too expensive to continue two separate development efforts. MC2 processes from ENDF/B straight through to

a finished multi-group set that can immediately be used in a neutron diffusion calculation. Unfortunately, MC2 does not go any further in the neutron transport business than a P1 effort, and so it is not widely used and will not be commented on further. Each of the code systems produces a different format for the final multi-group cross sections that are somewhat incompatible with each other. The only transport code system that reads more than one format multi-group data set is FEMP [18].

The most comprehensive system is the nuclear data processing system known as NJOY, so it will be followed from here on out (the SCALE approach will be referenced to the NJOY system). After converting all nuclides to a common energy grid, NJOY generates the actual cross sections in the resonance range from the parametric representation used in ENDF/B. Unfortunately these cross sections depend on two parameters that are usually part of a specific transport calculation. The very sharp resonances in nuclides like U^{238} are broadened by the random motion of the nuclei in a uranium medium because of a non-zero temperature. In fact as the temperature of the medium goes up, the resonances are broadened enough that the absorption in these resonances increases. This gives a negative feedback in low enriched reactors that is, called the Doppler coefficient.

The second factor that affects the processed cross sections is the actual concentration of the resonance absorber in the media. If the concentration of $U-238$ is very high, the neutron flux will be severely attenuated at the energies that correspond to the peaks of the $U-238$ absorption resonances. If the concentration of U^{238} is low, the neutron flux will be only moderately attenuated at the energies of these peaks. Since the actual number of absorption reactions is the product of the flux times the cross section, the average cross section will depend on the ratio of the U^{238} cross section to the cross sections of all of the other materials present in the media. The parameter that is used to characterize this effect is called the background scatter cross section. It is essentially the sum of all of the nuclide scattering cross sections, other than U^{238} (or the resonance nuclide), at the resonance energy per atom of U^{238} .

So when NJOY converts the nuclear data from the random grid in ENDF/B to a common grid for a transport calculation, it generates resonance range cross sections for a two-dimensional matrix of temperature and background scatter cross sections. The number of different temperatures is usually in the range of 3 to 5. The number of different background scatter cross sections is typically in the range of 5 to 9. Therefore for a given problem at a specific temperature and material composition, the code TRANXS (for transport cross-section code) can interpolate in the resonance grid that NJOY provides to get a problem-dependent cross section for each material. The output file that NJOY provides with the multiple values of cross sections is called a MATXS (for material cross-section library) file. The problem-specific file that TRANXS provides is called a DTF (one-dimensional transport theory code) library. NJOY can produce a DTF library directly, but it assumes one temperature and one concentration of resonance nuclide when it does this. Usually these are room temperature and an infinite dilute resonance nuclide concentration. The cross section of the resonance absorber does not perturb the neutron flux at all in the peak of the resonance. In the SCALE system, the equivalent library to the MATXS data file is

the AMPX master library. The equivalent library to the DTF data library in the SCALE system is the AMPX working library. The codes that perform the TRANSX calculation for SCALE are called BONAMI and NITAWL. (Most of the SCALE modules are named after common household products.) SCALE can also produce a data library very similar to the DTF format in what is called ANISN format. DTF and ANISN were early one-dimensional SN transport codes developed by Los Alamos National Laboratory (LANL) and ORNL/Westinghouse, respectively.

The SCALE system has many more modules for manipulating multi-group data libraries than the NJOY-TRANSX system. TRANSX performs multiple functions for NJOY libraries that are performed by separate modules in the SCALE system. The AMPX library formats are much more compact than the MATXS and DTF formats, but both contain comparable data.

In summary then, NJOY converts ENDF/B data to a common energy grid and generates multiple data sets for resonance nuclides for a matrix of temperatures and background scatter cross sections. The output is called a MATXS library. TRANSX reads a MATXS library and generates problem-dependent (temperature and background scatter cross section) DTF cross sections. SCALE uses NJOY to produce an AMPX master library and uses BONAMI/NITAWL to produce an AMPX working library for a specific design problem. FEMP will read either output.

An overview of INAS (IRI-NJOY-AMPX-SCALE) code system is presented as Fig. 1.8 above.

The NJOY code and ENDF itself is somewhat of an ongoing effort in that the work started here is based on the 1999 version of the NJOY code and ENDF/B-V. But it is desirable that any capability developed should be compatible with the 2005 NJOY version and ENDF/B-VI. In fact, the starting point for code modifications initially was a version of the NJOY-99 code modified at Sandia National Laboratories for enhanced recoil analysis capability. The code at Sandia is maintained with the UPD (Update Deck) processor, so that any modifications generated should be in the form of UPD decks that can be incorporated into a UPD input stream to produce a final source code for compilation [19].

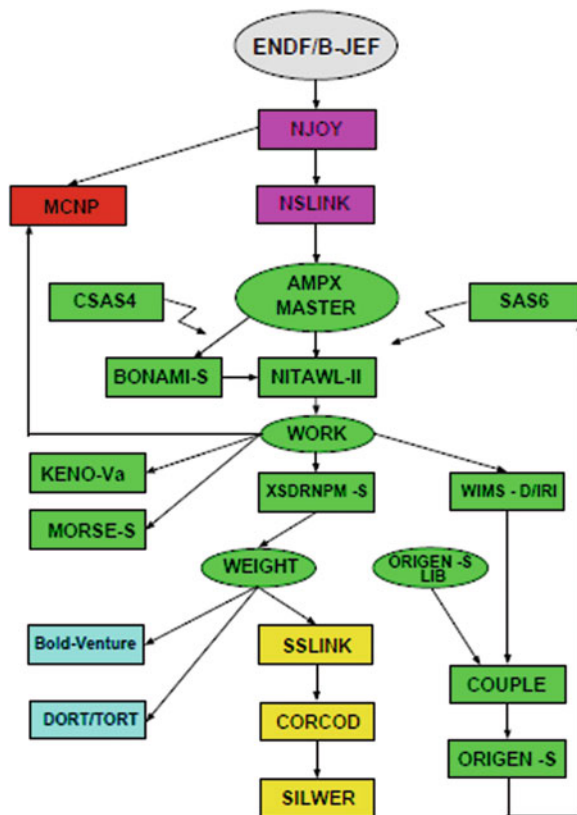
It is important to recognize at the outset that since neutrons are electrically neutral, they are not affected by the electrons in an atom or by the positive charges of the nucleus. Consequently, neutrons pass through the atomic electron cloud and interact directly with the nucleus. In short, neutrons collide with nuclei, not with atoms.

Neutrons may interact with nuclei in one or more of the following ways

Elastic scattering: In this process, the neutron strikes the nucleus, which is usually in its ground state, the neutron reappears, and the nucleus is left in its ground state. The neutron in this case is said to have been *elastically scattered* by the nucleus. In the notation of nuclear reactions, this interaction is abbreviated by the symbol (n, n) .

Inelastic scattering: This process is identical to elastic scattering except that the nucleus is left in an excited state. Because energy is retained by the nucleus, this is

Fig. 1.8 Overview of the INAS code system



clearly an endothermic interaction. Inelastic scattering is denoted by the symbol (n, \hat{n}) . The excited nucleus decays by the emission of γ -rays. In this case, since these γ -rays originate in inelastic scattering, they are called *inelastic γ -rays*.

Radiation capture: Here the neutron is captured by the nucleus, and one or more γ -rays – called *capture γ -rays* – are emitted. This is an exothermic interaction and is denoted by (n, γ) . Since the original neutron is absorbed, this process is examples of a class of interactions know as *absorption reaction*.

Charged-particle reaction: Neutron may also disappear as the result of absorption reaction of the type (n, α) and (n, p) . Such reactions may be either exothermic or endothermic.

Neutron-producing reaction: Reaction of the type $(n, 2n)$ and $(n, 3n)$ occur with energetic neutrons. These reactions are clearly endothermic since in the $(n, 2n)$ reaction on neutron, and in the $(n, 3n)$ reaction two neutrons are extracted from the struck nucleus. The $(n, 2n)$ reaction is especially important in reactors containing heavy water or beryllium since ${}^2\text{H}$ and ${}^9\text{Be}$ have loosely bound neutron which can easily be ejected.

Numerical data for microscopic cross sections of many nuclides are available as computer data files (ENDF/B, Evaluated Nuclear Data File or JEF, Joint Evaluated File). Various computer programs making use of these data files can represent the microscopic cross sections for many nuclides and various reactions graphically.

1.4.4 Energy Dependence of Neutron Cross Sections

Besides a ground state, atomic nuclei also have higher energy levels, which can be excited. The lowest energy levels of the compound nucleus, which is formed in a neutron-nucleus interaction, are relatively far apart; for medium-weighted nuclei ($A = 100 - 150$) circa 0.1 MeV. The high energy levels become closer and closer to each other. For an excitation energy of about 8 MeV, as is the case after capture of a neutron with low kinetic energy, the separation between the levels is only 1–10 eV. Figure 1.9 schematically indicates the position of the energy levels during the formation of a compound nucleus.

The energy levels of a nucleus are no sharp “lines” but show a certain width Γ , which according to the uncertainty principle of Heisenberg is connected with the average time before a nucleus in an excited state decays by emission of a photon or other particle. If there are several decay possibilities for the compound nucleus (emission of a photon, neutron, etc. or fission), we distinguish partial level widths $\Gamma_\gamma, \Gamma_n, \Gamma_f$, etc., which summed yield the total level width Γ .

If the excitation energy of the compound nucleus corresponds with one of the level energies, the probability of an interaction is large: resonance occurs. As the excitation energy depends on the kinetic energy of the neutron, the probability of an interaction and thus the microscopic cross section vary strongly with the energy of

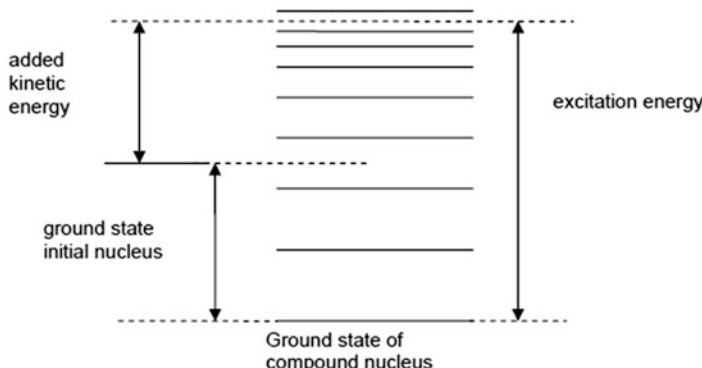


Fig. 1.9 Energy diagram of a neutron-nucleus interaction

the neutron. Breit and Wigner, on the ground of quantum-mechanic considerations, have derived the following expression for the microscopic cross section σ_{na} for an interaction whereby the neutron is included in the nucleus and a particle a (possibly the same neutron again) is emitted:

$$\sigma_{na}(E) = \frac{\lambda^2}{4\pi} \frac{\Gamma_n \Gamma_a}{(E - E_r)^2 + (\Gamma/2)^2} \quad (1.30)$$

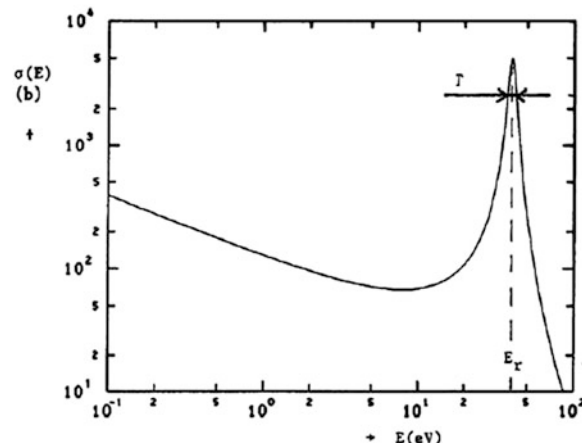
in which $\lambda = h/p = h/mv$ (where p is neutron momentum, h is Planck's constant, m is mass of neutron, and v is the presentation of neutron velocity) is the de Broglie wavelength of the neutron and E_r the resonance energy. The microscopic cross section shows a maximum if the kinetic energy E of the neutron equals E_r . If $E = E_r \pm \Gamma/2$, the value of the microscopic cross section is halved, so that Γ indicates the width of the resonance peak at half height. As the level widths are often small, the resonance peaks can be very sharp. Figure 1.10 gives an example.

According as the neutron energy increases, the peak height of the resonance decreases and the resonances become relatively closer to each other, so that they finally cannot be distinguished anymore (see Fig. 1.11).

Note that the resonances bunch together because the energy scale is drawn in logarithmic scale in Fig. 1.10. Normally resonances are processed with a constant average energy spacing in the unresolved resonance region.

For the derivation of the Breit-Wigner equation, the starting point is an unmoving nucleus, which is struck by a neutron. In reality, the nucleus will also have a kinetic energy as a result of thermal excitation. This expresses itself in the microscopic cross section, because averaging over the energy distribution of the nuclei must take place. Although the average energy of the nuclei is small, at room temperature 0.025 eV, this averaging still has noticeable consequences for the resonances, because the width of the resonances can be of the same order of magnitude. This leads to

Fig. 1.10 Microscopic cross section at a resonance



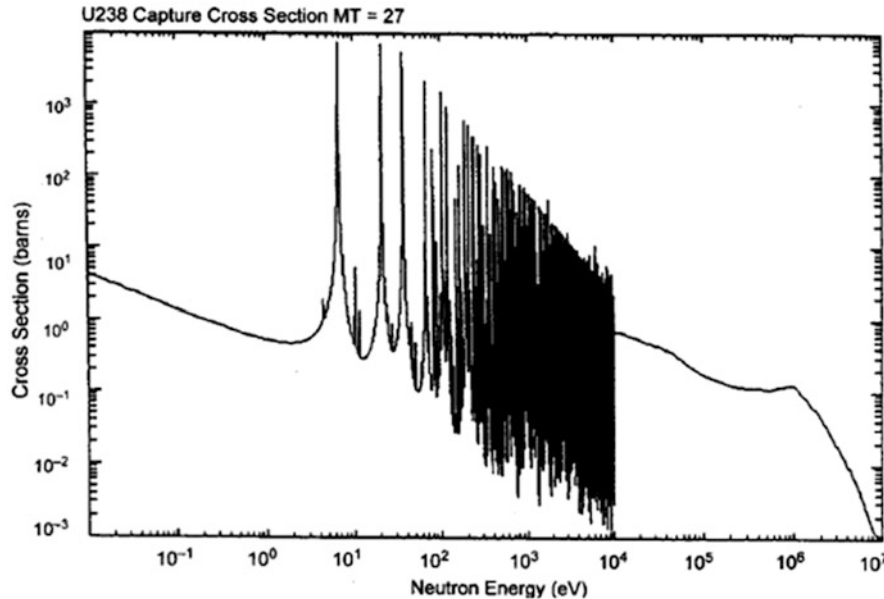


Fig. 1.11 Microscopic cross section of a U^{238} nucleus for neutron capture

broadening of the resonances and lowering of the top value. This so-called Doppler effect is thus temperature dependent and plays an important role in reactors.

The microscopic cross section outside the resonance is also, determined by the behavior of the level widths $\Gamma_\gamma, \Gamma_n, \Gamma_f, \dots$ as a function of the neutron energy. The level widths Γ_γ and Γ_f appear to be rather constant, whereas Γ_n increases approximately proportional to \sqrt{E} . From this, it can be derived that for energies much lower than the lowest resonance energy, the capture and fission cross sections behave as follows:

$$\sigma_\gamma, \sigma_f(E) \propto \frac{1}{\sqrt{E}} \propto \frac{1}{v} \quad (1.31)$$

One finds this “ v -relation” for many nuclides, and it means that the probability of such a reaction is proportional to the time that the incident neutron spends in the proximity of the nucleus.

For scattering, the microscopic cross section decreases sharply outside the resonance, and the so-called potential scattering will predominate, whereby the neutron is scattered by the potential field of the nucleus and does not form a compound nucleus. The potential scattering cross section is constant over a large energy range but decreases at high energies. For light nuclides, at low energies chemical bonding effects can occur, by which the microscopic cross section is larger than that of the free atomic nucleus (e.g., H in H_2O).

In addition to elastic scattering, whereby the total kinetic energy of the particles is conserved, also inelastic scattering can occur. In that case, the nucleus remains in an excited state after emission of the neutron and rapidly decays to the ground state under emission of a photon. The incident neutron then must have sufficient energy to be able to excite this level, so that inelastic scattering is a threshold reaction.

The energy dependence of the microscopic cross section can be summarized as:

Captured and fission:	$\frac{1}{v}$ + resonances
Elastic scattering:	constant/decreasing + resonances
Inelastic scattering:	threshold reaction; for light nuclides a few MeV, for heavy nuclides 10–100 keV
Resonances:	width Γ_γ, Γ_f constant; $\Gamma_n \div \sqrt{E}$ peak width decreasing with E for light nuclides $E_\gamma > 1$ MeV, for heavy nuclides $E_\gamma > 1$ eV as a result of resonances at very low energy e.g. 0.1 eV deviations occur in the $1/v$ relation

1.4.5 Types of Interactions

When a neutron comes into collision with a nucleus, three types of interaction are possible and they are:

1. Formation of a compound nucleus
2. Potential scattering
3. Direct interaction

Each of these three above possibilities is described in details below.

1. Compound Nucleus

In compound nucleus formation, the incident neutron is absorbed by the target nucleus and a system called compound nucleus is formed. The neutron's kinetic energy is shared among all nucleons. If the target nucleus is $_Z X^A$, where Z is the number of protons, A the number of nucleons (also called the “mass number”), and X is the chemical symbol of the element, then the compound-nucleus formation can be represented as:



The energy of excitation (i.e., above the ground state) of the compound nucleus E^* is, however, larger than the incident neutron's kinetic energy (much larger if the incident neutron is in the thermal energy range). This is so for the following reason. The binding energy of a nucleon in a nucleus is the energy which must be supplied to the nucleon to free it from the nucleus. In the reverse process, this energy reappears when the neutron is captured into the nucleus [20]. Therefore, when the incident

Table 1.2 De-excitation pathways for the compound nucleus

Elastic resonant scattering (n, n)	$(_{Z}X^{A+1})^* \rightarrow _Z X^A + _0 n^1$
Inelastic resonant scattering (n, n')	$(_{Z}X^{A+1})^* \rightarrow _Z X^A + _0 n^1 + \gamma$
Radiative capture (n, g)	$(_{Z}X^{A+1})^* \rightarrow _Z X^A + \gamma$
Fission (n, f)	$(_{Z}X^{A+1})^* \rightarrow _C PF_1^B + _{Z-C} PF_2^{A+1-B-v} + v_0 n^1 + \gamma$
Transmutation (n, p)	$(_{Z}X^{A+1})^* \rightarrow _{Z-1} Y^A + _1 H^1$
(n, a) reaction	$(_{Z}X^{A+1})^* \rightarrow _{Z-1} Y^A - {}^3_2 He^4$
($n, 2n$), ($n, 3n$)...reactions	--

neutron is absorbed into the target nucleus to form the compound nucleus, it contributes its binding energy E_b to the compound nucleus. The energy of excitation of the compound nucleus is consequently the sum of the incident neutron's kinetic energy and its binding energy in the compound nucleus:

$$E^* = E + E_b \quad (1.33)$$

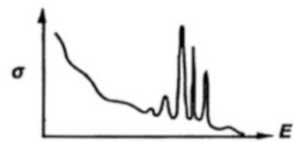
The compound nucleus is highly unstable. It is in an excited state and lives only about 10^{-14} fs before de-excitation. This occurs by particle and/or photon emission. The type of nuclear reaction allowing the compound nucleus to reach stability is called a de-excitation pathway. The main de-excitation pathways of the compound nucleus are shown in Table 1.2.

The compound nucleus can also de-excite by re-emitting a neutron. If the residual nucleus ${}_Z X^A$ is in its ground state, the process is called elastic scattering. More often the residual nucleus is left in an excited state (later de-exciting by emitting a photon), and the kinetic energy of the emitted neutron is smaller than that of the incident neutron: this is inelastic scattering.

The compound nucleus can also de-excite to the ground state of the nuclide ${}_Z X^{A+1}$ by emitting one or more γ rays. This is called radiative capture. In addition, depending on the random collisions between nucleons in the highly excited compound nucleus, one or more nucleons (a proton, a deuteron, two or three neutrons, an α particle, ...) can be ejected. These reactions generally require that the kinetic energy E supplied be above a minimum value. These are termed threshold-type reactions.

In general, cross sections involving the capture or absorption of the neutron vary inversely with the neutron speed. This illustrated the fact that it is generally more difficult to hit a moving target than a stationary one. Also, according to quantum mechanics, a nucleus can exist only in certain states called quantum states. For a compound nucleus to be formed, it must be in an allowed intermediate state. If there is an excited state of the nucleus ${}_Z X^{A+1}$ in the vicinity of $E^* = E + E_b$, the probability of compound-nucleus formation will be great, and the cross section for the reaction will be large. But if there is no allowed level close to E^* , the cross section will be much smaller. The dependence of the cross sections on the kinetic energy of the incident neutron will therefore exhibit resonances, which lead to sudden variations of the cross sections with neutron energy. The presence of resonances is illustrated in Fig. 1.12.

Fig. 1.12 Nuclear cross section with resonances



2. Potential Scattering

While the cross section for elastic scattering is significant only near a resonance, potential scattering is a type of elastic scattering which can take place for any energy of the incident neutron.

This mode of interaction does not involve the formation of a compound nucleus. It appears simply as a result of the presence of the nucleus. It is a collision of the “billiard ball” type, in which the total energy is conserved. Potential scattering is a function only of the forces which act on the neutron in the vicinity of the target nucleus, and these forces depend on the dimensions and the shape of the nucleus.

If we assume the target nucleus to be at rest, energy conservation can be shown to imply that the kinetic energy E' of the neutron after the collision is always smaller than the incident energy E and must be in the range:

$$\alpha E \leq E' \leq E \quad (1.34a)$$

where:

$$\alpha \approx \left(\frac{A-1}{A+1} \right)^2 \quad (1.34b)$$

The neutron loses therefore a fraction of its energy in each collision: we have neutron moderation (slowing down). We further discuss this under slowing down of neutron due to scattering.

3. Direct Interaction

High-energy neutrons can also interact with nuclei by direct interaction. In this type of interaction, a direct collision between the neutron and the nucleus results in the ejection of one or more nucleons (protons or neutrons) and in the absorption of the incident neutron. However, very few neutrons in a reactor possess sufficient energy to enter into direct interaction. This type of interaction is thus of little interest in reactor physics.

1.5 Mean Free Path

We proved this by Eq. 1.26 above. Now, if a neutron has a certain probability of undergoing a particular interaction in one centimeter of travel, then the inverse of this value describes how far the neutron will travel (in the average case) before

undergoing an interaction. This average distance traveled by a neutron before interaction is known as the *mean free path* for that interaction and is represented by the symbol λ . The relationship between the mean free path (λ) and the macroscopic cross section (Σ) is shown below.

$$\lambda = \frac{1}{\Sigma} \quad (1.35)$$

1.6 Nuclear Cross Section and Neutron Flux Summary

The important information so far summarized below:

- Atom density (N) is the number of atoms of a given type per unit volume of material.
- Microscopic cross section (Σ) is the probability of a given reaction occurring between a neutron and a nucleus.
- Microscopic cross sections are measured in units of barns, where 1 barn = 10^{-24} cm 2 .
- Macroscopic cross section (Σ) is the probability of a given reaction occurring per unit length of travel of the neutron. The unit Σ s for macroscopic cross section are cm $^{-1}$.
- The mean free path (λ) is the average distance that a neutron travels in a material between interactions.
- Neutron flux (ϕ) is the total path length traveled by all neutrons in one cubic centimeter of material during 1 s.
- The macroscopic cross section for a material can be calculated using the equation below.

$$\Sigma = N\sigma$$

- The absorption cross section for a material usually has three distinct regions. At low neutron energies (<1 eV), the cross section is inversely proportional to the neutron velocity.
- Resonance absorption occurs when the sum of the kinetic energy of the neutron and its binding energy is equal to an allowed nuclear energy level of the nucleus.
- Resonance peaks exist at intermediate energy levels. For higher neutron energies, the absorption cross section steadily decreases as the neutron energy increases.
- The mean free path equals $1/\Sigma$.

- The macroscopic cross section for a mixture of materials can be calculated using the equation below.

$$\sum = N_1\sigma_1 + N_2\sigma_2 + \dots + N_n\sigma_n \quad (1.36)$$

- Self-shielding is where the local neutron flux is depressed within a material due to neutron absorption near the surface of the material.

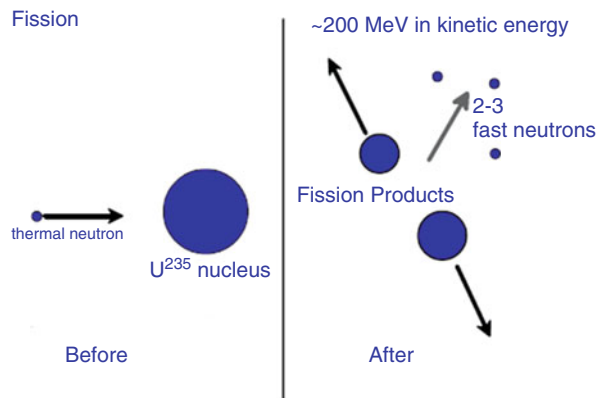
1.7 Fission

To make sense of nuclear reactor design in general, and any reactor design in particular, the reader needs to have some familiarity with a few key nuclear concepts and phenomena. In a nutshell, slow neutrons (called thermal neutrons) can initiate a fission of uranium 235 (U-235), an isotope of uranium that occurs in nature. Natural uranium that is mined from the ground is 0.7% U-235 and 99.3% U-238. The result of fission is fission products that are radioactive, radiation, fast (or energetic) neutrons and heat as shown in Fig. 1.13. The fast neutrons have a low probability of inducing further fissions, and hence have a low probability of generating more neutrons and thus sustaining a chain reaction. So we need to slow down the neutrons (i.e., thermalize or moderate them), which we do by using a moderator such as water. We also need to remove the heat generated. We control the process by controlling the number of neutrons since the number of fissions per second (and hence the heat produced) is proportional to the number of neutrons present to induce the fissions.

From this we can directly derive the basic functional requirements of a reactor. We need:

- A fuel such as U-235
- A moderator to thermalized (i.e., slow down) the fast neutrons

Fig. 1.13 A fission process



- A coolant to remove the heat
- A control system to control the number of neutrons
- A shielding system to protect equipment and people from radiation
- A system that pulls all this together into a workable device

1.8 Fission Spectra

The nuclear fission process is the fundamental reason that nuclear reactors can produce energy. It also determines all of the characteristics of a reactor from criticality to control to waste disposal. Understanding fission is fundamental to understanding reactor design, operation, and licensing. Fission occurs when a neutron enters the nucleus and forms a compound nucleus. The compound nucleus divides into two unsymmetrical parts about two magic number kernels. These kernels “bounce” apart until they are far enough apart to separate based on the Coulomb repulsion of their respective protons. Once the split occurs, the newly formed fission products are rich in energy and neutrons. They boil off 1~6 neutrons until there is not enough excitation energy left to release another neutron with its binding energy. The remaining excitation energy is released as prompt gamma rays. The fission products are still rich in neutrons having approximately six excess neutrons between them. These two nuclei then beta decay back to stability. This process can take a long time and is the reason that radioactive waste takes a long time to give up its energy. Associated with most beta decays are several gamma decays. Some of the beta decays produce residual nuclei that have enough energy to release another neutron, thus a neutron is then promptly released. Therefore, the half-life for delayed neutrons is determined by the intermediate beta decay.

1. Neutron contributes 6.0–7.5 MeV excitation energy
2. Two magic number kernels form

Magic numbers	
Protons	Neutrons
2	2
8	8
20	20
28	28
50	50
82	82
114	126

Light kernel: 28 protons, 50 neutrons – $A = 78$

Heavy kernel: 50 protons, 82 neutrons – $A = 132$

U^{235} = 92 protons, 143(+1) neutrons: $A = 235(+1)$

Excess protons = 14

Excess neutrons = 12

Consider a Typical Fission Product Split

Xe¹⁴⁰ - 54 protons, 86 neutrons

Sr⁹⁶ - 38 protons, 58 neutrons

Average Binding Energies

U²³⁵ - 7.6 Mev/nucleon

Xe¹⁴⁰ - 8.4 Mev/nucleon

Sr⁹⁶ - 8.7 Mev/nucleon

Binding Energy Available from Thermal Neutron Fission

U²³⁶ 7.6 Mev/nucleon \times 236 nucleons = -1793.6 MeV

Xe¹⁴⁰ 8.4 Mev/nucleon \times 140 nucleons = 1176.0 MeV

Sr⁹⁶ 8.7 Mev/nucleon \times 96 nucleons = 835.2 MeV

Energy available from incoming neutron = 7.6 MeV

Net Binding Energy Released = 225.2 MeV

Prompt Emissions

Nucleus Splits into Two Fission Products

1. Kernels repel each other due to Coulomb energy.
2. Each Kernel is neutron rich.
3. The stable nuclides are determined by:

$$Z_{st} = 0.5 * A_{st} / (1.0 + 0.007826 * A_{st}^{2/3})$$

$$A_{st}(54) = 130, N_{st} = 76, 10 \text{ excess neutrons}$$

$$A_{st}(38) = 88, N_{st} = 50, 8 \text{ excess neutrons}$$

Prompt Neutrons Boil Off

1. Neutrons evaporate until excitation energy is too low.
2. Remaining energy released as prompt gammas.
3. Evaporation spectrum.

$$\chi(E) \sim E^{1/2} e^{-E/T} \quad [E \text{ in MeV}] \quad \text{In the Center of Mass (CM) system}$$

Maxwellian Spectrum A fit in the laboratory reference system to the correct shape for a single fission product in the center of mass system.

The excitation energy of the nucleons in the two fission fragments can be given by:

$$E^* = E_r + B_n + E_n - \langle E_f \rangle^{\text{tot}}$$

E^* = Energy available for internal excitation of fission products

E_r = Total difference in binding energies of the fissioning nucleus and the two fission products

B_n = Binding energy of neutron added to nucleus to cause fission

E_n = Kinetic energy of neutron added to nucleus to cause fission

$\langle E_f \rangle^{\text{tot}}$ = Total kinetic energy of fission products

The expected kinetic energy per nucleon of the light fission fragment is given by:

$$\langle E_f \rangle^L = (A_H/A_L) * (\langle E_f \rangle^{\text{tot}}/A)$$

A_L = Mass number of light fission fragment

A_H = Mass number of heavy fission fragment

A = Mass number of compound nucleus undergoing fission

The kinetic energy of the heavy fragment is given by the converse relation.

Inside the nucleus assuming a Fermi gas model for the statistical distribution of nucleon energies:

$$T_m = (E^*/a)^{1/2}$$

Where a is the nuclear level density parameter, nominally $A/11 \text{ MeV}^{-1}$ to $A/8 \text{ MeV}^{-1}$, and E^* is the residual energy of the nucleus after fission.

We can then estimate an average Maxwellian temperature given by:

$$T_M = \frac{1}{3} (\langle E_f \rangle^H + \langle E_f \rangle^L) + 8/9 T_m$$

If we use the same average kinetic energy per nucleon for both the heavy and light fragments and neglect the center of mass to lab transformation, we have a laboratory Maxwellian spectrum given by:

$$\chi(E) = 2E^{1/2*} e^{-E/T_M} / \left(\pi^{1/2} T_M^{3/2} \right) \quad [E \text{ in Mev}]$$

The following parameters (in MeV) are extracted from the paper by Madlang and Nix [1] for a value of $a = A/9$.

Nuclide	E_r	B_n	$\langle E_f \rangle^{\text{tot}}$	T_m	T_M	T_w
U^{233}	188.971	6.844	172.1	0.955	1.339	0.849
U^{235}	186.980	6.546	171.8	0.910	1.294	0.809
Pu^{239}	198.154	6.534	177.1	1.017	1.396	0.904

For ^{235}U this gives,

$$\chi(E) = 0.7665E^{1/2}e^{-E/1.293} \quad [E \text{ in MeV}]$$

Watt spectrum If we use the calculated T_m for both nuclei and transform the Maxwellian from the center of mass to the laboratory system for the average fission fragment, we obtain the Watt spectrum:

$$T_w = 8/9T_m$$

$$\langle E_f \rangle^{\text{ave}} = (\langle E_f \rangle^H + \langle E_f \rangle^L)/2$$

$$\chi(E) = \frac{e^{-(E + \langle E_f \rangle^{\text{ave}})/T_w} \sinh((2 \langle E_f \rangle^{\text{ave}} E)^{1/2}/T_w)}{(\pi \langle E_f \rangle^{\text{ave}} T_w)^{1/2}} \quad [E \text{ in MeV}]$$

For U^{235} this gives:

$$\chi(E) = 0.271e^{-E/0809} \sinh(2.38E)^{1/2} \quad [E \text{ in MeV}]$$

A better fit to the experimental data gives:

$$\chi(E) = 0.4527e^{-5/0.965} \sinh(2.29E)^{1/2} \quad [E \text{ in MeV}]$$

Madlang-Nix spectrum The Madlang-Nix spectrum [1] is the most accurate spectrum used today and can be obtained from their paper referenced at the end of these notes. It computes average light and average heavy nuclei from fission and calculates an evaporation spectrum for each in the center of mass system. Then it translates both to the laboratory system and averages them. However, there is not a closed form representation, which is easily computable on a hand calculator. It is given by:

$$\chi(E) = \frac{1}{2} \left\{ N(E, E_f^L) + N(E, E_f^H) \right\}$$

where:

$$N(E, E_f) = \frac{1}{3(E_f T_m)^{1/2}} \left\{ u_2^{3/2} E_1(u_2) - u_1^{3/2} E(u_1) + \gamma\left(\frac{3}{2}, u_2\right) - \gamma\left(\frac{3}{2}, u_1\right) \right\}$$

and:

E_f = Average kinetic energy of the fission product in MeV

T_m = Fermi gas model temperature of the nucleus

$E_1(x)$ = the exponential integral of x

$$E_1(x) = \int_x^{\infty} \frac{\exp(-u)}{u} du$$

$\gamma(a, x)$ = the incomplete gamma function of order a:

$$\gamma(a, x) = \int_0^x u^{a-1} \exp(-u) du$$

$$u_1 = \left(E^{1/2} - E_f^{1/2} \right)^2 / T_m$$

$$u_2 = \left(E^{1/2} + E_f^{1/2} \right)^2 / T_m$$

Average energy of neutrons released in fission ~ 2.0 MeV

Average number of prompt neutrons ~ 2.5

Most probable energy ~ 0.8 MeV

Average number of neutrons increases with the energy of the neutron causing fission.

Nuclide	N_{thermal}	dN/dE	$N(14 \text{ MeV})$
U^{233}	2.493	0.136	4.393
U^{235}	2.425	0.150	4.525
Pu^{239}	2.877	0.133	4.737

Prompt Gammas Boil Off

Prompt Gamma Spectrum

$$\begin{aligned} N_{\gamma}(E) &= 6.6 \gamma/\text{MeV}, & 0.1 \text{ MeV} < E < 0.6 \text{ MeV} \\ &= 20.2e^{-1.78E} \gamma/\text{MeV}, & 0.6 \text{ MeV} < E < 1.5 \text{ MeV} \\ &= 7.2e^{-1.09E} \gamma/\text{MeV}, & 1.5 \text{ MeV} < E < 10.5 \text{ MeV} \\ & \quad [E \text{ in MeV}] \end{aligned}$$

Approximately 7.4 prompt gammas per fission

Approximately 7.2 MeV in prompt gammas per fission

This corresponds to about 3.6 MeV per fission product, which is about half the binding energy of a neutron. When the neutrons finish boiling off, each fission product is left with some residual energy. If the actual energy left is randomly distributed in value between its peak (the energy required to release another neutron) and zero, then the average energy left per fission product will be about half the binding energy of the last neutron or 7.0–8.5 MeV.

Decay Emissions

Delayed Betas

Assume that two neutrons are boiled off from Sr^{96} and one neutron is boiled off from Xe^{140} . To estimate the number of beta decays required to reach stability assume that each neutron converted to a proton moves the nucleus toward the stability line. This means that each beta decay reduces the number of excess neutrons and increases the number of protons in the fission products. This gives the following:

Number of excess neutrons remaining		
Beta decays	Sr^{94}	Xe^{139}
1	3.72 (Y^{94})	6.64(Cs^{139})
2	1.16 (Zr^{94})	3.93(Ba^{139})
3	−1.40(Nb^{94})	1.20(La^{139})
4		−1.53(Ce^{139})

For this case, Zr^{94} and La^{139} are stable. Five beta decays will be required to reach stability. The three neutrons boiled off meant fewer than average beta decays were required. Of course, fewer or more neutrons could have been boiled off. On the average, considering all fission products, there are nominally six beta decays per fission required to reach two stable fission products.

Beta Decay

Beta decay occurs in groups of reactions given by Sagan's equation:

$$\log_{10}(f^* \tau) = C_\beta \quad \text{or,} \quad \tau = \frac{10^{C_\beta}}{f_0 E_\beta^5}$$

where:

$$f = f_0(E_\beta)^5$$

$$f_0 = 0.676$$

E_β = Maximum decay energy in MeV

τ = Mean life in seconds = (half-life)/0.693

C_β = A constant associated with the forbiddings of the β decay

$C_\beta \sim 2.0 - 3.0$ for super allowed decays

~ 4.0 - 6.0 for allowed decays

~ 6.0 - 8.0 for first level forbidden decays

~ 8.0–10.0 for second level forbidden decays

Note for neutron decay, we have:

$$E_\beta = 0.782 \text{ MeV}$$

$$t_{1/2} = 624 \text{ s}$$

$$\tau = 900 \text{ s}$$

$$C_\beta = 2.25$$

The total energy released in beta decay is approximately 8.0 MeV per fission.

Delayed Neutrons

Delayed neutrons are given off some time after fission and have decay e-folding times in the range of ~ 0.25 s to ~ 80.0 s (half-lives from ~ 0.17 s to ~ 55 s). In order for a delayed neutron to be given off, a beta decay must occur first, and the beta decay must leave the new compound nucleus with enough excitation energy to emit a neutron. This is possible due to the difference in binding energy required between even-even and odd-odd nuclei. The beta decays that offer this possibility fall into the “Allowed” decay category. Even if they were to be “Super Allowed” decays, the shortest possible mean lifetime would be about 3–3.5 milliseconds. This corresponds to a maximum beta decay energy of 8.4–8.7 MeV or roughly the binding energy of an additional neutron in the fission product nucleus. If the nucleus had more energy than this, it would emit another neutron rather than waiting for a beta decay to occur. The fact that we have not measured decay constants shorter than this is probably not due to a lack of fast instrumentation but rather due to the physics of the decay process.

Nominally, six families of delayed neutrons can be measured. There are far more than six delayed neutron precursors, but their decay constants can be conveniently represented by no more than six decay constants that vary slightly with the fissioning species. The following data are taken from the text by Lewins [3].

The data for thermal fission of U^{235} , $\beta = 0.00700$, $\beta/\lambda = 0.089$ s

Family	Yield fraction (β_I)	Decay constant (λ_I)
1	0.000266	0.0127
2	0.001492	0.0317
3	0.001317	0.115
4	0.002851	0.311
5	0.000897	1.40
6	0.000182	3.87

for thermal fission of Pu^{239} , $\beta = 0.00227$, $\beta/\lambda = 0.033$ s

Family	Yield fraction (β_I)	Decay constant (λ_I)
1	0.000086	0.0129
2	0.000637	0.0311
3	0.000491	0.134
4	0.000746	0.331
5	0.000234	1.26
6	0.000080	3.21

for thermal fission of U^{233} , $\beta = 0.00281$, $\beta/\lambda = 0.050$ s

Family	Yield fraction (β_I)	Decay constant (λ_I)
1	0.000241	0.0126
2	0.000769	0.0334
3	0.000637	0.131
4	0.000890	0.302
5	0.000205	1.27
6	0.000065	3.13

Unfortunately, in real reactors, there are usually several species of delayed neutrons present and trying to predict time-dependent reactor behavior by keeping track of each fissioning nuclide, and its measured delay families can get very messy. Ott [4] has presented a convenient scheme for presenting effective delayed yields based on the decay constants of Pu^{239} that matches the experimental curves very accurately. However, assuming the following sets of decay constants:

Family	Decay constant (s^{-1})	e-folding(s)	half-life(s)
1	0.0129 ± 0.0002	77.5	53.7
2	0.0311 ± 0.0005	32.2	22.3
3	0.134 ± 0.003	7.5	5.2
4	0.331 ± 0.012	3.0	2.1
5	1.26 ± 0.12	0.8	0.6
6	3.21 ± 0.26	0.3	0.2

The yields for each of the delay families by nuclide are:

Family	U^{233}	U^{235}	U^{238}	Th^{232}
1	0.00053	0.00060	0.00049	0.00143
2	0.00197	0.00364	0.00540	0.00776
3	0.00175	0.00349	0.00681	0.00843
4	0.00212	0.00628	0.01526	0.02156
5	0.00047	0.00179	0.00836	0.00838
6	0.00016	0.00070	0.00488	0.00204

	Pu^{239}	Pu^{240}	Pu^{241}	Pu^{242}
1	0.00024	0.00028	0.00019	0.00036
2	0.00176	0.00237	0.00369	0.00263
3	0.00136	0.00162	0.00276	0.00270
4	0.00207	0.00314	0.00534	0.00607
5	0.00065	0.00106	0.00310	0.00279
6	0.00022	0.00039	0.00032	0.00145

The average number of delayed neutrons given off varies with the fissioning species. Some typical numbers for thermal fission are:

Nuclide	Delayed yield	Total yield	Delayed fraction
U^{233}	0.000698	2.493	0.0028
U^{235}	0.00170	2.425	0.0070
Pu^{239}	0.000662	2.877	0.0023

The delayed yield is fairly constant from thermal energies up to about 4 MeV, and then it falls off to about 50% of its thermal value by 14 MeV. Since the total yield and prompt yield increase as a function of the fissioning neutron energy, β actually decreases slightly as energy increases. However this is such a small effect that it is neglected and β is assumed constant for most neutronics calculations.

The delayed neutron energy spectrum actually varies with the delayed family under consideration, but a convenient average spectrum can be calculated by using a Maxwellian at a lower temperature than the prompt spectrum temperature.

$$\chi_d(E) \sim E^{1/2} e^{-E/T} \quad [E \text{ in MeV}]$$

$$T(U^{235}) \sim 0.29 \text{ MeV} \quad T(Pu^{239}) \sim 0.27 \text{ MeV} \quad T(U^{233}) \sim 0.26 \text{ MeV}$$

The energy carried away by the delayed neutrons is negligible compared to the accuracy of the other energies generated during fission.

Delayed Gammas

The spectrum of delayed gammas is generally assumed to be similar to the prompt gamma spectrum.

The energy carried away by the delayed gammas is also about 7.0 MeV.

Fission Energy Summary

Total energy available	225.2 MeV
Neutron binding energy (2.43*7.5)	18.3
Neutron kinetic energy (2.43*2.0)	4.9
Fission product kinetic energy	172.0
Prompt gammas	6.0
Delay gammas	6.0
Decay betas	6.0
Neutrinos	12.0
	225.2 MeV
Less neutrinos and binding energy	30.2
Sensible energy	195.0 MeV

Average Energies Available From Fission (Mev)

Nuclide	Thermal	Fast	14 MeV
Th ²³²	—	196.98	216.75
Pa ²³³	—	200.27	—
U ²³³	200.32	200.91	225.06
U ²³⁴	—	202.14	—
U ²³⁵	202.64	203.41	228.47
U ²³⁶	—	205.14	—
U ²³⁸	—	208.96	229.77
Np ²³⁷	—	203.93	—
Pu ²³⁸	208.88	—	—
Pu ²³⁹	211.44	212.26	237.67
Pu ²⁴⁰	—	211.21	—
Pu ²⁴¹	213.44	214.38	—
Pu ²⁴²	—	215.50	—
Am ²⁴¹	213.62	—	—
Am ²⁴²	213.62	—	—
Am ²⁴³	—	221.25	—
Cm ²⁴³	218.65	—	—
Cm ²⁴⁴	218.03	—	—

Time History of Decay Energy Release

Traditionally the decay energy release has been described by formulas of the form:

$$P_{decay} = 2.66/t^{1/2} \text{ MeV/Fiss/Sec}, \quad [t \text{ in sec}], \quad 1.0 < t < 10^6 \text{ sec}$$

This gives a total decay energy release from 1 s on of 13.3 MeV per fission.

A more recent formula that is somewhat more accurate is given by the work of R. J. Labauve, T. R. England, and D. C. George of Los Alamos National Laboratory [2].

$$P_{decay} = \sum_i \alpha_i e^{-\beta_i t} \text{ MeV/Fiss/sec}, \quad [t \text{ in sec}], \quad 0 < t < 10^9 \text{ s}$$

where the α_i 's and β_i 's for ^{235}U are given by:

Beta decays			Gamma decays		
α_i	β_i	α_i/β_i	α_i	β_i	α_i/β_i
6.169E-11	7.953E-10	7.757E-02	2.808E-11	7.332E-10	3.830E-02
2.249E-09	2.758E-08	8.154E-01	6.038E-10	4.335E-08	1.393E-02
2.365E-08	2.082E-07	1.136E-01	3.227E-08	1.932E-07	1.670E-01
2.194E-07	1.846E-06	1.189E-01	4.055E-07	1.658E-06	2.446E-01
1.140E-05	2.404E-05	4.742E-01	8.439E-06	2.147E-05	3.931E-01
1.549E-04	2.337E-04	6.628E-01	2.421E-04	2.128E-04	1.138E+00
1.991E-03	1.897E-03	1.050E+00	1.792E-03	1.915E-03	9.358E-01
3.256E-02	1.926E-02	1.691E+00	2.810E-02	1.769E-02	1.588E+00
2.227E-01	1.573E-01	1.416E+00	1.516E-01	1.652E-01	9.177E-01
5.381E-01	1.264E+00	4.257E-01	4.162E-01	1.266E+00	3.288E-01
1.282E-01	5.196E+00	2.481E-02	1.053E-01	5.222E+00	2.016E-02
Total		6.869 MeV			5.785 MeV

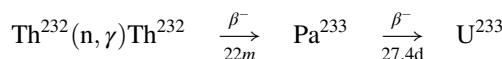
This method gives a total decay energy per fission of 12.654 MeV per fission.

1.9 The Nuclear Fuel

When we start talking about fuel for nuclear power reactor as a source of fissile material for starting the reactor, we encounter some ambiguity since actual fissile material are mixed with some fertile material or diluents (see next section for definition of fertile material), and normally this is the mixture that is referred to as fuel. Therefore, this provides fuels of 15% Pu^{49}O_2 in natural form of UO_2 , or “slightly enriched” UO_2 where uranium oxide has a content of 2 or 3 percent U^{235} rather than 0.7% in the natural ore, or “highly enriched” uranium-zirconium alloy with uranium being in 93% U^{235} included [5].

Given the chemical property of uranium isotopes such as U^{238} cannot alone to be used as fissionable source with energetic neutron for fuel of nuclear reactors. It is the fissile isotopes U^{233} , U^{235} , and Pu^{239} that are practical enough to be used for nuclear power plant fuels. Among all these nuclei, only U^{235} can be found as ore in the nature, does exist as 0.71 atom percent in natural uranium, and can be extracted by various means of separation processes in the related industries to bring it to level of desired enrichment [6], which is any specified atom percent of U^{235} . The isotope U^{233} can be produced by the absorption of neutrons by Th^{232} .

The reactions involved are:

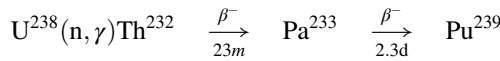


U^{233} holds considerable potential for fueling certain advanced types of reactors, in particular as part of Generation IV (GEN-IV) reactors. The molten salt reactor (MSR) uses nuclear fuel, which is dissolved in the molten fluoride salt as uranium tetrafluoride (UF_4) or thorium tetrafluoride (ThF_4), where also a part of this fuel can be used as primary coolant in form of molten salt mixture. The GEN-IV is playing a big rule in future existence of nuclear power plants, and it is a very promising technological approach to replace the existing old operational and experimental plants. In some cases such a gas-cooled fast reactor (GFR), by providing the high temperature output of $850\text{ }^{\circ}\text{C}$, justifies better thermal efficiencies using a direct Brayton cycle gas turbine [7–12]. For more details of each GEN-IV reactors refer to Chap. 17 of this book.

The fuel for a nuclear power reactor is the source of energy by the fission process. The probability of neutron capture leading to fission is larger for slow neutrons than for fast neutrons. Hence, most practical reactors are “thermal” reactors, that is, they utilize the higher thermal cross sections. Possible fuels include some of the various isotopes of uranium (U) and plutonium (Pu). The only naturally occurring fuel with suitable properties of significant quantities is U^{235} ; hence most reactors use this fuel (see Fig. 1.14) 0.7% U-235. The rest is U^{238} . This percentage is too low to sustain a chain reaction when combined with most practical moderators. Hence either the probability of fission must be enhanced or the moderator effectiveness must be enhanced. One group of reactor types (PWR, BWR, and HTGR) enriches the fuel (a costly task) and use a cheap moderator (ordinary water or graphite).

It should be mentioned that isotopes such as Th232 which are not themselves fissile (though they may be fissionable) but which can be used as the raw materials for production of fissile isotopes are called *fertile*. See the next section for definition of fertile material.

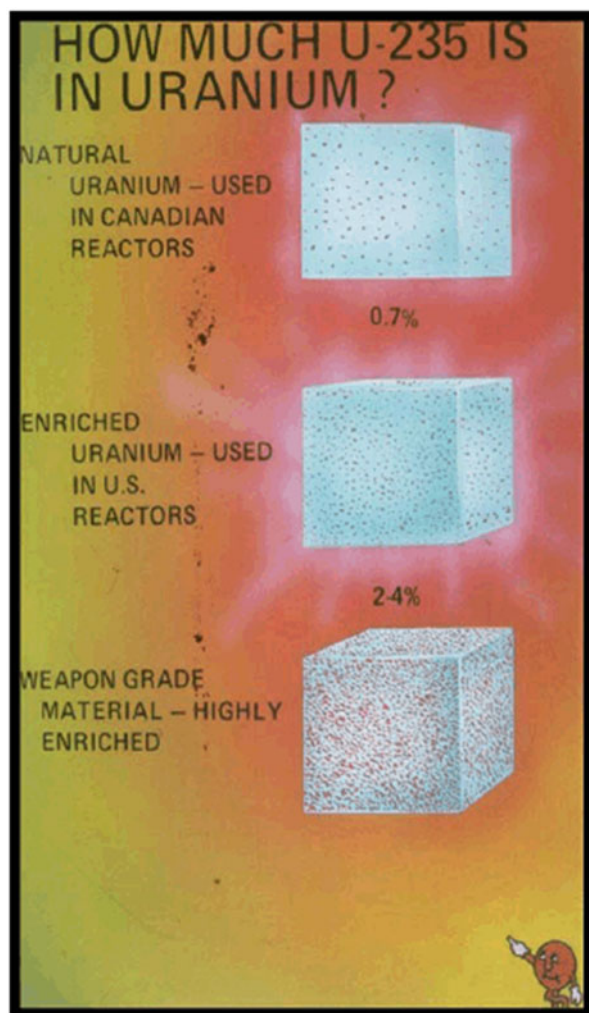
Pu^{239} is produced by the absorption of neutrons by U^{235} via the following reactions:



Manhattan project during World War II and for nuclear weapon rushed production of plutonium, and it has been continued since the war on an even greater scale. For the following reasons, plutonium production is still very active, although comparatively has little application as a fuel reactor. The reasons are [6]:

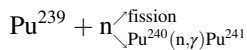
1. Pu^{239} is more expensive to produce than U^{235} .
2. It is less satisfactory than U^{235} for fueling most of reactors built since World War II, because of its high value α .
3. The physical and chemical properties of plutonium make it a difficult material to work with.
4. Little Pu^{239} has been available because of the competing demand of the weapons program.

Fig. 1.14 Uranium enrichment



Nevertheless, as in the case of U^{233} , Pu^{239} appears to be a far better fuel than U^{235} for certain advanced types of reactor, and the future will undoubtedly see increased use of this isotope.

Note that a certain amount of Pu^{239} accumulates in any reactor containing U^{238} , as the result of neutron absorption. In a similar fashion, the fissile isotope Pu^{241} accumulates in reactors containing Pu^{239} by the absorption of two additional neutrons, and bear in your mind that at this point, the absorption of a neutron by Pu^{239} does not always lead to fission. The reactions involved are [6]:



Note that the operation of a reactor is certainly will be impacted by the presence of Pu^{241} , and therefore it should be taken into account in design of Pu^{239} -fueled reactor or reactors containing large amounts of U^{238} .

1.9.1 Fertile Material

All of the neutron absorption reactions that do not result in fission lead to the production of new nuclides through the process known as *transmutation*. These nuclides can, in turn, be transmuted again or may undergo radioactive decay to produce still different nuclides. The nuclides that are produced by this process are referred to as transmutation products. Because several of the fissile nuclides do not exist in nature, they can only be produced by nuclear reactions (transmutation).

The target nuclei for such reactions are said to be fertile. *Fertile materials* are materials that can undergo transmutation to become fissile materials. Figure 1.15 traces the transmutation mechanism by which two fertile nuclides, thorium-232 and uranium-238, produce uranium-233 and plutonium-239, respectively; see Fig. 1.15.

If a reactor contains fertile material in addition to its fissile fuel, some new fuel will be produced as the original fuel is burned up. This is called conversion. Reactors that are specifically designed to produce fissionable fuel are called “breeder” reactors. In such reactors, the amount of fissionable fuel produced is greater than the amount of fuel burnup. If less fuel is produced than used, the process is called conversion, and the reactor is termed a “converter.”

It is important to remember that the “fuel” generally refers to a mixture of fissile material with fertile or diluents.

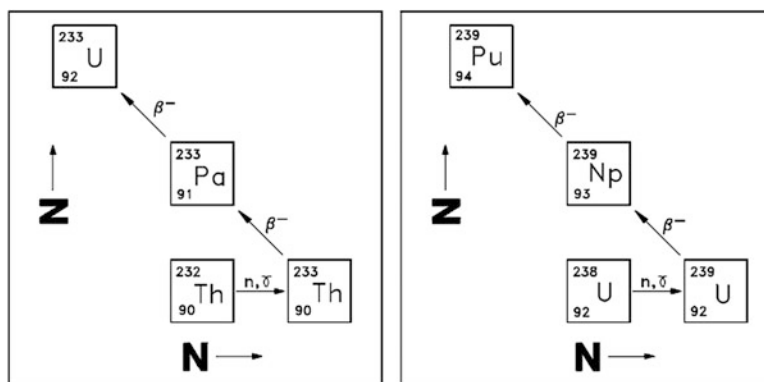


Fig. 1.15 Conversion of fertile nuclides to fissile nuclides

1.10 Liquid Drop Model of a Nucleus

The nucleus is held together by the attractive nuclear force between nucleons, which was discussed in a previous chapter. The characteristics of the nuclear force are listed below.

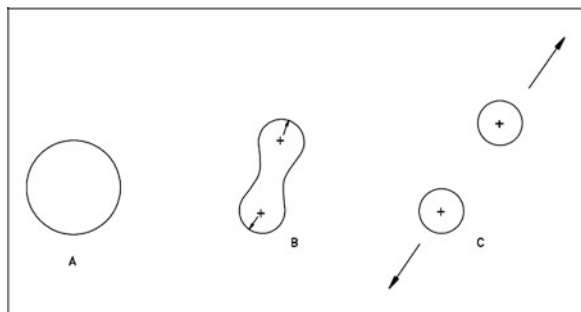
- (a) Very short range, with essentially no effect beyond nuclear dimensions (10^{-13} cm)
- (b) Stronger than the repulsive electrostatic forces within the nucleus
- (c) Independent of nucleon pairing, in that the attractive forces between pairs of neutrons are no different than those between pairs of protons or a neutron and a proton
- (d) Saturable, that is, a nucleon can attract only a few of its nearest neighbors

One theory of fission considers the fissioning of a nucleus similar in some respects to the splitting of a liquid drop. This analogy is justifiable to some extent by the fact that a liquid drop is held together by molecular forces that tend to make the drop spherical in shape and that try to resist any deformation in the same manner as nuclear forces are assumed to hold the nucleus together. By considering the nucleus as a liquid drop, the fission process can be described.

Referring to Fig. 1.16a, the nucleus in the ground state is undistorted, and its attractive nuclear forces are greater than the repulsive electrostatic forces between the protons within the nucleus.

When an incident particle (in this instance a neutron) is absorbed by the target nucleus, a compound nucleus is formed. The compound nucleus temporarily contains all the charge and mass involved in the reaction and exists in an excited state. The excitation energy added to the compound nucleus is equal to the binding energy contributed by the incident particle plus the kinetic energy possessed by that particle. Figure 1.16b illustrates the excitation energy thus imparted to the compound nucleus, which may cause it to oscillate and become distorted. If the excitation energy is greater than a certain critical energy, the oscillations may cause the compound nucleus to become dumbbell-shaped. When this happens, the attractive

Fig. 1.16 Liquid drop model of fission



nuclear forces (short range) in the neck area are small due to saturation, while the repulsive electrostatic forces (long range) are only slightly less than before. When the repulsive electrostatic forces exceed the attractive nuclear forces, nuclear fission occurs, as illustrated in Fig. 1.16c.

1.11 Summary of Fission Process

The important information for nuclear fission is summarized as follows:

- The fission process can be explained using the liquid drop model of a nucleus. In the ground state, the nucleus is nearly spherical in shape. After the absorption of a neutron, the nucleus will be in an excited state and will start to oscillate and become distorted. If the oscillations cause the nucleus to become shaped like a dumbbell, the repulsive electrostatic forces will overcome the short-range attractive nuclear forces, and the nucleus will split in two.
- Excitation energy is the amount of energy a nucleus has above its ground state.
- Critical energy is the minimum excitation energy that a nucleus must have before it can fission.
- Fissile material is a material for which fission is possible with neutrons that have zero kinetic energy. Fissionable material is material for which fission caused by neutron absorption is possible provided the kinetic energy added with the binding energy is greater than the critical energy. Fertile material is a material that can undergo transmutation to become fissile material.
- Transmutation is the process of neutron absorption and subsequent decay, which changes one nuclide to another nuclide. Conversion is the process of transmuting fertile material into fissile material in a reactor, where the amount of fissile material produced is less than the amount of fissile material consumed. Breeding is the same as conversion, except the amount of fissile material produced is more than the amount of fissile material consumed.
- The curve of binding energy per nucleon increases quickly through the light nuclides and reaches a maximum at a mass number of about 56. The curve decreases slowly for mass numbers greater than 60.
- The heaviest nuclei are easily fissionable because they require only a small distortion from the spherical shape to allow the Coulomb forces to overcome the attractive nuclear force, forcing the two halves of the nucleus apart.
- Uranium-235 fissions with thermal neutrons because the binding energy released by the absorption of a neutron is greater than the critical energy for fission. The binding energy released by uranium-238 absorbing a neutron is less than the critical energy; therefore, additional, kinetic energy must be possessed by the neutron for fission to be possible.

1.12 Reactor Power Calculation

Multiplying the reaction rate per unit volume by the total volume of the core, results in the total number of reactions occurring in the core per unit time. If the amount of energy involved in each reaction were known, it would be possible to determine the rate of energy release (power) due to a certain reaction.

In a reactor where the average energy per fission is 200 MeV, it is possible to determine the number of fissions per second that are necessary to produce 1 watt of power using the following conversion factors.

$$1 \text{ fission} = 200 \text{ MeV}$$

$$1 \text{ MeV} = 1.602 \times 10^{-6} \text{ ergs}$$

$$1 \text{ erg} = 1 \times 10^{-7} \text{ watt-sec}$$

$$\begin{aligned} 1 \text{ watt} & \left(\frac{1 \text{ erg}}{1 \times 10^{-7} \text{ watt-sec}} \right) \left(\frac{1 \text{ MeV}}{1.602 \times 10^{-6} \text{ erg}} \right) \left(\frac{1 \text{ fission}}{200 \text{ MeV}} \right) \\ & = 3.12 \times 10^{10} \frac{\text{fissions}}{\text{second}} \end{aligned}$$

This is equivalent to stating that 3.12×10^{10} fissions release 1 watt-second of energy.

The power released in a reactor can be calculated based on the relation $R = \phi \sum$; here R is reaction rate (reactions/sec), ϕ is neutron flux (neutron/cm²-sec), and \sum is macroscopic cross section (cm⁻¹). Multiplying, the reaction rate by the volume of the reactor results in the total fission rate for the entire reactor. Dividing the number of fissions per watt-second results in the power released by fission in the reactor in units of watts. This relationship is shown mathematically in Eq. 1.37 below.

$$P = \frac{\phi_{th} \sum_f V}{3.12 \times 10^{10} \frac{\text{fission}}{\text{second}}} \quad (1.37)$$

where:

P = Power (watts)

ϕ_{th} = Thermal neutron flux (neutron/cm²-sec)

$\sum_f V$ = Macroscopic cross section for fission (cm⁻¹)

V = Volume of core (cm³)

1.13 Relationship Between Neutron Flux and Reactor Power

In an operating reactor, the volume of the reactor is constant. Over a relatively short period of time (days or weeks), the number density of the fuel atoms is also relatively constant. Since the atom density and microscopic cross section are constant, the macroscopic cross section must also be constant. Examining Eq. 1.35, it is apparent that if the reactor volume and macroscopic cross section are constant, then the reactor power and the neutron flux are directly proportional. This is true for day-to-day operation. The neutron flux for a given power level will increase very slowly over a period of months due to the burnup of the fuel and resulting decrease in atom density and macroscopic cross section.

In summary, the reaction rate is:

- The reaction rate is the number of interactions of a particular type occurring in a cubic centimeter of material in a second.
- The reaction rate can be calculated by the equation below.

$$R = \phi \sum$$

- Over a period of several days, while the atom density of the fuel can be considered constant, the neutron flux is directly proportional to reactor power.

Problems

Problem 1.1 If the atomic mass unit is designated by u , where 1 u is exactly one 12th of the mass of the ^{12}C atom, equal to 1.661×10^{-27} kg, then, calculate the energy equivalent to a conventional mass equal to $1u$.

Problem 1.2 Calculate the energy as Problem 1.1 using MeV as units.

Problem 1.3

- (a) Calculate the mass defect and the binding energy for a nucleus of an isotope of tin ^{120}Sn (atomic mass $M = 119.9022$ u) and for an isotope of uranium-235 (U^{235}) (atomic mass $M = 235.0439$). Assume the measured mass of the atom is M ; the mass defect ΔM is given by:

$$\Delta M = Z \cdot (m_p + m_e) + (A - Z) \cdot m_n - M$$

$Z \cdot m_p$ = Total mass of proton

$Z \cdot m_e$ = Total mass of electron

$(A - Z) \cdot m_n$ = Total mass of neutrons.

- (b) Assume the total binding energy for uranium is approximately same as Tin; what would be the total energy that will be released after fission of a single ^{235}U nucleus?

Problem 1.4 Calculate the mass defect for lithium-7. The mass of lithium-7 is 7.016003 amu. Assuming that:

m_p = Mass of a proton (1.007277 amu)

m_n = Mass of neutron (1.008665 amu)

m_e = Mass of an electron (0.000548597 amu)

Problem 1.5 Consider that 1 amu is equivalent to 931.5 MeV of energy; the binding energy can be calculated using the following relationship.

$$\text{Binding Energy} = \Delta m \left(\frac{931.5 \text{ MeV}}{1 \text{ amu}} \right)$$

Then calculate the mass defect and binding energy for uranium-235. One uranium-235 atom has a mass of 235.043924 amu.

Problem 1.6 Calculate the decay constant, mean life and half-life of a radioactive isotope which radioactivity after 100 days is reduced 1.07 times.

Problem 1.7 A block of aluminum has a density of 2.699 g/cm^3 . If the gram atomic weight of aluminum is 26.9815 gram, then calculate the atom density of aluminum.

Problem 1.8 Since the activity and the number of atom are always proportional, they may be used interchangeably to describe any given radionuclide population. Therefore, the following is true:

$$A = A_0 e^{-\lambda t}$$

where:

A = Activity present at time t

A_0 = Activity initially present

λ = Decay constant (time^{-1})

t = Time

Assuming a sample of material contains 20 micrograms of californium-252 and this element has a half-life of 2.638 years, then calculate:

- The number of californium-252 atoms initially present.
- The activity of californium-252 in curies. Assume the relationship between the activity, number of atoms, and decay constant is shown in $A = \lambda N$, where A is activity of nuclide (disintegrations/seconds), λ is the decay constant of the nuclide (1/second), and finally N is number of atoms of the nuclide in the sample.
- The number of californium-252 atoms that will remain in 12 years.
- The time it will take for the activity to reach 0.001 curies.

Problem 1.9 Plot the radioactive decay curve for nitrogen-16 over a period of 100 s. The initial activity is 142 curies and the half-life of nitrogen-16 is 7.13 s. Plot the curve on both linear rectangular coordinates and on a semi-log scale.

Problem 1.10 Find the macroscopic thermal neutron absorption cross section for iron, which has a density of 7.86 g/cm. The microscopic cross section for absorption of iron is 2.56 barns, and the gram atomic weight is 55.847 g.

Problem 1.11 An alloy is composed of 95% aluminum and 5% silicon (by weight). The density of the alloy is 2.66 g/cm. Properties of aluminum and silicon are shown below.

Element	Gram atomic weight	σ_a (barns)	σ_s (barns)
Aluminum	26.9815	0.23	1.49
Silicon	28.0855	0.16	2.20

1. Calculate the atom densities for the aluminum and silicon.
2. Determine the absorption and scattering macroscopic cross sections for thermal neutrons.
3. Calculate the mean free paths for absorption and scattering.

Problem 1.12 What is the value of σ_f for uranium-235 for thermal neutrons at 500 °F? Uranium-235 has σ_f of 583 barns at 68 °F.

Problem 1.13 If a one cubic centimeter section of a reactor has a macroscopic fission cross section of 0.1 cm^{-1} , and if the thermal neutron flux is $10^{13} \text{ neutrons/cm}^2\text{-sec}$, what is the fission rate in that cubic centimeter?

Problem 1.14 A reactor operating at a flux level of $3 \times 10^{13} \text{ neutrons/cm}^2\text{-sec}$ contains 10^{20} atoms of uranium-235 per cm³. The reaction rate is $1.29 \times 10^{12} \text{ fission/cm}^3$. Calculate \sum_f and σ_f .

Problem 1.15 The microscopic cross section for the capture of thermal neutrons by hydrogen is 0.33 barn and for oxygen 2×10^{-4} barn. Calculate the macroscopic capture cross section of the water molecule for thermal neutrons.

Problem 1.16 Calculate the minimum energy that a neutron with energy 1 MeV can be reduced to after collision with:

- (a) Nucleus of hydrogen
- (b) Nucleus of carbon

References

1. D.G. Madland, J.R. Nix, New calculation of prompt fission neutron spectra and average prompt neutron multiplicities. *Nucl. Sci. Eng.* **81**, 213–271 (1982)
2. R.J. LaBouve, T.R. England, D.C. George, C.W. Maynard, Fission product analytic impulse source functions. *Nucl. Technol.* **56**, 332–339 (1982)

3. J. Lewins, *Nuclear Reactor Kinetics and Control* (Pergamon Press, Oxford, UK, 1978)
4. K. Ott, R.J. Neuhold, *Nuclear Reactor Dynamics* (American Nuclear Society, LaGrange Park, 1985)
5. A.F. Henry, *Nuclear Reactor Analysis* (The MIT Press, Cambridge, MA/London, UK, 1975)
6. J.R. Lamarsh, *Introduction to Nuclear Reactor Theory* (Addison Wesley Publishing Company, Inc, New York, NY, 1966)
7. B. Zohuri, *Combined Cycle Driven Efficiency for Next Generation Nuclear Power Plants: An Innovative Design Approach* (Springer.; 2015 edition, New York, NY, 2015)
8. B. Zohuri, P. McDaniel, A Comparison of a Recuperated Open Cycle (Air) Brayton Power Conversion System with the Traditional Steam Rankine Cycle for the Next Generation Nuclear Power Plant" will be published in Nuclear Science
9. B. Zohuri, *Innovative Open Air Brayton Combined Cycle Systems for the Next Generation Nuclear Power Plants* (University of New Mexico Publications, New York, NY, 2014)
10. P.J. McDaniel, B. Zohuri, C.R.E. de Oliveira, *A Combined Cycle Power Conversion System for Small Modular LMFBRs* (ANS Transactions, 2014)
11. B. Zohuri, *Cycle Power Conversion System for the Next Generation Nuclear Power Plant* (ANS Transactions, 2012)
12. C. Forsberg, P. McDaniel, B. Zohuri, Variable Electricity and steam from salt, helium, and sodium cooled base-load reactors with gas turbines and heat storage, Proceedings of ICAPP 2015
13. P.E. Hodgson, E. Gadioli, E. Gadioli Erb, *Introductory Nuclear Physics* (Oxford Science Publications). Paperback – November 27, New York, NY, 1997
14. You can get the data from <http://ie.lbl.gov/toimass.html>
15. Nuclear Data Center, JAEA <http://wwwndc.tokai-sc.jaea.go.jp/nucldata/index.html>, Chart of the Nuclides here is based on the compilation of experimental data until 2008 by H. Koura (JAEA), T. Tachibana (Waseda University), and J. Kataura (JAEA), beta-decay half-lives
16. Nuclear Data Center, JAEA <http://wwwndc.tokai-sc.jaea.go.jp/nucldata/index.html>. this is estimated, by T. Tachibana, with the Gross Theory [T. Tachibana, M. Yamada, Proc. Int. Conf. on exotic nuclei and atomic masses, Arles, 1995, p.763], and alpha-decay half-lives based on the reference of V.E. Vola, Jr. and G.T. Seaborg, J. Inorg. Nucl. Chem., 28, 741 (1966) and newly adjusted parameter values
17. The speed of neutrons in a reactor is sufficiently low that one can neglect relativistic effects therefore $m = m_0$, the neutron rest mass (1.6748×10^{-27} kg)
18. FEMP computer code has been developed by Professor Patrick McDaniel of University of New Mexico, Nuclear Engineering Department
19. This effort was taken in place under contract by McDaniel and Zohuri in time period of 2001-2003 but never was a finished effort, although a lot of work was put into it and somewhat a new modified version NJOY with recoil capability was developed
20. One can calculate the total binding energy of a nucleus from the mass defect, Δm which is the difference between the mass of the bound nucleus and the sum of the masses of the nucleons, using Einstein's equation $E_{b\text{Total}} = \Delta mc^2$

Chapter 2

Modeling Neutron Transport and Interactions



It is essential to know the spatial and energy distributions of the neutrons in a field in a nuclear fission reactor, D-T (or D-D) fusion reactor, or other nuclear reactors populated with large numbers of neutrons. It is obvious why the spatial distribution should be known, and because neutron reactions vary widely with energy, the energy distribution is also a critical parameter. The neutron energy distribution is often called the neutron spectrum. The neutron distribution satisfies transport equation. It is usually difficult to solve this equation, and often approximated equation so-called diffusion equation is solved instead. In this chapter only overview of transport equation and diffusion equation of neutrons is presented, and methods for solving these equations are presented in the following sections.

2.1 Transport Equations

In order to predict the reaction rates in a nuclear reactor, we need to know two entities. We need to know the nuclear cross sections as a function of space and position, and we need to know the neutron population as a function of time, space, and position. We can calculate this neutron population if we can develop a balance equation, or conservation equation, to describe the neutron population. Actually, there are two approaches to deriving the balance or conservation equation. There is the integrodifferential equation approach and the complete integral equation approach. We will use the integrodifferential approach for most of this class because with suitable approximations it reduces to the multi-group diffusion equations or simply the diffusion equation. The complete integral equation is the equation solved by Monte Carlo transport codes and therefore is used in more advanced analyses. Further discussion of transport equations will take place in Chap. 3 of the book.

Before we move on further, we need to define few concepts in neutronics analysis which falls under the category of *neutron transport analysis* concept and reactor design process that one should know, and they are as follows.

2.2 Reaction Rates

It is possible to determine the rate at which a nuclear reaction will take place based on the neutron flux, cross section for the interaction, and atom density of the target. This relationship illustrates how a change in one of these items affects the reaction rate.

If the total path length of all the neutrons in a cubic centimeter in a second is known, neutron flux (ϕ), and if the probability of having an interaction per centimeter path length is also known, which we called it macroscopic cross section (Σ), multiply them together to get the number of interactions taking place in that cubic centimeter in 1 s. This value is known as the reaction rate and is denoted by the symbol R . The reaction rate can be calculated by the equation shown below.

$$R = \phi\Sigma \quad (2.1)$$

where:

R = reaction rate (reactions/sec)

ϕ = neutron flux (neutron/ $\text{cm}^2\text{-sec}$)

Σ = macroscopic cross section (cm^{-1})

Substituting the fact that $\Sigma = N\sigma$ into Eq. 2.1 yields the following equation as:

$$R = \phi N\sigma \quad (2.2)$$

where:

σ = microscopic cross section (cm^2)

N = atom density (atoms/ cm^3)

The reaction rate calculated will depend on which macroscopic cross section is used in the calculation. Normally, the reaction rate of greatest interest is the fission reaction rate.

In addition to using Eq. 2.1 to determine the reaction rate based on the physical properties of the material, it is also possible to algebraically manipulate the equation to determine physical properties if the reaction rate is known.

2.3 Reactor Power Calculation

If we multiply the reaction rate per unit volume by the total volume of the core results in the total number of reactions occurring in the core per unit time and if the amount of energy involved in each reaction were known, it would be possible to determine the rate of energy release (power) due to a certain reaction.

In a reactor where the average energy per fission is 200 MeV, it is possible to determine the number of fissions per second that are necessary to produce 1 watt of power using the following conversion factors:

$$\begin{aligned}1 \text{ fission} &= 200 \text{ MeV} \\1 \text{ MeV} &= 1.602 \times 10^{-6} \text{ ergs} \\1 \text{ erg} &= 1 \times 10^{-7} \text{ watt- sec}\end{aligned}$$

$$\begin{aligned}1 \text{ watt} & \left(\frac{1 \text{ erg}}{1 \times 10^{-7} \text{ watt- sec}} \right) \left(\frac{1 \text{ MeV}}{1.602 \times 10^{-6} \text{ erg}} \right) \left(\frac{1 \text{ fission}}{200 \text{ MeV}} \right) \\&= 3.12 \times 10^{10} \frac{\text{fission}}{\text{second}}\end{aligned}$$

This is equivalent to stating that 3.12×10^{10} fissions release 1 watt-second of energy.

The power released in a reactor can be calculated based on Eq. 2.1. Therefore, multiplying the reaction rate by the volume of the reactor would result in the total fission rate for the entire reactor. Dividing by the number of fissions per watt-sec would result in the power released by fission in the reactor in units of watts. This relationship is shown mathematically in Eq. 2.3.

$$P = \frac{\phi_{th} \Sigma_f V}{3.12 \times 10^{10} \frac{\text{fissions}}{\text{watt- sec}}} \quad (2.3)$$

where:

P = power (watts)

ϕ_{th} = thermal neutron flux (neutrons/cm²-sec)

Σ_f = macroscopic cross section for fission (cm⁻¹)

V = volume of core (cm³)

2.4 Relationship Between Neutron Flux and Reactor Power

In an operating reactor, the volume of the reactor is constant. Over a relatively short period of time (days or weeks), the number density of the fuel atoms is also relatively constant. Since the atom density and microscopic cross section are constant, the macroscopic cross section must also be constant. Examining Eq. 2.3, it is apparent that if the reactor volume and macroscopic cross section are constant, then the reactor power and the neutron flux are directly proportional. This is true for day-to-day operation. The neutron flux for a given power level will increase very slowly

over a period of months due to the burnup of the fuel and resulting decrease in atom density and macroscopic cross section.

2.5 Neutron Slowing Down and Thermalization

In thermal reactors, the neutrons that cause fission are at a much lower energy than the energy level at which they were born from fission. In this type of reactor, specific materials must be included in the reactor design to reduce the energy level of the neutrons in an efficient manner.

Fission neutrons are produced at an average energy level of 2 MeV and immediately begin to slow down as the result of numerous scattering reactions with a variety of target nuclei. After a number of collisions with nuclei, the speed of a neutron is reduced to such an extent that it has approximately the same average kinetic energy as the atoms (or molecules) of the medium in which the neutron is undergoing elastic scattering. This energy, which is only a small fraction of an electron volt at ordinary temperatures (0.025 eV at 20°C), is frequently referred to as the thermal energy, since it depends upon the temperature. Neutrons whose energies have been reduced to values in this region (less than 1 eV) are designated thermal neutrons. The process of reducing the energy of a neutron to the thermal region by elastic scattering is referred to as *thermalization*, slowing down, or moderation. The material used for the purpose of thermalizing neutrons is called a moderator. A good moderator reduces the speed of neutrons in a small number of collisions, but does not absorb them to any great extent. Slowing the neutrons in as few collisions as possible is desirable in order to reduce the amount of neutron leakage from the core and also to reduce the number of resonance absorptions in nonfuel materials. Neutron leakage and resonance absorption will be discussed in the next module.

The ideal moderating material (moderator) should have the following nuclear properties:

- Large scattering cross section.
- Small absorption cross section.
- Large energy loss per collision.

A convenient measure of energy loss per collision is the logarithmic energy decrement. The *average logarithmic energy decrement* is the average decrease per collision in the logarithm of the neutron energy. This quantity is represented by the symbol ξ (Greek letter xi), and it is shown as:

$$\xi = \ln E_i - \ln E_f$$

$$\xi = \ln \left(\frac{E_i}{E_f} \right) \quad (2.4)$$

where:

ξ = average logarithmic energy decrement

E_i = average initial neutron energy

E_f = average final neutron energy

The symbol ξ is commonly called the average logarithmic energy decrement because of the fact that a neutron loses, on the average, a fixed fraction of its energy per scattering collision. Since the fraction of energy retained by a neutron in a single elastic collision is a constant for a given material, is also a constant. Because it is a constant for each type of material and does not depend upon the initial neutron energy, it is a convenient quantity for assessing the moderating ability of a material.

The values for the lighter nuclei are tabulated in a variety of sources. The following commonly used approximation may be used when a tabulated value is not available:

$$\xi = \frac{2}{A + \frac{2}{3}} \quad (2.5)$$

This approximation is relatively accurate for mass numbers (A) greater than 10, but for some low values of A , it may be in error by over 3%.

Since ξ represents the average logarithmic energy loss per collision, the total number of collisions necessary for a neutron to lose a given amount of energy may be determined by dividing into the difference of the natural logarithms of the energy range in question. The number of collisions (N) to travel from any energy, E_{high} , to any lower energy, E_{low} , can be calculated as shown below.

$$N = \frac{\ln E_{high} - \ln E_{low}}{\xi} = \frac{\ln \left(\frac{E_{high}}{E_{low}} \right)}{\xi} \quad (2.6)$$

Sometimes it is convenient, based upon information known, to work with an average fractional energy loss per collision as opposed to an average logarithmic fraction. If the initial neutron energy level and the average fractional energy loss per collision are known, the final energy level for a given number of collisions may be computed using the following formula:

$$E_N = E_0(1 - x)^N \quad (2.7)$$

where:

E_0 = initial neutron energy

E_N = neutron energy after N collisions

x = average fractional energy loss per collision

N = number of collision

2.6 Macroscopic Slowing Down Power

Although the logarithmic energy decrement is a convenient measure of the ability of a material to slow neutrons, it does not measure all necessary properties of a moderator. A better measure of the capabilities of a material is the macroscopic slowing down power. The *macroscopic slowing down power* (MSDP) is the product of the logarithmic energy decrement and the macroscopic cross section for scattering in the material. Equation 2.8 illustrates how to calculate the macroscopic slowing down power:

$$\mathbf{MSDP} = \xi \Sigma_s \quad (2.8)$$

2.7 Moderate Ratio

Macroscopic slowing down power indicates how rapidly a neutron will slow down in the material in question, but it still does not fully explain the effectiveness of the material as a moderator. An element such as boron has a high logarithmic energy decrement and a good slowing down power, but it is a poor moderator because of its high probability of absorbing neutrons.

The most complete measure of the effectiveness of a moderator is the moderating ratio. The *moderating ratio* is the ratio of the macroscopic slowing down power to the macroscopic cross section for absorption. The higher the moderating ratio, the more effectively the material performs as a moderator. Equation 2.9 shows how to calculate the moderating ratio of a material:

$$\mathbf{MR} = \frac{\xi \Sigma_s}{\Sigma_a} \quad (2.9)$$

Moderating properties of different materials are compared in Table 2.1.

Table 2.1 Moderating properties of materials

Material	ξ	Number of collision thermalized	Macroscopic slowing down power	Moderating ratio
H^2O	0.927	19	1.425	62
D^2O	0.510	35	0.177	4830
Helium	0.427	42	9×10^{-6}	51
Beryllium	0.207	86	0.154	126
Boron	0.171	105	0.092	0.00086
Carbon	0.158	114	0.083	216

2.8 Integrodifferential Equation (Maxwell-Boltzmann Equation)

The integrodifferential equation is also called the Maxwell-Boltzmann equation after its original developers. However, they developed it in its most complete nonlinear form wherein each particle could interact with every other particle in the solution space. Here we will only deal with the linear form, wherein we only consider neutron interactions with nuclei. We will not consider nuclei interactions with other nuclei or neutron interactions with other neutrons. There are, on the order, of 10^{21-22} nuclei per cubic centimeter in a typical reactor and on the order of 10^{13-15} neutrons in the same reactor. The interactions of neutrons with themselves are very low probability events compared with their interactions with nuclei. In addition, nuclei are held in place and do not interact with each other except as characterized by an equilibrium temperature model.

Consider the Fig. 2.1,

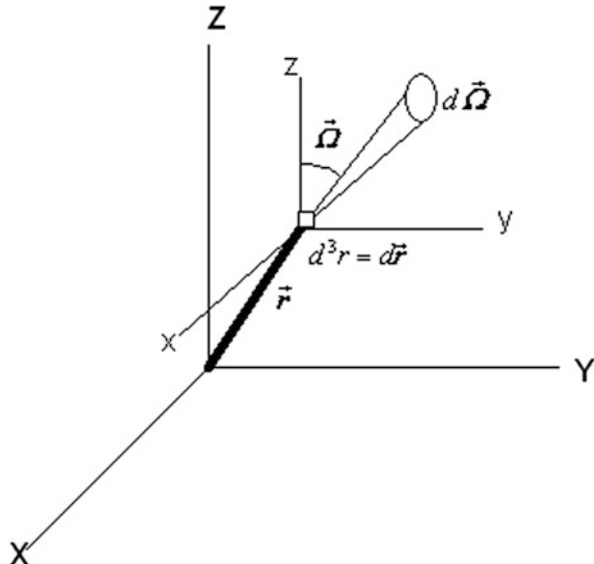
Now define:

$n(\vec{r}, \vec{\Omega}, E, t) d^3r d\vec{\Omega} dE dt$ = the number of neutrons in a differential spatial volume $d^3r = d\vec{r}$ about \vec{r} , moving in direction $d\vec{\Omega}$ about direction $\vec{\Omega}$ with an energy within dE about E , in a time interval dt about time t . This quantity will be called the neutron angular density. Note bold quantities indicate a vector. Thus, n is dependent on seven variables.

Now we can write a balance equation for n as simply:

$$\frac{dn}{dt} = \text{Gains} - \text{Losses} \quad (2.10)$$

Fig. 2.1 Solid angle



The principle gains will be composed of three terms. These are:

1. Inhomogeneous sources or direct production of neutrons.
2. In-scatter sources where at a point, a neutron shows up with energy E and going in direction $\vec{\Omega}$ as the result of scattering \vec{r} .
3. Fission sources that are the result of a fission occurring at \mathbf{r} .

The inhomogeneous source is given by:

$$IS = q(\vec{r}, \vec{\Omega}, E, t) d \vec{r} d \vec{\Omega} dE \quad (2.11)$$

The in-scatter source term is given by:

$$SS = \int_{E'} \int_{\vec{\Omega}'} \Sigma_s(E', \vec{\Omega}' \rightarrow E, \vec{\Omega}) v(E') n(\vec{r}, E', \vec{\Omega}', t) dE' d\vec{\Omega}' d \vec{r} d \vec{\Omega} dE \quad (2.12)$$

And the fission source is given by:

$$\int_{E'} \int_{\vec{\Omega}'} \chi(E) \frac{v(E')}{4\pi} \Sigma_f(E') v(E') n(\vec{r}, E', \vec{\Omega}', t) dE' d\vec{\Omega}' d \vec{r} dE d \vec{\Omega} \quad (2.13)$$

The two loss terms correspond to particles that have a collision at \vec{r} or leak out of $d \vec{r}$. The collision term is:

$$CL = \Sigma_T(\vec{r}, E) v(E) n(\vec{r}, E, \vec{\Omega}, t) d \vec{r} d \vec{\Omega} dE \quad (2.14)$$

And the leakage term is:

$$LL = \vec{v}(E) n(\vec{r}, E, \vec{\Omega}, t) \cdot d \vec{S} d \vec{\Omega} dE \quad (2.15)$$

where $d \vec{S}$ is the surface area of the differential volume $d \vec{r}$ and the vector dot product of $\vec{v}(E)$ with $d \vec{S}$ gives the net leakage through the surface surrounding $d \vec{r}$.

Note that in order to get reaction rates per unit time, each of the cross sections with units of 1/cm had to be multiplied by $\vec{v}(E)$ to get units of 1/sec. It is easier to group the $\vec{v}(E)$ with $n(\vec{r}, E, \vec{\Omega}, t)$ and call the new quantity $\psi = (\vec{r}, E, \vec{\Omega}, t) = \vec{v}(E) n(\vec{r}, E, \vec{\Omega}, t)$ the neutron angular flux density.

Now note that we can apply Gauss's theorem to the leakage loss term to get:

$$\vec{\psi}(\vec{r}, E, \vec{\Omega}, t) \cdot d \vec{S} = \nabla \cdot \vec{\Omega} \psi(\vec{r}, E, \vec{\Omega}, t) d \vec{r} \quad (2.16)$$

This allows us to delete the $d\vec{S} d\vec{\Omega} dE$ factor from each term. The complete equation then becomes:

$$\begin{aligned} \frac{1}{v(E)} \frac{\partial \psi(\vec{r}, E, \vec{\Omega}, t)}{\partial t} &= q(\vec{r}, E, \vec{\Omega}, t) + \int_{E'} \int_{\vec{\Omega}} \sum_S (\vec{r}, E', \vec{\Omega}' \rightarrow E, \vec{\Omega}) \\ &\psi(\vec{r}, E', \vec{\Omega}', t) dE' d\vec{\Omega}' + \int_{E'} \int_{\vec{\Omega}} \chi(E) \frac{v(E')}{4\pi} \sum_f (\vec{r}, E') \psi(\vec{r}, E', \vec{\Omega}', t) dE' d\vec{\Omega}' \\ &- \sum_T \left((\vec{r}, E) \psi(\vec{r}, E, \vec{\Omega}, t) - \nabla \cdot \vec{\Omega} \psi(\vec{r}, E, \vec{\Omega}, t) \right) \end{aligned} \quad (2.17)$$

Now note that $\nabla \cdot \vec{\Omega} \psi(\vec{r}, E, \vec{\Omega}, t) = \psi(\vec{r}, E, \vec{\Omega}, t) \nabla \cdot \vec{\Omega} + \vec{\Omega} \cdot \nabla \psi(\vec{r}, E, \vec{\Omega}, t)$. In addition, the first term on the left-hand side is zero due to the constancy of $\vec{\Omega}$. Thus, the divergence term is often written as $\vec{\Omega} \cdot \nabla \psi(\vec{r}, E, \vec{\Omega}, t)$. However, for many numerical schemes, it is conservative to keep it in its original form. If we move the two loss terms to the left-hand side of the equation, we can write it as:

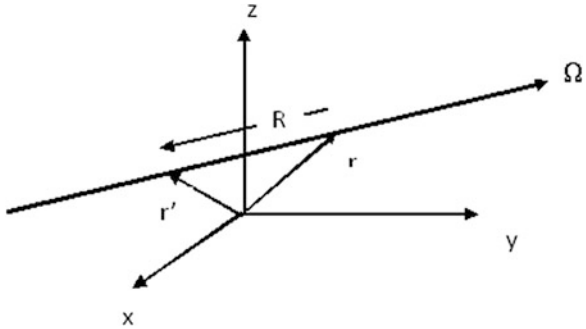
$$\begin{aligned} \frac{1}{v(E)} \frac{\partial \psi(\vec{r}, E, \vec{\Omega}, t)}{\partial t} + \nabla \cdot \vec{\Omega} \psi(\vec{r}, E, \vec{\Omega}, t) + \Sigma_T(\vec{r}, E) \psi(\vec{r}, E, \vec{\Omega}, t) &= q(\vec{r}, E, \vec{\Omega}, t) + \\ \int_{E'} \int_{\vec{\Omega}} \sum_S (\vec{r}, E', \vec{\Omega}' \rightarrow E, \vec{\Omega}) \psi(\vec{r}, E', \vec{\Omega}', t) dE' d\vec{\Omega}' + \chi(E) \int_{E'} \int_{\vec{\Omega}'} \frac{\nu(E')}{4\pi} \Sigma_f(\vec{r}, E') \psi(\vec{r}, E', \vec{\Omega}', t) dE' d\vec{\Omega}' & \end{aligned} \quad (2.18)$$

The time-independent form can be obtained by dropping the derivative term with respect to time. Then if the inhomogeneous term is omitted, we will have the term of most interest for reactor analysis. However, in this form the equation becomes homogenous, and every term depends on the angular flux density. So in order to obtain a solution, an eigenvalue, $1/k$, has to be introduced. This gives the following equation:

$$\begin{aligned} \nabla \cdot \vec{\Omega} \psi(\vec{r}, E, \vec{\Omega}) + \Sigma_T(\vec{r}, E) \psi(\vec{r}, E, \vec{\Omega}) &= \int_{E'} \int_{\vec{\Omega}'} \Sigma_S(\vec{r}, E', \vec{\Omega}' \rightarrow E, \vec{\Omega}) \psi(\vec{r}, E', \vec{\Omega}') dE' d\vec{\Omega}'' \\ + \frac{\chi(E)}{k} \int_{E'} \int_{\vec{\Omega}'} \frac{\nu(E')}{4\pi} \Sigma_f(\vec{r}, E') \psi(\vec{r}, E', \vec{\Omega}') dE' d\vec{\Omega}' & \end{aligned} \quad (2.19)$$

which is the version of the transport equation that is of most concern for reactor criticality analyses.

Fig. 2.2 Three-dimensional configuration for integral equation derivations



2.9 Integral Equation

Consider now the following diagram (Fig. 2.2):

We have:

$$\vec{R} = R \vec{\Omega}$$

$$\frac{d\psi(\vec{r}, E, \vec{\Omega}, t)}{dR} = \frac{\partial x}{\partial R} \frac{\partial \psi}{\partial x} + \frac{\partial y}{\partial R} \frac{\partial \psi}{\partial y} + \frac{\partial z}{\partial R} \frac{\partial \psi}{\partial z} + \frac{\partial t}{\partial R} \frac{\partial \psi}{\partial t}$$

$$\frac{\partial x}{\partial R} = -\vec{\Omega}_x$$

$$\frac{\partial y}{\partial R} = -\vec{\Omega}_y$$

$$\frac{\partial z}{\partial R} = -\vec{\Omega}_z$$

$$\vec{v} = -\frac{\partial \vec{R}}{\partial t}$$

or:

$$\frac{d\psi(\vec{r}, E, \vec{\Omega}, t)}{dR} = -\vec{\Omega} \cdot \nabla \psi(\vec{r}, E, \vec{\Omega}, t) - \frac{1}{v} \frac{\partial \psi(\vec{r}, E, \vec{\Omega}, t)}{\partial t} \quad (2.20)$$

Substituting this into the integrodifferential form gives:

$$\begin{aligned} -\frac{d\psi(r, E, \Omega, t)}{dR} + \Sigma_t(r, E)\psi(r, E, \Omega, t) &= q(r, E, \Omega, t) \\ + \int_{E'} \int_{\Omega'} \Sigma_s(r, E', \Omega' \rightarrow E, \Omega) \psi(r, E', \Omega', t) dE' d\Omega' & \\ + \frac{\chi(E)}{4\pi} \int_{E'} \int_{\Omega'} v(E') \Sigma_f(r, E') \psi(r, E, \Omega', t) dE' d\Omega' & \end{aligned} \quad (2.21)$$

Now with the integrating factor:

$$e^{-\int_0^R \Sigma_t(r-R', \vec{\Omega}, E) dR'} \quad (2.22)$$

the equation becomes:

$$\frac{d}{dR} \left\{ \psi(\vec{r}, E, \vec{\Omega}, t) e^{-\int_0^R \sum_t(\vec{r} - R', \vec{\Omega}, E) dR'} \right\} = e^{-\int_0^R \sum_t(\vec{r} - R', \vec{\Omega}, E) dR'} \left\{ \begin{array}{l} q(\vec{r}, E, \vec{\Omega}, t) \\ + \int_{E'} \int_{\Omega'} \sum_s(\vec{r}, E', \vec{\Omega}' \rightarrow E, \vec{\Omega}) \psi(\vec{r}, E', \vec{\Omega}', t) dE' d\vec{\Omega}' \\ + \frac{\chi(E)}{4\pi} \int_{E'} \int_{\Omega'} v(E') \sum_f(\vec{r}, E') \psi(\vec{r}, E', \vec{\Omega}', t) dE' d\vec{\Omega}' \end{array} \right\} \quad (2.23)$$

Integrating over R gives the following equation (note the equation $R = vt$ must be satisfied at all points along the ray defined by $\vec{R} = R \vec{\Omega}$):

$$\begin{aligned} \psi(\vec{r}, E, \vec{\Omega}, t) - \psi(\infty, E, \vec{\Omega}, t) e^{-\int_0^\infty \sum_t(\vec{r} - R', \vec{\Omega}, E) dR'} \\ = \int_0^\infty dRe^{-\int_0^R \sum_t(\vec{r} - R', \vec{\Omega}, E) dR'} \\ \left\{ \begin{array}{l} q(\vec{r}, E, \vec{\Omega}, t) \\ + \int_{E'} \int_{\Omega'} \sum_s(\vec{r}, E', \vec{\Omega}' \rightarrow E, \vec{\Omega}) \psi(\vec{r}, E', \vec{\Omega}', t) dE' d\vec{\Omega}' \\ + \frac{\chi(E)}{4\pi} \int_{E'} \int_{\Omega'} v(E') \sum_f(\vec{r}, E') \psi(\vec{r}, E', \vec{\Omega}', t) dE' d\vec{\Omega}' \end{array} \right\} \end{aligned} \quad (2.24)$$

and hoping that we can find a location at infinity along the ray such that $\psi = (\vec{r}, E, \vec{\Omega}, t)$ can be neglected and defining the optical thickness as:

$$\beta(\vec{r}, R, E, \vec{\Omega}, t) = \int_0^R \sum_t(\vec{r} - R', \vec{\Omega}, E) dR' \quad (2.25)$$

We have:

$$\psi(\vec{r}, E, \vec{\Omega}, t) = \int_0^\infty dR e^{-\beta(\vec{r} - R, E, \vec{\Omega}, t)} \left\{ \begin{array}{l} q(\vec{r}, E, \vec{\Omega}, t) \\ + \int_{E'} \int_{\vec{\Omega}'} \sum_s (\vec{r}, E', \vec{\Omega}' \rightarrow E, \vec{\Omega}) \psi(\vec{r}, E', \vec{\Omega}', t) dE' d\vec{\Omega}' \\ + \frac{\chi(E)}{4\pi} \int_{E'} \int_{\vec{\Omega}'} v(E') \sum_f (\vec{r}, E') \psi(\vec{r}, E', \vec{\Omega}', t) dE' d\vec{\Omega}' \end{array} \right\} \quad (2.26)$$

Note that the time dependence is tied up in β and the equation $R = vt$ must still be satisfied. However, this is a purely integral equation. It can be multi-grouped simply by integrating over a set of energy group intervals. We can also find the isotropic flux simply by integrating ψ over $\vec{\Omega}$. That is:

$$\phi(r, E, t) = \int_{\vec{\Omega}} \psi(r, E, \vec{\Omega}, t) d\vec{\Omega} \quad (2.27)$$

2.10 Multi-group Diffusion Theory

In this section, the multi-group form of the neutron diffusion equation is developed and explored with the aim to relate the mathematics to the physical meaning. Keep in your mind that the diffusion theory model of neutron transport has a crucial input and plays a major role in reactor theory since its simplification allows scientific insight and it is sufficiently realistic enough to study many important design problems in real world of reactor design and manufacturing. In order to simplify the complex mathematics of multi-group diffusion theory, one can assume neutrons can be characterized by a single energy or speed if need be, and a model then allows preliminary design problem estimations. In that case, the mathematical methods used to analyze such a model are the same as those applied in more sophisticated methods that are applied in multi-group diffusion theory and transport theory which are our intention in this section and chapter. There are enough literature and notes of references that can be found on the Internet, which shows the derivation of such a simple diffusion equation which depends on Fick's law, even through a direct derivation from the transport equation is also possible, and as a result the Helmholtz equation can easily be derived in this simple case. In this simple case approach, the limitation on diffusion equation as well as the boundary conditions can be applied in its application to realistic engineering and physics problem of reactor theory [1].

Back to our subject of multi-group diffusion theory, we start by asking question of why we need the *multi-group model* to start with. In order to answer this question, we know that neutrons have a wide energy spectrum, ranging from a fraction of an

eV to a few MeV. The cross sections vary over decades in this range, so we can hardly expect the one-group approximation to be very accurate. To illustrate this, consider a simple cell model as shown in Fig. 2.3 for a tank-type experimental reactor as:

The height, H , of the D_2O moderator was varied to achieve criticality. Then a void was introduced in the coolant by bubbling air into it. The height, H , of the moderator was again varied to keep the reactor critical. A range of void fraction was introduced. Figure 2.4 gives the experimental results (Buckling, $(\pi/H)^2$ vs. void fraction, α) and the predictions of a number of simple reactor models. One-group theory does not

Fig. 2.3 Schematic of the nuclear reactor model showing the top view of the lattice structure of fuel bundles and a side view of the two-region cell

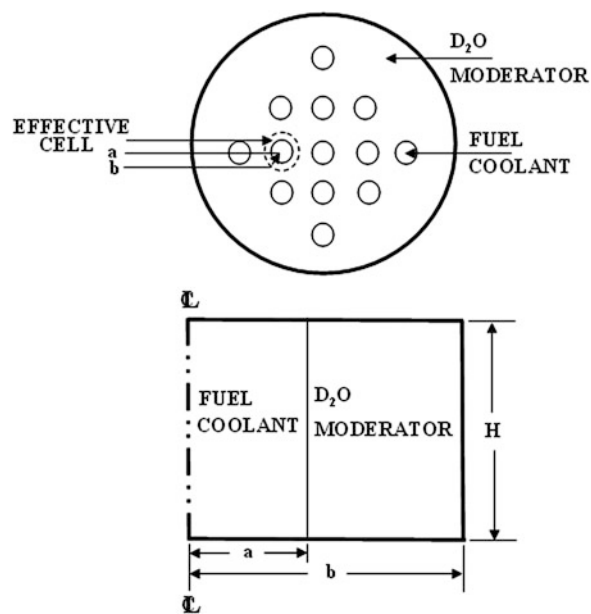


Fig. 2.4 Comparison between experimentally observed and calculated buckling

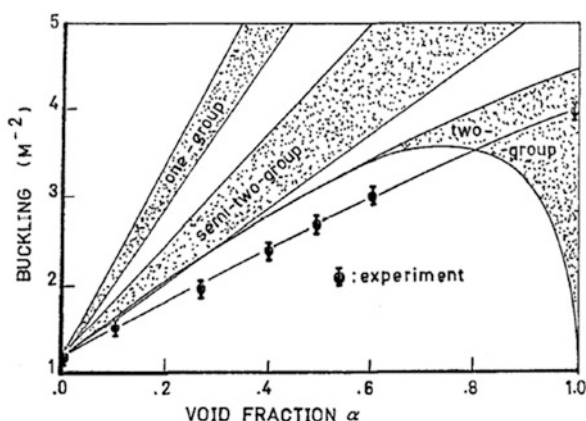
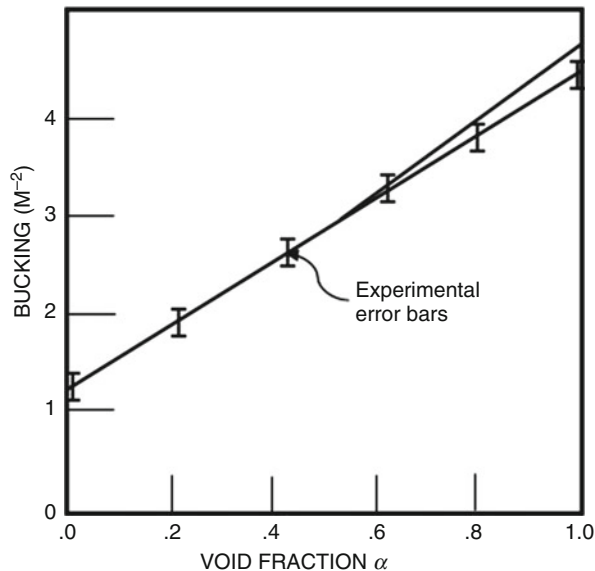


Fig. 2.5 Comparison of experimentally observed buckling and predictions of the two-group model using adjusted parameters



come close to predicting the buckling, even if the cross sections are varied within their experimental error. The semi-two-group theory does better, and the two-group model does better still.

The two-group model can be further improved by using energy-averaged cross sections obtained by a comprehensive cell code that employs a detailed energy structure. The improved comparison is shown in Fig. 2.5 which shows what can be achieved with a few-group model (in this case, two) if the “appropriate” average cross sections can be found that represent the cell in question. We shall see that we can only get good values if we first perform a many-group model calculation.

This work is detailed in B. Garland (1975) [2], but for the present discussion, the main point to note is the inadequacy of the one-group model or even the two-group model since the appropriate cross sections are not explicitly available and since these low-order models do not come close to capturing the energy structure. Accurate cell calculations are done typically with up to 150 neutron energy groups to obtain cell-averaged cross sections. Then, few-group approximations are used for the full-core calculation based on the cell-averaged cross sections. Few-group calculations can be successfully done but only if they are backed up by detailed multi-group cell calculations.

This chapter is all about the governing equations for the multi-group model that are the essence of all these calculations.

2.11 The Multi-group Equations

To form the multi-group neutron diffusion equations, we first divide the energy range for the neutrons up into groups as shown in Fig. 2.6.

Thus, we have:

$$\phi_g(\bar{r}, t) \quad \text{for } E \in (E_g, E_{g-1}) \quad \text{where } E_g < E < E_{g-1} \quad (2.28)$$

The multi-group form of the neutron diffusion equation is then given by:

$$\frac{1}{v_g} \frac{\partial}{\partial t} \phi_g(\bar{r}, t) = \underbrace{\nabla \cdot D_g(r) \nabla \phi_g(\bar{r}, t)}_{\text{leakage}} - \underbrace{\sum_{ag}(r) \phi_g(\bar{r}, t)}_{\text{loss by absorption}} - \underbrace{\sum_{sg}(r) \phi_g(\bar{r}, t)}_{\text{removal by scattering}} + \underbrace{\sum_{g'=1}^G \sum_{sg'}(r) \phi_{g'}(\bar{r}, t)}_{\text{scattering into group } g} + \underbrace{\chi_g}_{\text{fraction appearing in group } g} \underbrace{\sum_{g'=1}^G v_{g'} \sum_{fg'}(r) \phi_{g'}(\bar{r}, t)}_{\text{total fission production}} + \underbrace{S_g^{\text{ext}}}_{\text{external source}} \quad (2.29)$$

Note that the neutrons are born with no knowledge of their parents. Thus, we write the total fission production as a sum that is independent of the index g . From there, we split out the fraction, χ_g , that appear in group g .

As we know that the cross sections and flux can vary greatly as a function of neutron energy, E , Fig. 2.7 shows an illustrative five-group approximation. So we will have to use some average flux and cross section that have been averaged over the property in the group energy range in question.

We will see how to do this soon, but for now, we want to concentrate on each of the terms in Eq. 2.20 to make sure you understand what each term represents in a physical sense.

The fission terms are as follows:

$$\underbrace{\sum_{g'=1}^G v_g \sum_{fg'}(r) \phi_{g'}(\bar{r}, t)}_{\text{total fission production}} = \underbrace{v_5 \sum_{f5} \phi_5 + v_4 \sum_{f4} \phi_4}_{\text{thermal fission (about 97\%)}} + \underbrace{v_3 \sum_{f3} \phi_3 + v_2 \sum_{f2} \phi_2 + v_1 \sum_{f1} \phi_1}_{\text{fast fission (about 3\%)}} \quad (2.30)$$

Fig. 2.6 Neutron energy group numbering schema

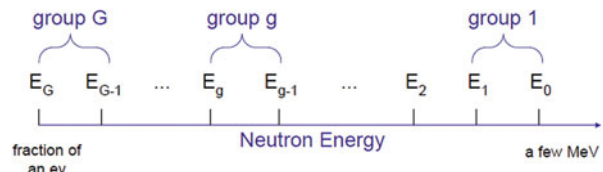


Fig. 2.7 Illustrative flux and cross-sectional variation with energy

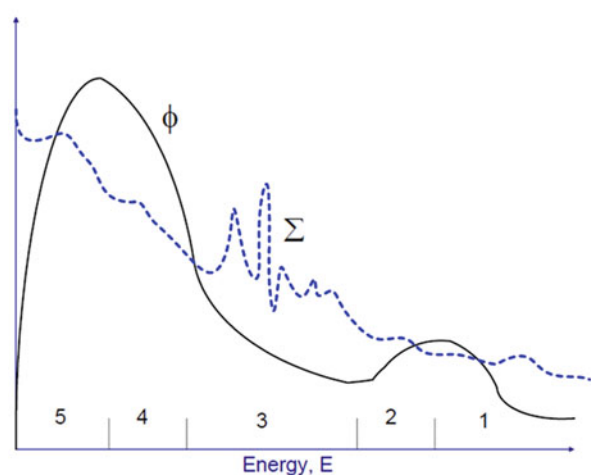
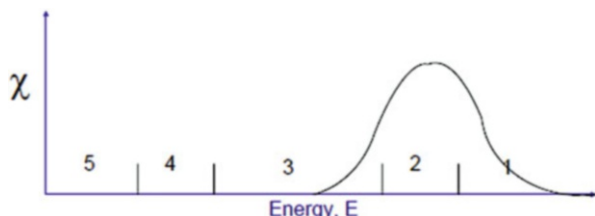


Fig. 2.8 Fission neutron energy spectrum



These fission neutrons, arising mostly from the fissions that are induced by thermal neutrons, have energies in the MeV range, for the most part. Figure 2.8 illustrates this.

So, for the illustrated five-group examples, $\chi_5 = \chi_4 = 0$ and the other χ s are non-zero. So, for the thermal groups (i.e., groups 5 and 4), there are no fission source neutrons. The summation term contains contributions from all five fission terms, but the biggest contributors are from the thermal group. This sum of fission neutrons will only show up as sources for groups 1, 2, and 3.

Now would be a good time to look back at the governing equations and write them out for the five-group cases. It is important that you get it right.

Now, let us look at the scattering terms. These are new. They add complexity, but, taken step-by-step, they are not that hard to understand. In previous chapters, which assumed monoenergetic neutrons, we did not have to consider the loss and gain of neutrons by the scattering process because when a scattering event occurs, the neutron is simply deflected. It is not absorbed; hence there is no gain or loss of neutrons *in total* because of scattering. However, now that we have subdivided the neutrons up into groups, the scattered neutrons emerge from the scattering process at some energy different, in all likelihood, from the incident energy.

The scattering removal term in Eq. 2.29 is straightforward. It says that all the neutrons in group g scatter to some other energy and, so, disappear from the g^{th} neutron balance equation. Some of the scattered neutrons will emerge with a new energy that is within the range of the energies represented by group g . Therefore, we have to add those back in. We will do that via the scattering in term, discussed next and that is as follows.

The scattering in term is given as:

$$\sum_{g'=1}^G \sum_{sg'g} (r) \phi_{g'}(\bar{r}, t) = \sum_{s1g} \phi_1 + \sum_{s2g} \phi_2 + \sum_{s3g} \phi_3 + \sum_{s4g} \phi_4 + \sum_{s5g} \phi_5 \quad (2.31)$$

that is, neutrons are scattered into group g from all the five groups. Note that we have a term representing scattering from group g to group g , i.e., the ones that stay in the group even after scatter. This effectively adds back in the neutrons that were erroneously subtracted by the scattering removal term of the previous paragraph. Figure 2.9 illustrates the process.

Of course, the total scattering out of group 3 is just the sum total of all the scattering out processes, i.e.:

$$\begin{aligned} \sum_{s3} \phi_3 &= \sum_{s31} \phi_3 + \sum_{s32} \phi_3 + \sum_{s33} \phi_3 + \sum_{s34} \phi_3 + \sum_{s35} \phi_3 \\ &= \left(\sum_{g'=1}^G \sum_{s3g'} (r) \right) \phi_3(\bar{r}, t) \end{aligned} \quad (2.32)$$

Fig. 2.9 Scattering into group [3]

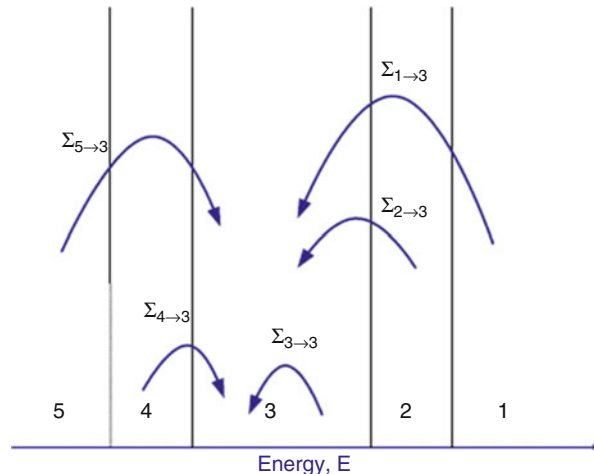
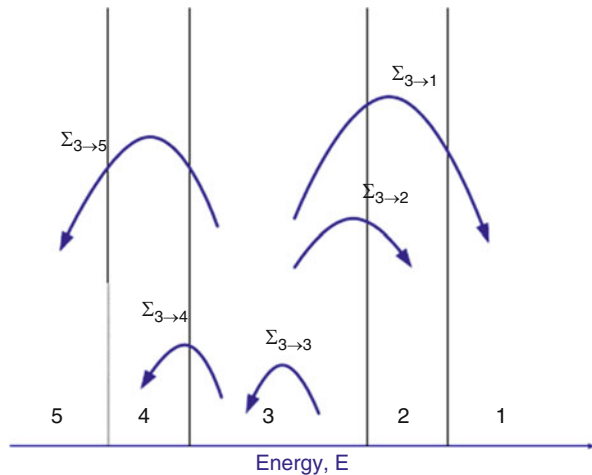


Fig. 2.10 Scattering out of group [3]



Or for the general group g , we can write:

$$\sum_{sg} \phi_g = \sum_{sg1} \phi_g + \sum_{sg2} \phi_g + \sum_{sg3} \phi_g + \sum_{sg4} \phi_g + \sum_{sg5} \phi_g \\ = \left(\sum_{g'=1}^G \sum_{sgg'}(r) \right) \phi_g(\bar{r}, t) \quad (2.33)$$

This is illustrated in Fig. 2.10 as:

Now we can plug Eqs. 2.31 and 2.33 into Eq. 2.29, using group 3 as an example to obtain the following relationship as:

$$\frac{1}{v_3} \frac{\partial}{\partial t} \phi_3(\bar{r}, t) = \underbrace{\nabla \cdot D_3(r) \nabla \phi_3(\bar{r}, t)}_{\text{leakage}} - \underbrace{\sum_{a3}(r) \phi_3(\bar{r}, t)}_{\text{loss by absorption}} \\ - \underbrace{\sum_{s31}(r) \phi_3(\bar{r}, t) + \sum_{s32}(r) \phi_3(\bar{r}, t) + \underbrace{\sum_{s33}(r) \phi_3(\bar{r}, t)}_{\text{scattering out}}}_{\text{scattering out}} \\ + \underbrace{\sum_{s13}(r) \phi_1(\bar{r}, t) + \sum_{s23}(r) \phi_2(\bar{r}, t) + \underbrace{\sum_{s33}(r) \phi_3(\bar{r}, t)}_{\text{scattering in}}}_{\text{scattering in}} \\ + \underbrace{\chi_3 \sum_{g'=1}^G v_{g'} \sum_{f_{g'}}(r) \phi_{g'}(\bar{r}, t)}_{\text{fraction appearing in group 3}} + \underbrace{S_3^{\text{ext}}}_{\text{external source}} \quad (2.34)$$

Notice how the “in-group” scattering terms cancel.

Just to confuse matter a bit more, the *removal cross section* is often used. It is defined as for group 3:

$$\begin{aligned}
 \sum_{r3} &\equiv \sum_{a3} + \sum_{s3} - \sum_{s33} \\
 &= \sum_{a3} + \sum_{s31} + \sum_{s32} + \sum_{s34} + \sum_{s35} \\
 &= \sum_{a3} + \sum_{g'=1}^G \sum_{sg'g}(r) \\
 &\quad g' \neq 3
 \end{aligned} \tag{2.35}$$

i.e., it is the net removal of neutron from group 3 by scattering and absorption. If we use this definition, the governing equation becomes:

$$\begin{aligned}
 \frac{1}{v_g} \frac{\partial}{\partial t} \phi_g(\bar{r}, t) &= \underbrace{\nabla \cdot D_g(r) \nabla \phi_g(\bar{r}, t)}_{\text{leakage}} - \underbrace{\sum_{rg}(r) \phi_g(\bar{r}, t)}_{\text{removal}} - \underbrace{\sum_{sgg}(r) \phi_g(\bar{r}, t)}_{\text{in-group scattering}} \\
 &+ \underbrace{\sum_{g'=1}^G \sum_{sg'g}(r) \phi_{g'}(\bar{r}, t)}_{\text{scattering into group } g} + \underbrace{\chi_g \sum_{g'=1}^G v_{g'} \sum_{fg'g}(\bar{r}) \phi_{g'}(\bar{r}, t)}_{\text{fraction appearing in group } g} \\
 &+ \underbrace{S_g^{\text{ext}}}_{\text{external source}} \quad g = 1, 2, \dots, G
 \end{aligned} \tag{2.36}$$

or, more simply:

$$\begin{aligned}
 \frac{1}{v_g} \frac{\partial}{\partial t} \phi_g(\bar{r}, t) &= \underbrace{\nabla \cdot D_g(r) \nabla \phi_g(\bar{r}, t)}_{\text{leakage}} - \underbrace{\sum_{rg}(r) \phi_g(\bar{r}, t)}_{\text{removal}} - \underbrace{\sum_{sgg}(r) \phi_g(\bar{r}, t)}_{\text{in-group scattering}} \\
 &+ \underbrace{\sum_{\substack{g'=1 \\ g' \neq 3}}^G \sum_{sg'g}(r) \phi_{g'}(\bar{r}, t)}_{\text{net scattering into group } g} + \underbrace{\chi_g \sum_{g'=1}^G v_{g'} \sum_{fg'g}(\bar{r}) \phi_{g'}(\bar{r}, t)}_{\text{fraction appearing in group } g} \\
 &+ \underbrace{S_g^{\text{ext}}}_{\text{external source}}
 \end{aligned} \tag{2.37}$$

Maybe the use of the removal form is unnecessary and bit confusing, and some folks like to use and remember just the relationship in Eq. 2.29. Everything else discussed above flows readily from that equation. There is no need to memorize any of this. If you take the time to visualize the processes that are occurring, then you should be able to state Eq. 2.29 as you go through the accounting of the sinks and sources of neutrons. *Try it! Do not be afraid to spend some time making sure that you have it clear in your mind. It is a milestone concept in reactor physics, and the subject won't make sense unless you grasp it.*

2.12 Generating the Coefficients

The raw cross-sectional data is available in libraries like ENDF/B in the public domain. This data gives the experimental values as a function of energy in far too much detail for our multi-group model. We need to come up with good estimates of the group-averaged cross sections. To do that we step back and use the more general form of the neutron diffusion equation, one that has energy represented as a continuum, rather than as discrete bins:

$$\frac{1}{v} \frac{\partial \phi}{\partial t} = \underbrace{\nabla \cdot D(r) \nabla \phi}_{\text{leakage}} - \underbrace{\sum_a(r) \phi}_{\text{loss by absorption}} - \underbrace{\sum_s(r) \phi}_{\text{removal by scattering}} + \underbrace{\int_0^\infty \sum_s(E' \rightarrow E) \phi(r, E', t) dE'}_{\text{scattering into } E \rightarrow E + dE \text{ range}} \\ + \underbrace{\chi(E)}_{\substack{\text{fraction} \\ \text{appearing} \\ E \rightarrow E + dE \\ \text{range}}} \underbrace{\int_0^\infty v(E') \sum_f(E') \phi(\bar{r}, E', t) dE'}_{\text{total fission production}} + \underbrace{S^{\text{ext}}}_{\text{external source}} \quad (2.38)$$

Note that $\phi = \phi(\bar{r}, E', t)$.

The term $\sum_s(E' \rightarrow E) dE'$ is the cross section for neutrons at energy E' scattering to energy E . Note that $\sum_s(E' \rightarrow E) dE'$ has units of cm^{-1} so $\sum_s(E' \rightarrow E)$ as units of $\text{cm}^{-1} \text{ ev}^{-1}$.

We define the group flux as:

$$\phi_g(\bar{r}, t) \equiv \int_{E_g}^{E_{g-1}} \phi(\bar{r}, E, t) dE \quad (2.39)$$

This prompts us to perform the same integral for each term of Eq. 2.38 and to equate what we get to Eq. 2.29 to generate a rigorous definition of the group-averaged cross sections. Thus Eq. 2.38 becomes, term by term:

$$\frac{\partial}{\partial t} \left(\int_{E_g}^{E_{g-1}} \frac{1}{v(E)} \phi(\bar{r}, E, t) dE \right) \equiv \frac{\partial}{\partial t} \left(\frac{\phi_g}{v_g} \right) = \frac{1}{v_g} \frac{\partial \phi_g}{\partial t} \quad (2.40)$$

$$\text{where: } \frac{1}{v_g} \equiv \frac{\int_{E_g}^{E_{g-1}} \frac{1}{v(E)} \phi(\bar{r}, E, t) dE}{\int_{E_g}^{E_{g-1}} \phi(\bar{r}, E, t) dE}$$

Notice how the coefficient, $1/v_g$, is determined simply as the flux-weighted integral over the group energy range. As we go through the integral term by term, we will see the same pattern.

Now for the diffusion coefficient:

$$\nabla \cdot \left(\int_{E_g}^{E_{g-1}} D(E) \nabla \phi(\bar{r}, E, t) dE \right) \equiv \nabla \cdot D_g \nabla \phi_g \quad (2.41)$$

$$\text{i.e.: } D_g \equiv \frac{\int_{E_g}^{E_{g-1}} D(E) \nabla \phi(\bar{r}, E, t) dE}{\int_{E_g}^{E_{g-1}} \nabla \phi(\bar{r}, E, t) dE}$$

This time, the weighting is $\nabla \phi(\bar{r}, E, t)$ since that is how the flux factor appears in the term.

The absorption term is just:

$$\int_{E_g}^{E_{g-1}} \sum_a(E) \phi(\bar{r}, E, t) dE \equiv \sum_{ag} \phi_g \quad (2.42)$$

$$\text{i.e.: } \sum_{ag} \equiv \frac{\int_{E_g}^{E_{g-1}} \sum_a(E) \phi(\bar{r}, E, t) dE}{\int_{E_g}^{E_{g-1}} \phi(\bar{r}, E, t) dE}$$

The scattering removal term is similar.

The scattering down term is a bit messier:

$$\begin{aligned} \int_{E_g}^{E_{g-1}} \left(\int_0^\infty \sum_s (E' \rightarrow E) \phi(\bar{r}, E', t) dE' \right) dE &= \int_{E_g}^{E_{g-1}} \left(\sum_{g'=1}^G \int_{E_{g'}}^{E_{g'-1}} \sum_s (E' \rightarrow E) \phi(\bar{r}, E', t) dE' \right) dE \\ &= \sum_{g'=1}^G \int_{E_g}^{E_{g-1}} \left(\int_{E_{g'}}^{E_{g'-1}} \sum_s (E' \rightarrow E) \phi(\bar{r}, E', t) dE' \right) dE \\ &\equiv \sum_{g'=1}^G \sum_{sg'} \phi_{g'} \end{aligned} \quad (2.43)$$

So we have:

$$\sum_{sg'g} = \frac{1}{\phi_{g'}} \int_{E_g}^{E_{g-1}} \left(\int_{E_{g'}}^{E_{g-1}} \sum_s (E' \rightarrow E) \phi(\bar{r}, E', t) dE' \right) dE \quad (2.44)$$

The fission term is:

$$\begin{aligned} \int_{E_g}^{E_{g-1}} \chi(E) \int_0^\infty v(E') \sum_f (E') \phi(\bar{r}, E', t) dE' dE &= \int_{E_g}^{E_{g-1}} \chi(E) dE \int_0^\infty v(E') \sum_f (E') \phi(\bar{r}, E', t) dE' \\ &= \chi_g \int_0^\infty v(E') \sum_f (E') \phi(\bar{r}, E', t) dE' \\ &= \chi_g \sum_{g'=1}^G \int_{E_g}^{E_{g-1}} v(E') \sum_f (E') \phi(\bar{r}, E', t) dE' \\ &= \chi_g \sum_{g'=1}^G v_{g'} \sum_{f g'} \phi_{g'} \end{aligned} \quad (2.45)$$

where: $\chi_g \equiv \int_{E_g}^{E_{g-1}} \chi(E) dE$

Dropping the summation, we finally arrive at:

$$\begin{aligned} v_{g'} \sum_{f g'} &\equiv \frac{1}{\phi_{g'}} \int_{E_g}^{E_{g-1}} v(E') \sum_f (E') \phi(\bar{r}, E', t) dE' \\ \chi_g &\equiv \int_{E_g}^{E_{g-1}} \chi(E) dE \end{aligned} \quad (2.46)$$

The accuracy of the multi-group model depends very much on the group constants chosen.

Note that the constants depend on ϕ which depends on the constants. This is a circular argument. To compensate, the typical practice is to follow a scheme as outlined in Fig. 2.11.

A fine energy structure (many groups, perhaps of the order of 100 or more) is assumed by taking the flux as Maxwellian in the thermal range and $1/E$ in the midrange and a fission spectrum for the high end. A coarse spatial grid is assumed, or a small representative region is chosen (usually a representative cell). The multi-group equations can then be solved numerically (high G , small number of spatial mesh points). This yields ϕ_g for the cell, $g = 1, 100$ (say). This flux can be used to calculate weighted cross sections and other constants for a coarse energy structure, perhaps $G=5$ or so. Now, with a manageable number of neutron equations per spatial mesh point, the whole core (or a typical cell) can numerically be solved with a large number of spatial mesh points, giving good spatial detail, albeit with a coarse energy resolution. Once these calculations are done, there is the possibility that a re-weighting of the group constants might have to be done to account for flux-dependent effects like Xe, burnup, temperature, control rod position, etc. Therefore, iteration might be required.

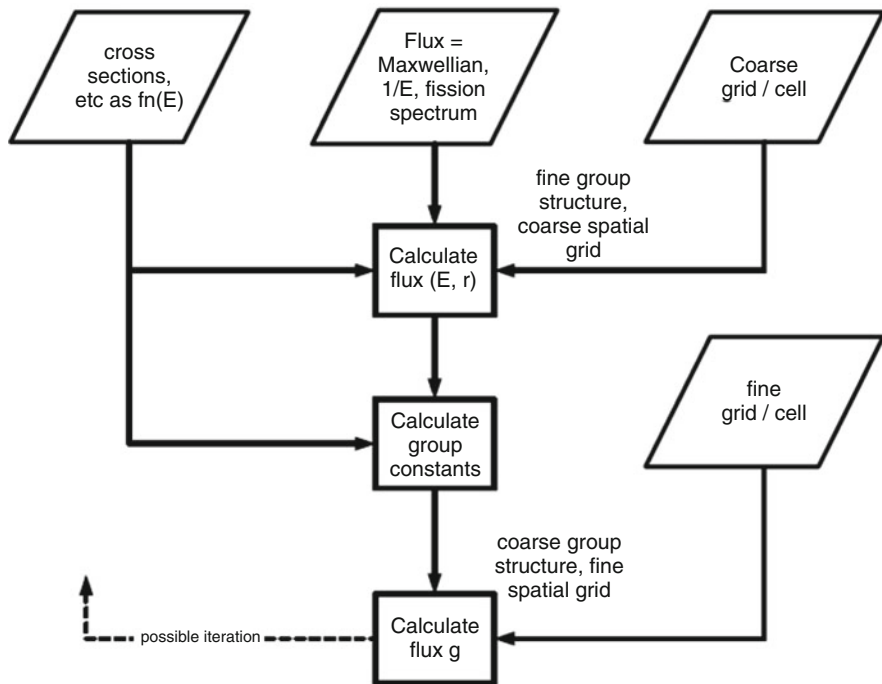


Fig. 2.11 Typical calculation schema

We could use the same basic equation (i.e., Eq. 2.29) for both the fine energy calculation and the fine spatial mesh calculation. The more typical route, however, is to not use diffusion-based calculation for the fine energy mesh/cell calculation because diffusion theory is not accurate near interfaces that involve large changes in cross sections (like water/control rod interfaces, for instance). Rather, a transport-based code such as *WIMS* [3] is used (i.e., *VIMS* is a general purpose reactor physics program for core physics calculations). The fine spatial mesh/core calculations typically do use the diffusion approximation propped up by the group-averaged coefficients based on transport calculations. Herein, we will assume that the proper flux-weighted coefficients have been found, and we explore some simplifications and criticality calculations.

2.13 Simplifications

Most neutrons lose energy when they scatter. Only the low energy thermal neutrons experience any significant upscatter (that is what the Maxwellian is all about, after all). Therefore, it is a reasonable approximation to assume that all groups do not

upscatter if the thermal breakpoint is kept above ~ 1 eV. That will keep the thermal upscatter restricted to itself. Thus:

$$\sum_{sg'g} (r) \approx 0 \quad \text{for } g' > g \quad \textbf{No up-stream assumption}$$

This simplifies the group in-scattering term:

$$\underbrace{\sum_{g'=1}^G \sum_{sg'g} (r) \phi_{g'}(\bar{r}, t)}_{\text{scattering into group } g} \rightarrow \sum_{g'=1}^{g-1} \sum_{sg'g} (r) \phi_{g'}(\bar{r}, t) + \underbrace{\sum_{sgg} (r) \phi_g(\bar{r}, t)}_{\substack{\text{can lump this into} \\ \text{the removal term}}} \quad (2.47)$$

We can also sometimes assume that scattering down is to the next lowest group only, i.e., no groups are skipped when scattering down. Thus:

$$\underbrace{\sum_{g'=1}^G \sum_{sg'g} (r) \phi_{g'}(\bar{r}, t)}_{\text{scattering into group } g} \rightarrow \sum_{sg_{-1}g} (r) \phi_{g-1}(\bar{r}, t) + \sum_{sgg} (r) \phi_g(\bar{r}, t) \quad (2.48)$$

This is called “directly coupled.”

Consider that in a scattering event:

$$E_f = \alpha E_i \quad \text{where} \quad \alpha \equiv \left(\frac{A-1}{A+1} \right)^2 \quad (2.49)$$

Therefore, if we maintain a group separation such that:

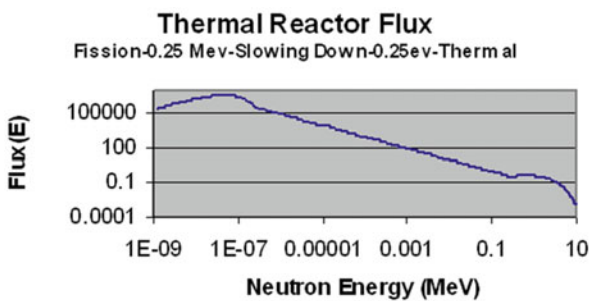
$$\frac{E_g}{E_{g-1}} \leq \alpha \quad (2.50)$$

then the scattered neutron cannot have a final energy that is below the next group down. For hydrogen, which has $A=1$, there is a problem because $\alpha=0$. But it can be shown that, even then, the error is $<1\%$ if $E_g/E_{g-1} < 1/150$.

2.14 Nuclear Criticality Concepts

A nuclear reactor works on the principle of a chain reaction. An initial neutron is absorbed by a fissile nuclide and during the process of fission; additional neutrons are released to replace the neutron that was consumed. If more neutrons are produced than are consumed, then the neutron population grows. If fewer neutrons are

Fig. 2.12 LWR neutron flux spectrum



produced than are consumed, the neutron population shrinks. The number of fissions caused by the neutron population determines the energy released.

In order to quantify this concept, let us define a multiplication factor k . We will define k as the ratio of the production to consumption of neutrons.

$$k = \text{Multiplication Factor} = \frac{\text{Production}}{\text{Consumption}} \quad (2.51)$$

Now both production and consumption are reaction rates. Reaction rates are products of neutron fluxes and nuclide cross sections. And since the neutrons are produced at high energies (~ 2 MeV) and are consumed at thermal energies (~ 0.05 eV) at least in light water reactors (LWRs), it is important to integrate these reaction rates over all energies. Consider the neutron flux spectrum in a typical LWR, as plotted in Fig. 2.12 here.

It is basically composed of three main functions. At the high end, it looks like a fission spectrum; in the intermediate range (0.25 MeV to 0.25 eV), it looks like a $1/E$ spectrum; and in the thermal range, it looks like a Maxwellian. Since cross sections also vary significantly as a function of energy, the true production and destruction rates must be integrals over energy. In real reactors, some neutrons are destroyed by absorption in the fuel, moderator, and structure, and some leak out. All of these processes depend on the energy distribution of the neutrons within the reactor.

2.15 Criticality Calculation

The criticality calculation follows the same itinerary as the one-speed neutron case except that we now have to sweep through the energy groups as well as through space. The basic steady-state equation to solve is (assuming no upscatter):

$$\begin{aligned}
& -\nabla \cdot D_g(r) \nabla \phi_g(\bar{r}, t) + \underbrace{\sum_{rg}(r) \phi_g(\bar{r}, t)}_{\text{removal}} - \sum_{g'=1}^G \sum_{sg'g} (r) \phi_{g'}(\bar{r}, t) \\
& = \frac{1}{k} \chi_g \sum_{g'=1, g' \neq g}^G v_{g'} \sum_{fg'}(\mathbf{r}) \phi_{g'}(\bar{r}, t)
\end{aligned} \tag{2.52}$$

Note that $\sum_{rg} = \sum_{tg} - \sum_{sg'g} = \sum_{ag} + \sum_{sg} - \sum_{sg'g}$. We can write this in a matrix form:

$$M\phi = \frac{1}{k} F\phi \tag{2.53}$$

where:

$$\underline{\underline{M}} = \begin{pmatrix} -\nabla \cdot D_1 \nabla + \sum_{r1} & 0 & 0 \\ -\sum_{s12} & -\nabla \cdot D_2 \nabla + \sum_{r2} & 0 \\ -\sum_{s13} & & -\nabla \cdot D_3 \nabla + \sum_{r3} \\ \vdots & \vdots & \vdots \end{pmatrix} \tag{2.54}$$

$$\underline{\phi} = \begin{bmatrix} \phi_1 \\ \phi_2 \\ \phi_3 \\ \vdots \end{bmatrix} \tag{2.55}$$

$$\underline{\underline{F}} = \begin{pmatrix} \chi_1 v_1 \sum_{f1} & \chi_1 v_2 \sum_{f2} & \chi_1 v_3 \sum_{f3} & \cdots \\ \chi_2 v_1 \sum_{f1} & \chi_2 v_2 \sum_{f12} & \chi_2 v_3 \sum_{f3} & \cdots \\ \chi_3 v_1 \sum_{f1} & \chi_3 v_2 \sum_{f2} & \chi_3 v_2 \sum_{f2} & \cdots \\ \vdots & \vdots & \vdots & \end{pmatrix} \tag{2.56}$$

Please note that the span is over the groups, *not* space. Imbedded in the diffusion term is the space mesh. Two-dimensional papers cannot do justice to the complexity of the structure in matrix form. With the assumption of no upscatter, the M matrix is lower triangular. If we further assume that the neutrons are directly coupled, M would be two-striped, i.e.:

$$M = \underbrace{\begin{pmatrix} X & & & \\ X & X & & \\ X & X & X & \\ X & X & X & X \end{pmatrix}}_{\text{no up-scatter}} = \underbrace{\begin{pmatrix} X & & & \\ X & X & & \\ X & X & X & \\ X & X & X & X \end{pmatrix}}_{\text{directly coupled}} \quad (2.57)$$

Solution, numerically, proceeds are for the one-speed case. The right-hand side (RHS) of Eq. 2.53 is evaluated from a guess at the flux in space and energy. The RHS is the source term. The flux is found using Gauss-Seidel or SOR to complete the inner iteration for the first iteration. Typically, the spatial grid is swept sequentially, starting with the equation for group 1, then 2, ...G since the faster neutrons are essentially the source terms for the slower neutrons, but we suspect that it really does not matter what order the equations are swept.

Next, the source terms and k are updated, and the iteration is repeated until both k and the flux have converged. It is a straightforward procedure, just be careful to properly account for all the scattering terms.

2.16 The Multiplication Factor and a Formal Calculation of Criticality

We are now at the point that we need to pay some attention to the calculation of k or four-factor formula that allows the analysis of the multiplication factor for pile of uranium that are possibly used in a nuclear reactor. In order to hold the core of reactor together, we probably need to add some coolant to remove fission-produced heat and maybe some structural materials as well. We also need to define *multiplication factor* k that characterized the chain reaction in reactor core as:

$$k \equiv \text{Multiplication Factor} \equiv \frac{\text{Number of neutron in one generation}}{\text{Number of neutron in preceding generation}}$$

A simple chain reaction also can schematically depicted in Fig. 2.13.

Using definition of multiplication factor k above, then we can declare the chain reaction is time-independent, if $k=1$, where the number of neutrons in any two consecutive fission generations is the same and at this point the reactor is in critical mode. By the same talking if $k<1$, then the reactor is in subcritical condition, and similarly if $k>1$ the core is under supercritical operating mode.

In summary reactor core can operate under three following conditions:

$$\begin{aligned} k > 1 & \text{ Subcritical} \\ k = 1 & \text{ Critical} \\ k < 1 & \text{ Supercritical} \end{aligned}$$

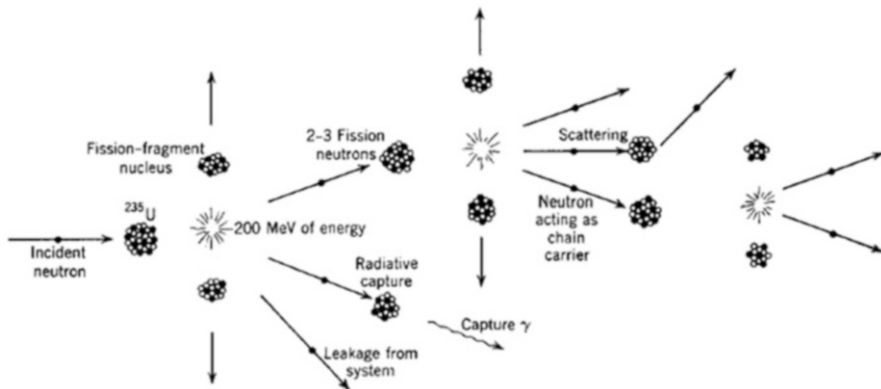


Fig. 2.13 A simple schematic of fission chain reaction for ^{235}U . (Courtesy of Duderstadt and Hamilton [4])

For purpose of reactor design, all the chosen materials and related subsystem within core (i.e., fuel rods) should be considered as part of criticality analysis, so we can meet our primary objective of reactor design, which is having a reactor that can be in critical mode. Sometime we need reiterate our analysis and material that reactor finally goes critical as part of design and criticality condition is met, where $k=1$.

Note that sometime the multiplication factor k in terms of successive fission neutron generation is called and known as *life cycle*. Also bear in your mind that in process of a chain reaction, some neutrons may not induce fission reactions at all but instead absorbed in a nonproductive capture or leak out of the core system; under these conditions we can somewhat have a better definition for multiplication factor k in order to have a neutron balance, as follows:

$$k \equiv \text{Multiplication Factor} \equiv \frac{\text{Rate of neutron production in reactor}}{\text{Rate of neutron loss or absorption plus capture in reactor}}$$

The above definition is explicitly indicating that the production and loss rate are functions of time due to fuel consumption and they may vary accordingly [4].

We can also at this stage define the neutron lifetime l which is as follows:

$$l \equiv \frac{N(t)}{L(t)} \quad (2.58)$$

where $N(t)$ is the total neutron population or the number of neutron count and $L(t)$ is loss rate in reactor at time t . And in order to have a better understanding of $N(t)$ in a nuclear reactor at a time t , we can take under consideration a simple *kinetics of chain reactions*, using the following analysis as:

$$\frac{dN(t)}{dt} = \text{Production Rate} - \text{Loss Rate} = P(t) - L(t) \quad (2.59)$$

By the definition of multiplication factor k for balancing neutron, Eq. 2.59 further can be expanded to the following form of Eq. 2.60 as:

$$\frac{dN(t)}{dt} = \left[\frac{P(t)}{L(t)} - 1 \right] L(t) = (k - 1)L(t) \quad (2.60)$$

To proceed further, we can write:

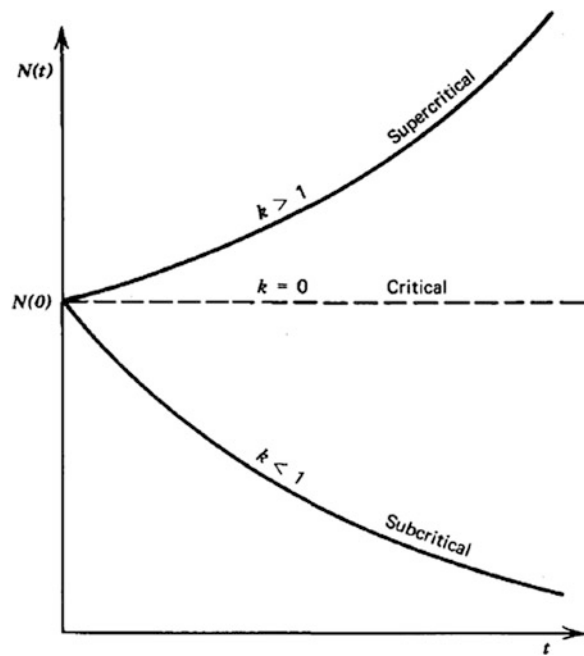
$$\frac{dN(t)}{dt} = \frac{(k - 1)}{l} N(t) \quad (2.61)$$

If we set initial condition for the above ordinary differential Eq. 2.61 that there are N_0 neutrons in the reactor at time $t = 0$ and assuming that both k and l are time-independent and in general they are not, we write a solution for Eq. 2.61 as:

$$N(t) = N_0 \exp \left[\left(\frac{k-1}{l} \right) t \right] \quad (2.62)$$

The above simple approach to model a nuclear reactor kinetic agrees with reactor criticality in terms of k and depicted in Fig. 2.14 below as well.

Fig. 2.14 Time behavior of the neutrons in a reactor



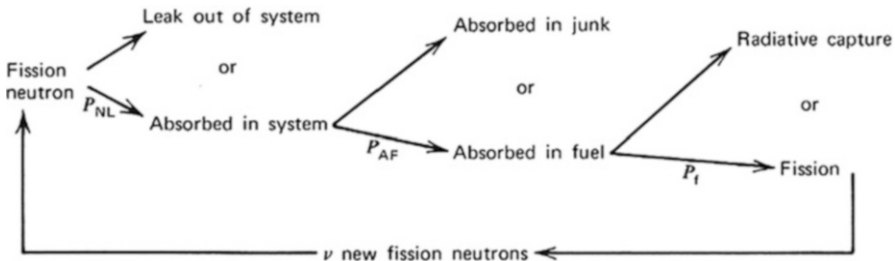


Fig. 2.15 Schematic of new fission neutron generation and possible event sequence. (Courtesy of Duderstadt and Hamilton [4])

Note that the power level of a nuclear reactor is proportional to its neutron population; therefore, we are in position to regard the time behavior of the reactor power level as an exponential with a time constant or *reactor period* T given by:

$$T = \frac{l}{k - 1} \quad (2.63)$$

Analyzing Eq. 2.63, we can observe if $k \rightarrow$, then $T \rightarrow \infty$, which corresponds to a time-independent neutron population or react power level and is in agreement with our previous arguments above. However, if we want to expand our simple kinetic model, then we need to study the subject of nuclear reactor kinetic analysis which is beyond the scope of this book.

Before, we continue with our analysis to calculate k ; we need to investigate what is going with the neutrons in a given fission reaction or generation. Such fission neutron and probabilities for each of these possible events such as leak out of the reactor, and be lost to the chain reaction and eventually absorbed that might be due to nonproductive capture event in either fuel or other materials can be depicted as shown in Fig. 2.15.

To make it more formal, we define the probabilities for each of these possible events presented by Fig. 2.15 as follows: [4]

$P_{NL} \equiv$ Probability that neutron will not leak out of system before absorption

$P_{AF} \equiv$ Conditional probability that *if* neutron is absorbed, it will be absorbed in the fuel

$P_f \equiv$ Conditional probability that *if* neutron is absorbed in fuel, it will induce a fission reaction

We can easily calculate the last two probability conditions, and the conditional probability for absorption in the fuel P_{AF} can be expressed as the ratio of the macroscopic absorption cross section for the fuel \sum_a^F and for the fuel plus the rest of the material in the core Σ_a [4].

Note that in Chap. 1 we defined the general form of macroscopic cross section as Σ . However, here we show the superscript to refer to material which we are concerned with (i.e., fuel), and absence of the superscript will indicate that the macroscopic cross section is the total for all of the material in system and we use symbol of Σ_t ; thus, for probability of absorption, we can write:

$$P_{AF} = \frac{\sum_a^F}{\sum_a} \quad (2.64)$$

Equation 2.64 holds only for the situation where the reactor has a uniform composition. Although in reality most of the reactor design engineers encounter non-uniform compositions with modern reactor analysis, which varies from point to point due to fuel elements, coolant channels, support structure, etc., usage of macroscopic cross sections is shown as symbol Σ_a in respect to spatial average over all the reactor in more general case. Considering that we need to evaluate neutron energy at which these cross sections are under consideration, Eq. 2.55 is valid for appropriately averaged over energy, just as they are over space.

It is a common knowledge that the probability of absorption to be called as *thermal utilization factor* of reactor denotes it by f as below and will be discussed further in Sect. 2.23:

$$P_{AF} \equiv f \quad (2.65)$$

The term in Eq. 2.65 historically comes from early analysis of thermal reactors in which essentially all fissions in the fuel were induced by thermal neutrons. Under these circumstances, the cross sections in f would be evaluated at thermal neutron energies and would represent the effectiveness of the fuel in competing with other materials in the reactor. For the absorption of thermal neutrons, that is, the effectiveness with which the reactor utilized the thermal neutrons in the fuel and Eq. 2.64 usually holds for any type of reactor [4].

Now, we are getting back to our definition above, about conditional probability for inducing a fission reaction in the fuel. Thus, we can express it in terms of cross sections, which in that case we simply take the ratio of the fission cross section to that of the absorption cross section due to both fission and radiative capture in the fuel material as:

$$P_f = \frac{\sum_f^F}{\sum_a^F} = \frac{\sigma_f^F}{\sigma_a^F} \quad (2.66)$$

Now we are at the stage where we can utilize all these probabilities in order to determine the multiplication factor k defined above in order to follow the neutrons.

We start with N_1 neutrons present in the reactor in a given fission generation process; then using Eq. 2.66 along with Fig. 2.15, we can compute the number of neutrons N_2 in the next step generation as:

$$N_2 = vP_f P_{AF} P_{NL} N_1 \quad (2.67)$$

So if we substitute both Eqs. 2.65 and 2.66 into Eq. 2.67 and use the definition of number of fission neutrons produced per absorption in the fuel as $\eta = v(\sigma_t^F / \sigma_a^F)$, then we get:

$$N_2 = \eta f P_{NL} N_1 \quad (2.68)$$

Note that η is also known as reproduction factor and most of the neutron absorbed in the fuel causes fission, but some do not. The reproduction factor η is defined as the ratio of the number of fast neutrons produced by thermal fission to the number of thermal neutrons absorbed in the fuel. The reproduction factor is shown below as:

$$\eta = \frac{\text{number of fast neutrons produced by thermal fission}}{\text{number of thermal neutrons absorbed in the fuel}}$$

The reproduction factor can also be stated as ratio of rated as shown below as well:

$$\eta = \frac{\text{rate of production of fast neutrons by thermal fission}}{\text{rate of absorption of thermal neutrons by the fuel}}$$

The rate of production of fast neutrons by thermal fission can be determined by the product of the fission reaction rate ($\sum_f^u \phi^u$) and the average number of neutrons produced per fission (n). The average number of neutrons released in thermal fission of uranium²³⁵ is 2.42. The rate of absorption of thermal neutrons by the fuel is $\sum_f^u \phi^u$. By substituting these terms into the definition in above results in the following equation as:

$$\eta = \frac{\sum_f^U \phi^U v}{\sum_f^u \phi^u} \quad (2.69)$$

Table 2.2 lists values of v and η for fission of several different materials by thermal neutrons and fast neutrons.

Table 2.2 Average number of neutrons liberated in fission

Fissile nucleus	Thermal neutrons		Fast neutrons	
	v	η	v	η
Uranium-233	2.49	2.29	2.58	2.40
Uranium-235	2.42	2.07	2.51	2.35
Uranium-239	2.93	2.15	3.04	2.90

In the case where the fuel contains several fissionable materials, it is necessary to account for each material. In the case of a reactor core containing both uranium²³⁵ (²³⁵U) and uranium²³⁸ (²³⁸U), the reproduction factor would be calculated as shown below.

$$\eta = \frac{N^{U-235} \sigma_f^{U-235} \nu^{U-235}}{N^{U-235} \sigma_a^{U-235} + N^{U-238} \sigma_a^{U-238}} \quad (2.70)$$

To determine the reproduction factor for a single nuclide rather than for a mixture, the calculation may be further simplified to the one shown below.

$$\eta = v(\sigma_t^F / \sigma_a^F) \quad (2.71)$$

Note that superscript is referring to uranium.

Now again utilizing the definition of multiplication factor k as being the ratio of the number of neutrons in two successive fission generations to write the following as:

$$k = \frac{N_2}{N_1} = \frac{\eta f P_{NL} N_1}{N_1} = \eta f P_{NL} \quad (2.72)$$

In this equation the non-leakage probability P_{NL} characterizing neutron leakage from the core of reactor is very difficult to compare, and it will require more accurate analysis, and further analysis should be in place. However, since no neutrons could leak out, we can immediately come to conclusion that we should set the non-leakage probability $P_{NL}=1$, and therefore, the corresponding multiplication factor is then known as the *infinite medium multiplication factor* and expressed by the following form of equation by substituting this value of P_{NL} in Eq. 2.69.

$$k_\infty = \eta f \quad (2.73)$$

However, we have to bear in mind that no reactor is of infinite size, but k_∞ is a useful parameter in reactor analysis since it characterizes the multiplication properties of the *material* used in reactor as distinct from the *geometry* of the reactor core. Of course since $P_{NL}<1$ more generally for a finite reactor from which some neutron leakage can occur, then we must have $k_\infty>1$ in order to have any chance for critical chain reaction in reactor, which is in agreement with what we expressed previously.

2.17 Fast Fission Factor ϵ Definition

Another definition that we need to know for our further discussion in neutronics analysis *fast fission factor ϵ* as part of the first process that the neutron of one generation may undergo is fast fission. Fast fission is fission caused by neutrons that are in the fast energy range, slowing down to thermal energies. Fast fission results in

the net increase in the fast neutron population of the reactor core. This factor as part of four-factor formula takes into account of the fact that although most fission will be induced in fissile materials by thermal neutrons, some fissions will be induced in both fissile and fissionable materials by fast neutrons and will be related to multiplication factor k as shown in Eq. 2.72. The cross section for fast fission in uranium²³⁵ (²³⁵U) or uranium²³⁸ (²³⁸U) is small; therefore, only a small number of fast neutrons cause fission. The fast neutron population in one generation is therefore increased by a factor called the *fast fission factor*. The fast fission factor (ϵ) is defined as the ratio of the net number of fast neutrons produced by all fissions to the number of fast neutrons produced by thermal fissions. The mathematical expression of this ratio is shown below.

$$\epsilon = \frac{\text{Total number of fission neutrons (from both fast and thermal fission)}}{\text{Number of fission neutrons from thermal fissions}}$$

Furthermore, the above definition can be presented by the following equation as:

$$\epsilon \equiv \frac{\int_{fuel} dV \int_0^\infty v \Sigma_f(\vec{r}, E) dE}{\int_{fuel} dV \int_0^{E_2} v \Sigma_f(\vec{r}, E) \phi_1(\vec{r}, E) dE} \quad (2.74)$$

where $\Phi(\vec{r}, E)$ is flux and will be presented for infinite lattice of cells, where these cells are for given square-shaped fuel rod and its associated moderator and will be the same as that for any other cell. Thus, if we know $\Phi(\vec{r}, E)$ for one cell, we know it for all [5].

Note that, just as, if we know $\Phi(E)$ at one *point* in an infinite homogeneous medium, we know it for all points. The relationship that is given by the fraction in Eq. 2.74 is the definition of fast fission factor ϵ . The above relation is the ratio of the total rate of production of fission neutrons in the lattice to the rate of production due to fission in the thermal energy range, and what is presented in Eq. 2.70 is clear from the definition that ϵ depends directly only on $v^j \sigma_f^j(E) n^j(\vec{r}, E)$ of the various fissionable isotopes contained in the fuel rod [5].

Also in order for a neutron to be absorbed by a fuel nucleus as a fast neutron, it must pass close enough to a fuel nucleus, while it is a fast neutron. The value of ϵ will be affected by the arrangement and concentrations of the fuel and the moderator. The value of ϵ is essentially 1.00 for a homogeneous reactor where the fuel atoms are surrounded by moderator atoms. However, in a heterogeneous reactor, all the fuel atoms are packed closely together in elements such as pins, rods, or pellets. Neutrons emitted from the fission of one fuel atom have a very good chance of passing near another fuel atom before slowing down significantly. The arrangement of the core elements results in a value of about 1.03 for ϵ in most heterogeneous reactors. The value of ϵ is not significantly affected by variables such as temperature, pressure, enrichment, or neutron poison concentrations. Poisons are nonfuel materials that easily absorb neutrons and will be discussed in more detail later.

To further enhance our analysis, we need to introduce a second factor in the next section that will characterize the possibility, where neutron might be absorbed while slowing down from fission to thermal energies.

2.18 Resonance Escape Probability p

After increasing in number as a result of some fast fission, the neutrons continue to diffuse through the reactor. As the neutrons move, they collide with nuclei of fuel and nonfuel material and moderator in the reactor losing part of their energy in each collision and slowing down. While they are slowing down through the resonance region of uranium²³⁸, which extends from about 6 eV to 200 eV, there is a chance that some neutrons will be captured. The probability that a neutron will not be absorbed by a resonance peak is called the resonance escape probability. The *resonance escape probability* (p) is defined as the ratio of the number of neutrons that reach thermal energies to the number of fast neutrons that start to slow down. This ratio is shown below:

$$p = \frac{\text{number of neutron that reach thermal energy}}{\text{number of fast neutrons that start to slow down}}$$

The value of the resonance escape probability is determined largely by the fuel-moderator arrangement and the amount of enrichment of uranium²³⁵ (²³⁵U) (if any is used). To undergo resonance absorption, a neutron must pass close enough to a uranium²³⁸ (²³⁸U) nucleus to be absorbed while slowing down. In a homogeneous reactor, the neutron does its slowing down in the region of the fuel nuclei, and this condition is easily met. This means that a neutron has a high probability of being absorbed by uranium²³⁸ (²³⁸U) while slowing down; therefore, its escape probability is lower. In a heterogeneous reactor, however, the neutron slows down in the moderator where there are no atoms of uranium²³⁸ (²³⁸U) present. Therefore, it has a low probability of undergoing resonance absorption, and its escape probability is higher.

The value of the resonance escape probability is not significantly affected by pressure or poison concentration. In water-moderated, low uranium²³⁵ (²³⁵U) enrichment reactors, raising the temperature of the fuel will raise the resonance absorption in uranium²³⁸ (²³⁸U) due to the Doppler effect (an apparent broadening of the normally narrow resonance peaks due to thermal motion of nuclei). The increase in resonance absorption lowers the resonance escape probability, and the fuel temperature coefficient for resonance escape is negative (explained in detail later). The temperature coefficient of resonance escape probability for the moderator temperature is also negative. As water temperature increases, water density decreases. The decrease in water density allows more resonance energy neutrons to enter the fuel and be absorbed. The value of the resonance escape probability is always slightly less than one (normally 0.95 to 0.99).

The product of the fast fission factor and the resonance escape probability (ϵp) is the ratio of the number of fast neutrons that survive slowing down (thermalization) compared to the number of fast neutrons originally starting the generation.

Finally as a useful step, we modify our definition of the non-leakage probability to take under consideration the fact that there would be two distinct phases of neutron leakage that will require two rather different types of analysis in our later work. First the neutron may leak out while slowing down. In reality the neutron mean free path is relatively large for high energies; such fast neutron leakage may quite slow down to thermal energies. After slowing down, the neutron may continue to scatter and eventually leak out before it has had an opportunity to be absorbed. To take account of these two processes, we will break up our earlier non-leakage probability P_{NL} as follows: [4]

$$P_{NL} = P_{FNL}P_{TNL} \quad (2.75)$$

where P_{FNL} and P_{TNL} are defined below as:

$P_{FNL} \equiv$ Probability that fast neutron will not leak out (fast nonleakage)

$P_{TNL} \equiv$ Probability that thermal neutron will not leak out (thermal nonleakage)

Inserting these two above definitions in Eq. 2.71 along with Eq. 2.72 and Eq. 2.74, we get a new form for infinite medium multiplication factor as follows:

$$k_{\infty} = \eta f p \epsilon \quad (2.76)$$

This equation is known as the *four-factor formula* that is defined as before in Sect. 2.16 of this book, and furthermore one can write multiplication factor k of Eq. 2.69 in the following form:

$$k = \eta f p \epsilon P_{FNL} P_{TNL} \quad (2.77)$$

which, this form of Eq. 2.77, is surprisingly known as the *six-factor formula*.

Note that one can vary the non-leakage probability P_{NL} by changing the geometry of larger reactor or changing the materials surrounding the reactor with larger scattering cross section so that some of the neutrons leaking out will scatter back into the reactor [4].

As matter of fact, when leakage is changed, there will be some changes in the parameters that consists of four-factor formula as well since these are actually averages over the various neutron energies in the reactor and this cause distribution of energies to vary with the amount of leakage. Thus, such consideration deduces somewhat different notation for multiplication factor characterizing a finite system

which is occasionally referred to as the *effective multiplication factor* and denoted by k_{eff} and written as:

$$k_{eff} = k_\infty P_{FNL} P_{TNL} \quad (2.78)$$

More details and mathematical analysis can be found in Henry [5], and we encourage the reader to refer to that book.

2.19 Group Collapsing

Herein we will collapse the multi-group equations to one group just to show that the two forms are consistent with each other. Then we will look at the two-group approximation because it is commonly used and it is illustrative without being overly complex.

2.19.1 Multi-group Collapsing to One Group

We have the general multi-group equation as:

$$\begin{aligned} \frac{1}{v_g} \frac{\partial}{\partial t} \phi_g &= \nabla \cdot D_g \nabla \phi_g - \sum_{ag} \phi_g - \sum_{sg} \phi_g + \sum_{g'=1}^G \sum_{sg'} \phi_{g'} \\ &+ \chi_g \sum_{g'=1}^G v_{g'} \sum_{fg'} \phi_{g'} + S_g^{ext} \end{aligned} \quad (2.79)$$

And we have the definitions of the coefficients as well in the form of:

$$\phi_g(\vec{r}, t) \equiv \int_{E_g}^{E_{g-1}} \phi(\vec{r}, E, t) dE \Rightarrow \phi(\vec{r}, t) \equiv \int_0^\infty \phi(\vec{r}, E, t) dE \quad (2.80)$$

But in one group, we can write:

$$\frac{1}{v_g} \equiv \frac{\int_{E_g}^{E_{g-1}} \frac{1}{v(E)} \phi(\vec{r}, E, t) dE}{\int_{E_g}^{E_{g-1}} \phi(\vec{r}, E, t) dE} \Rightarrow \frac{1}{v} \equiv \frac{\int_0^\infty \frac{1}{v(E)} \phi(\vec{r}, E, t) dE}{\int_0^\infty \phi(\vec{r}, E, t) dE} \quad (2.81)$$

and we can claim as well that:

$$D_g \equiv \frac{\int_{E_g}^{E_{g-1}} D(E) \phi(\vec{r}, E, t) dE}{\int_{E_g}^{E_{g-1}} \nabla \phi(\vec{r}, E, t) dE} \Rightarrow D \equiv \frac{\int_0^\infty D(E) \nabla \phi(\vec{r}, E, t) dE}{\int_0^\infty \nabla \phi(\vec{r}, E, t) dE} \quad (2.82)$$

$$\sum_{ag} \equiv \frac{\int_{E_g}^{E_{g-1}} \sum_a(E) \phi(\vec{r}, E, t) dE}{\int_{E_g}^{E_{g-1}} \phi(\vec{r}, E, t) dE} \Rightarrow \sum_a \equiv \frac{\int_0^\infty \sum_a(E) \phi(\vec{r}, E, t) dE}{\int_0^\infty \phi(\vec{r}, E, t) dE} \quad (2.83)$$

The scattering terms are:

$$-\sum_{sg} \phi_g + \sum_{g'=1}^G \sum_{sg'g} (r) \phi_{g'}(\vec{r}, t) \rightarrow \sum_s \phi_g + \sum_s \phi_g = 0 \quad (2.84)$$

Note that the Eq. 2.83 hold when $G = 1$.

The fission term is:

$$\begin{aligned} \chi_g &\equiv \int_{E_g}^{E_{g-1}} \chi(E) dE \Rightarrow \chi \equiv \int_0^\infty \chi(E) dE = 1 \\ \sum_{g'=1}^G \chi_{g'} &\sum_{fg'} \phi_{g'} \Rightarrow \chi \sum_f \phi \end{aligned} \quad (2.85)$$

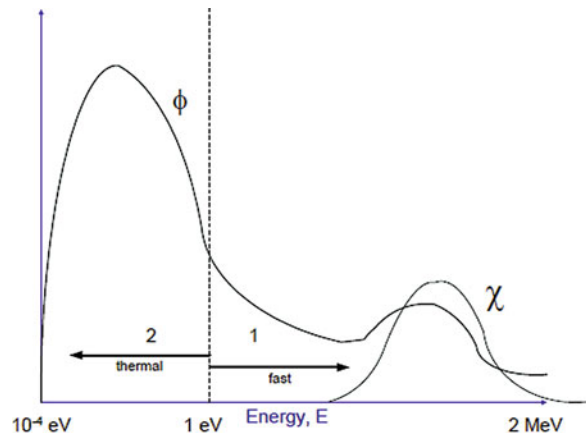
Putting all these terms together, we get back the one-group equation:

$$\frac{1}{v} \frac{\partial}{\partial t} \phi(\vec{r}, t) = \nabla \cdot D(r) \nabla \phi(\vec{r}, t) - \sum_a (r) \phi(\vec{r}, t) + v \sum_f \phi(\vec{r}, t) \quad (2.86)$$

2.19.2 Multi-group Collapsing to Two Group

The two-group approximation is a common and illustrative one. We divide the neutrons into a thermal group and a fast group with the division at 1 eV, as shown in Fig. 2.16.

Fig. 2.16 Two-group approximation



Note that:

$$\chi_2 = \int_0^{1eV} \chi(E) dE = 0 \quad \text{and} \quad \chi_1 = 1 \quad (2.87)$$

Thus, the general fission source term:

$$S_g = \underbrace{\chi_g}_{\substack{\text{fraction} \\ \text{appearing} \\ \text{in group } g}} \underbrace{\sum_{g'=1}^G v_{g'} \sum_{fg'} (\vec{r}) \phi_{g'} (\vec{r}, t)}_{\text{total fission production}} \quad (2.88)$$

For the simple two-group case is:

$$\begin{aligned} S_1 &= v_1 \sum_{f1} \phi_1 + v_2 \sum_{f2} \phi_2 \\ S_2 &= 0 \end{aligned} \quad (2.89)$$

There is no upscattering so:

$$\sum_{s21} = 0 \Rightarrow \sum_{s2} + \sum_{s22} \Rightarrow \sum_{s2} = \sum_{s22} \quad (2.90)$$

Therefore:

$$\sum_{s21} = \sum_{t2} - \sum_{s22} = \sum_{a2} \quad (2.91)$$

Thus, the two-group equations are:

$$\begin{aligned} \frac{1}{v_1} \frac{\partial \phi_1}{\partial t} - \nabla \cdot D_1 \phi_1 - \sum_{r1} \phi_1 &= v_1 \sum_{f1} \phi_1 + v_2 \sum_{f2} \phi_2 \text{ no up-scatter} \\ \frac{1}{v_2} \frac{\partial \phi_2}{\partial t} &= \nabla \cdot D_2 \phi_2 - \sum_{a2} \phi_2 + \sum_{s12} \phi_1 \text{ no direct fission source} \end{aligned} \quad (2.92)$$

In steady state, adding the k fudge factor, we have:

$$\begin{aligned} -\nabla \cdot D_1 \phi_1 - \sum_{r1} \phi_1 &= \frac{1}{k} \left[v_1 \sum_{f1} \phi_1 + v_2 \sum_{f2} \phi_2 \right] \text{ no up-scatter} \\ -\nabla \cdot D_2 \phi_2 - \sum_{a2} \phi_2 &= \sum_{s12} \phi_1 \text{ no direct fission source} \end{aligned} \quad (2.93)$$

Notice how the fast flux is the source term for the thermal neutrons (by scattering down in energy), while the thermal flux is the source for the fast neutrons by the fission event. This is illustrated in Fig. 2.17.

So, it follows that you would expect to see an abundance or peak of fast neutrons in the fuel region (because that is where the fissions take place). They diffuse to the moderator where there is a high probability of slowing down (because of the materials used there for just that purpose). Hence, you would expect to see a peak of thermal neutrons in the moderator. This is illustrated in Fig. 2.18.

Thus, the fast and thermal neutrons not only have a vastly different energy distribution, but also they have different spatial distributions in general.

Fig. 2.17 Thermal fast exchange

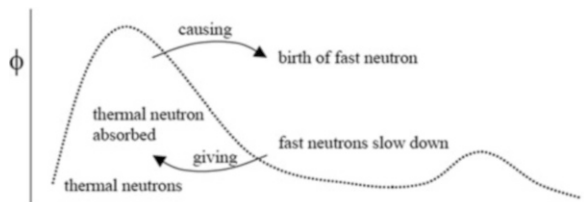
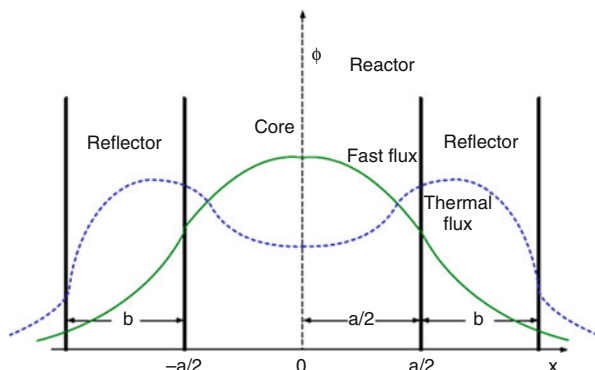


Fig. 2.18 Spatial distribution of flux



2.19.3 Two-Group Criticality

We consider the case of a bare (i.e., unreflected) reactor so that we can develop the criticality condition for the two-group case and compare it to the one-speed case developed earlier. Because the moderator and fuel are mixed together, the thermalization and fission processes are not physically separated. We can expect that both the fast and the thermal fluxes will have the same fundamental cosine shape for a simple slab reactor. The basic equations are:

$$\begin{aligned} -\nabla \cdot D_1 \phi_1 - \sum_{r1} \phi_1 &= \frac{1}{k} \left[v_1 \sum_{f1} \phi_1 + v_2 \sum_{f2} \phi_2 \right] \\ -\nabla \cdot D_2 \phi_2 - \sum_{a2} \phi_2 &= \sum_{s12} \phi_1 \end{aligned} \quad (2.94)$$

We write the flux as a product of an amplitude factor and a shape factor:

$$\phi_1(\bar{r}) = \varphi_1 \psi(\bar{r}) \quad \text{and} \quad \phi_2(\bar{r}) = \varphi_2 \psi(\bar{r}) \quad (2.95)$$

Defining the buckling for homogeneous reactor as usual:

$$\nabla^2 \psi(\bar{r}) + B^2 \psi(\bar{r}) = 0 \quad (2.96)$$

We find that Eq. 2.95 becomes:

$$\begin{aligned} +D_1 B^2 \varphi_1 + \sum_{r1} \varphi_1 &= \frac{1}{k} \left[v_1 \sum_{f1} \varphi_1 + v_2 \sum_{f2} \varphi_2 \right] \\ +D_2 B^2 \varphi_2 - \sum_{a2} \varphi_2 &= \sum_{s12} \varphi_1 \end{aligned} \quad (2.97)$$

Or in matrix form Eq. 2.97 can be written as:

$$\begin{pmatrix} \left(D_1 B^2 - \sum_{r1} - \frac{v_1 \sum_{f1}}{k} \right) & -\frac{v_2 \sum_{f2}}{k} \\ -\sum_{s12} & (D_2 B^2 + \sum_{a2}) \end{pmatrix} = 0 \quad (2.98)$$

$$\text{i.e. : } \bar{\bar{A}} \bar{\varphi} = 0 \quad (2.99)$$

which has a nontrivial solution for the flux amplitudes only if the following relationship is imposed:

$$|\bar{\bar{A}}| = 0 \quad (2.100)$$

Thus:

$$\left(D_1 B^2 - \sum_{r1} - \frac{v_1 \sum_{f1}}{k} \right) \left(D_2 B^2 + \sum_{a2} \right) - \frac{v_2 \sum_{f2} \sum_{s12}}{k} = 0 \quad (2.101)$$

Solving for multiplication factor k , we get:

$$\begin{aligned} k &= \frac{v_1 \sum_{f1}}{\underbrace{\sum_{r1} + D_1 B^2}_{\text{fast fission}}} + \frac{\sum_{s12}}{(\sum_{r1} + D_1 B^2)} \frac{v_2 \sum_{s12}}{(\sum_{a2} + D_2 B^2)} \\ &= 1 \text{ at criticality} \end{aligned} \quad (2.102)$$

The first term on the RHS (right-hand side) is the fast fission contribution. We can lump it into the second term via the fast fission factor ϵ which is defined below and recognize that:

- The resonance escape probability is just the ratio of the number of neutrons that successfully scatters down to group 2 over the number that leaves group 1.
- Likewise ηf is just the ratio of neutrons born to the number of thermal absorbed, and further discussion is given in Sect. 2.9.4 as well.

Thus, we can reconstruct the four-factor formula, with additional factors for fast and thermal leakage:

$$\begin{aligned} k &= \frac{\sum_{s12}}{(\sum_{r1} + D_1 B^2)} \frac{v_2 \sum_{f2}}{(\sum_{a2} + D_2 B^2)} \\ &= \frac{\sum_{s12}/\sum_{r1}}{(1 + L_1^2 B^2)} \frac{v_2 \sum_{f2}/\sum_{a2}}{(1 + L_2^2 B^2)} = \frac{p}{(1 + L_1^2 B^2)} \frac{\eta f}{(1 + L_2^2 B^2)} \\ &= p \eta f P_{NL1} P_{NL2} \end{aligned} \quad (2.103)$$

where $L^2 \equiv D/\sum_{a2}$.

Note that as again, we mentioned previously the fast fission factor ϵ is usually quite close to unity in a thermal reactor with typical values ranging between $\epsilon = 1.03$ and $\epsilon = 1.15$.

2.20 The Infinite Reactor

To simplify analysis and separate effects, begin by considering an infinitely large reactor. This means that leakage could be ignored for the moment. The above spectrum is a characteristic of such a reactor. The multiplication factor can be written:

$$k = \frac{\int v\Sigma_f(E)\phi(E)dE}{\int \Sigma_a(E)\phi(E)dE} = \frac{\text{Production}}{\text{Absorption}} \quad (2.104)$$

Now if we define an average fission production rate as:

$$v\Sigma_f = \frac{\int v\Sigma_f(E)\phi(E)dE}{\int \phi(E)dE} \quad (2.105)$$

and an average consumption rate as:

$$\Sigma_a = \frac{\int \Sigma_a(E)\phi(E)dE}{\int \phi(E)dE} \quad (2.106)$$

we can write k as:

$$k_\infty = \frac{v\Sigma_f}{\Sigma_a} \quad (2.107)$$

where k is identified with the subscript for infinity to identify this multiplication factor as applying to an infinitely large reactor.

2.21 Finite Reactor

In order to consider a finite reactor, we must introduce the concept of leakage out of the reactor as a destruction process. This can be written as:

$$k = \frac{\text{Production}}{\text{Absorption} + \text{Leakage}} \quad (2.108)$$

or:

$$k = \frac{\int v\Sigma_f(E)\varphi(E)dE}{\int \Sigma_a(E)\varphi(E)dE + \int L(E)dE} = \frac{\int v\Sigma_f(E)\varphi(E)dE}{\int \Sigma_a(E)\varphi(E)dE} \frac{1}{1 + \frac{\int L(E)dE}{\int \Sigma_a(E)\varphi(E)dE}} \quad (2.109)$$

$$k = k_\infty P_{NL} \quad (2.110)$$

or the multiplication factor with leakage is equal to the infinite multiplication factor times the probability of non-leakage. This multiplication factor is called k_{eff} , which is in agreement with what we presented before.

2.22 Time Dependence

These are static concepts. In order to make it more realistic, we need to introduce time dependence. To introduce time dependence, we need some estimate of how long it takes a generation to be produced or consumed. This concept can be defined as the average neutron lifetime and given the symbol l . Then a simple balance equation can be written as:

$$\frac{d\phi(t)}{dt} = \frac{\text{Differential Production}}{\text{Consumption Rate}} = \frac{v\Sigma_f\phi - \Sigma_a\phi}{\Sigma_a l} = \frac{(k-1)\Sigma_a}{\Sigma_a l} \phi \quad (2.111)$$

$$\frac{d\phi(t)}{dt} = \frac{(k-1)}{l} \phi(t) \quad (2.112)$$

whose solution is:

$$\phi(t) = \phi(0)e^{-\frac{k-1}{l}t} \quad (2.113)$$

Thus, the flux level in a reactor (and therefore the power level) will exponentially increase or decrease depending on the sign of $k - 1$. The following table applies:

$k > 1$, flux exponentially increases

$k = 0$, flux is stable

$k < 1$, flux exponentially decreases

Since even thermal neutrons move at speeds over a thousand meters per second, neutron lifetimes are very short. A typical lifetime in a thermal reactor is on the order of tenths of a millisecond. In a fast reactor, lifetimes can be as short as tenths of a microsecond. If there were no delayed neutrons, these short-time constants would make a nuclear reactor almost uncontrollable. However, delayed neutrons add a significant delay to control actions so that most reactors are easily controllable by human manipulation. The time required for reactor power (or neutron flux) to increase or decrease by a factor of exponential is called the reactor “period.” For this simple model, this is given by $l/k - 1$.

The four-, five-, or six-factor formulas can give a slightly more detailed model of the chain reaction process. The four-factor formula breaks down the chain reaction into a factor that takes into account the efficiency of the fuel nuclide itself, called η , and defined by:

$$\eta = \frac{v\sigma_f^F}{\sigma_a^F}$$

Again, this is in agreement with the previous discussion and presented in Eq. 2.71.

A second factor quantifies the ratio of the absorption of thermal neutrons in the fuel to the absorption of thermal neutrons in the fuel and moderator. This factor is called thermal utilization factor and given by f as:

$$f = \frac{\sum_a^F}{\sum_a^F + \sum_a^M} \quad (2.114)$$

This factor is defined in more detail in section References below.

In a homogeneous reactor, the neutron flux seen by the fuel, moderator, and poisons will be the same. In addition, since they are spread throughout the reactor, they all occupy the same volume. This allows the previous equation to be rewritten as shown below:

$$f = \frac{\sum_a^F}{\sum_a^F + \sum_a^M + \sum_a^P} \quad (2.115)$$

The superscripts F , M , and P refer to fuel such as uranium, moderator, and poison, respectively.

A third factor takes into account the fraction of fast neutrons that slow down from fission energies to thermal energies without being absorbed. This factor is called the probability of resonance escape and given the symbol p_{re} . The fourth factor takes into account the fact that not all fissions are caused by thermal neutrons. It is simple called the fast fission factor and is given the symbol ϵ . The four-factor formula is then written as:

$$k_\infty = \eta f p_{re} \epsilon \quad (2.116)$$

For a finite reactor, this must be modified by including the probability of leakage. We get five terms if an integral non-leakage probability is considered. If we separate out fast and thermal leakage, then we get two non-leakage terms. This is often done to emphasize the fast leakage, as thermal leakage is usually insignificant for a large reactor. The formula for k_{eff} becomes:

$$k_{\text{eff}} = \eta f p_{re} \epsilon P_{NL} = \eta f p_{re} \epsilon P_{NL}^F P_{NL}^{Th} \quad (2.117)$$

Perhaps the real reasons for trying to understand the four- or six-factor formulas are historical ones. They were an attempt to isolate effects, so that they could be measured separately. Typical values for any of the parameters are no longer tabulated for any of these quantities. Their values can be obtained from multi-group calculations for specific configurations. And multi-group calculations are so inexpensive today that tabulating these parameters does not produce a useful analysis approach.

2.23 Thermal Utilization Factor f

Once thermalized, the neutrons continue to diffuse throughout the reactor and are subject to absorption by other materials in the reactor as well as the fuel. The thermal utilization factor describes how effectively thermal neutrons are absorbed by the fuel or how well they are utilized within the reactor. The *thermal utilization factor* (f) is defined as the ratio of the number of thermal neutrons absorbed in the fuel to the number of thermal neutrons absorbed in any reactor material. This ratio is shown below:

$$f = \frac{\text{number of thermal neutrons absorbed in the fuel}}{\text{number of thermal neutrons absorbed in all reactor materials}}$$

The thermal utilization factor will always be less than one because some of the thermal neutrons are absorbed within the reactor which will be absorbed by atoms of nonfuel materials.

An equation can be developed for the thermal utilization factor in terms of reaction rates as follows:

$$f = \frac{\text{rate of absorption of thermal neutrons by the fuel}}{\text{rate of absorption of thermal neutrons by all reactor materials}}$$

or in general mathematically can be written as:

$$f = \frac{\sum_a^F \phi^F V^F}{\sum_a^F \phi^F V^F + \sum_a^M \phi^M V^M + \sum_a^P \phi^P V^P} \quad (2.118)$$

The superscripts F , M , and P refer to fuel, moderator, and poison, respectively. In a heterogeneous reactor, the flux will be different in the fuel region than in the moderator region due to the high absorption rate by the fuel. Also, the volumes of fuel, moderator, and poisons will be different. Although they are not shown in the above equation, other nonfuel materials, such as core construction materials, may absorb neutrons in a heterogeneous reactor. These other materials are often lumped together with the superscript designation OS for “other stuff.” To be completely accurate, the above equation for the thermal utilization factor should include all neutron-absorbing reactor materials when dealing with heterogeneous reactors. However, for the purposes of this text, the above equation is satisfactory.

However, as we said before, in a homogeneous reactor, the neutron flux seen by the fuel, moderator, and poisons will be the same. In addition, since they are spread throughout the reactor, they all occupy the same volume. This allows Eq. 2.116 to reduce to Eq. 2.115.

Equation 2.118 gives an approximation for a heterogeneous reactor if the fuel and moderator are composed of small elements distributed uniformly throughout the reactor.

Since absorption cross sections vary with temperature, it would appear that the thermal utilization factor would vary with a temperature change. But, substitution of the temperature correction formulas in Eq. 2.115 will reveal that all terms change by the same amount and the ratio remains the same. In heterogeneous water-moderated reactors, there is another important factor. When the temperature rises, the water moderator expands, and a significant amount of it will be forced out of the reactor core. This means that N^M , the number of moderator atoms per cm^3 , will be reduced, making it less likely for a neutron to be absorbed by a moderator atom. This reduction in N_m results in an increase in thermal utilization as moderator temperature increases because a neutron now has a better chance of hitting a fuel atom. Because of this effect, the temperature coefficient for the thermal utilization factor is positive. The amount of enrichment of uranium²³⁵ and the poison concentration will affect the thermal utilization factor in a similar manner as can be seen from the equation above.

Problems

Problem 2.1 If a 1 cubic centimeter section of a reactor has a macroscopic fission cross section of 0.1 cm^{-1} , and if the thermal neutron flux is $10^{13} \text{ neutrons/cm}^2\text{-sec}$, what is the fission rate in that cubic centimeter?

Problem 2.2 A reactor operating at a flux level of $3 \times 10^{13} \text{ neutrons/cm}^2\text{-sec}$ contains 1020 atoms of uranium-235 per cm^3 . The reaction rate is $1.29 \times 10^{12} \text{ fission/cm}^3$. Calculate Σ_f and σ_f , assuming 1 barn = 10^{-24} cm^2 .

Problem 2.3 How many collisions are required to slow a neutron from energy of 2 MeV to a thermal energy of 0.025 eV and using water as the moderator. Water has a value of 0.948 for M .

Problem 2.4 If the average fractional energy loss per collision in hydrogen is 0.63, what will be the energy of a 2 MeV neutron after (a) 5 collisions and (b) 10 collisions?

Problem 2.5 A block of aluminum has a density of 2.699 g/cm^3 . If the gram atomic weight of aluminum is 26.9815 g, calculate the atom density of the aluminum.

Problem 2.6 How long on average for a given nuclei to suffer a neutron interaction?

Problem 2.7 Find the macroscopic thermal neutron absorption cross section for iron, which has a density of 7.86 g/cm^3 . The microscopic cross section for absorption of iron is 2.56 barns, and the gram atomic weight is 55.847 g.

Problem 2.8 Calculate the reproduction factor for a reactor that uses 10% enriched uranium fuel. The microscopic absorption cross section for uranium-235 is 694 barns. The cross section for uranium-238 is 2.71 barns. The microscopic fission

cross section for uranium-235 is 582 barns. The atom density of uranium-235 is 4.83×10^{21} atoms/cm³. The atom density of uranium-238 is 4.35×10^{22} atoms/cm³. n is 2.42.

Problem 2.9 Calculate the thermal utilization factor for a homogeneous reactor. The macroscopic absorption cross section of the fuel is 0.3020 cm^{-1} , the macroscopic absorption cross section of the moderator is 0.0104 cm^{-1} , and the macroscopic absorption cross section of the poison is 0.0118 cm^{-1} .

Problem 2.10 Determine the infinite multiplication factor k_{∞} for a uniform mixture of uranium-235 and beryllium oxide in the atomic or molecular ratio of 1 to 10,000. The value of absorption cross section for beryllium is $\sigma_a = 0.010$ (barn) and for uranium is $\sigma_U = 683$ (barn). Assume the resonance escape probability and the fast-fission factor may be taken to be unity and ratio of average number of neutrons liberated per neutron absorbed for uranium-235 at thermal (2200 m/sec) is $\eta = 2.06$.

References

1. M. Ragheb, *Neutron Diffusion Theory*. <http://mragheb.com/NPRE%20402%20ME%20405%20Nuclear%20Power%20Engineering/Neutron%20Diffusion%20Theory.pdf>
2. B. Garland., <http://www.nuceng.ca/ep4d3/ep4d3home.htm>
3. WIMS can provide simple pin cell calculations of reactivity to whole core estimates of power and flux distributions. The user can benefit from the flexibility of using predefined calculation routes or providing customized methods of solution using diffusion theory, discrete-ordinates, collision probability, characteristics or Monte Carlo methods
4. J. Duderstadt, L. Hamilton, *Nuclear Reactor Analysis* (John Wiley Publishing Company, New York, NY, 1976)
5. A. Henry, *Nuclear Reactor Analysis* (The MIT Press, Cambridge, Massachusetts, and London, England, 1975)

Chapter 3

Spatial Effects in Modeling Neutron Diffusion: One-Group Models



The fundamental aspect of keeping a reactor critical was discussed in Chap. 2, and we found out that the most principal evaluation quantity of the nuclear design calculation is the effective multiplication factor $(\bar{\sigma}(v, T) = \frac{1}{v} \int d^3 V |v - V| \sigma(|v - V|) M(V, T))$ and neutron flux distribution. We also so far have noticed that the excess reactivity, control rod worth, reactivity coefficient, power distribution, etc. are undoubtedly inseparable from the nuclear design calculation. Some quantities among them can be derived by secondary calculations from the effective multiplication factor or neutron flux distribution that was also discussed in Sect. 2.15 of Chap. 2 so far. In this chapter we treat the theory and mechanism to be able to analyze and calculate the effective multiplication factor and neutron flux distribution and possibly show numerical analysis and computer codes involved with solving the diffusion equation in one-dimensional and one-group models. The goal of this chapter is also for the reader to understand simple reactor systems, the notion of criticality, what it means both physically and mathematically, how to analytically solve for the steady-state flux for simple geometries, and finally how to numerically solve the steady state for more arbitrarily complex geometries.

3.1 Nuclear Reactor Calculations

The fundamental tool for reactor design analyses is multi-group diffusion theory. The ability of Monte Carlo methods to accurately calculate criticality in complex geometry has grown significantly with the advent of very high-speed computers with megabytes of fast memory. However, improved computing capability means that multi-group deterministic methods also run faster and more questions can be asked during the design process. The design process really is one of synthesis, and therefore a deterministic method guides the thought patterns required to understand

the complex interplay of materials and physical processes. Monte Carlo methods perform the analysis task very well, but often do not provide this insight into the interplay of the physical processes involved. In addition, there is always the concern that the effects observed by varying a design parameter are not really real, but rather the result of some unlucky statistical occurrence due to the random numbers chosen. Running enough histories can always minimize this, but it is sometimes hard to determine the required number ahead of time. Finally, deterministic multi-group calculations are based on a set of tested cross sections that behave the same way every time. Monte Carlo cross sections can also be tested multiple times, but they never give exactly the same answer for the same problem starting with different random numbers.

A well-thought-out process has been developed over the years for performing high-quality multi-group diffusion calculations for reactor design. The *ENDF/B* point-wise data is processed through a number of steps to obtain problem-dependent “group constants” appropriate for the design of the reactor under consideration. This process goes as follows:

1. The point-wise *ENDF/B data* is processed to a set of many (~200–1000) group cross sections so that every material has the same group boundaries for its linear and 2-D arrays. The within-group weighting spectrum for this processing is normally chosen to be either the fission slowing down thermal Maxwellian asymptotic spectrum or a constant.
2. An infinite medium or zero-dimensional calculation is performed for all core compositions of interest. The individual group fluxes from this calculation are used as the within-group spectrum to collapse the material cross sections to a broad group set typically in the range of 10–50 groups.
3. These cross sections are then used in a cell calculation to determine spatial self-shielding factors for various geometric configurations within the reactor assembly. The cell fluxes are used for this collapse and self-shielding subject to the requirement to match reaction rates as closely as possible in going from broad groups to few groups.
4. Finally, the multidimensional reactor design calculations are performed with the few-group cross sections.

In some cases, steps 2 and 3 can be combined, but they will be dealt with separately in this book to demonstrate the difference between spatial and energy-dependent effects.

The nuclear reactor calculation is classified broadly into the reactor core calculation and the nuclear plant characteristic calculation. The former is done to clarify nuclear, thermal, or their composite properties. The latter is done to clarify dynamic and control properties, startup and stability, and safety by modeling pipes and valves of the coolant system, coolant pump, their control system, steam turbine and condenser, etc., connected with the reactor pressure vessel as well as the reactor core. The reactor core, plant dynamics, safety analysis, and fuel rod analysis are described in the later part of this book.

The collective behavior of neutrons in a reactor core is described by the neutron transport equation presented in Eq. 3.1 which is also referred to as the Boltzmann equation.

$$\frac{1}{v(E)} \frac{\partial}{\partial t} \phi(\vec{r}, \vec{\Omega}, E, t) = S(\vec{r}, \vec{\Omega}, E, t) - \vec{\Omega} \cdot \nabla \phi(\vec{r}, \vec{\Omega}, E, t) - \Sigma_t(\vec{r}, E, t) \phi(\vec{r}, \vec{\Omega}, E, t) \quad (3.1)$$

Here, S is the neutron source, Σ_t is the macroscopic total cross section, and ϕ is the angular neutron flux being calculated. And finally $v(E)$ is the neutron velocity corresponding to energy, E . This equation represents the balance between gain and loss in the unit volume of neutrons that are characterized by a specific kinetic energy E with velocity v and are traveling in a specific direction $\vec{\Omega}$ at a time t and a position \vec{r} . That is, the time change of the target neutrons which is the first term in the *left-hand side* (LHS) is given by the balanced relation among the gain of neutrons appearing from the neutron source S , which is the first term in the *right-hand side* (RHS). The net loss of neutrons traveling is the second term in the RHS, and the loss of neutrons due to nuclear collisions is the third term in the RHS. It should be noted that the changes in angle and energy of neutrons are also included in the gain and loss.

We expand upon this equation in Chap. 2, and the target neutrons are gained from three mechanisms: scattering, fission, and external neutron sources. Each gain is represented as follows in Eq. 3.2:

$$S(\vec{r}, \vec{\Omega}, E, t) = \int_0^\infty dE' \int_{4\pi} \Sigma_s(\vec{r}, \vec{\Omega}' \rightarrow \vec{\Omega}, E' \rightarrow E, t) \phi(\vec{r}, \vec{\Omega}', E', t) d\vec{\Omega}' + \frac{\chi(E)}{4\pi} \int_0^\infty dE' \int_{4\pi} \chi(E) v \Sigma_f(\vec{r}, E', t) \phi(\vec{r}, \vec{\Omega}', E', t) d\vec{\Omega}' + S_{ex}(\vec{r}, \vec{\Omega}, E, t) \quad (3.2)$$

A very similar form of Eq. 3.2 was also presented in Chap. 2, where Σ_s and Σ_f are the macroscopic scattering and fission cross sections, respectively, v is the average number of neutrons released per fission, and the product $v\Sigma_f$ is treated as a production cross section. The cross sections were described in Chap. 2 of this book.

The first term in the RHS of Eq. 3.2 is called the *scattering source*, and it totals the number of the target neutrons scattering into E and $\vec{\Omega}$ from another energy E and direction $\vec{\Omega}'$ by integrating the number for E and $\vec{\Omega}'$. The second term is the fission source, and it indicates that the neutrons produced by fission over the whole range of energies are distributed with the isotropic probability in direction ($1/4\pi$) and the probability $\chi(E)$ in energy. $\chi(E)$ is called the *fission spectrum*, and it is dependent on the nuclide undergoing fission and the energy of incident neutrons. For instance, the

fission spectrum in an enriched uranium-fueled in case of light water reactor (LWR) is well described by the function of Eq. 3.3 as below.

$$\chi(E) = \sinh(\sqrt{2.29E}) e^{(-E/0.965)} \quad (3.3)$$

Since $\chi(E)$ is a probability distribution function, it is normalized so that we can write the following form of Eq. 3.4 as:

$$\int_0^{\infty} \chi(E) dE = 1.0 \quad (3.4)$$

The third term in the RHS of Eq. 3.2, S_{ex} , expresses the external neutron source for reactor startup which may be such species as ^{252}Cf or Am-Be. Therefore, it is not used in the nuclear design calculation of a reactor in operation.

More details of the neutron transport equation are not handled here. If the cross-sectional data (\sum_t , \sum_s , and $v\sum_f$) in Eqs. 3.1 and 3.2 are provided, the angular neutron flux $\phi(\vec{r}, \vec{\Omega}, E, t)$, which depends on location, traveling direction, energy, and time, can be calculated by properly solving the equation.

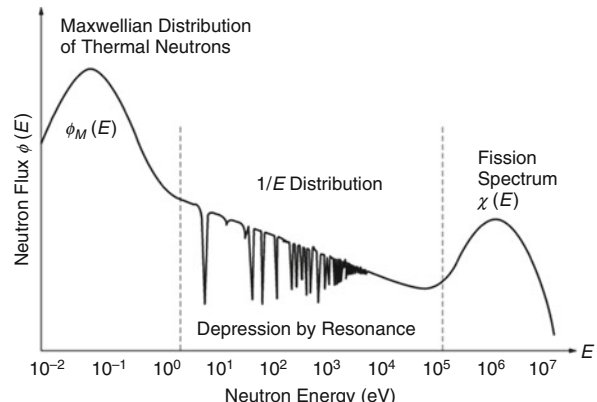
The information on traveling direction of neutrons is finally unimportant in the nuclear design calculation. The scalar neutron flux integrated over the angle is rather meaningful and presented as Eq. 3.5 here.

$$\phi(\vec{r}, E, t) = \int_0^{4\pi} \phi(\vec{r}, \vec{\Omega}, E, t) d\vec{\Omega} \quad (3.5)$$

3.1.1 Neutron Spectrum

The function characterizing the energy dependence of neutron flux $\phi(\vec{r}, E, t)$ is called the *neutron spectrum*, and it varies with fuel enrichment, moderator density, void fraction, burnup, and so on. Figure 3.1 shows a neutron spectrum of a thermal

Fig. 3.1 Neutron spectrum of a thermal reactor



reactor. The neutron spectrum of thermal reactors is divided into three distinct energy regions. In the high-energy region above 105 eV, since the prompt neutrons released by fission are dominant, the neutron spectrum is approximately proportional to the fission spectrum $\chi(E)$. In the energy region below several hundred of keV, the fast neutrons from fission lose their energies mainly through *elastic scattering* reaction with light moderator nuclides such as hydrogen. According to neutron slowing down theory [1], when fast-neutron sources are in an infinite homogeneous medium which is an ideal moderator with negligible absorption, the neutron energy spectrum behaves as $1/E$.

The above definition proportionality can be presented in Eq. 3.6:

$$\phi(E) \propto \frac{1}{E} \quad (3.6)$$

In the practical medium of fuel and moderator, the $1/E$ distribution is characterized by the occurrence of fairly sharp depressions due to the resonance absorption of U^{238} , etc. as shown in Fig. 3.1.

Moreover, if the resonance absorption is large, the neutron flux becomes somewhat smaller than the $1/E$ distribution in the low-energy region [1].

If neutrons are moderated below several eV of kinetic energy, the kinetic energy by thermal vibration of nuclei cannot be ignored. In other words, if the kinetic energies of neutrons become appropriately small, the neutrons collide with the thermally vibrating moderator nuclei, and their kinetic energies become reversely large. This is called *upscattering* against moderation which is the *downscattering*. In this energy region, the neutron spectrum is characterized in a thermal equilibrium at a temperature T by a balance between downscattering and upscattering. Further, in the ideal infinite medium without absorption, the thermal equilibrium neutron spectrum is described by the following Maxwellian distribution function, where it is presented by Eq. 3.7 here.

$$\phi_M(E) \propto E \exp\left(-\frac{E}{kT}\right) \quad (3.7)$$

where k is the Boltzmann constant. At room temperature ($T = 300$ K), $\phi_M(E)$ is maximized at $E = 0.0253$ eV for which the corresponding velocity is 2200 m/s. On being absorbed, the thermal neutron spectrum deviates a little from $\phi_M(E)$ forward the high-energy region because absorption cross sections are larger in lower energies. This is called *absorption hardening*. To compensate the Maxwellian distribution for the absorption hardening, neutron temperature, which is a little higher than moderator temperature, is used as T of Eq. 3.7 [1].

3.2 Control Rods in Reactors

Early approach to nuclear industry and making reactor going critical were designed around controlling comparatively few rods, and naturally they were around invariable cylindrical shape made of a strong thermal neutron absorber such as cadmium with absorption cross section of $\sigma_a = 0.025 \text{ eV} = 245 \text{ b}$. These cylindrical rods were called *black rods* and had substantial diameter greater than the absorption mean free path of thermal neutrons, and all thermal neutrons striking the rod were thus absorbed [2].

In today's nuclear reactor design technologies, these black rods are not utilized as frequent because of the following reasons, and they are listed as follows:

- (a) Strong absorbing rods are having undesirable distorting flux in their vicinity, and this gives rise to undesirable power and temperature distributions.
- (b) Less strong absorbing materials such as hafnium with absorbing cross section of $\sigma_a = 0.025 \text{ eV} = 105 \text{ b}$ or steel containing small amount of boron are therefore used for the rods in most modern reactors. These rods are also comparatively thin, so that while they are providing a good neutron absorbent conditions, all the thermal neutrons striking them are not absorbed, and these rods are called *gray rods*.

In today's modern reactors, the control rods no longer are in cylindrical shape, but are fabricated in various shapes such as the cruciform or cross-like rods, and they fit closely into an array of fuel assemblies and widely used in reactors of water, moderated reactor in particular, that have tight fuel lattices. As results proper lattice calculation and analysis are desired using high-performance computer codes, and a direct core calculation with several tens of thousands of fuel pins is difficult to perform in its heterogeneous geometry model form, where one needs to use fine-group analysis to prepare a reactor constant library. The gray rods have additional advantages over the cylindrical rod in that they can be cooled more easily. This is particularly important in power reactors where a rod may become very hot unless properly cooled [2].

When we remove the rods from a solid-moderated reactor, the region originally occupied by the rod remains behind as space vacancy, while in a liquid-moderated reactor, the region may be filled with moderator. In either case when the void is replacing the strongly absorbing rod or a weak absorber tends to peak the flux in this region. To avoid this situation, it is common practice to attach a region of fuel or mildly absorbing structural material to the end of the rod [1].

Such rod *followers*, as these extensions to a control rod are called, reduce the peaking of the flux, and if the followers are fueled, they may substantially increase the reactivity equivalent of the rod, and then under this condition, fuel is simultaneously introduced into the system as the rod is extracted.

When we insert the control rod in a reactor, it changes its multiplication factor in two possible ways, and they are:

1. The rod simply absorbs neutrons, while simultaneously the rod distorts the flux such that the leakage of neutrons from the system is increased. Figure 3.2 demonstrates these processes where the flux is presented in the bare cylindrical reactor before and after insertion of a single rod takes place.
2. Observation of the curvature or buckling of the flux is *greater* when the rod is present, and the gradient of the flux at the surface of the reactor, thus, is greater and so is the leakage current.

With many reactors these two above effects of a control rod, increases the absorption and increases leakage, are very important and play important roles in determining the impact of the rod upon the multiplication factor of the system [1].

In summary the effectiveness of a control rod totally depends mainly upon the value of the ratio of the neutron flux of the location of the rod to the average neutron flux ϕ in the reactor. The control rod has maximum effect, which inserts the most negative reactivity, if it is placed in the reactor where the flux has maximum value. If reactor has only one control rod, the rod must be placed in the center of the reactor core as shown in Figs. 3.2 and 3.3. The effect of such a rod on the flux is illustrated as one can in Fig. 3.3 as well.

Fig. 3.2 Flux in a reactor with and without central control rod [1]

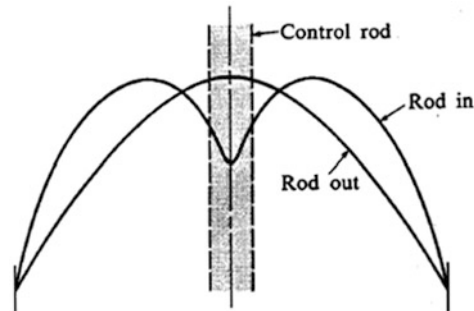
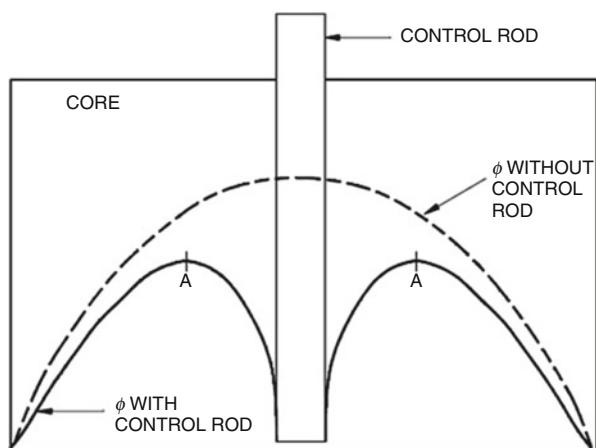


Fig. 3.3 Effect of control rod on radial flux distribution



In case of additional rod scenario, if they are added to such simple reactor, the most effective location is where the flux is maximum, which is shown as point A in Fig. 3.3. Numerous control rods are required for a reactor that has a large amount of excessive reactivity that is required for the reactor to go critical. The exact amount of reactivity that each control rod inserts depends upon the reactor design and core shape. The change in reactivity caused by control rod motion is referred to as control rod worth. Note that the exact effect of control rods on reactivity can be determined via experiment such that a control rod can be withdrawn in small increments, for example, about 0.5 inch, and the change in reactivity can be determined following each increment of withdrawal. Consequently, by plotting the resulting reactivity versus the rod position as shown in Fig. 3.4, one can illustrate the integral control rod worth over the full range of withdrawal. This way we can define the *integral control rod worth* as the total reactivity worth of the rod at that particular degree of withdrawal and is usually defined to be greatest when the rod is fully withdrawn.

As it can be seen in Fig. 3.4, the slope of the curve $\Delta\rho/\Delta x$, and hence the amount of reactivity inserted per unit of withdrawal, is greatest when the control rod is midway out of the core of the reactor of our example here. This situation takes place due to the area of greatest neutron flux, which is near the center of the core; therefore, the amount of change in neutron absorption is greatest in this area. If the slope of the curve for integral rod worth in Fig. 3.4 is taken, the result is a value for the rate of change of control rod worth as a function of control rod position.

Fig. 3.4 Integral control rod worth

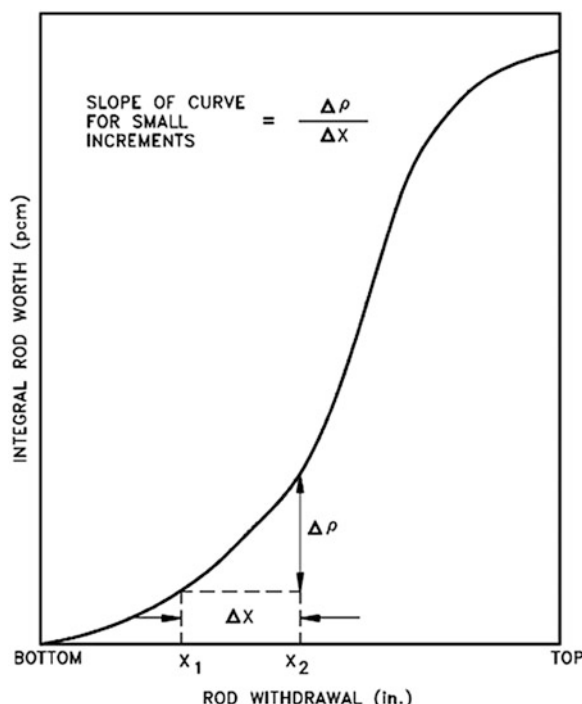


Fig. 3.5 Differential control rod worth

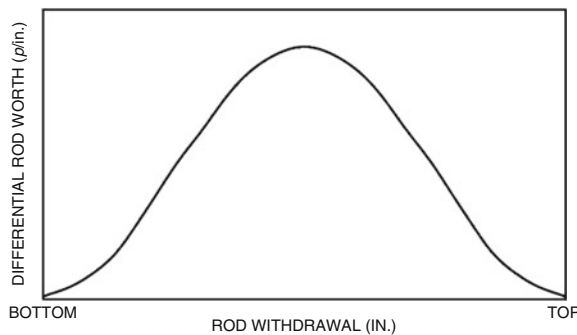
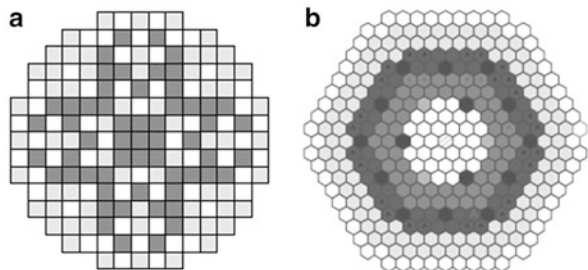


Fig. 3.6 Reactor cores consisting of square and hexagonal fuel assemblies. (a) Square fuel assemblies, (b) hexagonal fuel assemblies. (Courtesy of W. S. Yang, Argonne National Laboratory)



A plot of the slope of the integral rod worth curve is also known as the *differential control rod worth*, which is illustrated in Fig. 3.5. As one can see, in this figure at the bottom of the core, where there are few neutrons, rod movement has little effects so the change in rod worth per inch varies little. As the rod approaches the center of the core, its effect becomes greatest, and the change in rod worth per inch is greater. At the center of the core, the differential rod worth is greatest and varies a little with rod motion. From the center of the core to the top, the rod worth per inch is basically the inverse of the rod worth per inch from the center to the bottom.

Based on the above discussion, we now can define *differential control rod worth* as the reactivity change per unit movement of a rod and is normally expressed as ρ /inch, $\Delta k/k$ per inch, or pcm/inch. The integral rod worth at a given withdrawal is merely the summation of the entire differential rod worth up to that point of withdrawal. It is also the area under the differential rod worth curve at any given withdrawal position.

Some classes of power reactors contain space for the control rods as channels reserved for them within designated fuel assemblies; the assemblies shown in Fig. 3.6a and b fall into this category. In other systems, the control rods are inserted between the fuel assemblies. For better understanding of the above issues, refer to Problems 3.3 and 3.4 at the end of the chapter.

Control rods with cruciform cross sections may be placed at the intersections of square assemblies, or control rods maybe inserted into moderator regions between assemblies.

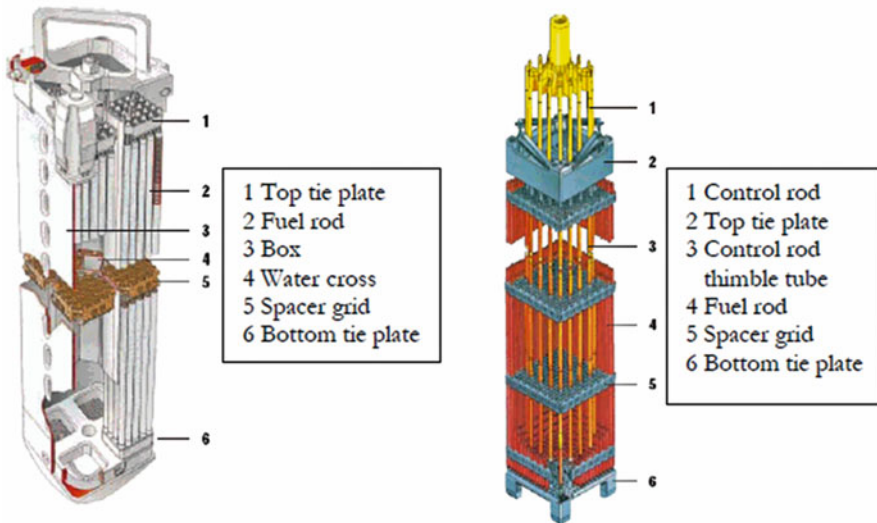


Fig. 3.7 Typical fuel assemblies used in BWRs (left) and PWRs (right)

Typical reactor core and fuel assemblies are consist of a number of fuel assemblies fixed in the pressure vessel between the lower and the upper core support plates. Fuel assemblies typical for pressurized water reactors (PWRs) and boiling water reactors (BWRs) are shown in Fig. 3.7.

Bear in your mind that the control rods are manufactured from materials that are strong absorbers of neutrons. These are usually special alloys, for example, 80% silver, 15% indium, and 5% cadmium. Generally, the material selected should have a good absorption cross section for neutrons and have a long lifetime as an absorber (not burn out rapidly).

The ability of a control rod to absorb neutrons can be adjusted during manufacture. A control rod that is referred to as a *black absorber* absorbs essentially all incident neutrons. A gray absorber absorbs only a part of them. While it takes more *gray rods* than black rods for a given reactivity effect, the gray rods are often preferred because they cause smaller depressions in the neutron flux and power in the vicinity of the rod.

This leads to a flatter neutron flux profile and more even power distribution in the core.

If gray rods are desired, the amount of material with a high absorption cross section that is loaded in the rod is limited. A material with a very high absorption cross section may not be desired for use in a control rod, because it will burn out rapidly due to its high absorption cross section. The same amount of reactivity worth can be achieved by manufacturing the control rod from a material with a slightly lower cross section and by loading more of the material. This also results in a rod that does not burn out as rapidly.

Another factor in control rod material selection is that materials that are resonantly absorbing neutrons are often preferred to those that merely have high thermal neutron absorption cross sections. Resonance neutron absorbers absorb neutrons in the epithermal energy range. The path length traveled by the epithermal neutrons in a reactor is greater than the path length traveled by thermal neutrons. Therefore, a resonance absorber absorbs neutrons that have their last collision farther (on the average) from the control rod than a thermal absorber. This has the effect of making the area of influence around a resonance absorber larger than around a thermal absorber and is useful in maintaining a flatter flux profile.

In summary, the control rod insertion rates on a reactor scram situation for a reactor operation that encounter such circumstances are designed to be sufficient to protect the reactor against damage in all transients mode that are expected to occur during the life cycle of the reactor.

During a normal reactor operation rod motion, the control rods must be able to move fast enough to compensate for the most rapid rate at which positive reactivity is expected to build within the reactor in order to provide positive control. The transient that is normally considered when setting this minimum rod speed is the burnout of maximum peak xenon while at full power. Xenon burnout which is usually the most rapid, non-accident transient circumstances is expected. The maximum rod speed is normally limited in order to reduce the severity of a reactor accident involving the continuous withdrawal of control rods.

3.2.1 *Lattice Calculation Analysis*

The purpose of lattice calculation as we said above is using a high-performance computer. A direct core calculation with several tens of thousands of fuel pins is difficult to perform in its heterogeneous geometry model form. Using fine groups (e.g., 107 groups in *SRAC* which is a Japanese Atomic Energy Agency (JAEA) code for Research Group for Reactor Physics and Standard Nuclear Code System using *NJOY 99* to produce cross-sectional library for thermal reactor analysis) of a prepared reactor constant library.

To do lattice calculation analysis, the Monte Carlo method can handle such a core calculation, but it is not easy to obtain enough accuracy for a local calculation or small reactivity because of accompanying statistical errors. Hence, the Monte Carlo method is not employed for nuclear design calculations requiring a fast calculation time. Instead, the nuclear design calculation is performed in two steps: lattice calculation in a two-dimensional (2-D) infinite arrangement of fuel rods or assemblies and core calculation in a three-dimensional (3-D) whole core. The lattice calculation prepares few-group homogenized cross sections, which maintain the important energy dependence (neutron spectrum) of nuclear reactions, as shown in Fig. 3.8, and this reduces the core calculation cost in terms of time and memory. Since final design parameters in the core calculation are not concerned with the

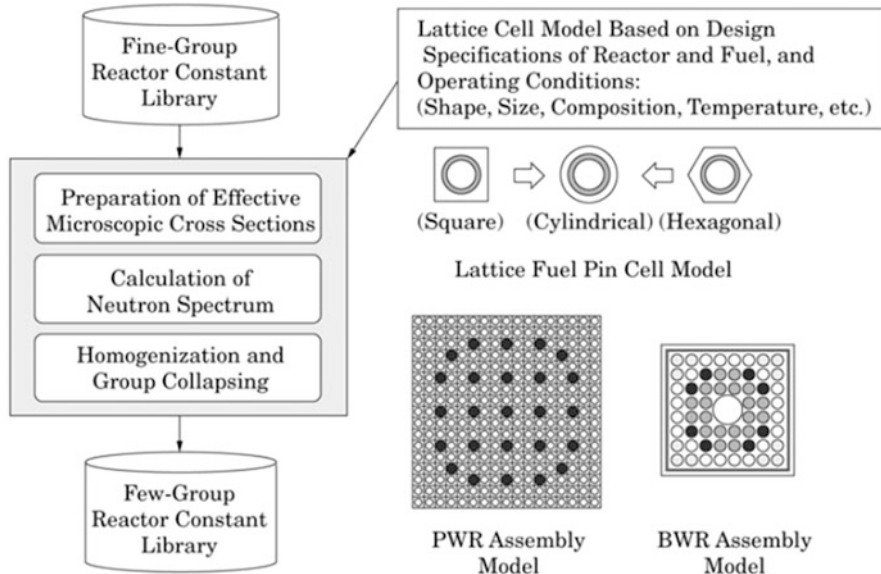


Fig. 3.8 Lattice calculation flow

energy dependence, the spatial dependence such as for the power distribution is important.

Multi-group neutron transport equation is also playing an important role where the neutron transport equation in the lattice calculation is a steady-state equation without the time differential term in Boltzmann Equation 3.1. Further, the neutron energy variable is discretized in the equation, and therefore a multi-group form is used in designing computer codes as in Eq. 3.8.

$$-\vec{\Omega} \cdot \nabla \phi_g(\vec{r}, \vec{\Omega}) - \Sigma_{t,g}(\vec{r}) \phi_g(\vec{r}, \vec{\Omega}) + S_g(\vec{r}, \vec{\Omega}) = 0 \quad (3.8)$$

The neutron source of Eq. 3.9 is the multi-group form without the external neutron source of Eq. 3.2 at the critical condition.

$$S_g(\vec{r}, \vec{\Omega}) = \int_{4\pi} d\Omega' \sum_{g'} \Sigma_{s,g' \rightarrow g}(\vec{r}, \vec{\Omega}' \rightarrow \vec{\Omega}) \phi_{g'}(\vec{r}, \vec{\Omega}') + \frac{\chi_g}{4\pi} \sum_{g'} v \Sigma_{f,g'}(\vec{r}) \int_{4\pi} \phi_{g'}(\vec{r}, \vec{\Omega}') d\Omega' \quad (3.9)$$

The system to which the multi-group transport equation is applied is an infinite lattice system of a 2-D fuel assembly (including assembly gap) with a reflective boundary condition. For a complicated geometry, two lattice calculations corresponding to a single fuel rod and a fuel assembly are often combined.

In practically solving Eq. 3.8 in the lattice model, the space variable (\vec{r}) is also discretized in the equation, and each material region is divided into several sub-regions where neutron flux is regarded to be flat. In liquid-metal-cooled fast reactors (LMFRs), neutron flux in each energy group has an almost flat spatial distribution within the fuel assembly because the mean free path of the fast neutrons is long. A simple hexagonal lattice model covering a single fuel rod or its equivalent cylindrical model simplified to one dimension is used in the design calculation of LMFRs. The spatial division can also be simplified by assigning the macroscopic cross section by material.

On the other hand, thermal reactors have a highly nonuniform distribution (called the spatial self-shielding effect) of neutron flux in a fuel assembly as thermal neutron flux rises in the moderator region or steeply falls in the fuel and absorber as shown in Fig. 3.9. Moreover, control rod guide tubes or water rods are situated within fuel assemblies, and differently enriched fuels or burnable poison (Gd_2O_3) fuels are loaded. In such a lattice calculation, therefore, it is necessary to make an appropriate spatial division in the input data predicting spatial distribution of thermal neutron flux and its changes with burnup.

In lattice calculation codes, effective microscopic cross sections are first prepared from fine-group infinite dilution cross sections based on input data such as material compositions, dimensions, temperatures, and so on. The effective cross sections are provided in solving Eqs. 3.8 and 3.9 by the use of the collision probability method, etc., and then multi-group neutron spectra are obtained in each divided region (neutron spectrum calculation).

3.3 An Introduction to Neutron Transport Equation

Now we turn our attention to the original subject of this chapter and to the central issue of nuclear reactor theory, including the determination of the neutron distribution in the reactor as well as the rate at which various nuclear reactions take place within the core of the reactor. In that case, one needs then to understand the fundamental of *neutron transport equation* as indicated in this section of the chapter. This way we are able to investigate the process and the motion of the neutrons as they stream about the reactor core and frequently scatter off atomic nuclei, eventually either being absorbed or leaked out of the reactor. Considering that neutrons have tendency of diffusion behavior from regions of high to low temperature, analogous to gas of molecules would diffuse through another to reduce spatial variations in concentration. However, in the case of neutrons, they have the tendency of traveling or streaming a large distance between interactions, which is typically called the *mean free path* (MFP), as characterized by the path of fast neutrons on order of centimeters. This is where the dimensions characterizing changes in reactor core composition comparable to a neutron MFP, knowing that a reactor fuel pin or rod is typically about 1 cm in diameter. Ultimately our goal is to determine the

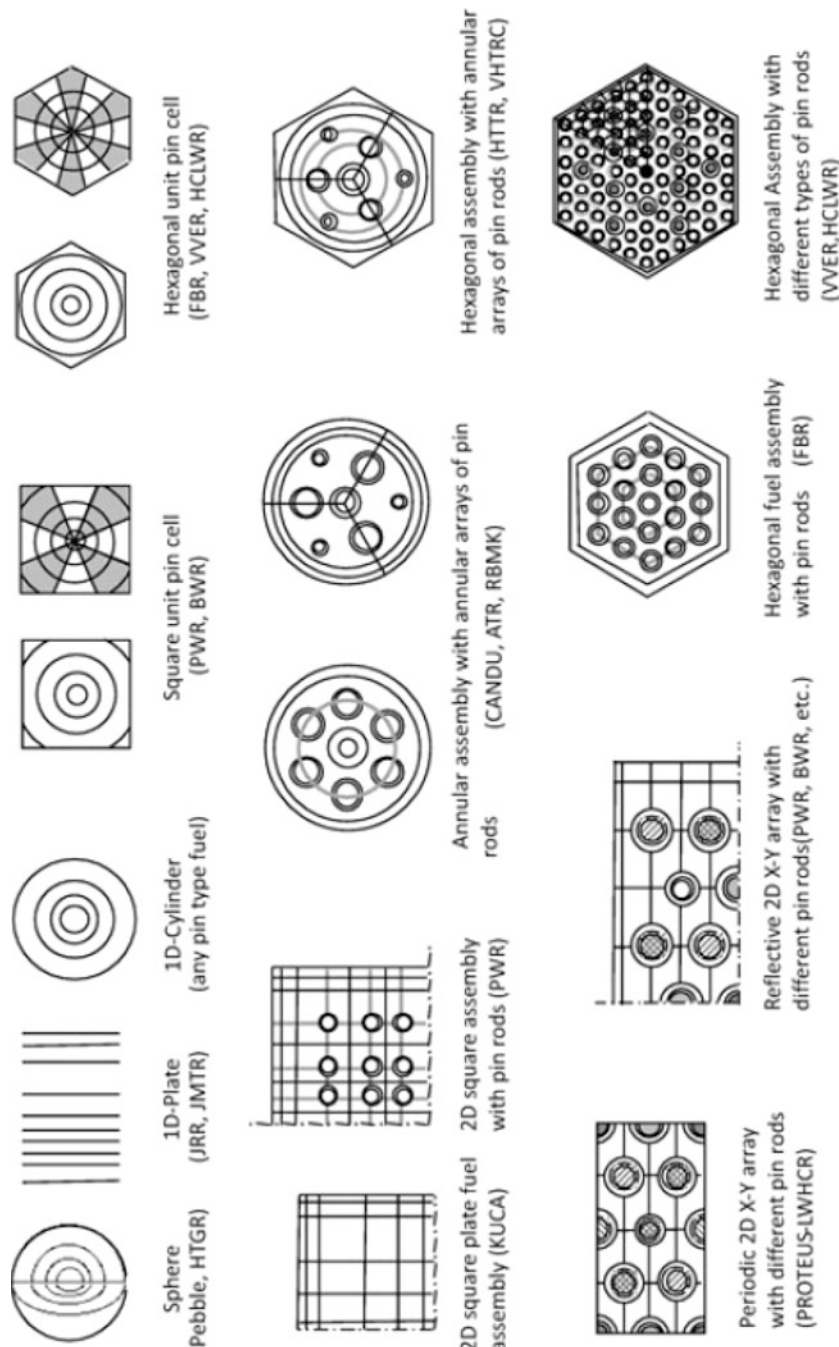


Fig. 3.9 Lattice models of SRAC [3]

distribution of neutrons in a nuclear reactor core, which also requires understanding of the neutron motion about the core and neutron interactions with nuclei in the core.

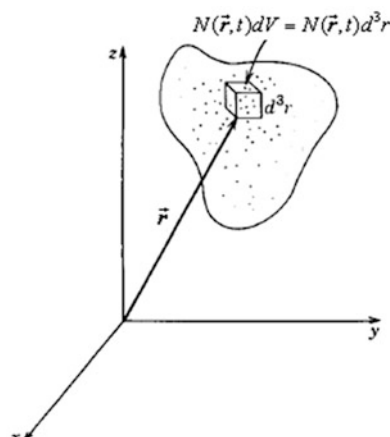
The most fundamental equation in the study of neutron interactions and migration in any media is the neutron transport equation. This equation has as its solution the time-dependent distribution function for neutrons in configuration-velocity (phase) space. Knowledge of this distribution function is sufficient to solve almost all problems of interest in the reactor theory. However, most of the time one does not need to know the distribution function itself; the integrals over some of the phase-space coordinates such as velocity direction, energy, or position are usually sufficient.

We consider a brief derivation of the transport equation to show that it is just a balance relation. One can give a more elaborate derivation than what we do here, including a quantum mechanical formulation, but we believe this is not necessary for the basic understanding of the physical content of the equation. To start with, statistically speaking, we define the number density at any point \vec{r} in the reactor core as follows using Fig. 3.10 which depicts the neutron density $N(\vec{r}, t)$:

$$\left[N(\vec{r}, \vec{v}, t) d^3 r \right] \vec{v} = N(\vec{r}, \vec{v}, t) d^3 r d^3 v \equiv \begin{cases} \text{expected number of neutrons in } d^3 r \\ \text{about } \vec{r}, \text{ with velocities in } d^3 v \\ \text{about } \vec{v} \text{ at time } t \end{cases} \quad (3.10)$$

Note that the vector variable \vec{v} for velocity has been used and it is often more convenient to use the scalar variable for neutron energies E where we will be able to further analyze the reaction rate density $F(\vec{r}, E, t)$. This is taking place in both space and energy for a given neutron nuclear reaction in terms of macroscopic cross section characterizing that reaction Σ_f and the neutron speed v to further define the

Fig. 3.10 The neutron density $N(\vec{r}, t)$



neutron flux $\phi(\vec{r}, \vec{\Omega}, E, t)$ in the same domain. This also leads to vector solid angle $\vec{\Omega}$, so that vector velocity \vec{v} of neutron can be presented as $\vec{v} = (v_x, v_y, v_z) \rightarrow (v, \theta, \phi) \rightarrow (E, \theta, \phi)$. Correspondingly, $d^3v = v^2 dv d\Omega$, with $d\Omega = \sin \theta d\theta d\phi$.

As one notices, the word “expected” has been applied to Eq. 3.10. This is simply because the definition of this equation on the right-hand side (RHS) indicates that it falls into the statistical theory concept in which only mean or average values for neutron density can be calculated when we deal with masses as small as neutron at the velocity \vec{v} and volume dV that we are calculating the neutron density. In reality one is able to measure through series of events where such measurements are fluctuating around the mean values. By measuring the neutron density $N(\vec{r}, \vec{v}, t)$ or calculating it, we are able to analyze the *rate* at which nuclear reactions are taking place at any point in the space core of the reactor.

Now recall from the above that the frequency of neutron encountering a given neutron nuclear reaction in terms of the macroscopic cross section and neutron speed can be expressed as:

$$v \sum_f = \text{Interaction frequency} \quad (3.11)$$

Thus the reaction rate density $F(\vec{r}, t)$ at any point in the system space in the absence of energy can be defined by merely multiplying the neutron density $N(\vec{r}, t)$ with no energy involved by the interaction frequency of Eq. 3.11, using Fig. 3.10 again, as:

$$F(\vec{r}, t) d^3r \equiv v \sum_f N(\vec{r}, t) d^3r \equiv \begin{cases} \text{expected rate at which} \\ \text{interactions are occurring} \\ \text{in } d^3r \text{ about } \vec{r} \text{ at time } t \end{cases} \quad (3.12)$$

This concept easily can be extended to the case in which the neutron density is different for various neutron energies E by defining Eq. 3.11 in new form as:

$$N(\vec{r}, E, t) d^3r d^3v \equiv \begin{cases} \text{expected number of neutrons in } d^3r \\ \text{about } \vec{r}, \text{ energies in } dE \text{ about } E \\ \text{at time } t \end{cases} \quad (3.13)$$

And again note here that neutron density is expressed as function of space and energy as well as time and we can generalize this concept of reaction rate density to include energy dependency as we showed in the form of $F(\vec{r}, E, t)$; thus, we can establish Eq. 3.14 by utilizing Eq. 3.12 and write it as:

$$F(\vec{r}, E, t) d^3r dE = v \sum_f N(\vec{r}, E, t) d^3r dE \quad (3.14)$$

The product of $vN(\vec{r}, dE, t)$ in terms of generalizing neutron of various energies that is shown in Eqs. 3.12 and 3.14 takes place more often in reactor theory analysis, and therefore it can be assigned a special name as *neutron flux* and in terms of energy can be defined as:

$$\phi(\vec{r}, E, t) \equiv vN(\vec{r}, E, t) \equiv \text{Neutron flux} \quad (3.15)$$

and in the absence of energy is written as:

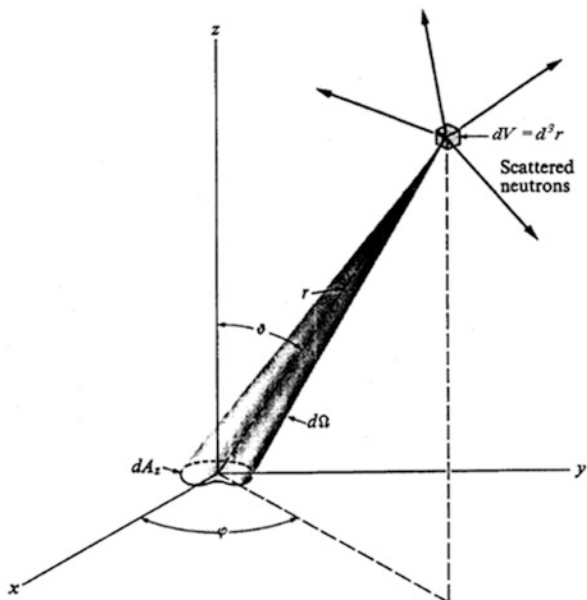
$$\phi(\vec{r}, t) \equiv vN(\vec{r}, t) \equiv \text{Neutron flux (cm}^2/\text{s}) \quad (3.16)$$

which will prove to be very convenient to work with either form of neutron flux $\phi(\vec{r}, E, t)$ for further analysis in reactor theory rather than neutron density $N(\vec{r}, E, t)$.

If we now take the solid angle $\vec{\Omega}$ into consideration and establish Fig. 3.11 below for driving Fick's law later on, then Eq. 3.13 can have a new form generalization as:

$$N(\vec{r}, \vec{v}, t) d^3 r d^3 v \equiv N(\vec{r}, E, \vec{\Omega}, t) d^3 r dE d\vec{\Omega} = \left| \begin{array}{l} \text{expected number of neutrons in } d^3 r \\ \text{about } \vec{r}, \text{ with energies in } dE \text{ about } E \\ \text{and going in direction in } d\vec{\Omega} \\ \text{about } \vec{\Omega} \text{ at time } t \end{array} \right. \quad (3.17)$$

Fig. 3.11 Schematic for deriving Fick's law



Consider a subsystem of volume V and surface S . Suppose we want to calculate the change in the number of neutrons in V with energies in dE about E and direction in $d\Omega$ about $\vec{\Omega}$ during a time interval Δt . This is given by:

$$\int_V N(\vec{r}, E, \vec{\Omega}, t + \Delta t) - N(\vec{r}, E, \vec{\Omega}, t) d^3 r dE d\Omega = \text{Gains} - \text{Losses} \quad (3.18)$$

There are two contributions to gains as follows:

1. *Fission and external source*

$$\frac{v\chi(E)dE d\Omega}{4\pi} \iiint_{V, E', \vec{\Omega}} \Sigma_f(E') \phi(\vec{r}, \vec{\Omega}', E', t) dE' d\Omega' d^3 r \Delta t + \int_V S(\vec{r}, E, \vec{\Omega}, t) d^3 r dE d\Omega \Delta t \quad (3.19)$$

where $\chi(E)$ is the fission spectrum as is defined before, $\phi(\vec{r}, E, \vec{\Omega}, t) \equiv vN(\vec{r}, E, \vec{\Omega}, t)$ is the *neutron flux*, and S is the external source distribution.

2. *Scattering*

$$\iiint_{V, E', \vec{\Omega}'} \Sigma_s(E') \phi(\vec{r}, \vec{\Omega}', E', r) dE' d\Omega' d^3 r \Delta t F(E' \vec{\Omega}' \rightarrow E \vec{\Omega}) dE d\Omega \quad (3.20)$$

where $F(E' \vec{\Omega}' \rightarrow E \vec{\Omega})$ is the conditional probability that is given to a neutron scattered at $(E' \vec{\Omega}')$, its energy will be in dE about E , and its direction will be in $d\Omega$ about $\vec{\Omega}$.

For losses, there are also two terms, one for collisions and other convective flow.

3. *Collisions*

$$\int_V \Sigma_t(E) S(\vec{r}, E, \vec{\Omega}, t) d^3 r dE d\Omega \Delta t \quad (3.21)$$

4. *Net flow outward*

$$\int_S \vec{\Omega} \cdot \hat{n} N(\vec{r}, E, \vec{\Omega}, t) ds dE d\Omega \Delta t = \int_V \vec{\Omega} \cdot \nabla \phi(\vec{r}, E, \vec{\Omega}, t) d^3 r ds dE d\Omega \Delta t \quad (3.22)$$

where $\hat{\vec{N}}$ is the outward normal at \vec{r} , and the divergence theorem $\int_S d\vec{s} \cdot \vec{F} = \int_V (\nabla \cdot \vec{F}) d^3r$ has been applied. Putting together the gains and losses, dividing by Δt , and taking the limit of $\Delta t \rightarrow 0$, we can write the balance Eq. 3.18 as $\int_V [] = 0$. Since volume V can be any arbitrary part of the system, the integral $\int_V []$ must vanish identically if the integral is to vanish for any V . Thus, we can write the following relationship:

$$\begin{aligned} \frac{\partial N(\vec{r}, E, \vec{\Omega}, t)}{\partial t} &= \frac{v\chi(E)}{4\pi} \int_{E', \vec{\Omega}} dE d\Omega' \Sigma_f(E') \phi(\vec{r}, E, \vec{\Omega}, t) + S(\vec{r}, E, \vec{\Omega}, t) \\ &+ \int_{E', \vec{\Omega}} dE' d\Omega' \Sigma_s(E') \phi(\vec{r}, E', \vec{\Omega}', t) F(E' \vec{\Omega}' \rightarrow E \vec{\Omega}) \\ &+ \Sigma_t(E) \phi(\vec{r}, E, \vec{\Omega}, t) - \vec{\Omega} \cdot \nabla \phi(\vec{r}, E, \vec{\Omega}, t) \end{aligned} \quad (3.23)$$

Equation 3.23 is what is known as the neutron transport equation for a homogeneous medium. For a heterogeneous system, we simply let $\Sigma(E) \rightarrow \Sigma(\vec{r}, E)$. Notice that this is a *linear* equation because we have ignored the neutron-neutron interaction (the mean free path for such events is 10^8 cm or greater). Sometimes the neutron transport equation is also called the Boltzmann equation; one should be careful when using this terminology since the Boltzmann equation in kinetic theory of gases treats explicitly the collisions among the particles and is in general *nonlinear*.

The transport equation is an integrodifferential equation in seven variables. While it is much too complicated for us to attempt any kind of solution directly, either as a boundary value or initial value problem, all the equations in the reactor theory that we will encounter can be derived from the transport equation in one approximation or another.

3.4 Neutron Current Density Concept in General

The term current has been used to denote a stream of particles flowing in a certain direction; it frequently appears in discussions of scattering of a particle beam or some kind of transport process. To be precise, one should begin with the definition in terms of the neutron flux $\phi(\vec{r}, E, \vec{\Omega}, t)$, which, as we have just seen, is the solution to the neutron transport equation, which we will be discussing in the next section. Since the current and the flux have the same dimensions, what then are the differences between these two quantities? Let:

$$\begin{aligned} \vec{J}(\vec{r}, E, t) &\equiv \int_{\vec{\Omega}} \vec{\Omega} \phi(\vec{r}, E, \vec{\Omega}, t) d\Omega \\ &= \int_{\vec{\Omega}} v N(\vec{r}, E, \vec{\Omega}, t) d\Omega \end{aligned} \quad (3.24)$$

If we recall the meaning of a particle flux from previous section as:

$$vN(\vec{r}, E, \vec{\Omega}, t) dEd\Omega\Delta t dA \cos \theta = \begin{cases} \text{expected number in } dE \text{ about } E \text{ and } d\Omega \\ \text{about } \vec{\Omega} \text{ crossing } dA \text{ during } \Delta t \end{cases} \quad (3.25)$$

Let:

$$\begin{aligned} J_+(\vec{r}, E, t) dEdA\Delta t &= \text{expected number in } dE \text{ about } E \text{ crossing } dA \text{ during } \Delta t \\ &\quad \text{from ' - ' to ' + ' in the sense of a normal vector } \hat{n} \\ &= \int_{\hat{n}, \vec{\Omega} > 0} \hat{n} \cdot \vec{\Omega} \phi(\vec{r}, E, \vec{\Omega}, t) dEd\Omega\Delta t dA \end{aligned} \quad (3.26)$$

or

$$J_+(\vec{r}, E, t) = \int_{\hat{n}, \vec{\Omega} > 0} \hat{n} \cdot \vec{\Omega} \phi(\vec{r}, E, \vec{\Omega}, t) d\Omega \quad (3.27)$$

Similarly, those going in the opposite direction become as:

$$J_-(\vec{r}, E, t) = \int_{\hat{n}, \vec{\Omega} < 0} (-\hat{n} \cdot \vec{\Omega}) \phi(\vec{r}, E, \vec{\Omega}, t) d\Omega \quad (3.28)$$

We can define the vector $\vec{J}(\vec{r}, E, t)$ such that:

$$\hat{n} \cdot \vec{J}(\vec{r}, E, t) = J_+(\vec{r}, E, t) - J_-(\vec{r}, E, t) = \hat{n} \cdot \int_{\vec{\Omega}} \vec{\Omega} \phi(\vec{r}, E, \vec{\Omega}, t) d\Omega \quad (3.29)$$

As one can see, Eq. 3.29 is consistent with Eq. 3.24 and allows us to arrive at the interpretation.

$$\begin{aligned} \hat{n} \cdot \vec{J}(\vec{r}, E, t) dEdA\Delta t &= \text{net number neutron in } dE \text{ about } E \text{ crossing } dA \text{ during } \Delta t \\ &\quad \text{from ' - ' to ' + ' during } \Delta t \end{aligned} \quad (3.30)$$

The difference between $\hat{n} \cdot \vec{J}$ and J_+ lies in the word *net*.

3.5 Neutron Current Density and Fick's Law

In order to have better understanding of the nuclear reactor theory filed, one should deal with the general and very complicated problem of neutron transport in it. In order to do that for the first step, we can show that the neutron flux ϕ and current \vec{J} are associated with each other in a simple manner if certain conditions could be met.

When such conditions are established, then it is possible to obtain very elementary solutions to neutron transport problem, and this where we lay the ground in order to be able to deal with this complicated problem.

Fick's law is establishing the relationship between neutron flux ϕ and current \vec{J} , which is known for very many years and is used in order to describe diffusion phenomena in fluid dynamics of liquid and gas analysis. Similarly in reactor theory, Fick's law leads to understand what is known as the *diffusion approximation*, which will be the subject of our discussion in the next few following sections of this chapter.

However in order to be able to derive and apply Fick's law in reactor theory simple number of simplifications assumptions need to take place, where the neutron current density at any point in core of reactor or medium where the neutrons do exist. For that matter at minimum, the following assumption will be made as:

1. We assume that the medium is finite and uniform; thus all the cross sections are constants and independent of position.
2. There exist no neutron sources in the medium.
3. In *laboratory coordinate system*, the neutron scattering is isotropic.
4. The neutron flux is a function of time and yet slowly varying function of position.

For us to continue with the derivation of Fick's law, it would be possible to relax certain of these above restrictions in the future discussion. We start our computation of the current density vector \vec{J} at the center of the laboratory coordinate system as it was shown in Fig. 3.11, where we can identify the three components of current density vector as J_x , J_y , and J_z , so we are able to evaluate them as well. To begin with we take component of J_x into consideration where the neutron current flow rate through cross-sectional area dA_z laying in the xy -plane at the origin can be evaluated. For this matter based on our above assumptions, it is very clear that there are no neutron sources that are present in the medium and then every neutron which passes through dA_z has just arrived from scattering collisions event and as result the neutrons flow downstream through dA_z above the xy -plane and they flow upstream through dA_z from these collisions below the xy -plane.

Before we go on with our further discussion of the problem in hand, consider the following statement in the following box.

Note that:

The central problem of reactor physics can be stated quite simply. It is to compute, for any time t , the characteristics of the free-neutron population throughout an extended region of space containing an arbitrary, but known, mixture of materials. Specifically we wish to know the number of neutrons in any infinitesimal volume dV that have kinetic energies between E and $E+\Delta E$ and are traveling in directions within an infinitesimal solid angle of a fixed direction specified by the unit vector $\vec{\Omega}$.

Considering Fig. 3.11 and volume element dV located at the point \vec{r} and the number of scattering collisions per second that take place in it can be presented as $\sum_s \phi(\vec{r})$, where \sum_s is the macroscopic scattering cross section and $\phi(\vec{r})$ is the neutron flux at point \vec{r} , then scattering in this case is assumed to be isotropic in the laboratory coordinate system that we assumed at the beginning. However, the fraction of these neutrons that are scattered in the direction of surface element dA_z in xy -plane is just the fraction of the total solid angle $\vec{\Omega}$ subtended by surface element dA_z at volume element dV , and from the definition of solid angle, one can write the following equation for this fraction as:

$$\text{Fraction of neutrons occupied in solid angle } \vec{\Omega} = \frac{dA_z \cos \theta}{4\pi r^2} \quad (3.31)$$

From this equation then, the number of neutrons scattered per second in volume element dV which is headed toward surface element dA_z is then demonstrated by the following relationship as:

$$\frac{\Sigma_s \phi(\vec{r}) \cos \theta dA_z dV}{4\pi r^2} \quad (3.32)$$

Not all of these neutrons reach the surface element dA_z ; some are scattered or absorbed in the process, and the number of which that do reach dA_z per second is expressed as:

$$\frac{e^{-\Sigma_t r} \Sigma_s \phi(\vec{r}) \cos \theta dA_z dV}{4\pi r^2} \quad (3.33)$$

where Σ_t is the macroscopic total cross section of the medium. For convenience, we take into consideration the contributions of current neutrons of J_z separately, which are passing downward through dA_z , and those which pass upward through the same surface element as well. With volume element dV written in spherical coordinates and using Fig. 3.11 as $dV = r^2 \sin \theta dr d\theta d\phi$, the total number of neutrons which flow downward through dA_z per second is written as:

$$\frac{\Sigma_s dA_z}{4\pi} \int_{\phi=0}^{2\pi} \int_{\theta=0}^{\pi/2} \int_{r=0}^{\infty} e^{-\Sigma_t r} \phi(\vec{r}) \cos \theta \sin \theta dr d\theta d\phi \quad (3.34)$$

Now if take under the consideration the number of neutrons passing per second in the negative direction of z coordinate through a unit area and denote it with J_z^- , which is just Eq. 3.34 divided by surface element dA_z , then we get the following mathematical form as:

$$J_z^- = \frac{\Sigma_s}{4\pi} \int_{\phi=0}^{2\pi} \int_{\theta=0}^{\pi/2} \int_{r=0}^{\infty} e^{-\Sigma_t r} \phi(\vec{r}) \cos \theta \sin \theta dr d\theta d\phi \quad (3.35)$$

Since the flux $\phi(\vec{r})$ is an unknown function of Eq. 3.35, therefore the integral in that equation cannot be evaluated as it stands in the above form. In order to perform this integral, we fall on our assumption that this flux varies slowly with position as we expressed before as part of our assumption above. Thus we can use Taylor's series properties, and we expand $\phi(\vec{r})$ in the following form as:

$$\phi(\vec{r}) = \phi_0 + x \left(\frac{\partial \phi}{\partial x} \right)_0 + y \left(\frac{\partial \phi}{\partial y} \right)_0 + z \left(\frac{\partial \phi}{\partial z} \right)_0 + \dots, \quad (3.36)$$

In Eq. 3.35 the subscript zero is an indication of that ϕ , and its derivatives are going to be evaluated at the origin. However considering the spherical coordinate and writing the component of x , y , and z in that coordinate, we have:

$$x = r \sin \vartheta \cos \varphi \quad y = r \sin \vartheta \sin \varphi \quad z = r \cos \vartheta$$

Now by inserting Eq. 3.36 into Eq. 3.35, it can easily be found that the terms containing $\cos \varphi$ and $\sin \varphi$ immediately integrate to zero; hence, the J_z^- reduces to the following form:

$$J_z^- = \frac{\Sigma_s}{4\pi} \int_{\varphi=0}^{2\pi} \int_{\vartheta=0}^{\pi/2} \int_{r=0}^{\infty} e^{-\Sigma_t r} \left[\phi_0 + \left(\frac{\partial \phi}{\partial z} \right)_0 r \cos \vartheta \right] \cos \vartheta \sin \vartheta dr d\vartheta d\varphi \quad (3.37)$$

Where the evaluation of integral in Eq. 3.37 results in J_z^- to be as:

$$J_z^- = \frac{\Sigma_s \phi_0}{4\Sigma_t} + \frac{\Sigma_s}{6\Sigma_t^2} \left(\frac{\partial \phi}{\partial z} \right)_0 \quad (3.38)$$

Similarly we can evaluate the J_z^+ , which is the number of neutrons moving per second in the positive z -direction through a unit area in the xy -plane as:

$$J_z^+ = \frac{\Sigma_s \phi_0}{4\Sigma_t} + \frac{\Sigma_s}{6\Sigma_t^2} \left(\frac{\partial \phi}{\partial z} \right)_0 \quad (3.39)$$

Then the z -component of current density \vec{J} which refers to the *net flow* of neutrons per unit area can be expressed as:

$$\begin{aligned} J_z &= J_z^+ - J_z^- = \left\{ \frac{\Sigma_s \phi_0}{4\Sigma_t} - \frac{\Sigma_s}{6\Sigma_t^2} \left(\frac{\partial \phi}{\partial z} \right)_0 \right\} - \left\{ \frac{\Sigma_s \phi_0}{4\Sigma_t} - \frac{\Sigma_s}{6\Sigma_t^2} \left(\frac{\partial \phi}{\partial z} \right)_0 \right\} \\ &= -\frac{\Sigma_s}{3\Sigma_t^2} \left(\frac{\partial \phi}{\partial z} \right)_0 \end{aligned} \quad (3.40)$$

We performed the above analysis for the z -component of current density vector \vec{J} , and since the orientation of the coordinate system is purely arbitrary, thus the other components \vec{J} in both x and y directions can be analyzed the same way, and the results are as follows:

$$J_x = -\frac{\Sigma_s}{3\Sigma_t^2} \left(\frac{\partial \phi}{\partial x} \right)_0 \quad (3.41)$$

and

$$J_y = -\frac{\Sigma_s}{3\Sigma_t^2} \left(\frac{\partial \phi}{\partial y} \right)_0 \quad (3.42)$$

Based on Eqs. 3.40, 3.41, and 3.42, the current density vector \vec{J} is now written as:

$$\begin{aligned} \vec{J} &= J_x \hat{i} + J_y \hat{j} + J_z \hat{k} = -\frac{\Sigma_s}{3\Sigma_t^2} \left[\left(\frac{\partial \phi}{\partial x} \right)_0 \hat{i} + \left(\frac{\partial \phi}{\partial y} \right)_0 \hat{j} + \left(\frac{\partial \phi}{\partial z} \right)_0 \hat{k} \right] \\ &= -\frac{\Sigma_s}{3\Sigma_t^2} \text{grad}\phi \end{aligned}$$

or in a final form is given as:

$$\vec{J} = -\frac{\Sigma_s}{3\Sigma_t^2} \text{grad}\phi = D \text{grad}\phi \quad (3.43)$$

As we note the subscript of zero has been dropped in Eq. 3.43 since the location of the origin of coordinates in this derivation is also arbitrary, so this indicates that Eq. 3.43 is valid at any point in the medium where the initial assumption at the beginning of this discussion is a valid one as well.

Equation 3.43 is known as Fick's law, which states that *the current density vector \vec{J} is proportional to the negative gradient of the flux $\phi(\vec{r})$* . The proportionality constant $D = \Sigma_s/3\Sigma_t^2$ is called the *diffusion constant* and is as you can see denoted by the symbol D , and this final form of Fick's law is becoming as:

$$\vec{J} = -D \text{grad}\phi \quad (3.44)$$

3.6 Problem Classification and Neutron Distribution

To understand this problem better, we classify the neutron distribution as function of seven variables, where three of these variables are associated with neutron position \vec{r} at any point in space of medium, while the other three variables are representing

the velocity of neutron in a three-dimensional space, and finally the last variable can either count for neutron energy. We can consider one for energy and two for direction of travel in laboratory coordinate system as it was described under Fick's law assumption in the previous section, and last but not least, statistically speaking time is playing as another variable in neutron distribution if we want to be more accurate.

One can define several reduced distributions by integrating out one or more of the variables or by setting a variable such as the energy at a particular value. By doing this we can break down the transport problem into several simpler problems such as:

1. Neutron slowing down
2. Neutron diffusion
3. Neutron thermalization and one-speed neutron transport

Each then can be studied separately with further simplifying approximations. Not only does each problem have physical interest by itself, but also the problems can be combined to give understanding of the essence of neutron transport phenomena.

For steady-state problems, one simply postulates that the neutron distribution and the external source are both time-independent. The left-hand side of Eq. 3.23 vanishes; what is left is the time-independent neutron transport equation. Two kinds of problems can be investigated, one with an external source and the other without. The former corresponds to a subcritical reactor system since a source is needed to maintain a steady-state neutron density. The latter describes a critical reactor, a system in which one can have steady-state neutron density in the absence of a source.

Suppose one is not interested in the neutron direction of travel, then in that case Eq. 3.23 can be integrated over $\vec{\Omega}$. In steady state and in the absence of a source, this gives:

$$\begin{aligned} -\nabla \cdot \vec{\mathbf{J}}(\vec{\mathbf{r}}, E) + \int dE' \Sigma_s(E') \phi(\vec{\mathbf{r}}, E) F(E' \rightarrow E) + v\chi(E) \int dE \Sigma_f(E') \phi(\vec{\mathbf{r}}, E') \\ -\Sigma_t(E) \phi(\vec{\mathbf{r}}, E) = 0 \end{aligned} \quad (3.45)$$

where we have used Eq. 3.24. The equation describes the distribution of neutrons in configuration space and energy. It is not a closed equation in that it involves two unknown quantities, the neutron flux and the net current. To take another step in simplification, one commonly makes the approximation that the current is related to the flux by Fick's law of diffusion, which was proven as presented in Eq. 3.44:

$$\vec{\mathbf{J}} = -D \vec{\nabla} \phi$$

which then leads to the diffusion equation for a multiplying system in steady state:

$$\begin{aligned} [D\nabla^2 - \Sigma_t]\phi(\vec{r}, E) + v\chi(E) \int dE' \Sigma_f(E') \phi(\vec{r}, E') \\ + \int dE' \Sigma_s(E') \phi(\vec{r}, E') F(E' \rightarrow E) = 0 \end{aligned} \quad (3.46)$$

This is the energy-dependent diffusion equation, and still it is not the simplest diffusion equation that one can solve, since this equation also treats the process of neutron energy moderation where neutron slowing down and further reductions can be considered.

At this stage, one can go in two directions of simplification. One is to get rid of the energy dependence by integrating over E . The result is then the problem of neutron diffusion:

$$\vec{D} \nabla^2 \vec{\phi}(\vec{r}) + [v\bar{\Sigma}_f - \bar{\Sigma}_a] \vec{\phi}(\vec{r}) = 0 \quad (3.47)$$

where we are using the overhead bar that denotes two kinds of energy-integrated quantities, an effective flux-averaged cross section and the integrated flux:

$$\bar{\Sigma} = \frac{\int dE \Sigma(E) \phi(\vec{r}, E)}{\int dE \phi(\vec{r}, E)} \quad \text{and} \quad \vec{\phi}(\vec{r}) = \int \phi(\vec{r}, E) dE \quad (3.48)$$

This is the starting point for the discussion of neutron diffusion. For simplicity we will not bother to write out explicitly the overhead bar, but the origin of Eq. 3.47 should be kept in mind. We will return later on to consider the different solutions to this equation, including the treatment of boundary conditions. Notice that Eq. 3.47 is still a balance relation – the difference between what flows into and out of a volume element whereby diffusion is balanced by the difference between production and absorption in the volume element dV . The other simplification of Eq. 3.46 is to get rid of the spatial dependence by integrating over the volume of the system. The first term in Eq. 3.46 then vanishes because the integral gives:

$$\int_V D \nabla^2 \phi(\vec{r}, E) d^3r = -D \int_V \nabla \cdot \vec{J}(\vec{r}, E) d^3r = -D \int_V \vec{J}(\vec{r}, E) \cdot d\vec{S} \quad (3.49)$$

which is proportional to the current integrated over the surface of the system. The latter is taken to be zero for large or infinite systems. The remaining terms in Eq. 3.46 become:

$$[v\Sigma_f(E) - \Sigma_t(E)]\phi(E) + \int \Sigma_s(E') \phi(E') F(E' \rightarrow E) dE' = 0 \quad (3.50)$$

where we continue to use the same symbol for the spatially integrated flux:

$$\phi(E) = \int_V \phi(\vec{r}, E) d^3r \quad (3.51)$$

For further discussion of neutron slowing down, we can use Eq. 3.50 as the starting point, which is a balance in energy space – the loss of neutrons at energy E by all kinds of interactions, represented by \sum_t , is balanced by gains from neutrons produced directly from fission and neutrons which scatter into energy E from some other energy. We will analyze the various solution of Eq. 3.50 later on in this chapter.

In addition to Eqs. 3.47, 3.50 and two other equations can be derived from the transport equation, Eq. 3.23. Suppose we assume that all neutrons can have only energy, E_0 . This is tantamount to setting the following:

$$\phi(\vec{r}, E, \vec{\Omega}) = \phi(\vec{r}, \vec{\Omega}) \delta(E - E_0) \quad (3.52)$$

$$F(E' \vec{\Omega}' \rightarrow E, \vec{\Omega}) = F(\vec{\Omega}' \rightarrow \vec{\Omega}) \delta(E - E_0) \quad (3.53)$$

$$\chi(E) = \delta(E - E_0) \quad (3.54)$$

$$\Sigma(E) = \Sigma \quad \text{a constant} \quad (3.55)$$

Here $\delta(x)$ is the Dirac delta function – it is zero everywhere except at the point where its argument vanishes, and there its value is infinite. Note that the integral of the delta function is unity provided the point where it is infinite lies within the range of integration. Some properties of $\delta(x)$ are:

$$\int_{a-\delta}^{a+\delta} \delta(x - a) dx = 1 \quad \int_{a-\delta}^{a+\delta} f(x) \delta(x - a) dx = f(a) \quad (3.56)$$

$$\delta(x) = \delta(-x) \quad x\delta(x) = 0 \quad \delta(ax) = \frac{1}{a} \delta(x) \quad (3.57)$$

Inserting Eqs. 3.52 through 3.55 into Eq. 3.23 and integrating over E , we obtain:

$$\begin{aligned} [\Sigma_t + \vec{\Omega} \cdot \vec{\nabla}] \phi(\vec{r}, \vec{\Omega}) &= \frac{\nu \Sigma_f}{4\pi} \int_{\vec{\Omega}} \phi(\vec{r}, \vec{\Omega}) d\Omega + S(\vec{r}, \vec{\Omega}) \\ &+ \Sigma_s \int_{\vec{\Omega}} \phi(\vec{r}, \vec{\Omega}') d\Omega' F(\vec{\Omega}' \rightarrow \vec{\Omega}) \end{aligned} \quad (3.58)$$

This is the one-speed, time-independent transport equation. It can be simplified further if we restrict our attention to a slab system (system is infinite in two directions

and finite in the third, or x , direction). Let the angle between $\vec{\Omega}$ and the x -axis be the polar angle θ . Then:

$$\vec{\Omega} \cdot \vec{\nabla} \phi = \mu \frac{\partial \phi}{\partial x} + \sin \theta \cos \varphi \frac{\partial \phi}{\partial y} + \sin \theta \sin \varphi \frac{\partial \phi}{\partial z} \quad (3.59)$$

We then integrate over y and z and the azimuthal angle φ to obtain:

$$\left[\mu \frac{\partial}{\partial x} + \Sigma_t \right] \phi(x, \mu) = \frac{v \Sigma_f}{4\pi} \int_{-1}^1 d\mu' \phi(x, \mu') + \Sigma_s \int_{-1}^1 d\mu' \phi(x, \mu') F(\mu_0) + S(x, \mu) \quad (3.60)$$

where:

$$\phi(x, \mu) = \iint dy dz \int_0^{2\pi} \phi(xyz\mu\varphi) d\varphi \quad (3.61)$$

and $\mu = \cos \theta$, and we have put $F(\vec{\Omega}' \rightarrow \vec{\Omega}) = F(\vec{\Omega} \cdot \vec{\Omega}') \equiv F(\mu_0)/2\pi$. Equation 3.60 is the one-speed transport equation for a slab. It is the simplest transport equation which one can consider. It is however still as rigorous as the original transport equation since we have made *no approximations* in the reduction. Equation 3.60 can be solved in an infinite medium problem or in problems involving boundaries. These solutions are useful mainly for checking approximate solutions and also in cases where energy dependence is of no interest.

3.7 Neutron Slowing Down

We are at the point to tackle neutron slowing down subject before we go on with the rest of this chapter and the following sections. In order to understand this matter, we now turn our attention to the topic of neutron energy moderation, the slowing down of a fast neutron to the thermal energy region. The equation that describes the slowing down process, as we can expect by now, can be obtained by reducing the transport equation, Eq. 3.23 in Sect. 3.4. There are two simple ways to get rid of the spatial dependence of the flux. One is to integrate the transport equation over a large system and then take the system size to be infinite, thus we can write the following relationship as:

$$\phi(E) = \int \phi(\vec{r}, E) d^3 r \quad (3.62)$$

and

$$\int_s \vec{\nabla} \cdot \vec{J} d^3r = \int_s (\hat{n} \cdot \vec{J}) dS \rightarrow 0 \quad (3.63)$$

The other situation we need to pay attention and take under consideration is “point reactor” condition, defined as:

$$\phi(\vec{r}, E) = \phi(E) \delta(\vec{r}) \quad (3.64)$$

Here again we integrate over space along with invoking help from Fick’s law above to obtain the following result as:

$$\int_{-\infty}^{+\infty} \frac{\partial^2}{\partial x^2} \delta(x) dx = \frac{1}{2\pi} \int_{-\infty}^{+\infty} \frac{\partial^2}{\partial x^2} dx \int_{-\infty}^{+\infty} e^{ikx} dk = - \int_{-\infty}^{+\infty} k^2 \delta(k) dk = 0 \quad (3.65)$$

In either, we get the equivalent result in Eq. 3.50 as:

$$\Sigma_t(E) \phi(E) = S(E) + \int \Sigma_s(E') \phi(E') dE' F(E' \rightarrow E) \quad (3.66)$$

which is known as the slowing down equation for an infinite medium. In writing Eq. 3.66, we have combined the external source with the fission source in $S(E)$. Without specifying the scattering kernel F , an equation having the same form as Eq. 3.66 is also applicable to the thermal energy region, where upscattering of the neutron must be considered. In that case the energy balance problem would be called neutron thermalization, which will be the topic of a later lecture.

Further study of Eq. 3.65 reveals that using the energy transfer kernel, we have previously derived under the conditions of elastic scattering, target nucleus at rest, and isotropic scattering in center of mass coordinate system (CMCS) [4]. This kernel is perfectly valid in the slowing down region where the neutron loses energy every time it is scattered by the nucleus. Then we can recall the following relation as:

$$\begin{aligned} F(E' \rightarrow E) &= \frac{1}{E'(1-\alpha)} & \text{for } \alpha E' \leq E \leq E' \\ F(E' \rightarrow E) &= 0 & \text{otherwise} \end{aligned} \quad (3.67)$$

where $\alpha = (A - 1)^2/(A+1)^2$ and $A = M/m$.

Isotropic Source and Scattering [5]

Note that one major simplification that can be introduced into the neutron transport equation arises when one assumes both isotropic neutron sources as:

$$s(\vec{r}, \vec{\Omega}, t) = \frac{1}{4\pi} S(\vec{r}, t) \quad (1)$$

and isotropic scattering in laboratory frame system:

$$\Sigma_s(\vec{\Omega}' \rightarrow \vec{\Omega}) = \frac{1}{4\pi} \Sigma_s \quad (2)$$

The assumption of isotropic neutron source is usually not too restrictive since most sources such as fission are indeed essentially isotropic. Unfortunately although neutron scattering is usually isotropic in the center of mass (CM) system, it is far from isotropic in the laboratory system, particularly for low mass number scatters such as hydrogen. Undeterred by such physical considerations, we will assume for the moment that isotropic scattering is present. Then the one-speed transport equation simplifies still further to:

$$\frac{1}{v} \frac{\partial \phi}{\partial t} + \vec{\Omega} \cdot \nabla \phi + \Sigma_t(\vec{r}, \vec{\Omega}, t) = \frac{\Sigma_s}{4\pi} \int_{4x} d\vec{\Omega}' \phi(\vec{r}, \vec{\Omega}', t) + \frac{S(\vec{r}, t)}{4\pi} \quad (3)$$

However, even this equation is extremely difficult to solve in general.

Before discussing the solution of Eq. 3.66, we first consider the problem of estimating the escape probability $P(E' \rightarrow E)$ that a neutron, scattered at E' , will cross E , with no restriction on how large is the interval from E' to E and how many collisions are involved. Notice that $P(E' \rightarrow E)$ differs from $F(E' \rightarrow E)$ in that the latter is for one collision and is a distribution function in the variable E . (In contrast P is not a distribution function, although it is a probability.) The exercise of estimating $P(E' \rightarrow E)$ will also help to make clear this distinction. Since the energy range (E', E) is arbitrary, we divide this interval into a number of subintervals ΔE_j where $j = 1, \dots$, such that for each subinterval we can write:

$$\{p_a(\Delta E_j)\} = [\text{Average number collision required to cross}] \times [\text{probability absorp per cell}] \quad (3.68)$$

where $p_a(\Delta E_j)$ is the probability of neutron absorption while crossing ΔE_j . The second term in Eq. 3.68, which is the probability of absorption each time the neutron collides, is just:

$$[\text{Probability absorp per cell}] = \Sigma_a(\Delta E_j) = \Sigma_t(\Delta E_j) \quad (3.69)$$

Equation is an indication of the strategy we are following in making our estimate of P . To find the probability of no absorption while crossing the interval (E', E) , we write it as a product of probabilities, in a format as below:

$$P(E' \rightarrow E) = \prod_j [1 - p_a(\Delta E_j)] \quad (3.70)$$

where $p_a(\Delta E_j)$ is to be obtained according to Eqs. 3.68 and 3.69. The advantage of doing this is that once we have Eq. 3.70, we can rewrite it as follows:

$$\ln(P) = - \sum_{j=1, \dots} p_a(\Delta E_j) \rightarrow \int_E^{E'} p_a(E'') dE'' \quad (3.71)$$

using the logarithmic properties of $\ln(ab) = \ln(a) + \ln(b)$ and $\ln(1 - x) \approx -x$ for $x \ll 1$. Now we see that the condition on the subinterval division ΔE_j has to be chosen small enough to make $p_a(\Delta E_j)$ small compared to unity. Equation 3.71 means that the probability we are seeking is given by the expression:

$$P(E' \rightarrow E) = \exp\left(- \int_E^{E'} p_a(E'') dE''\right) \quad (3.72)$$

To turn equation 3.72 into an explicit expression, we can use Eqs. 3.68 and 3.69 to find $p_a(\Delta E_j)$, which means we need to make an estimate of the average number of collisions a neutron should make in going from energy E' to energy E .

As a simple way to estimate the number of collisions a neutron should make, on average, in crossing an energy interval, we need only the average energy that a neutron will lose in a collision at a given energy. Suppose the neutron collision occurs at energy E' and the neutron has energy E after the collision. The probability of such an event is just given by the energy transfer kernel $F(E' \rightarrow E)$. The energy the neutron would have, on average, after a collision at E' then becomes:

$$\bar{E} = \int E F(E' \rightarrow E) dE = (1 + \alpha)E'/2 \quad (3.73)$$

where we have used Eq. 3.67. The energy loss per collision is $E' - \bar{E} = (1 + \alpha)E'/2$. Thus the average number of collisions required to cross an interval ΔE is:

$$[\text{Average number collision required to cross}] = \frac{2}{1 - \alpha} \frac{\Delta E}{E} \quad (3.74)$$

With this result, we have an explicit expression for the escape probability $P(E' \rightarrow E)$ from Eq. 3.72, and then we can write the following relation as:

$$P(E' \rightarrow E) = \exp \left(-\frac{2}{1-\alpha} \int_E^{E'} \frac{\Sigma_a(E'')}{\Sigma_t(E'')} \frac{dE''}{E''} \right) \quad (3.75)$$

This expression contains the parameter α whose numerical value depends on the mass number of the target nucleus A. In the case of a hydrogenous medium, $A = 1$ and $\alpha = 0$.

Note that for a heavy target nucleus, $A \gg 1$, then $\alpha \approx 1 - (4/A)$, and the coefficient in front of the integral in Eq. 3.75 becomes $A/2$.

Before closing this discussion, we take the opportunity to introduce another energy-like quantity, called the lethargy, in the reactor physics literature;

$$u = \ln(E_0/E) \quad (3.76)$$

where E_0 is some constant energy. Notice that there is a one-to-one correspondence between energy and lethargy and the two variables move in opposite directions in that when the energy decreases the lethargy would increase. Given that we have just calculated the average energy loss per collision, it is perhaps not surprising that the corresponding average lethargy increase per collision turns out to be a rather useful quantity:

$$\langle \Delta u \rangle = \langle u - u' \rangle = \langle \ln(E'/E) \rangle = \int_{\alpha E'}^{E'} \ln(E'/E) F(E' \rightarrow E) dE = 1 + \frac{\alpha \ln \alpha}{1 - \alpha} \equiv \xi \quad (3.77)$$

In the two limits which are always of interest:

$$\begin{aligned} A = 1 & \quad \alpha = 1 & \xi = 1 \\ A \gg 1 & \quad \alpha \approx 1 & \xi = 2/(A + 2/3) \approx 2/A \end{aligned} \quad (3.78)$$

Now we can use Eq. 3.77 to estimate the average number of collisions to cross an interval ΔE and write the following relationship:

$$\begin{aligned} [\text{Number collisions required to cross } \Delta E] &= \frac{\ln(E) - \ln(E - \Delta E)}{\xi} = \frac{1}{\xi} \ln \left(\frac{E}{E - \Delta E} \right) \\ &= \frac{1}{\xi} \ln \left(1 + \frac{\Delta E}{E} \right) \approx \frac{1}{\xi} \frac{\Delta E}{E} \end{aligned} \quad (3.79)$$

Notice that if we insert the estimate as Eq. 3.79 into Eq. 3.68, we would arrive at the estimate for P as:

$$P(E' \rightarrow E) = \exp \left(- \int_E^{E'} \frac{\Sigma_a(E'')}{\Sigma_t(E'')} \frac{dE''}{\xi E''} \right) \quad (3.80)$$

which agrees with Eq. 3.75 in the case of heavy target nucleus, but not when $A = 1$. We conclude that when $A > 1$ one can use either Eq. 3.75 or 3.80, whereas for $A = 1$ our present discussion indicates that Eq. 3.75 should be preferred since it involves fewer approximations.

We now turn our attention to the solution of the slowing down equation, Eq. 10.5, for the special case of hydrogenous medium, $A = 1$, a monoenergetic source at E_0 , $S(E) = S_0\delta(E - E_0)$, and furthermore we neglect absorption. Equation 3.66 then reads the following form as:

$$\Sigma_s(E)\phi(E) = \frac{S_0}{E_0} + \int_E^{E_0} \Sigma_s(E')\phi(E') \frac{dE'}{E'} \quad (3.81)$$

This is a simple integral equation, which can be solved readily. Let $G(E) = \Sigma_s(E)\phi(E)$; Eq. 3.66 is then of the following form:

$$G(E) = \text{constant} + \int_E^{E_0} G(E') \frac{dE'}{E'} \quad (3.82)$$

Now differentiating both sides of Eq. 3.82 with respect to E gives the following:

$$\frac{dG(E)}{dE} = -\frac{G(E)}{E} \quad \text{Or} \quad \frac{dG}{G} = -\frac{dE}{E} \quad (3.83)$$

Therefore, we can write that:

$$G(E) = \frac{\text{cte}}{E} = \frac{c}{E} \quad (3.84)$$

where c is an integration constant. To find c , take the limit as E approaches E_0 in which case $G(E)$ should approach S_0 , thus $c = S_0$.

We have shown that in the energy region of neutron slowing down, the flux is given by the following relationship as:

$$\phi(E) = \frac{S_0}{\Sigma_s(E)E} \quad (3.85)$$

The $1/E$ behavior of the flux is very characteristic of the neutron distribution during energy moderation by elastic collisions with the target nuclei. Equation 3.85 has been obtained for the case of the hydrogenous medium. We can extend it to an arbitrary medium, $A > 1$, by writing in the same spirit as Eqs. 3.79 and 3.80, where for flux $\phi(E)$ we can write:

$$\phi(E) \simeq \frac{1}{\Sigma_s(E)\xi E} \quad (3.86)$$

In summary, we have obtained an expression for the probability that a neutron will undergo energy moderation by elastic scattering across an arbitrary interval in the form of Eq. 3.80, which involves the quantity ξ , the average lethargy increase per collision. We have also shown that the flux in the slowing down region, the region of energy below the fission spectrum and above thermal energy where neutrons can be upscattered, is $1/E$.

3.8 Neutron Diffusion Concept

To study neutron diffusion we go back to the neutron transport equation and obtain an equation only in the spatial variable. We first eliminate the $\vec{\Omega}$ dependence by integrating the transport equation over $\vec{\Omega}$, getting an equation with two unknowns:

$$\phi(\vec{r}, E, t) = \int \phi(\vec{r}, E, \vec{\Omega}, t) d\vec{\Omega} \quad (3.87)$$

$$\vec{J}(\vec{r}, E, t) = \int \phi(\vec{r}, E, \vec{\Omega}, t) \vec{\Omega} d\vec{\Omega} \quad (3.88)$$

Then we invoke Fick's law to eliminate \vec{J} , thus obtaining:

$$\begin{aligned} \frac{1}{v} \frac{\partial \phi(\vec{r}, E, t)}{\partial t} &= [D(E) \nabla^2 - \Sigma_t(E)] \phi(\vec{r}, E, t) + S(\vec{r}, E, t) \\ &+ vf(E) \int \Sigma_f(E') \phi(\vec{r}, E', t) dE' \\ &+ \int \Sigma_s(E') \phi(\vec{r}, E', t) dE' (E' \rightarrow E) \end{aligned} \quad (3.89)$$

To reduce further, we consider only steady-state solutions and integrate over all energy to arrive at following results as:

$$[\bar{D} \nabla^2 + (v \bar{\Sigma}_f - \bar{\Sigma}_a)] \phi(\vec{r}) = -S(\vec{r}) \quad (3.90)$$

where:

$$\phi(\vec{r}) = \int \phi(\vec{r}, E) dE \quad (3.91)$$

$$\bar{D} \equiv \frac{\int D(E) \phi(\vec{r}, E) dE}{\int \phi(\vec{r}, E) dE} \quad (3.92)$$

and a similar expression like Eq. 3.92 for the macroscopic cross section $\bar{\Sigma}$. The overhead denotes energy average weighed by the flux as indicated in Eq. 3.92 (recall also Eq. 3.48 as well). In writing Eq. 3.90, we have made use of the statement of neutron conservation as follows:

$$\int F(E' \rightarrow E) dE = 1 \quad (3.93)$$

We need to keep in mind that in Eq. 3.90, we are also assuming that the external source is time-independent and more significantly that D is independent of position, which would be the case if $\phi(\vec{r}, E)$ were separable in r and E (this is not true in general).

Equation 3.90 is a second-order differential equation with constant coefficients. Since the *Schrödinger equation*, in the case of constant potential, is also of this form, it is worthwhile to make note of the analogy between the problem of neutron diffusion and the problem of a particle confined in a potential well, particularly in the role of the boundary conditions.

To keep the notations simple, we will drop the overhead bar on the material constants with the understanding that they are to be regarded as energy-averaged quantities.

3.9 The One-Group Model and One-Dimensional Analysis

In the above at the beginning of this chapter, we talked and discussed about control rod in the reactor. When we insert the control rod in a reactor, it changes its multiplication factor in two possible ways, and further we pointed out that for many reactors, these two effects of a control rod, increases the absorption and increases leakage, are very important and play important roles in determining the impact of the rod upon the multiplication factor of system [1]. However, in summary, we took under consideration that the effectiveness of a control rod totally depends mainly upon the value of the ratio of the neutron flux of the location of the rod to the average neutron flux ϕ in the reactor. We also said that the control rod has maximum effect, which inserts the most negative reactivity, if it is placed in the reactor where the flux has maximum value. Now, we will further talk about the one-group model and the one-dimensional analysis of the problem in hand, so we can lay out the foundation for the diffusion theory and boundary conditions associated with it. To do so, we pay our attention to a simple reactor system as before and take the notion of criticality under consideration. In this case, we have a better understanding of what it means from the point of view of both physics and mathematics of the problem, and then we see how we can solve analytically the steady-state flux for simple geometries and present the numerical solution for steady state for a more arbitrary complex form of these geometries.

Therefore, we start our opening discussion with the time-dependent, one-speed model where we ignore the delay neutrons with *source distribution function* $S_f(\vec{r}, t)$, which is equal to the number of neutrons emitted per cm^3/s by sources at the point \vec{r} and the time t , along with its associated *fuel fusion cross section* $\Sigma_f(\vec{r})$. Thus, the diffusion equation in the following forms as:

$$S_f(\vec{r}, t) \Rightarrow v \Sigma_f(\vec{r}) \phi(\vec{r}, t) \quad (3.94)$$

$$\frac{1}{v} \frac{\partial}{\partial t} \phi(\vec{r}, t) = \nabla \cdot D(\vec{r}) \nabla \phi(\vec{r}, t) - \Sigma_a(\vec{r}) \phi(\vec{r}, t) + v \Sigma_f(\vec{r}) \phi(\vec{r}, t) \quad (3.95)$$

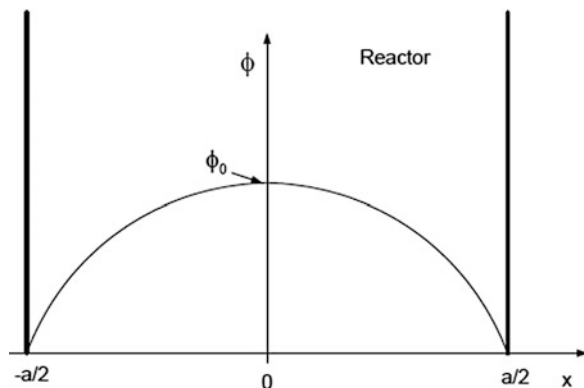
In the above relationships, the absorption term $\Sigma_a(\vec{r})$ is a local parameter that may vary in space, depending on the material at hand (moderator, structure, coolant, fuel, etc.), and the fuel fission cross section $\Sigma_f(\vec{r})$ is part of the fuel absorption cross section as:

$$\Sigma_a^{fuel}(\vec{r}) = \Sigma_\gamma^{fuel}(\vec{r}) + \Sigma_f^{fuel}(\vec{r}) \quad (3.96)$$

where $\Sigma_\gamma^{fuel}(\vec{r})$ is the neutron capture cross section for radiative capture reaction as it was defined previously [2].

Note that we also treat both $\Sigma_a^{fuel}(\vec{r})$ and $D(\vec{r})$ as constant over time since typically they do not vary substantially over the short time span that the flux can vary significantly in time. The details of the problem at hand will guide you. As an example of the above consideration, we look at a simple one-dimensional slab reactor as demonstrated in Fig. 3.12, a case that readily yields an analytical solution. The reactor is composed of a homogeneous mixture of fuel and moderator. The slab thickness is a centimeter. We assume the dimensions represent the extrapolated distances at which the flux goes to zero.

Fig. 3.12 A simple slab reactor



The steady-state equation for constant coefficients is:

$$D \frac{\partial^2 \phi(x)}{\partial x^2} + (-\Sigma_a + v\Sigma_f) \phi(x) = 0 \quad (3.97)$$

The solution to the one-dimensional partial differential equation will be of the form:

$$\phi(x) = \phi_0 \cos(Bx) \quad (3.98)$$

and for the flux to go to zero at the extrapolated boundaries, we must have:

$$B = \frac{\pi}{a} \quad (3.99)$$

Substituting Eq. 3.98 into Eq. 3.97 and after dropping the common $\phi_0 \cos(Bx)$ factor, we find that:

$$\begin{aligned} -DB^2 - \Sigma_a + v\Sigma_f &= 0 \quad \Rightarrow \quad DB^2 = v\Sigma_f - \Sigma_a \\ \text{and} \quad B_g^2 &= (\pi/a)^2 = \frac{v\Sigma_f - \Sigma_a}{D} = B_m^2 \end{aligned} \quad (3.100)$$

where the subscript g refers to the geometric buckling and the subscript m refers to the material buckling.

This Is the Criticality Condition

Referring back to Eq. 3.97 and using $\frac{v\Sigma_f - \Sigma_a}{D} = B^2$, we find that:

$$\frac{\partial^2 \phi(x)}{\partial x^2} + B^2 \phi(x) = 0 \quad (3.101)$$

As we can see, this form of equation that is used quite often and in three-dimensional form in Eq. 3.101 can be written as:

$$D \left(\frac{\partial^2 \phi}{\partial x^2} + \frac{\partial^2 \phi}{\partial y^2} + \frac{\partial^2 \phi}{\partial z^2} \right) + (-\Sigma_o + v\Sigma_f) \phi(x) = 0 \quad (3.102)$$

and the general solution to Eq. 3.102 is the form of the following relation as:

$$\phi(x) = \phi_0 \cos(B_x x) \cos(B_y y) \cos(B_z z) \quad (3.103)$$

which leads to the criticality condition as:

$$B_g^2 = B_x^2 + B_y^2 + B_z^2 = \left(\frac{\pi}{a}\right)^2 + \left(\frac{\pi}{b}\right)^2 + \left(\frac{\pi}{c}\right)^2 = \frac{v\Sigma_f - \Sigma_a}{D} = B_m^2 \quad (3.104)$$

where a , b , and c are the slab dimensions in the three directions. Note that the basic equality of geometric and material buckling holds even though the exact form of the equality is case dependent.

It is important to stop for a moment and reflect on what this means. This is a statement of the balance between neutron production by fission and neutron loss by leakage and absorption. A unique slab thickness ensures that the ratio of net production to loss (i.e., production/loss) is zero for the given material properties. Any other size will result in a net loss or gain of neutrons over time.

It is also important to realize that this critical size is the size that is *predicted* by the model. Reality will be something else. For the remainder of this section, we spend some of our effort to establish a way of solving the diffusion equation as we started at the beginning of this section as well as with subsections below. We also deal with boundary conditions related to the steady-state diffusion equation for simple slab geometry as we started as part of our opening discussion in this chapter. These include sections and then extend to more complex geometries and included the time variable with more sophisticated boundary conditions that handles both space and time as derivatives to diffusion theory and neutron diffusion equation.

3.9.1 Boundary Conditions for the Steady-State Diffusion Equation

As we have seen so far, the neutron diffusion equation is a type of partial diffusion equation that has derivatives in both space \vec{r} and time t . Since the steady-state diffusion equation is a *partial differential equation* (PDE) as function of space t only, then infinite numbers of solutions can be found for such form of PDEs, or basically there are infinite numbers of functions which satisfy the partial differential equation in hand, but in our case there is just *one* function that correctly represents the neutron flux given the boundary conditions corresponding to the problem of interest. These boundary conditions are restrictions that must be imposed on the solution of the problem or differential equation by nature of physical problem. In other words the boundary conditions cannot be imposed arbitrarily; however, it can be demonstrated that for each or every differential equation or partial differential equation, a corresponding set of boundary conditions will help to find a reasonable solution. For a typical Helmholtz scalar-type equation, the following can be stated as [6]:

On the boundaries of a region in which ϕ satisfies the differential equation, either ϕ , or the normal derivative of ϕ , or a linear combination of the two must be specified; both ϕ and its normal derivative cannot be specified independently.

Therefore for any imposing boundary conditions based on physical argument, the above definition or requirement must not and will not be violated under any circumstances, given the physical problem in hand. Now if we assume a boundary condition *at the surface* of the medium of the form:

$$\frac{1}{\phi} \frac{d\phi}{dn} = -\frac{1}{d} \quad (3.105)$$

where $d\phi/dn$ is the normal derivative of the neutron flux and d is a parameter known as the *reciprocal logarithm derivative* considering that Eq. 3.104 can be written as $d/dn(\ln\phi) = -1/d$ which is sometimes referred to as logarithmic boundary condition. Normally, these types of boundary conditions apply in reactor problems that are comparatively dense and essentially vacuous media [2].

In the above case, the exterior surface of a reactor represents a situation that the surrounding atmosphere is a vacuum in reality and the mean free path of neutrons in air is much larger than in nongaseous materials. It is usually possible to treat it as a vacuum in reactor analysis, and we have to bear in mind that as we mentioned before, the related diffusion theory is not valid near such a surface and it is required to for our further analysis of such problem to take special care and handling of the solution.

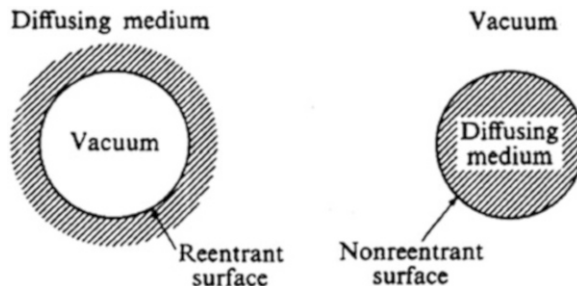
In the case of special handling, the value of distance d is also known as the *extrapolation distance* or *extrapolation length*, and it can be chosen so that the solution to the diffusion equation satisfies the boundary condition given by Eq. 3.105. This solution can be as close as possible to the rigorous solution that is given by neutron transport theory in the interior of the reactor media. It should be also noted that when Eq. 3.105 is written as the following form:

$$\frac{d\phi}{dn} + \frac{\phi}{d} = 0 \quad (3.106)$$

then this boundary condition is of the form required by the above theorem in hand [2].

To find an appropriate value for d that is also shown in Fig. 3.14, we need to apply the condition that is necessary to take under consideration two types of surfaces that are known as *reentrant* and *non-reentrant*, respectively, and they are demonstrated in Fig. 3.13 as well.

Fig. 3.13 Simple reentrant and non-reentrant surface [2]



Each of these surfaces is described as follows:

1. *Reentrant surface*

A surface is called reentrant if it is possible to draw, through any point on the surface, one straight line outward, which eventually reenters the medium.

2. *Non-reentrant surface*

A surface is called non-reentrant if no straight line that reenters the medium can be drawn through the surface.

The essential differences between these two surfaces are that a neutron leaving a reentrant surface may *reappear* elsewhere in the system, whereas a neutron that passes through a non-reentrant surface is *permanently* lost from the same system [2].

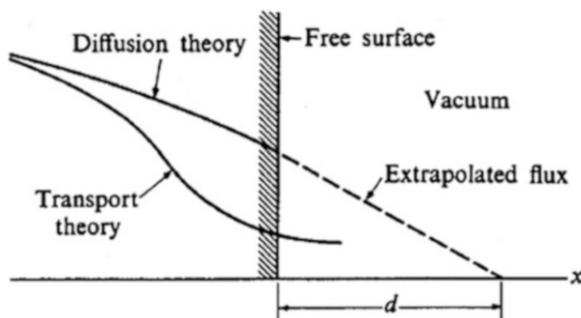
Note that the value of extrapolation distance/length d at a reentrant depends in a complicated way upon the size and the shape of the space adjacent to the surface, which is by far simpler in a non-reentrant surface situation, which is identically known as a *free surface* in a reactor analysis or theory as well. In particular planner free surface it can be demonstrated by transport theory that for the value of d as per following equation.

$$d = 0.7\lambda_{Tran.} \quad (3.107)$$

where $\lambda_{Tran.}$ is the *transport mean free path* of the medium; therefore the solution of neutron flux diffusion equation will be subject to the above boundary condition that provides a good approximation to the actual flux ϕ everywhere within the medium except near the surface of the reactor, in which the situation is plotted in Fig. 3.14.

Further analysis of Fig. 3.14 reveals that the flux ϕ is shown near a free surface as calculated by exact transport theory and by diffusion theory using similar boundary conditions as above. It also demonstrates that, while the two solutions are very nearly the same in the interior of the reactor, they also differ from each other. This difference is quite evident in the immediate vicinity of the surface and with curved free surface as it can be found for the outer edge of a cylindrical or spherical shape of simple reactor case. The extrapolation distance d is given by a somewhat more complex formula than the one we see in Eq. 3.107 and that depends on the radius of curvature R of the reactor surface. However, for extrapolation distance

Fig. 3.14 Neutron flux as a function of position near a free surface according to diffusion theory and transport theory [2]



d approaching the planar value for the larger limit of curvature radius of reactor surface, i.e., $d/R \rightarrow 0$, it is possible to use Eq. 3.107. This situation can be implemented at the surface of cylindrical and spherical reactors providing that $d \ll R$ [2].

In quest of simple solution for diffusion equation using the condition provided by Eq. 3.106, we notice this solution does vanish at the extrapolation distance d from the surface if the solution gets extended beyond the surface of the reactor by means of linear extrapolation. However, such approach for the quest of the solution for flux ϕ does introduce negligible error into diffusion equation solution, and it can be shown that ordinarily the extrapolation distance d is very small compared with the dimensions of practical reactor design system. In that case, it is possible to replace the above boundary condition to be a simple statement as below:

The solution to the diffusion equation vanishes at the extrapolation distance d beyond the edge of a free surface.

We use this simple statement as a mathematical tool to be able to simplify the neutron diffusion equation for quest of simpler solutions. Note that the neutron flux *does not* vanish at the extrapolation distance anymore and solutions of this type of approach do not provide the correct flux near the boundary. If we use the diffusion coefficient D that is validating Fick's law for its value of $D = \lambda_{Tran.}/3$, the extrapolation distance is then about $d = 2D$ [2].

Lamarsh [2] further makes statement that for most diffusing media in a reactor, diffusion coefficient D is in the order of 1 cm or less, and consequently the extrapolation distance d is never more than 2 cm and more often is less than such value. He also indicates that the most reactors, however, are of the order of meters in size, so that in many reactor analyses and calculations, the extrapolation distance d can be neglected altogether; thus the neutron flux ϕ presumably will vanish at the actual surface of the reactor of concern.

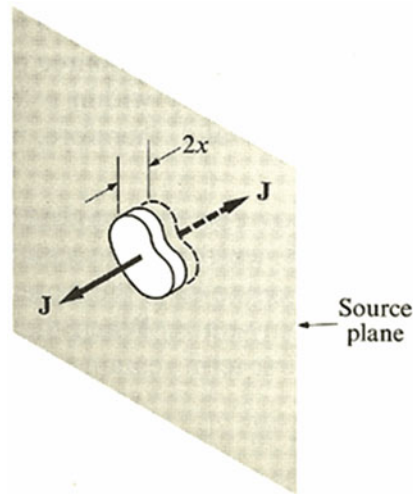
Further boundary condition types for different circumstances such as multilayer of materials at the interface for handling the problems involving neutron diffusion can be found in Lamarsh [2], and we encourage the readers to refer to his book. Interface boundary condition is discussed in details in that reference, and an elementary solution of the steady-state diffusion equation is provided as follows given the modified version of neutron diffusion equation of 2.96 in the form of the following that is satisfying the preceding boundary conditions.

$$D\nabla^2\phi - \Sigma_a\phi + S = 0 \quad (3.108)$$

We can rewrite Eq. 3.107 in the form of:

$$\nabla^2\phi - \frac{1}{L^2}\phi + S = -\frac{S}{D} \quad (3.109)$$

Fig. 3.15 Construction to drive the planar source condition



where the constant L^2 is defined as:

$$L^2 = \frac{D}{\Sigma_a} \quad (3.110)$$

The constant quantity L appears very frequently in the equations of reactor theory and is known as the *diffusion length*, and the dimension of it is in centimeter range based on the dimension of D and Σ_a being in range of cm and cm^{-1} , respectively. Again, we encourage readers to refer themselves to Lamarsh [2] book for more detailed discussion; however in summary the steady-state solution is of linear type as:

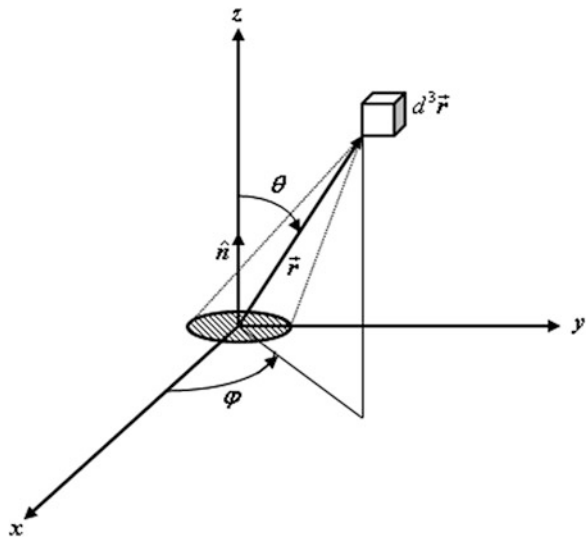
$$\phi(x) = Ae^{-x/L} + Ce^{-x/L} \quad (3.111)$$

This solution is provided based on the following limitation current density $J(x)$ in x -direction and utilizing Fig. 3.15:

$$\lim_{x \rightarrow 0} J(x) = \frac{S}{2} \quad (3.112)$$

Note that A and C are the constants that need to be determined for the given boundary conditions, and we purposely did not use letter B since it has different meaning and designation in the reactor theory as it was demonstrated in Eq. 3.105.

Fig. 3.16 Three-dimensional space presenting diffusion equation problem



3.9.2 Boundary Conditions: Consistent and Approximate

In general in a three-dimensional space, a non-steady-state diffusion equation has a derivative of both space $\vec{r} = x\hat{i} + y\hat{j} + z\hat{k}$ and time t (see Fig. 3.16) as we have indicated in the previous section, and one must assign the proper boundary and initial conditions to complete the specification of any particular problem. To solve such general problem in hand knowing that the diffusion equation itself is only approximation to the more exact neutron transport equation in our case, we might expect that we can use the transport theory boundary conditions as a direction to our development for appropriate diffusion boundary conditions. However, in the previous section, we saw it was sufficient to consider this development in a one-speed (one-dimensional) or one-group approximation, and we can express the neutron transport theory boundary condition to be defined as:

$$\text{Initial condition : } \phi(\vec{r}, \vec{\Omega}, 0) \Big|_{t=0} = \phi_0(\vec{r}, \vec{\Omega}) \quad (3.113)$$

$$\text{Boundary condition : } \phi(\vec{r}, \vec{\Omega}, t) = 0 \quad \text{for } \vec{\Omega} \cdot \hat{n}_s \quad \text{all } \vec{r} \text{ on } S \quad (3.114)$$

We are able to obtain the appropriate initial condition for the diffusion equation by merely integrating the transport condition over solid angle $\vec{\Omega}$ to have the following initial condition.

$$\text{Initial condition : } \phi(\vec{r}, 0) \Big|_{t=0} = \phi_0(\vec{r}) \quad (3.115)$$

As we mentioned in the previous section, the boundary conditions are getting setup for specific problem in the reactor theory, and several types of them are discussed by Lamarsh [2] as well as Duderstadt and Hamilton [5].

Depending on the particular physics problem of interest in nuclear reactor analysis, these boundary conditions can be grouped in several classes, but as we have said, the boundary conditions to be imposed on $\phi(\vec{r})$ are quite similar to those imposed on the wave function in solving the Schrödinger equation. Because we are dealing with a physical quantity, the neutron distribution in space $\phi(\vec{r})$ must be positive and finite everywhere or zero. In addition, the distribution must reflect the symmetry of the problem, such as $\phi(x) = \phi(-x)$ in a slab system with $x = 0$ being at the center of the slab. Then there are the usual boundary conditions at a material interface; flux and currents must be continuous since there are no sources or sinks at such interfaces. All these conditions have counterparts in solving the wave equation.

One boundary condition, which requires some discussion, is the statement of no reentrant current across the boundary between a medium and vacuum. Let this surface be located at the position $x = x_0$ in slab geometry. The physical condition is $J_-(x_0) = 0$. While the definition of J_- given in Eq. 3.28, Sect. 3.4, is perfectly correct, we can evaluate J_- according to its physical meaning and by making the assumptions that the scattering is isotropic in *laboratory coordinate system* (LCS), the medium is non-absorbing, and the flux is slowly varying. Then J_- is approximately given by the following integral (see Fig. 3.16). In this figure the geometrical setup for estimating the current of neutrons crossing a unit area A shown in the shaded area at the origin with normal unit \hat{n} after scattering isotropically in the volume element d^3r about vector space \vec{r} is given by [2]:

$$\hat{z} \cdot \mathbf{J}_- \int_{UHS} \sum_s \phi(\vec{r}) \left(\frac{A \cos \theta}{4\pi r^2} \right) e^{-\sum_i r} d^3r \quad (3.116)$$

where the integral extends over the upper half-space (UHS) of the medium because we are interested in all those neutrons which can cross the unit area A from above (in the direction opposite to the unit normal). The part of the integrand in the parenthesis is a fraction of neutron going through the unit area A if there were no collisions along the way, with A being subtended at an angle θ from the elemental volume d^3r at \vec{r} . The fact that neutrons can collide on the way to the unit area is taken into account by the factor $\exp(-\sum_i r)$. To carry out the indicated integral, we need to know $\phi(\vec{r})$; since we have assumed the flux is slowly varying, we can expand about the origin (the location of the unit area) and keep only the first term in the expansion:

$$\phi(\vec{r}) \simeq \phi(0) + \vec{r} \cdot \vec{\nabla} \phi \Big|_{x=0} \quad (3.117)$$

Then:

$$J_z^z(0) = \frac{\Sigma_s}{4\pi} \int_{\varphi=0}^{2\pi} d\varphi \int_{\theta=0}^{2\pi} \cos \theta \sin \theta d\theta \int_{r=0}^{2\pi} dr e^{-\Sigma_s r} \left[\phi_0 + x(\partial\phi/\partial x)_{x=0} + y(\partial\phi/\partial y)_{y=0} + z(\partial\phi/\partial z)_{z=0} \right] \quad (3.118)$$

where we have taken $A = 1$. Writing out the Cartesian component x , y , and z in terms of the spherical coordinates (r, θ, φ) , $x = r \sin \theta \cos \varphi$, $y = r \sin \theta \sin \varphi$, and $z = r \cos \theta$ as before, we find the ϕ -integration renders the terms containing x or y equal to zero. The term containing z can be easily integrated to give the following forms after shifting the unit area from being at the origin as in Fig. 3.16 to a slab geometry with the unit area on the surface at $x = x_0$.

$$J_z^z(x_0) = \frac{\phi(x_0)}{4} + \frac{D}{2} \left(\frac{d\phi}{dx} \right)_{x_0} \quad (3.119)$$

or

$$\left(\frac{d\phi}{dx} \right)_{x_0} = -\frac{1}{2D} \phi(x_0) \quad (3.120)$$

Equation 3.120 is not really a bona fide condition on $\phi(x_0)$ because the gradient $d\phi/dx$ is not known. To find another relation between the flux and gradient, we interpret the latter as a finite difference:

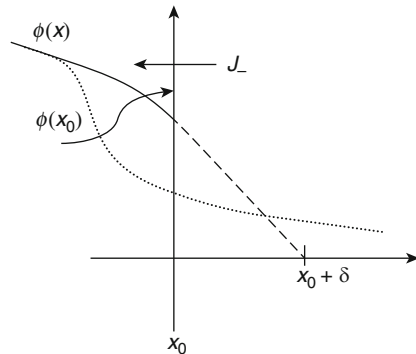
$$\left(\frac{d\phi}{dx} \right)_{x_0} = -\frac{\phi(x_0) - \phi(x')}{x' - x_0} \quad x' > x_0 \quad (3.121)$$

where we use the negative sign because we know the gradient must be negative. Now we choose x' such that we know the value of the flux at this position. How is this possible? Suppose we choose x' to be the distance where the flux linearly extrapolates from $x = x_0$ to zero. Calling this distance $x' = x_0 + \delta$ (see Fig. 3.17), we then have from Eq. 3.121.

As it can be seen from Fig. 3.17, the schematic of the extrapolated boundary condition with δ being the distance beyond the actual boundary where a linear extrapolation of the flux at $x = x_0$ would vanish as it was explained before in the previous section and the dotted curve shows the variation of the flux that would be obtained from transport theory [2].

$$\left(\frac{d\phi}{dx} \right)_{x=x_0} = -\frac{1}{\delta} \phi(x_0) \quad (3.122)$$

Fig. 3.17 Schematic of the extrapolated boundary condition



Combining this with Eq. 3.117, we obtain for the extrapolated distance $\delta = 2D$. Conventionally instead of the physical condition of no reentrant current, one often applies the simpler mathematical (and approximate) condition of the following form:

$$\phi(x_0 + 2D) = \phi(\tilde{x}_0) = 0 \quad (3.123)$$

where $\tilde{x}_0 = x_0 + 2D$. Equation 3.12 is called the extrapolated boundary condition; it is commonly adopted because of its simplicity. One can use transport theory to do a better calculation of the extrapolated distance δ . We have seen that in simple diffusion theory, this turns out to be $2D$ or $2/3\sum_a$. The transport theory result, when there is no absorption, is $0.71/\sum_{tran.}$, where again $\sum_{tran.}$ is transport mean free path. The rather small difference between diffusion theory and transport theory should not be taken to mean that the flux near the surface is always accurately given by diffusion theory. As can be seen in Fig. 3.17, diffusion theory typically overestimates the flux at the surface relative to transport theory. All these were discussed differently in the previous section.

Note that as part of the infinite planar source which emits at a constant rate of neutrons per second per unit area into an infinite homogeneous medium, where the source plane and medium are both infinite, the flux at any point in the medium can be a function of distance explicitly from the plane, and we can write Eq. 3.108 in the form of:

$$\frac{d^2\phi}{dx^2} - \frac{1}{L^2}\phi = -\frac{s(x)}{D} \quad (3.124)$$

In this equation the source density function $s(x)$ is an orthodox function of x , and since there are no sources present in the medium itself, then $s(x)$ is zero everywhere in that medium. However at $x = 0$, the source density function $s(x)$ is infinite. This is because the source density function is the number of neutrons emitted per plane, and thus the source density is necessarily infinite at the plane, simply because a finite number of neutrons are produced in zero volume [2].

Function such as $s(x)$, which are zero everywhere except at $x = 0$, can be represented in terms of the *Dirac delta function* $\delta(x)$, which is defined by the equations.

$$\delta(x) = 0 \quad x \neq 0$$

$$\int_a^b \delta(x) = \begin{cases} 1 & a < 0 < b \\ 0 & \text{otherwise} \end{cases} \quad (3.125)$$

In any case, $s(x)$ can be written as:

$$s(x) = S\delta(x) \quad (3.126)$$

In view of Eq. 3.125, the total number of neutrons emitted per second per unit area of the source plane is just in the form of the following, where ϵ has any value [2].

$$\int_{-\epsilon}^{+\epsilon} s(x)dx = S \int_{-\epsilon}^{+\epsilon} \delta(x)dx = S \quad (3.127)$$

Inserting Eq. 3.126 into diffusion Eq. 3.124, then we get the following result.

$$\frac{d^2\phi}{dx^2} - \frac{1}{L^2}\phi = -\frac{S\delta(x)}{D} \quad (3.128)$$

The above equation is an ordinary, inhomogeneous, linear differential equation which easily can be solved by all the known methods of solving differential equation in mathematics, and for all the value of x , except for $x = 0$, the above equation can be converted to a simple equation of homogeneous form as:

$$\frac{d^2\phi}{dx^2} - \frac{1}{L^2}\phi = 0 \quad \text{for } x \neq 0 \quad (3.129)$$

Note that at $x = 0$ can now be taken into account by means of a *source condition*, rather than using the source density function directly.

3.9.3 An Approximate Method for Solving the Diffusion Equation

Now let us consider an approximate method for solving the diffusion equation for an inhomogeneous problem in slab geometry. We know that the eigenfunctions for this problem are the *exponentials* or the *sinh* and *cosh*. But suppose we did not know this

or that the actual eigenfunctions were unknown. Let us try an approximate approach that often gives very good answers.

Let us choose a set of functions that satisfy the boundary conditions automatically. The easiest set to choose, because most people are familiar with them, is the sin and cos functions. However, since we will put the plane source at the middle of our inhomogeneous slab and require the solution to be symmetric, the sin functions are not acceptable. This leaves only the cos functions.

Now in order for the $\cos(\alpha z)$ to be zero at the boundary where $z = H/2$, we must have the following:

$$\frac{\alpha H}{2} = \frac{(2k+1)\pi}{2} \quad \text{or} \quad \alpha = \frac{(2k+1)\pi}{H} \quad (3.130)$$

Now since the cos functions are not eigenfunctions of the operator for an attenuation problem, we will want to use more than one of them in our approximate solution. We might even want to use an infinite number if we are mathematicians and want the best accuracy. However, since we are engineers, we will only take a few if they work. So we can choose for our solution:

$$\phi(z) = \sum_{k=0}^N C_k \cos\left(\frac{(2k+1)\pi}{H}z\right) \quad (3.131)$$

If we substitute this equation into our differential equation, we obtain:

$$\sum_{k=0}^N \left(\frac{(2k+1)\pi}{H}\right)^2 C_k \cos\left(\frac{(2k+1)\pi}{H}z\right) + \frac{1}{L^2} \sum_{k=0}^N C_k \cos\left(\frac{(2k+1)\pi}{H}z\right) = \frac{S_D}{D} \delta(0) \quad (3.132)$$

So now we would like to choose the C_k in such a way that we get the best solution we can get with the fewest terms. What we will do is to require the equation to be satisfied in an integral sense. However if we want to use N terms to approximate our solution, we must have N equations to solve for the N coefficients. Therefore, to get N equations, we will multiply the equation by each of the solution functions, one at a time. This will give us N equations, and luckily, since the cos functions are orthogonal on the interval of our problem, we will get a simple equation for each coefficient. Thus we have:

$$\begin{aligned} & \int_{-H/2}^{H/2} \cos\left(\frac{(2n+1)\pi}{H}z\right) \sum_{k=0}^N \left(\left[\frac{(2k+1)\pi}{H}\right]^2 + \frac{1}{L^2}\right) C_k \cos\left(\frac{(2k+1)\pi}{H}z\right) dz \\ &= \int_{-H/2}^{H/2} \frac{S_D}{D} \delta(0) \cos\left(\frac{(2n+1)\pi}{H}z\right) dz \end{aligned} \quad (3.133)$$

$$\begin{aligned}
\int_{-H/2}^{H/2} \cos^2 \left(\frac{(2n+1)\pi}{H} z \right) dz &= \frac{H}{(2n+1)\pi} \int_{-H/2}^{H/2} \cos^2 \beta d\beta \\
&= \frac{H}{(2n+1)\pi} (2n+1) \int_{-H/2}^{H/2} \cos^2 \beta d\beta = \frac{H}{\pi} \frac{1}{2} \pi
\end{aligned} \tag{3.134}$$

or

$$\int_{-H/2}^{H/2} \frac{S_D}{D} \delta(0) \cos \left(\frac{(2n+1)\pi}{H} z \right) dz = \frac{S_D}{D} \tag{3.135}$$

So each of the coefficients must satisfy:

$$\left(\left[\frac{(2n+1)\pi}{H} \right]^2 + \frac{1}{L^2} \right) C_n \frac{H}{2} = \frac{S_D}{D} \tag{3.136}$$

or

$$C_n = \frac{2S_D}{HD \left(\frac{1}{L^2} + \left[\frac{(2n+1)\pi}{H} \right]^2 \right)} \tag{3.137}$$

So we have an approximate solution that satisfies the differential equation in an integral sense. Let us see how good it is. Consider a stainless steel slab that has a planar source at its center. Let the slab be 60 cm thick, and we will use the one-group fast energy spectrum cross sections.

$$\Sigma_a = 0.002963 \text{ cm}^{-1}$$

$$D = 0.6962 \text{ cm}$$

$$L^2 = 234.96 \text{ cm}^2$$

and let

$$S_D = 100 \text{ particles/s/cm}^2.$$

In Fig. 3.18 are plotted the exact solution, the approximate solution with one term, the approximate solution with two terms, and the approximate solution with five terms. Two terms give a solution that looks close, and five terms cannot be distinguished from the exact solution on this chart.

Of course all approximate solutions match the exact solution at the boundary because each of the terms is exactly equal to zero. However, if the slab thickness is broken up into 26 mesh points or 25 intervals, the largest difference between the exact solution and the five-term approximate solution occurs at the last mesh point in the slab, and at this point the approximate solution is off by 21% of the exact value, which is pretty small.

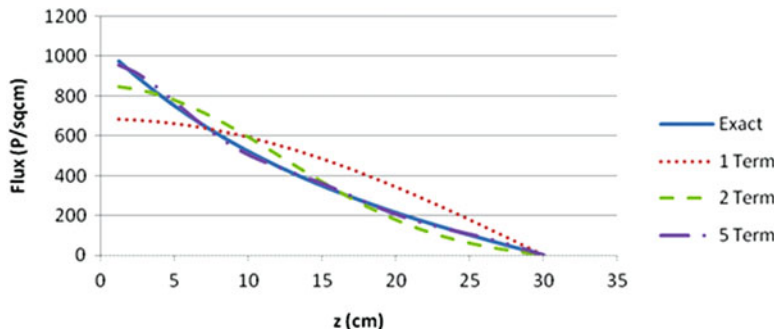


Fig. 3.18 Approximation accuracy by number of included terms

If ten terms are used, the largest difference also occurs at the same mesh point and the difference is 8%. If 25 terms are used, the largest difference is 0.2%, and it occurs at the first mesh point near the center of the slab.

We now continue with further analysis approximation in transport theory.

3.9.4 The P_1 Approximate Methods in Transport Theory

Referring to Eq. 3.60, we see that this equation is still an integrodifferential equation that cannot be solved easily. One of the most common methods of extracting a more tractable description of transport is to expand the distribution function in a series of angular functions and then truncate the series. This is reminiscent of the use of partial wave expansion as a means of reducing the Schrödinger equation to a more manageable form. For this discussion we can ignore the fission without any loss of generality. We write the following relationship:

$$\phi(x, \mu) = \sum_{\ell=0}^{\infty} \frac{2\ell+1}{2} \phi_{\ell}(x) P_{\ell}(\mu) \quad (3.138)$$

$$F(\mu_0) = \sum_{\ell=0}^{\infty} \frac{2\ell+1}{2} F_{\ell} P_{\ell}(\mu_0) \quad (3.139)$$

where $P_{\ell}(\mu)$ is the ℓ th-order Legendre polynomial. This expansion leads to an infinite set of coupled equations for the functions:

$$\phi_{\ell}(x) = \int_{-1}^{+1} P_{\ell}(\mu) \phi_l(x, \mu) d\mu \quad (3.140)$$

$$F_{\ell} = \int_{-1}^{+1} P_{\ell}(\mu) F(\mu) d\mu \quad (3.141)$$

The first two such equations are:

$$\frac{d\phi_1(x)}{dx} + \Sigma_t \phi_0(x) = \Sigma_s F_0 \phi_0(x) + S_0(x) \quad (3.142)$$

$$\frac{2}{3} \frac{d\phi_2(x)}{dx} + \frac{1}{3} \frac{d\phi_0}{dx} + \Sigma_t \phi_1(x) = \Sigma_s F_1 \phi_1(x) \quad (3.143)$$

If somehow we are justified in ignoring the term containing $\phi_2(x)$, then we would have a closed set of equations in which we can solve for the flux coefficients ϕ_0 and ϕ_1 :

$$\frac{d\phi_1(x)}{dx} + (\Sigma_t - \Sigma_s F_0) \phi_0(x) = S_0(x) \quad (3.144)$$

$$\frac{1}{3} \frac{d\phi_0(x)}{dx} + (\Sigma_t - \Sigma_s F_1) \phi_1(x) = 0 \quad (3.145)$$

The truncation of the Legendre polynomial expansion at $\ell = 1$ is called the P_1 approximation. In general, retaining the $N+1$ terms in the series leads to a coupled set of $N+1$ equations – the P_N approximation.

The two scattering kernel coefficients, which appear in the P_1 equations, have quite simple meanings:

$$F_0 = \int_{-1}^{+1} F(\mu) d\mu = 1 \quad (\text{Particle conservation}) \quad (3.146)$$

$$F_1 = \int_{-1}^{+1} F(\mu) \mu d\mu = \langle \mu \rangle \quad (3.147)$$

An immediate consequence of the P_1 approximation is that we obtain a relation between the current and the gradient of the flux from Eq. 3.145 as follows:

$$\phi_1(x) = -\frac{1}{3} [\Sigma_t - \Sigma_s \langle \mu \rangle]^{-1} \frac{d\phi_0(x)}{dx} \quad (3.148)$$

where ϕ_0 and ϕ_1 are the neutron flux distribution in position space (position flux) and the neutron net current, respectively. Such a relation defines a transport coefficient, in this case, the neutron diffusion coefficient:

$$D = [3(\Sigma_t - \Sigma_s) \langle \mu \rangle]^{-1} \quad (3.149)$$

Equation 3.148 is the P_1 approximation to Fick's law of diffusion, generally written as:

$$\vec{J} = -D \vec{\nabla} \phi \quad (3.150)$$

As we said in the previous sections, this relation is also well known in the kinetic theory of gases, with one difference. In neutron transport, the diffusion coefficient

has dimension of cm, whereas in kinetic theory its dimension would be cm²/s. This distinction arises from a factor of the thermal speed, that is, in kinetic theory one uses number density rather than flux.

If the absorption is weak, $(\Sigma_a/\Sigma_t) \ll 1$, the diffusion coefficient simplifies to:

$$D \simeq \frac{1}{3\Sigma_s(1 - \langle \mu \rangle)} \equiv \frac{1}{3\Sigma_{tran.}} \quad (3.151)$$

with $\Sigma_{tran.}$ being an effective “transport cross section.” Since $\langle \mu \rangle$ is the average of the cosine of the scattering angle in laboratory coordinate system (LCS), it would have a larger value if the scattering were preferentially biased in the forward direction. Then D and the net current would increase as one would intuitively expect. On the one hand, if the medium has a large scattering cross section, D would decrease since the neutron would be scattered more frequently thus impeding its forward progress. These simple physical interpretations apply to neutron diffusion transport as well as particle diffusion in general. Another remark is that we can go back to the transport equation without making the P_1 approximation and derive a Fick’s law relation between the current and the flux gradient. This however would take us to Sect. 3.5 discussion.

Further discussion of this topic and derivation of the one-dimensional multi-group P_N equations will be referred to further down in this book.

3.10 Further Analysis Methods for One Group

Now let us try to perform a little more sophisticated analysis of the spatial variation, of the flux, in a nuclear reactor. To make things simple and focus on one part of the problem at a time, assume that a suitable within-group spectrum can be found such that the multi-group equations can be reduced to one equivalent group and reasonable estimates of reaction rates can be obtained. We will assume that this spectrum can vary with material, but within a given material, it is constant across all space. The one-group diffusion equation becomes:

$$-\frac{\partial}{\partial z} D \frac{\partial}{\partial z} \phi(z) + \Sigma_a \phi(z) = \frac{1}{k} v \Sigma_f \phi(z) \quad (3.152)$$

Since we have assumed that the spectrum is constant for any given material, then each of the coefficients appearing in the equation will be constant, and in particular the diffusion coefficient will not change with location, and it can be brought out of the first derivative operation. This will give:

$$-D \frac{\partial^2}{\partial z^2} \phi(z) + \Sigma_a \phi(z) = \frac{1}{k} v \Sigma_f \phi(z) \quad (3.153)$$

Now the second derivative with respect to z in the first term is the same as the $-\nabla^2$ operator in one spatial dimension. In fact if the multi-group diffusion equations were derived in three dimensions or in any other coordinate system, this first term would always come out to be the $-\nabla^2$ operator. So let us write the equations that way.

$$-D\nabla^2\phi(z) + \Sigma_a\phi(z) = \frac{1}{k}v\Sigma_f\phi(z) \quad (3.154)$$

We will deal with the changes in group cross sections across different materials by applying boundary, or interface, conditions at those boundaries. This simplifies the analysis somewhat and allows some problems to be solved analytically.

Note that this equation is still a homogeneous equation as the flux, $\phi(z)$, appears in every term. If the flux is exactly zero at every point, then the equation is completely satisfied. However, this is a very uninteresting result. Therefore, in order for the flux to be non-zero, a unique relationship must exist between the operators and constants in the equation. Note that the equation can be rewritten in the following fashion:

$$-\nabla^2\phi(z) = \frac{\frac{1}{k}v\Sigma_f - \Sigma_a}{D}\phi(z) \quad (3.155)$$

This is the form of:

$$-\nabla^2\phi(z) = \lambda\phi(z), \quad \lambda = \frac{\frac{1}{k}v\Sigma_f - \Sigma_a}{D}$$

a classic eigenvalue problem. The question becomes does there exist a set of functions that will satisfy this equation such that operating on the functions with the $-\nabla^2$ operator will reproduce the same functions multiplied by a constant. It is also worth noting that the constant, λ , can be either positive or negative depending on the relative values of Σ_a and $v\Sigma_f$. Of course there exist functions that will replicate themselves multiplied by a non-zero constant when operated on by the $-\nabla^2$ operator. These functions will depend on exactly how the $-\nabla^2$ operator is expressed.

We will deal with the $-\nabla^2$ operator in three one-dimensional geometries, two two-dimensional geometries, and a one three-dimensional geometry altogether. There are an infinite variety of ways that three-dimensional space can be measured, and just because we do not address a three-dimensional spherical coordinate system geometry does not mean that it would not be appropriate for certain problems. The coordinate systems that we will use for one-dimensional problems and the appropriate expression of the $-\nabla^2$ operator are:

1. *Infinite slab*

$$-\nabla^2\phi(z) = -\frac{\partial^2}{\partial z^2}\phi(z) \quad (3.156)$$

2. *Infinite cylinder*

$$-\nabla^2 \phi(\rho) = -\frac{1}{\rho} \frac{\partial}{\partial \rho} \rho \frac{\partial}{\partial \rho} \phi(\rho) \quad (3.157)$$

3. *Sphere*

$$-\nabla^2 \phi(r) = -\frac{1}{r^2} \frac{\partial}{\partial r} r^2 \frac{\partial}{\partial r} \phi(r) \quad (3.158)$$

The two-dimensional coordinate systems and the appropriate $-\nabla^2$ operators are:

1. *Finite Cylinder*

$$-\nabla^2 \phi(\rho, z) = -\frac{1}{\rho} \frac{\partial}{\partial \rho} \rho \frac{\partial}{\partial \rho} \phi(\rho, z) - \frac{\partial^2}{\partial z^2} \phi(\rho, z) \quad (3.159)$$

2. *Infinite rectangular column*

$$-\nabla^2 \phi(x, y) = -\frac{\partial^2}{\partial x^2} \phi(x, y) - \frac{\partial^2}{\partial y^2} \phi(x, y) \quad (3.160)$$

We will consider two three-dimensional $-\nabla^2$ operators, the rectilinear one based on Cartesian coordinates (x, y, z) and the spherical coordinate one based on the (r, θ, φ) system:

1. *Rectangular parallelepiped*

$$-\nabla^2 \phi(x, y, z) = -\frac{\partial^2}{\partial x^2} \phi(x, y, z) - \frac{\partial^2}{\partial y^2} \phi(x, y, z) - \frac{\partial^2}{\partial z^2} \phi(x, y, z) \quad (3.161)$$

2. *Nonhomogeneous sphere*

$$\begin{aligned} -\nabla^2 \phi(r, \theta, \varphi) = & -\frac{\partial}{\partial r} \left(r^2 \frac{\partial}{\partial r} \phi(r, \theta, \varphi) \right) + \frac{1}{\sin \theta} \frac{\partial}{\partial \theta} \left(\sin \theta \frac{\partial}{\partial \theta} \phi(r, \theta, \varphi) \right) \\ & + \frac{1}{\sin^2 \theta} \frac{\partial^2}{\partial \varphi^2} \phi(r, \theta, \varphi) \end{aligned} \quad (3.162)$$

Each of these coordinate systems and $-\nabla^2$ operators will have different eigenfunctions that will satisfy the above homogeneous equation. Note that the one-dimensional spherical system is a way of representing a physically realizable object, as are the two-dimensional finite cylinder and three-dimensional box. Ultimately, these two coordinate systems will allow us to build simple models that can be used in real experiments to test our mathematical theories.

3.10.1 Slab Geometry

Now consider the eigenfunctions that will satisfy the one-dimensional slab problem. The simplest case corresponds to when λ is a negative constant. Note that the units on λ are $(\text{length})^{-2}$. So the physical constant that will non-dimensionalized our solutions should really be the square root of λ . We will use a different symbol for this constant depending on whether λ is positive or negative. If λ is negative, the constant will be imaginary, and we will give it a different interpretation than if λ were positive. Consider first the case where λ is negative. We will let our fundamental constant be the square root of $1/|\lambda|$. Thus we will write $|\lambda| = 1/L^2$. We will call L the diffusion length. For this case the eigenfunctions are the exponential functions with positive or negative exponents.

$$\hat{\Phi}_1(z) = e^{z/L}, \quad \hat{\Phi}_2(z) = e^{-z/L} \quad (3.163)$$

These functions can also be expressed as the hyperbolic sine and cosine functions such that,

Both representations are equivalent, and the one that we will choose to solve a given problem will depend on the geometry and boundary conditions for the problem. The exponentials are often easier to use if one boundary condition is at infinity; the hyperbolic functions are often easier to use if symmetry about the origin is a natural boundary condition. Either set will work in all cases, but the solutions are usually simpler if the appropriate basis set is chosen.

Next consider the case where λ is a positive number. We can still set it equal to the square of another number, but now this number is imaginary. We will let $\lambda = B^2$ where we will call B the buckling and its nominal units will be $1/\text{cm}$. If we use the exponential functions for the eigenfunctions (we will talk about the eigenfunction expansion in the next section) for this case, they replicate themselves, but their arguments must be imaginary. This really does not present a problem, as the exponential of an imaginary argument can be transformed to the trigonometric functions, sin and cosine, by the de Moivre identities as below:

$$\hat{\Phi}_1(z) = \sin Bz = \frac{e^{iBz} - e^{-iBz}}{2i}, \quad \hat{\Phi}_2(z) = \cos Bz = \frac{e^{iBz} + e^{-iBz}}{2} \quad (3.164)$$

Thus any time we have $-\nabla^2$ operator operating on a single Cartesian dimension, the eigenfunctions will be either the exponential functions or the trigonometric functions depending on the sign of the constant, λ .

3.10.2 Cylindrical Geometry

For the cylindrical geometry, $-\nabla^2$ operator, consider the case of a positive λ first. The eigenfunctions for a positive λ are the Bessel functions. The first and most

common of these is the $J_0(\rho)$ function. It is called the Bessel function of the first kind of order zero. It has a value of 1.0 at $\rho = 0$ and has a value of 0.0 at $\rho = 2.4048255577\dots$. After that, it goes negative and continues to oscillate with a slightly decreasing period out to infinity. It is a solution to Bessel's equation:

$$\frac{\partial^2}{\partial \rho^2} \phi(p) + \frac{1}{\rho} \frac{\partial}{\partial \rho} \phi(\rho) + \left(1 - \frac{n^2}{\rho^2}\right) \phi(\rho) = 0 \quad (3.165)$$

for $n = 0$. Moreover, it can be computed from the general series expansion form as:

$$\hat{\Phi}_1(\rho) = J_n(B\rho) = \frac{\left(\frac{B\rho}{2}\right)^n}{\Gamma(n+1)} \left\{ 1 - \frac{\left(\frac{B\rho}{2}\right)^2}{1 \cdot (n+1)} + \frac{\left(\frac{B\rho}{2}\right)^4}{1 \cdot 2 \cdot (n+1)(n+2)} \dots \right\} \quad (3.166)$$

where the only case of interest is $n = 0$ case. Note that $\Gamma(n+1)$ is the gamma function of order n . It is given by:

$$\Gamma(n) = \int_0^\infty t^{n-1} e^{-t} dt \quad (3.167)$$

and when n is an integer, $\Gamma(n+1) = n!$, i.e., $\Gamma(5) = 5^*4^*3^*2^*1$.

Since we have a second-order differential equation, then there must be a second solution that also satisfies it. This solution in our notation will be called $Y_0(\rho)$, or Neumann's function, and its properties are that it is a negative infinity for $\rho = 0$ and it passes through zero at $\rho = 0.89357697\dots$.

It continues to oscillate out to infinity interlacing its zeroes with $J_0(\rho)$. A expansion for $J_0(\rho)$ is given by:

$$\hat{\Phi}_2(\rho) = Y_0(B\rho) = J_0(B\rho) \log(B\rho) + \left\{ \left(\frac{B\rho}{2}\right)^2 - \frac{\left(\frac{B\rho}{2}\right)^4}{2!} \left(1 + \frac{1}{2}\right) + \frac{\left(\frac{B\rho}{2}\right)^6}{3!} \left(1 + \frac{1}{2} + \frac{1}{3}\right) \dots \right\} \quad (3.168)$$

For the case of a negative λ in our original differential equation, we will obtain the modified Bessel functions of integer order. These are identified as $I_n(\rho)$ and $K_n(\rho)$. $I_0(\rho)$ starts at 1.0 for $\rho = 0.0$ and increases without bound, much as a positive exponential function. It is given by:

$$\hat{\Phi}_1(\rho) = I_n(B\rho) = \frac{\left(\frac{B\rho}{2}\right)^n}{\Gamma(n+1)} \left\{ 1 + \frac{\left(\frac{B\rho}{2}\right)^2}{1 \cdot (n+1)} + \frac{\left(\frac{B\rho}{2}\right)^4}{1 \cdot 2 \cdot (n+1)(n+2)} \dots \right\} \quad (3.169)$$

$I_n(\rho)$ starts at 0.0 and increases without bound in a similar fashion.

All of the $K_n(\rho)$ start at a positive infinity and decrease to zero as their argument goes from 0.0 to infinity, paralleling the behavior of a negative exponent. $K_0(\rho)$ is given by:

$$\begin{aligned}\hat{\Phi}_2(\rho) = K_0(B\rho) &= -\left\{ \gamma + \log\left(\frac{B\rho}{2}\right) \right\} I_0(B\rho) \\ &+ \left(\frac{B\rho}{2}\right)^2 + \frac{\left(\frac{B\rho}{2}\right)^4}{2!} \left(1 + \frac{1}{2}\right) + \frac{\left(\frac{B\rho}{2}\right)^6}{3!} \left(1 + \frac{1}{2} + \frac{1}{3}\right) \dots\end{aligned}\quad (3.170)$$

where γ is Euler's constant ($\gamma = 0.5772156649\dots$). Probably the only real thing to remember about the Bessel functions for this course is that they are the eigensolutions in cylindrical geometry for the $-\nabla^2$ operator and that the first zero of $J_0(\rho)$ is 2.4048.... Most students are not that facile with Bessel functions for solving differential equations, and they are only useful when exact analytic solutions can be obtained. Unfortunately, in nuclear engineering, most solutions wind up being numerical, and trying to compute Bessel functions numerically is the *WRONG* way to solve the problem.

3.10.3 Spherical Geometry

Moving on to spherical geometry, the one-dimensional eigenfunctions for the $-\nabla^2$ operator with a negative λ are the exponential functions divided by the radius variable:

$$\hat{\Phi}_1(r) = \frac{e^{r/L}}{r}, \quad \hat{\Phi}_2(r) = \frac{e^{-r/L}}{r} \quad (3.171)$$

These can be shown to be the eigenfunctions by simply plugging them into the differential equation and verifying that they repeat themselves multiplied by a constant when operated on by the $-\nabla^2$ operator.

$$\begin{aligned}\frac{1}{r^2} \frac{\partial}{\partial r} r^2 \frac{\partial}{\partial r} \frac{e^{r/L}}{r} &= \frac{1}{r^2} \frac{\partial}{\partial r} r^2 \left(\frac{1}{L} \frac{e^{r/L}}{r} - \frac{e^{r/L}}{r^2} \right) = \frac{1}{r^2} \frac{\partial}{\partial r} \left(\frac{r}{L} e^{r/L} - e^{r/L} \right) \\ &= \frac{1}{r^2} \left\{ \frac{e^{r/L}}{L} + \frac{1}{L^2} r e^{r/L} - \frac{e^{r/L}}{L} \right\} = \frac{1}{L^2} \frac{e^{r/L}}{r}\end{aligned}\quad (3.172)$$

Equation 3.172 is a quod erat demonstrandum, meaning “which is what had to be proven.”

Of course the hyperbolic functions can be substituted for the exponential functions by using linear combinations of exponential functions, as for the slab geometry case:

$$\hat{\Phi}_1(r) = \frac{\sinh^r/\ell}{r}, \quad \hat{\Phi}_2(r) = \frac{\cosh^r/\ell}{r} \quad (3.173)$$

This is particularly useful when the problem under consideration contains the origin, as both the positive and negative exponential functions divided by the radius give an unbounded answer at the origin. The hyperbolic sine function, however, goes to zero at the origin and therefore produces a bounded eigenfunction at the origin for this operator.

The spherical geometry case for a positive λ parallels the slab geometry case, and the standard trigonometric functions are substituted for the exponential functions to give the eigenfunctions for this operator.

$$\hat{\Phi}_1(r) = \frac{\sin Br}{r}, \quad \hat{\Phi}_2(r) = \frac{\cos Br}{r} \quad (3.174)$$

3.11 Eigenfunction Expansion Methods and Eigenvalue Equations

For solving the linear but nonhomogeneous ordinary differential equation (ODE), one can use the method of variation that helps to determine the constants, and it will be useful for finding the solution in more general problems of that sort. Using this method allows one to find both auxiliary and particular solution of nonlinear differential equation solution. (See Problems 3.19 and 3.20 at the end of this chapter.) In this case one must be able to guess the particular solution for such ODEs by inspection; hence for most problems, Green's function techniques are more convenient.

Green's functions are particularly helpful in quest of the solution of partial differential equations. However, they can be used to solve ordinary differential equations. Few examples here can briefly show the ideas that are extended to the solution of partial differential equations.

Example 3.1 Let us reconsider the following linear nonhomogeneous differential equation, namely:

$$y'' + \omega^2 y = f(t) \quad \text{With boundary condition} \quad y_0 = y'_0 = 0 \quad (1)$$

Note that this equation might describe the oscillations of a mass suspended by a spring or a simple series electric circuit with negligible resistance.

Solution Considering the differential equation given by the example, we can write:

$$f(t) = \int_0^x f(t') \delta(t' - t) dt' \quad (2)$$

This is based on thoughts that the force $f(t)$ is a whole sequence of impulses. You might reflect that, on the molecular level, air pressure is the force per unit area to a tremendous number of impacts of individual molecules. Now suppose that we have solved the given differential equation with $f(t)$ replaced by $\delta(t' - t)$, that is, we find the response of the system to a unit impulse at $G(t', t)$. Let us call this response $G(t', t)$, that is, t' is the solution of:

$$\frac{d^2}{dt^2} G(t, t') + \omega^2 G(t, t') = \delta(t' - t) \quad (3)$$

Then, given some forcing function $f(t)$, we try to find a solution of differential equation of the example by “adding up” the responses of many such impulses. We shall show that this solution is:

$$y(t) = \int_0^x G(t, t') f(t') dt' \quad (4)$$

Substituting Eq. (4) into differential Eq. (1) of the problem in hand provides the following results as:

$$\begin{aligned} y'' + \omega^2 y &= \left(\frac{d^2}{dt^2} + \omega^2 \right) y = \left(\frac{d^2}{dt^2} + \omega^2 \right) \int_0^x G(t, t') f(t') dt' \\ &= \int_0^x \left(\frac{d^2}{dt^2} + \omega^2 \right) G(t, t') f(t') dt' \\ &= \int_0^x \delta(t' - t) f(t') dt' = f(t) \end{aligned} \quad (5)$$

Thus, the function $G(t, t')$ is called a *Green's function*. Green's function is the response of the system to a unit impulse at $t = t'$. Solving Eq. (3) with initial conditions $G = 0$ and $(dG/dt) = 0$ at $t = 0$, we find that:

$$G(t, t') = \begin{cases} 0 & 0 < t < t' \\ (1/\omega) \sin \omega(t - t') & 0 < t' < t \end{cases} \quad (6)$$

Then Eq. (4) gives the solution of Eq. (1) with $y_0 = y'_0 = 0$, namely:

$$y(t) = \int_0^t \left(\frac{1}{\omega} \right) \sin \omega(t - t') f(t') dt' \quad (7)$$

The upper limit is $t = t'$ since $G = 0$ for $t' > t$; thus, given a forcing function $f(t)$, we can find the response $y(t)$ of the system Eq. (1) by increasing Eqs. (7)–(6). Similarly, for other differential equations, we can find the solution in terms of an appropriate Green's function.

Note that in general, once a Green's function has been obtained for a given ordinary differential equation of $d^2y/dx^2 + y = f(x)$, and boundary conditions, one can apply Eq. (4) to provide the solution for the problem in hand.

One of the most powerful methods available for solving boundary value problems is to search the right solution as an expansion in the set of *normal modes* or *eigenfunctions* characterizing the geometry of interest. The problem of finding the solution of a given differential equation subject to given boundary conditions is called a *boundary value problem* (BVP). Such problems often lead to *eigenvalue problems* or *characteristic value problem*. Under these conditions, there are parameters that their values are to be selected so that the solutions of boundary value problems of these ODEs could meet the given requirements, and these parameters could be the separation constants that we need in order to solve our BVPs. Then their values are determined by demanding that the solutions satisfy some of the boundary conditions (BCs). The resulting values of the separation constants are called *eigenvalues*, and the basic solutions of the differential equation corresponding to the eigenvalues are called *eigenfunctions*.

To further enhance the understanding of the boundary value and eigenvalue problems, we continue to look at the solutions of second-order ordinary differential equations of the following form exists under general conditions.

$$y'' = f(t, y, y') \quad (3.175)$$

It becomes unique if we specify initial values for $y(t_0)$ and $y'(t_0)$, which is the foundation of *initial value problem* (IVP).

In many applications, we are seeking a solution for Eq. 3.175, in which one specifies the *values* of the solution $y(t)$ at two separate points $t_0 < t_1$ rather than specifying the value of $y(t)$ and its derivative at a single point.

This leads to the subject of boundary value problems, a very large and important area of mathematics dealing with differential equation of different subjects such as heat transfer, fluid mechanics, reactor theory and diffusion equations. The subject is studied for both ordinary and partial differential equations. In the case of partial differential equations, one deals with solutions which are defined on subsets of various Euclidean spaces, and, hence, there are many interesting regions for which to specify boundary conditions.

In most applications, the independent variable of the differential equation represents a spatial condition along a real interval rather than time, so we use x for the independent variable of our functions instead of t . The general linear second-order boundary value problems have the form of the following format:

$$\begin{cases} \frac{d^2y}{dx^2} + p(x)\frac{dy}{dx} + q(x)y = h(x) & \text{Including boundary conditions} \\ y'' + p(x)y' + q(x)y = h(x) \end{cases} \quad (3.176)$$

Here, x is in some interval $I = (a, b) \subset \mathfrak{R}$ and $p(x)$, $q(x)$, and $h(x)$ are continuous real valued functions on I with $\alpha < \beta$ are two fixed real numbers in I , and boundary condition (BC) refers to specific boundary conditions.

Let us use the letters BVP to denote the *boundary value problem*. We wish to study all solutions of such a problem. In the cases considered here, we can replace x by $x+\alpha$ if necessary and assume that $\alpha = 0$. We will denote the right boundary point by L .

For the purpose of this subject and further study of it, we will consider four types of boundary conditions, which we denote by the expressions 00, 01, 10, and 11. These are defined by:

$$\begin{cases} \text{type 00 : } y(0) = 0, y(L) = 0 \\ \text{type 01 : } y(0) = 0, y'(L) = 0 & \text{Where } L > 0 \\ \text{type 10 : } y'(0) = 0, y(L) = 0 \end{cases} \quad (3.177)$$

Then the boundary value problem of the following form:

$$y'' + p(x)y' + q(x)y = 0 \quad \text{with BC } y(0) = 0, y(L) = 0 \quad (3.178)$$

is called a *homogeneous boundary value problem* (HBVP), and it was denoted as HBVP; thus any BVP which is not homogeneous will be called a nonhomogeneous boundary value problem (NHBVP).

Given a BVP of the form as Eq. 3.176 of type 00, 01, or 10, there is an associated HBVP of type 00 obtained by replacing $h(x)$ by the zero function and replacing the boundary conditions by $y(0) = 0, y(L) = 0$.

From our experience with initial value problems (IVPs), we might expect that the solutions to a general NHBVP are related to those of its associated HBVP. It turns out that BVPs behave very differently than IVPs. For instance, a BVP may have no solution at all, infinitely many solutions, or it may have a unique solution. In a certain sense, BVPs behave more like systems of linear algebraic equations than IVPs.

For comparison, let us recall some general properties of linear algebraic equations. Consider the matrix equation:

$$Ax = b \quad (3.179)$$

where A is an $n \times n$ matrix and x are $n \times 1$ matrices, which we think of as column vectors. Here, A and b are known, and we wish to find x .

Based on the given situation, we have the following facts:

1. If $\det(A) \neq 0$, then:

- (a) $Ax = 0$ has only the trivial solution.
- (b) $Ax = b$ has a unique solution for every b .

2. If $\det(A) = 0$, then:

- (a) $Ax = 0$ has infinitely many solutions.
- (b) $Ax = b$ has either no solutions at all or infinitely many solutions.

Now if we impose a constraint on our study of BVPs upon the case where $p(x) = p$ and $q(x) = q$ are constants (i.e., not function of variable x) and the boundary conditions are of the types 00, 01, and 11, then we can begin with HBVP of the following form.

$$y''(x) + py'(x) + qy(x) = 0 \quad \text{for boundary conditions } y(0) \text{ and } y(L) = 0 \quad (3.180)$$

If Eq. 3.180 has a *nontrivial* solution, then $p^2 - 4q < 0$, which is the *characteristic polynomial* $z(r) = r^2 + pr + q$, has no real roots. Under these conditions of the assumption that by way of the contradiction that $z(r)$ has real roots, then the following two cases can be considered for our analysis purpose here.

Case 1: $z(r) = (r - r_1)(r - r_2)$ where $r_1 \neq r_2$.

In this case the general solution to the differential equation of Eq. 3.180 has the form of the following shape:

$$y(x) = c_1 e^{r_1 x} + c_2 e^{r_2 x}$$

Assume that it is a nontrivial solution, so that either $c_1 \neq 0$ or $c_2 \neq 0$.

The first BC $y(0) = 0$ gives $c_1 + c_2 = 0$, so that $c_1 = -c_2$.

The second BC $y(L) = 0$ gives:

$$e^{r_1 L} = e^{r_2 L}$$

But, the function $x \rightarrow e^x$ is strictly increasing, so this implies that $r_1 = r_2$, which is a contradiction situation.

Case 2: $z(r) = (r - r_1)^2$

Here, the general solution is the form of the following shape:

$$y(x) = c_1 e^{r_1 x} + c_2 x e^{r_1 x}$$

The first BC, $y(0) = 0$, gives $c_1 = 0$.

Then, the second BC, $y(L) = 0$, gives $c_2 L e^{r_1 L} = 0$. But, since $L > 0$, we have that $L e^{r_1 L} > 0$, so $c_2 = 0$ also. This is a contradiction and the above proposition is proved.

Remark In a similar manner, one can prove that the BVPs $y'' + py' + qy = 0$ of types 01, 10, and 11 only have nontrivial solutions if $z(r)$ has no real roots. We leave the proof as an exercise (see Problem 3.7 at the end of this chapter). Thus, in considering constant coefficient BVPs of types 00, 01, 10, and 11, we might as well assume that $p^2 - 4q < 0$. The quadratic formula gives that the roots have the form:

$$r = -p/2 \pm \sqrt{p^2 - 4q}/2$$

Letting $a = -p/2$ and $b = \sqrt{p^2 - 4q}/2$, we get the general solution to the differential equation as:

$$y(x) = e^{ax} [c_1 \cos(bx) + c_2 \sin(bx)]$$

It turns out that the methods and ideas in the study of this expression with BCs of types 00, 01, 10, and 11 are not much different when $a \neq 0$ or $a = 0$. So, for simplicity, we only consider the case when $a = 0$. That is, the case in which $z(r)$ has purely imaginary roots.

This can be interpreted as that our differential equation has the form of:

$$y''(x) + qy(x) = 0 \quad (3.181)$$

where $q > 0$. It will simplify things if we follow other differential equation and boundary value problems book to write $q = \lambda^2$, where $\lambda > 0$.

Thus, we consider the boundary value problem of the following form as:

$$y''(x) + \lambda^2 y(x) = 0 \quad (3.182)$$

where boundary condition is one of the four types 00, 01, 10, and 11.

3.11.1 *Eigenvalues and Eigenfunctions Problems*

As we did in the previous section, we need to again note that we are only going to give a brief look at the topic of eigenvalues and eigenfunctions for boundary value problems. Generally speaking again from linear algebra that we are familiar with, for a given matrix A , if we could find values of λ for which we could find non-zero solutions, i.e., $\vec{x} \neq 0$, to the following relation:

$$A \vec{x} = \lambda \vec{x} \quad (3.183)$$

then we call λ an eigenvalue of A and \vec{x} is its corresponding eigenvector. It is important to recall here that in order for λ to be an eigenvalue, then we had to be able to find non-zero solutions to the equation.

So, just what does this have to do with boundary value problems? Well go back to the previous section and look at Examples 3.2 and 3.3. In these two examples, we solved homogeneous BVPs in the form:

$$y'' + \lambda y = 0 \quad y(0) \quad \text{and} \quad y(2\pi) = 0 \quad (3.184)$$

Example 3.2 Solve the following BVP along with its boundary conditions.

$$y'' + 4y = 0 \quad y(0) \quad \text{and} \quad y(2\pi) = 0$$

Solution: Here the general solution is of the following shape:

$$y(x) = c_1 \cos(2x) + c_2 \sin(2x)$$

Applying the boundary conditions gives:

$$\begin{aligned} c_1 &= y(0) = 0 \\ c_1 &= y(2\pi) = 0 \end{aligned}$$

Thus c_2 is arbitrary and the solution is:

$$y(x) = c_2 \sin(2x)$$

and in this case we will get infinitely many solutions.

Example 3.3 Solve the following BVP along with its boundary conditions.

$$y'' + 3y = 0 \quad y(0) \quad \text{and} \quad y(2\pi) = 0$$

Solution: Here the general solution is of the following shape:

$$y(x) = c_1 \cos(\sqrt{3}x) + c_2 \sin(\sqrt{3}x)$$

Applying the boundary conditions gives:

$$\begin{aligned} c_1 &= y(0) = 0 \\ c_2 \sin(2\sqrt{3}x) &= y(2\pi) = 0 \quad \Rightarrow \quad c_2 = 0 \end{aligned}$$

In this case, we will both constants to be zero and so the solution is of the following form:

$$y(x) = 0$$

To further analyze the two above examples, we can see that we have solved the homogeneous boundary value problem (HBVP) of the form as in Eq. 3.182, where in Example 3.1 we had $\lambda = 4$ and we found nontrivial (i.e., non-zero) solutions to BVP. However, in Example 3.2 we use $\lambda = 3$, and the only solution was the trivial solution (i.e., $y(x) = 0$), so that the homogeneous BVP seems to exhibit similar behavior to the behavior in the matrix equation given by Eq. 3.181. Recall that it also means the boundary conditions are zero as well. There are values of λ that will give nontrivial solutions to this BVP and values of λ and will only admit the trivial solutions.

From what we have learned so far, those values of λ that give nontrivial solutions will be called λ and the *eigenvalue* for the BVP and the nontrivial solutions will be called *eigenfunctions* for the BVP corresponding to the given eigenvalue.

We know by now that for homogeneous boundary value problem of Eq. 3.182 type given, $\lambda = 4$ is an eigenvalue with eigenfunction $y(x) = c_2 \sin(2x)$ and $\lambda = 3$ is not an eigenvalue.

Eventually, we will try to determine if there are any other eigenvalues for Eq. 3.182; however, before we do that let us comment briefly on why it is so important for the BVP to be homogeneous in this discussion. In Examples 3.4 and 3.5, we solve the homogeneous differential equation of such type as in Eq. 3.182 with two boundary conditions of $y(0) = a$ and $y(2\pi) = b$.

Example 3.4 Solve the BVP of the following form along with its given boundary conditions.

$$y'' + 4y = 0 \quad y(0) = -2 \quad \text{and} \quad y(2\pi) = -2$$

Solution: We are working with the same differential equation that is given in Eq. 3.182 with eigenvalue of $\lambda = 4$, so we have a general solution of the following form:

$$y(x) = c_1 \cos(2x) + c_2 \sin(2x)$$

Upon applying the given boundary conditions, we get:

$$\begin{cases} y(0) = -2 = c_1 \\ y(2\pi) = -2 = c_1 \end{cases}$$

So in this case, unlike the previous example, both boundary conditions tell us that we have to have $c_1 = -2$ and neither one of them tell us anything about them. Remember however that all we are asking for is a solution to the differential equation

that satisfies the two given boundary conditions and the following function will do that:

$$y(x) = -2 \cos(2x) + c_2 \sin(2x)$$

In other words, regardless of the value of c_2 , we get a solution, and so, in this case, we get infinitely many solutions to the boundary value problem.

Example 3.5 Solve the BVP of following form along with its given boundary conditions.

$$y'' + 4y = 0 \quad y(0) = -2 \quad \text{and} \quad y(2\pi) = 3$$

Solution: Again, we have the following general solution below, given the eigenvalue of $\lambda = 4$:

$$y(x) = c_1 \cos(2x) + c_2 \sin(2x)$$

However, this time the boundary conditions are providing the following result:

$$\begin{cases} y(0) = -2 = c_1 \\ y(2\pi) = 3 = c_1 \end{cases}$$

In this case, we have a set of boundary conditions each of which requires a different value of c_1 in order to be satisfied. This, however, is not possible and so in this case has *no solution*.

If we now introduce the boundary value problem of Example 3.6 below and its associated boundary conditions, we get totally a different eigenfunction as its solution. The only difference between this example and the other two examples of 3.4 and 3.5 is the boundary conditions.

Example 3.6 Solve the BVP of following form along with its given boundary conditions.

$$y'' + 4y = 0 \quad y(0) = -2 \quad \text{and} \quad y(\pi/4) = 10$$

Solution: Again, the general solution to this differential equation and given eigenvalue of $\lambda = 4$ is in the form of:

$$y(x) = c_1 \cos(2x) + c_2 \sin(2x)$$

and applying the two boundary conditions provided the eigenfunction solution of the following form as well:

$$\begin{cases} y(0) = -2 = c_1 \\ y(\pi/4) = 10 = c_2 \end{cases}$$

With final solution of:

$$y(x) = -2 \cos(2x) + 10 \sin(2x)$$

In the two examples of 3.3 and 3.4, we saw that by simply changing the value of a and/or b , we were able to get either nontrivial solutions or to force no solution at all. In the discussion of eigenvalues and associated eigenfunctions, we need solutions to exist and the only way to assure this behavior is to require that the boundary conditions also be homogeneous. In other words, we need for the BVP to be homogeneous.

There is one final topic that we need to discuss before we move into the topic of eigenvalues and eigenfunctions, and this is more of a notational issue that will help us with some of the work that we'll need to do.

Let us suppose that we have a second-order differential equations and its characteristic polynomial has two real, distinct roots and that they are in the form of:

$$\begin{cases} r_1 = \alpha \\ r_2 = -\alpha \end{cases} \quad (3.185)$$

Then we know that the solution is:

$$y(x) = c_1 e^{r_1 x} + c_2 e^{r_2 x} = c_1 e^{\alpha x} + c_2 e^{-\alpha x} \quad (3.186)$$

While there is nothing wrong with this solution, let us do a little rewriting of this. We will start by splitting up the terms as follows:

$$\begin{aligned} y(x) &= c_1 e^{\alpha x} + c_2 e^{-\alpha x} \\ &= \frac{c_1}{2} e^{\alpha x} + \frac{c_1}{2} e^{\alpha x} + \frac{c_2}{2} e^{-\alpha x} + \frac{c_2}{2} e^{-\alpha x} \end{aligned} \quad (3.187)$$

Now we will add and subtract the following terms as well as notice we are “mixing” the c_i for $i = 1, 2$ and $\pm\alpha$ up in the new terms to obtain the following mathematical relationship for general solution of our boundary value problem as:

$$y(x) = \frac{c_1}{2} e^{\alpha x} + \frac{c_1}{2} e^{\alpha x} + \frac{c_2}{2} e^{-\alpha x} + \frac{c_2}{2} e^{-\alpha x} + \left(\frac{c_1}{2} e^{\alpha x} - \frac{c_1}{2} e^{\alpha x} \right) + \left(\frac{c_2}{2} e^{-\alpha x} + \frac{c_2}{2} e^{-\alpha x} \right) \quad (3.188)$$

Next, rearrange terms around a little with the help of mathematical manipulation, and we have:

$$y(x) = \frac{1}{2}(c_1 e^{\alpha x} + c_1 e^{-\alpha x} + c_2 e^{\alpha x} + c_2 e^{-\alpha x}) + \frac{1}{2}(c_1 e^{\alpha x} - c_1 e^{-\alpha x} - c_2 e^{\alpha x} + c_2 e^{-\alpha x}) \quad (3.189)$$

Finally, the quantities in parenthesis factor and we will move the location of the fraction as well. Doing this, as well as renaming the new constants, we get:

$$\begin{aligned} y(x) &= (c_1 + c_2) \left[\frac{e^{\alpha x} + e^{-\alpha x}}{2} \right] + (c_1 - c_2) \left[\frac{e^{\alpha x} - e^{-\alpha x}}{2} \right] \\ &= A \left[\frac{e^{\alpha x} + e^{-\alpha x}}{2} \right] + B \left[\frac{e^{\alpha x} - e^{-\alpha x}}{2} \right] \end{aligned} \quad (3.190)$$

All this work probably seems very mysterious and unnecessary. However, there really was a reason for it. In fact, you may have already seen the reason, at least in part. The two “new” very well-known hyperbolic functions that we have in our solution are in fact two of the hyperbolic functions that we discussed previously as $\sinh(x)$ and $\cosh(x)$. In particular, they can be mathematically presented by:

$$\begin{cases} \sinh(\alpha x) = \frac{e^{\alpha x} - e^{-\alpha x}}{2} \\ \cosh(\alpha x) = \frac{e^{\alpha x} + e^{-\alpha x}}{2} \end{cases} \quad (3.191)$$

So, another way to write the solution to a second-order differential equation presented as Eq. 3.184 whose characteristic polynomial has two real, distinct roots in the form $r_1 = \alpha$ and $r_2 = -\alpha$ is:

$$y(x) = c_1 \cosh(\alpha x) + c_2 \sinh(\alpha x) \quad (3.192)$$

Note that we switched both constants A and B back to c_1 and c_2 , which is totally acceptable.

Having the solution in this form for some or actually in most of the problems we will be looking would make our life a lot easier. The hyperbolic functions have some very nice properties that we can and will take advantage of the two forms of trigonometric relationships in differential calculus. Since we are going to need these forms, we write the derivative of the two hyperbolic functions as:

$$\begin{cases} \frac{d}{dx}[\cosh(x)] = \sinh(x) \\ \frac{d}{dx}[\sinh(x)] = \cosh(x) \end{cases} \quad (3.193)$$

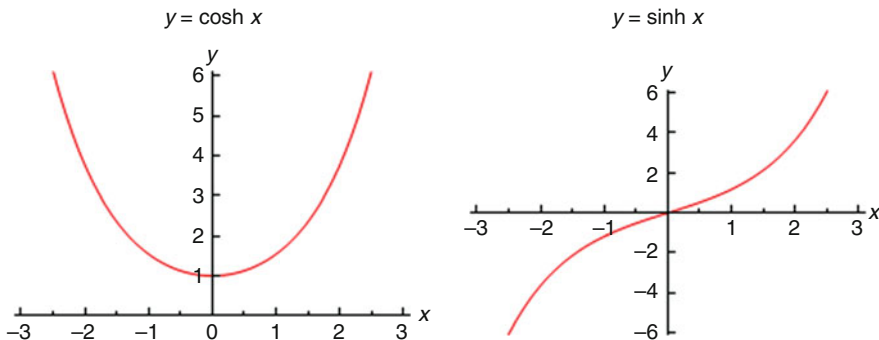


Fig. 3.19 Depiction of hyperbolic cosine and sine functions

Next, let us take a quick look at the graphical depiction of these two functions give in Eq. 3.191 with the value of $\alpha = 1$.

Note that $\cosh(0) = 1$ and $\sinh(0) = 0$. Since most of the time in reactor analysis and neutron diffusion equations we will be working with boundary conditions at the edge of reactor core for distance $x = 0$, these figures will be useful evaluations.

Now if also look at possibility more important case such, as when $\cosh(x) > 0$ for all value of x and so the hyperbolic cosine will never be zero. Similarly, we can see that $\sinh(x) = 0$ only if $x = 0$. We will be using both of these facts in some of our work so we should not forget them (Fig. 3.19).

Only, we have all we need to understand all the above examples and be able to work on some of the homework's problem that is provided at the end of this chapter for boundary value problems.

3.12 Multidimensional Models and Boundary Conditions

The basic multidimensional neutron kinetics model that is currently the state of the art and is expected to be applicable to LWR applications for the expected future is based on the three-dimensional neutron diffusion equation for two neutron energy groups and with six groups of delayed neutron precursors. Several solution methods are considered state of the art although those that are expected to be most applicable in the future utilize a nodal method to handle the spatial dependence and direct integration to handle the temporal dependence.

For light water reactors (LWRs), a two-group diffusion theory approach has proven to be adequate for steady-state applications, and, for those transient applications where direct validation is possible, it also has been found to be adequate. One could argue that more energy groups or a higher-order approximation to the angular dependence of the neutron flux (i.e., a more rigorous approximation to the transport equation than diffusion theory) might improve the rigor of the methodology.

However, since there is an interest in making the transient analysis compatible with steady-state core calculations, and since there is no direct evidence that these higher-order methods give more accurate results for two-group diffusion theory and should continue to be the standard approach.

Six delayed neutron precursor groups are the standard for treating LWRs, and no change should be made in this area either. However, it should be noted that these properties should be defined for each computational cell throughout the core. Although this is the practice in some state-of-the-art codes, some transient codes currently use global averages for the delayed neutron parameters.

Computer codes such as NESTLE solve a few-group neutron diffusion equations utilizing the nodal expansion method (NEM) for eigenvalue, adjoint, and fixed-source steady-state and transient problems.

The NESTLE code can solve the eigenvalue (criticality), eigenvalue adjoint, external fixed-source steady state, and external fixed-source or eigenvalue initiated transient problems. The eigenvalue problem allows criticality searches to be completed, and the external fixed-source steady-state problem can search to achieve a specified power level. Transient problems model delayed neutrons via precursor groups. Several core properties can be input as time-dependent. Two- or four-energy groups can be utilized, with all energy groups being thermal groups (i.e., upscatter exists) if desired. Core geometries modeled include Cartesian and hexagonal. Three-, two-, and one-dimensional models can be utilized with various symmetries. The thermal conditions predicted by the thermal-hydraulic model of the core are used to correct cross sections for temperature and density effects. Cross sections are parameterized by color, control rod state (i.e., in or out), and burnup, allowing fuel depletion to be modeled. Either a macroscopic or a microscopic model maybe employed.

The nonlinear iterative strategy associated with the NEM method is employed. An advantage of the nonlinear iterative strategy is that NESTLE can be utilized to solve either the nodal or finite difference method representation of the few-group neutron diffusion equation. Thermal-hydraulic feedback is modeled employing a homogeneous equilibrium mixture (HEM) model, which allows two-phase flow to be treated. However, only the continuity and energy equations for the coolant are solved, so they are implying a constant pressure treatment.

The slip is assumed to be one in the HEM model. A lumped parameter model is employed to determine the fuel temperature. Decay heat groups are used to model decay heat. All cross sections are expressed in terms of a Taylor's series expansion in coolant density, coolant temperature, effective fuel temperature, and soluble poison number density.

Note that this does not preclude the use of point kinetics models when the neutronic response of the core is not of primary importance. A code which models the nuclear steam supply system (NSSS) should have the ability to use point kinetics with parameters supplied by the user or calculated from the three-dimensional neutronic model – an approach not conducive to automation. One aspect of the point model mat is easy to relate to the multidimensional core model.

The equations are to be solved in three dimensions using rectangular or hexagonal geometry. Multidimensional kinetics should be equated with three-dimensional kinetics for the simple reason that there is no need to consider one-dimensional or two-dimensional models. The latter two approximations are only applicable for certain transients when there is separation between the axial and radial changes during a transient. Furthermore, both of these approximations require considerable analysis in order to obtain nuclear data that have been properly averaged over the remaining dimensions (e.g., over the radial plane when the axial direction is explicitly modeled). This complicates the analysis and negates any simplification that might result from using a lower-order spatial representation. Hence, it has become well established that only three-dimensional methods are of interest.

The treatment of multidimensional systems, other than the spherical geometry, is an important topic since reactor systems normally have finite cylinder geometry. Two approaches are possible: numerical methods and, in the simplest case, the separation of variable method can be used for homogeneous systems. The method of separation of variables is then used to study the criticality and the flux distribution for the parallelepiped reactor geometry, of which the cube is a special case, and the finite cylinder reactor core, which is the geometric configuration of most existing nuclear power reactors.

Hence, in the following content of this section, we deal with this kind of geometry for reactor core and show the related analysis using the separation of variable method, as well as taking orthogonal and orthonormal functions under consideration where we are going to use their advantages.

First, we look at two simple functions $\phi_m(x)$ and $\phi_n(x)$ which are said to be orthogonal over an interval $[a, b]$ if the integral of the product of two functions over that interval vanishes where it can be seen mathematically as Eq. 3.194:

$$\int_a^b \phi_m(x)\phi_n(x)dx = 0 \quad (3.194)$$

Or generally speaking, the two functions of $\phi_m(x)$ and $\phi_n(x)$ are said to be orthogonal with respect to a weighting function $r(x)$, over an interval $[a, b]$, if the following equation is satisfied.

$$\int_a^b r(x)\phi_m(x)\phi_n(x)dx = 0 \quad (3.195)$$

So in summary, a set of functions is said to be orthogonal in interval $[a, b]$, if all pairs of distinct functions in the set are orthogonal in same interval $[a, b]$.

In the previous section, we did fairly discussed the eigenvalues and eigenfunction solution of general one-dimensional differential equation of form such as Eq. 3.182, and now we write the same equation in the following form to later on match it with

our separation of variable method of solving these types of ordinary differential equations. Hence as an application of one-dimensional problem, we can write:

$$\frac{d^2X(x)}{dx^2} + \alpha^2 X(x) = 0 \quad (3.196)$$

with the boundary conditions such as 00 in the form of $X(0) = X(a) = 0$ having the eigenvalues or characteristic values:

$$\alpha_n^2 = \left(\frac{n\pi}{a}\right)^2 \quad (3.197)$$

With corresponding characteristic functions or eigenfunctions of the following form:

$$X_n(x) = \sin\left(\frac{n\pi x}{a}\right) \quad (3.198)$$

Where in this case the weighting function $r(x) = 1$, thus it follows the orthogonality of the following form:

$$\int_0^a X_m(x)X_n(x)dx = \int_0^a \sin\left(\frac{m\pi x}{a}\right) \sin\left(\frac{n\pi x}{a}\right)dx = 0 \quad \text{for } m \neq n \quad (3.199)$$

where m and n are positive integers and the weighted integral of the square of characteristic function $\varphi_n(x)$ has a positive numerical value as follows:

$$C_n = \int_a^b r(x)[\varphi_n(x)]^2dx \quad (3.200)$$

If the arbitrary multiplicative factor involved in the definition of $\varphi_n(x)$ is so chosen that this integral has the value unity, the function $\varphi_n(x)$ is said to be normalized with respect to the weighting function $r(x)$; hence, a set of normalized orthogonal functions is said to be orthonormal.

By direct integration of Eq. 3.200, we get the following:

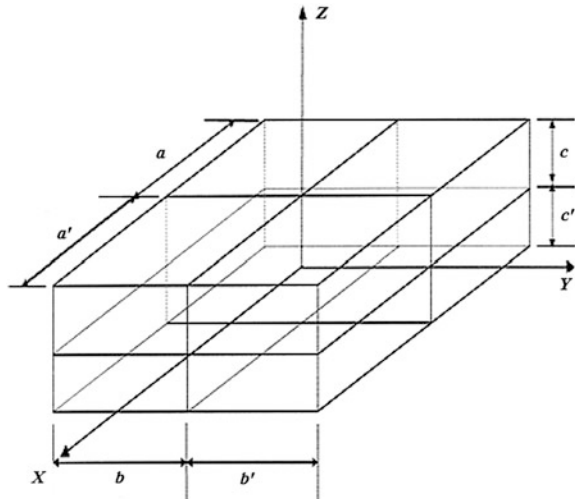
$$C_n = \int_0^a X_n^2(x)dx = \int_0^a \sin^2\left(\frac{n\pi x}{a}\right)dx = \frac{a}{2} \quad (3.201)$$

Thus in order to normalize the functions $\sin(n\pi x/a)$ over the interval $[0, a]$, we would divide them by the normalizing factor $\sqrt{a/2}$, and the set of eigenfunction will yield as:

$$X_n(x) = \sqrt{\frac{a}{2}} \sin\left(\frac{n\pi x}{a}\right) \quad (3.202)$$

Equation 3.202 is an orthonormal set in the interval $[0, a]$.

Fig. 3.20 Unreflected or bare parallelepiped reactor core



3.12.1 The Unreflected Reactor Parallelepiped Core

The unreflected reactor parallelepiped core geometry configuration as depicted in Fig. 3.20 is the simplest possible model of a nuclear fission reactor, where a reflector is not used and the coordinate axes are $2a$, $2b$, and $2c$, respectively. The diffusion equation to be solved is the eigenvalue equation of the following form:

$$\frac{\partial^2 \phi(x, y, z)}{\partial x^2} + \frac{\partial^2 \phi(x, y, z)}{\partial y^2} + \frac{\partial^2 \phi(x, y, z)}{\partial z^2} + B_g^2 \phi(x, y, z) = 0 \quad (3.203)$$

The boundary conditions associated with this partial differential equation are in the form of:

$$\phi(\pm a, y, z) = \phi(x, \pm b, z) = \phi(x, y, \pm c) = 0 \quad (3.204)$$

To solve the partial differential Eq. 3.203 via the separation of variable methods, by assuming the following equation:

$$\phi(x, y, z) = X(x)Y(y)Z(z) \quad (3.205)$$

and substituting Eq. 3.205 into Eq. 3.203, will yield:

$$Y(y)Z(z) \frac{\partial^2 X(x)}{\partial x^2} + X(x)Z(z) \frac{\partial^2 Y(y)}{\partial y^2} + X(x)Y(y) \frac{\partial^2 Z(z)}{\partial z^2} + B_g^2 X(x)Y(y)Z(z) = 0 \quad (3.206)$$

Or simply we can write Eq. 3.206 as:

$$YZ \frac{\partial^2 X}{\partial x^2} + AZ \frac{\partial^2 Y}{\partial y^2} + XY \frac{\partial^2 Z}{\partial z^2} + B_g^2 XYZ = 0 \quad (3.207)$$

We should replace the partial derivatives by total derivatives. Dividing by XYZ yields:

$$\frac{1}{X} \frac{d^2 X}{dx^2} + \frac{1}{Y} \frac{d^2 Y}{dy^2} + \frac{1}{Z} \frac{d^2 Z}{dz^2} = -B_g^2 \quad (3.208)$$

Each term must be separately equal to a constant if it is to hold for all allowed values of x , y , and z . This results in three ordinary rather than partial differential equations:

$$\begin{cases} \frac{1}{X} \frac{d^2 X}{dx^2} = -\alpha^2 \\ \frac{1}{Y} \frac{d^2 Y}{dy^2} = -\beta^2 \\ \frac{1}{Z} \frac{d^2 Z}{dz^2} = -\gamma^2 \end{cases} \quad (3.209)$$

With the condition:

$$\alpha^2 + \beta^2 + \gamma^2 = B_g^2 \quad (3.210)$$

Considering the first ordinary second-order differential equation in variable x :

$$\frac{d^2 X(x)}{dx^2} = -\alpha^2 X(x) \quad (3.211)$$

Equation 3.211 is known to have the solution of the following form as we have seen in the previous section.

$$X(x) = A \cos(\alpha x) + C \sin(\alpha x) \quad (3.212)$$

Note again in Eq. 3.211, we purposely have not used the constant, since it has a special meaning in the reactor theory and it is usually reserved for that purpose as demonstrated before in Eq. 3.104.

Applying the boundary condition $X(\pm a) = 0$ enforces that:

$$A \cos(\alpha a) \pm C \sin(\alpha a) = 0 \quad (3.213)$$

Since we are not interested in the trivial solution $A = C = 0$, this can be satisfied if:

$$C = 0 \rightarrow \alpha a = \frac{n\pi}{2} \quad \text{For all } n \text{ odd}$$

or by

$$A = 0 \rightarrow \alpha a = \frac{n\pi}{2} \quad \text{For all } n \text{ even}$$

Therefore:

$$\alpha^2 = \left(\frac{n\pi}{2a}\right)^2 \quad (3.214)$$

The even and odd solutions can be taken as members of the normalized set:

$$\begin{aligned} X_n(x) &= \frac{1}{\sqrt{a}} \cos\left(\frac{n\pi x}{2a}\right) & \text{For all } n \text{ odd} \\ X_n(x) &= \frac{1}{\sqrt{a}} \sin\left(\frac{n\pi x}{2a}\right) & \text{For all } n \text{ even} \end{aligned} \quad (3.215)$$

Similarly, for the variables y and z cases we can write the following results:

$$\begin{aligned} Y_p(y) &= \frac{1}{\sqrt{b}} \cos\left(\frac{p\pi y}{2b}\right) & \text{For all } p \text{ odd} \\ Y_p(y) &= \frac{1}{\sqrt{b}} \sin\left(\frac{p\pi y}{2b}\right) & \text{For all } p \text{ even} \end{aligned} \quad (3.216)$$

Therefore:

$$\beta^2 = \left(\frac{p\pi}{2b}\right)^2 \quad (3.217)$$

and

$$\begin{aligned} Z_q(z) &= \frac{1}{\sqrt{c}} \cos\left(\frac{q\pi z}{2c}\right) & \text{For all } q \text{ odd} \\ Z_q(z) &= \frac{1}{\sqrt{c}} \sin\left(\frac{q\pi z}{2c}\right) & \text{For all } q \text{ even} \end{aligned} \quad (3.218)$$

Therefore:

$$\gamma^2 = \left(\frac{q\pi}{2b}\right)^2 \quad (3.219)$$

The geometric buckling is the sum of the $B_{g(npq)}^2$ given by Eqs. 3.214, 3.217, and 3.219, and it is shown as below which is matching what we said and expressed as Eq. 3.104:

$$B_{g(npq)}^2 = \left(\frac{n\pi}{2a}\right)^2 + \left(\frac{p\pi}{2b}\right)^2 + \left(\frac{q\pi}{2c}\right)^2 \quad (3.220)$$

and the corresponding eigenfunction solution is:

$$\phi_{npq}(x, y, z) = X_n(x)Y_p(y)Z_q(z) \quad (3.221)$$

The only choice of n, p , and q which gives a nonnegative flux over the whole core is:

$$n = p = q = 1 \quad (3.222)$$

Thus for a solution, we use:

$$B_g^2 = B_{g(1,1,1)}^2 = \left(\frac{\pi}{2a}\right)^2 + \left(\frac{\pi}{2b}\right)^2 + \left(\frac{\pi}{2c}\right)^2 \quad (3.223)$$

Since B_g^2 is fixed by the medium, thus, there are many choices of the dimensions of the medium to reach criticality, but these dimensions must satisfy the condition presented in Eq. 3.223.

Finally, the solution for the critical system becomes from Eqs. 3.215, 3.216, 3.218, and 3.221 as:

$$\phi(x, y, z) = A\phi_{111}(x) = A\frac{1}{\sqrt{abc}} \cos\left(\frac{\pi x}{2a}\right) \cos\left(\frac{\pi y}{2b}\right) \cos\left(\frac{\pi z}{2c}\right) \quad (3.224)$$

3.12.2 The Minimum Volume of the Critical Parallelepiped

Let us minimize the volume V of the parallelepiped as below subject to the condition presented in Eq. 3.223:

$$V = 8abc \quad (3.225)$$

To introduce the constraint, let us solve for one of the dimensions in terms of B_g and the other two dimensions:

$$a' = a + d = \left[\left(\frac{2B_g}{\pi} \right)^2 - \frac{1}{b^2} - \frac{1}{c^2} \right]^{\frac{1}{2}} \quad (3.226)$$

where d is the extrapolation distance. On substitution for “a” into the expression of volume V given by Eq. 3.225, we get:

$$V = 8 \left\{ \left[\left(\frac{2B_g}{\pi} \right)^2 - \frac{1}{(b+d)^2} - \frac{1}{(c+d)^2} \right] - d \right\} \cdot bc \quad (3.227)$$

The minimization processed by setting:

$$\frac{\partial V}{\partial b} = \frac{\partial V}{\partial c} = 0 \quad (3.228)$$

This results in two equation in the two unknown b and c :

$$\begin{aligned} \frac{\partial V}{\partial b} &= 8c \left\{ \left[\left(\frac{2B_g}{\pi} \right)^2 - \frac{1}{(b+d)^2} - \frac{1}{(c+d)^2} \right]^{-\frac{1}{2}} - d \right\} \\ &\quad - \frac{8cb}{(b+d)^3} \left(\frac{1}{2} \right) (2) \left[\left(\frac{2B_g}{\pi} \right)^2 - \frac{1}{(b+d)^2} - \frac{1}{(c+d)^2} \right]^{\frac{3}{2}} = 0 \end{aligned} \quad (3.229)$$

$$\begin{aligned} \frac{\partial V}{\partial c} &= 8b \left\{ \left[\left(\frac{2B_g}{\pi} \right)^2 - \frac{1}{(b+d)^2} - \frac{1}{(c+d)^2} \right]^{-\frac{1}{2}} - d \right\} \\ &\quad - \frac{8cb}{(c+d)^3} \left(\frac{1}{2} \right) (2) \left[\left(\frac{2B_g}{\pi} \right)^2 - \frac{1}{(b+d)^2} - \frac{1}{(c+d)^2} \right]^{\frac{3}{2}} = 0 \end{aligned} \quad (3.230)$$

Using Eq. 3.226 and applying the above two equations yield the following result.

$$\begin{aligned} a &= \frac{b}{(b+d)^3} (a+d)^3 \\ a &= \frac{c}{(c+d)^3} (a+d)^3 \end{aligned} \quad (3.231)$$

Equating the two above expressions presented by set of Eq. 3.231 for a , we get:

$$\frac{b}{(b+d)^3} = \frac{c}{(c+d)^3} \quad (3.232)$$

Equation 3.232 implies that:

$$b = c \quad (3.233)$$

If we would have started by eliminating b instead of a , we would have obtained $a = c$; thus, we can say that:

$$a = b = c \quad (3.234)$$

The critical parallelepiped with minimum volume is found to be a cube with:

$$a = b = c = \sqrt{3} \frac{\pi}{2B_g} \quad (3.235)$$

3.12.3 The Peak-to-Average Flux Ratio

This is an important quantity for heat transfer and fuel management design considerations. This ratio should be as small as possible in order to make the heat generation and the fuel burnup as uniform as possible. Otherwise, larger cooling ducts or orifices must be used in the central parts of the reactor core, and shorter refueling and fuel shuffling times will ensue. However, the average flux is given by:

$$\begin{aligned} \bar{\phi} &= \frac{A}{V} \int_{-c}^{+c} \int_{-b}^{+b} \int_{-a}^{+a} \cos\left(\frac{\pi x}{2a'}\right) \cos\left(\frac{\pi y}{2b'}\right) \cos\left(\frac{\pi z}{2c'}\right) dx dy dz \\ &= A \cdot \left(\frac{2}{\pi}\right)^3 \frac{a'b'c'}{8abc} \left[\sin\left(\frac{\pi x}{2a'}\right) \right]_{-a}^a \left[\sin\left(\frac{\pi y}{2b'}\right) \right]_{-b}^b \left[\sin\left(\frac{\pi z}{2c'}\right) \right]_{-c}^c \\ &= A \cdot \left(\frac{4}{\pi}\right)^3 \frac{a'b'c'}{8abc} \left[\sin\left(\frac{\pi x}{2a'}\right) \right] \left[\sin\left(\frac{\pi y}{2b'}\right) \right] \left[\sin\left(\frac{\pi z}{2c'}\right) \right] \end{aligned} \quad (3.236)$$

Then the maximum flux is as follows:

$$\phi_{\max} = \phi(x = y = z = 0) = A \quad (3.237)$$

Thus, we can write:

$$\frac{\phi_{\max}}{\bar{\phi}} = \left(\frac{\pi}{2}\right)^3 \frac{abc}{a'b'c'} \sqrt{\left[\sin\left(\frac{\pi a}{2a'}\right) \right] \left[\sin\left(\frac{\pi b}{2b'}\right) \right] \left[\sin\left(\frac{\pi c}{2c'}\right) \right]} \quad (3.238)$$

If d is small, then $a' \approx a$, $b' \approx b$, $c' \approx c$, and Eq. 3.238 becomes to be as:

$$\frac{\phi_{\max}}{\bar{\phi}} = \left(\frac{\pi}{2}\right)^3 \quad (3.239)$$

which is a quantity that is independent of the values of a , b , and c .

3.12.4 The Finite Height Cylindrical Core

This is the geometry adopted by most reactor nuclear power plants in today's fission reactors. In this case the equation to be solved is:

$$\frac{1}{r} \frac{\partial}{\partial r} \left[r \frac{\partial \phi(r, z)}{\partial r} \right] + \frac{\partial^2 \phi(r, z)}{\partial z^2} + B_g^2 \phi(r, z) = 0 \quad (3.240)$$

Assuming a separable solution of the form as:

$$\phi(r, z) = R(r)Z(z) \quad (3.241)$$

Substitution of Eq. 3.241 into Eq. 3.240 would yield as:

$$\frac{1}{R} \frac{1}{r} \frac{\partial}{\partial r} \left(r \frac{\partial R}{\partial r} \right) + \frac{1}{Z} \frac{\partial^2 Z}{\partial z^2} + B_g^2 = 0 \quad (3.242)$$

In Eq. 3.242, each term must be a constant; therefore, we can conclude the following relationships as:

$$\frac{1}{R} \frac{1}{r} \frac{d}{dr} \left(r \frac{\partial R}{\partial r} \right) = -\gamma^2 \quad (3.243)$$

$$\frac{1}{Z} \frac{d^2 Z}{dz^2} = -\delta^2 \quad (3.244)$$

With the constraint of the following form:

$$\gamma^2 + \delta^2 = B_g^2 \quad (3.245)$$

Equation 3.245 has a solution for $Z(z)$ as follows as well:

$$Z(z) = A \cos(\delta z) + C \sin(\delta z) \quad (3.246)$$

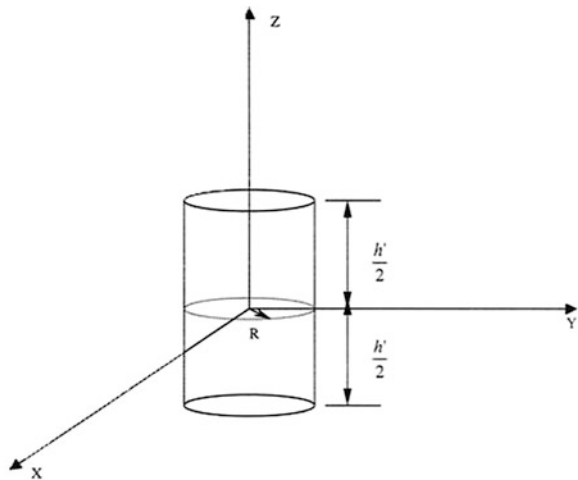
At the extrapolated height of the cylinder and then with the help from Fig. 3.21, we can write the following relationship as:

$$Z\left(\pm \frac{h'}{2}\right) = A \cos\left(\frac{\delta h'}{2}\right) \pm C \sin\left(\frac{\delta h'}{2}\right) = 0 \quad (3.247)$$

Because of the symmetry around $z = 0$, the terms with C are ruled out, thus $C = 0$, and we have:

$$Z(z) = A \cos(\delta z) \quad (3.248)$$

Fig. 3.21 The unreflected finite height cylindrical reactor core



and:

$$\frac{\delta h'}{2} = \frac{n\pi}{2} \quad \text{For all } n = 1, 2, 5, \dots \text{being odd} \quad (3.249)$$

or:

$$\delta^2 = \left(\frac{n\pi}{h'}\right)^2 \quad \text{For all } n \text{ odd} \quad (3.250)$$

The equation for R is then going to be of the following form:

$$\frac{d^2R}{dr^2} + \frac{1}{r} \frac{dR}{dr} = -\gamma^2 R \quad (3.251)$$

which is a Bessel equation of order zero.

This equation derives its name from the German mathematician and astronomer Friedrich Bessel (1784–1846) who reported it while studying planetary motions. In modern engineering practice, it is encountered whenever cylindrical geometry arises in engineering analysis.

The general form of the Bessel equation of order n , which is a variable coefficient equation, is written as:

$$x^2 \frac{d^2y}{dx^2} + x \frac{dy}{dx} + (x^2 - n^2)y = 0 \quad (3.252)$$

where n is a constant.

Equation 3.153 has a general solution of the following form as:

$$y(x) = EJ_n(x) + FY_n(x) \quad (3.253)$$

where E and F are constants of integration to be determined by the boundary conditions and $J_n(x)$ is the Bessel function of the first kind of order n , while $Y_n(x)$ is the Bessel function of the second kind of order n which is also designated as the Neumann function.

If x is replaced by jx where $j = \sqrt{-1}$, Bessel's equation modifies into the form such as:

$$x^2 \frac{d^2 y}{dx^2} + x \frac{dy}{dx} + (x^2 + n^2)y = 0 \quad (3.254)$$

This in turn has a general solution as:

$$y(x) = E'I_n(x) + F'K_n(x) \quad (3.255)$$

where E' and F' are constants of integration to be determined by the boundary conditions and $I_n(x)$ is the modified Bessel function of the first kind of order n , while $K_n(x)$ is the modified Bessel of the second kind of order n .

The four Bessel functions of zero order are shown in Fig. 3.22 and are compared to the $\cos(x)$ function. It can be noticed that both $J_0(x)$ and $Y_0(x)$ are oscillatory. The distance between the roots, or the values at which the functions have a value of zero when they cross the x -axis, become larger and approach the value of π as x increases. The amplitudes of these two functions decrease as x increases, and they are bounded and not infinite everywhere except for $Y_0(x)$ at $x = 0$, which reaches $-\infty$. It is of interest to note that the first root or zero of the function J_0 occurs at $x = 2.405$.

The two functions, $I_0(x)$ and $K_0(x)$, are non-oscillatory and unbounded, the former going to infinity at $x = \infty$ and the latter at $x = 0$.

Per our discussion so far, the general solution of Eq. 3.255 in terms of the Bessel functions of the first and second kinds of zeroth order is:

$$R(r) = EJ_0(\gamma r) + FY_0(\gamma r) \quad (3.256)$$

For the flux to be finite, $F = 0$, and, thus, Eq. 3.256 reduces to the following form:

$$R(r) = EJ_0(\gamma r) \quad (3.257)$$

For the flux to vanish at the extrapolated $EJ_0(\gamma a') = 0$, we must have the following relation as:

$$J_p a' = j_{0,p} \quad \text{for all } p = 1, 2, 3, \dots \quad (3.258)$$

where $j_{0,p}$ is the argument at which J_0 becomes zero at the p -th time.

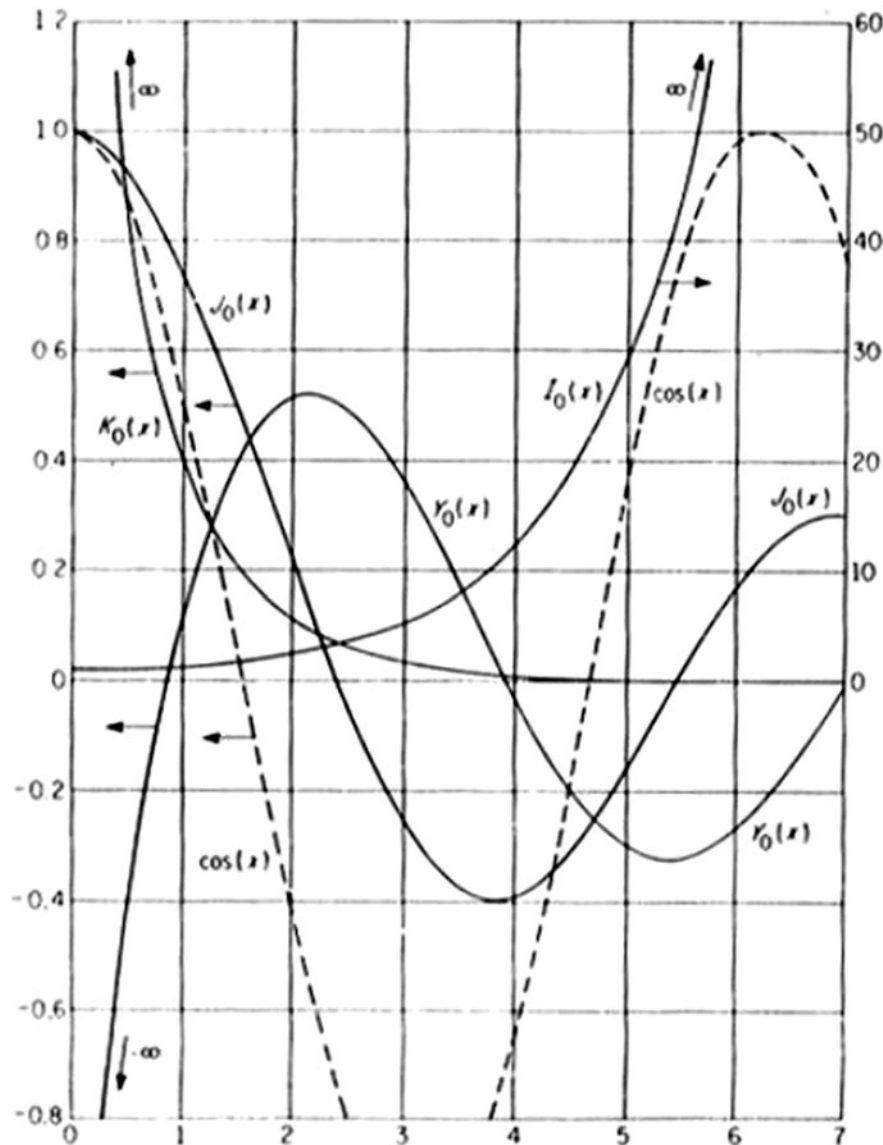


Fig. 3.22 Bessel functions of zero order compared with the cosine function

For the flux to remain positive, we only take $p = 1$ and $j_{0,p} = 2.405$. Thus, we can write the following conclusion, where we have:

$$\gamma = \frac{2.405}{a'} \quad (3.259)$$

and

$$R(r) = EJ_0\left(\frac{2.405}{a'}r\right) \quad (3.260)$$

Choosing also $n = 1$ in Eq. 3.250:

$$\phi(r, z) = \phi_{\max} J_0\left(\frac{2.405}{a'}r\right) \cos\left(\frac{\pi z}{h'}\right) \quad (3.261)$$

where ϕ_{\max} is the flux at the origin.

However then the criticality conditions will be as:

$$B^2 = \delta_1^2 + \gamma_1^2 = \left(\frac{\pi}{h'}\right)^2 + \left(\frac{2.405}{a'}\right)^2 \quad (3.262)$$

The average flux is then given by:

$$\begin{aligned} \bar{\phi} &= \frac{\phi_{\max}}{\pi a^2 h} \int_0^a \int_{-h/2}^{+h/2} \cos\left(\frac{\pi z}{h'}\right) J_0\left(\frac{2.405r}{a'}\right) \cdot (2\pi r dr dz) \\ &= \frac{\phi_{\max}}{\pi a^2 h} \left[\frac{h'}{\pi} 2 \sin\left(\frac{\pi h}{2h'}\right) \right] \cdot \left[2\pi \left(\frac{a'}{2.405}\right)^2 \left(\frac{2.405a}{a'}\right) J_1\left(\frac{2.405a}{a'}\right) \right] \end{aligned} \quad (3.263)$$

Where $\int r J_0(r) dr = r J_1(r)$, thus we can write the following equation as:

$$\frac{\phi_{\max}}{\bar{\phi}} = \sqrt{\left[\left(\frac{4}{2.405\pi}\right) \left(\frac{a'}{a}\right) \left(\frac{h'}{\pi}\right) J_1\left(\frac{2.405a}{a'}\right) \right]} \quad (3.264)$$

and for $a' \approx a$ and $h' \approx h$, it becomes:

$$\frac{\phi_{\max}}{\bar{\phi}} = \frac{2.405\pi}{4J_1(2405)} \approx 1.15\pi \quad (3.265)$$

Table 3.1 below shows all the geometric bucking and flux distribution in different nuclear reactor core geometries

Table 3.1 Geometrical bucking and flux distribution in different nuclear reactor core geometries

Reactor core shape	Geometric bucking	Flux distribution
Sphere radius R	$B_g^2 = \left(\frac{\pi}{R}\right)^2$	$\phi(r) = A \left\{ \frac{\sin\left(\frac{\pi r}{R}\right)}{\left(\frac{\pi r}{R}\right)} \right\}$
Rectangular parallelepiped with side lengths of a, b , and c	$B_g^2 = \left(\frac{\pi}{a}\right)^2 + \left(\frac{\pi}{b}\right)^2 + \left(\frac{\pi}{c}\right)^2$	$\phi(x, y, z) = A \cos\left(\frac{\pi x}{a}\right) \cos\left(\frac{\pi y}{b}\right) \cos\left(\frac{\pi z}{c}\right)$
Cube side length of a	$B_g^2 = 3\left(\frac{\pi}{a}\right)^2$	$\phi(x, y, z) = A \cos\left(\frac{\pi x}{a}\right) \cos\left(\frac{\pi y}{a}\right) \cos\left(\frac{\pi z}{a}\right)$
Finite height cylinder radius R and height H	$B_g^2 = \left(\frac{2.405}{R}\right)^2 + \left(\frac{\pi}{H}\right)^2$	$\phi(x) = AJ_0\left(\frac{2.405r}{R}\right) \cos\left(\frac{\pi z}{H}\right)$
Semi-infinite cylinder radius R	$B_g^2 = \left(\frac{2.405}{R}\right)^2$	$\phi(x) = AJ_0\left(\frac{2.405r}{R}\right)$
Semi-infinite slab thickness a	$B_g^2 = \left(\frac{\pi}{a}\right)^2$	$\phi(x) = A \cos\left(\frac{\pi x}{a}\right)$

3.13 Relating k to the Criticality Condition

We have $-DB^2 - \Sigma_a + v\Sigma_f = 0$. Since there is uncertainty in the material parameters and since $v\Sigma_f$ is the dominant source of error, we introduce a fudge factor to ensure criticality:

$$-DB^2 - \Sigma_a + \frac{v\Sigma_f}{k_{\text{fudge}}} = 0 \quad (3.266)$$

Rearranging, we obtain:

$$\frac{v\Sigma_f}{k_{\text{fudge}}} = DB^2 + \Sigma_a \quad \Rightarrow \quad k_{\text{fudge}} = \frac{v\Sigma_f}{\Sigma_a + DB^2} = \frac{v\Sigma_f / \Sigma_a}{1 + L^2 B^2} \quad (3.267)$$

where $L^2 = D/\Sigma_a$ and Eq. 3.267 has the look of the four-factor formula with a leakage term after we manipulate the above equation a bit.

We can now write:

$$k = k_\infty P_{NL} = p \eta f P_{NL} \quad (3.268)$$

Now:

$$1, \quad p \sim 1 \quad \text{and} \quad \eta f = \frac{v\Sigma_f^{\text{final}}}{\Sigma_a^{\text{fuel}}} \frac{\Sigma_a^{\text{fuel}}}{v\Sigma_f^{\text{final}}} = \frac{v\Sigma_f}{\Sigma_a} \quad (3.269)$$

and

$$\begin{aligned}
 P_{NL} &= \frac{\int \Sigma_a \phi dV}{\int \Sigma_a \phi dV + \int \nabla \cdot \vec{J} dV} = \frac{\int \Sigma_a \phi dV}{\int \Sigma_a \phi dV - \int D \nabla^2 \phi dV} \\
 &= \frac{\int \Sigma_a \phi dV}{\int \Sigma_a \phi dV - \int DB^2 \phi dV} \approx \frac{1}{1 + L^2 B^2}
 \end{aligned} \tag{3.270}$$

So in Eq. 3.267, if we find that for a given size (i.e., B^2) and material properties $(D, \Sigma_a, v\Sigma_f, k_{\text{fudge}})$ must be, say, 1.1 to make the model critical, this is equivalent that the multiplication factor $k = 1.1$, i.e., the arrangement is supercritical as specified and the $v\Sigma_f$ term must be reduced or downgraded to bring the reactor model to the critical state.

[Note that in the above equation, we used the relationship $D\nabla^2\phi(x) + DB^2\phi(x) = D\nabla^2\phi + DB^2\phi = 0$.]

3.14 Analytical Solution for the Transient Case for Reactor

We had the general one-speed neutron balance equation as:

$$\frac{1}{v} \frac{\partial}{\partial t} \phi(\vec{r}, t) = \nabla \cdot D(\vec{r}) \nabla \phi(\vec{r}, t) - \Sigma_a(\vec{r}) \phi(\vec{r}, t) + v\Sigma_f(\vec{r}) \phi(\vec{r}, t) \tag{3.271}$$

For the homogeneous case in one-dimensional, we can write the following:

$$\frac{1}{v} \frac{\partial}{\partial t} \phi(x, t) = D \frac{\partial^2 \phi(x, t)}{\partial x^2} - \Sigma_a \phi(x, t) + v\Sigma_f \phi(x, t) \tag{3.272}$$

Now, we will try to solve Eq. 3.272 by separation of variables; thus, we define $\phi(x, t)$ as:

$$\phi(x, t) = X(x)T(t) \tag{3.273}$$

and substituting Eq. 3.273 into Eq. 3.272 and all the rearrangement as before, we get:

$$\frac{1}{v} X \frac{\partial T}{\partial t} = TD \frac{\partial^2 X}{\partial x^2} - \Sigma_a X T + v\Sigma_f X T \tag{3.274}$$

Or dividing Eq. 3.274 by XT , it yields:

$$\frac{1}{v} \frac{\partial T}{\partial t} = \frac{v}{X} \left[D \frac{\partial^2 X}{\partial x^2} + (\Sigma_f - \Sigma_a) X \right] \equiv -\lambda = \text{constant} \quad (3.275)$$

The left-hand side (LHS) of Eq. 3.275 is a function of T only and has a solution as follows:

$$T(t) = T(0) e^{-\lambda t} \quad (3.276)$$

While the right-hand side (RHS) of Eq. 3.275 is a function of X only and can be rewritten as follows:

$$D \frac{\partial^2 X}{\partial x^2} + (v\Sigma_f - \Sigma_a) X = -\frac{\lambda}{v} X = 0 \quad \text{When reactor is critical} \quad (3.277)$$

i.e.:

$$D \frac{\partial^2 X}{\partial x^2} + \left(\frac{\lambda}{v} + v\Sigma_f - \Sigma_a \right) X = 0 \quad \Rightarrow \quad \frac{\partial^2 X}{\partial x^2} + B^2 X = 0 \quad (3.278)$$

Thus:

$$\frac{\lambda}{v} + v\Sigma_f - \Sigma_a = DB^2 \quad \Rightarrow \quad \lambda = v(\Sigma_a + DB^2 - v\Sigma_f) \quad (3.279)$$

Now the flux goes to zero at the boundaries of the slab $x = \pm \frac{a}{2}$, and we try a cosine solution:

$$X_n(x) = \cos(B_n x) \Rightarrow B_n^2 = \left(\frac{\pi n}{a} \right)^2 \quad \text{for all } n = 1, 3, 5, \dots \quad (3.280)$$

This is an eigenvalue problem and we see the eigenvalues as:

$$\lambda \Rightarrow \lambda_n = v(\Sigma_a + DB_n^2 - v\Sigma_f) \quad (3.281)$$

With the following eigenfunction then as solution:

$$\phi(x, t) = \sum_{n \text{ odd}} A_n e^{-\lambda_n t} \cos\left(\frac{n\pi x}{a}\right) \quad (3.282)$$

where A_n is the amplitude function of the n th term. We use the initial flux and the orthogonal nature of the cosine function to determine A_n . The initial condition for $t = 0$ then is presented as:

$$\phi(x, 0) = \sum_{n \text{ odd}} A_n \cos\left(\frac{n\pi x}{a}\right) \quad (3.283)$$

We multiply both sides by $\cos\left(\frac{m\pi x}{a}\right)$ and integrate over the slab:

$$\begin{aligned} & \int_{-\frac{a}{2}}^{+\frac{a}{2}} \phi(x, 0) \cos\left(\frac{m\pi x}{a}\right) dx \\ &= \sum_{n \text{ odd}} \int_{-\frac{a}{2}}^{+\frac{a}{2}} A_n e^{-\lambda_n t} \cos\left(\frac{n\pi x}{a}\right) \cos\left(\frac{m\pi x}{a}\right) dx \\ &= \frac{a}{2} A_m \end{aligned} \quad (3.284)$$

Therefore, we have:

$$A_n = \frac{2}{a} \int_{-\frac{a}{2}}^{+\frac{a}{2}} \phi(x, 0) \cos\left(\frac{n\pi x}{a}\right) dx \quad (3.285)$$

For long times of t , then we can write the general solution as:

$$\phi(x, t) \approx A_1 e^{-\lambda_1 t} \cos\left(\frac{\pi x}{a}\right) = A_1 e^{-\lambda_1 t} \cos B_1 x \quad (3.286)$$

Since the higher-order modes (larger n) decay faster than the lower-order modes (low n), i.e.,:

$$\lambda_1 < \lambda_2 < \lambda_3 < \dots \quad (3.287)$$

Because:

$$B_1^2 < B_2^2 < B_3^2 < \dots \quad (3.288)$$

[Note that we ignore the even terms in the summation simply because they give non-zero terms at the boundaries $x = \pm \frac{a}{2}$.]

3.15 Criticality

We had found $\lambda \Rightarrow \lambda_n = v(\Sigma_a + DB_n^2 - v\Sigma_f)$ for the transient case. We also found that the slowest decaying mode was that associated with the fundamental eigenvalue, λ_1 . It follows that in the steady state:

$$\lambda_1 = 0 = v(\Sigma_a + DB_1^2 - v\Sigma_f) \quad (3.289)$$

For example, only the fundamental cosine mode remains, and all the other higher-order modes have died away. Thus, we can write the following relationship:

$$B_1^2 = \underbrace{B_g^2}_{\text{geometric buckling}} = \underbrace{\frac{v\Sigma_f - \Sigma_a}{D}}_{\text{material buckling}} \quad (3.290)$$

To summarize the reactor criticality, we can write:

$$\begin{aligned} B_m^2 > B_g^2 &\Rightarrow \lambda_1 < 0 && \text{Supercritical} \\ B_m^2 = B_g^2 &\Rightarrow \lambda_1 = 0 && \text{Critical} \\ \underbrace{B_m^2}_{\text{fission source}} &< \underbrace{B_g^2}_{\text{leakage}} \Rightarrow \lambda_1 > 0 && \text{Subcritical} \end{aligned} \quad (3.291)$$

3.16 Bare Critical Reactor One-Group Model

Now consider the implications of the eigensolutions for reactor design. For the slab reactor, we have:

$$\hat{\Phi}_1(z) = \sin(Bz) \quad \text{and} \quad \hat{\Phi}_2(z) = \cos(Bz) \quad (3.292)$$

Note however that the spatial boundary conditions will determine the value of B^2 . That is, for a given eigenfunction to solve the differential equation, it must:

1. Replicate itself multiplied by a constant
2. Satisfy the boundary conditions imposed by the geometry

The boundary conditions that we will use most often are that the flux goes to zero on the outer boundary of the reactor. In the slab case in z -direction, this means that the flux is 0.0 at $z = 0$ and at $z = H$, where H is the thickness of the slab. The natural eigenfunction for this case is the $\sin(Bz)$ eigenfunction as the \sin function starts at zero, goes to a maximum, and then returns to zero when its argument reaches and the solution is always positive in between. (Frequently this solution is referred to as a cosine function due to the placement of the origin at the center of the slab. All that is important is to remember that the solution must be symmetric about the center of the slab, and depending on where the origin is placed determines which function is used.) For the origin at the center of the slab, the equations are:

$$\begin{aligned}\varphi(z) &= A\hat{\Phi}_1(z) + C\hat{\Phi}_2(z) = A \sin(Bz) + C \cos(Bz) \\ \phi\left(\frac{-H}{2}\right) &= \phi\left(\frac{H}{2}\right) = 0, \text{ therefore } A = 0 \quad \varphi(z) = C \cos(Bz) \\ B \cdot \frac{H}{2} &= \frac{\pi}{2}, \text{ therefore } B = \frac{\pi}{H}\end{aligned}\quad (3.293)$$

Now referring back to the one-group diffusion equation, we have:

$$-\nabla^2\phi(z) = \frac{\frac{1}{k}v\Sigma_f - \Sigma_a}{D}\phi(z) = B^2\phi(z) \quad (3.294)$$

So if:

$$B^2 = \frac{\left(\frac{v\Sigma_f}{k} - \Sigma_a\right)}{D} \quad (3.295)$$

After dividing $\phi(z)$ out of both sides, this can be rewritten as:

$$\begin{aligned}DB^2 &= \frac{v\Sigma_f}{k} - \Sigma_a \\ DB^2 + \Sigma_a &= \frac{v\Sigma_f}{k} \\ \frac{1}{k} &= \frac{(DB^2 + \Sigma_a)}{v\Sigma_f}\end{aligned}\quad (3.296)$$

Finally, mathematical manipulation gives the following:

$$k = \frac{v\Sigma_f}{(DB^2 + \Sigma_a)} \quad (3.297)$$

Now for the infinite reactor with one-group, we have:

$$k_\infty = \frac{v\Sigma_f}{\Sigma_a} \quad (3.298)$$

Therefore, the term DB^2 must represent a leakage effect. We can define:

$$L^2 = \frac{D}{\Sigma_a} = \text{Diffusion area, and } L = \text{Diffusion length} \quad (3.299)$$

and

$$k = \frac{v\Sigma_f}{\Sigma_a} \cdot \left(\frac{\Sigma_a}{DB^2 + \Sigma_a}\right) = \frac{v\Sigma_f}{\Sigma_a} \cdot \left(\frac{1}{1 + L^2B^2}\right)$$

and finally, we can write:

$$k = \frac{v\Sigma_f}{\Sigma_a} \cdot P_{NL} \quad \Rightarrow \quad P_{NL} = \frac{1}{(1 + L^2 B^2)} \quad (3.300)$$

Therefore, we can express that:

$$k_{eff} = k_{\infty} \cdot P_{NL} = k \cdot \frac{1}{(1 + L^2 B^2)}$$

where:

P_{NL} = non-leakage probability

This leads to the traditional two design questions that are asked of most reactor neutronic calculations:

1. How close to critical is a given geometry and configuration? (k ?)
2. What is the required geometry for criticality? (B^2 ?)

Consider an example problem. The following one-group constants are appropriate for a fast, liquid-metal-cooled core.

$$\Sigma_a = 0.004154 \text{ cm}^{-1}$$

$$v\Sigma_f = 0.006007 \text{ cm}^{-1}$$

$$3\Sigma_{tr} = 0.68493 \text{ cm}^{-1}, \text{ and } D = 1.4599 \text{ cm}$$

$$k = \frac{v\Sigma_f}{\Sigma_a} = \frac{0.006007}{0.004154} = 1.45$$

Now consider an infinite slab that is 200 cm thick.

$$B = \frac{\pi}{200} = 0.015708$$

$$B^2 = 0.000247$$

$$DB^2 = 0.000360$$

$$DB^2 + \Sigma_a = 0.004514$$

$$k_{eff} = \frac{v\Sigma_f}{(DB^2 + \Sigma_a)} = \frac{0.006007}{0.004514} = 1.33$$

However, 200 cm is still too thick for criticality. Therefore, let us calculate the exact width required for criticality.

$$k_{eff} = 1.0 = \frac{v\Sigma_f}{(DB^2 + \Sigma_a)}$$

$$(DB^2 + \Sigma_a) = v\Sigma_f$$

Thus, we can write the following result as:

$$B^2 = \frac{(v\Sigma_f - \Sigma_a)}{D} \quad (3.301)$$

$$B^2 = \frac{(0.006007 - 0.004154)}{(1.4599)}$$

$$B^2 = 0.001269$$

$$B = 0.035626$$

$$H = (\pi/B) = 88.18 \text{ cm}$$

For this case with one group and one medium, we can calculate an analytic solution for the thickness required to achieve criticality. When the problem gets more complicated, we will still want to ask the question: “How thick should the reactor be to achieve criticality?” In this case, we will answer the question with an implicit approach. We will choose a set of sizes covering the range required for criticality and interpolate between values on either side of $k_{eff} = 1.0$. Consider the following table for this problem.

H	B^2	k_{eff}
200	0.000247	1.330
150	0.000439	1.253
100	0.000987	1.0736
75	0.001755	0.8944
50	0.003948	0.6057

Note that the analytic value for $k_{eff} = 1.0$ falls between 75.0 and 100.0 cm as expected. The advantage of solving the problem implicitly is that only one computational scheme will be required to answer both design questions. It will become apparent why this is important as our study moves along.

3.17 Bare Critical Reactor One-Group Model: Finite Geometries

Of course, most reactors are not built as infinite slabs. The above example was provided just for simplicity. Consider how it would have to be modified if we were dealing with a finite reactor. We would have to write the diffusion equation in three dimensions as:

$$-D \frac{\partial^2}{\partial x^2} \phi(x, y, z) - D \frac{\partial^2}{\partial y^2} \phi(x, y, z) - D \frac{\partial^2}{\partial z^2} \phi(x, y, z) + \Sigma_a \phi(x, y, z) = \frac{1}{k} v \Sigma_f \phi(x, y, z) \quad (3.302)$$

Now, if the x and y dimensions are each 200 cm and we want to find the z thickness that makes the reactor exactly critical as before, we can choose our origin at the geometric center of the reactor and assume a product form for the flux solution in the reactor. The assumed flux shape would be:

$$\phi(x, y, z) = C \cos B_x x \cdot \cos B_y y \cdot \cos B_z z \quad (3.303)$$

Since the flux will have to go to zero on all boundaries and the x and y dimensions are 200 cm, we have:

$$\begin{aligned} B_x &= \pi/200 & \Rightarrow B_x^2 &= 0.000247 \\ B_y &= \pi/200 & \Rightarrow B_y^2 &= 0.000247 \end{aligned} \quad (3.304)$$

Since these two dimensions are known, the values for B_x^2 and B_y^2 can be substituted back into the differential equation to get:

$$\begin{aligned} &+DB_x^2\phi(x, y, z) + DB_y^2\phi(x, y, z) \\ &- \frac{\partial^2}{\partial z^2}\phi(x, y, z) + \Sigma_a\phi(x, y, z) = \frac{1}{k}v\Sigma_f\phi(x, y, z) \end{aligned} \quad (3.305)$$

Rewriting slightly gives:

$$-\frac{\partial^2}{\partial z^2}\phi(x, y, z) + \left\{DB_x^2 + DB_y^2 + \Sigma_a\right\}\phi(x, y, z) = \frac{1}{k}v\Sigma_f\phi(x, y, z) \quad (3.306)$$

So that the leakage in the other two finite dimensions looks like an increase in absorption when the diffusion calculation is performed in the z -direction.

Now performing the differentiation with respect to z on the z dimension eigenfunction and then dividing out the flux eigenfunction from each term give:

$$DB_z^2 + \left\{DB_x^2 + DB_y^2 + \Sigma_a\right\} = \frac{1}{k}v\Sigma_f \quad (3.307a)$$

or:

$$B_z^2 = \frac{\frac{1}{k}v\Sigma_f - \Sigma_a - \left\{DB_x^2 + DB_y^2\right\}}{D} = \frac{\frac{1}{k}v\Sigma_f - \Sigma_a}{D} - B_x^2 - B_y^2 \quad (3.307b)$$

Thus:

$$B^2 = 0.001269 - 0.000494 = 0.000775$$

$$H_z = 112.8 \text{ cm}$$

The leakage in the two transverse dimensions required a thicker z dimension to compensate, as compared with the infinite slab.

3.18 Reflected Critical Reactors: One-Group Model

Now consider the same core material in a spherical assembly. The fundamental eigenfunction for the flux in a bare core is:

$$\phi(r) = A \frac{\sin Br}{r} \quad (3.308)$$

The $\cos(Br)$ eigenfunction does not show up because it is not bounded at the center of the sphere. The boundary condition at the outer surface requires that the flux goes to zero. This gives:

$$BR = \pi, \text{ and } B = \frac{\pi}{R} \quad (3.309)$$

Using the above value of B gives:

$$B^2 = 0.001269 \text{ cm}^2 \quad \text{and} \quad R = 88.19 \text{ cm} \quad (3.310)$$

This corresponds to $2.873 \times 10^6 \text{ cm}^3$ of the material. If this amount of material provides more than enough volume to transfer the heat produced by the fissile material to a working fluid, it is possible to reduce the size of the core by adding a reflector. The reflector will reduce the number of neutrons lost through leakage and therefore increase k_{eff} for a constant size. We will have the same one-group diffusion equation in the reflector, but the coefficients will be different. In fact for most “reflector” materials, fissile nuclides are not present. This gives the following diffusion equation.

$$\begin{aligned} -D\nabla^2\phi(z) + \Sigma_a\phi(z) &= 0 \\ -\nabla^2\phi(z) &= (\Sigma_a/D)\phi(z) \\ \Sigma_a/D &= 1/L^2 = 3\Sigma_{tr}\Sigma_a \end{aligned} \quad (3.311)$$

For example, consider one-group constants appropriate for a stainless steel reflector.

$$\Sigma_a = 0.002963$$

$$3\Sigma_{tr} = 1.4364, \quad D = 0.6962$$

$$1/L^2 = \frac{\Sigma_a}{D} = \frac{0.002963}{0.6962} = 0.04256$$

$$1/L = 0.06524$$

$$L = 15.33 \text{ cm}$$

Now the differential equation is satisfied in both media, the core and the reflector, if the solutions use the constants derived from the cross sections in both media. All that remains is that the solutions satisfy the boundary conditions. We want to treat the interface between the core and reflector as a boundary condition, rather than worrying about infinite derivatives as the solution jumps from the core to the reflector. This can be done if we require the physical quantities of interest to behave appropriately. At the interface, we must have continuity of the angular flux density. This means that each of the spatial coefficients in the expansion of the angular flux density in Legendre polynomials must be continuous across the interface. For the P_1 approximation, this means that $\phi_0(z)$ and $\phi_1(z)$ must be continuous across the interface. It is obvious how to apply the continuity equation to $\phi_0(z)$. To apply the continuity condition on $\phi_1(z)$, we have to refer back to the P_1 equation. We have:

$$\phi_{1c}(R_c) = -D_c \frac{\partial}{\partial R_c} \phi(R_c) = -D_R \frac{\partial}{\partial R_c} \phi(R_c) = \phi_{1R}(R_c) \quad (3.312)$$

The general solution in the reflector is given by:

$$\phi_R(r) = A_R \frac{e^{-r/L}}{r} + C_R \frac{e^{r/L}}{r} \quad (3.313)$$

3.19 Infinite Reflector Case

Consider first adding an infinite reflector. This will show the largest effect and assumes that the material of the reflector is much cheaper than the core material. For this case the increasing exponential must have zero coefficient ($C_R = 0$) to keep the solution finite. This leaves one function in each material. Applying the interface conditions at the core-reflector interface gives:

(i) *Continuity of flux*

$$A_c \frac{\sin BR_c}{R_c} = A_R \frac{e^{-R_c/L}}{R_c} \quad (3.314)$$

(ii) *Continuity of current*

$$-D_c A_c \left(B \frac{\cos BR_c}{R_c} - \frac{\sin BR_c}{R_c^2} \right) = -D_R A_R \left(-\frac{1}{L} \frac{e^{-R_c/L}}{R_c} - \frac{e^{-R_c/L}}{R_c^2} \right) \quad (3.315)$$

Dividing the flux equation into the current equation gives:

$$-D_c B \frac{\cos BR_c}{\sin BR_c} + \frac{D_c}{R_c} = \frac{D_R}{L} + \frac{D_R}{R_c} \quad (3.316)$$

or:

$$\tan BR_c = \frac{BR_c}{1 - \frac{D_c}{D_c} \left(\frac{R_c}{L} + 1 \right)} \quad (3.317)$$

This equation is a transcendental equation because the unknown R_c occurs on both sides of the equation. The easiest way to find an acceptable solution is to compute both sides of the equation for various values of the unknown R_c and find the value of R_c where both sides attain the same value.

Consider the following table:

Core radius (cm)	Left-hand side	Right-hand side
80.0	-0.30006	-1.45005
70.0	-0.75670	-1.50736
60.0	-1.57131	-1.59122
55.0	-2.44225	-1.64962
59.0	-1.70228	-1.60179
59.8	-1.59631	-1.59329

This gives a core radius of about 59.8 cm which is a very significant reduction from the 88.19 cm of the bare core (or the 85.27 cm if the extrapolation distance is subtracted). The active core volume is only 31.2% (34.5%) of the bare core active volume.

Now consider the effect of a finite reflector. Choose the reflector thickness to be one diffusion length or about 15.33 cm. We now must solve for the coefficient of the rising exponential in the reflector based on the boundary condition at the outer surface. Setting the flux equal to zero at the outer boundary gives:

$$\begin{aligned} \phi(R_c + t_c) = 0 &= A_R \frac{e^{-\frac{R_c+t_R}{L}}}{R_c + t_R} + C_R \frac{e^{\frac{R_c+t_R}{L}}}{R_c + t_R} \\ C_R &= -A_R e^{-\frac{2(R_c+t_R)}{L}} = -\alpha A_R \end{aligned} \quad (3.318)$$

Then at the core-reflector interface, the continuity of the flux gives:

$$A_C \frac{\sin BR_C}{R_C} = A_R \left(\frac{e^{-R_C/L}}{R_C} - \alpha \frac{e^{R_C/L}}{R_C} \right) \quad (3.319)$$

And the continuity of the current gives:

$$-D_C A_C \left(B \frac{\cos BR_C}{R_C} - \frac{\sin BR_C}{R_C^2} \right) = -D_R A_R \left\{ -\frac{e^{-R_C/L}}{LR_C} - \frac{e^{R_C/L}}{R_C^2} - \alpha \left(\frac{e^{R_C/L}}{LR_C} - \frac{e^{R_C/L}}{R_C^2} \right) \right\} \quad (3.320)$$

or:

$$D_C A_C \sin BR_C (1 - BR_C ctn BR_C) = D_R A_R d^{-R_C/L} \left\{ 1 + \frac{R_C}{L} - \left(1 - \frac{R_C}{L} \right) e^{-R_C/L} \right\} \quad (3.321)$$

And the flux equation becomes:

$$A_C \sin BR_C = A_R e^{-R_C/L} \left(1 - e^{-2t_R/L} \right) \quad (3.322)$$

Dividing the flux equation into the current equation gives:

$$D_C (1 - BR_C ctn BR_C) = D_R \frac{\left\{ 1 + \frac{R_C}{L} - \left(1 - \frac{R_C}{L} \right) e^{-2t_R/L} \right\}}{\left\{ 1 - e^{-2t_R/L} \right\}} \quad (3.323)$$

or

$$BR_C ctn BR_C = 1 - \frac{D_R}{D_C} \left\{ \frac{1 + \frac{R_C}{L} - \left(1 - \frac{R_C}{L} \right) e^{-2t_R/L}}{1 - e^{-2t_R/L}} \right\} \quad (3.324)$$

When this is solved for the core thickness with a one diffusion length thick reflector, the core radius comes out to be 65.0 cm. This corresponds to a reduction in volume for the core to 40% of the bare core and is only 28.4% greater than the infinite reflector core.

3.20 Criticality for General Bare Geometries

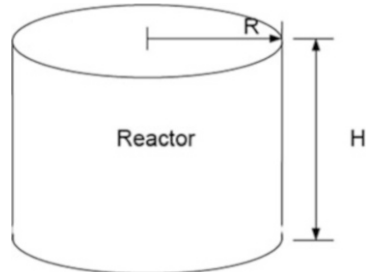
Consider the following equation as:

$$\frac{1}{v} \frac{\partial}{\partial t} \phi(\vec{r}, t) = \nabla \cdot D(\vec{r}) \nabla \phi(\vec{r}, t) - \Sigma_a(\vec{r}) \phi(\vec{r}, t) + v \Sigma_f(\vec{r}) \phi(\vec{r}, t) \quad (3.325)$$

In the steady state with homogeneous properties, we have:

$$\nabla^2 \nabla \phi(\vec{r}, t) + \left(\frac{v \Sigma_f(\vec{r}) - \Sigma_a(\vec{r})}{D(\vec{r})} \right) \phi(\vec{r}, t) = 0 \quad (3.326)$$

Fig. 3.23 Cylindrical reactor



or

$$\nabla^2 \nabla \phi(\vec{r}, t) + \underbrace{\left(\frac{k_\infty - 1}{L^2} \right)}_{\equiv B^2} \phi(\vec{r}, t) = 0 \quad \text{where } L^2 \equiv \frac{D}{\Sigma_a} \text{ and } k_\infty \equiv \frac{\nu \Sigma_f}{\Sigma_a} \quad (3.327)$$

The boundary condition is zero flux at the extrapolated boundary (surface):

$$\phi(\tilde{r}_s) = 0 \quad (3.328)$$

Consider, for example, a reactor made in the shape of a right cylinder as shown in Fig. 3.23.

The one-speed, neutron balance equation is then given by:

$$\frac{1}{r} \frac{\partial}{\partial r} \left(r \frac{\partial \phi(r, z)}{\partial r} \right) + \frac{\partial^2 \phi(r, z)}{\partial z^2} + B^2 \phi(r, z) = 0 \quad (3.329)$$

With the boundary conditions that are given as:

$$\begin{aligned} \phi(\tilde{R}, z) &= 0 \\ \phi(r, \pm \tilde{H}/2) & \end{aligned} \quad (3.330)$$

We use the separation of variable methods as before and write:

$$\phi(r, z) = R(r)Z(z) \quad (3.331)$$

Substituting Eq. 3.331 into Eq. 3.329, we obtain two sets of independent variables for r and z as follows:

$$\begin{aligned} \frac{d}{dr} \left(r \frac{dR}{dr} \right) + \alpha^2 R &= 0 \\ \frac{d^2 Z}{dr^2} + \lambda^2 Z &= 0 \end{aligned} \quad (3.332)$$

The solution to the radial equation is:

$$R(r) = AJ_0(\alpha r) + CY_0(\alpha r) \quad (3.333)$$

The constant C must be 0, because $Y_0(\alpha r) \rightarrow \infty$ as $r \rightarrow 0$. Since the flux must go to zero at the extrapolated boundary, $\alpha = \frac{2.405}{\tilde{R}}$, the first root of J_0 .

The solution to the axial equation is also going to be:

$$Z(z) = \cos(\lambda z) \quad (3.334)$$

where $\lambda^2 = (\pi/H)^2$ since the flux goes to zero at the extrapolated boundaries. Thus, the full solution to Eq. 3.331 is given by:

$$\phi(r, z) = AJ_0\left(\frac{2.405}{\tilde{R}}r\right) \cos\left(\frac{\pi}{H}z\right) \quad (3.335)$$

And as a result, the criticality condition is:

$$\underbrace{\left(\frac{2.405}{R}\right)^2 + \left(\frac{\pi}{H}\right)^2}_{B_g^2} = \underbrace{\frac{v\Sigma_f - \Sigma_a}{D}}_{B_m^2} \quad (3.336)$$

3.21 Reflected Reactor Geometries

Now let us look at a slab reactor with a reflector on each side. As before, we can write the following as we have seen in Eq. 3.325:

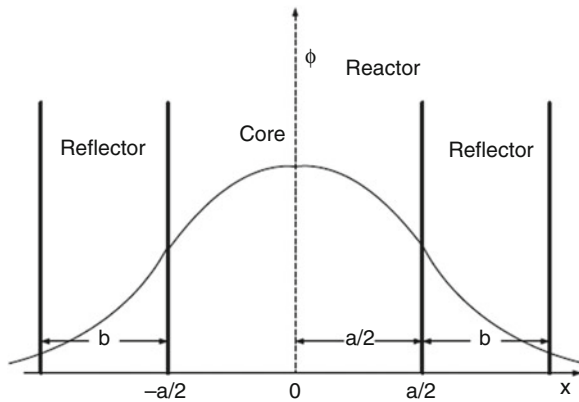
$$\frac{1}{v} \frac{\partial}{\partial t} \phi(\vec{r}, t) = \nabla \cdot D(\vec{r}) \nabla \phi(\vec{r}, t) - \Sigma_a(\vec{r}) \phi(\vec{r}, t) + v\Sigma_f(\vec{r}) \phi(\vec{r}, t) \quad (3.337)$$

Assuming again the steady state, homogeneous properties within each region, and one-dimensional case, we can write:

$$D \frac{\partial^2 \phi(x)}{\partial x^2} + (-\Sigma_a + v\Sigma_f) \phi(x) = 0 \quad (3.338)$$

This will apply to both the core region and the reflected region, as we can see in Fig. 3.24.

Fig. 3.24 Reflected slab reactor



The governing equation of this problem is given by:

$$\begin{aligned} \text{Core : } & D^C \frac{d^2 \phi^C(x)}{dx^2} + \left(-\Sigma_a^C + v \Sigma_f^C \right) \phi^C(x) = 0 \\ \text{Reflector : } & D^R \frac{d^2 \phi^R(x)}{dx^2} + -\Sigma_a^R \phi^R(x) = 0 \end{aligned} \quad (3.339)$$

With given boundary condition as:

$$\begin{cases} \phi^R\left(\frac{a}{2} + b\right) = 0 \\ \phi^C\left(\frac{a}{2}\right) = \phi^R\left(\frac{a}{2}\right) \\ J^C\left(\frac{a}{2}\right) = J^R\left(\frac{a}{2}\right) \\ \text{Symmetry} \end{cases} \quad (3.340)$$

We will just solve for $x > 0$ since, by symmetry, the solution is the same for $x < 0$. We try:

$$\phi^C(x) = A^C \cos(B_m^C x) \quad \text{where } (B_m^C)^2 = \frac{v \Sigma_f^C - \Sigma_a^C}{D^C} \quad (3.341)$$

and

$$\phi^C(x) = A^R \sinh\left[\frac{\frac{a}{2} + b - x}{L^R}\right] \quad \text{where } (L^R)^2 = \frac{D^R}{\Sigma_a^R} \quad (3.342)$$

And Eq. 3.342 is equal to 0 at $x = \frac{a}{2} + b$ since $\sinh(t) = \frac{e^{+t} - e^{-t}}{2}$.

Applying the boundary conditions given by Eq. 3.340 provides the following results:

$$\phi \text{ equal at interface} \Rightarrow A^C \cos(B_m^C x) = A^R \sinh\left(\frac{b}{L^R}\right) \quad (3.343)$$

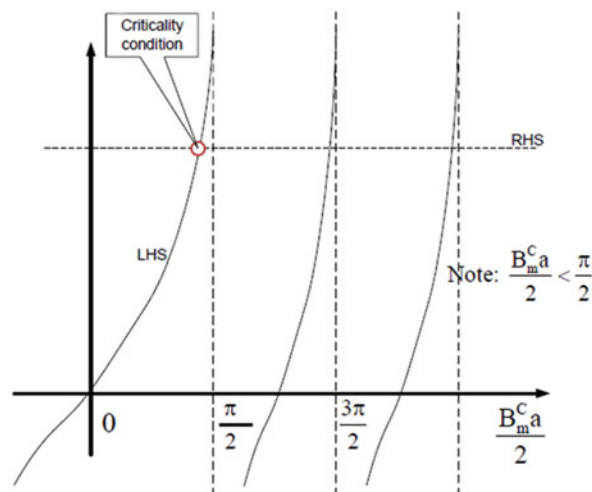
$$J \text{ equal at interface} \Rightarrow D^C B_m^C A^C \sin\left(\frac{B_m^C a}{2}\right) = \frac{D^R}{L^R} A^R \cosh\left(\frac{b}{L^R}\right) \quad (3.344)$$

We divide Eq. 3.350 by Eq. 3.349 to eliminate the unknown A coefficients to give the *criticality condition*:

$$D^C B_m^C \tan\left(\frac{B_m^C a}{2}\right) = \frac{D^R}{L^R} \coth\left(\frac{b}{L^R}\right) \quad (3.345)$$

This relates the geometry of the reactor to the material properties of the reactor. To graphically illustrate this, we plot the LHS and the RHS against $\frac{B_m^C a}{2}$ in Fig. 3.25. Where the LHS and the RHS are equal, the reactor is critical. This occurs at multiple values of $\frac{B_m^C a}{2}$, but the lowest value (i.e., smallest core size, a) occurs at just less than $\pi/2$. If you recall, the bare reactor went critical at $B_m = \pi/a$ or equivalently at $B_m a/2 = \pi/2$. Thus, the core size for a reflected reactor is smaller than a non-reflected reactor, which resulted in a fuel “savings.”

Fig. 3.25 Criticality for a reflected slab reactor



3.22 Reactor Criticality Calculations

As you no doubt noticed from the previous analytical solutions, any real reactor model would be too complex to be solved analytically. Therefore, we resort to numerical means.

You will recall that we had:

$$\frac{1}{v} \frac{\partial}{\partial t} \phi(\vec{r}, t) = \nabla \cdot D(\vec{r}) \nabla \phi(\vec{r}, t) - \Sigma_a(\vec{r}) \phi(\vec{r}, t) + v \Sigma_f \phi(\vec{r}, t) \quad (3.346)$$

If we postulate that:

$$\phi(x, t) = e^{\lambda t} \Psi(x) \quad (3.347)$$

then:

$$\frac{\lambda}{v} \Psi(\vec{r}, t) = \nabla \cdot D(\vec{r}) \nabla \Psi(\vec{r}) - \Sigma_a(\vec{r}) \Psi(\vec{r}) + v \Sigma_f(\vec{r}) \Psi(\vec{r}) \quad (3.348)$$

and we get a steady-state solution when $\lambda = 0$. Therefore, the basic idea is to adjust the equation parameters until $\lambda = 0$. However, which parameters and how to adjust them are the questions.

Generally, you start with a *fixed* geometry and basic design, i.e., the materials are known. Thus, the free variable is the fuel, i.e., reactivity. Therefore, vary v or, equally, introduce a fudge factor:

$$\begin{aligned} -\nabla \cdot D(\vec{r}) \nabla \phi(\vec{r}) + \Sigma_a(\vec{r}) \phi(\vec{r}) &= \underbrace{\frac{v}{k} \Sigma_f(\vec{r}) \phi(\vec{r})}_{\text{source term}} \\ \Downarrow \\ M\phi &= \frac{1}{k} F\phi \end{aligned} \quad (3.349)$$

where M and F are operators and the fudge factor is k . If you rearrange the equation, solving for k as we did in Sect. 3.14 of this chapter, you will see that k takes on a form like the multiplication factor k that we introduced earlier. The k generated satisfies:

$$k_{\text{fudge}} = \frac{v \Sigma_f / \Sigma_a}{1 + \underbrace{L^2 B^2}_{\text{from the } \nabla \cdot D \nabla \phi \text{ term}}} \quad (3.350)$$

The numerical algorithm for a fixed design is as follows:

1. Set up a spatial grid as we did for the fixed-source case in *Reactor Physics: Numerical Methods*.
2. Guess $k^{(0)}$ and $\phi^{(0)}$ for the initial or zeroth iteration.
3. Calculate the source term $\frac{1}{k} F\phi^{(0)}$.
4. Solve as per the previous numerical methods (G-S or SOR, etc.) with this known source. This involves iteration on ϕ to get a converged spatial distribution of ϕ for this fixed-source estimate. This generates $\phi^1(\vec{r})$. This is the *inner loop*. Note that this flux distribution is based on a guess of the source term which is a function of ϕ . Mathematically:

$$M\phi^{(1)} = \frac{1}{k^{(0)}} F\phi^{(0)} = \frac{S^{(0)}}{k^{(0)}} \Rightarrow \phi^{(1)} \\ S^{(1)} = F\phi^{(1)} \quad (3.351)$$

5. Now we need to update the source and the value of the fudge factor k . The source is easy – just recalculate $F\phi$ as per Eq. 3.349 or 3.351 using the latest flux values. But what about k ? We will see in a minute that $k^1 = k^0 S^1 / S^0$.
6. With an updated source term, we now recalculate the flux as above. This is the outer loop. The algorithm can be summarized as:

Guess $\phi^{(0)}$ and $k^{(0)}$.

[outer loop] on i

$$M\phi^{(i+1)} = \frac{1}{k^{(i)}} F\phi^{(i)} = \frac{S^{(i)}}{k^{(i)}} \Rightarrow \text{inner loop} \Rightarrow \phi^{(i+1)} \\ \text{Update } S^{(i+1)} = F\phi^{(i+1)} \\ \text{Update } k^{(i+1)} = \frac{k^{(i)} S^{(i+1)}}{S^{(i)}} \quad (3.352)$$

[outer loop] until flux converges

If we are clever, we can combine the inner and outer iterations by updating k and S every time we make an inner loop sweep. There is hardly any sense in converging the inner loop to a fine tolerance only to make big changes in the fudge factor and source term and then recompute the flux again to a fine tolerance. It is far better to update k and S as you go.

Now, on to how to update k , we note that:

$$k \equiv \frac{\text{Fission sources}}{\text{Sinks}} = \frac{F\phi}{M\phi} \quad (3.353)$$

Thus:

$$k \equiv \frac{\int_{\text{volume}} F\phi^{(i+1)} dV}{\int_{\text{volume}} M\phi^{(i+1)} dV} \quad (3.354)$$

However, in our procedure:

$$M\phi^{(i+1)} = \frac{1}{k^{(i)}} F\phi^{(i)} = \frac{S^{(i)}}{k^{(i)}} \quad (3.355)$$

Therefore:

$$k^{(i+1)} \equiv \frac{\int_{\text{volume}} S^{(i+1)} dV}{\frac{1}{k^{(i)}} \int_{\text{volume}} S^{(i)} dV} \quad (3.356)$$

We can improve on this by looking ahead based on the past trend (extrapolation). What does adjusting the k mean physically? Let us say that the converged value of k that you get for a particular case is 1.1. That means that the source term, $v\Sigma_f(\vec{r})\phi(\vec{r})$, was too big, causing the reactor to be supercritical. To make the reactor critical, it had to be reduced by 10%. Then, and only then, did the source and sink terms balance. Obviously, we could have made the reactor critical in a number of other ways, such as adjusting the absorption term or changing the size of the reactor. But since we typically start with a physical reactor of the given (or proposed) dimensions and materials, it is convenient to control the criticality in the way we did. If you run into a case where it makes more sense to adjust another term, by all means, go for it. The overall procedure is similar, and it should work just as well. Just make sure that you are not attempting to find criticality by adjusting a term that is of little influence on the equation set. For instance, a control rod (absorber) at the very edge of a reactor sees few neutrons so it would be ineffective in affecting overall criticality. Use your common sense.

Problems

Problem 3.1 Assuming that the reactivity drop in dollars can be measured by taking the ratio of the neutrons immediately before to immediately after the control rod insertion and is given by the following relationship as:

$$\frac{|\rho|}{\beta} = \frac{n_0}{n_1} - 1$$

where n_0 is initial condition and n_1 is the final one, then consider that a critical reactor operates at a power level of 80 W. Dropping a control rod into the core causes the flux to undergo a sudden decrease to 60 W. How many dollars is the control rod worth?

Problem 3.2 An infinite, bare cylindrical reactor is critical with a cylindrical control rod along its axis.

- (a) Using one-group theory, derive expressions for the probability that a thermal neutron:
- (i) Is absorbed by the rod
 - (ii) Escapes from the surface of the reactor
 - (iii) Is absorbed in the reactor core material
- (b) Show that the increase in the number of neutrons leaking per second from the surface due to the presence of the rod is comparable to the number of neutrons absorbed per second in the rod.

Solution: I need to write a solution for this problem.

Problem 3.3 Using the integral rod worth curve plotted in the following Fig. 3.26, find the reactivity inserted by moving the rod from 12 inches withdrawn out to 18 inches withdrawn.

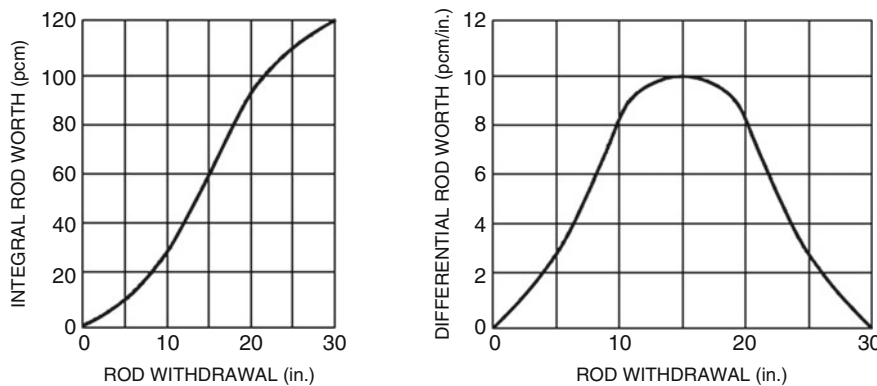


Fig. 3.26 Rod worth curves for Problem 3.3

Problem 3.4 Using the differential rod worth curve provided in Fig. 3.26, calculate the reactivity inserted by moving the rod from 10 inches withdrawn to 6 inches withdrawn.

Problem 3.5 For the differential rod worth data given below, construct differential and integral rod worth curves.

Interval (inches)	Reactivity inserted (pcm)
0–2	10
2–4	20
4–6	40
6–8	60
8–10	60
10–12	40
12–14	20
14–16	10

Problem 3.6 Consider a thermal neutron density of $N = 10^8 \text{ cm}^{-3}$ in a graphite medium using the total cross section of $\Sigma_t = 0.385 \text{ cm}^{-1}$ and a corresponding neutron speed of $2.2 \times 10^5 \text{ cm/s}$, find the reaction rate density.

Problem 3.7 Determine all solutions, if any, to the boundary value problem:

$$y'' + 9y = 0 \quad 0 < x < \pi$$

with boundary conditions

$$y(0) = 0 \quad \text{and} \quad y'(\pi) = -6$$

by first finding a general solution to the differential equation.

Problem 3.8 Determine all solutions, if any, to the boundary value problem:

$$y'' + 2y' + y = 0 \quad -1 < x < 1$$

with boundary conditions

$$y(-1) = 0 \quad \text{and} \quad y(1) = 2$$

by first finding a general solution to the differential equation.

Problem 3.9 Find the eigenvalues and the corresponding eigenfunctions for the boundary value problem:

$$y'' + \lambda y = 0 \quad 0 < x < \pi$$

with boundary conditions

$$y'(0) = 0 \quad y(\pi) = 0.$$

Problem 3.10 Find the eigenvalues and the corresponding eigenfunctions for the boundary value problem:

$$y'' + \lambda y = 0 \quad 0 < x < \pi/2$$

with boundary conditions

$$y'(0) = 0 \quad y(\pi/2) = 0.$$

Problem 3.11 Find the eigenvalues and the corresponding eigenfunctions for the boundary value problem:

$$y'' - 2y' + \lambda y = 0 \quad 0 < x < \pi$$

with boundary conditions

$$y(0) = 0 \quad y(\pi) = 0.$$

Problem 3.12 Find the eigenvalues and the corresponding eigenfunctions for the boundary value problem:

$$y'' + \lambda y = 0$$

with boundary values $y(0) = 0$ and $y(L) = 0$.

Problem 3.13 Find the eigenvalues and the corresponding eigenfunctions for the boundary value problem:

$$y'' + \lambda y = 0$$

with boundary values $y'(0) = 0$ and $y'(L) = 0$.

Problem 3.14 Find the eigenvalues and the corresponding eigenfunctions for the boundary value problem:

$$y'' + \lambda y = 0$$

with boundary values $y(0) = 0$ and $y'(L) = 0$.

Problem 3.15 Find the eigenvalues and eigenfunctions for the boundary value problem:

$$y'' + \lambda y = 0$$

with boundary values $y(L_1) = 0$ and $y(L_2) = 0$, where $L_2 > L_1 > 0$.

Problem 3.16 Find the eigenvalues and eigenfunctions for the boundary value problem:

$$y'' + \lambda y = 0$$

with boundary values $y(0) = y(L)$ and $y'(0) = y'(L)$.

Problem 3.17 Find the eigenvalues and eigenfunctions for the boundary value problem:

$$y'' + \lambda y = 0$$

with boundary values $y(0) = 0$ and $y(L) + y'(L) = 0$.

Problem 3.18 Find the eigenvalues and eigenfunctions for the boundary value problem:

$$y'' - \frac{2}{x}y' + \left(\lambda + \frac{2}{x^2}\right)y = 0$$

with boundary values $y(1) = 0$ and $y(2) = 0$.

Hint: Let $y = xu(x)$.

Problem 3.19 Consider a uniform source as $S(x) = S_0$ in an infinite medium represented by differential equation of the following form:

$$\frac{d^2\phi(x)}{dx^2} - \frac{1}{L^2}\phi(x) = -\frac{S_0}{D}$$

with boundary conditions such that $\phi(x) < \infty$ as $x \rightarrow \pm\infty$. Find the solution for such equation.

Problem 3.20 We will try to determine the neutron flux resulting from an arbitrary distribution source in a finite slab of width a . This results in to solve the following nonlinear differential equation:

$$\frac{d^2\phi(x)}{dx^2} - \frac{1}{L^2}\phi(x) = -\frac{S_0}{D} \quad -\frac{a}{2} \leq x \leq \frac{a}{2}$$

Subject to the vacuum boundary conditions as:

$$\phi\left(\frac{a}{2}\right) = 0$$

$$\phi\left(-\frac{a}{2}\right) = 0$$

Hint: Since we have taken the source $S(x)$ to be arbitrary, we cannot assume symmetry to restrict our attention to the range $0 \leq x \leq \tilde{a}/2$.

Problem 3.21 Use Green's function to solve the following problem:

$$\frac{d^2y}{dx^2} + y = \operatorname{cosec}(x)$$

Subject to the boundary conditions $y(0) = y(\pi/2) = 0$.

Hint: Green's function $G(x, z)$ must satisfy the original ordinary differential equation with the right-hand side (RHS) set equal to a *delta function* such as $\mathcal{E}\{G(x, z)\} = \delta(x - z)$. Thus, $G(x, z)$ may be thought of physically as the response of a system to unit impulse at $x = z$.

Problem 3.22 Solve the heat flow problem:

$$\begin{aligned}\frac{\partial u}{\partial t}(x, t) &= 3 \frac{\partial^2 u}{\partial x^2}(x, t) & 0 < x < \pi \quad t > 0 \\ u(0, t) &= u(\pi, t) = 0 & t < 0 \\ u(x, 0) &= \sin 4x + 3 \sin 6x - \sin 10x & 0 < x < \pi\end{aligned}$$

Problem 3.23 Show that if $u(x, t) = X(x)T(t)$ is a solution of the partial differential equation:

$$\frac{\partial^2 u(x, t)}{\partial t^2} + \frac{\partial u(x, t)}{\partial t} + u(x, t) = \alpha^2 \frac{\partial^2 u(x, t)}{\partial x^2}$$

then $X(x)$ and $T(t)$ must satisfy the following ordinary differential equations:

$$\begin{aligned}X''(x) - \lambda X(x) &= 0 \\ T''(t) + T'(t) + (1 - \lambda \alpha^2)T(t) &= 0\end{aligned}$$

where λ is a constant.

Problem 3.24 Show that if $u(r, \theta, z) = R(r)T(\theta)Z(z)$ is a solution of the partial differential equation:

$$\frac{\partial^2 u}{\partial r^2} + \frac{1}{r} \frac{\partial u}{\partial r} + \frac{1}{r^2} \frac{\partial^2 u}{\partial \theta^2} + \frac{\partial^2 u}{\partial z^2} = 0$$

then $R(r)$, $T(\theta)$, and $Z(z)$ must satisfy the following ordinary differential equations:

$$T''(\theta) + \mu T(\theta) = 0 \quad (1)$$

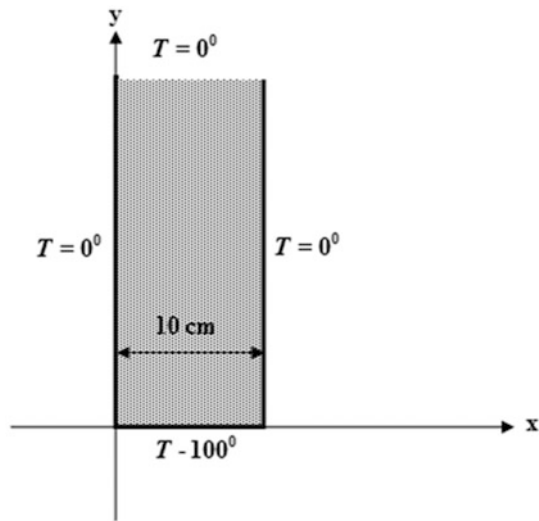
$$Z''(z) + \lambda Z(z) = 0 \quad (2)$$

$$r^2 R''(r) + r R'(r) - (r^2 \lambda + \mu) R(r) = 0 \quad (3)$$

where λ and μ are constants.

Problem 3.25 Problem of steady-state temperature in a rectangular plate (Laplace's equation) with two long sides and the far end at 0 and the base at 1000. See Fig. 3.27.

Fig. 3.27 Problem 3.25



The heat flow equation is given by:

$$\begin{cases} \nabla^2 T(x, y) = 0 \\ \frac{\partial^2 T(x, y)}{\partial x^2} + \frac{\partial^2 T(x, y)}{\partial y^2} = 0 \end{cases}$$

Solve this problem for the boundary conditions associated with this problem as shown in the figure provided by finding the steady-state temperature distribution inside the plate.

Problem 3.26 Solve Problem 3.25 for a finite plate of height 30 cm with top edge at $T = 0^\circ$ and other dimensions and temperatures as given in Fig. 3.27.

Problem 3.27 Problem of diffusion or heat flow equation in a bar or slab.

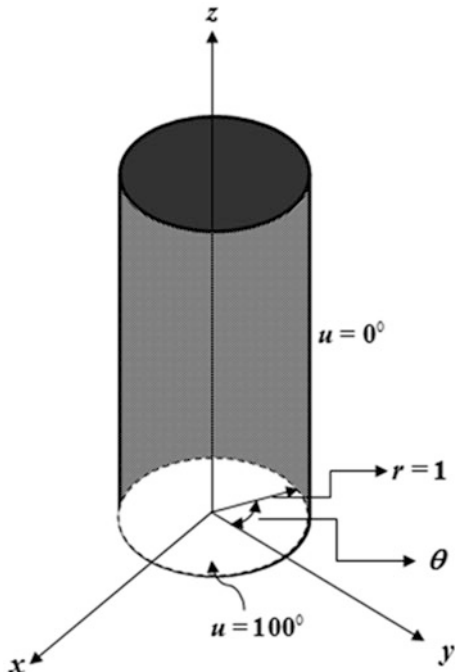
The heat flow equation is given by:

$$\nabla^2 u(x, y, z) = \frac{1}{\alpha^2} \frac{\partial u(x, y, z)}{\partial t} \quad (1)$$

where u is the temperature and α^2 is a constant characteristic of the material through which the heat is flowing. Using separation methods, argue why the separation constant has to be chosen as $-k^2$.

Problem 3.28 Problem of steady-state temperature in a cylinder.

Consider the following problem by finding the steady-state temperature distribution u in a semi-infinite solid cylinder (see Fig. 3.28) of radius $r = 1$ if the base is held at 100° and the curved sides at 0° .

Fig. 3.28 Problem 3.28

Problem 3.29 Suppose the given temperature of the base of the cylinder in Problem 3.24 is more complicated than just a constant value, say $f(r, \theta)$, some function of r and θ .

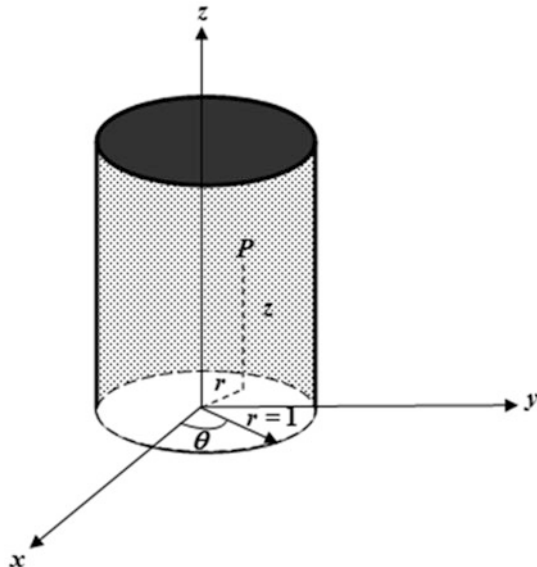
Problem 3.30 Steady-state temperature in sphere Bois page 604.

Find the steady-state temperature inside a sphere of radius 1 when the surface of the upper half is held at 100° and the surface of the lower half at 0° .

Problem 3.31 Use Laplace's transform to solve heat conduction problem in an infinitely long circular cylinder of unit radius (i.e., $r = 1$) that has a constant initial temperature T . At the time $t = 0$ a temperature of 0°C is applied to the surface and is maintained. Find the temperature at any point of the cylinder such as P at any later time t . Use fire below (Fig. 3.29).

Hint: Replace the t by kt .

Fig. 3.29 Problem 3.31



Problem 3.32 Consider a bare homogeneous cylindrical core with material composition typical of modern pressurized water reactor (PWR) operating at full power conditions. The reactor contains a concentration of 2.21 particle per billion (PPB) of natural boron as boric acid dissolved in the coolant water and is fueled with UO_2 at 2.78% enrichment in U^{235} .

Based on thermal design considerations, if the core height is fixed at $H = 3.7$ m, then compute the critical core volume and estimate the neutron leakage fraction from the critical core. The macroscopic cross sections for the materials composing this core are given in the table below.

Element/ isotope	Transport cross section (cm^{-1}) Σ_{tr}	Absorption cross section (cm^{-1}) Σ_a	Product of average number of neutrons released in fission and fission cross section, ($\text{neutron}\cdot\text{cm}^{-1}$) $\nu\Sigma_f$
H	1.79×10^{-2}	8.08×10^{-3}	—
O	7.16×10^{-3}	4.90×10^{-6}	—
Zr	2.91×10^{-3}	7.01×10^{-4}	—
Fe	9.46×10^{-4}	3.99×10^{-3}	—
U^{235}	3.08×10^{-4}	9.24×10^{-2}	1.45×10^{-1}
U^{238}	6.95×10^{-3}	1.39×10^{-2}	1.20×10^{-2}
B^{10}	8.77×10^{-6}	3.41×10^{-2}	—

Problem 3.33 The infinite multiplication factor k_∞ for a heterogeneous lattice of natural uranium fuel is 1.28 for heavy water D_2O moderator. In this particular lattice

L^2 for thermal neutron is 175 cm^2 and Fermi age of neutron $\tau = 120 \text{ cm}^2$. Determine the critical buckling using:

- (a) The one-group thermal critical equation
- (b) The criticality for a large reactor
- (c) The age-diffusion equation
- (d) Criticality for the age-diffusion in part c, which is an approximation of the age-diffusion equation for a large reactor and is written as follows:

$$\frac{k_\infty}{(1 + \tau B_c^2)(1 + L^2 B_c^2)} = 1$$

Problem 3.34 The system to which Problem 3.33 refers to consists of i -inch diameter rods of natural uranium metal arranged in a square lattice with a pitch of 6 inches, suspended in a cylindrical vessel containing the heavy water moderator. The ratio of the height to diameter of the bare core is 1.2. Estimate the mass of uranium which will make this bare reactor just critical. Assume the bulking B_c^2 for finite cylinder is given by following equation.

$$B_c^2 = \left(\frac{2.405}{R_c}\right)^2 + \left(\frac{\pi}{H_c}\right)^2$$

References

1. Y. Oka, T. Kiguchi, *Nuclear Reactor Design (An Advanced Course in Nuclear Engineering)* (Springer, Tokyo, June 2014)
2. J.R. Lamarsh, *Introduction to Nuclear Reactor Theory* (Addison-Wesley, Reading, 1966)
3. K. Okumura, T. Kugo, K. Kaneko, K. Tsuchihashi, *SRAC2006: A Comprehensive Neutronic Calculation Code System, JAEA-Data/Code 2007-004* (Japan Atomic Energy Agency, Tokaimura, 2007)
4. A.F. Henry, *Nuclear-Reactor Analysis*. Chapter 2 (MIT Press, Cambridge, MA, 1975)
5. J.J. Duderstadt, L.J. Hamilton, *Nuclear Reactor Analysis* (Wiley, New York, 1976)
6. P.M. Morse, H. Feshbach, *Method of Theoretical Physics*. Chapter 6 (McGraw-Hill, New York, 1963)

Chapter 4

Energy Effects in Modeling Neutron Diffusion: Two-Group Models



In this chapter, we derive the multi-group diffusion equation (MGDE) and we illustrate how do we solve them in a way that allows us to calculate an accurate eigenvalue and accurate reaction rates. Since the cross sections vary wildly by multiple orders of magnitude over the energy range in a typical nuclear reactor, the major problem becomes one of determining accurate multi-group cross sections for the design problem under consideration.

4.1 One-Group Diffusion Theory

If we set up the one-group diffusion equation by defining $E_0 = \infty$ and $E_1 = 0$, then we can write the following notation:

$$\int_0^\infty dE \chi(E) = 1 \quad (4.1)$$

and

$$\begin{aligned} \text{1 group} \left\{ \begin{array}{l} \cdots \cdots \cdots E_0 = \infty \\ \cdots \cdots \cdots E_1 = 0 \end{array} \right. \\ \int_0^\infty dE' \sum_s (E \rightarrow E') = \sum_s (E) \end{aligned} \quad (4.2)$$

Thus, the multi-group equations yield converts to the one-speed diffusion equation as:

$$\frac{1}{v} \frac{\partial \phi}{\partial t} - \vec{\nabla} \cdot D \vec{\nabla} \phi + \sum_a \phi(\vec{r}, t) = v \sum_f \phi \quad (4.3)$$

Note that the Eq. 4.3 is important once we provide some means for calculating the group constants of intragroup flux, which is presented as $\phi(\vec{r}, E, t)$. It is also important to know if we chose the group constant properly, then even one speed diffusion theory could provide an accurate description of nuclear reactor behavior.

4.2 Two-Group Diffusion Theory

One of the interesting applications of neutronic analysis for reactor system is about application that involves the scenarios of two energy groups, which are characterizing the fast neutrons and associated thermal neutrons respectfully.

For the thermal group that is selected for sufficiently high such that upscattering out of thermal group can be ignored based on the cutoff energy of this thermal group. The corresponding energy in that case is around 0.5–1.0 eV in a water-moderated reactor as an example. However, this may range as high as 3 eV in high-temperature gas-cooled reactors. Figure 4.1 is presentation of the group structure that one can identify the following relationship as:

$$\phi_1(\vec{r}, t) = \int_{E_1}^{E_0} \phi(\vec{r}, E, t) dE \equiv \text{Fast Flux} \quad (4.4)$$

$$\phi_2(\vec{r}, t) = \int_{E_2}^{E_1} \phi(\vec{r}, E, t) dE \equiv \text{Thermal Flux} \quad (4.5)$$

Given the Eqs. 4.4 and 4.5, we can simplify the group constants for this model considering first the fission spectrum. Since essentially all fission neutrons are born in the fast group therefore, we can write the following relationship for the fission spectrum $\chi(E)$ that is also illustrated in Fig. 4.2.

$$\begin{aligned} \chi_1(E) &= \int_{E_1}^{E_0} dE \chi(E) = 1 \\ \chi_2(E) &= \int_{E_2}^{E_1} dE \chi(E) = 0 \end{aligned} \quad (4.6)$$

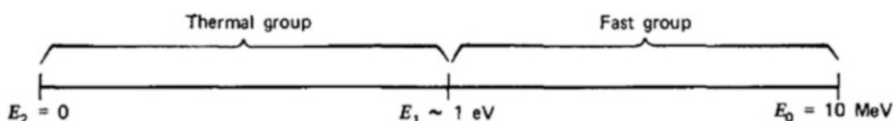
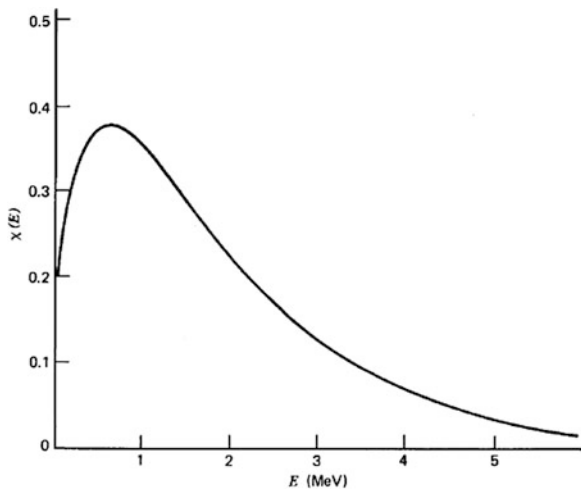


Fig. 4.1 Group structure depiction

Fig. 4.2 Fission spectrum for thermal neutron-induced fission in ^{235}U . (Courtesy of Duderstadt and Hamilton [1])



Hence, the fission source will only appear in the fast group equation:

$$S_f^1 = v_1 \Sigma_f^1 \phi_1 + v_2 \Sigma_f^2 \phi_2 \quad (\text{Fast Neutron}) \quad (4.7)$$

$$S_f^2 = 0 \quad (\text{Thermal Neutron}) \quad (4.8)$$

With two sets of equations in above, we can go ahead and calculate the scattering and removal cross section. First, since there is no upscattering out of the thermal group:

$$\int_{E_2=0}^{E_1-1\text{eV}} dE \Sigma_s(E' \rightarrow E) = \Sigma_s(E') \quad E_2 \leq E' \leq E_1 \quad (4.9)$$

Hence, we can eventually find the following:

$$\begin{aligned} \Sigma_s^{2 \rightarrow 2} &= \frac{1}{\phi_2} \int_{E_2}^{E_t} dE \int_{E_2}^{E_t} \Sigma_s(E' \rightarrow E) \phi(\vec{r}, E') \\ &= \frac{1}{\phi_2} \int_{E_2}^{E_t} dE' \Sigma_s(E') \phi(\vec{r}, E') = \Sigma_s^2 \end{aligned} \quad (4.10)$$

Therefore, the removal cross section for the thermal group is just:

$$\Sigma_R^2 = \Sigma_t^2 - \Sigma_s^{2 \rightarrow 2} = \Sigma_t^2 - \Sigma_s^2 = \Sigma_a^2 \quad (4.11)$$

This is what we are expecting to happen anyway. In practice first performing a fine spectrum calculation for the group of interest, and then averaging the appropriate cross-sectional data over this spectrum would calculate the remainder of the group constant. This allows us to obtain the group constants, for example, a *fast*

spectrum calculation would be performed to calculate the *fast group constant* v_1, Σ_f^1 , Σ_R^1 , $\Sigma_s^{1 \rightarrow 2}$, and D_1 , while *a thermal group constants* v_2, Σ_f^2, D_2 , and Σ_a^2 handles the situation [1].

If we consider the application of two-group diffusion theory to a reactor criticality analysis as described by Zweifel, [2] then we can set both the time derivatives and the external source terms equal to zero to write the two-group diffusion equation as:

$$\begin{aligned} -\vec{\nabla} \cdot D_1 \vec{\nabla} \phi_1(\vec{r}, t) + \sum_R^1 \phi_1(\vec{r}, t) &= \frac{1}{k} \left[v_1 \sum_f^1 \phi_1 + v_2 \sum_f^2 \phi_2 \right] \\ -\vec{\nabla} \cdot D_2 \vec{\nabla} \phi_2(\vec{r}, t) + \sum_a^2 \phi_2(\vec{r}, t) &= \sum_s^{1 \rightarrow 2} \phi_1 \end{aligned} \quad (4.12)$$

However, in first equation of Eq. 4.12, we have inserted a multiplication factor $1/k$ in front of the fission source terms since we are eventually analyzing a criticality conditions and search. Also, note that while the source terms in the fast group correspond to fission neutrons, the source term in the thermal group is due only to slowing down from the fast group [1].

Now we apply the two-group diffusion equations that are presented in as a set in Eq. 4.12, in order to analyze and illustrate the criticality of a bare yet uniform reactor assuming that both fast and thermal fluxes can be characterized by the same spatial shape as $\psi(\vec{r})$:

$$\nabla^2 \psi(\vec{r}) + B^2 \psi(\vec{r}) = 0 \quad \psi(\vec{r}) = 0 \quad (4.13)$$

In above relationship, we have omitted the subscript g from the geometric bucking $B_g^2 = B^2$ so as not to confuse it with the group index g , so we can write:

$$\begin{aligned} \phi_1(\vec{r}) &= \phi_1 \psi(\vec{r}) \\ \phi_2(\vec{r}) &= \phi_2 \psi(\vec{r}) \end{aligned} \quad (4.14)$$

Then if we substitute the sets of Eq. 4.14 into Eq. 4.12, we can get the following algebraic equations as:

$$\begin{cases} \left(D_1 B^2 + \Sigma_R^1 - \frac{1}{k} v_1 \Sigma_f^1 \right) \phi_1 - \frac{1}{k} v_2 \Sigma_f^2 \phi_2 = 0 \\ \Sigma_{s_0}^{1 \rightarrow 2} \phi_1 + (D_2 B^2 + \Sigma_a^2) \phi_2 = 0 \end{cases} \quad (4.15)$$

However, the solution of Eq. 4.15 can be found as:

$$\left(D_1 B^2 + \Sigma_R^1 - \frac{v_1 \Sigma_f^1}{k} \right) (D_2 B^2 + \Sigma_a^2) - \frac{v_2 \Sigma_f^2 \Sigma_{s_0}^{1 \rightarrow 2}}{k} = 0 \quad (4.16)$$

Now, if we solve for the value of the multiplication factor k , which will yield a nontrivial solution of the two-group equations:

$$k = \frac{v_1 \Sigma_f^1}{(\Sigma_R^1 + D_1 B^2)} + \frac{\Sigma_{s_0}^{1 \rightarrow 2}}{(\Sigma_R^1 + D_1 B^2)} \frac{v_2 \Sigma_f^2}{(\Sigma_a^2 + D_2 B^2)} \quad (4.17)$$

The Eq. 4.17 is easily can be related to our earlier expression for k notably the six-factor formula. The first term in Eq. 4.17 is representing the neutron multiplication due to fissions occurring in the fast group, and the second term in same equation represents multiplication due to thermal fission.

In case of the thermal fission contribution, we anticipate that to be the dominant factor in these situations in which such a two-group analysis makes sense, let us first examine the following:

$$\begin{aligned} k_2 &= \frac{\Sigma_{s_0}^{1 \rightarrow 2}}{(\Sigma_R^1 + D_1 B^2)} \frac{v_2 \Sigma_f^2}{(\Sigma_a^2 + D_2 B^2)} \\ &= \frac{\Sigma_{s_0}^{1 \rightarrow 2} / \Sigma_R^1}{(1 + L_1^2 B^2)} \frac{v_2 (\Sigma_f^2 / \Sigma_a^2)}{(1 + L_2^2 B^2)} \end{aligned} \quad (4.18)$$

Note that reader should not be deceived into believing that such criticality calculations are always so straightforward and we should take under consideration that for the non-leakage probability $P_{NL} = (1 + L^2 B^2)^{-1}$ holds only for uniform, bare reactor geometries (i.e., single-region cores). In addition, one should note that is no longer possible to derive simple expressions for P_{NL} or k in terms of the reactor geometry and composition for multiregional reactors as reflected one.

From our above discussion, it is evident that:

$$P_{NL}^1 = (1 + L_1^2 B^2)^{-1} \quad \text{and} \quad P_{NL}^2 = (1 + L_2^2 B^2)^{-1} \quad (4.19)$$

are just the fast and thermal non-leakage probabilities. Notice that the diffusion length L_1 characterizing the fast group is defined somewhat differently as: [1].

$$L_1^2 \equiv \frac{D_1}{\Sigma_R^1} = \frac{D_1}{\Sigma_a^2 + \Sigma_{s_0}^{1 \rightarrow 2}} \quad (4.20)$$

As we can see, Eq. 4.20 is inconsistent with our earlier definition of the diffusion length, since both Σ_a^2 and $\Sigma_{s_0}^{1 \rightarrow 2}$ act to remove neutrons from the fast group. Note that the only common term in Eq. 4.18 is the ratio $\Sigma_{s_0}^{1 \rightarrow 2} / \Sigma_R^1$; however, for a homogeneous-type reactor design, we have concluded in previous chapters that this ratio is defined as below:

$$\frac{\text{Rate at which neutrons slow down to thermal group}}{\text{Rate at which neutrons are removed from fast group}} = \frac{\int \Sigma_{s_{12}} \phi_1(\vec{r}) d^3r}{\int \Sigma_R^1 \phi_1(\vec{r}) d^3r} = \frac{\Sigma_{s_0}^{1 \rightarrow 2}}{\Sigma_R^1} = p \quad (4.21)$$

where p is representing the resonance escape probability characterizing slowing down from group 1 to group 2. Hence, we can write the following conclusion based on above analysis:

$$k_2 = \eta_2 f_2 p P_{NL}^1 P_{NL}^2 \quad (4.22)$$

Similarly, we can identify the fast multiplication factor as:

$$k_1 = \frac{v_2 \left(\sum_f^1 / \sum_R^1 \right)}{(1 + L_1^2 B^2)} = \eta_1 f_1 P_{NL}^1 \quad (4.23)$$

where $\eta_1 = v_1 \left(\sum_{f_1}^F / \sum_{a_1}^F \right)$ and we have defined a “fast utilization factor” as $f_1 = \sum_{a_1}^F / \sum_R^1$ in analogy to the thermal utilization f_2 .

With above analysis in place, we can easily identify the fast fission factor ϵ with usual six-factor formula as before and write the following relationship:

$$\epsilon = \left(1 + \frac{k_1}{k_2} \right) = \left\{ 1 + \left(\frac{v_1 \Sigma_f^1}{v_2 \Sigma_f^2} \right) \left[\frac{\Sigma_a^2 + D_2 B^2}{\Sigma_{s_0}^{1 \rightarrow 2}} \right] \right\} \quad (4.24)$$

where we can find that the six-factor formula is as it was shown in Chap. 2 (Eq. 2.77) and it is written here again:

$$k = k_1 + k_2 = \epsilon k_2 = \eta_2 f_2 p \epsilon P_{NL}^1 P_{NL}^2 \quad (4.25)$$

Going forward, we can conclude similar result as above by using a few-group analysis as presented in the next section.

4.3 Few-Group Analysis

We discussed one group theory and the typical solutions to the diffusion equation. Then we talked about the energy dependence of nuclear interaction cross sections. This led to a discussion of the variable energy transport equation, which could be reduced to the multi-group diffusion equations by making three approximations:

1. The P_1 approximation
2. The multi-group approximation
3. The diffusion approximation

In order to make multi-group approximation work in a reasonable fashion, we had to know a little about the actual neutron spectrum in the reactor. Therefore, we used the infinite-medium- or zero-dimensional spectra to collapse a very fine group cross-sectional structure to a few-group structures for spatially dependent calculations. A few-group model constructed in this fashion is the easiest way to deal with the large variation in cross sections as a function of the neutron energy in a nuclear reactor.

In order to demonstrate the difference between a one energy group model and a few-group energy model, let us consider the simplest of all few-group models – the two-group model. We can write the multi-group diffusion equations in the compact form as:

$$[-D^g \nabla^2] \{\Phi\} + \left[\sum_r^g \right] \{\Phi\} = \left[\sum_{s0}^{g' \rightarrow g} \right] \{\Phi\} + [\chi^g] \left[v \sum_f^g \right] \{\Phi\} \quad (4.26)$$

Or, in terms of matrix formation, Eq. 4.26 can be written as:

$$\begin{bmatrix} -D^1 \nabla^2 & \\ & -D^2 \nabla^2 \end{bmatrix} \begin{Bmatrix} \phi_1 \\ \phi_2 \end{Bmatrix} + \begin{bmatrix} \sum_r^1 & \\ & \sum_r^2 \end{bmatrix} \begin{Bmatrix} \phi_1 \\ \phi_2 \end{Bmatrix} = \begin{bmatrix} \sum_{s0}^{2 \rightarrow 1} & \\ \sum_{s0}^{1 \rightarrow 2} & \end{bmatrix} \begin{Bmatrix} \phi_1 \\ \phi_2 \end{Bmatrix} + \begin{bmatrix} \chi^1 v \sum_f^1 & \chi^1 v \sum_f^2 \\ \chi^2 v \sum_f^1 & \chi^2 v \sum_f^2 \end{bmatrix} \begin{Bmatrix} \phi_1 \\ \phi_2 \end{Bmatrix} \quad (4.27)$$

Note that both matrices on the left are diagonal; the group scatter matrix can be full with the exception of the diagonal, and the fission source matrix can be full. However and most importantly, the matrices on the left are not symmetric. Using the above analysis, we can easily conclude the two-group thermal reactor equation as we discussed in Sect. 4.1.

4.3.1 Two-Group Thermal Reactor Equations

The most interesting two-group problem is one fast group and one thermal group. Typical energy ranges for these two groups would be:

Group 1: 20 MeV – 0.125 eV
 Group 2: 0.125 eV – 10^{-5} eV

These are chosen because thermal cross sections are usually much larger than fast or epithermal cross sections. When these choices are made, we will have:

1. $\chi^2 = 0.0, \chi^1 = 1.0$
2. $\sum_{s0}^{2-1} = 0.0$

Note that epithermal cross section is result of epithermal neutrons. However, the epithermal neutron is defined as an **Epithermal Neutrons** (0.025 eV, 0.4 eV). These are neutrons of kinetic energy greater than thermal. Some of reactor designs operate with epithermal neutron's spectrum. This design allows reaching higher fuel breeding ratio than in thermal reactors.

The two-group equations become:

$$\begin{bmatrix} -D^1 \nabla^2 & \\ & -D^2 \nabla^2 \end{bmatrix} \begin{Bmatrix} \phi^1 \\ \phi^2 \end{Bmatrix} + \begin{bmatrix} \sum_r^1 & \\ & \sum_r^2 \end{bmatrix} \begin{Bmatrix} \phi_1 \\ \phi_2 \end{Bmatrix} = \begin{bmatrix} & \\ \sum_{s0}^{1-2} & \end{bmatrix} \begin{Bmatrix} \phi_1 \\ \phi_2 \end{Bmatrix} + \begin{bmatrix} \chi^1 v \sum_f^1 & \chi^1 v \sum_f^2 \end{bmatrix} \begin{Bmatrix} \phi_1 \\ \phi_2 \end{Bmatrix} \quad (4.28)$$

Now since the size of the reactor does not depend on the group structure so if the flux shape is a cosine in an infinite slab reactor, then it must be a cosine shape for each group. If we make the approximate diffusion theory boundary condition assumption that the flux goes to zero on the boundary, we must assume that the flux for each group goes to zero on the boundary and has the same shape within the material of the reactor. Thus, our solution for the flux becomes a product of a spatial function and an energy function. The energy function is a discrete vector with a number for each energy group. We will write it as:

$$\{\Phi(E, z)\} = \begin{Bmatrix} \phi_1(z) \\ \phi_2(z) \end{Bmatrix} = \begin{Bmatrix} \phi_1 \cos Bz \\ \phi_2 \cos Bz \end{Bmatrix} = \begin{Bmatrix} \phi^1 \\ \phi^2 \end{Bmatrix} \cos Bz \quad (4.29)$$

where we will use the script $\phi(\vec{r})$ to indicate the energy group constant vector components.

Now in order to obtain a non-zero solution for the flux, we must have a unique relationship between the parameters in the equation. If we substitute the product solution we have identified above into the two-group equation, we can get rid of the del-squared operator. This gives:

$$\begin{bmatrix} D_1 B^2 & \\ & D^2 B^2 \end{bmatrix} \begin{Bmatrix} \phi^1 \\ \phi^2 \end{Bmatrix} + \begin{bmatrix} \sum_r^1 & \\ & \sum_r^2 \end{bmatrix} \begin{Bmatrix} \phi^1 \\ \phi^2 \end{Bmatrix} = \begin{bmatrix} & \\ \sum_{s0}^{1-2} & \end{bmatrix} \begin{Bmatrix} \phi^1 \\ \phi^2 \end{Bmatrix} + \begin{bmatrix} \chi^1 v \sum_f^1 & \chi^1 v \sum_f^2 \end{bmatrix} \begin{Bmatrix} \phi^1 \\ \phi^2 \end{Bmatrix} \quad (4.30)$$

This can be considered an eigenvalue equation for B^2 as all terms depend on the $\phi(\vec{r})$ vector. With only two groups, the easiest way to set up the problem is to transfer all terms to the left-hand side.

$$\begin{bmatrix} D^1 B^2 + \sum_r^1 -\chi^1 v \sum_f^1 & -\chi^1 v \sum_f^2 \\ -\sum_{s_0}^{1 \rightarrow 2} & D^2 B^2 + \sum_r^2 \end{bmatrix} \begin{Bmatrix} \phi^1 \\ \phi^2 \end{Bmatrix} = \begin{Bmatrix} 0 \\ 0 \end{Bmatrix} \quad (4.31)$$

In order to obtain a non-zero solution for the $\phi(\vec{r})$ vector, we can set the determinant of the multiplying matrix to zero and solve for the two values of B^2 that will make the determinant equal to zero. This will give:

$$\begin{bmatrix} D^1 B^2 + \sum_r^1 -\chi^1 v \sum_f^1 & -\chi^1 v \sum_f^2 \\ -\sum_{s_0}^{1 \rightarrow 2} & D^2 B^2 + \sum_r^2 \end{bmatrix} = 0 = (D^1 B^2 + \sum_r^1 -\chi^1 v \sum_f^1) (D^2 B^2 + \sum_r^2) - (\chi^1 v \sum_f^2) (\sum_{s_0}^{1 \rightarrow 2}) \quad (4.32)$$

Then we can divide the equation by $\sum_r^1 \sum_f^2$ and make the following definitions.

$$\begin{aligned} L_1^2 &= \frac{D^1}{\sum_r^1} \\ L_2^2 &= \frac{D^2}{\sum_r^2} \\ \eta f &= \frac{v \sum_f^2}{\sum_r^2} \\ P_{re} &= \frac{\sum_{s_0}^{1 \rightarrow 2}}{\sum_r^1} \end{aligned} \quad (4.33)$$

This gives:

$$\left(L_1^2 B^2 + 1 - \frac{v \sum_f^1}{\sum_r^1} \right) (L_2^2 B^2 + 1) - \eta f P_{re} = 0 \quad (4.34)$$

Now dividing by both L^2 and collecting terms in powers of B^2 gives:

$$B^4 + \left[\frac{1}{L_1^2} \left(1 - \frac{v \sum_f^1}{\sum_r^1} \right) + \frac{1}{L_2^2} \right] B^2 - \frac{1}{L_1^2 L_2^2} \left(\eta f P_{re} + \frac{v \sum_f^1}{\sum_r^1} - 1 \right) = 0 \quad (4.35)$$

This can be written as:

$$\begin{aligned}
 B^4 + C_1 B^2 - C_0 &= 0 \\
 C_1 &= \left[\frac{1}{L_1^2} \left(1 - \frac{v \Sigma_f^1}{\Sigma_r^1} \right) \right] + \frac{1}{L_2^2} \\
 C_0 &= \frac{1}{L_1^2 L_2^2} \left(\eta f p_{re} + \frac{v \Sigma_f^1}{\Sigma_r^1} - 1 \right)
 \end{aligned} \tag{4.36}$$

Moreover, the solution:

$$B^2 = -\frac{C_1}{2} \pm \sqrt{\left(\frac{C_1}{2}\right)^2 + C_0}$$

This will give two solutions for B^2 . The largest value must be greater than zero in order to obtain a critical reactor. It is possible for both values to be greater than zero for very highly enriched reactors that have a predominately fast spectrum.

Consider the following parameters for the AGN-201 reactor.

Coefficient	Fast group	Thermal group
Removal cross section	0.05704	0.09583
Diffusion coefficient	0.71514	0.11283
Absorption cross section	0.00193	0.09583
Downscatter cross section	0.05511	-----
Nu fission cross section	0.002562	0.15179
L^2	12.5375	1.17740
ηf	-----	1.58395
p_{re}	0.96616	-----
$v \sum_f^1 / \sum_r^1$	0.04492	-----

$$B_1 = 0.92551$$

$$B_0 = 0.03897$$

$$B^2 = +0.040347, -0.96586$$

$$B_+ = 0.2008656, B_- = 0.98278i$$

This gives a bare critical radius of $R_c = 15.64$ cm (diameter equal to 31.28 cm) for the AGN-201, or the equivalent thickness for an infinite slab reactor made of the same material. The radius for an infinite cylinder would be 11.97 cm (diameter equal to 23.94 cm). A right circular cylinder with height equal to diameter would be 28.60 cm tall, and a cube would be 27.09 cm on a side.

Consider now the solution for the energy eigenfunction corresponding to this value of the criticality eigenvalue. The thermal equation can be written:

$$\begin{aligned} -\Sigma_{s_0}^{1 \rightarrow 2} \phi_1 + (D^2 B^2 + \Sigma_r^2) \phi_2 &= 0 \\ \phi_1 &= \frac{(D^2 B^2 + \Sigma_r^2)}{\Sigma_{s_0}^{1 \rightarrow 2}} \phi_2 \end{aligned} \quad (4.37)$$

So if the group vector is normalized such that $\phi_2 = 1.0$, then ϕ_1 must be equal to 1.822 (i.e., $\phi_1 = 1.822$). For the case of the negative B^2 , we would get that $\phi_1 = -0.2386$. Therefore, we have:

$$\begin{aligned} B_+^2 \\ \Phi_+ &= \begin{Bmatrix} 1.822 \\ 1.0 \end{Bmatrix} \cos 0.20086z \\ B_-^2 \\ \Phi_- &= \begin{Bmatrix} -0.2386 \\ 1.0 \end{Bmatrix} \cos 0.98278iz \end{aligned} \quad (4.38)$$

Realizing that the imaginary argument can be converted to a real argument by switching the *cos* to the *cosh* function, the general solution can be written as:

$$\begin{Bmatrix} \phi_1(z) \\ \phi_2(z) \end{Bmatrix} = A \begin{Bmatrix} \phi_+^1 \\ \phi_+^2 \end{Bmatrix} \cosh B_+ z + C \begin{Bmatrix} \phi_-^1 \\ \phi_-^2 \end{Bmatrix} \cosh B_- z = A \begin{Bmatrix} 1.822 \\ 1.0 \end{Bmatrix} \cosh 0.20086z + C \begin{Bmatrix} -0.2386 \\ 1.0 \end{Bmatrix} \cosh 0.98278z \quad (4.39)$$

Realize that since we are operating in an eigenvalue state, one of the coefficients, either A or C , cannot be determined by this type of calculation. The power level of the reactor will determine the overall magnitude of the flux in the reactor. However, we can eliminate the C coefficient in terms of the A coefficient by applying boundary conditions. C must be zero if we truly stick to the zero flux on the boundary condition. If we are willing to consider extrapolation lengths though, it is possible to evaluate C in terms of A and we will do that shortly.

k eigenvalue equation.

So far we have answered the criticality question. “Given the material and the requirement for exact criticality, how big is the reactor?” The other criticality question that we are often concerned with is, “given the material and size of the reactor, how far from exactly critical are we?”. To answer this question, we must

introduce the k eigenvalue. We do this by writing the multi-group diffusion equation (MGDE) in the following fashion:

$$[-D^g \nabla^2] \{\Phi\} + [\Sigma_r^g] \{\Phi\} = \left[\Sigma_{s_0}^{g' \rightarrow g} \right] \{\Phi\} + \frac{1}{k} [\chi^g] \left[v \Sigma_f^g \right] \{\Phi\} \quad (4.40)$$

For the two-group, thermal reactor problem, this becomes:

$$\begin{bmatrix} D_1 B^2 & \\ D_2 B^2 & \end{bmatrix} \begin{Bmatrix} \phi_1 \\ \phi_2 \end{Bmatrix} + \begin{bmatrix} \sum_r^1 & \\ \sum_r^2 & \end{bmatrix} \begin{Bmatrix} \phi_1 \\ \phi_2 \end{Bmatrix} = \begin{bmatrix} \sum_{s_0}^{1 \rightarrow 2} & \\ \sum_{s_0}^{1 \rightarrow 2} & \end{bmatrix} \begin{Bmatrix} \phi_1 \\ \phi_2 \end{Bmatrix} + \frac{1}{k} \begin{bmatrix} v \sum_f^1 & v \sum_f^2 \end{bmatrix} \begin{Bmatrix} \phi_1 \\ \phi_2 \end{Bmatrix} \quad (4.41)$$

In addition, the expanded determinant equation becomes:

$$\begin{bmatrix} D_1 B^2 + \Sigma_r^1 - \frac{1}{k} v \Sigma_f^1 & -\frac{1}{k} v \Sigma_f^2 \\ -\Sigma_{s_0}^{1 \rightarrow 2} & D_2 B^2 + \Sigma_r^2 \end{bmatrix} = 0 = \left(D_1 B^2 + \Sigma_r^1 - \frac{1}{k} v \Sigma_f^1 \right) \left(D_2 B^2 + \Sigma_r^2 \right) - \left(\frac{1}{k} v \Sigma_f^2 \right) \left(\Sigma_{s_0}^{1 \rightarrow 2} \right) \quad (4.42)$$

We can then solve this equation for k to get:

$$\begin{aligned} (D_1 B^2 + \Sigma_r^1) (D_2 B^2 + \Sigma_r^2) &= \frac{1}{k} \left\{ v \Sigma_f^2 \Sigma_{s_0}^{1 \rightarrow 2} + v \Sigma_f^1 (D_2 B^2 + \Sigma_r^2) \right\} \\ k &= \frac{v \Sigma_f^2 \Sigma_{s_0}^{1 \rightarrow 2} + v \Sigma_f^1 (D_2 B^2 + \Sigma_r^2)}{(D_1 B^2 + \Sigma_r^1) (D_2 B^2 + \Sigma_r^2)} \end{aligned} \quad (4.43)$$

This can then be solved iteratively by plugging in values for B^2 and finding a value that gives $k = 1.0$.

It is also useful to divide numerator and denominator by $\Sigma_r^1 \Sigma_r^2$ and inserting the definitions of the diffusion lengths and ηfp_{re} to obtain:

$$k = \frac{\eta fp_{re} + \frac{v \Sigma_f^1}{\Sigma_r^1} (L_2^2 B^2 + 1)}{(1 + L_1^2 B^2) (1 + L_2^2 B^2)} \quad (4.44)$$

Then defining the fast fission factor as:

$$\varepsilon = \frac{\text{Total Fissions}}{\text{Thermal Fissions}} = \frac{v \Sigma_f^1 \phi^1 + v \Sigma_f^2 \phi^2}{v \Sigma_f^2 \phi^2} = 1 + \frac{v \Sigma_f^1 \phi_1}{v \Sigma_f^2 \phi_2} \quad (4.45)$$

And remembering that the thermal equation gives:

$$\phi_1 = \frac{(D_2 B^2 + \Sigma_r^2)}{\Sigma_{s_0}^{1 \rightarrow 2}} \phi_2 \quad (4.46)$$

This becomes:

$$\epsilon = 1 + \frac{v \Sigma_f^1 \frac{D_2 B^2 + \Sigma_r^2}{\Sigma_{s_0}^{1 \rightarrow 2}}}{v \Sigma_f^2} = 1 + \frac{v \Sigma_f^1}{\Sigma_r^1} \frac{(1 + L_2^2 B^2)}{\frac{\Sigma_{s_0}^{1 \rightarrow 2}}{\Sigma_r^1} v \Sigma_f^2} = 1 + \frac{v \Sigma_f^1}{\Sigma_r^1} \frac{(1 + L_2^2 B^2)}{\eta f p_{re}} \quad (4.47)$$

Then,

$$k = \frac{\eta f p_{re} \epsilon}{(1 + L_1^2 B^2)(1 + L_2^2 B^2)} \quad (4.48)$$

And defining:

$$\begin{aligned} P_{NL}^1 &= \frac{1}{1 + L_1^2 B^2} = \text{Fast Non-Leakage Probability} \\ P_{NL}^2 &= \frac{1}{1 + L_2^2 B^2} = \text{Thermal Non-Leakage Probability} \end{aligned} \quad (4.49)$$

This gives the classic six-factor formula:

$$k = \eta f p_{re} \epsilon P_{NL}^1 P_{NL}^2 \quad (4.50)$$

This is exactly same equation as it was derived in previous section as Eq. 4.25.

4.3.2 Two-Group Fast Reactor Equations

Now consider the two-group equations for a fast reactor where fission neutrons show up in both groups.

$$\begin{aligned} & \begin{bmatrix} -D_1 B^2 & \\ & -D_2 B^2 \end{bmatrix} \begin{Bmatrix} \phi_1 \\ \phi_2 \end{Bmatrix} + \begin{bmatrix} \sum_r^1 & \\ & \sum_r^2 \end{bmatrix} \begin{Bmatrix} \phi_1 \\ \phi_2 \end{Bmatrix} \\ &= \begin{bmatrix} \sum_{s0}^{1 \rightarrow 2} & \\ & \end{bmatrix} \begin{Bmatrix} \phi_1 \\ \phi_2 \end{Bmatrix} + \begin{bmatrix} \chi_1 \nu \sum_f^1 & \chi_1 \nu \sum_f^2 \\ \chi_2 \nu \sum_f^1 & \chi_2 \nu \sum_f^2 \end{bmatrix} \begin{Bmatrix} \phi_1 \\ \phi_2 \end{Bmatrix} \end{aligned} \quad (4.51)$$

or

$$\begin{bmatrix} D_1 B^2 + \sum_r^1 -\chi_1 \nu \sum_f^1 & -\chi_1 \nu \sum_f^2 \\ -\sum_{s_0}^{1 \rightarrow 2} -\chi_2 \nu \sum_f^1 & D_2 B^2 + \sum_r^2 -\chi_2 \nu \sum_f^2 \end{bmatrix} \begin{Bmatrix} \phi_1 \\ \phi_2 \end{Bmatrix} = \begin{Bmatrix} 0 \\ 0 \end{Bmatrix} \quad (4.52)$$

Three- and Four-Group Equations.

The equations for three groups without upscatter are:

$$\begin{bmatrix} D_1 B^2 + \sum_r^1 \\ -\sum_{s_0}^{1 \rightarrow 2} & D_2 B^2 + \sum_r^2 \\ -\sum_{s_0}^{1 \rightarrow 3} & -\sum_{s_0}^{2 \rightarrow 3} & D_3 B^2 + \sum_r^3 \end{bmatrix} \begin{Bmatrix} \phi_1 \\ \phi_2 \\ \phi_3 \end{Bmatrix} = \frac{1}{k} \begin{bmatrix} \chi_1 v \sum_f^1 & \chi_1 v \sum_f^2 & \chi_1 v \sum_f^3 \\ \chi_2 v \sum_f^1 & \chi_2 v \sum_f^2 & \chi_2 v \sum_f^3 \\ \chi_3 v \sum_f^1 & \chi_3 v \sum_f^2 & \chi_3 v \sum_f^3 \end{bmatrix} \begin{Bmatrix} \phi_1 \\ \phi_2 \\ \phi_3 \end{Bmatrix} \quad (4.53)$$

The equations for four groups without upscatter are:

$$\begin{bmatrix} D_1 B^2 + \sum_r^1 \\ -\sum_{s_0}^{1 \rightarrow 2} & D_2 B^2 + \sum_r^2 \\ -\sum_{s_0}^{1 \rightarrow 3} & -\sum_{s_0}^{2 \rightarrow 3} & D_3 B^2 + \sum_r^3 \\ -\sum_{s_0}^{1 \rightarrow 4} & -\sum_{s_0}^{2 \rightarrow 4} & -\sum_{s_0}^{3 \rightarrow 4} & D_4 B^2 + \sum_r^4 \end{bmatrix} \begin{Bmatrix} \phi_1 \\ \phi_2 \\ \phi_3 \\ \phi_4 \end{Bmatrix} = \frac{1}{k} \begin{bmatrix} \chi_1 v \sum_f^1 & \chi_1 v \sum_f^2 & \chi_1 v \sum_f^3 & \chi_1 v \sum_f^4 \\ \chi_2 v \sum_f^1 & \chi_2 v \sum_f^2 & \chi_2 v \sum_f^3 & \chi_2 v \sum_f^4 \\ \chi_3 v \sum_f^1 & \chi_2 v \sum_f^2 & \chi_3 v \sum_f^3 & \chi_3 v \sum_f^4 \\ \chi_4 v \sum_f^1 & \chi_4 v \sum_f^2 & \chi_4 v \sum_f^3 & \chi_4 v \sum_f^4 \end{bmatrix} \begin{Bmatrix} \phi_1 \\ \phi_2 \\ \phi_3 \\ \phi_4 \end{Bmatrix} \quad (4.54)$$

In general, we will write the MGDE in shorthand notation for an arbitrary number of groups as:

$$[\mathbf{M}]\{\boldsymbol{\Phi}\} = \frac{1}{k} [\mathbf{F}]\{\boldsymbol{\Phi}\} \quad (4.55)$$

where $[\mathbf{M}]$ is called the migration operator or matrix, and $[\mathbf{F}]$ is called the fission operator or matrix.

4.4 Transverse Buckling Approximation

Note that in the migration matrix, the $\mathbf{D}^g \mathbf{B}^2$ terms play the same role and show up in the same places as the Σ_r^g terms do. Typically, in multidimensional problems, we will get a buckling term that corresponds to each of the dimensions. For instance, in $R - Z$ geometry for a homogeneous media, the \mathbf{DB}^2 term can be written as the sum of a \mathbf{B}^2 for the r direction and a B^2 term for the z -direction.

$$\mathbf{DB}^2 = \mathbf{D}(\mathbf{B}_r^2 + B_z^2) \quad (4.56)$$

Also for $X - Y - Z$ geometry, we have:

$$\mathbf{DB}^2 = \mathbf{D}(\mathbf{B}_x^2 + \mathbf{B}_y^2 + B_z^2) \quad (4.57)$$

Now in a real reactor design problem where fuel assemblies is changing material properties in the radial direction, but do not change significantly in the z -direction due to the requirement for fuel pins and coolant channels. This configuration can easily be manufactured, and it is often possible to reduce the two-dimensional calculation in the r and z -directions to a one-dimensional calculation in the r -direction by assuming the flux in the z -direction to be cosine shaped and correcting for leakage in this direction with a \mathbf{DB}_z^2 term. This term is then added to the Σ_f^g term and the calculation conducted in the radial direction, with an increased removal due to the transverse leakage in the z -direction.

4.5 Consistent Diffusion Theory Boundary Conditions

Now let us return to the issue of applying the Consistent Diffusion Theory Boundary Conditions. Consider the slab case and realize that the extrapolation distance is given by $2D_g$ or $2/3(\lambda_g)$. For the AGN-201, this gives the following two distances:

Fast group: $z_{ex} = 2*D_1 = 2*0.71514 = 1.43028$ cm

Thermal group: $z_{ex} = 2*D_2 = 2*0.11283 = 0.22566$ cm

We can then write the general solution as:

$$A \left\{ \begin{array}{l} 1.822 \cos[0.20086(H/2 + 1.43028)] \\ 1.0 \cos[0.20086(H/2 + 0.22566)] \end{array} \right\} + C \left\{ \begin{array}{l} -0.2386 \cosh[0.9278(H/2 + 1.43028)] \\ 1.0 \cosh[0.9278(H/2 + 0.22566)] \end{array} \right\} = \left\{ \begin{array}{l} 0 \\ 0 \end{array} \right\}$$

We have two equations in three unknowns, so we cannot completely solve for all of the unknowns. However, if we divide the second equation into the first, we can eliminate both A and C and come up with one equation in one unknown, $H/2$. So we get:

$$\frac{1.822 \cos[0.20086(H/2 + 1.43028)]}{\cos[0.20086(H/2 + 0.22566)]} = -\frac{0.2386 \cosh[0.9728(H/2 + 1.43028)]}{\cosh[0.9728(H/2 + 0.22566)]} \quad (4.58)$$

We can solve for the critical $H/2$ by plugging in values for the right-hand side and the left-hand side as a function of H . When they are equal, we have the critical H .

H	RHS	LHS
15.64	11.4091	-0.7296
15.60	12.3494	-0.7296
15.50	15.7590	-0.7296
15.00	-21.1808	-0.7296
14.50	-4.5265	-0.7296
14.00	-1.8684	-0.7296
13.50	-0.7794	-0.7296
13.40	-0.6343	-0.7296
13.46	-0.7193	-0.7296
13.48	-0.7490	-0.7296
13.467	-0.7296	-0.7296

So the $2^*z_{ex} = 15.64 - 13.467 = 2.173$ cm. $z_{ex} = 1.0865$ cm. This value of z_{ex} is in between the value for the fast and thermal groups. Now that we have a H , we can go back and evaluate C in terms of A from either of the equations. From the thermal equation, we have:

$$C = A \frac{1.822 \cos[0.20086^*7.82]}{0.2386 \cosh[0.9728^*7.82]} = -5.4 \times 10^{-7}A$$

Therefore, our final solution is:

$$\begin{Bmatrix} \phi_1(z) \\ \phi_2(z) \end{Bmatrix} = A \begin{Bmatrix} 1.822 \\ 1.0 \end{Bmatrix} \cos(0.20086z) - 5.4 \times 10^{-7} A \begin{Bmatrix} -0.2386 \\ 1.0 \end{Bmatrix} \cosh(0.9278z)$$

The A coefficient must be determined by the power level.

4.6 Derivation of the One-Dimensional Multi-group P_N Equations

The most accurate description of the behavior of neutrons in a nuclear reactor is obtained by solving the three-dimensional, energy-dependent, time-dependent Boltzmann transport equation. However, solutions to this equation are time-consuming and expensive for simple reactors and impossible for very complicated ones. Therefore, approximations are necessary and very useful. For many problems of interest in reactor design and safety, the general time-dependent equation can be simplified to a time-independent eigenvalue problem. A critical reactor maintains the flux level at which it becomes critical indefinitely, and therefore the time-dependent part of the Boltzmann equation can be neglected. This time-independent equation is still too complicated to solve in all of its generality, so further approximations are usually made. For preliminary design analysis and scoping studies, one-dimensional approximations are often very useful. With this in mind, it is very instructive to derive the one-dimensional, multi-group P_N equations from the one-dimensional Boltzmann equation. This derivation will cover all of the main points required to perform the same reduction for the two- or three-dimensional problem and save on a great deal of extraneous and confusing notation. The one-dimensional P_1 equations can be reduced to the multi-group diffusion equations, which by analogy can easily be extended to two or three dimensions. The multi-group diffusion equations are by far the most extensively used description of neutron behavior in nuclear reactors, though they suffer in accuracy for small reactors and near strong absorbers.

Therefore, let us begin with the three-dimensional, time-dependent, energy-dependent Boltzmann transport equation, and it is given by:

$$\begin{aligned} \frac{1}{v(E)} \frac{d\phi(\vec{r}, E, \vec{\Omega})}{dt} = & S(\vec{r}, E, \vec{\Omega}) + \int \int \sum_s (\vec{r}, E', \vec{\Omega}' \rightarrow E, \vec{\Omega}') \phi(\vec{r}, E, \vec{\Omega}') dE d\vec{\Omega}' \\ & + \int_{E'} \int_{\vec{\Omega}'} \frac{\chi(E)}{4\pi} v \sum_f (\vec{r}, E') \phi(\vec{r}, E, \vec{\Omega}') dE' d\vec{\Omega}' \\ & - \nabla \cdot \vec{\Omega} \phi(\vec{r}, E, \vec{\Omega}') - \sum_T (\vec{r}, E) \phi(\vec{r}, E, \vec{\Omega}) \end{aligned} \quad (4.59)$$

where:

$\phi(\vec{r}, E, \vec{\Omega})$ = neutron angular flux density

$\sum_T (\vec{r}, E)$ = total interaction cross section

$\sum_s (\vec{r}, E, \vec{\Omega}' \rightarrow E, \vec{\Omega})$ = scattering cross section for transfer from energy E' and angle $\vec{\Omega}'$ to energy E and angle $\vec{\Omega}$

$\chi(E)v\sum_f(\vec{r}, E) =$ number of neutrons produced per fission at energy E times the fission cross section for a neutron of energy E' , (i.e., fission is generally considered to be isotropic in the laboratory reference frame, and it will be treated that way here)

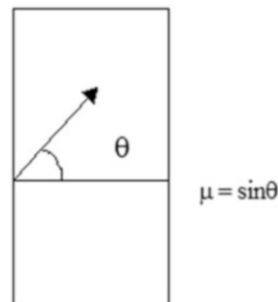
$S(\vec{r}, E, \vec{\Omega}) =$ the time-independent source of neutrons at position \vec{r} , with energy E , and moving in direction $\vec{\Omega}$.

Note this is simply a balance equation that says the rate of change of the neutron density at a point, with energy and direction specified, is the difference between the sources and the sinks. It is essentially a linear equation, as none of the cross sections depends on the neutron angular flux density. This is an excellent approximation for the most reactor analysis questions; moreover, since criticality questions are the first priority, the time-derivative term can be neglected by setting the sum of sources equal to the sum of sinks. This gives the time-independent equation.

Also, $S(\vec{r}, E, \vec{\Omega})$ is generally insignificant and changes dramatically the type of problem to be solved if it is significant. To show how it could be treated, it will be carried along for a while. If this term is present, the equation is called an inhomogeneous equation. If it is not present, the equation is called homogeneous, or an eigenvalue equation. In this case, all terms depend on the neutron angular flux density and for only certain values of the cross-sectional parameters can a non-zero flux density solution be found.

The general three-dimensional transport equation is a function of six independent variables. These are the three position coordinates, two angular directions, and the neutron energy. In order to conserve effort and still reflect the essence of the reduction from this general equation to a coupled set of multi-group P_N equations, it is useful to simplify to a one-dimensional problem. For the one-dimensional problem, consider a slab of thickness L in the z -dimension and infinite in the x -dimension and y -dimension. This simplification allows us to get rid of the spatial dependence on x and y , and only the angular dependence relative to the z -axis need be considered. Consider Fig. 4.1 (Fig. 4.3).

Fig. 4.3 Slab reactor



Then, the transport equation immediately simplifies to:

$$\begin{aligned} \mu \frac{\partial \phi(z, E, \mu)}{\partial z} + \Sigma_t(z, E) \phi(z, E, \mu) &= q(z, E, \mu) \\ + \int_{E'} \int_{\vec{\Omega}'} \Sigma_s(z, E', \mu' \rightarrow E, \mu) \phi(z, E', \vec{\Omega}') dE' d\vec{\Omega}' \\ + \frac{\chi(E)}{4\pi} \int_{E'} \int_{\vec{\Omega}'} v(E') \Sigma_f(z, E') \phi(z, E', \vec{\Omega}') dE' d\vec{\Omega}' \end{aligned} \quad (4.60)$$

This equation is still exact for the problem we are considering.

At this point, it is useful to digress slightly and introduce the Legendre polynomials and the associated Legendre functions. These are defined as follows:

Legendre Polynomials: Definition

$$P_n(\mu) = \frac{1}{2^n n!} \frac{d^n}{d\mu^n} (\mu^2 - 1)^n \quad (4.61)$$

Associated Legendre Functions: Definition

$$P_n^k(\mu) = (-1)^k (1 - \mu^2)^{k/2} \frac{d^k}{d\mu^k} P_n(\mu) \quad (4.62)$$

These functions are introduced because they have some very useful properties for expanding solutions to the transport equation. They possess recursion relationships that allow easy calculation on the computer and allow one order to be related to another:

Legendre Polynomials: Recursion Relation

$$nP_n(\mu) = (2n - 1)\mu P_{n-1}(\mu) - (n - 1)P_{n-2}(\mu), \quad P_0(\mu) = 1.0, \quad P_1(\mu) = \mu \quad (4.63)$$

Associated Legendre Functions: Recursion Relations

$$P_n^{k+2}(\mu) + 2(k + 2) \frac{\mu}{\sqrt{\mu^2 - 1}} P_n^{k+1}(\mu) = (n - k)(n + k + 1) P_n^k(\mu) \quad (4.64)$$

$$(2n + 1)\mu P_n^k(\mu) = (n - k + 1)P_{n+1}^k(\mu) + (n + k)P_{n-1}^k(\mu) \quad (4.65)$$

The Legendre polynomials and associated Legendre functions are orthogonal on the interval $(-1,1)$. The normalization relationships are given by:

Legendre Polynomials: Orthogonality and Normalization

$$\int_{-1}^1 P_n(\mu) P_m(\mu) d\mu = \begin{cases} \frac{2}{2n+1} & n = m \\ 0 & n \neq m \end{cases} \quad (4.66)$$

Associated Legendre Functions: Orthogonality and Normalization

$$\int_{-1}^1 \int_0^{2\pi} P_n^k(\mu) \cos(k\omega) P_m^p(\mu) \cos(p\omega) d\mu d\omega = \begin{cases} \frac{2\pi}{2n+1} \frac{(n+k)!}{(n-k)!}, & n = m, k = p \\ 0, & n \neq m, \text{ or } k \neq p \end{cases} \quad (4.67)$$

Finally, for the problem being considered here, they possess a very useful property called the expansion theorem, which is given by:

Legendre Polynomials: Expansion Theorem

$$P_n(\mu_{LAB}) = P_n(\mu) P_n(\mu) + 2 \sum_{k=1}^{k=l} P_n^k(\mu) P_n^k(\mu') \cos\{k(\omega - \omega')\} \quad (4.68)$$

where μ_{LAB} is the cosine of the angle in the laboratory system between the neutrons velocity vector prior to scattering and its velocity vector after scattering and μ' and μ are the polar angles before and after scattering.

For the slab problem considered here, the angular flux density can be expanded in terms of the Legendre polynomials as:

$$\psi(z, E, \mu) = \sum_{l=0}^{\infty} \frac{2l+1}{2} \phi_l(z, E) P_l(\mu)$$

and it is possible to expand the scattering cross section in terms of the angle of scattering in the lab system as:

$$\Sigma_s(z, E', \overline{\Omega'} \rightarrow E, \overline{\Omega}) = \sum_{m=0}^M \Sigma_{sm}(z, E' \rightarrow E) \frac{2m+1}{4\pi} P_m(\mu_{LAB}) \quad (4.69)$$

Then, the inhomogeneous source can also be expanded as:

$$S(z, E, \mu) = \sum_{l=0}^L \frac{2l+1}{2} s_l(z, E) P_l(\mu) \quad (4.70)$$

Substituting all of this into the transport equation and noting $d\vec{\Omega}' = d\mu' d\omega'$,

$$\begin{aligned} \mu \sum_{l=0}^{\infty} \frac{2l+1}{2} \frac{\phi_l(z, E)}{dz} P_l(\mu) + \Sigma_T(z, E) \sum_{l=0}^{\infty} \frac{2l+1}{2} \phi_l(z, E) P_l(\mu) &= \sum_{l=0}^L \frac{2l+1}{2} s_l(z, E) P_l(\mu) \\ + \int_{E'} \int_{\mu'} \int_{\omega'} \frac{\chi(E)}{4\pi} v \Sigma_f(z, E') \sum_{k=0}^{\infty} \frac{2k+1}{2} P_k(\mu') dE' d\mu' d\omega' \\ + \int_{E'} \int_{\mu'} \int_{\omega'} \sum_{m=0}^M \Sigma_{sm}(z, E') \frac{2m+1}{4\pi} P_m(\mu_{LAB}) \sum_{k=0}^{\infty} \frac{2k+1}{2} \phi_k(z, E') P_k(\mu) dE' d\mu' d\omega' \end{aligned} \quad (4.71)$$

We can immediately perform the integrals over μ' and ω' for the fission term on the right-hand side of the equation to obtain making use of the Orthogonality Relation:

$$\begin{aligned} & \int_{E'} \int_{\mu'} \int_{\omega'} \frac{\chi(E)}{4\pi} v \Sigma_f(z, E') \sum_{k=0}^{\infty} \frac{2k+1}{2} \phi_k(z, E') P_k(\mu') dE' d\mu' d\omega' \\ &= \frac{\chi(E)}{2} \int_{E'} v \Sigma_f(z, E') \phi_0(z, E') dE' \end{aligned} \quad (4.72)$$

The scattering integral can be reduced substituting in the expansion for $P_m(\mu_{LAB})$ and integrating over ω' to obtain, noting that a cosine function integrated over a full period or multiple full periods is always zero:

$$\begin{aligned} & \int_{E'} \int_{\mu'} \int_{\omega'} \sum_{m=0}^M \sum_{sm} (z, E') \frac{2m+1}{2} \left\{ \left\{ P_m(\mu) \right\} P_m(\mu') + 2 \sum_{j=1}^{j=m} P_m^j(\mu) P_m^j(\mu') \cos \{j(\omega - \omega')\} \right\} \\ & \cdot \sum_{k=0}^{\infty} \frac{2k+1}{2} \varphi_k(z, E') P_k(\mu') dE' d\mu' d\omega' \\ &= \int_{E'} \int_{\mu'} \sum_{m=0}^M \sum_{sm} (z, E') \frac{2m+1}{2} P_m(\mu) P_m(\mu') \sum_{k=0}^{\infty} \frac{2k+1}{2} \varphi_k(z, E') P_k(\mu') dE' d\mu' \end{aligned} \quad (4.73)$$

Then integrating over $d\mu'$ and applying the Orthogonality Relation, we obtain:

$$= \sum_{m=0}^M P_m(\mu) \frac{2m+1}{2} \int_{E'} \Sigma_{sm}(z, E') \phi_m(z, E') dE' \quad (4.74)$$

The divergence term can be manipulated to remove the $\mu P_1(\mu)$ term using the Recursion Relation:

$$\begin{aligned} \sum_{l=0}^{\infty} \frac{d\phi_l(z, E)}{dz} \frac{2l+1}{2} \mu P_l(\mu) &= \sum_{l=0}^{\infty} \frac{d\phi_l(z, E)}{dz} \frac{2l+1}{2} \left\{ \frac{l+1}{2l+1} P_{l+1}(\mu) + \frac{l}{2l+1} P_{l-1}(\mu) \right\} \\ &= \sum_{l=1}^{\infty} \frac{l}{2} \frac{d\phi_{l-1}(z, E)}{dz} P_l(\mu) + \sum_{l=0}^{\infty} \frac{l+1}{2} \frac{d\phi_{l+1}}{dz} P_l(\mu) \end{aligned} \quad (4.75)$$

After multiplying by 2, the transport equation for the one-dimensional slab becomes:

$$\begin{aligned} &\sum_{l=1}^{\infty} l \frac{d\phi_{l-1}(z, E)}{dz} P_l(\mu) + \sum_{l=0}^{\infty} (l+1) \frac{d\phi_{l+1}(z, E)}{dz} P_l(\mu) \\ &+ \Sigma_T(z, E) \sum_{l=0}^{\infty} (2l+1) \phi_l(z, E) P_l(\mu) = \sum_{l=0}^L (2l+1) s_l(z, E) P_l(\mu) \\ &+ \chi(E) \int_{E'} v \Sigma_f(z, E) \phi_0(z, E') dE' + \sum_{m=0}^M (2m+1) P_m(\mu) \int_{E'} \Sigma_{sm}(z, E' \rightarrow E) \phi_m(z, E') dE' \end{aligned} \quad (4.76)$$

At this point, there is still only one equation, but it is exact for the problem under consideration. However, it contains an infinite number of terms. In order to proceed, it is useful to multiply this equation by each of the Legendre polynomials in turn and integrate from -1 to $+1$. This will produce an infinite set of coupled equations with potentially an infinite number of terms in each. Luckily this turns out not to be the case, and after the multiplication and integration, only a few terms are left in any one equation. All of the terms but one in each of the summations are orthogonal to the polynomial used for the multiplication, and therefore they disappear from the resulting equation. The general equation obtained when this is done becomes:

$$\begin{aligned} &(n+1) \frac{d\phi_{n+1}(z, E)}{dz} + n \frac{d\phi_{n-1}(z, E)}{dz} + (2n+1) \Sigma_T(z, E) \phi_n(z, E) \\ &= (2n+1) s_n(z, E) + (2n+1) \int_{E'} \Sigma_{sn}(z, E' \rightarrow E) \phi_n(z, E') dE' \\ &+ \delta_{n0} \chi(E) \int_{E'} v \Sigma_f(z, E') \phi_0(z, E') dE' \end{aligned} \quad (4.77)$$

As an aside, if the same steps had been followed in cylindrical or spherical geometry, the following two general equations would have been obtained:

P_N Equation in Cylindrical Coordinates

$$\begin{aligned}
 & \frac{1}{2} \left[\frac{d}{dr} + \frac{k+1}{r} \right] \{ (n+k+2)(n+k+1) \phi_{n+1,k+1}(r, E) \} \\
 & \quad - (n-k-1)(n-k) \phi_{n+1,k+1}(r, E) \} \\
 & \quad + \frac{1}{2} \left[\frac{d}{dr} + \frac{k-1}{r} \right] \{ \phi_{n-1,k-1}(r, E) - \phi_{n+1,k-1}(r, E) \} \\
 & \quad + (2n+1) \sum_T(r, E) \phi_n(r, E) = (2n+1) s_n(r, E) \\
 & \quad + (2n+1) \int_{E'} \sum_{sn}(r, E' \rightarrow E) \phi_n(r, E') dE' \\
 & \quad + \delta_{0n} \chi(E) \int_{E'} v \sum_f(r, E') \phi_0(r, E') dE'
 \end{aligned} \tag{4.78}$$

P_N Equation in Spherical Coordinates

$$\begin{aligned}
 & (n+1) \left[\frac{d}{dr} + \frac{n+2}{r} \right] \phi_{n+1}(r, E) + n \left[\frac{d}{dr} + \frac{n-1}{r} \right] \phi_{n-1}(r, E) \\
 & + (2n+1) \sum_T(r, E) \phi_n(r, E) = (2n+1) s_n(r, E) \\
 & + (2n+1) \int_{E'} \Sigma_{sn}(r, E' \rightarrow E) \phi_n(r, E') dE' \\
 & + \delta_{0n} \chi(E) \int_{E'} v \Sigma_f(r, E') \phi_n(r, E') dE'
 \end{aligned} \tag{4.79}$$

Returning to the slab case, the first two equations are the P_0 and P_1 equations. They are:

For P_0

$$\begin{aligned}
 \frac{d\phi_1(z, E)}{dz} + \Sigma_T(z, E) \phi_0(z, E) &= s_0(z, E) + \int_{E'} \Sigma_{s_0}(z, E' \rightarrow E) \phi_0(z, E') dE' \\
 & + \chi(E) \int_{E'} v \Sigma_f(z, E') \phi_0(z, E') dE'
 \end{aligned} \tag{4.80}$$

For P_1

$$\begin{aligned}
 2 \frac{d\phi_2(z, E)}{dz} + \frac{d\phi_0(z, E)}{dz} + 3 \sum_T(z, E) \phi_1(z, E) &= 3s_1(z, E) \\
 & + 3 \int_{E'} \sum_{s_1}(z, E' \rightarrow E) \phi_1(z, E') dE'
 \end{aligned} \tag{4.80}$$

Note that these two equations contain three unknowns, ϕ_0 , ϕ_1 , and ϕ_2 . In order to solve them, an additional equation must be obtained or one of the unknowns neglected. The standard procedure is to neglect ϕ_2 . This approximation is known as the P_1 approximation. If the first six equations are considered, and ϕ_6 is neglected, the resulting approximation is known as the P_5 approximation. This is the first approximation that has been made for the slab problem and is known as the:

1. “ P_N Approximation”

Roughly, this approximation says that the magnitude of the expansion coefficients is decreasing with increasing N , and above some highest N , they will have negligible effect on the solution for the low-order coefficients, in particular, which are generally the quantities of most interest.

At this point, the inhomogeneous source terms will be dropped. If they are important, then the equations will require different solution techniques than will be used for reactor criticality analyses. Their inclusion is obvious in what follows, and the approach is straightforward, if they are required.

Next, the energy dependence must be considered. This is accomplished by breaking the energy region of interest (usually 0.00001 eV to 20 MeV) up into intervals called energy groups. As most neutron transport problems start with high-energy neutrons, born because of fission or fusion reactions, that slow down to lower energies, these intervals are generally numbered from highest energy to lowest energy. The lowest group number corresponds to the highest-energy neutrons. If the energy dependence of the angular flux density is mild over large energy ranges, then only a small number of groups are required for an accurate solution to the transport problem. However, if the energy dependence of the angular flux density is significant over many short energy intervals, then a large number of groups must be used. No matter how many groups are used, some estimate of the energy dependence within the group interval must be made, and this dependence is considered to remain constant throughout any given reactor material. That is, for the g^{th} energy group extending from energy E_{g+1} to E_g , the following holds:

$$\phi_n(z, E) = f(E)\phi_n^g(z), \quad E_{g+1} \leq E < E_g \quad (4.81)$$

$$\phi_n^g(z) = \frac{\int_{E_{g+1}}^{E_g} \phi_n(z, E) dE}{\int_{E_{g+1}}^{E_g} f(E) dE} \quad (4.82)$$

for all z and E of interest within any one material. This is known as the:

2. “Multi-group Approximation”

Essentially the energy and spatial dependence of the angular flux density expansion coefficients are assumed to be “separable” within the energy group width. This is the second major approximation that is made, and in the limit of an infinite number

of groups, it is not really an approximation at all. However, few computers have an infinite amount of storage, and therefore the assumed separability does become an approximation.

Group-averaged parameters are then defined in the following manner:

$$\sum_T^g(z) = \frac{\int_{E_{g+1}}^{E_g} f(E) \sum_T(z, E) dE}{\int_{E_{g+1}}^{E_g} f(E) dE} \quad (4.83)$$

and

$$\chi^g = \int_{E_{g+1}}^{E_g} \chi(E) dE \quad (4.84)$$

with

$$\sum_{sn}^{g'>g}(z) = \frac{\int_{E_{g11}}^{E_g} \int_{E_{g'+1}}^{E_{g'}} f(E') \sum_{sn}(z, E' \rightarrow E) dE' dE}{\int_{E_{g'+1}}^{E_g} f(E') dE'} \quad (4.85)$$

Having made this approximation and dropping the inhomogeneous terms, the multi-group P_1 equations can be written as:

$$\begin{aligned} \frac{d\phi_1^g(z)}{dz} + \Sigma_T^g(z) \phi_0^g(z) &= \sum_{g'=1}^{NOG} \Sigma_{s0}^{g'>g}(z) \phi_0^{g'}(z) + \chi^g \sum_{g'=1}^{NOG} v \Sigma_f^{g'}(z) \phi_0^{g'}(z), \quad 1 \leq g \leq NOG \\ \frac{d\phi_0^g(z)}{dz} + 3\Sigma_T^g(z) \phi_1^g(z) &= 3 \sum_{g'=1}^{NOG} \Sigma_{s1}^{g'>g}(z) \phi_1^{g'}(z), \quad 1 \leq g \leq NOG \end{aligned} \quad (4.86)$$

For most reactor problems, the summation over scattering is really only a summation over groups with higher energy than the group of interest (upscatter is impossible). If the term expressing scattering within the group is then pulled over to the left-hand side and combined with the total cross-sectional term, this can be written as:

$$\begin{aligned} \frac{d\phi_1^g(Z)}{dz} + \{\Sigma_T^g(z) - \Sigma_{s0}^{g>g}(z)\} \phi_0^g(z) &= \sum_{g'>g} \Sigma_{s0}^{g'>g}(z) \phi_0^{g'}(Z) + \chi^g \sum_{g'=1}^{NOG} v \Sigma_f^{g'}(z) \phi_0^{g'}(z) \\ \frac{d\phi_0^g(Z)}{dz} + 3\{\Sigma_T^g(z) - \Sigma_{s1}^{g>g}(z)\} \phi_1^g(z) &= 3 \sum_{g'>g} \Sigma_{s1}^{g'>g}(z) \phi_1^{g'}(z) \end{aligned} \quad (4.87)$$

Two of the within group cross sections have special names. They are:

3. Removal cross section

$$\Sigma_R^g(z) = \Sigma_T^g(z) - \Sigma_{s_0}^{g>g}(z) \quad (4.88)$$

4. Transport cross section

$$\Sigma_{TR}^g(z) = \Sigma_T^g(z) - \Sigma_{s_1}^{g>g}(z) \quad (4.89)$$

This coupled set of equations then becomes the multi-group P_1 equations. The slab case considered here is by far the simplest, but the steps and approximations are the same in reducing other one-dimensional geometries and two-/three-dimensional geometries. As a more concise notation, the multi-group P_1 equations can be written in matrix form by treating the expansion coefficients for all groups as a vector quantity of length equal to the number of groups, and the cross sections can be written as a square matrix in the following form:

$$\begin{aligned} \frac{d}{dz}\{\phi_1(z)\} + [\Sigma_R(z)]\{\phi_0(z)\} &= [\Sigma_{s0d}(z)]\{\phi_0(z)\} + [\chi v \Sigma_f(z)]\{\phi_0(z)\} \\ \frac{d}{dz}\{\phi_0(z)\} + [3\Sigma_{TR}(z)]\{\phi_1(z)\} &= [3\Sigma_{s1d}]\{\phi_1(z)\} \end{aligned} \quad (4.90)$$

This notation is a little obscure, but it makes it easier to emphasize the important parts for the following remarks.

The multi-group diffusion equations (MGDE) can be easily derived from the multi-group P_N equations. First, the P_1 approximation is made, and then the P_1 equation is solved for the coefficient vector.

$$\{\phi_1(z)\} = -[3\Sigma_{TR}(z) - 3\Sigma_{s1d}(z)]^{-1} \frac{d}{dz}\{\phi_0(z)\} \quad (4.91)$$

If anisotropic downscatter is neglected, and only the transport cross-sectional term retained, then the transport minus the anisotropic-downscatter matrix becomes a diagonal matrix, and its inverse can be instantly computed by finding the inverse of each diagonal term. This is called the:

“Diffusion Approximation”

It is the only difference between the multi-group P_1 equations and the multi-group diffusion equations. The P_1 group vector can be eliminated from the P_0 group equations to obtain:

$$-\frac{d}{dz}[3\Sigma_{TR}(z)]^{-1} \frac{d}{dz}\{\phi_0(z)\} + [\Sigma_R(z)]\{\phi_0(z)\} = [\Sigma_{s0d}(z)]\{\phi_0(z)\} + [\chi v \Sigma_f(z)] \times \{\phi_0(z)\} \quad (4.92)$$

These then are the multi-group diffusion equations for the slab problem. Conveniently, and it will not be shown here, the two-dimensional and three-dimensional multi-group diffusion equations can be obtained from the one-dimensional equations

by replacing the partial derivatives with respect to z , in the slab case, with the gradient operator in the general case. This gives for the general dimensional multi-group diffusion equations:

$$-\nabla \left[3\Sigma_{TR}(\vec{r}) \right]^{-1} \nabla \left\{ \phi_0(\vec{r}) \right\} + \left[\Sigma_R(\vec{r}) \right] \left\{ \phi_0(\vec{r}) \right\} = \left[\Sigma_{s_{0d}}(\vec{r}) \right] \left\{ \phi_0(\vec{r}) \right\} + \left[v\Sigma_f(\vec{r}) \right] \left\{ \phi_0(\vec{r}) \right\} \quad (4.93)$$

In addition, a group diffusion coefficient can be defined by:

$$D^g(\bar{r}) = \frac{1}{3 \sum_{TR}^g(\bar{r})} \quad (4.94)$$

In summary, the three major approximations made to derive the multi-group diffusion equations from the Boltzmann transport equation were:

1. **P₁ Approximation**
2. **Multi-group Approximation**
3. **Diffusion Approximation**

Two further simplifications can be considered. The first is simply the neglect of upscatter except for within the thermal group, and the second is the case of group structures wide enough such that the equations become direct coupled.

1. Downscatter-only case

The multi-group diffusion equations become:

$$-\frac{d}{dz} \left\{ 3 \sum_{TR}^g(z) \right\}^{-1} \frac{d}{dz} \phi_0^g(z) + \sum_R^g(z) \phi_0(z) = \sum_{g'=1}^{g-1} \sum_{s_0}^{g'>g}(z) \phi_0^{g'} + \chi^g \sum_{g'=1}^{NOG} v \sum_f^{g'}(z) \phi_0^{g'}(z) \quad (4.95)$$

2. Direct-coupled case

$$-\frac{d}{dz} \left\{ 3 \sum_{TR}^g(z) \right\}^{-1} \frac{d}{dz} \phi_0^g(z) + \sum_R^g(z) \phi_0(z) = \sum_{s_0}^{g-1>g}(z) \phi_0^{g-1} + \chi^g \sum_{g'=1}^{NOG} v \Sigma_f(z) \phi_0^{g'}(z) \quad (4.96)$$

Now that we are here, we can pay our attention to solution of multi-group diffusion equation in the next section.

4.7 Multi-group Diffusion Equations: Solution Approach

Now that we have derived the MGDE, how do we solve them in a way that allows us to calculate an accurate eigenvalue and accurate reaction rates, and this is the subject we are going to pay further attention to it. Since the cross sections vary wildly by multiple orders of magnitude over the energy range in a typical nuclear reactor, the major problem becomes one of determining accurate multi-group cross sections for the design problem under consideration.

The data for the cross sections for each individual nuclide are stored in the ENDF/B files as data points with interpolation schemes defined for representing the cross sections between the data points. Each nuclide has its unique basis set of energy values for representing its cross sections. Some cross sections are very smooth and don't require many basis points in the energy grid required to represent a nuclides cross section. The smoothly varying scattering cross section of hydrogen would be an example. Others have many data points to represent the multiple changes in cross-sectional values in both a positive and negative direction as the energy varies only slight amounts. An example of this type would be iron. Others vary so rapidly that a simple grid is inadequate, and specific functions must be chosen to represent the "resonance" structure of the nuclide. An example of this type of cross section would be U-238. We will ignore resonances for the present and come back to them later.

However, any reactor of interest involves multiple isotopes or nuclides, and it is impossible to perform a calculation on multiple energy grids. So initially a very fine group grid is established that can involve thousands of groups, but they are the same groups for each nuclide. The nuclide cross sections are each processed into multi-group form for this very fine grid. A first approximation is simply to use constant weighting or flux spectrum within these very fine groups. However, it is also possible to use a spectral shape that is characteristic of the likely flux shape in the energy region of interest. Usually this breaks down to three different flux shapes. Above about 100 keV, a fission spectrum is usually adequate. Below about 1 eV, a Maxwellian flux shape works, and in between a $1/E$ spectrum is the norm. Of course, we are now talking about the within-group spectrum for very narrow groups within which we do not expect the flux to vary much.

Once we have all of the cross sections for every nuclide converted to this several thousand-group grid, we can now start on generating an approximate energy spectrum for the reactor under consideration. We set up the MGDE in matrix form and introduce the k eigenvalue. We have:

$$-[D]\nabla^2\{\phi\} + [\Sigma_r]\{\phi\} = [\Sigma_d]\{\phi\} + \frac{1}{k} [v\Sigma_f]\{\phi\} \quad (4.97)$$

The simplest approximation is to choose an infinite medium spectrum by neglecting the first term.

4.7.1 *Infinite Medium for Group Collapse*

For the infinite medium case, the MGDE become:

$$[\Sigma_r]\{\phi\} = [\Sigma_d]\{\phi\} + \frac{1}{k} [v\Sigma_f]\{\phi\} \quad (4.98)$$

This can simply be solved by guessing a spectrum for the individual group fluxes and plugging that in on the left-hand side. Then we can calculate the fission source, setting $k = 1$, and the downscatter source. The Σ_r matrix is easy to invert because it is diagonal. So we can solve for a new flux vector on the left-hand side. If we call the flux guess we used on the right-hand side ϕ_0 and the solution we obtained on the left-hand side ϕ_1 , then the multiplication constant k -infinity can be written as:

$$k_{\infty} = \frac{\sum_{g=1}^{NOG} v \sum_f^g \phi_1^g}{\sum_{g=1}^{NOG} v \sum_f^g \phi_0^g} \quad (4.99)$$

This is really a fairly, straightforward process and essentially converges in one iteration. That means that as long as we choose a guessed spectrum ϕ_0 that contains a value in each group, the calculated spectrum will give us an estimate of the multiplication constant when substituted into the above formula. Of course, the easiest guess is to simply choose all of the ϕ_0^g to be equal to 1.0.

However since we get a k -infinity that is not equal to 1.0, the infinite medium spectrum is not the best approximation that we can obtain. (If k is less than 1.0, we need to reconsider what is going on because that says an infinite reactor will not be critical.) A better approximation can be obtained by using what is called the zero-dimensional approximation.

4.7.2 *Zero-Dimensional Spectrum for Group Collapse*

Remember when we considered an infinite slab reactor, we chose as a boundary condition that the flux would go to zero on the boundary of the reactor. If that is the case, then the flux is cosine shaped, and we have the following equation for the diffusion operator:

$$-D\nabla^2\phi(z) = B^2\phi(z) \quad (4.100)$$

converting the differential operator to multiplication by a constant. Of course when we did the same problem for the infinite cylinder or the homogeneous sphere, we

were able to do the same thing. In fact when we considered any of the forms of the ∇^2 operator, we were able to find eigenfunctions whose value went to zero on the surface and allowed us to replace the differential operator by a constant which we always called B^2 . Now if we do the same thing for the MGDE and require each group flux to go to zero on the boundary, we can replace the differential operator in each equation by the same constant. This allows us to take into account the effects of leakage on our very fine group calculation. The MGDE then become:

$$\begin{aligned} [DB^2]\{\phi\} + [\Sigma_r]\{\phi\} &= [\Sigma_d]\{\phi\} + \frac{1}{k}[\nu\Sigma_f]\{\phi\} \\ [DB^2 + \Sigma_r]\{\phi\} &= [\Sigma_d]\{\phi\} + \frac{1}{k}[\nu\Sigma_f]\{\phi\} \end{aligned} \quad (4.101)$$

The solution to this set of equations proceeds exactly the way the solution to the infinite media equations proceeds. But this time, we have to guess a value for B^2 and a flux vector for the right-hand side. Substitute the flux vector in and calculate the fission source term ($k = 1$) and the scattering source term. This gives a total source for each group. This source is then divided by the $[D^g B^2 + \sum_r^g]$ term to give the new flux. If the new flux is substituted into the k equation, it gives the multiplication constant k_{eff} in this case.

$$k_{eff} = \frac{\sum_{g=1}^{NOG} \nu \sum_f^g \phi_1^g}{\sum_{g=1}^{NOG} \nu \sum_f^g \phi_0^g} \quad (4.102)$$

Of course k_{eff} will not be exactly 1.0 unless we chose very accurately for B^2 . Since B^2 represents a leakage term, if k_{eff} is greater than 1.0, we need to increase B^2 and solve the equations again. If k_{eff} is less than 1.0, we need to decrease B^2 and solve the equations again. We can iterate on B^2 until we get k_{eff} exactly equal to 1.0. This then will give us our zero-dimensional spectrum, which takes into account the first-order effects of leakage appropriate to the reactor under consideration. Note that the iteration proceeds very quickly, and even for thousands of groups, it will never amount to more than a few seconds of computer time.

4.7.3 **Group Collapsing**

Once we have obtained a reasonable very fine group spectrum, we can now collapse this group structure to a more manageable form. The more manageable form will be a small number of broad groups. Typically, this number varies from 2 to say 20 or so,

depending on how large of a problem is to be solved. The basic formula for group collapsing of cross sections is:

$$\sum^G = \frac{\int_{E^{G+1}}^{E^G} \sum (E) \phi(E) dE}{\int_{E^{G+1}}^{E^G} \phi(E) dE} = \frac{\sum_{g \in G} \sum^g \phi^g}{\sum_{g \in G} \phi^g} \quad (4.103)$$

where g represents a very fine group and G represents a broad group.

This works well for the total, absorption, removal, and nu*fission cross sections.

$$\Sigma^G = \frac{\int_{E^{G+1}}^{E^G} \sum (E) \phi(E) dE}{\int_{E^{G+1}}^{E^G} \phi(E) dE} = \frac{\sum_{g \in G} \Sigma^g \phi^g}{\sum_{g \in G} \phi^g} \quad (4.104a)$$

$$\Sigma_a^G = \frac{\int_{E^{G+1}}^{E^G} \sum_a (E) \phi(E) dE}{\int_{E^{G+1}}^{E^G} \phi(E) dE} = \frac{\sum_{g \in G} \Sigma_a^g \phi^g}{\sum_{g \in G} \phi^g} \quad (4.104b)$$

$$\Sigma_r^G = \frac{\int_{E^{G+1}}^{E^G} \sum_r (E) \phi(E) dE}{\int_{E^{G+1}}^{E^G} \phi(E) dE} = \frac{\sum_{g \in G} \Sigma_r^g \phi^g}{\sum_{g \in G} \phi^g} \quad (4.104c)$$

$$v\Sigma_f^G = \frac{\int_{E^{G+1}}^{E^G} v \sum_f (E) \phi(E) dE}{\int_{E^{G+1}}^{E^G} \phi(E) dE} = \frac{\sum_{g \in G} v \Sigma_f^g \phi^g}{\sum_{g \in G} \phi^g} \quad (4.104d)$$

The downscatter cross sections are a little more subtle, they are given by:

$$\sum_s^{G' \rightarrow G} = \frac{\int_{E^{G+1}}^{E^G} dE \int_{E^{G'+1}}^{E^{G'}} \sum_s (E' \rightarrow E) \phi(E') dE'}{\int_{E^{G'+1}}^{E^{G'}} \phi(E') dE'} = \frac{\sum_{g \in G} \sum_{g' \in G'} \sum_s^{g' \rightarrow g} \phi^{g'}}{\sum_{g' \in G'} \phi^{g'}} \quad (4.105)$$

Note that in this case, g' must be a group in G' and g must be a group in G . In many cases, the very fine group that is being scattered out of and the very fine group that is being scattered into will belong to the same broad group. In this case, the scattering is not counted and the cross section is neglected. Only those very fine groups that scatter from one broad group to another broad group are counted. Thus as the group structure gets broader and broader, the downscatter cross sections decrease in magnitude.

Though χ is not really a cross section, a system needs to be defined for collapsing it from very fine groups to broad groups. This is really very simple, the solution is:

$$\chi^G = \sum_{g \in G} \chi^g \quad (4.106)$$

χ for a broad group is simply the sum of the χ 's for the very fine groups that make it up.

Finally the most difficult to understand is the diffusion coefficient. Many organizations and individuals have tried to collapse the very fine group D 's based on some sort of current model. This runs into difficulties because the current can in some cases be negative and that complicates the problem severely. The simplest and a suitably accurate approach is to collapse D by finding a broad group transport cross section and taking the inverse of that. The weighting spectrum will be used in the P_0 flux spectrum, ϕ . This gives:

$$\begin{aligned} \sum_{tr}^G &= \frac{\int_{E^{G+1}}^{E^G} \sum_{tr}(E) \phi(E) dE}{\int_{E^{G+1}}^{E^G} \phi(E) dE} = \frac{\sum_{g \in G} \sum_{tr}^g \phi^g}{\sum_{g \in G} \phi^g} \\ D^G &= \frac{1}{3 \sum_{tr}^G} \end{aligned} \quad (4.107)$$

Example 4.1 As an example problem, let us consider a BWR core with 2% enriched fuel. We will assume that we can simply mix the cross sections together based on their smeared volume fractions. This is not very accurate in many cases because heterogeneous effects can be important. However, for the sake of this example problem, let us simply mix the fuel and moderator and clad together based on volume fractions. For our very fine group calculation, we will use four groups to demonstrate the solution methods. For our broad group set of constants, we will choose two groups. Therefore, we are going to calculate an infinite medium spectrum and a zero-dimensional (ZD) spectrum with four groups and collapse based on the ZD spectrum to two broad groups.

The group constants for the four fine groups are:

	Group 1	Group 2	Group 3	Group 4
Chi	0.5503	0.4348	0.0149	0.0
Removal	0.10297	0.14361	0.09292	0.02569
3*Transport	0.46484	0.99536	1.82077	7.00474
Diff Coeff	2.15128	1.00466	0.54922	0.14276
Absorption	0.00169	0.00031	0.00220	0.02569
Nu*Fission	0.00288	0.00017	0.00122	0.04114
$\sum_{g \rightarrow g+1}$	0.09490	0.14330	0.09083	-----
$\sum_{g \rightarrow g+2}$	0.00646	-----	-----	-----

The fission sources by group can then be given by:

$$FS^1 = 0.5503 * (0.00288 * \phi_1 + 0.00017 * \phi_2 + 0.00122 * \phi_3 + 0.04114 * \phi_4)$$

$$FS^2 = 0.4348 * (0.00288 * \phi_1 + 0.00017 * \phi_2 + 0.00122 * \phi_3 + 0.04114 * \phi_4)$$

$$FS^3 = 0.0149 * (0.00288 * \phi_1 + 0.00017 * \phi_2 + 0.00122 * \phi_3 + 0.04114 * \phi_4)$$

$$FS^4 = 0.0 * (0.00288 * \phi_1 + 0.00017 * \phi_2 + 0.00122 * \phi_3 + 0.04114 * \phi_4)$$

Notice that the term in parentheses is constant which is essentially the total number of neutrons produced by the fluxes. We can now write the MGDE for the infinite medium case as:

$$\begin{aligned}
 0.10297 * \phi_1 &= & +FS^1 \\
 0.14361 * \phi_2 &= & +FS^2 \\
 0.09292 * \phi_3 &= & +FS^3 \\
 0.02569 * \phi_4 &= & +FS^4
 \end{aligned}$$

Choose the initial guess for the fluxes to be all equal to 1.0. This gives for the total fission source = $0.00288 + 0.00017 + 0.00122 + 0.04114 = 0.04541$. This then gives for the group fission sources:

$$FS^1 = 0.5503 * 0.04541 = 0.024989$$

$$FS^2 = 0.4348 * 0.04541 = 0.019744$$

$$FS^3 = 0.0149 * 0.04541 = 0.000677$$

$$FS^4 = 0.0$$

Then

$$\phi_1 = 0.024989/0.10297 = 0.24268$$

$$\phi_2 = (0.019744 + 0.0949 * 0.24268) / 0.14361 = 0.29785$$

$$\phi_3 = (0.000677 + 0.00646 * 0.24268 + 0.14330 * 0.29785) / 0.09292 = 0.48350$$

$$\phi_4 = 0.09083 * 0.48350 / 0.02569 = 1.70948$$

The new total fission source

$$= 0.00288 * 0.24268 + 0.00017 * 0.29785 + 0.00122 * 0.48350 \\ + 0.04114 * 1.70948 = 0.07167$$

Therefore, the multiplication constant is:

$$k\text{-infinity} = 0.07167 / 0.04541 = 1.57823$$

We will normally normalize the spectrum for a thermal reactor such that the thermal flux has a value of 1.0. When we do this, we get:

$$\phi_1 = 0.142$$

$$\phi_2 = 0.174$$

$$\phi_3 = 0.283$$

$$\phi_4 = 1.0$$

For the *ZD* case, the solution procedure proceeds in the same manner except in each case we add a DB^2 term to the \sum_r term before we divide it into the total source to that group on the right-hand side. A summary of the iteration is provided below, with a plot to follow giving k_{eff} as a function of B^2 .

B^2	FS ¹	ϕ_1	ϕ_2	ϕ_3	ϕ_4	FS ²	k
0	0.04541	0.24269	0.29787	0.48353	1.70959	0.07167	1.57823
0.002	0.04541	0.23295	0.28741	0.46128	1.61299	0.06764	1.48946
0.004	0.04541	0.22397	0.27773	0.44074	1.52444	0.06394	1.40808
0.006	0.04541	0.21565	0.26872	0.42174	1.44303	0.06054	1.33326
0.008	0.04541	0.20793	0.26033	0.40411	1.36799	0.05741	1.26429
0.01	0.04541	0.20075	0.25249	0.38771	1.29864	0.05452	1.20054
0.012	0.04541	0.19404	0.24514	0.37241	1.23441	0.05184	1.14149
0.014	0.04541	0.18777	0.23824	0.35812	1.17478	0.04935	1.08666

(continued)

B^2	FS ¹	ϕ_1	ϕ_2	ϕ_3	ϕ_4	FS ²	k
0.016	0.04541	0.18189	0.23175	0.34473	1.11932	0.04703	1.03566
0.017	0.04541	0.17908	0.22864	0.33835	1.09302	0.04593	1.01148
0.0174	0.04541	0.17798	0.22742	0.33585	1.08276	0.0455	1.00204
0.01742	0.04541	0.17793	0.22736	0.33573	1.08225	0.04548	1.00157
0.01744	0.04541	0.17788	0.2273	0.3356	1.08174	0.04546	1.00111
0.01746	0.04541	0.17782	0.22724	0.33548	1.08123	0.04544	1.00064
0.01748	0.04541	0.17777	0.22718	0.33536	1.08072	0.04542	1.00017
0.017486	0.04541	0.17775	0.22717	0.33532	1.08057	0.04541	1.00003
0.017487	0.04541	0.17775	0.22716	0.33531	1.08055	0.04541	1.00001
0.017488	0.04541	0.17774	0.22716	0.33531	1.08052	0.04541	0.99998
0.01749	0.04541	0.17774	0.22715	0.33529	1.08047	0.04541	0.99994
0.0175	0.04541	0.17771	0.22712	0.33523	1.08022	0.0454	0.9997
0.018	0.04541	0.17636	0.22563	0.33216	1.06763	0.04487	0.98813
0.02	0.04541	0.17117	0.21984	0.32035	1.01937	0.04286	0.94374
0.022	0.04541	0.16627	0.21437	0.30923	0.97424	0.04097	0.90223
0.024	0.04541	0.16164	0.20918	0.29875	0.93197	0.0392	0.86334

The normalized flux spectrum is:

$$\phi_1 = 0.164$$

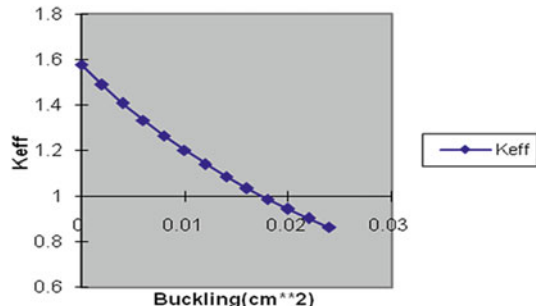
$$\phi_2 = 0.210$$

$$\phi_3 = 0.310$$

$$\phi_4 = 1.0$$

It is a little bit harder than the infinite medium spectrum. More high-energy neutrons are required to make up for leakage (Fig. 4.4).

Fig. 4.4 k_{eff} versus Buckling



4.7.4 Group Collapse

Now collapse the upper three groups to a fast group and leave the thermal group alone. Then we have for the nu*fission cross section.

$$v\Sigma_f^1 = (0.164*0.00288 + 0.210*0.00017 + 0.310*0.00122) / (0.164 + 0.210 + 0.310) = 0.0008862/0.684 = \mathbf{0.00130}$$

$$3\Sigma_{tr}^1 = (0.164*0.46484 + 0.210*0.99536 + 0.310*1.82077) / 0.684 = 0.8497/0.684 = \mathbf{1.2422}$$

$$D_1 = 1/1.2422 = \mathbf{0.805}$$

$$\chi_1 = 0.5503 + 0.4348 + 0.0149 = \mathbf{1.0}$$

$$\Sigma_r^1 = (0.164*0.10297 + 0.210*0.14361 + 0.310*0.09292) / 0.684 = 0.07585/0.684 = \mathbf{0.1109}$$

$$\Sigma_s^{1 \rightarrow 2} = 0.310*0.09083 / 0.684 = \mathbf{0.04117}$$

Problems

Problem 4.1 List and describe the three approximations made in deriving the multi-group diffusion equations from the neutron transport equation.

Problem 4.2 Listed below are a set of typical group constants for a BWR. Calculate the multiplication factor for this reactor if it can be treated as a right circular cylinder of height 370 cm and a diameter of 340 cm.

Group Constant	Group 1	Group 2
$v \sum_{\text{fission}}^g$	0.001348	0.040783
$\sum_{\text{absorption}}^g$	0.001469	0.040249
D_g	0.859599	0.142481
\sum_{removal}^g	0.044587	0.040249
χ_g	1.0	0.0

Problem 4.3 Using the group constants from the previous Problem 4.1, calculate k_∞ , the resonance escape probability, the fast fission factor, and the fast and thermal non-leakage probabilities for this reactor.

Problem 4.4 Calculate the critical radius for an unreflected right circular cylinder reactor characterized by the following group constants.

Group Constant	Group 1	Group 2
$v \sum_{\text{fission}}^g$	0.002562	0.15180
$\sum_{\text{absorption}}^g$	0.001930	0.09509
$\sum_{\text{transport}}^g$	0.466100	2.95420
$\sum_{\text{downstream}}^g$	0.055140	-----
χ_g	1.0	0.0

Reactor height = 25 cm.

Problem 4.5 Calculate the multiplication factor for an unreflected fast reactor with the following cross-sectional data and core size:

Group constant	Group 1	Group 2
$v \sum_{\text{fission}}^g$	0.011040	0.005486
$\sum_{\text{absorption}}^g$	0.004598	0.004108
$\sum_{\text{downstream}}^g$	0.023420	-----
$\sum_{\text{transport}}^g$	0.028020	0.242200
χ_g	0.55	0.45
Core Radius = 111 cm.	Core Height = 91.44 cm	

Problem 4.6 Derive an equation for k_{eff} in case of the three-group problem described by the following equations.

$$\begin{bmatrix} D_1 B^2 + \sum_r^1 & 0 & 0 \\ -\sum_{s_0}^{1 \rightarrow 2} & D_2 B^2 + \sum_r^2 & 0 \\ -\sum_{s_0}^{1 \rightarrow 3} & -\sum_{s_0}^{2 \rightarrow 3} & D_3 B^2 + \sum_r^3 \end{bmatrix} \begin{Bmatrix} \phi_1 \\ \phi_2 \\ \phi_3 \end{Bmatrix} = \begin{bmatrix} v \sum_f^1 & v \sum_f^2 & v \sum_f^3 \\ 0 & 0 & 0 \\ 0 & 0 & 0 \end{bmatrix} \begin{Bmatrix} \phi_1 \\ \phi_2 \\ \phi \end{Bmatrix}$$

Problem 4.7 Compute an infinite medium spectrum for the following 6 group fast reactor problem that is directly coupled.

	Group 1	Group 2	Group 3	Group 4	Group 5	Group 6
D	3.1348	2.5292	1.8095	0.7256	0.30601	0.1350
\sum_r	0.08175	0.05189	0.00813	0.03373	0.51380	0.37846
$\sum^{sg \rightarrow g+1}$	0.07066	0.041489	0.002214	0.015413	0.00192	-----
$v \sum_f$	0.037445	0.023684	0.010181	0.020241	0.42601	4.1648
χ	0.052579	0.52040	0.41085	0.016081	0.0008	0.0

Problem 4.8 Use the spectrum calculated as solution for Problem 4.7 to collapse the upper three groups to one group and the lower three groups to a second group for broad group cross sections. Calculate all five cross sections.

Problem 4.9 Estimate the minimum group spacing that will yield directly coupled multi-group for equations for C^{12} , D^2 , Be^9 , and Na^{22} .

Problem 4.10 What percentage of the neutrons slowing down in hydrogen will tend to skip groups if the group structure is chosen that $(E_{g-1}/E_g) = 100$?

Problem 4.11 Write out the details of the multi-group diffusion equations, $M\phi = k^{-1} F\phi$, for a four-group model in which:

- (a) There is direct coupling.
- (b) The fission source exists only in the upper two groups.
- (c) Only the lowest group contains thermal neutrons.

Problem 4.12 Solve the collision rate equation for Hydrogen as:

$$F(E) = \int_E^{E_0} dE' \frac{F(E')}{E'} + S_0 \delta(E - E_0)$$

By restricting our attention to $E < E_0$ and using the source as boundary condition as $E \rightarrow E_0$.

Problem 4.13 Determine the neutron flux $\phi(E)$ resulting from an arbitrary source in an infinite hydrogenous medium by solving the infinite medium slowing down equation with a general source term $S(E)$.

Problem 4.14 Show that for a mixture of N nuclides the collision rate density $F(E)$ can be written in asymptotic region as:

$$F(E) = \frac{S_0}{E\bar{\xi}} \quad \text{and} \quad \bar{\xi} = \frac{\sum_{i=1}^N \sum_{si} \xi_i}{\Sigma_s}$$

Problem 4.15 Show that for $A > 1$ and a monoenergetic source S_0 at E_0 we have the following relation:

$$F(E) = \frac{S_0 E_0^{(\alpha/(1-\alpha))}}{E \bar{\xi}} \frac{1}{E^{(1/(1-\alpha))}}, \quad \alpha E_0 < E < E_0$$

Problem 4.16 Show that for $A > 1$ compute and plot the collision density function $F_3(E)$ for neutrons that have had three collisions. Discuss the continuity of $F_3(E)$ and its derivatives at $E = E_0$, αE_0 , $\alpha^2 E_0$, and $\alpha^3 E_0$.

Problem 4.17 By means of the one-group treatment, estimate the critical radius of a spherical core of Uranium-235 surrounded by a thick reflector of Uranium-238. The

cross sections, etc. may be taken as the average values for neutrons in the energy range of 0.4 to 1.35 MeV, then:

Uranium-235:	$\sigma_f = 1.27$ (barn)	$\sigma_a = 1.40$ (barn)	$\sigma_{tr} = 5.7$ (barn)	$\nu = 2.52$
Uranium-238:	$\sigma_f = 1.27$ (barn)	$\sigma_a = 1.40$ (barn)	$\sigma_{tr} = 5.7$ (barn)	$\nu = 2.52$

Solution The solution to this problem is as follows:

The density of uranium is approximately 19 g/cm³, so that atoms N for both Uranium-235 and Uranium-238 are close to 0.048×10^{24} nuclei per cm³.

For the *core*,

$$\sum_a = 0.048 \times 1.40 = 0.067 \text{ cm}^{-1} \quad \text{and} \quad \sum_{tr} = 0.048 \times 5.7 = 0.27 \text{ cm}^{-1}$$

Thus:

$$L^2 = \frac{1}{3\sum_{tr}\sum_a} = \frac{1}{(3)(0.27)(0.067)} = 18 \text{ cm}^2$$

$$L = 4.24 \text{ cm}$$

For the *reflector*,

$$\sum_a = 0.048 \times 0.13 = 0.0062 \text{ cm}^{-1} \quad \text{and} \quad \sum_{tr} = 0.048 \times 5.8 = 0.28 \text{ cm}^{-1}$$

Thus.

$$L_{refl.}^2 = \frac{1}{3\sum_{tr}\sum_a} = \frac{1}{(3)(0.28)(0.0062)} = 190 \text{ cm}^2$$

$$L_{refl.} = 13.78 \text{ cm}$$

In Uranium-235 core, k_∞ is equal to η , i.e., to $\nu\sigma_f/\sigma_a$, so that:

$$k_\infty = (2.52)(1.27)/(1.40) = 2.3$$

Hence, by the one-group critical equation, we can write:

$$B_c^2 = \frac{k_\infty - 1}{L^2} = \frac{2.3 - 1}{18} = \frac{1.3}{18} = 0.072 \text{ cm}^{-2}$$

or

$$B_c = 0.27 \text{ cm}^{-1}$$

It is found that R_c/L_{refl} is not large in this case, so that for one-group critical equation for a spherical core with an infinitely thick reflector written as below must be used:

$$B_c R_c \coth(B_c R_c) = -\frac{D_r}{D} \left(1 + \frac{R_c}{L_{refl}}\right) + 1$$

However, since D and D_r are approximately equal, it reduces to:

$$\tan(B_c R_c) = -B_c L_{refl}.$$

Hence $\tan(0.27R_c) = -(0.27)(14) = -3.8$ and R_c is 6.8 cm. Note that the experimental value is close to 6.0 cm.

References

1. J.J. Duderstadt, L.J. Hamilton, *Nuclear Reactor Analysis* (Wiley). 1976 edition
2. P.F. Zweifel, *Reactor Physics* (McGraw-Hill, New York, 1973)

Chapter 5

Numerical Methods in Modeling Neutron Diffusion



The constructive techniques of functional analysis, using a computer code, allow us to build up directly, in their original domain of definition, solutions to linear transport equation. FEMP code is a computer code written in FORTRAN 77, to approximate the Boltzmann transport equation in one-dimensional form using a spherical harmonic for the angular variable and a linear finite element for the spatial variable.

5.1 Introduction

FEMP1D stands for Finite Element, Multi-Group, P_N , 1-Dimensional code. The code approximates the Boltzmann transport equation in one dimension using a spherical harmonic basis for the angular variable and a linear finite element (hat function) basis for the spatial variable. The energy variable is dealt with by the fairly standard multi-group approximation. In rectangular and spherical coordinates, the spherical harmonic basis reduces to the Legendre polynomials. The code was developed partly as a tutorial for a nuclear reactor analysis class, where this book is going to be used as a text. The code partly is providing a flexible code that could take its input to a number of forms, particularly cross-sectional data, and partly to provide a testing ground for algorithms to be implemented in the multidimensional versions of this code series. It has proven to be fairly, efficient and fairly, robust. It has been run on a number of mainframes, minis, workstations, and micros. FEMP1D is written in FORTRAN 77 and should be reasonably transportable.

5.2 Problem(s) Solved

FEMP1D solves a number of steady-state neutral particle radiation transport problems based on the Boltzmann model for the energy-dependent, angular flux density conservation equation. It approximates the energy-dependent, angular flux density with a spherical harmonic basis in the angle variables, with finite element hat functions in the spatial variable and with the standard multi-group coefficients for the energy variable. It will provide four types of strategies for iterating over the group structure to obtain solutions. The four outer iteration options are the following:

1. Inhomogeneous source only (no fission)
2. Inhomogeneous source with fission
3. Fission eigenvalue calculation
4. Fission eigenvalue searches

It will accept volume and surface sources. It will efficiently solve problems with a significant number of upscatter groups. It will accept cross-sectional input from ANISN style libraries, AMPX style libraries, and input stream data, as long as they have the same group structure. It will collapse ANISN and AMPX cross sections to generate problem-dependent libraries. FEMP will accept response functions as part of the input stream that can be multiplied against the isotropic flux solution. It is integrated over energy and possibly volume, to obtain macroscopic reaction rates. It also allocates core storage dynamically to make the most efficient use of high-speed memory no matter how much or how little is available.

5.2.1 Transport Equation

The steady-state Boltzmann transport equation for the multidimensional energy and angular dependent angular flux density is given by

$$\begin{aligned} \vec{\nabla} \cdot \vec{\Omega} \phi(\vec{r}, E, \vec{\Omega}) + \sum_T(\vec{r}, E, \vec{\Omega}) \phi(\vec{r}, E, \vec{\Omega}) &= S(\vec{r}, E, \vec{\Omega}) \\ + \int_{E'} \int_{\Omega'} \sum_S(\vec{r}, E', \vec{\Omega}' > E, \vec{\Omega}) \phi(\vec{r}, E', \vec{\Omega}') dE' d\vec{\Omega}' & \\ + \int_{E'} \int_{\Omega'} \frac{\chi(E')}{4\pi} v \sum_f(\vec{r}, E) \phi(\vec{r}, E', \vec{\Omega}') dE' d\vec{\Omega}' & \end{aligned} \quad (5.1)$$

where:

$\phi(\vec{r}, E, \vec{\Omega})$ = neutron angular flux density.

$\sum_T(\vec{r}, E, \vec{\Omega})$ = scattering cross section for transfer from energy E' and solid angle $\vec{\Omega}'$ to energy E and solid angle $\vec{\Omega}$.

$\sum_S(\vec{r}, E', \vec{\Omega}' > E, \vec{\Omega})$ = scattering cross section for transfer from energy.

$\chi(E')v \sum_f(\vec{r}, E)$ = number of neutrons produced per fission at energy E times the fission cross section for a neutron of energy E' (fission is generally considered to be isotropic in the laboratory reference frame, and it will be treated that way here), and this was explained in Chap. 3 of the book.

$S(\vec{r}, E, \vec{\Omega})$ = the time-independent source of neutrons at position \vec{r} , with energy E , and moving in direction of $\vec{\Omega}$ and for simplicity, it will be called inhomogeneous source.

5.2.2 Angle Discretization

Rather than deriving the general spherical harmonic approximation to the above equation, consider the case of a one-dimensional infinite slab.

Taking Fig. 5.1 under consideration, the transport Eq. 5.1 immediately simplifies to:

$$\begin{aligned} \mu\phi(z, E, \mu) + \sum_T(z, E, \mu)\phi(z, E, \mu) &= S(z, E, \mu) \\ + \int_{E'} \int_{\Omega'} \sum_S(z, E', \Omega' > E, \Omega) \phi(z, E', \Omega') dE' d\Omega' \\ + \int_{E'} \int_{\Omega'} \frac{\chi(E)}{4\pi} v \sum_f(z, E) \phi(z, E', \Omega') dE' d\Omega' \end{aligned} \quad (5.2)$$

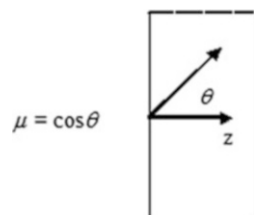
The angular flux density can be expanded in Legendre polynomials:

$$\phi(z, E, \mu) = \sum_{\ell=1}^{\infty} \phi_{\ell}(z, E) \frac{2\ell + 1}{2} P_{\ell}(\mu) \quad (5.3)$$

The scattering cross section can be expanded in terms of the angle of scattering in the lab system as:

$$\sum_S(z, E', \Omega' > E, \Omega) = \sum_{m=0}^M \Sigma_{sm}(z, E) \frac{2m + 1}{4\pi} P_m(\mu_{LAB}) \quad (5.4)$$

Fig. 5.1 Simple slab reactor



$$\mu = \cos \theta$$

In addition, the inhomogeneous source can be expanded as:

$$S(z, E, \mu) = \sum_{\ell=0}^L S_\ell(z, E) \frac{2\ell + 1}{2} P_\ell(\mu) \quad (5.5)$$

When these expansions are substituted into the transport equation and the addition theorem used to express the angle of scattering in the lab reference frame in terms of the incoming and outgoing cosines of the angle the scattered neutron makes with the fixed problem axis, a fairly, complicated equation with an infinite number of terms is obtained. In order to reduce this equation for solution on the computer, it is multiplied in term by each of the Legendre polynomials and integrated from $a-1$ to $a+1$. By making use of the orthogonality relationship for the Legendre polynomials, this reduces to a coupled set of equations infinite in extent. The general equation obtained when this is done becomes:

I. P_N Equation in Rectangular Coordinate

$$\begin{aligned} & (n+1) \frac{d\phi_{n+1}(z, E)}{dz} + n \frac{d\phi_{n-1}(z, E)}{dz} + (2n+1)\Sigma_T(z, E)\phi_n(z, E) \\ &= (2n+1) \int_{E'} \Sigma_{sn}(z, E' > E) \phi(z, E) dE' + \delta_{0n}\chi(E) \int_E v \Sigma_f(z, E') \phi_0(z, E') \\ & \quad + (2n+1)s_n(z, E) \end{aligned} \quad (5.6)$$

II. P_N Equation in Cylindrical Coordinate

$$\begin{aligned} & \frac{1}{2} \left(\frac{d}{dr} + \frac{k+1}{r} \right) \{ (n+k+2)(n+k+1)\phi_{n+1,k+1}(r, E) \\ & \quad - (n-k-1)(n-k)\phi_{n-1,k+1}(r, E) \} \\ & \quad + \frac{1}{2} \left(\frac{d}{dr} - \frac{k-1}{r} \right) \{ \phi_{n-1,k-1}(r, E) - \phi_{n+1,k-1}(r, E) \} + (2n+1)\Sigma_T(r, E)\phi_n(r, E) \\ &= (2n+1) \int_{E'} \Sigma_{sn}(z, E' > E) \phi_n(r, E) dE' + \delta_{0n}\chi(E) \int_E v \Sigma_f(z, E') \phi_0(z, E') dE' \\ & \quad + (2n+1)s_n(z, E) \end{aligned} \quad (5.7)$$

III. P_N Equation in Spherical Coordinate

$$\begin{aligned}
 & (n+1) \left(\frac{d}{dr} + \frac{n+2}{r} \right) \phi_{n+1}(r, E) + n \left(\frac{d}{dr} - \frac{n-1}{r} \right) \phi_{n-1}(r, E) \\
 & + (2n+1) \Sigma_T(r, E) \phi_n(r, E) = (2n+1) \int_{E'} \Sigma_{sn}(r, E' > E) \phi_n(r, E') dE' + \delta_{0n} \chi(E) \\
 & \int_E v \Sigma_f(z, E') \phi_0(z, E') dE' + (2n+1) s_n(z, E)
 \end{aligned} \tag{5.8}$$

Since each of the above equations contains terms from the previous order and the next highest order, there will always be more unknowns than there are equations. In order to obtain a finite set of equations, the highest-order coefficients are neglected, and a solvable system is achieved. The only way to determine if this produces an acceptable solution is obtain the same answer from at least two consecutive orders of solution. Normally the spherical harmonic expansion used here converges very rapidly, and with a little experience, an appropriate order can be chosen quickly. The highest order for the flux expansion must be chosen as an odd number. This is required by the code, as choosing an even order produces no better solution than the next lower odd order and allowing both even and odd highest orders would complicate the programming slightly.

5.2.3 Energy Discretization

The energy discretization is carried out using the standard multi-group approximation. That is, for the g th energy group extending from energy E_{g+1} to E_g the following holds:

$$\phi_n(z, E) = f(E) \phi_n^g \quad E_{g+1} \leq E \leq E_g \tag{5.9}$$

$$\phi_n^g(z) = \frac{\int_{E_{g+1}}^{E_g} \phi_n(z, E) dE}{\int_{E_{g+1}}^{E_g} f(E) dE} \tag{5.10}$$

$$\Sigma_T^g(z) = \frac{\int_{E_{g+1}}^{E_g} f(E) \Sigma_T(z, E) dE}{\int_{E_{g+1}}^{E_g} f(E) dE} \quad (5.11)$$

and

$$\chi_g = \int_{E_{g+1}}^E \chi(E) dE \quad (5.12)$$

with

$$\sum_{sn}^{g' > g}(z) = \frac{\int_{E_{g+1}}^{E_g} \int_{E_{g'+1}}^{E_{g'}} f(E') \Sigma_{sn}(z, E' > E) dE' dE}{\int_{E_{g'+1}}^{E_{g'}} f(E) dE} \quad (5.13)$$

Having made this approximation, the multi-group P_N equation (slab) can be written as:

$$(n+1) \frac{d\phi_{n+1}^g(z)}{dz} + n \frac{d\phi_{n-1}^g(z)}{dz} + (2n+1) \Sigma_T^g(z) \phi_n^g(z) = (2n+1) \sum_{g'=1}^{g'=NOG} \sum_{sn}^{g' > g}(z) \phi_n^{g'}(z) \phi_n^{g'}(z) + \delta_{0n} \chi_g \sum_{g'=1}^{g'=NOG} v \sum_f^{g'}(z) \phi_0^{g'}(z) + (2n+1) s_g^n(z) \quad (5.14)$$

where:

$$1 \leq g \leq NOG \quad (5.15)$$

This will give a set of $NOG^*(N+1)$ equations in the spatially dependent group flux expansion coefficients. This set could be solved directly by finite differencing these equations. However, further mathematical manipulation will reduce computer storage and run times by at least a factor of two.

Once the energy constants have been defined and calculated, the multi-group P_N equations can be reduced further by solving each of the odd order equations for the highest odd order flux coefficients and substituting each odd order coefficient solution into the next lower even order equation. This reduces the total number

of equations to be solved by a factor of 2. The g th order equation then becomes coupled to the 1–2 order and 1 + 2 order equations. This substitution also introduces second derivatives that can be integrated out by parts in the spatial discretization process.

5.2.4 Spatial Discretization

The spatial discretization is accomplished by expanding flux coefficients in a sum of linear splines or “hat” functions. Each “hat” function is defined as being equal to 1.0 at one mesh point and zero at all others. A picture of the i th “hat” function is given in Fig. 5.2.

The flux coefficient expansion can then be written as:

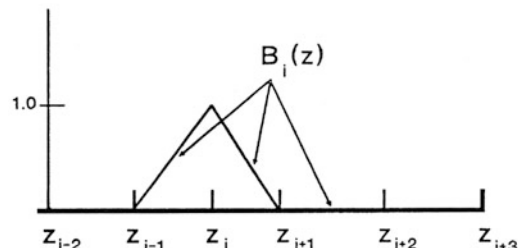
$$\phi_n^g(z) = \sum_{i=1}^{NZ} \phi_{li}^g B_i(z) \quad (5.16)$$

where each of the $B_i(z)$ is given by:

$$\begin{aligned} B_i(z) &= 0 & z \leq z_{i-1}, & z \geq z_{i+1} \\ &= \frac{z - z_{i-1}}{z - z_{i-1}}, & z_{i-1} \leq z \leq z_i \\ &= \frac{z_{i+1} - z}{z_{i+1} - z_i}, & z_i \leq z \leq z_{i+1} \end{aligned} \quad (5.17)$$

This expansion is inserted into each of the P_N equations, and a system of $NOG^*(N + 1)/2$ equations is obtained with $NOG^*(N + 1)/2$ unknowns. In order to obtain a solution, each of the P_N equations is multiplied by one of the $B_i(z)$ and an integration performed over all z as per the standard Galerkin procedure of finite element analysis. This will lead to a set of $NOG^*(N + 1)/2$ equations for the $NOG^*(N + 1)/2$ unknowns. That can then be solved by matrix methods.

Fig. 5.2 i th “hat” function



5.2.5 Matrix Formulation

Finally, the spatial, energy, and angle discretized equations can be written in the following symbolic matrix equation:

$$[\mathbf{M}]\{\boldsymbol{\Phi}\} = \{\mathbf{S}\} + (\mathbf{k}^{-1})[\mathbf{F}]\{\boldsymbol{\Phi}\} \quad (5.18)$$

where \mathbf{M} is the migration matrix that considers the effects of transfers between groups and transport in the spatial dimension. The \mathbf{S} vector is the inhomogeneous source. The \mathbf{F} matrix is the fission source matrix and corresponds to the generation of neutrons because of fission. The eigenvalue \mathbf{k} must be introduced if a solution is desired for the pure eigenvalue problem ($\mathbf{S} = 0$). It should be kept in mind that though the set of equations solved by FEMP1D only considers one spatial dimension, the equations are actually the solution to a three-dimensional problem in space, angle, and energy.

Each of the matrices is $\text{NZ}^* \{(N + 1)/2\}^* \text{NOG}$ by $\text{NZ}^* \{(N + 1)/2\}^* \text{NOG}$ with the majority of the elements identically equal to zero. In order to take advantage of this zero structure, the flux vector is ordered in a special way. Mesh point, Legendre order, and energy group index the flux vector. Thus the locations in the flux vector would start with the first energy group, lowest Legendre order, and run from the first to the last spatial index. Then the Legendre order would be incremented and the spatial mesh covered again. After the highest Legendre order is complete, the second group coefficients would be included. In order to make this ordering scheme a little clearer, consider an example problem that uses four groups, six Legendre orders, and five mesh points. This will be a matrix that is 60 by $60(5^* \{6/2\}^* 4)$.

The matrix ordering scheme can be clarified by considering the overall matrices to be made up of sub-matrices. At the first level, the problem matrices will be made up of the group sub-matrices. The above equation can be written:

$$\begin{bmatrix} M_{11} & 0 & 0 & 0 \\ M_{21} & M_{22} & 0 & 0 \\ M_{31} & M_{32} & M_{33} & 0 \\ M_{41} & M_{42} & M_{43} & M_{44} \end{bmatrix} \begin{bmatrix} \boldsymbol{\phi}_1 \\ \boldsymbol{\phi}_2 \\ \boldsymbol{\phi}_3 \\ \boldsymbol{\phi}_4 \end{bmatrix} = \begin{bmatrix} S_1 \\ S_2 \\ S_3 \\ S_4 \end{bmatrix} + 1/k \begin{bmatrix} F_{11} & F_{12} & F_{13} & F_{14} \\ F_{21} & F_{22} & F_{23} & F_{24} \\ F_{31} & F_{32} & F_{33} & F_{34} \\ F_{41} & F_{42} & F_{43} & F_{44} \end{bmatrix} \begin{bmatrix} \boldsymbol{\phi}_1 \\ \boldsymbol{\phi}_2 \\ \boldsymbol{\phi}_3 \\ \boldsymbol{\phi}_4 \end{bmatrix} \quad (5.19)$$

where the $M_{g,g'}$ matrix are now 15 by $15(5^* \{6/2\})$ square and the $\boldsymbol{\phi}_g$ vectors are 15 elements long. The equation for $\boldsymbol{\phi}_2$ vector can be written as:

$$[M_{22}]\{\boldsymbol{\phi}_2\} = [S_2] + 1/k[F S_2] - [M_{21}]\{\boldsymbol{\phi}_1\} \quad (5.20)$$

where:

$$[FS_2] = [F_{21}][\phi_1] + [F_{22}][\phi_2] + [F_{23}][\phi_3] + [F_{24}][\phi_4] \quad (5.21)$$

And the M_{22} and F_{22} matrices can be written as:

$$[M_{22}] = \begin{bmatrix} \mu_{00} & \mu_{02} & 0 \\ \mu_{20} & \mu_{22} & \mu_{24} \\ 0 & \mu_{42} & \mu_{44} \end{bmatrix}_{22} \quad [F_{22}] = \begin{bmatrix} f_{00} & 0 & 0 \\ 0 & 0 & 0 \\ 0 & 0 & 0 \end{bmatrix}_{22} \quad (5.22)$$

where each of the μ_k matrices is 5 by 5 square and the sub-vector that they multiply in the vector is 5 elements long. Finally, we obtain:

$$[FS_2] = [F_{21}][\phi_1] + [F_{22}][\phi_2] + [F_{23}][\phi_3] + [\mu_{00}]_{21}[\phi_0]_1 - [\mu_{02}]_{21}[\phi_2]_1 \quad (5.23)$$

And the μ_{00} matrix, for example, is given by:

$$[\mu_{00}]_{22} = \begin{bmatrix} m_{11} & m_{12} & 0 & 0 & 0 \\ m_{21} & m_{22} & m_{23} & 0 & 0 \\ 0 & m_{32} & m_{33} & m_{34} & 0 \\ 0 & 0 & m_{43} & m_{44} & m_{45} \\ 0 & 0 & 0 & m_{54} & m_{55} \end{bmatrix}_{22} \quad (5.24)$$

Not all options are complete for every case at this time. In a rectangular coordinate system, it is capable of dealing with angular approximations of (r, θ, z) cylindrical coordinate system; it is only capable of dealing with a P_1 spherical (r, θ, φ) of the angular flux density.

5.3 Solution Strategy

In order to efficiently solve for all of the coefficients of the energy-dependent angular flux density, a strategy must be implemented that takes advantage of the sparsity of the overall system matrices. This strategy can best be implemented by using a series of iterative sweeps through the spatial, angular, and energy meshes. The outermost iterative solution process is implemented with a sweep over the energy groups. The middle iterative process involves a sweep over the Legendre orders. And finally the inner solution over the spatial mesh can be implemented iteratively, but a direct solution is very rapid in 1-D and is used by FEMPID. (FEMP2D and FEMP3D use iterative techniques to solve the spatial mesh.)

The entire iterative process begins by assuming a fission source distribution is available and can be combined with any inhomogeneous sources that are to be

considered. Then the outer iteration process starts with the highest energy group and solves for the angular flux coefficients based on the “known” source. In most problems, these sources will be largely isotropic, so the isotropic flux coefficients are calculated assuming that the higher order coefficients are zero. The isotropic flux then provides a within group scatter source to the next higher Legendre order coefficients. The P_2 coefficients are found based on the P_0 isotropic flux components previously calculated and assuming that the P_4 components are zero. This process is then repeated for the P_4 components and on up until the highest-order coefficients have been found. Then the iteration (middle) is started over for the Po components using the calculated P , components from the previous sweep. This process is repeated until a convergence criterion is satisfied on the isotropic flux. At each Legendre order, the spatially dependent flux coefficients are found using a direct tri-diagonal solver. After a given group is converged, the process moves on to the next lower group. The recently completed group then provides an updated in scatter source to this group below it. Since most neutral particle radiation transport problems are dominated by downscatter, sweeping from high-energy to low-energy groups speeds the convergence of this type of outer iteration.

Once a sweep through the groups is completed, a new fission source is computed. This source is then rationed to the previous source for fission eigenvalue problems in order to obtain an estimate of K_{e1C} for the assembly. Once the fission source is calculated, the process can be repeated. The process continues until the fission source is converged. Then, one more outer, iteration is performed in order to obtain the flux coefficients for the converged fission source.

5.3.1 *Types of Outer Iterations*

FEM11D performs, basically, four types of outer iterations depending upon the type of problem data available and desired. It will perform a transport calculation for an inhomogeneous source without any fission present. It will perform a transport calculation for an inhomogeneous source with fission present. It will perform a fission eigenvalue calculation for a given geometry. Moreover, it will perform a fission eigenvalue calculation to achieve a desired k_{eff} by varying the problem data. Each of these calculations will now be discussed in more details.

5.3.2 *Inhomogeneous Source (No Fission)*

The inhomogeneous source calculation corresponds to calculating the transport of particles throughout an assembly that is emitted independent of the flux of those particles in the assembly. A typical example of this type of calculation is the calculation of the gamma fluxes produced by a radioactive gamma source in a shielded cavity.

For the inhomogeneous source case, the source of particles is specified for all energies and angles, so one outer iteration will generally be all that is required to completely solve the problem. However, since the middle iteration process is an iterative one, if the middle iterations do not converge for a given group, FEMPID will attempt to perform a second outer if the middle iterations do not converge for every group. If there is upscatter in the problem, a separate mini-outer iteration is performed over the upscatter groups. The most likely place that this will occur is if an adjoint problem is being run and the adjoint source is a thermal neutron detector that perturbs the flux. If the mini-outers over the upscatter groups converge during the first outer iteration, only one outer iteration will be performed.

Generally, there is not full upscatter involving all groups, and so a mini- or sub-outer iteration to converge only the upscatter groups is efficient.

FEMP1D accepts both volumetric and surface sources. Both types of sources must be represented by their Legendre component expansions. A fist scatter source is planned, but has not been implemented yet.

5.3.3 *Inhomogeneous Source (with Fission)*

The second type of outer that FEMPID performs is an inhomogeneous source with fission calculation for a subcritical assembly driven by an external source. If the assembly is critical, or supercritical, the FEMP1D calculation will not converge. For this case, FEMP1D starts out with a zero fission source for the first iteration and allows the fission source to build up over a series ofouters. This is not very efficient if the assembly is only slightly subcritical and some acceleration is attempted. For this type of problem, a large number of outer iterations (200 to 500) should be planned. FEMP1D has a very flexible restart capability, and periodic restart tapes may be useful in observing the solution progression for this type of problem.

No attempt is made to obtain rebalance factors to accelerate the fission source by treating this problem as if it were an upscatter one. This probably could be done, but source-driven fissionable assemblies near critical do not appear to be that common at this time.

5.3.4 *Fission Eigenvalue Calculation*

The third type of problem that FEMP1D solves is the fission eigenvalue problem. This entails solving for a multiplication constant, k_{eff} , for a defined assembly of interest. This is the classic fission reactor problem and is the major reason for structuring the FEMP1D solution strategy as it is.

The solution proceeds by guessing a flux and computing a fission source. It is essential that a non-zero flux be chosen so that a non-zero first fission source is obtained. It is not too critical how this flux is chosen, and a constant flux guess over

space and energy is about as good as on processing a nearly correct spatial shape with a poor energy shape. A flux guess can be obtained automatically from a previous FEMP1D run if the results of the previous run have been saved to a file. In fact it is possible to obtain an approximate flux shape with a very coarse mesh, save the calculation, restart with a fine mesh, and converge in less CPU time than using the fine mesh from the start in one long calculation. The question really comes down to how expensive the CPU time is relative to storage space and analyst effort.

FEMP1D attempts to estimate the condition number for the solution process so as to achieve a relative error in the calculated eigenvalue that represents its deviation from the “true” eigenvalue of the assembly, rather than simply the difference between two calculated eigenvalues in a converging sequence.

5.3.5 *Eigenvalue Search Calculation*

FEMP1D performs three types of searches to determine the appropriate assembly configuration to give a desired fission eigenvalue. These are a transverse buckling search, an overall dimension search, and a fissile material concentration search.

The transverse buckling search allows an assembly to be modeled quite accurately in one dimension, the dimension of the calculation, and approximates the transport in the opposite dimension by a buckling height. This often is a very useful technique to get an assembly close to critical and obtain a representative spectral shape in each of the materials in the calculation. This can often produce very accurate relative reaction rates. It also can be used to estimate the height that will be required for a critical assembly. However, since materials often change in the transverse direction as well as the calculation direction, this tends not to be a very accurate estimate.

The material outer dimension search is really an order of magnitude estimate for the amount of fissile material required for a critical assembly. It is simply an expansion of all boundaries by a constant factor to obtain a desired k_{eff} .

The fissile material search assumes the material of interest to be composed of three components represented by their respective volume fractions. The reactant material is the fissile material whose concentration per unit volume is required. The diluent material is the material that must be removed to make room for more reactant material. The volume fraction of diluents is decreased by the same volume as the reactant material is increased. The background material is always present and does not change as the search progresses.

This type of search can be used to determine the approximate fissile loading required to achieve a desired k_{eff} . All material thicknesses and the appropriate transverse buckling must be reasonably correct for this type of search to be useful in one dimension.

Obviously, the fission eigenvalue search is merely a loop over the standard fission eigenvalue calculation. However, it is broken out as a separate calculation so that efficient convergence parameters can be chosen easily.

5.4 Middle Iterations

Middle iterations are sweeps through the Legendre order coefficient matrices starting with the isotropic fluxes and increasing to the highest Legendre order required. Each set of Legendre order equations is coupled over three orders except for the lowest and highest which are only coupled over two. On the first sweep, all but the isotropic flux are assumed to be zero. Then as the sweep moves up in order, subsequent Legendre orders are filled in. When the highest order is solved, the next higher order is truly assumed to be zero, and it remains that way. Each sweep starts over with the isotropic flux and moves up in order. Convergence is achieved when two iterations of the isotropic flux match within the tolerance EPK. Two options are available for this tolerance. The tolerance check can be applied to the L_{inf} norm of the flux, or it can be applied to the L_{inf} norm of the relative deviation. The L norm is appropriate for fission eigenvalue problems, and the L L norm is appropriate for deep penetration problems where accuracy at flow flux levels is important.

5.5 Inner Iterations

FEMP1D does not perform inner iterations, but rather solves the diffusion matrix equation exactly because it has been reduced to a tri-diagonal matrix that can be solved very efficiently using vector methods.

5.6 Upscatter Iterations

Upscatter problems are handled by performing a mini-outer iteration over the upscatter groups. A rebalance matrix is developed by integrating the upscatter groups over all space and attempting to balance the flow in energy exactly. This accelerates convergence very significantly. The number of mini-outers per real outer is controlled by the parameter NUPS. It usually does not make much sense to perform more than about five mini-upscatter outers per real outer if the fission source has not been spatially converged. However, for a source-only problem, NUPS can be set as high as desired to get convergence in one true outer.

5.7 Inhomogeneous Sources

Inhomogeneous sources can be entered as incident on either the left or the right surface. These sources are represented by their Legendre expansions. Of course, for plane wave sources incident on a slab, a very high-order Legendre expansion will be required.

Volume sources are input as a tensor product in energy and space. Each source is assumed to have its own energy spectrum. The energy spectra should be normalized to 1.0 particle released; however, FEMP1D will attempt to normalize over the assembly to the total number of particles emitted equal to the variable SNORM particles/sec. Once the spectra have been input, the location of the sources by spatial interval is entered in the 46\$\$ array. Then the relative magnitude of the sources is entered by spatial interval in the 47** array. Thus to obtain the number of source particles emitted in a specific energy group and spatial interval, the value entered in the source spectrum group assigned to that interval is multiplied by the source strength for that spatial interval. This is a fairly flexible scheme but can be complicated if a number of multi-group source spectra are involved.

5.8 Background Concepts

In order to efficiently use a transport code, there are a number of algorithms and simplifications that are important to understand but have never been worthy of a separate publication. This section is an attempt to provide some documentation of these concepts that will make FEMP1D easier to use and understand.

5.8.1 *Mixing Tables*

Mixing tables are required to specify the correct material compositions for the macroscopic materials that make up the transport problem. In order to describe the composition of a given material to the code, three data pieces are required. The material that contains a particular nuclide, or cross-sectional set, must be identified, and the quantity of the nuclide, or cross section, set that will go into the material must be determined. Quantities are most easily specified in terms of atoms or molecules per cubic centimeter. However, since cross sections are specified in barns (cm^{-4}), it is usually easier to specify number densities (atoms/volume) in terms of atoms/barn/cm. This convention saves a lot of notation to carry along powers of 10 and makes the magnitude of typical number densities vary from 0.1 atom/barn/cm to 0.01 atom/barn/cm.

Returning to the problem of mixing materials together, the mixing table generally consists of three sets of numbers, two of which are integers and one which is a floating point in the range 0.2–0.0. These numbers can most easily be specified by setting up three arrays or columns and letting the same position in each array identify an operation that is to be performed on a specific nuclide. In FEMP1D these three arrays are the 10\$, 11\$, and the 12* arrays. The 10\$ array entry at a specific position identifies the macroscopic material that is under consideration. The 11\$ array entry at that position identifies the nuclide or cross-sectional array that will be mixed into that

macroscopic material, and the 12* array quantifies how much of that nuclide will be entered. Thus we might have the following three arrays:

10S\$	1	1	1	2	2
11S\$	1261	1262	1276	1269	1276
12**	0.00223	0.0201	0.0446	0.0670	0.0335

These arrays correspond to a problem with two materials – UO_2 and H_2O . The first material identified by the first three entries contains three cross-sectional sets. It contains U-235, U-238, and oxygen. The second material contains two cross-sectional sets – hydrogen and oxygen. The first set of three entries tells the code to take 0.00223 atoms/barn/cm of U-235 and place it in material 1. The number 1261 is a common identifier for U-235 in many cross-sectional libraries. The second set of three numbers tells the code to take 0.0201 atoms/barn/cm of U-238 and place it in material 1. The third set of three numbers tells the code to take 0.0446 atoms/barn/cm of oxygen and place it in material 1. Note that oxygen is an element composed of at least three nuclides. Oxygen is not treated in as much detail as uranium because the properties of the minor isotopes do not affect the transport properties significantly and seldom would there be an economic advantage to changing the isotopic composition of natural oxygen. This completes material 1, but additional numbers could be added to each of the three arrays to add (or subtract) more nuclides to (or from) material 1 if that was desirable at a later date. The fourth set of entries adds 0.067 atoms/barn/cm of hydrogen to material 2, and the last set of entries adds 0.0335 atoms/barn/cm of oxygen to material 2. Note that an individual cross-sectional set can occur as many times as necessary to complete the materials.

The mixing table length for this problem is five, and it bears no relationship to the number of materials in the problem. The mixing table length is determined simply by the number of instructions that the analyst wishes to give the code.

FEMP1D will accept cross-sectional sets from three sources. It can read an ANISN binary library tape. It can read an AMPX working library binary tape, and it can accept cross-sectional input as part of the input stream. It can mix if they have the same group structure. This makes inputting cross-sectional sets by hand an easy way of correcting cross-sectional sets stored on electronic media. The set ID numbers for the 11\$ array must match the numbers on the ANISN or AMPX library tapes in order to retrieve these data sets. The input nuclide ID numbers are chosen for the cross-sectional sets coming in through the input stream in the 13S array. The number in the first position in the 13\$ array corresponds to the first cross-sectional set read in the 20*, 21*, and 22* arrays. The number in the second position corresponds to the second set of these arrays. It is important to realize that each nuclide in a problem must have a unique nuclide ID number, and therefore, some care must be exercised in assigning nuclide ID numbers for the cross-sectional sets in the input stream.

In order to activate the reading of the ANISN library or the AMPX library, the variables MANSN and MAMPX must be non-zero. In order to mix the input stream cross sections, the variable MCRD must be non-zero.

Pre-mixed cross-sectional sets can be used by entering the cross-sectional sets in the 20*, 21*, and 22* arrays. Then the entries corresponding to these cross sections in the 12* array should be set to 1.0.

5.8.2 *Cross-Sectional Collapsing*

This will be provided at future data for the FEMP computer code series.

5.9 Input Description

The following annotated Input description is an attempted explanation of the input variables and data required by FEMP1D as of the writing of this manual. The current input requirements are always maintained in the first lines of the code listing. If the information in the code conflicts with what is printed here, believe the code listing. If an individual array is not needed for a particular problem, it should be skipped. If an individual variable is not needed for a particular problem, a default value of zero should be entered.

```
PROGRAM FEMP1D
C
C  INPUT DATA
C
C  TITLE CARD (18A4)
C
```

A title card is required to start each problem. More than one problem can be stacked, and the way the code knows to continue with a new problem is when it reads the new title card. If it hits an end of file, it quits.

```
C
C  1$ ARRAY (32)
C
C  MGEOM=1,  SLAB GEOMETRY
C          =2,  CYLINDRICAL GEOMETRY
C          =3,  SPHERICAL GEOMETRY
C
```

This variable describes the shape of the assembly modeled.

```
C  NOUTR=1,  INHOMOGENEOUS SOURCE
C          =2,  INHOMOGENEOUS SOURCE WITH FISSION
C          =3,  FISSION EIGENVALUE
C          =4,  EIGENVALUE SEARCH PROBLEM
C
```

NOUTR controls the type of problem solved.

```
C MADJ=0, FORWARD PROBLEM
C      =1, ADJOINT PROBLEM
C
```

MADJ decides whether the code will try to solve an adjoint problem or not.

```
C LPN=SPHERICAL HARMONIC ORDER
C
```

LPN tells the code how many Legendre orders to retain in the approximation to the angular flux density. It should always be an odd number, as even numbers give no better answer than the previous odd order approximation. In slab and spherical geometries, this can be set to any value. In cylindrical geometry, it can be set to any value, but the code will only perform a P_1 equivalent calculation.

```
C NMAT=NUMBER OF MATERIAL MIXTURE
C
```

This variable sets the number of mixtures to be generated in the mixing table. Note that all mixtures generated do not have to be used in any given calculation. For instance, one mixing table may be generated for a series of problems and the materials that are mixed and not chosen in the 33\$ array are mixed and ignored. This wastes core storage, but that is not usually a critical parameter.

```
C MNG=NUMBER OF NEUTRON GROUPS
C
```

The number of neutron groups used in the calculation. This must match the number of neutron groups on any AMPX libraries used for cross sections. The sum of NNG and NPG must equal the number of groups on an ANISN library or those read in through the input stream.

```
C MPN=PN ORDER OF CROSS SECTIONS RETAINED
C
```

The Legendre order of the cross-sectional expansion is used for the calculation. This must be equal to or less than the data available on any of the cross-sectional files used in the calculation.

```
C IHT=TOTAL CROSS SECTION POSITION (ANISM TAPE)
C
```

The location in the ANISN is cross-sectional table of the total cross section. Normally the default position is location 3. In this case it is preceded by the absorption and fission yield for the particular group. If additional 1-D cross sections are used, they are normally stored before the total cross section in the group vectors.

```
C IHT=WITHIN GROUP SCATTER CROSS SECTION POSITION (ANISM TAPE)
C
```

The location in the ANISN is cross-sectional table of the within group scattering cross section. If there is no upscatter, then the within group directly follows the total cross section, and IHS is normally 4. If there is upscatter, then a place between the total and the within group cross sections must be saved for the maximum number of upscatter transfers required.

C **LTBL=CROSS SECTION TABLE LENGTH (ANISN TAPE)**
 C

LTBL specifies the total length of the group vector for each group in an ANISN cross-sectional array. It is the sum of the number of 1-D cross sections (IHT) plus the upscatter and within group cross sections (IHS-IHT) plus the number of downscatters. If a complete downscatter problem including hydrogen is modeled, this works out to NOG-1 + IHS. Many truncated tables exist and the correct value of LTBL must usually be obtained by listing the data titles on an ANISN library file with DIAL.

C **MTL=MIXING TABLE LENGTH**
 C

MTL specifies the number of entries anticipated and required in the 10\$, 11\$, and 12* arrays. It is the total number of mixing instructions and bears no relationship to the number of materials used in the problem.

C **MCRD=NUMBER OF MATERIAL CROSS SECTIONS FROM CARDS**
 C

MCRD identifies the number cross-sectional descriptions to be in the 20*, 21*, and 22* arrays. Data Block 2 containing these arrays must be read MCRD times.

C **MAMPX=NUMBER OF MATERIAL CROSS SECTIONS TO BE READ IN AMPX**
 C **WORKING LIBRARY FORMAT FROM TAPE16**
 C

If MAMPX is greater than zero, FEMP1D will search for a file on LUN16 with cross sections in the AMPX Working Library format. The actual value greater than zero is not relevant.

C **NX=NUMBER OF MESH POINTS**
 C

NX is the total number of mesh points in the direction of the calculation. This must be 1 more than the number of intervals.

C **NZONE=NUMBER OF MATERIAL ZONE IN PROBLEM**
 C

NZONE is the total number of homogeneous material zones in the problem.

C **IBL=0, LEFT BOUNDARY IS VACUM**
 C **=1, LEFT BOUNDARY IS REFLECTING**

```
C      =2, LEFT BOUNDARY HAS SOURCE INCIDENT
C
```

IBL specifies how the left or inner boundary is to be treated with regard to an incident flux. IBL = 0 is not allowed in cylindrical or spherical geometry.

```
C  IBL=0, RIGHT BOUNDARY IS VACUM
C      =1, RIGHT BOUNDARY IS REFLECTING
C      =2, RIGHT BOUNDARY HAS SOURCE INCIDENT
C
```

IBR specifies how the right or outer boundary is to be treated with regard to an incident flux.

```
C  ISTRT=0, SET FLUX EQUAL TO ZERO EVERYWHERE
C      =1, SET FLUX EQUAL TO 1.0 EVERYWHERE
C      =2, SET FLUX EQUAL TO INPUT FROM TAPES
C
```

ISTRRT controls the initial flux estimate. It must be two or three for a fission eigenvalue or eigenvalue search problem. TAPE3 is the restart tape, and its group structure must match, but its spatial mesh structure does not have to match the actual calculation, as FEMP1D will perform an interpolation onto the selected calculation mesh.

```
C  MCT=0, USE INTEGRAL CONVERGENCE TEST FOR NIDDLE ITERATIONS
C      =1, USE POINTWISE CONVERGENCE TEST FOR MIDDLE ITERATIONS
C
```

The integral test computes the L_2 norm of the error vector for the P_0 component of the angular flux density. It compares this relative error with the input value for EPK. The point-wise test computes the L_{∞} norm of the error vector for the P_0 component of the angular flux density. This process is not vectorizable, and therefore it takes a bit longer than the integral test. The integral test is more appropriate for fission problems, and the point-wise test is more appropriate for shielding or deep penetration problems.

```
C  ITMX2=MAXIMUM NUMBER OF OUTER INTERATIONS FOR FISSION PROBLEMS
C
```

ITMX3 should be set large enough to get convergence. For inhomogeneous source problems, a value of 1 should be adequate; however, setting it higher will not mean that the code will use more than is required. For inhomogeneous source with fission problems, a fairly high value will be required, particularly if the assembly is nearly critical. Writing a restart file is highly recommended for this type of problem if a reasonable estimate of ITMX3 cannot be obtained a priori. For fission eigenvalue problems, a reasonably high value is also required. Several hundred is reasonable if the problem has been debugged to the extent that the input is correct. Upscatter will increase the number of outers required for convergence even if upscatter acceleration is elected. For eigenvalue search problems,

approximately ten times the number that would be required for similar fission eigenvalue problems is reasonable. This may seem like a very large number, but two things should always be kept in mind. First, the code will not iterate more than what is required for convergence, and second, the restart file can always be used to cover the case of ITMX3 set too low. If the code does not converge, and a restart file has not been written, the effort put into the calculation must be restarted from scratch.

```
C IACC=0, NO FISSION SOURCE ACCELERATION
C      =1, SINGLE STEP CHEBYCHEV ACCELERATION
C      =2, MULTIPLE STEP CHEBYCHEV ACCELERATION
C
```

FEMP1D will accelerate the fission source with either 1 step or 2 step Chebychev acceleration. This process is covered in *Applied Iterative Methods* by Hageman and Young.

```
C NPOW=NUMBER OF POWER ITERATIONS PERFORMED BEFORE STARTING
C      THE CHEBYCHEV ACCELERATION
C
```

In order to obtain estimates of the parameters to be used for fission source acceleration, a number of unaccelerated outer (power) iterations must be performed first. It is recommended that approximately ten outers be performed before attempting to accelerate the fission source.

```
C NUPS=0, NO UPSCATTER SCALING
C      =N, NUMBER OF SUB-OUTERS PER OUTER TO SACLE UPSCATTER
C
```

Upscatter scaling is very efficient and highly recommended if the cross sections include upscatter. For inhomogeneous source only problems, NUPS should be set quite high, 30 or greater. For fission problems, a value of 3–8 has been found to work quite well.

```
C NS=NIUMBER OF SOURCE SPECTRA
C
```

NS is the number of different source spectra to be input in the 47* array.

```
C IPX=-2, DO NOT PRINT CROSS SECTIONS
C      =-1, PRINT 10 CROSS SECTIONS
C      = N, PRINT 20 CROSS SECTIONS THRU PM
C
```

IPX controls the printing of the mixed cross sections. Note that large group structures and numerous materials can produce very large output files, and the printing of every mixed cross section is not recommended.

```
C NPPUT=NUMBER OF POINTS FOR FLUX PRINT
C
```

After FEMP1D achieves a converged solution, it will print the flux at selected points if desired. NPOUT specifies the number of these points to be input in the 36* array.

```
C  MRF=NUMBER OF CARD INPUT RESPONSE FUNCTIONS
C
```

MRF specifies the number of response functions that will be read in the 39* array. These response functions will be integrated over the flux at the desired flux output points, and they will be multiplied by the zone fluxes and integrated over energy to obtain the zone and energy-integrated response.

```
C  IPFLX=0, DO NOT PRINT FLUX OUTPUT
C      =1, PRINT FLUX AT REQUESTED OUTPUT POINTS
C      =2, PRINT FLUX AT CALCULATION MESH POINTS
C
```

IPFLX determines if and where the final isotropic flux will be printed.

```
C  IWFIL=0, DO NOT WRITE SAVE FILE
C      =1, WRITE SAVE FILE TO FORT 4
C      =2, WRITE SAVE FILE TO (4TH) FILE NAMED AFTER BLOCK 0
C
```

IWFIL determines if a SAVE file will be written. The easiest way to write a SAVE file is to set IWFIL = -1. The SAVE file will be written to FORT.4. However, if the SAVE file is to be used later, it can be identified as the fourth file name in the input file after the Block 0 data. If the three previous files are not required, then it will move up in position depending on how many are not required.

```
C  2* ARRAY (3)
C
C  EPK=CONVERGENCE TOLERANCE ON EIGENVALUE
C
```

EPK is the relative error convergence test to be used on the fission eigenvalue, the isotropic flux during middle iterations, and the eigenvalue search, parameter during searches.

```
C  XK=EIGENVALUE ESTIMATE
C
```

XK is the initial estimate for K_{eff} . A non-zero value must be specified for all eigenvalue calculations.

```
C  SNORM=SOURCE NORMALIZATION
C
```

SNORM specifies the total number of source particles to be produced per centimeter of transverse length for the problem specified. At the end of the calculation, FEMP1D renormalizes all output values based on this value.

```

C  3$ ARRAY(5)
C
C  KSRCH=1, BUCKLING SEARCH
C      =2, DIMENSION SEARCH
C      =3, MIXTURE SEARCH
C

```

KSRCH specifies the type of search performed. A buckling search changes the input transverse bucklings to achieve the desired k_{eff} . All material bucklings are multiplied by the same factor. A dimension search scales all of the mesh points by the same factor to achieve the desired k_{eff} . A mixture search scales the volume fraction for the reactant to achieve the desired k_{eff} . The diluent volume fraction is reduced appropriately, and the background volume fraction remains constant.

```

C  MSRCH=MATERIAL TO BE MIXED FOR SEARCH
C

```

MRS is the material in the mixing table whose volume fraction in MSRCH will be adjusted to increase fissile content.

```

C  MDS=MATERIAL TO BE USED FOR DILUENT IN SEARCH
C

```

MDS is the material in the mixing table whose volume fraction in MSRCH will be adjusted downward to account increased for fissile content in MRS.

```

C  MBS=MATERIAL TO BE USED FOR BACKGROUND IN SEARCH
C

```

MBS is a background material that retains the same volume fraction in MSRCH throughout the mixing process. A search example might involve determining the enrichment of ^{335}U required in a UO_2 fuel to achieve criticality. For this case, ^{235}U would be the reactant, ^{235}U would be the diluent, and O would be the background material.

```

C  4* ARRAY(4)
C
C  DKEFF=DESIRED KEFF FOR SEARCH
C

```

DKEFF is the desired eigenvalue for the search. Often this will be greater than 1.0 in order to provide a control margin and a burnup lifetime.

```

C  VFR=INITIAL VOLUME FRACTION FOR REACTION MATERIAL
C

```

VFR is the initial volume fraction of material MRS in MSRCH. The factor found during the search to achieve the desired k_{eff} multiplies this volume fraction for the final volume fraction for this material.

```

C  VFD=INITIAL VOLUME FRACTION FOR DILUENT MATERIAL
C

```

VFD is the initial volume fraction of MDS in MSRCH. It is adjusted during the search such that VFR + VFD = Constant = 1.0 - VFB.

C **VFB=INITIAL VOLUME FRACTION FOR BACKGROUND MATERIAL**
C

VFB is the volume fraction in MSRCH for material MBS used during the search. It is not adjusted by the search.

C **5\$ ARRAY (4)**
C
C **NAN=NUMBER OF COLLAPSED ANISN CROSS SECTION SETS**
C

NAN is the number of cross-sectional sets from LUN15 that will be collapsed and written to LUN25. It is the number of input cross sections, not the number of output sets.

C **NAW=NUMBER OF COLLAPSED WORKING LIBRARY CROSS SECTION SETS**
C

NAW is the number of cross-sectional sets from LUN16 that will be collapsed and ten to LUN26. It is the number of input cross sections, not the number of output sets.

C **NBNG=NUMBER OF BROAD NEUTRON GROUPS**
C

NBNG is the number of broad, or few, neutron groups that the collapsing process will reduce to in the output library.

C **NBPG=NUMBER OF BROAD PHOTON GROUPS**
C

NBPG is the number of broad or few photon groups that the collapsing process will reduce to the output library.

C **LTBLB=ANISN TABLE LENGTH FOR COLLAPSED LIBRARY**
C

LTBLB is the length of the broad group library table for the collapsed ANISN library if one is produced. This is the end of Data Block 0 specifying the major parameters of the desired calculation.

C **DATA BLOCK NO. 1 (MIXING TABLE)**
C
C **10\$ ARRAY (MTL)**
C
C **MATERIAL NUMBERS**
C

The 10\$ array is made up of the material numbers to which cross-sectional sets will be assigned during the mixing process. The values at the same relative position in the 10\$, 11\$, and 12* arrays determine a specific mixing action.

```
C 11$ ARRAY (MTL)
C
C  NUCLIDE NUMBERS
C
```

The 11\$ array lists cross-sectional sets that are to be used in the mixing operation. ANISN, AMPX, and input stream numbers can be mixed so long as no two sets have the same number.

```
C 12$ ARRAY (MTL)
C
C  NUMBER DENSITIES (ATOMS/BARN/CM)
C
```

The 12* array contains the number densities for the cross-sectional sets identified in the 11\$ array that are to be mixed into the materials specified in the 10\$ array. The units to be used are atoms/barn/cm.

```
C 13$ ARRAY (MCRD)
C
C  NUCLIDE IDS FOR CROSS SECTIONS INPUT ON CARDS
C
```

These are the ID numbers to be assigned to the input stream cross-sectional sets. The first number entered corresponds to the cross sections read in the first Data Block 2. The second number entered corresponds to the second Data Block 2 read in the input stream. These numbers should not be the same as any of the numbers on the ANISN or AMPX data files.

```
C 14* ARRAY (NOG)
C
C  CHI SPECTRUM
C
```

These are the fractional neutron yields for fission by group.

```
C 15* ARRAY (NNG+1)
C
C  NEUTRON GROUP BOUNDARIES
C
```

These are the energy bounds for the neutron group boundaries. They are used to compute the average neutron group velocity. They can also be used to compute a chi spectrum if one is not inputted.

```
C 16* ARRAY (NPG+1)
C
C  NEUTRON GROUP BOUNDARIES
C
```

These are the energy bounds for the gamma group boundaries.

```
C 17* ARRAY (NOG)
C
C GROUP AVERAGE VELOCITIES
C
C T
```

The group *average* velocities can be input and the 17* array will override the code calculation. This is the last array in Data Block 1.

```
C DATA BLOCK NO. 2 (CROSS SECTIONS-ONE BLOCK FOR NUCLIDE/MATERIAL)
C
C 20* ARRAY (NOG*4)
C
C NOTE THE 1D CROSS SECTIONS ARE STORED IN THE FOLLOWING ORDER
C 1. TOTAL
C 2. TOTAL FISSION YIELD (NU*SIGF)
C 3. ABSORPTION
C 4. GROUP FRACTIONAL YIELD (CHI)
C
C 1D CROSS SECTIONS FOR THIS MATERIAL
```

Data Block 2 is optional, but it must be entered MCRD times if cross sections are to be read in from the input stream. The 20* array is the input for the 1-D cross sections. Based on the way numbers are processed in FORTRAN, the total cross section for all groups is read first, then the NU*SIGF cross section for all groups, etc.

```
C 21* ARRAY (NOG*NOG)
C
C P0 SCATTERING ARRAY FOR THIS NUCLIDE
C
```

The P_0 scattering cross-sectional array is read in the 20* array. The first set of NOG numbers are the cross sections for scattering within and out of the first or highest energy group. The second set of NOG numbers are the within and outscatter cross sections for the second group. This process repeats itself until all groups have been read. Due to the way numbers are stored and used, the look of the 20* array data stream can be confusing. When printed out by FEMP1D, the 2-D cross-sectional sets should look like a standard matrix to be multiplied by a flux vector ordered from high to low energy.

```
C 22* ARRAY (NOG*NOG)
C
C P1 SCATTERING ARRAY FOR THIS NUCLIDE
C
C T
C
```

The P_1 scattering array is read in the 22* array exactly analogous to the way the 21* array is read. No provision is made to read higher than P_1 expansions, as it is not likely that the large number of numbers required will often be manipulated hand input.

Note: A Data Block 2 must be entered for each data set to be entered from the input stream.

```
C  DATA BLOCK NO. 3 (MESH POINTS AND MATERIAL ZONES)
C
C  30• ARRAY (NK)
C
C  X MESH POINTS
C
```

This array contains the mesh point values in centimeters. Values should be entered in increasing numerical order. The 31* and 32* arrays are skipped in FEMP1D in an attempt to keep array numbering consistent between FEMP1D, FEMF2D, and FEMP3D.

```
C  33$ ARRAY (NZONE)
C
C  MACROSCOPIC MATERIALS BY ZONE
C
```

The 33\$ array identifies the macroscopic materials mixed in the 10S array to be assigned to each zone. The number entered in the first position in the 33S array will be the material assigned to the first zone. The number entered in the second position in the 33\$ array will be the material entered in the second zone, etc.

```
C  34$ ARRAY (NX-1)
C
C  ZONE NUMBERS BY MESH INTERVAL
C
```

Since a given material zone will often be more than one mean free path thick, it is usually required to have more than one mesh interval per zone. The 34\$ array assigns mesh intervals to zones. The first value in the 34\$ array is the zone to which the first interval is assigned. The second value in the 34S array is the zone to which the second interval is assigned, etc.

```
C  35* ARRAY (NMAT)
C
C  TRANSVERSE DIMENSIONS FOR BUCKLING CORRECTION BY MATERIAL
C
```

The values entered in the 35* array are the dimensions for the assembly transverse to the direction of calculation. These are entered by material. This gives some flexibility in allowing an assembly without a constant transverse dimension and an assembly with a very low density material to be modeled. For the low density materials, an attempt should be made to have the same transverse leakage per material across the assembly. Obviously this is an approximate technique, and the 1-D results computed should be evaluated with that in mind. The transverse dimension in the slab calculation case is assumed to represent a radius for a cylindrical assembly. The transverse dimension in the cylindrical calculation case is assumed to

represent a height for a cylindrical assembly. The transverse dimension in a spherical calculation is ignored by the code.

```
C 36* ARRAY (NPOUT)
C
C  OUTPUT X MESH POINTS FOR FLUX PRINT OUT
C
```

The 36* array contains values for the spatial points at which a flux print out or a response function evaluation is desired.

```
C 39* ARRAY (NOG*MRF)
C
C  RESPONSE FUNCTIONS
C
C  T
C
```

The 39* array contains the energy group-dependent response functions that can be multiplied times the group fluxes to obtain a measured response at a point in the assembly. They are also multiplied times the zone integrated fluxes to give an integral reaction rate over each zone. Note that the code does not know which response applies to which zone, so it evaluates all responses for all zones.

```
C  DATA BLOCK NO. 4 (INHOMOGENEOUS SOURCES)
C
C  40* ARRAY ( (LPNT1) *NOG)
C
C  LEFT MMDARY Sa) RCE SPECTRUM
C
```

The 40* array is the Legendre expansion for the source incident on the left side of the assembly, ordered by Legendre order and group number.

```
C  41*ARRAY ( (LPN+1) *NOG)
C
C  RIGHT BOUNDARY SOURCE SPECTRUM
C
```

The 41* array is the Legendre expansion for the source incident on the left side of the assembly, ordered by Legendre order and group number.

```
C  46*ARRAY (NOG*NS)
C
C  FIXED SOURCE SPECTRA
C
```

The 46* array contains the energy-dependent information for inhomogeneous sources. It is ordered by group and then spectrum. The spectra can be unnormalized or normalized, but if more than one spectrum is input, the relative normalization must be correct. The volume sources are assumed to be isotropic. The 42* through 45* arrays are reserved for input to FEMP2D and FEMP3D.

```

C  47$ ARRAY (NX-1)
C
C  INHOMOGENEOUS SOURCES BY MESH INTERVAL
C
C  T
C

```

The 47\$ array assigns the spectra input in the 46* array to mesh intervals. This completes Data Block 4.

```

C  DATA BLOCK NO. 5 (COLLAPSING INSTRUCTIIXIS)
C
C  50$ ARRAY (NNG)
C
C  BROAD NEUTRON GROUP NUMBERS BY FINE GROUP
C

```

These are essentially the instructions that assign the neutron fine group identified by position within the array to the neutron broad group identified by the numerical value entered. For instance, if the fifth entry in this array is a 2, that would direct that the fifth fine group be included in the second broad group.

```

C  51$ ARRAY (MPG)
C
C  BROAD GAMMA GROUP NUMBERS BY FINE GROUP
C

```

These are essentially the instructions that assign the photon fine group identified by position within the array to the photon broad group identified by the numerical value entered. For instance, if the fifth entry in this array is a 2, that would direct that the fifth fine group be included in the second broad group.

```

C  52$ ARRAY (NAN)
C
C  ANISN FINE GROUP LIBRARY IDS FM COLLAPSE
C

```

The 52\$ array identifies the ANISN sets on LUN15 that will be collapsed.

```

C  53$ ARRAY (NAN)
C
C  ANISN BROAD GROUP LIBRARY IDS
C

```

The 53\$ array gives the new ID Numbers that are to be assigned to the ANISN broad group sets.

```

C  54$ ARRAY (NAN)
C
C  ZONES FOR COLLAPSING ANISN CROSS SECTION SETS
C

```

The 54\$ array identifies the zone fluxes to be used to collapse the ANISN sets.

```
C 55$ ARRAY(18*NAN)
C
C  TITLES OF COLLAPSED AMISS CROSS SECTION SETS
C
```

The 55* array identifies the titles to be used for the ANISN broad group sets to be created.

```
C 56$ ARRAY(NAW)
C
C  WORKING LIBRARY FINE GROUP LIBRARY IDS
C
```

The 56\$ array identifies the AMPX sets on LUN16 that will be collapsed.

```
C 57$ ARRAY(NAW)
C
C  WORKING LIBRARY BROAD GROUP LIBRARY IDS
C
```

The 57\$ array gives the new ID numbers that are to be assigned to the AMPX broad group sets.

```
C 58$ ARRAY(NAW)
C
C  ZONES FOR COLLAPSING WORKING LIBRARY CROSS SECTION SETS
C
```

The 58\$ array identifies the zone fluxes to be used to collapse the AMPX sets.

```
C 59* ARRAY(18*NAM)
C
C  TITLES FOR COLLAPSED LURKING LIBRARY SETS
C
C  T
C
```

The titles for the AMPX collapsed data sets are read as character data and cannot be free form. This completes the input data stream for one problem.

```
C FEMP1D QTTPUT TAPE FORMAT - (LUN4)
C
C RECORD 1: TITLE
C FORMAT - (1BA4)
C DATA - (CODE(I), I=1,6), (TITLE(I), I=1,18)
```

The output tape is a convenient way of electronically saving the output of a calculation for additional processing or to restart a calculation. It is written in ASCII format to facilitate reading by a number of processors including the eyeball if required. The first record is the problem title.

Note that provisions are made for a three-dimensional format. This allows some passing of information between different dimension-level calculations.

```
C RECORD 2: INTEGER PARAMETERS
C FORMAT - (1216)
C DATA - MADJ, NGEOM, NZOIE, NX, NZ, NOG1 YNG, NPG, LPN, ITER, IDU(
C MADJ=FORWARD/ADJOINT INDICATOR (0/1-FORWARD/ADJOINT)
C NGEOM=GEOMETRY INWICATWR (1/2/3-XZ/RZT/RTZ)
C NZOME=NUMBER OF DISTINCT MATERIAL ZONES
C NX=NUMBER OF FIRST DIMENSION MESH POINTS
C NY=NUMBER OF SECOND DIMENSION MESH POINTS
C NZ=MONGER OF THIRD DIMENSION MESH POINTS
C NOGI=NUMBER OF ENERGY GR JP BOUNDS
C NNG=NUMBER OF NEUTRON ENERGY GROUPS
C MPG=NUMBER OF GANIA ENERGY GROUPS
C LPN=SPHERICAL HARMONIC ORDER (0/1-P0/P1)
C ITER=WINGER OF COMPLETED OUTER ITERATIONS
C IDLAM=SPARE
```

The second record is a listing of the integer problem control parameters.

```
C RECORD 3: REAL PARAIEIERS
C FORMAT - (1P6E12.4)
C DATA - XKEFF, DMRT0, OMEGA, SNORM, DUM1, DUM2
C XKEFF=CRITICALITY EIGENVALUE
C DMRT0=LOINNANCE RATIO
C OMEGA=UPSCATTER OVER-RELAMTION FACTOR
C SNORM=SOURCE NORMALIZATION FACTO
C DUM1=SPARE
C DUM2=SPARE
```

The third record is a listing of the floating point problem control parameters.

```
C RECORD 4: (NEUTRON, GAMA) ENERGY GROUP BONNDS
C FORMAT - (1P6E12.4)
C DATA - (EN(IG), IG=1, NNG+1), (EN(IG), I=1, NPG+1)
```

The fourth record gives the group energy bounds.

```
C RECORD 5: MESH BOUNDRIES
C FORMAT - (1P6E12.4)
C DATA - (X(I), I=1, NX), (Y(J), J=1, NY), (Z(K), K=1, NZ)
```

The fifth record gives the calculation mesh boundaries.

```
C RECORD 6: ZONE MAP, MATERIAL BY ZONE ARRAY
C FORMAT - (2413)
C DATA - ((NZ(I, J, K), I=1, NX-1), J=1, NY), K=1, NZ-1), (NZ(L), L=1, NZONE)
```

The sixth record specifies the material map.

```
C RECORD 7-NOG+6: GROW FLUX MOMENTS
C FOMAT - (1P6E12.4)
C DATA - (((FLXM (I,J,K),I=1,NX),J=1,NY),K=1,NZ)
C CODING - DO 10 IG=1,NOG
C      DO 10 L=1,LPN
C      READ(NTFLX,FORMAT) (((ELXM(I,J,K),I=1,NX),J=1,NY),K=1,NZ)
C      10 CONTINUE
C
```

The seventh and subsequent records are the Legendre flux expansions generated during the calculation.

5.10 Output Description

The best description of the output to be expected from a typical problem can be obtained by perusing the sample problems contained in the code package. Please contact this author for further information. Further information is provided in the user's manual of FEMP computer code [1].

Reference

1. McDaniel P. Finite element multi-group PN 1-dimensional computer code, User's manual. Albuquerque: University of New Mexico; 2007

Chapter 6

Slowing Down Theory



In neutronic analysis for nuclear reactor systems, we look at three types of reactors depending upon the average energy of neutrons, which cause the bulk of the fission in the system:

Thermal reactors, in which most fission are induced by neutron, and these neutrons more or less are in thermal equilibrium with the atoms in reactor and maintain energy below approximately 0.3 eV.

Intermediate reactor or resonance reactors, in which neutrons have energy above thermal up to 10 keV, and most of these neutrons are responsible for fission lying in the resonance region of the heavy elements. This type of reactor is also largely responsible for producing fissions.

Finally, the third one is *fast reactor*, in which fissions are induced primarily by neutrons with energy of the order of 100 keV and above.

Yet importantly, one should be aware of the fact that in a thermal reactor, the fission neutrons are slowed down by the use of a *moderator* and that is a mass of material, such as carbon, beryllium, or water, which is distributed throughout the fueled region or *core* of the reactor.¹

6.1 Neutron Elastic and Inelastic Scattering for Slowing Down

Over a broad range of energies from about 1.0 MeV down to just above thermal energies, the energy spectrum in a thermal reactor is dominated by elastic scattering interactions. This single fact allows a number of approximations to be made that are generally very accurate and of great use in analyzing the behavior of this type of reactor. In fact, the process of slowing down that goes on in most reactors, and large light water power reactors in particular, can be approximated by considering the

slowing down medium to be infinite in extent. This allows the consideration of neutron energy changes to separate from spatial density changes and decouple the isotropic neutron flux equation from higher order terms. Therefore, a solution can be obtained for the isotropic flux for an infinite medium that should be a good approximation to the actual spectrum in the slowing down range of an actual reactor.

6.2 Derivation of the Energy and Transfer Cross Section

Derivation of the energy and transfer cross section will be discussed in this section, and they are approached from two point of views as:

1. Elastic scattering
2. Inelastic scattering

Both topics are discussed in the following subsections.

6.2.1 Elastic Scattering

In order to derive the fundamental spectrum that is produced by elastic scattering in the slowing down region, the following diagram relating the angle of scattering in the laboratory and the center of mass reference frames is of great use.

The laboratory and center of mass reference frames are defined as follows:

Laboratory frame of reference (L): This is a fixed frame of reference with a neutron moving with velocity u and a stationary nucleus. Thermal motions of the nucleus can be neglected, when the neutron's energy is in the slowing down range.

Center of mass frame of reference(C): The moving frame of reference is a frame, in which the sum of the momentum of both particles is equal to zero. This frame of reference is moving toward the nucleus prior to the collision, and since no external forces act on the particles during the collision, it continues moving at the same velocity after the collision. The neutron and nucleus themselves also have the same velocity magnitudes after the collision as they did before the collision in order to satisfy conservation of momentum. The only thing that the collision change has is their relative direction of motion.

Velocities before collision will be identified by u and U and after collision by v and V . A subscript C will identify velocities measured in the center of mass frame, and a subscript L will identify velocities measured in the lab frame.

Consider now the total momentum in the C frame, then we can write:

$$mu_C + MU_C = 0 \quad (6.1)$$

$$U_C = -\frac{m}{M} u_C \quad (6.2)$$

$$u_L = u_C - U_C = \left(1 + \frac{m}{M}\right) u_C \quad (6.3)$$

Or the velocity of the nucleus in the **C** frame can be related to its **L** frame velocity by:

$$u_C = \frac{1}{1 + \frac{m}{M}} u_L \quad (6.4)$$

Now since a neutron is approximately 1 amu and a nucleus with atomic number *A* is approximately *A* amu:

$$\frac{M}{m} = A \quad (6.5)$$

$$u_C = \frac{A}{A + 1} u_L = v_C \quad (6.6)$$

$$U_C = -\frac{1}{A} u_C \quad (6.7)$$

The velocity of the **C** frame relative to the **L** frame can be found by:

$$u_{CM} = -U_C = \frac{1}{A} u_C = \frac{1}{A + 1} u_L \quad (6.8)$$

The reduced mass, μ , is defined by:

$$\mu = \frac{mM}{m + M} = \frac{A}{A + 1} m \quad (6.9)$$

Then from the angle relationships of Fig. 6.1:

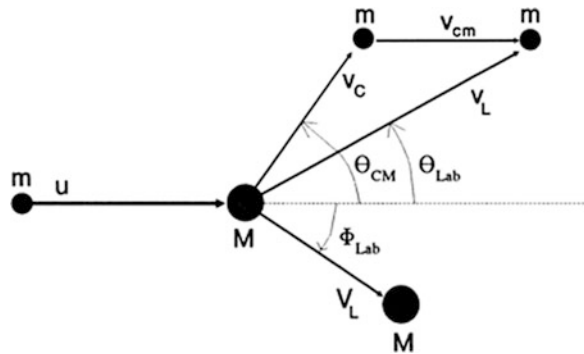
$$v_L \sin \theta_L = v_C \sin \theta_C \quad (6.10)$$

$$v_L \cos \theta_L = v_{CM} + v_C \cos \theta_C \quad (6.11)$$

Dividing the second into the first gives:

$$\frac{\sin \theta_L}{\cos \theta_L} = \frac{\sin \theta_C}{\frac{v_{CM}}{v_C} + \cos \theta_C} \quad (6.12)$$

Fig. 6.1 Laboratory and center of mass reference frames



Or

$$\tan \theta_L = \frac{\sin \theta_C}{\frac{1}{A} + \cos \theta_C} \quad (6.13)$$

This gives a method for obtaining the angle of scattering in the **L** frame, given an angle of scattering in the **C** frame. However, a more useful relationship for neutron scattering purposes can be obtained by squaring both equations and adding:

$$v_L^2 (\cos^2 \theta_L + \sin^2 \theta_L) = v_C^2 \sin^2 \theta_C + (v_{CM} + v_C \cos \theta_C)^2 \quad (6.14)$$

$$v_L^2 = v_C^2 + v_{CM}^2 + 2v_C v_{CM} \cos \theta_C \quad (6.15)$$

$$\frac{1}{2} m v_L^2 = \frac{1}{2} m v_C^2 + \frac{1}{2} m v_{CM}^2 + 2 \frac{1}{2} m v_C v_{CM} \cos \theta_C \quad (6.16)$$

$$E = \left[\frac{A}{A+1} \right]^2 E' + \left[\frac{1}{A+1} \right]^2 E' + 2 \left[\frac{1}{A+1} \frac{A}{A+1} \right] E' \cos \theta_C \quad (6.17)$$

where the usual notation of E' is the neutron energy before the collision and E as the neutron energy after collision (both measured in the lab frame) has been introduced. This can be written as:

$$\frac{E}{E'} = \frac{A^2 + 2A \cos \theta_C + 1}{(A+1)^2} \quad (6.18)$$

Considering the two extremes for θ_c gives:

(a)

$$\theta_c = 0$$

$$\frac{E}{E'} = \frac{A^2 + 2A + 1}{(A + 1)^2} = 1.0 \quad (6.19)$$

(b)

$$\theta_c = \pi$$

$$\frac{E}{E'} = \frac{A^2 - 2A + 1}{(A + 1)^2} = \frac{(A - 1)^2}{(A + 1)^2} \quad (6.20)$$

This then leads to the definition of a convenient new variable, α :

$$\alpha = \frac{(A - 1)^2}{(A + 1)^2} \quad (6.21)$$

The energy change equation can then be written as:

$$E = \frac{(1 + \alpha) + (1 - \alpha) \cos \theta_C}{2} E' \quad (6.22)$$

Differentiating this equation gives:

$$dE = -\frac{(1 - \alpha)}{2} E' \sin \theta_C d\theta_C \quad (6.23)$$

This can be written as:

$$dE = \frac{(1 - \alpha)}{2} E' d\mu_C \quad \mu_C = \cos \theta_C \quad (6.24)$$

Now defining a cross section for scattering through a given μ_{CM} as $\sigma_s(\mu_{CM})$ and realizing that it can be related to the total scattering cross section by:

$$\sigma_s = 2\pi \int_{-1}^1 \sigma_s(\mu_C) d\mu_C \quad (6.25)$$

The probability of scattering through a given μ_{CM} into an incremental $d\mu_{CM}$ is given by:

$$P(\mu_C) d\mu_C = 2\pi \frac{\sigma_s(\mu_C)}{\sigma_s} d\mu_C \quad (6.26)$$

And the probability of going from energy E' to a differential energy dE about energy E is the same as scattering through a CM angle corresponding to μ_C :

$$P(E' \rightarrow E)dE' = P(\mu_C)d\mu_C \quad (6.27)$$

Or

$$P(E' \rightarrow E)dE' = 2\pi \frac{\sigma_s(\mu_C)}{\sigma_s} d\mu_C \quad (6.28)$$

Then the differential relationship between dE and $d\mu_C$ can be used:

$$dE = \frac{(1 - \alpha)}{2} E' d\mu_C \quad (6.29)$$

This gives:

$$P(E' \rightarrow E) \frac{(1 - \alpha)}{2} E' d\mu_C = 2\pi \frac{\sigma_s(\mu_C)}{\sigma_s} d\mu_C \quad (6.30)$$

which reduces to:

$$P(E' \rightarrow E) = \frac{\sigma_s(\mu_C)}{\sigma_s} \frac{4\pi}{(1 - \alpha)E'} \quad (6.31)$$

This can be used for an arbitrary scattering distribution in the C frame. However, for isotropic scattering in the C frame (by far the most common case for realistic moderators):

$$\sigma_s(\mu_C) = \frac{\sigma_s}{4\pi} \quad (6.32)$$

Then the energy transfer probability reduces to:

$$P(E' \rightarrow E) = \frac{1}{(1 - \alpha)E'} \quad (6.33)$$

In addition, the isotropic transfer cross section from energy E' to energy E is given by:

$$\sigma_{s0}(E' \rightarrow E) = \sigma_{s0}P(E' \rightarrow E) = \frac{\sigma_{s0}}{(1 - \alpha)E'} \quad (6.34)$$

6.2.2 Inelastic Scattering

For the case of inelastic scattering, everything remains the same except the excitation energy must be introduced into the conservation of energy equation. The excitation energy will be identified by the symbol Q . For inelastic scattering, Q will be negative as the energy of excitation is removed from the kinetic energy of the system. The energy balance equation in the center of mass frame is then:

$$\frac{1}{2}mu_C^2 + \frac{1}{2}MU_C^2 + Q = \frac{1}{2}mv_C^2 + \frac{1}{2}MV_C^2 \quad (6.35)$$

This can be simplified by multiplying by 2 and dividing by m . Then:

$$u_C^2 + \frac{M}{m}U_C^2 + \frac{2Q}{m} = v_C^2 + \frac{M}{m}V_C^2 \quad (6.36)$$

and remembering that:

$$mu_C = -MU_C \quad \text{and} \quad mv_C = -MV_C \quad (6.37)$$

$$u_C^2 + \frac{2QA}{m(1+A)} = v_C^2 = \left(\frac{A}{A+1}\right)^2 u_L^2 + \frac{2QA}{m(A+1)} \quad (6.38)$$

$$v_C^2 = \left(\frac{A}{A+1}\right)^2 u_L^2 \left(1 + \frac{Q}{\frac{1}{2}mu_L^2} \frac{A+1}{A}\right) \quad (6.39)$$

In addition, from Eq. 6.15 we have:

$$v_L^2 = v_C^2 + 2v_C v_{CM} \cos \theta_C + v_{CM}^2 \quad (6.40)$$

$$v_L^2 = u_L^2 \left\{ \left(\frac{A}{A+1}\right)^2 \left(1 + \frac{Q}{\frac{1}{2}mu_L^2} \frac{A+1}{A}\right) + \frac{2A}{(A+1)^2} \sqrt{1 + \frac{Q}{\frac{1}{2}mu_L^2} \frac{A+1}{A}} \cos \theta_C + \left(\frac{1}{A+1}\right)^2 \right\} \quad (6.41)$$

Or

$$E = E' \left\{ \left(\frac{A}{A+1} \right)^2 \left(1 + \frac{Q}{E'} \frac{A+1}{A} \right) + \frac{2A}{(A+1)^2} \sqrt{1 + \frac{Q}{E'} \frac{A+1}{A}} \cos \theta_C + \left(\frac{1}{A+1} \right)^2 \right\} \quad (6.42)$$

Note that the lowest energy that can excite a level with an excitation energy of Q is:

$$E' = \frac{A+1}{A} Q \quad (6.43)$$

When this happens, we will have that:

$$E = \frac{E'}{(A+1)^2} \quad (6.44)$$

Note that this is a significantly greater energy loss than elastic scattering.

6.3 Derivation of the Isotropic Flux in an Infinite Hydrogen Moderator

Now in order to obtain the energy-dependent flux in an infinite reactor, begin by considering the balance equation for an infinite medium where the only scattering element is hydrogen. Hydrogen is chosen first because it will be assumed that a neutron and a proton are of equal mass and a collision between a neutron and a hydrogen atom will allow the neutron to lose all of its energy. The balance equation can be, written as:

$$\Sigma_T(E)\phi(E) = \int_E^\infty \Sigma_s(E' \rightarrow E)\phi(E')dE' + S(E) \quad (6.45)$$

For the sake of simplicity, assume that all neutrons are introduced at a single energy, E_0 , by a delta function source, $S(E) = S^* \delta(E - E_0)$. This approximates the fission spectrum and can be handled analytically, as well as producing reasonable results. It will also allow treatment of the high-energy source as a boundary condition. Then, for isotropic scattering in the center of mass reference frame for hydrogen, the energy transfer cross section is:

$$\Sigma_s(E' \rightarrow E) = \frac{\Sigma_s(E')}{(1-\alpha)E'} = \frac{\Sigma_s^H(E')}{E'} \quad (6.46)$$

Inserting this into the balance equation, and considering a source and absorption free region below the delta function source, gives:

$$\Sigma_s^H(E)\phi(E) = \int_E^{E_0} \frac{\Sigma_s^H(E')\phi(E')}{E'} dE' \quad (6.47)$$

It will prove useful to define a new quantity, $F(E)$, called the collision density as:

$$F(E) = \Sigma_s(E)\phi(E) \quad (6.48)$$

Inserting this quantity into the P_0 equation and differentiating with respect to E gives:

$$F'(E) = -\frac{F(E)}{E} \quad (6.49)$$

This can be written as:

$$EF'(E) + F(E) = 0 \quad (6.50)$$

And is of the form:

$$\frac{d}{dE}[EF(E)] = 0 \quad (6.51)$$

This can be integrated directly to obtain:

$$EF(E) = \text{Constant} = Q_0 \quad (6.52)$$

Therefore, in pure hydrogen the collision density varies as $1/E$:

$$F(E) = \frac{Q_0}{E} \quad (6.53)$$

The flux varies as:

$$\phi(E) = \frac{Q_0}{\Sigma_s(E)E} = \frac{\text{Constant}}{\Sigma_s E} \quad (6.54)$$

If the total scattering cross section is constant, then the flux varies as $1/E$ also.

At this point it is useful to introduce a new variable called lethargy and defined by:

$$u = \ln \frac{E_0}{E} \quad (6.55)$$

The lethargy will vary from near zero to some maximum value, as a neutron slows down; thus, it is a conceptually useful concept in terms of following the life of a neutron. Because it is a logarithmic variable, it condenses the 8 or 9 orders of magnitude change in energy into a number less than 30.

In addition, since a neutron tends to lose a fraction of its energy in any given collision, scattering phenomena will be more constant when expressed on a lethargy scale. In order to relate the flux as a function of energy to the flux as a function of lethargy, the following mathematical relationship for the two collision densities can be used:

$$|F(E)dE| = |F(u)du| \quad (6.56)$$

Or

$$F(E) \left| \frac{dE}{du} \right| = F(u) \quad (6.57)$$

And noting:

$$\left| \frac{dE}{du} \right| = E \quad (6.58)$$

Gives:

$$F(u) = EF(E) \quad (6.59)$$

Thus $F(u)$ is a constant. Moreover, since over broad expanses of the slowing down range, the total cross section of hydrogen is only elastic scattering and relatively constant; this gives:

$$\phi(u) = \frac{Q_0}{\Sigma_s^H(u)} \quad (6.60)$$

This result means that for multi-group cross sections used in typical light water reactors, the weighting spectrum within group can be very adequately represented as a constant in the lethargy variable.

In order to evaluate the constant Q_0 , a new quantity, $q(E)$, called the “slowing down density” must be defined. This is basically the number of neutrons per unit volume that slow past a given energy on a continuous basis. It is defined by the integral equation:

$$q(E) = \int_0^E dE'' \int_E^{E_0} \Sigma_s(E' \rightarrow E'') \phi(E') dE' + \int_0^E dE'' \int_E^{E_0} \Sigma_s(E' \rightarrow E'') S(E') dE' \quad (6.61)$$

For isotropic scattering in hydrogen, this can be written as:

$$q(E) = E \int_E^{E_0} \frac{F(E')}{E'} dE' + E \int_E^{E_0} \frac{\Sigma_s^H(E')S(E')}{E'} dE' \quad (6.62)$$

As indicated above, consider the source at energy E_0 to be a delta function. This allows integration over the source energy:

$$q(E) = E \int_E^{E_0} \frac{F(E')}{E'} dE' + \frac{E}{E_0} \Sigma_s^H(E_0)S_0 \quad (6.63)$$

Moreover, performing the inscatter integration between the source energy and the energy of interest, E , gives:

$$q(E) = E \left[\frac{1}{E} - \frac{1}{E_0} \right] Q_0 + \frac{E}{E_0} \Sigma_s^H(E_0)S_0 \quad (6.64)$$

At the source energy, E_0 , this will give:

$$q(E_0) = \frac{E_0}{E_0} \Sigma_s^H(E_0)S_0 = \Sigma_s^H(E_0)S_0 \quad (6.65)$$

For an infinite medium with no absorption, the same number of neutrons must slow past the energy E as it starts out at energy E_0 , and $q(E) = q(E_0)$. The general slowing down density becomes:

$$q(E) = \Sigma_s^H(E_0)S(E_0) = \left[1 - \frac{E}{E_0} \right] Q_0 + \frac{E}{E_0} \Sigma_s^H(E_0)S_0 \quad (6.66)$$

$$\left[1 - \frac{E}{E_0} \right] \Sigma_s^H(E_0)S_0 = \left[1 - \frac{E}{E_0} \right] Q_0 \quad (6.67)$$

$$Q_0 = \Sigma_s^H(E_0)S_0 \quad (6.68)$$

So for slowing down in an infinite medium:

$$\phi(E) = \frac{Q_0}{E \Sigma_s^H(E)} = \frac{S_0 \Sigma_s^H(E_0)}{E \Sigma_s^H(E)} \quad (6.69)$$

6.4 Derivation of the Isotropic Flux in a Moderator Other than Hydrogen $A > 1$

Consider now the case of a single moderator with $A > 1$. The balance equation becomes:

$$\Sigma_s(E)\phi(E) = \int_E^{E/\alpha} \frac{\Sigma_s(E')}{(1-\alpha)E'} \phi(E') dE' + S(E) \quad (6.70)$$

where the isotropic, in the center of mass, scattering transfer function has been used. This is a good approximation for most light moderators. For fast reactors, and all-metal assemblies, this is not a good approximation, *a priori*. However, experience has shown that even for these cases, the results obtained by making this approximation are quite good, when a large enough number of groups are used.

Once again, the high-energy source of neutrons can be assumed to be a delta function and the homogeneous problem solved first. Defining the collision density, $F(E)$, as before, the balance equation becomes:

$$F(E) = \int_E^{E/\alpha} \frac{F(E') dE'}{(1-\alpha)E'} \quad (6.71)$$

Differentiating this equation gives:

$$F'(E) = \frac{1}{(1-\alpha)} \left[\frac{F(E/\alpha)}{E/\alpha} \frac{1}{\alpha} - \frac{F(E)}{E} \right] \quad (6.72)$$

Now due to the presence of the $F(E/\alpha)$ term in this equation, it is difficult to easily proceed beyond this point. This equation cannot be solved in a direct manner. It has been solved in the literature for the case of a true delta function source at energy, E_0 . The solution in terms of so-called Placzek functions is discontinuous at the end of the first scattering interval below the source. At the boundary to each subsequent scattering interval, a higher-order derivative is discontinuous. Though the Placzek functions produce the correct mathematical solution to the approximate problem, the introduction of the delta function source causes too much of a simplification in this case and produces the unphysical result of a discontinuous flux at the energy αE_0 . The actual fission source, spread over a range of energies, will smooth this effect out and the discontinuity will not be seen. Therefore, the approach taken here will be to assume a form for the asymptotic spectrum at a number of scattering intervals below the source and show that the assumed spectrum is a solution to the differential-difference equation. This solution is also the Placzek solution for energies removed by more than three scattering intervals from a delta function source.

The solution assumed will be:

$$F(E) = \frac{\text{Constant}}{E} = \frac{C_0}{E} \quad (6.73)$$

Then differentiating:

$$\frac{dF(E)}{dE} = -\frac{C_0}{E^2} \quad (6.74)$$

And evaluating:

$$F\left[\frac{E}{\alpha}\right] = \frac{\alpha C_0}{E} \quad F(E) = \frac{C_0}{E} \quad (6.75)$$

$$-\frac{C_0}{E^2} = \frac{1}{(1-\alpha)} \left[\frac{\frac{\alpha C_0}{E} \frac{1}{\alpha}}{\frac{E}{\alpha}} - \frac{\frac{C_0}{E}}{E} \right] \quad (6.76)$$

$$-\frac{C_0}{E^2} = \frac{1}{(1-\alpha)} \left[\frac{(\alpha-1)C_0}{E^2} \right] \quad (6.77)$$

$$-\frac{C_0}{E^2} = -\frac{C_0}{E^2} \quad QED \quad (6.78)$$

Therefore, the solution $EF(E) = C_0$ is clearly an acceptable solution.

Now consider the slowing down density:

$$q(E) = \int_{\alpha E'}^E dE'' \int_E^{E/\alpha} \Sigma_s(E' \rightarrow E) \phi(E') dE' \quad (6.79)$$

Note that only one scattering interval above and below the energy of interest is all that must be considered for this case. This means that a neutron cannot scatter from the source energy, E_0 , to an energy below αE_0 without first scattering in the interval above αE_0 .

Transforming to the lethargy variable and continuing to assume isotropic scattering in the center of mass reference frame give the following equation for $q(E)$:

$$q(u) = \int_{u' - \ln \alpha}^u du'' \int_u^{u + \ln \alpha} \frac{\Sigma_s(u')}{(1-\alpha)} \phi(u') e^{-(u'' - u')} du' \quad (6.80)$$

Pulling out the constant cross section-flux product and reversing the order of integration give:

$$q(u) = \frac{\Sigma_s(u)\phi(u)}{(1-\alpha)} \int_{u+\ln\alpha}^u e^{u'} du' \int_u^{u'-\ln\alpha} e^{-u''} du'' \quad (6.81)$$

$$q(u) = \frac{\Sigma_s(u)\phi(u)}{(1-\alpha)} \int_{u+\ln\alpha}^u e^{u'} [e^{-u} - \alpha e^u] du' \quad (6.82)$$

$$q(u) = \Sigma_s(u)\phi(u) \left[1 + \frac{\alpha}{1-\alpha} \right] \ln\alpha \quad (6.83)$$

And then defining:

$$\xi = 1 + \frac{\alpha}{1-\alpha} \ln\alpha \quad (6.84)$$

Finally gives:

$$q(u) = \xi \Sigma_s(u)\phi(u) = \xi F(u) \quad (6.85)$$

6.5 Summary of Slowing Down Equations

Summarizing the above analysis, the following relationships apply to the slowing down fluxes in an infinite medium dominated by moderators that scatter isotropically in the center of mass reference frame.

1.

$$A = 1$$

$$\phi(E) = \frac{Q_0}{E \Sigma_s^H(E)} \quad (6.86)$$

$$\phi(u) = E\phi(E) = \frac{Q_0}{\Sigma_s^H} \approx \text{Constant} \quad (6.87)$$

$$q(u) = \Sigma_s^H(u)\phi(u) \quad (6.88)$$

2.

$$A > 1$$

$$\phi(E) = \frac{Q_0}{\xi E \Sigma_s(E)} \quad (6.89)$$

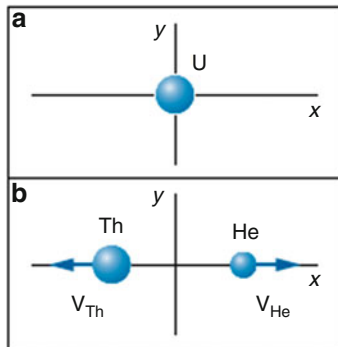
$$\varphi(u) = \frac{Q_0}{\xi \Sigma_s(u)} \approx \text{Constant} \quad (6.90)$$

$$q(u) = \xi \Sigma_s(u) \phi(u) \quad (6.91)$$

Problems

Problem 6.1 An atom of uranium (U) with mass of 3.9529×10^{-25} kg (i. e., $m = 3.9529 \times 10^{-25}$ kg) at rest decays spontaneously into an atom of helium (He) mass of 3.8864×10^{-27} kg (i.e., $m = 3.8864 \times 10^{-27}$ kg). The helium atom is observed to move in the positive x -direction with velocity of 1.423×10^7 m/sec Fig. 6.2. Do the following analyses as:

Fig. 6.2 (a) Before decay and (b) after decay

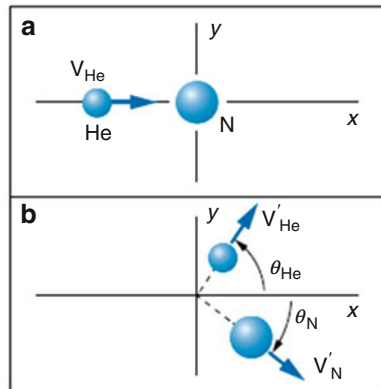


- (a) Find the velocity (i.e., magnitude and direction) of the thorium atom.
- (b) Find the total kinetic energy of the two atoms after the decay.

Problem 6.2 A helium atom ($m = 6.6465 \times 10^{-27}$ kg) moving at a speed of $V_{He} = 1.518 \times 10^6$ m/s collides with an atom of nitrogen ($m = 2.3253 \times 10^{-26}$ kg) at rest. After the collision, the helium atom is found to be moving with a velocity of $V'_{He} = 1.199 \times 10^6$ m/s at an angle of $\theta_{He} = 78.75^\circ$ relative to the direction of the original motion of the helium atom.

- (a) Find the velocity (magnitude and direction) of the nitrogen atom after the collision.
 (b) Compare the kinetic energy before the collision with the total kinetic energy of the atoms after the collision. Use Fig. 6.3 to solve this problem.

Fig. 6.3 (a) Before collision and (b) after collision



Problem 6.3 A particle of mass M is elastically scattered from a stationary proton of mass m . The proton is projected at an angle $\varphi = 22.1^\circ$, while the incident particle is scattered through an angle $\theta = 5.6^\circ$ with the incident direction. Calculate M in atomic mass units. (This event was recorded in photographic emulsions in the Wills Lab., Bristol.)

Problem 6.4 A particle of mass M is elastically scattered through an angle θ from a target particle of mass m initially at rest ($M > m$).

- (a) Show that the largest possible scattering angle θ_{max} in the lab. System is given by $\sin\theta_{\text{max}} = m/M$, the corresponding angle in the center of mass system (CMS) being $\cos\theta_{\text{max}}^* = -m/M$.
 (b) Further show that the maximum recoil angle for m is given by $\sin\varphi_{\text{max}} = [(M-m)/2M]^{1/2}$.
 (c) Calculate the angle $\theta_{\text{max}} + \varphi_{\text{max}}$ for elastic collisions between the incident deuterons and target protons.

Problem 6.5 A deuteron of velocity u collides with another deuteron initially at rest. The collision results in the production of a proton and a triton (${}^3\text{H}$), the former moving at an angle 45° with the direction of incidence. Assuming that this rearrangement collision may be approximated to an elastic collision (quasi-scattering), calculate the speed and direction of triton in the lab and center of mass (CM) system.

Problem 6.6 An α -particle from a radioactive source collides with a stationary proton and continues with a deflection of 10° . Find the direction in which the proton moves (α -mass = 4.004 amu; proton mass = 1.008 amu).

Problem 6.7 An α -particle of kinetic energy of 20 MeV passes through a gas, and they are found to be elastically scattered at angles up to 30° but not beyond. Explain this, and identify the gas. In what way, if any, does the limiting angle vary with energy?

Problem 6.8 A perfectly smooth sphere of mass m_1 moving with velocity v collides elastically with a similar but initially stationary sphere of mass m_2 ($m_1 > m_2$) and is deflected through an angle θ_L . Describe how this collision would appear in the center of mass frame of reference and show that the relation between θ_L and the angle of deflection θ_M , in the center of mass frame is $\tan \theta_L = \sin \theta_M / [m_1/m_2 + \cos \theta_M]$. Show also that θ_L cannot be greater than about 15° if $(m_1/m_2) = 4$.

Problem 6.9 Show that the maximum velocity that can be imparted to a proton at rest by nonrelativistic alpha particle is 1.6 times the velocity of the incident alpha particle.

Problem 6.10 Show that the differential cross section $\sigma(\theta)$ for scattering of protons by protons in the lab system is related to $\sigma(\theta^*)$ corresponding to the center of mass system (CMS) by the formula $\sigma(\theta) = 4 \cos(\theta^*/2) \sigma(\theta^*)$.

Problem 6.11 If E_0 is the neutron energy and σ the total cross section for low energy n-p scattering assumed to be isotropic in the center of mass system (CMS), then show that in the laboratory system (LS), the proton energy distribution is given by $(d\sigma_p/dE_p) = (\sigma/E_0) = \text{constant}$.

Problem 6.12 Particles of mass m are elastically scattered off target nuclei of mass M initially at rest. Assuming that the scattering in the center of mass system (CMS) is isotropic shows that the angular distribution of M in the laboratory system (LS) has $\cos\varphi$ dependence.

Problem 6.13 A beam of particles of negligible size is elastically scattered from an infinitely heavy hard sphere of radius R . Assuming that the angle of reflection is equal to the angle of incidence in any encounter shows that $\sigma(\theta)$ is constant, that is, scattering is isotropic and the total cross section is equal to the geometric cross section, π/R^2 .

Problem 6.14 Calculate the maximum wavelength of γ -rays which, in passing through matter, can lead to the creation of electrons.

Problem 6.15 A positron and an electron with negligible kinetic energy meet and annihilate one another, producing two γ -rays of equal energy. What is the wavelength of these γ -rays?

Problem 6.16 Show that electron-positron pair cannot be created by an isolated photon.

Problem 6.17 In dealing with diffusion of monoenergetic neutrons from a point source, the source diffusion equation for the flux distribution for a spherical symmetry is given in the following form:

$$\frac{d^2\phi}{dr^2} + \frac{2}{r} \frac{d\phi}{dr} - k^2 \phi = 0 \quad (\text{a})$$

Solve the differential equation (a) and show that the general solution is in form of the following type as:

$$\phi(r) = A \left(\frac{e^{-kr}}{r} \right) \quad (\text{b})$$

where in Eq. (b), the parameter A can be evaluated based on what is so-called source condition. Hint: Assume $\phi(r) \equiv y/r$.

Problem 6.18 Determine the value of parameter A , in Problem 6.17, if \bar{J} is the neutron current density at the surface of a sphere of radius r , with the source at the center. Utilize Fick's law that you have learned in Chap. 3 in r -direction due to symmetrical condition. Assume the source strength is Q neutrons per second, i.e., to the number of neutrons emitted by the point source in all directions per second.

Problem 6.19 A hypothetical source of thermal neutrons emits 10^6 neutrons per second into a surrounding “infinite” graphite block. Determine the neutron flux at distances of 27, 54, and 108 cm from this source. For graphite $\kappa = 1/L$ is 0.0185 cm^{-1} and the appropriate diffusion coefficient D is 0.94 cm. Hint: Use the result of the solution that you found in Problem 6.18.

Reference

1. J.R. Lamarsh, *Introduction to nuclear reactor theory* (Addison-Wesley, Publishing Company, 1966)

Chapter 7

Resonance Processing



In this chapter, we will study the Doppler broadening of resonances. Doppler effect improves reactor stability. Broadened resonance or heating of a fuel results in a higher probability of absorption, thus causing negative reactivity insertion or reduction of reactor power. One of the most important virtues of the optical model is that it takes into account the existence of *giant* or *broad resonances* in the total cross section as part of neutronic analysis for nuclear reactor systems. For resonances of energy levels, which are spaced widely apart, we can describe the energy dependency of the absorption cross section via *Breit-Wigner single-level resonance formula*.

7.1 Difficulties Presented by Resonance Cross Sections

Interactions between neutrons and nuclei in nuclear reactors can be classified broadly into scattering and absorption reactions as shown in Table 7.1 and were described in Chap. 1.

Scattering is further classified into elastic scattering in which the kinetic energy is conserved before and after the reaction and inelastic scattering in which a part of the kinetic energy is used in exciting a target nucleus. In absorption, the main reactions are capture, fission, charged-particle emission, and neutron emission. Thus, the microscopic cross sections of the total, scattering, and absorption reactions are given by:

$$\text{Total cross section} : \sigma_t(E) = \sigma_s(E) + \sigma_a(E) \quad (7.1)$$

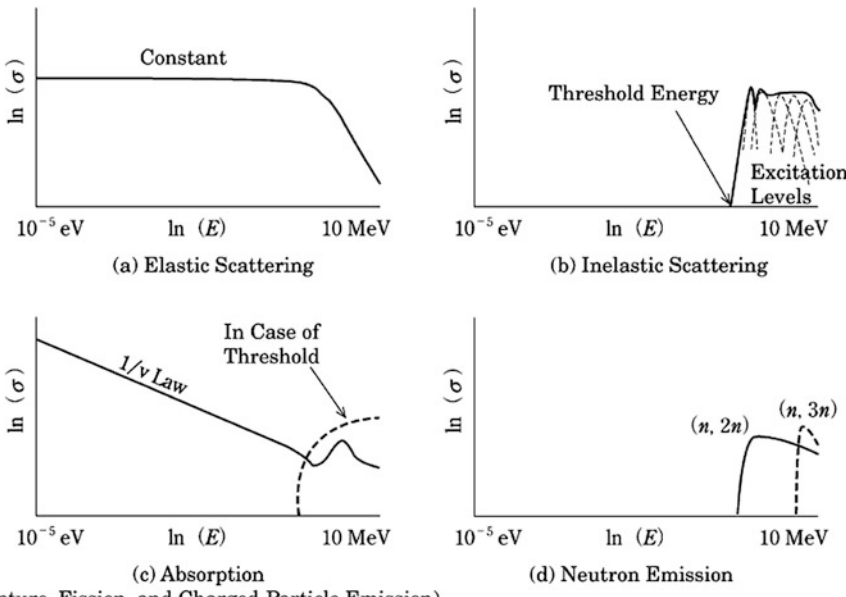
$$\text{Scattering cross section} : \sigma_s(E) = \sigma_e(E) + \sigma_{in}(E) \quad (7.2)$$

$$\text{Absorption cross section} : \sigma_a(E) = \sigma_r(E) + \sigma_f(E) + \sigma_p(E) + \sigma_\alpha(E) + \sigma_{(n,2n)}(E) \quad (7.3)$$

Table 7.1 Classification of key nuclear reactions in nuclear reactor [1]

Classification	Reaction	Transcription	Cross-sectional symbol	Reaction example
Scattering (σ_s)	Elastic scattering	(n, n)	σ_e	$H^1(n, n)$
Absorption (σ_a)	Inelastic scattering	(n, n')	σ_{in}	$U^{238}(n, n')$
	Radiative capture	(n, γ)	σ_γ	$U^{238}(n, \gamma)$
	Fission	(n, f)	σ_f	$U^{235}(n, f)$
	Charged-particle emission	(n, p)	σ_p	$N^{14}(n, p)$
	(n, α)	(n, α)	σ_α	$B^{10}(n, \alpha)$
	Neutron emission	$(n, 2n)^a$	$\sigma_{(n, 2n)}$	$Be^9(n, 2n)$

^aThe $(n, 2n)$ reaction can be treated as a special scattering reaction. Here this reaction, which transmits the nuclide, is classified as an absorption reaction.

**Fig. 7.1** Energy dependence of cross sections [1]

To further have a general discussion of energy dependency of these microscopic cross sections and neutron energy range for design of nuclear reactors, the neutron energy range to be considered in design of nuclear reactors is from the Maxwellian distribution of the thermal neutrons at room temperature to the fission spectrum of the prompt neutrons. As we have learned in reactor design, most nuclear design codes handle the range of 10^{-5} eV to 10 MeV. In this energy range, the microscopic cross sections are introduced in Eq. 7.1 through Eq. 7.3, and they behave as shown in Fig. 7.1. [1]

In Chap. 6, we learned that the elastic scattering cross section is mostly constant in all the energies except for the MeV region. Meanwhile, in inelastic scattering, the

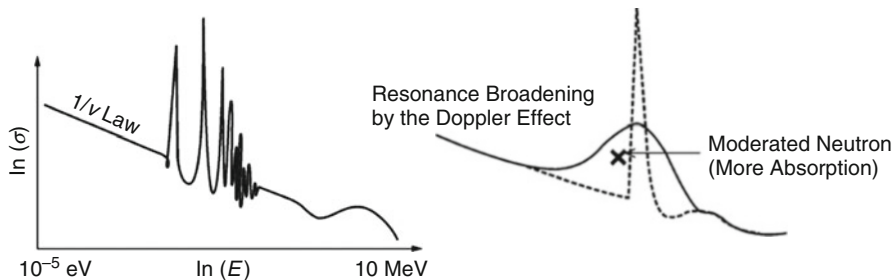


Fig. 7.2 Resonance absorption cross section and Doppler effect [1]

incident neutron should have sufficient kinetic energy to place the target nucleus in its excited state. Hence, the inelastic scattering cross section is zero up to some threshold energy of several MeV. Fast neutrons can be moderated by inelastic scattering with heavy nuclides, but by elastic scattering with light nuclides below threshold energies of the heavy nuclides [1].

Most absorption cross sections including the fission cross section appear as a straight line with a slope of $-1/2$ on a log-log scale. This means that the absorption cross sections are inversely proportional to the neutron speed ($1/v$ law) and therefore increase as the neutron energy decreases. Using such large fission cross sections at low neutron energies and thermal neutrons in the Maxwellian distribution makes it possible that natural or low-enrichment uranium-fueled reactors reach a critical state. The current thermal reactors, represented by LWRs, use the characteristics of the cross section.

For heavy nuclides such as fuel materials, many resonances are observed in elastic scattering and absorption cross section as shown in Fig. 7.2. The widths of the resonances broaden as fuel temperature increases. This is called the Doppler effect, which is the subject of our next section (i.e., Sects. 7.2 and 7.3) in this chapter. The width broadening facilitates resonance absorption of neutrons under moderation. Most low-enrichment uranium fuel is composed of fertile U^{238} , and thermal neutrons escaping from the resonance of capture reaction induce fissions for the next generation.

Hence, a rise in fuel temperature leads to a decrease in resonance escape probability of moderated neutrons, and then fission events in the reactor decrease with thermal neutrons. Such a mechanism is called negative temperature feedback. The temperature dependence is not described in the Boltzmann equation of Eq. 3.1, however, reflected in the cross sections of the equation.

The Doppler effect arises from the dependence of neutron cross sections on the relative velocity between the neutron and nucleus. The probability of the radiative capture depends on the center of mass energy and therefore depends on the kinetic energy of the incident neutron and the velocity of the target nucleus. Target nuclei are themselves in continual motion owing to their thermal energy. Because of these thermal motions, neutrons impinging on a target appear to the nuclei in the target to have a continuous spread in energy. This, in turn, has an effect on the observed shape

of resonance. Raising the temperature causes the nuclei to vibrate more rapidly within their lattice structures, effectively broadening the energy range of neutrons that may be resonantly absorbed in the fuel. The resonance becomes shorter and wider than when the nuclei are at rest.

7.2 What Is Nuclear Resonance: Compound Nucleus

For us to be able to write about this topic, we start our discussion with the subject of *radiative capture*, in which its reactions play significant roles in reactor analysis because they remove neutrons from the chain reaction, and we briefly did expand upon it in both Chaps. 1 and 2.

“Further we can see that such reactions proceed via compound nucleolus formation in which the incident neutron is first absorbed to form the compound nucleolus of atomic mass number $A+1$, and this nucleolus subsequently decays by eliminating a cascade of high-energy gammas.” [2]

For reason stated in the above capture, cross section is a function of the neutron kinetic energy E and illustrates a resonance behavior at those energies at which the center of mass (CM) energy E_c plus the neutron binding energy E_b do match an energy level of the compound nucleolus. Such definition can be demonstrated for neutron capture in U^{238} and schematically can be depicted in Fig. 7.3.

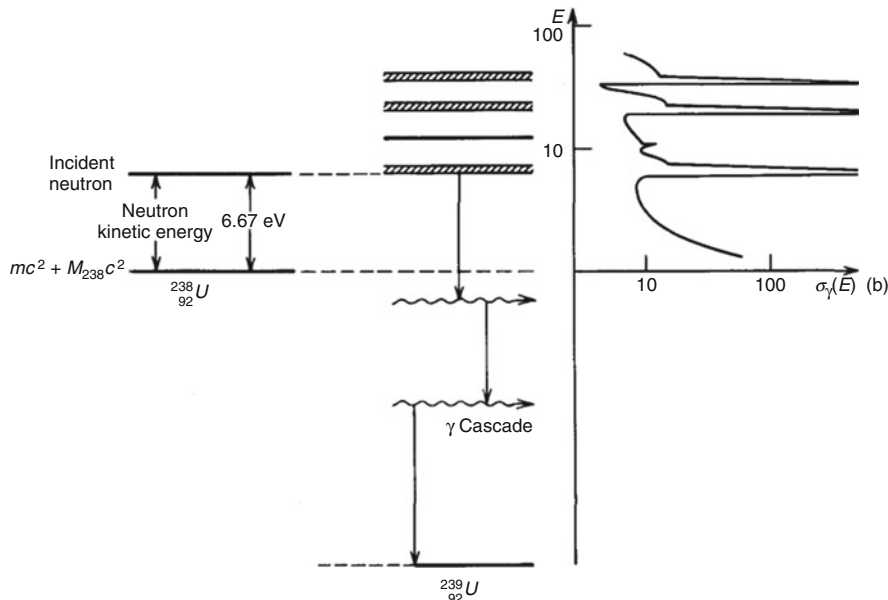


Fig. 7.3 An energy-level diagram of the capture resonance in U^{238} at $E = 6.67$ eV. (Courtesy of Duderstadt and Hamilton [2])

Figure 7.3, in particular, demonstrates the energy-level diagram for the U^{239} for one of the low-lying resonances at $E = 6.67$ eV. Since the excited energy levels are typically in the MeV range, the total energy of the emitted gammas will be quite large.

For resonance, energy levels are presented by Fig. 7.3 and are spaced widely apart. It is possible to describe the absorption cross-sectional dependency by a very simple mathematical formula, which is known as the Breit-Wigner single-level resonance formula as it was expressed in form of Eq. 1.30, which is again shown here as follows:

$$\sigma_r(E_c) = \sigma_0 \frac{\Gamma_\gamma}{\Gamma} \left(\frac{E_0}{E_c} \right)^{1/2} \frac{1}{1 + y^2} \quad \text{and} \quad y = \frac{2}{\Gamma} (E_c - E_b) \quad (7.4)$$

In Eq. 7.4, E_0 is the energy at the level where the resonance takes place, that is, the energy E_c at which $E_c + E_b$ matches the energy level of the compound nucleus. The symbol Γ is so-called *total line width* of resonance, and it characterizes the width of the energy level and the full width at half maximum (FWHM) of the resonance, while Γ_γ is the *radiative line width*, and this one characterizes the probability that the compound nucleus will decay via gamma emission.

In Eq. 7.4, the symbol σ_0 is the value of the *total cross section* $\sigma_{\text{tot}}(E)$ at the resonance energy E_0 and can be expressed in terms of the reduced neutron wavelength λ_0 at E_0 and atomic mass A as:

$$\sigma_0 = 4\pi\lambda_0^2 \frac{\Gamma_n}{\Gamma} g = 2.608 \times 10^6 \frac{(A+1)^2}{A^2 E_0(\text{eV})} \frac{\Gamma_n}{\Gamma} g \quad (7.5)$$

In Eq. 7.5, $g = (2J+1)/(2I+1)$ is a statistical spin factor that is given in terms of the nuclear spin I and total spin J , while Γ_n is the *neutron line width* and varies in energy as presented in following equation:

$$\Gamma_n \sim E^{1/2} \quad (7.6)$$

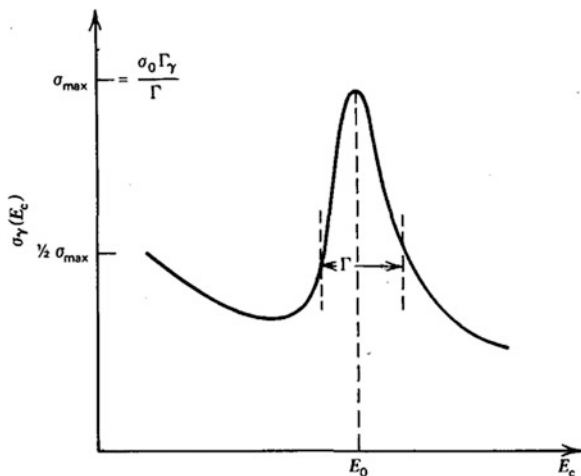
The Breit-Wigner resonance shape versus the center of mass (CM) kinetic energy E_c is depicted in Fig. 7.4, and note that the resonance absorption is in order of importance in heavy nuclei, and we can approximate $E_c \sim E$.

Note as well that for low energies, i.e., $E \ll E_0$, the cross section behaves as essentially $1/E^{1/2} = E^{-1/2}$ or $1/v$ velocity of neutron, and for large energy, i.e., $E \gg E_0$, the cross section drops off quite rapidly as $1/E^{5/2} = E^{-5/2}$, and it is also important to know that such absorption cross sections are largest at low energies.

In summary, if we ask “What is Compound Nucleus and What is Resonance?” we can answer that by saying, “there is really no difference between the compound nucleus and the nuclear resonance.”

The compound nucleus is the intermediate state formed in a compound nucleus reaction. It is normally one of the excited states of the nucleus formed by the

Fig. 7.4 A single-level capture resonance.
(Courtesy of Duderstadt and Hamilton [2])



combination of the incident particle and target nucleus. If a target nucleus with atomic mass number A is bombarded with particles x , it is sometimes observed that the ensuing nuclear reaction takes place with appreciable probability only if the energy of the particle x is in the neighborhood of certain definite energy values. These energy values are referred to as resonance energies. The compound nuclei of these certain energies are referred to as nuclear resonances. Resonances are usually found only at relatively low energies of the projectile. The widths of the resonances increase in general with increasing energies. At higher energies, the widths may reach the order of the distances between resonances, and then no resonances can be observed. The narrowest resonances are usually the compound states of heavy nuclei (such as fissionable nuclei) and thermal neutrons (usually in (n, γ) capture reactions; see Table 7.1 as well). The observation of resonances is by no means restricted to neutron nuclear reactions, and both illustrations (a) and (b) in Fig. 7.5, in general, show energy levels of the compound state. For neutron absorption reaction of U^{238} , the first resonance E_1 corresponds to the excitation energy of 6.67 eV as we said, and E_0 is a base state of U^{239} . [3]

7.2.1 Breit-Wigner Resonance Reaction Cross Sections

We have the formula that the total cross section is given by:

$$\sigma_t = 4\pi\lambda^2 \sin^2\delta_0 \quad (7.7)$$

For the orbital angular momentum quantum number $l = 0$ total cross section. Now if we assume a Lorentzian shape for the $\sin^2\delta_0$ term at an interaction resonance at energy E_r and a full width at half maximum Γ , such that:

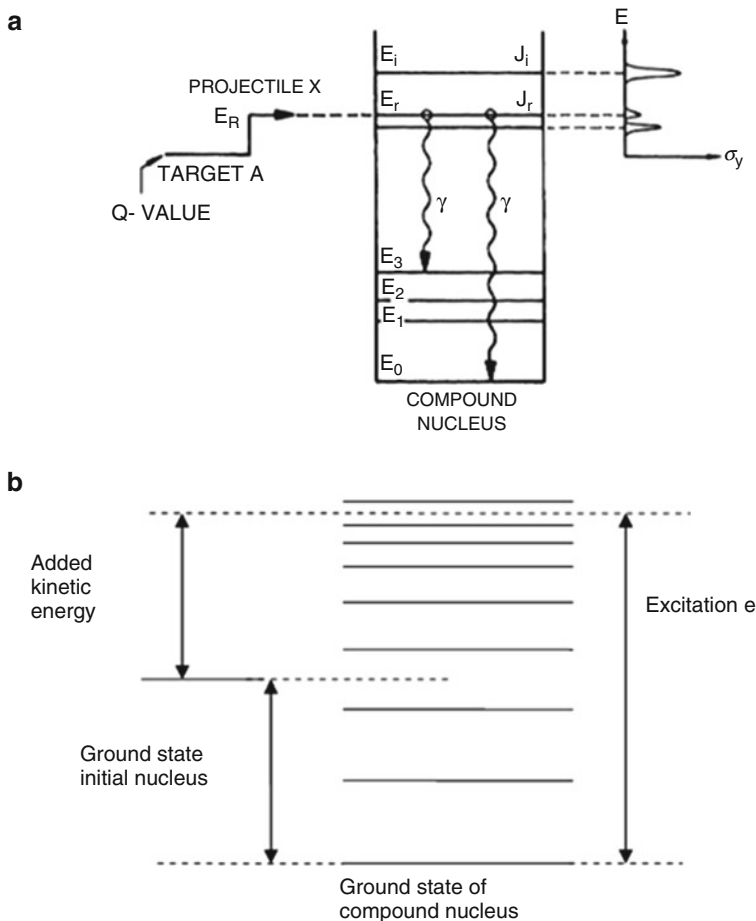


Fig. 7.5 Energy levels of compound state

$$\sin^2 \delta_0 = \frac{\left(\frac{\Gamma}{2}\right)^2}{(E - E_r)^2 + \left(\frac{\Gamma}{2}\right)^2} \quad (7.8)$$

And realizing that for an absorption, the fraction of time the compound nucleus can be formed is Γ_n/Γ and the fraction of time it can decay by an absorption (gamma decay) is given by Γ_γ/Γ , we get that the cross section for neutron absorption is given by:

$$\sigma_a = \sigma_\gamma = 4\pi\lambda^2 \frac{\frac{\Gamma_n\Gamma_\gamma}{\Gamma}\left(\frac{\Gamma}{2}\right)^2}{(E - E_r)^2 + \left(\frac{\Gamma}{2}\right)^2} = \pi\lambda^2 \frac{\Gamma_n\Gamma_\gamma}{(E - E_r)^2 + \left(\frac{\Gamma}{2}\right)^2} \quad (7.9)$$

This is the correct equation but it does not include the effects of neutron or nucleus spin. The effects of spin are included by multiplying by the g factor, where g is given by:

$$g = \frac{J+1}{(2s+1)(2l+1)} \quad (7.10)$$

$$J = s + l + I$$

where:

s = spin quantum number of the neutron

l = orbital angular momentum quantum number

J = total angular momentum quantum number

I = ground state spin quantum number of the nucleus

Therefore, we have the absorption cross section written as:

$$\sigma_\gamma = \pi \hat{\lambda}^2 g \frac{\Gamma_n \Gamma_\gamma}{(E - E_r)^2 + \left(\frac{\Gamma}{2}\right)^2} = \frac{\Gamma_\gamma}{\Gamma} \frac{\sigma_o}{1 + y^2} \quad (7.11)$$

$$\sigma_o = 4\pi \hat{\lambda}^2 g \left(\frac{\Gamma_n}{\Gamma} \right)$$

$$y = \frac{2}{\Gamma} (E - E_r)$$

Note that the neutron width varies with the square root of energy such that $\Gamma_n = \Gamma_n^0 E^{1/2}$ and $\hat{\lambda} \sim 1/E^{1/2}$. Thus, as the energy goes to zero, the cross section behaves as $E^{1/2}$, which is the classic $1/v$ behavior that is observed in many nuclides.

The resonance scattering cross section is slightly different as the potential scattering cross section interferes with the compound nucleus resonance scattering cross section. The complete scattering cross section is given by:

$$\sigma_n(E) = 4\pi R^2 + 4\pi \hat{\lambda}^2 g \left[\left| \frac{\Gamma_n/2}{E - E_r + i\Gamma/2} + \frac{R}{\hat{\lambda}} \right|^2 - \left(\frac{R}{\hat{\lambda}} \right)^2 \right] \quad (7.12)$$

$$\sigma_n(E) = \sigma_p + \frac{\Gamma_n}{\Gamma} \frac{\sigma_o}{1 + y^2} + \left(\sigma_{on} \sigma_p \frac{\Gamma_n}{\Gamma} \right)^{1/2} \frac{2y}{1 + y^2}$$

$$\sigma_o = 4\pi \hat{\lambda}^2 g \left(\frac{\Gamma_n}{\Gamma} \right)$$

$$\sigma_p = 4\pi R^2$$

This gives the total resonance cross section as:

$$\begin{aligned}\sigma_t(E) &= \sigma_p + \frac{\Gamma_n}{\Gamma} \frac{\sigma_o}{1+y^2} + \left(\sigma_{on} \sigma_p g \frac{\Gamma_n}{\Gamma} \right)^{1/2} \frac{2y}{1+y^2} + \frac{\Gamma_\gamma}{\Gamma} \frac{\sigma_o}{1+y^2} \\ \sigma_t(E) &= \frac{\sigma_o}{1+y^2} + \left(\sigma_o \sigma_p \frac{\Gamma_n}{\Gamma} \right)^{1/2} \frac{2y}{1+y^2} + \sigma_p\end{aligned}\quad (7.13)$$

7.2.2 Resonance and Neutron Cross Section

For the compound nucleus, peaks in the cross section are typical. Each peak is manifesting a particular compound state of the nucleus. These peaks and the associated compound nuclei are usually called resonances. The behavior of the cross section between two resonances is usually strongly affected by the effect of nearby resonances.

Resonances (particular compound states) are mostly created in neutron nuclear reactions, but they are by no means restricted to neutron nuclear reactions. The formation of resonances is caused by the quantum nature of nuclear forces. Each nuclear reaction is a transition between different quantum discrete states and energy levels. The discrete nature of energy transitions plays a key role. If the energy of the projectile (the sum of the Q value and the kinetic energy of the projectile) and the energy of target nucleus are equal to a compound nucleus at one of the excitation states, a resonance can be created, and peak occurs in the cross section. For light nucleus, the allowable state density in this energy region is much lower, and the “distance” between states is higher. For heavy nuclei, such as U^{238} , we can observe large resonance region in the neutron absorption cross section.

As illustrated in Fig. 7.6, this figure shows the region of resonance of U^{238} nuclei, while Fig. 7.7 is the presentation of uranium-235 comparison of total fission cross section and cross section for radiative capture, which was described in the previous section.

It is obvious the compound states (resonances) are observed at low excitation energies. This is due to the fact that the energy gap between the states is large. At high excitation energy, the gap between two compound states is very small, and the widths of resonances may reach the order of the distances between resonances. Therefore, at high energies, no resonances can be observed, and the cross section in this energy region is continuous and smooth.

Here, both Figs. 7.8 and 7.9 illustrate the comparison of radiative capture cross sections, both for gadolinium-155 and gadolinium-157 nuclei that have region of resonance, and, for boron-10, comparison of total cross section and cross section for (n, α) , respectively. B^{10} does not have any region of resonance.

Now, we are in position to go forward with describing the Doppler effect and Doppler broadening of resonances in the next section.

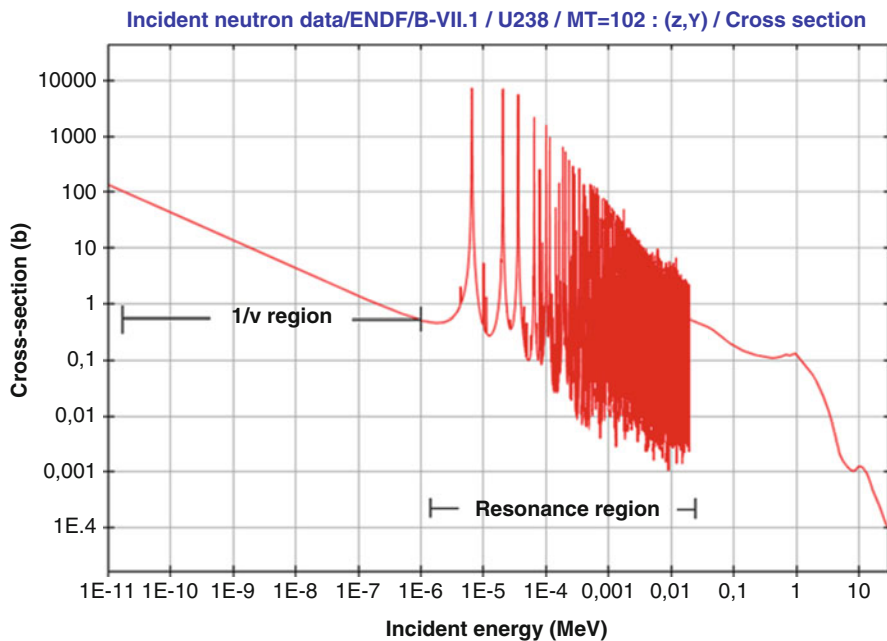


Fig. 7.6 Region of resonance of U^{238} nuclei. Source: JANIS (Java-based Nuclear Data Information Software); The ENDF/B-VII.1 Nuclear Data Library

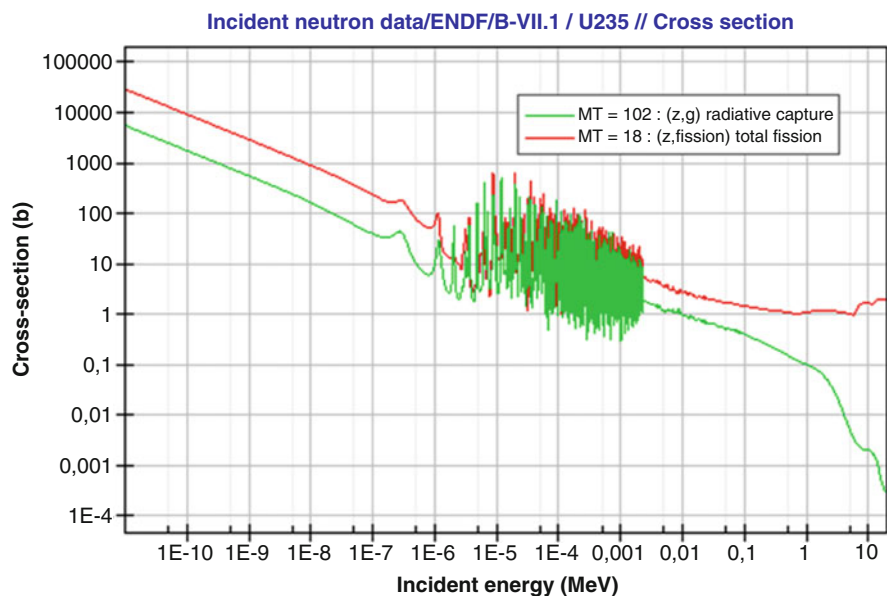


Fig. 7.7 Comparison of total fission cross section and cross section for radiative capture for U^{238} . Source: JANIS (Java-based Nuclear Data Information Software); The ENDF/B-VII.1 (Nuclear Data Library)

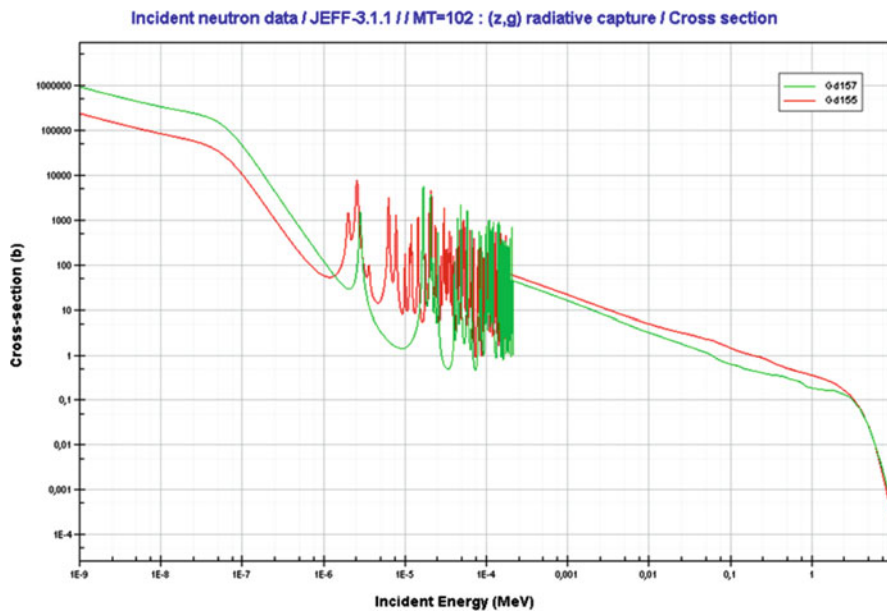


Fig. 7.8 Gadolinium-155 and gadolinium-157 incident neutron data. Source: JANIS (Java-based Nuclear Data Information Software); The JEFF-3.1.1 Nuclear Data Library

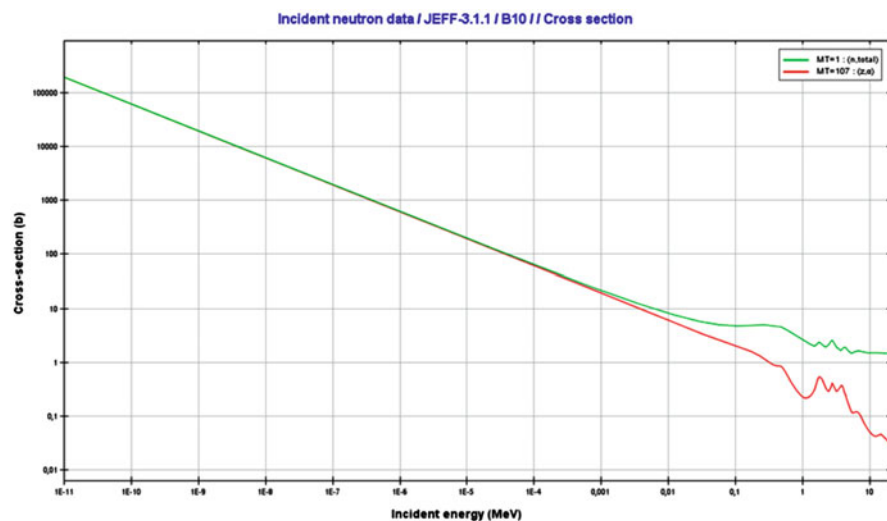


Fig. 7.9 Boron-10 incident neutron data. Source: JANIS (Java-based Nuclear Data Information Software); The JEFF-3.1.1 Nuclear Data Library

7.3 Doppler Effect and Doppler Broadening of Resonance

The Doppler-broadened Breit-Wigner resonance cross section was first derived many years ago by Beth and Placzek [5], which is more commonly found in textbooks. In general, Doppler broadening is the broadening of spectral lines due to the Doppler effect caused by a distribution of kinetic energies of molecules or atoms. In reactor physics, a particular case of this phenomenon is the thermal Doppler broadening of the resonance capture cross sections of the fertile material (e.g., U^{238} or Pu^{240}) caused by thermal motion of target nuclei in the nuclear fuel.

Doppler effect improves reactor stability. Broadened resonance (heating of a fuel) results in a higher probability of absorption, thus causing negative reactivity insertion (reduction of reactor power), and this can be seen as illustrated in Fig. 7.10 schematically.

For heavy nuclides such as fuel materials, many resonances are observed in elastic scattering and absorption cross section as shown in Fig. 7.2. The widths of the resonances broaden as fuel temperature increases. This is called the Doppler effect, and the width broadening facilitates resonance absorption of neutrons under moderation. As we have mentioned previously, most low-enrichment uranium fuel is composed of fertile U^{238} , and thermal neutrons escaping from the resonance of capture reaction induce fissions for the next generation.

Hence, a rise in fuel temperature leads to a decrease in resonance escape probability of moderated neutrons, and then fission events in the reactor decrease with thermal neutrons. Such a mechanism is called negative temperature feedback. Note that the temperature dependence is not described in the Boltzmann equation of Eq. 3.1; however, it is reflected in the cross sections of the equation.

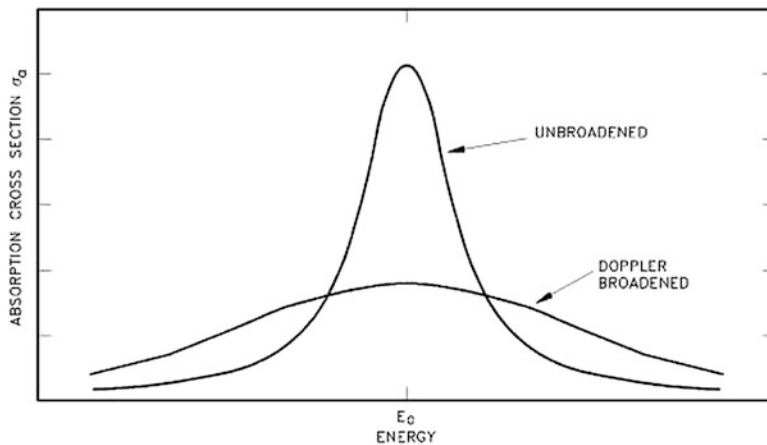


Fig. 7.10 Doppler effect improves reactor stability [4]

The Doppler broadening of resonances is a very important phenomenon, which improves reactor stability, because it accounts for the dominant part of the fuel temperature coefficient (the change in reactivity per degree change in fuel temperature) in thermal reactors and makes a substantial contribution in fast reactors as well. This coefficient is also called the prompt temperature coefficient because it causes an immediate response on changes in fuel temperature. The prompt temperature coefficient of most thermal reactors is negative.

A negative fuel temperature coefficient is generally considered to be even more important than a negative moderator temperature coefficient. Especially in case of reactivity-initiated accidents (RIA), the Doppler coefficient of reactivity would be the first and most important effect in the compensation of the inserted positive reactivity. The time for heat to be transferred to the moderator is usually measured in seconds, while the Doppler coefficient is effective almost instantaneously. Therefore, the moderator temperature cannot turn the power rise for several seconds, whereas the fuel temperature coefficient starts adding negative reactivity immediately. The fuel temperature coefficient α_f may be defined as:

$$\alpha_f = \frac{1}{k} \frac{\partial k}{\partial \bar{T}_f} \quad (7.14)$$

Although the shape of a resonance changes with temperature, the total area under the resonance remains essentially constant. Nevertheless, this does not imply constant neutron absorption. Despite the constant area under resonance, the resonance integral, which determines the absorption, increases with the increasing target temperature. The broadened resonances result in a larger percentage of neutrons having energies that are susceptible to capture in the fuel pellets. On the other hand, with colder fuel, only neutrons very close to the resonance energy are absorbed.

Moreover, there is a further phenomenon closely connected with “Doppler broadening.” The vicinity of the resonance causes an increase in the neutron absorption probability, when a neutron has energy near a resonance. This results in a reduction of the effective absorption per nucleus due to the depression of the energy-dependent flux $\phi(E)$ near the resonance in comparison to a flat flux. At energies just below the resonance, where $\Sigma_a(E)$ becomes small again, the neutron flux reaches almost the same value just above the resonance. This reduction in the energy-dependent neutron flux near the resonance energy is known as energy self-shielding. These two phenomena provide negative reactivity feedback against fuel temperature increase. See Fig. 7.11 for the thermally averaged capture cross section as determined by Doppler broadening of a resonance with increasing temperature.

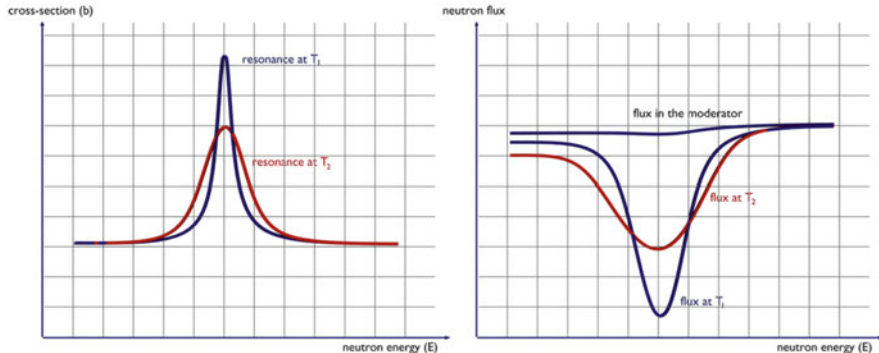


Fig. 7.11 Cross section and neutron flux versus neutron energy [4]

This effect can be mathematically derived by utilizing Maxwell-Boltzmann distribution of target nuclei, if we perform the integration over nuclear velocity V of the nucleus with mass of M in the following equation and that the relationship for thermally averaged cross section as [2]:

$$\bar{\sigma}(v, T) = \frac{1}{v} \int d^3V |v - V| \sigma(|v - V|) M(V, T) \quad (7.15)$$

In Eq. 7.15 the element v is the neutron velocity, while $\sigma(|v - V|) = \gamma/v - V$, which is the relationship based on nuclear cross-sectional behavior below a capture resonance as $1/v$, if nuclear motion behaves as such and $\gamma \equiv 2(E_C - E_0)/\Gamma$. [2]

Note that it is sufficient for most purposes to represent the nuclear velocity distribution by the Maxwell-Boltzmann distribution that was discussed in Chaps. 1 and 2, characterizing an ideal gas in thermal equilibrium at a temperature T .

Now if we integrate Eq. 7.15 over the nuclear velocity of V and apply the Maxwell-Boltzmann distribution of target nuclei, then we can write:

$$\bar{\sigma}_\gamma(v, T) = \frac{1}{\sqrt{\pi} v_{th}^2 v} \int_0^\infty v_r^2 \sigma_\gamma(v_r) dv_r \left[\exp\left(-\frac{(v - v_r)^2}{2v_{th}^2}\right) - \exp\left(-\frac{(v + v_r)^2}{2v_{th}^2}\right) \right] \quad (7.16)$$

where $v_r = |v - V|$ while $v_{th} = (kT/m)^{1/2}$, and if we substitute the Breit-Wigner formula defined by Eq. 7.4 into Eq. 7.16 for $\sigma_r(v_r)$, we find an exact expression for the averaged cross section as below:

$$\bar{\sigma}_\gamma(v, T) = \sigma_0 \frac{\Gamma_\gamma}{\Gamma} \frac{1}{\sqrt{\pi} v_{th}^2 v} \int_0^\infty \frac{v_r dv_r}{1 + y^2} \left[\exp\left(-\frac{(v - v_r)^2}{2v_{th}^2}\right) - \exp\left(-\frac{(v + v_r)^2}{2v_{th}^2}\right) \right] \quad (7.17)$$

Note that in relation for v_{th} and k in form of $v_{th} = (kT/m)^{1/2}$, constant k is known as Boltzmann constant, and $k = 0.8617E-4$ eV/K = 1/11600 eV/K.

We already have defined γ , where we recall that the *CM* energy is $E_C = \frac{1}{2}\mu v_r^2$; now if we define the following variables such as:

$$x \equiv 2(E - E_0)/\Gamma \quad \text{and} \quad \xi \equiv \Gamma/\Gamma_D \quad (7.18)$$

where Γ_D is the so-called Doppler width of the resonance as we have described before as:

$$\Gamma_D \equiv \left(\frac{4E_0 k T}{A} \right)^{1/2} \quad (7.19)$$

with Eq. 7.19 on hand, one can write the following result:

$$\bar{\sigma}_\gamma(E, T) = \sigma_0 \frac{\Gamma_\gamma}{\Gamma} \left(\frac{E_0}{E} \right)^{1/2} \Psi(\xi, x) \quad (7.20)$$

where:

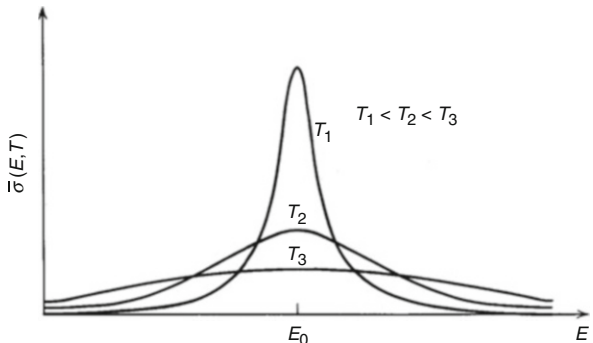
$$\Psi(\xi, x) = \int_{-2E/\Gamma}^{\infty} \frac{dy}{1 + y^2} \left[\exp\left(-\frac{(v - v_r)^2}{2v_{th}^2}\right) - \exp\left(-\frac{(v + v_r)^2}{2v_{th}^2}\right) \right] \quad (7.21)$$

Using any numerical integration technique, one is able to calculate the value of ξ and x in real world of reactor design.

The sketch of thermally averaged capture cross section is determined by Eq. 7.20, and it is presented by Fig. 7.12 here, which provides better understanding of the matter.

Figure 7.12, in particular, shows the dependence of cross section on energy for several different temperatures T .

Fig. 7.12 Doppler broadening of a resonance with increasing temperature. (Courtesy of Duderstadt and Hamilton [2])



Further analysis of Fig. 7.12 reveals that as the temperature T increases, the resonance broadens, while its peak magnitude decreases. For this reason, one frequently refers to resonance cross sections that have been averaged over the distribution of nuclear velocities as “Doppler-broadened” cross sections.

Duderstadt and Hamilton [2] show that at the high temperature limit, $T \rightarrow \infty$ implies that $\xi \rightarrow 0$, and in this case, Eq. 7.21 reduces to the following form, which is a Gaussian shape characterized by Doppler width Γ_D rather than the “natural” line width Γ . Hence, as the temperature increases, the resonance broadens out from its natural width to eventually approach a width that depends on the temperature as $T^{1/2}$. [2]

7.4 Doppler Coefficient in Power Reactors

In power reactors, the Doppler coefficient is always negative. It is ensured by the fuel composition. In PWRs, the Doppler coefficient can range, for example, from -5 pcm/K to -2 pcm/K. The value of the Doppler coefficient α_f in Eq. 7.14 depends on the temperature of the fuel and depends on the fuel burnup as well, and the following points do apply. See Fig. 7.13.

- *Fuel temperature:* The dependency on the fuel temperature is determined by the fact the rate of broadening diminishes at higher temperatures. Therefore, the Doppler coefficient becomes less negative (but always remains negative) as the reactor core heats up.

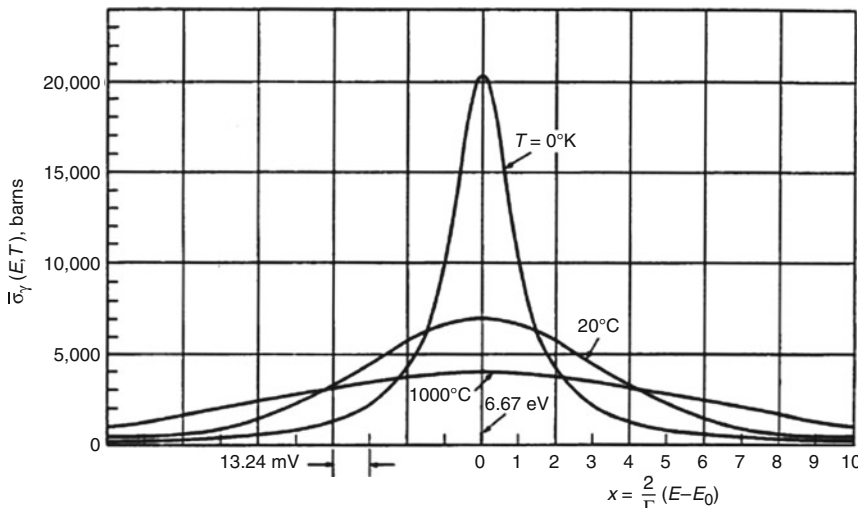


Fig. 7.13 Doppler broadening of the capture cross section of U^{238} at the 6.67 eV. (Courtesy of Lamarsh [6])

- *Fuel-cladding gap*: There is also one very important phenomenon, which influences the fuel temperature. As the fuel burnup increases, the fuel-cladding gap reduces. This reduction is caused by the swelling of the fuel pellets and cladding creep. Fuel pellets' swelling occurs because fission gases cause the pellet to swell resulting in a larger volume of the pellet. At the same time, the cladding is distorted by outside pressure (known as the cladding creep). These two effects result in direct fuel-cladding contact (e.g., at burnup of 25 GWd/tU). The direct fuel-cladding contact causes a significant reduction in fuel temperature profile, because the overall thermal conductivity increases due to conductive heat transfer.
- *Fuel burnup*: During fuel burnup, the fertile materials (conversion of U^{238} to fissile Pu^{239} known as fuel breeding) partially replace fissile U^{235} . The plutonium content rises with the fuel burnup. For example, at a burnup of 30 GWd/tU (gigawatt-days per metric ton of uranium), about 30% of the total energy released comes from bred plutonium. However, Pu^{239} raises also the content of Pu^{240} , which has significantly higher resonance cross sections than U^{238} . Therefore, the Doppler coefficient becomes more negative as the Pu^{240} content raises. See Fig. 7.14.

In fast neutron reactors, the Doppler effect becomes less dominant (due to the minimization of the neutron moderation), but strongly depends on the neutron spectrum (e.g., gas-cooled reactors have harder spectra than other fast reactors) and the type of the fuel matrix (metal fuel, ceramic fuel, etc.). In fast reactors, other effects, such the axial thermal expansion of fuel pellets or the radial thermal

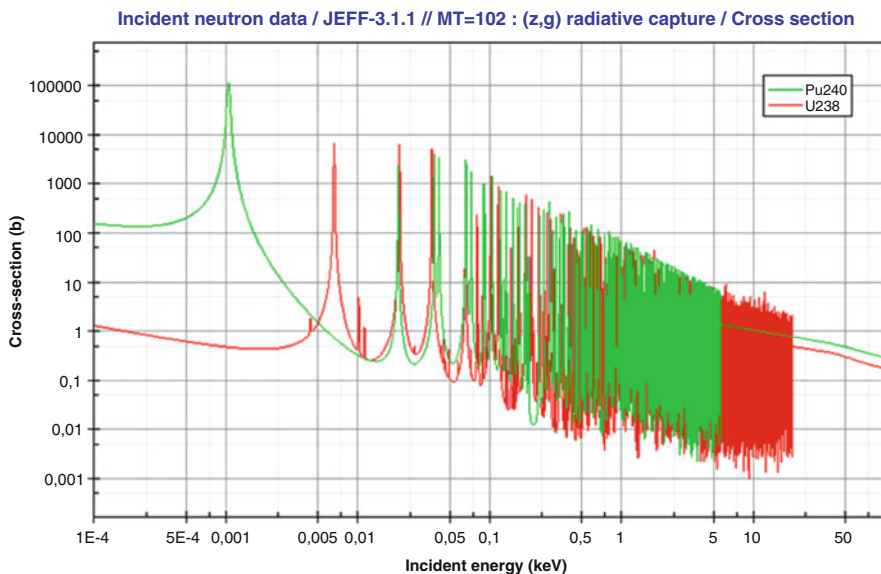


Fig. 7.14 Doppler broadening of Pu^{240} and U^{238}

expansion of reactor core, may also contribute to the fuel temperature coefficient. In thermal reactors, these effects tend to be small relative to that of Doppler broadening.

Figure 7.14 here presents the schematic of comparison of resonance capture cross section of U^{238} and Pu^{240} .

Note that in summary, it is difficult to define the dependency, because these effects have opposite directions.

7.5 Infinite Resonance Integrals and Group Cross Section

Here we can study the resonance absorption due to an infinity massive absorber distributed uniformly through an infinite medium of hydrogen that is mixed with U^{238} . The infinite absorber mass implies that all neutron slowing down due to elastic scattering will be due to hydrogen, while we are ignoring any inelastic scattering circumstances. However, we want to include an absorption term in an infinite medium slowing down equation, which was described previously, knowing that in real situation, the absorption cross section of hydrogen will be assumed negligible, but the physical situation we want to describe is that of a strongly absorbing isotope mixed in hydrogen such as U^{238} .

However, for simplicity of our analysis here, we assume the absorber to be “infinitely massive,” so it does not slow down neutron, yet it only absorbs them. This assumption comes from the fact that the mentioned isotope can also scatter, and since its atomic mass number is not unity, it will be difficult to validate our analysis of resonance integral and group cross section, so that is why the assumption of an infinite mass will be a reasonable approach.

Then, the appropriate slowing down equation with a monoenergetic source at energy E_0 is written as:

$$[\Sigma_a(E) + \Sigma_s(E)]\phi(E) = \int_E^{E_0} dE' \frac{\Sigma_s(E')\phi(E')}{E'} + S_0(E_0)\delta(E - E_0) \quad (7.22)$$

where the factor $S_0(E_0)$ is the rate at which source neutrons are emitted at energy level E_0 .

To seek a solution for Eq. 7.22, Duderstadt and Hamilton [2] show more details of the analysis for the total collision density as the sum of collided and uncollided contribution, and we refer our readers to their book.

Furthermore, in open literature and available computer codes such as NJOY, which is dealing with group self-shielding for studying the neutron slowdown in a medium with resonance absorption presence, for calculating the flux spectrum. The code NJOY looks at methods known as self-shielding to analyze the flux calculator method in an infinite medium spectrum or another one that is known as Bondarenko method.

There is another method which is used by NJOY computer code and that is known as the **CENTRM** (Continuous ENergy TRansport Module) method, where code solves the Boltzmann transport equation using both point-wise and multi-group cross sections in defined energy range, to compute a point-wise flux spectrum. [7]

7.5.1 The Flux Calculator Method

The flux calculator method expresses Eq. 7.15 in a general form as follows, by assuming that $\Sigma_t(E) = \Sigma_a(E) + \Sigma_s(E)$, so we can write:

$$\Sigma_t(E)\phi(E) = \int_0^\infty dE' \Sigma_s(E' \rightarrow E)\phi(E') + S(E) \quad (7.23)$$

where the term on the left-hand side (LHS) of Eq. 7.16 represents the collision, the integral on the right-hand side (RHS) is the scattering source, and finally $S(E)$ is the external source.

Next, we can write Eq. 7.23 by considering a homogeneous medium consisting of two materials, an absorber and a moderator, represented by a and m , respectively, and write it in form of Eq. 7.24. Elastic scattering cross sections that are isotropic in the center of mass are used. Neutron slowing down in a single resonance of the absorber material is assumed:

$$\Sigma_t(E)\phi(E) = \int_E^{E/\alpha_m} dE' \frac{\Sigma_{sm}(E')}{(1 - \alpha_m)E'} \phi(E') + \int_E^{E/\alpha_a} dE' \frac{\Sigma_{sa}(E')}{(1 - \alpha_a)E'} \phi(E') \quad (7.24)$$

where α_a and α_m are the absorber and moderator collision parameter, respectively, and in terms of atomic mass number A are defined as:

$$\alpha = \left(\frac{A - 1}{A + 1} \right)^2 \quad (7.25)$$

Note that to be able to establish and write down Eq. 7.24, the following approximations are introduced:

- The moderator scattering cross section is assumed to be constant and equal to the potential scattering cross section, i.e., $\Sigma_s^M(E') = \Sigma_p^M$.
- The moderator absorption cross section is assumed to be negligible, i.e., $\Sigma_a^M(E') = \Sigma_p^M$.
- The narrow resonance approximation is used for the moderator. This states that the resonance width is very small, compared to the energy loss from scattering with the moderator nucleus. Therefore, the flux distribution in the moderator integral is assumed to have an asymptotic form. In general, the moderator integral is assumed to be a smooth function of energy represented as $C(E)$.

- The moderator is assumed to represent all nuclides other than the absorber. This enables the inclusion of the dilution microscopic cross section of the absorber, σ_d , in Eq. 7.24. The dilution (or background) cross section of an isotope i is defined to be all cross sections representing isotopes other than the isotope i . The dilution cross section is a measure of energy self-shielding. It determines the significance of a resonance compared to other cross sections. If the dilution cross section (σ_d) is small, it indicates that the resonance has a significant impact on the flux and a large self-shielding effect exists. If σ_d is very large (infinite dilution), the cross sections of the absorber do not affect the flux spectrum, and the flux may be represented as a smooth function of energy.

Taking all the above approximations under consideration, then Eq. 7.24 becomes:

$$[\sigma_d + \sigma_{ta}] \phi(E) = C(E) \sigma_d + \int_E^{E/\alpha_a} dE' \frac{\sigma_{sa}(E')}{(1 - \alpha_a) E'} \phi(E') \quad (7.26)$$

The dilution cross section for an isotope i is then given as:

$$\sigma_d = \frac{1}{\rho_i} \sum_{j \neq i} \rho_j \sigma_{tj} \quad (7.27)$$

where i and j represent isotope indexes and ρ is atomic density. Equations such as Eq. 7.26 are used in codes such as NJOY for computing the flux with the flux calculator option. In NJOY, several dilution cross sections are provided as input. Depending on a system of interest, the cross sections corresponding to the appropriate dilution cross section are used [7].

7.5.2 The Bondarenko Method: The Bondarenko Factor

Prof. Bondarenko of the USSR came up with a very efficient method for calculating fast reactor cross sections for a specific reactor design from pre-calculated tables of what have come to be called self-shielding factors. Bondarenko's insight for fast reactor cross sections got the technique started, and it has been widely applied to many problems.

The Bondarenko method is obtained by using the narrow resonance approximation in the absorber integral of Eq. 7.26. The practical width of a resonance of the absorber is considered to be much smaller than the energy loss due to a collision with the absorber. This enables the absorber integral to be represented as a smooth function of energy. Therefore, the flux is represented by:

$$\phi(E) = \frac{C(E)}{(\sigma_{ta}(E) + \sigma_d)} \quad (7.28)$$

Consider the general form for resonance absorption cross sections.

$$\begin{aligned}
 \Sigma_a^g &= N_a \sigma_a^g = \frac{N_a}{\Delta u} \sum_i \frac{\sigma_{di} \Gamma_{\gamma i}}{E_{ri}} \beta_i J(\theta_i, \beta_i) \\
 \sigma_a^g &= \frac{1}{\Delta u} \sum_i \frac{\sigma_{di} \Gamma_{\gamma i}}{E_{ri}} \beta_i J(\theta_i, \beta_i) \\
 \beta_i^{NR} &= \frac{\Sigma_{sm} + \Sigma_{pa}}{\Sigma_{di}} \quad \text{or} \quad \frac{\Sigma_{sm} + \Sigma_{pa} + \Sigma_e}{\Sigma_{di}} \\
 \beta_i^{WR} &= \frac{\Sigma_{sm}}{\Sigma_{di} \frac{\Gamma_{\gamma i}}{\Gamma_i}} \quad \text{or} \quad \frac{\Sigma_{sm} + \Sigma_e}{\Sigma_{di} \frac{\Gamma_{\gamma i}}{\Gamma_i}}
 \end{aligned} \tag{7.29}$$

The β_i can be written as:

$$\begin{aligned}
 \beta_i^{NR} &= \frac{\sigma_b}{\sigma_{di}} \\
 \sigma_b &= \frac{N_m \sigma_{sm} + N_a \sigma_{pa}}{N_A} \\
 \beta_i^{WR} &= \frac{\sigma_b}{\sigma_{di}} \\
 \sigma_b &= \frac{N_m \sigma_{sm}}{N_a}
 \end{aligned} \tag{7.30}$$

Then we can write the cross section as:

$$\begin{aligned}
 \sigma_a^g &= \frac{1}{\Delta u} \sum_i \frac{\sigma_{oi} \Gamma_{\gamma i}}{E_{ri}} \frac{\sigma_b}{\sigma_{oi}} J\left(\theta_i, \frac{\sigma_b}{\sigma_{oi}}\right) \\
 &= \frac{1}{\Delta u} \sum_i \frac{\sigma_{oi} \Gamma_{\gamma i}}{E_{ri}} \frac{\pi}{2} f(\theta_i, \sigma_b) \\
 &= \sigma_{a,\infty}^g f(T, \sigma_b)
 \end{aligned} \tag{7.31}$$

Or the absorption cross section can be expressed in terms of the infinite dilute cross section times some sort of self-shielding or Bondarenko factor that is only a function of the background scatterer and the temperature. This will allow the calculation of the infinite dilute cross section and a table of f factors as accurately as desired. The narrow resonance and wide resonance approximations are no longer required. This will allow the interpolation of the resonance effects for any mixture of nuclides that is physically possible. There are two advantages of this approach. First, the infinite dilute cross section and f factor cross section table can be computed for a single nuclide without specifically considering other nuclides present. Second, when it comes to setting up cross sections for a design mixture, the f factor table can be easily interpolated to get the appropriate cross sections for that specific mixture. This

approach requires a large amount of computation to be performed one time, and the results of that calculation are used many times in short design-specific calculations.

A typical f factor table for an absorption cross section might look like:

$\Sigma_b(b)$	10^0	10^1	10^2	10^3	10^4	10^5	10^6
T(K)							
300	0.75	0.85	0.89	0.93	0.96	0.98	1.0
600	0.78	0.87	0.90	0.94	0.96	0.98	1.0
900	0.81	0.89	0.91	0.95	0.97	0.99	1.0
1200	0.84	0.90	0.93	0.96	0.97	0.99	1.0
1500	0.87	0.91	0.94	0.97	0.98	0.99	1.0
1800	0.90	0.92	0.96	0.98	0.99	1.0	1.0
2100	0.93	0.94	0.96	0.98	0.99	1.0	1.0

Bondarenko extended the concept to fission and scattering cross sections. Since that time, the concept has been extended to almost all cross sections. The concept of a background scattering cross section has been extended to a background total cross section. Since the total cross section in the resonance range is dominated by scattering except in the resonances, basing everything on a total background cross section is a logical extension.

By basing everything on a total cross section, this simplified a number of things.

In particular, if a given mixture requires two or more resonance absorbers, then the calculation to solve for the appropriate background total cross section will require iteration. Consider the case of a mixture containing both U^{235} and U^{238} in the compound UO_2 . We have:

$$\begin{aligned}
 \sigma_t^{g,235} &= \sigma_t^{g,235,\infty} f\left(T, \sigma_{t,b}^{g,235}\right) \\
 \sigma_{t,b}^{g,235} &= \frac{N_O \sigma_{sO}^g + N_{238} \sigma_{t,238}^g}{N_{235}} \\
 \sigma_t^{g,238} &= \sigma_t^{g,238,\infty} f\left(T, \sigma_{t,b}^{g,238}\right) \\
 \sigma_{t,b}^{g,238} &= \frac{N_O \sigma_{sO}^g + N_{235} \sigma_{t,235}^g}{N_{238}}
 \end{aligned} \tag{7.32}$$

Note that the total cross section for U^{238} appears in the background cross section used to calculate the total cross section for U^{235} . The total cross section for U^{235} appears in the background cross section used to calculate the total cross section for U^{238} . Therefore, iteration will be necessary to get both total cross sections. The iteration proceeds as follows:

1. Use the infinite dilute total cross sections to calculate a background cross section for each absorber.
2. Estimate new total cross sections for all absorbers based on these background cross sections.

3. Calculate new background cross sections based on these updated total cross sections.
4. Repeat the process until the total cross sections converge.
5. When the total cross sections have converged, use the estimated background cross sections to calculate scattering, absorption, and fission cross sections.

This process is fairly efficient and converges in less than three or four iterations in most cases. Note that all subordinate cross sections must be calculated based on the same background cross section to ensure that they add up to the correct total.

The iterative process when two or more resonance species are present does correct slightly for resonance overlap, but a strong theoretical justification for its accuracy is lacking.

7.5.3 *The CENTRM Method*

The CENTRM code in NJOY divides the energy range into three intervals: upper multi-group range, point-wise range, and lower multi-group range. The user can control the energy boundaries of these ranges. However, it is desirable to set the boundaries of the point-wise energy range such that it includes the resonance structure of an important isotope. This way, a detailed flux calculation in the resonance range can be obtained. Calculations can be performed for an infinite homogeneous medium or for one-dimensional problems having a slab, cylindrical, or spherical geometry. Several methods are available for solving the transport equation in the multi-group and point-wise energy ranges. The methods for multi-group calculations are discrete ordinates (SN), diffusion, homogenized infinite medium, zone-wise infinite medium, and BN. For the point-wise calculations, the SN, collision probability, homogenized infinite medium, and zone-wise infinite medium methods exist. [7]

7.6 Infinite Resonance Integrals and Group Cross Sections

In this section, we introduce infinite resonance integrals (RIs), very briefly, as flux weighted, and that is weighted with $1/E$ spectrum when $\phi(E) \sim 1/E$ considering microscopic cross section $\sigma(E)$:

$$\begin{aligned}
 \text{RI} &= - \int_{E_1}^{E_2} \sigma(E) dE \\
 E &= \ln \left(\frac{E_2}{E_1} \right) = \ln(E_2) - \ln(E_1) \\
 dE &= -\frac{1}{E} dE \\
 \text{RI} &= \int \sigma(E) dE
 \end{aligned} \tag{7.33}$$

Notice that:

- RI is defined directly from cross-sectional data; no flux calculation is required because $1/E$ spectrum is assumed.
- RI depends on the normalization of the $1/E$ flux spectrum; it is also implicitly assumed that flux equals 1 when $E = 1$ through normalization.
- RI is independent of energy bounds for isolated resonances.
- RI is independent of temperature. This is because if the energy bound is large enough, then as temperature increases, the spectrum would broaden, but because the area under the curve remains the same, assuming the cross section is constant, then RI is essentially integrating the spectrum, which would not change upon temperature change.
- RI is useful for intercomparing libraries or cross-sectional models. It is a classic way to evaluate new resonance data typically from 0.5 eV to 10 keV. We use RI to check our resonance data, in particular the three big resonances at 6.67, 20.9, 36.7, and 66 eV. Numerical test of the SLBW RIs shows that the RI comes out to be within 1% of ENDF/B-VII Reich-Moore data.

Group cross section is a similar but much more useful quantity. From its definition, we see g does not depend on the flux normalization:

$$\sigma_g = \frac{\int_{E_1}^{E_2} \sigma(E) \phi(E) dE}{\int_{E_1}^{E_2} \phi(E) dE} \quad (7.34)$$

If we make assumption on the flux spectrum, then we can relate group cross section σ_g to effective resonance integral RI_{eff} as:

$$\begin{aligned} \phi(E) &\sim \frac{1}{E} \\ \sigma_g &= \frac{\int_{E_1}^{E_2} \sigma(E) \frac{1}{E} dE}{\int_{E_1}^{E_2} \frac{1}{E} dE} = \frac{RI_{eff}}{\ln(E_2) - \ln(E_1)} = \frac{RI_{eff}}{\ln(E_2/E_1)} \\ RI_{eff} &= \sigma_g \ln(E_2/E_1) \end{aligned} \quad (7.35)$$

Notice that:

- Group cross section by definition depends on both cross section and flux spectrum.
- Group cross section depends on the flux, but not on the normalization of flux (i.e., only the shape matters, not the magnitude).

- Group cross section depends explicitly on energy bounds (widths) of the groups.
- Effective RI can be computed from group cross sections and group energy bounds as in Eq. 7.31; as spectrum approaches $1/E$, the effective resonance integrals (RIs) computed from group cross sections will approach infinite RI.

7.7 Dilution Cross Section: Dilution Factor

In an infinite homogeneous medium with one resonance absorber and one moderator, we write removal rates equals scattering rates very similar to Eq. 7.15 as before:

$$\begin{aligned}
 [N_r \sigma_r(E) + N_m \sigma_m(E)] \phi(E) &= \int_{-\infty}^E N_m \sigma_m(E') \phi(E') P(E' \rightarrow E) dE' \\
 &= N_m \sigma_m(E) \int_{-\infty}^E \phi(E') P(E' \rightarrow E) dE' \\
 &= N_m \sigma_m(E) C
 \end{aligned} \tag{7.36a}$$

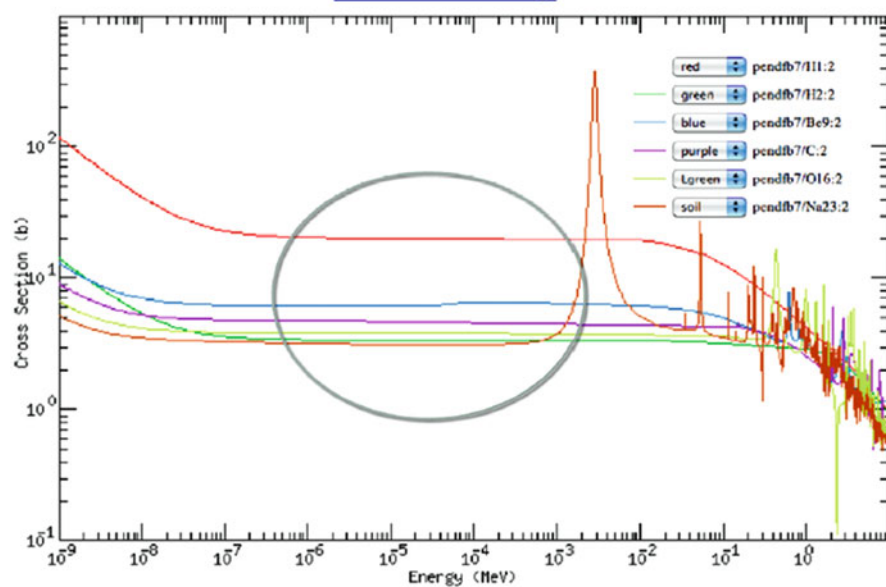
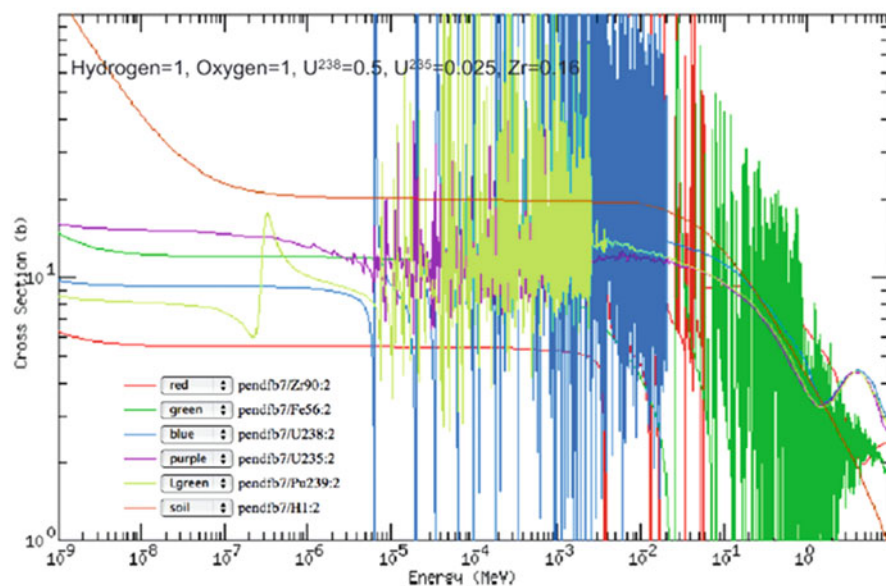
where:

$$\begin{aligned}
 \phi(E) &\propto \frac{N_m \sigma_m(E)}{N_r \sigma_r(E) + N_m \sigma_m(E)} \\
 \phi(E) &\propto \frac{\frac{N_m}{N_r} \sigma_m(E)}{\sigma_r(E) + \frac{N_m}{N_r} \sigma_m(E)}
 \end{aligned} \tag{7.36b}$$

In the above derivation, we made two assumptions as:

- The moderator's cross section is independent of energy near resonances. For almost any moderators, we can pick the assumption that the elastic scattering cross section is constant and is valid in the thermal range as in Fig. 7.15.
- $\int_{-\infty}^E \phi(E') P(E' \rightarrow E) dE'$ is constant (i.e., C). We know that the flux above the resonance is $1/E$ and hence constant in lethargy. If we assume scattering into the resonance comes from this constant lethargy region, then the resonance lethargy is constant as well.

Equation 7.32(b) suggests that *in infinite medium, the flux shape near resonance depends only on the ratio of the number density of the moderator to the resonance absorber and the moderator cross section*. However, once we move into a finite medium or we take into account leakage, then the absolute number densities are needed.

a**Moderators: Elastic Scattering Cross Sections****b****H plus Non-Moderators: Elastic Scattering Cross Sections****Fig. 7.15** Elastic scattering cross sections

To capture the ratio of number densities and the moderator cross section, we define *dilution cross section* as:

$$\sigma_d = \frac{N_m \sigma_m}{N_r} \quad (7.37)$$

Then, the flux shape near resonance is:

$$\phi(E) \propto \frac{\sigma_d}{\sigma_r + \sigma_d} \quad (7.38)$$

These flux shapes in Eq. 7.38 let us compare approximated effective resonance integrals (RIs). Recall resonance integrals (RIs) are defined in Eq. 7.33 as $RI = \int \sigma(E)dE$, and then the approximated effective resonance integrals RI_{eff} are given as:

$$RI_{eff} = \int \sigma_r(E) \frac{\sigma_d}{\sigma_r + \sigma_d} dE \quad (7.39)$$

Based on what we have derived so far, the two extremes of RI_{eff} and σ_d are:

- As $\sigma_d \rightarrow \infty$, the entire media is moderator, and we reach the limit of infinite dilute, $RI_{eff} \rightarrow RI$; we should get within 1% of the ENDFVII cross-sectional data.
- As $\sigma_d \rightarrow 0$, analytically our assumptions do not hold true anymore, but the MC is true such that $RI_{eff} \rightarrow 0$ and $\phi(E) \rightarrow 0$ as seen in Fig. 7.16. Interpretation: As we have no moderator, every atom is essentially self-shield because they are all resonant isotopes, hence infinite flux depression.

<u>Numerical</u>	<u>U/H = .00001</u>	<u>U/H = .001</u>	<u>U/H = .01</u>	<u>U/H = .1</u>	<u>U/H = 1.0</u>
5.09	4.39	4.39	4.39	4.38	4.32
1.70	1.71	1.71	1.71	1.71	1.69
1.45	1.48	1.48	1.48	1.47	1.41
126.84	124.8	101.0	47.1	14.0	3.96
65.88	67.3	54.4	21.2	6.8	2.15
41.58	40.0	31.1	11.5	5.2	1.60
12.2	11.7	10.7	6.4	2.8	0.73
271.61	264	216	99.4	38.0	12.2

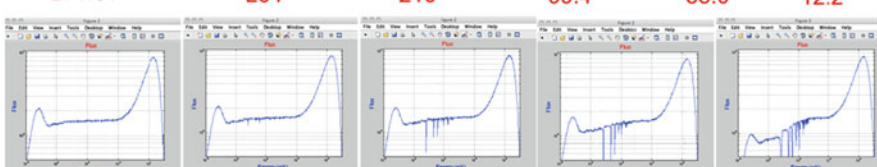
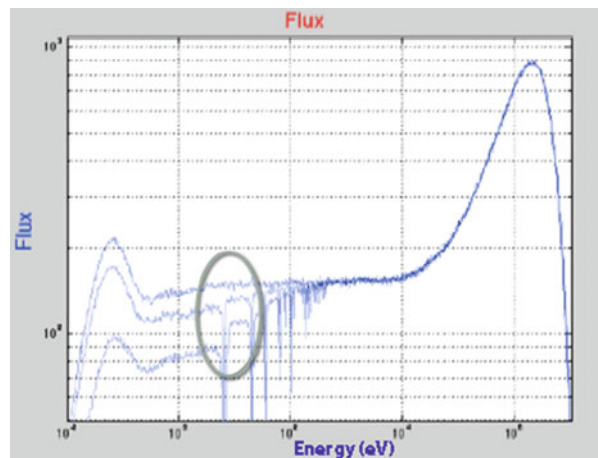


Fig. 7.16 Impact of energy self-shielding on effective resonance integrals

Fig. 7.17 The $1/E$ spectrum above a resonance suggests group cross section independent of higher energy absorption



The scattering down to resonance is independent of the resonance. In other words, if the spectrum above a resonance returns to $1/E$ as in Fig. 7.17, the group cross sections will be independent of higher energy absorptions. This may be related to what we talked about in the previous sections.

7.8 Resonance Effects

Cross sections, much like spectra, can be broken down into three major regions. Absorption cross sections tend to vary as $1/v$ in the thermal energy range below about 0.5 eV. In the slowing down region from 0.5 eV to about 0.1 MeV, absorption is dominated by resonance effects with very large peaks at the resonance energies and zero absorption between resonances. Above 0.1 MeV, absorption cross sections tend to be smoothly varying and close to constant. There are still resonances in this range, but they tend to be so close together that they cannot be resolved and their effects are simply averaged out. The thermal range and fast range are fairly easily handled in the multi-group approach, but the resonance region presents some difficulties. Scattering cross sections are dominated by a fairly constant potential scattering cross section over most of the region of interest for nuclear reactors and do not show a significant variation with energy.

The resonance range is normally split into two regions identified as resolved resonances and unresolved resonances. The energy span of the resolved resonance range varies with nuclide and tends to be a function of both the atomic number and the spacing of the resonances. For instance, in a low mass number A nuclide like aluminum, the entire range is essentially resolved. In a high mass number A nucleus like U^{238} with fairly, widely separated resonances, the resolved resonance range extends up to about ~ 10 keV. In U^{235} however, the resolved resonance range only goes up to about 500 eV as its resonances are much closer spaced.

The sharpness of the resonance cross sections causes problems in producing multi-group data sets. The absorption cross section can vary several orders of magnitude over a range of less than 0.025 eV. The standard procedure of choosing very narrow groups and calculating an infinite medium or zero-dimensional spectrum becomes very difficult if a range of 0.5 eV to 1.0 MeV must be spanned with say 0.005 eV wide groups. This would require $\sim 2E+8$ groups. This is still too large of a number even for today's computers. So a fundamental spectrum must be calculated analytically within fairly, broad groups. The techniques for accomplishing this are fairly well developed.

However, like any infinite medium or zero-dimensional spectrum, the actual spectrum will depend on all of the nuclides present in the material zone of interest. Consider what happens to the total cross section and the neutron flux near the 6.67 eV resonances in U^{238} as a function of the materials present in the material region.

Start by considering that the material is a one-to-one mixture of U^{238} to hydrogen with a scattering cross section of 20 barns per atom. The total cross section and flux in the resonance region are given in Fig. 7.18. The cross section varies by approximately a factor of one million over an energy range of a few eV. The flux takes a very strong dip at the resonance energy, going down by a factor of several hundred thousand. Since the absorption is the product of the flux and the cross section, it is important to get a good estimate for the flux in the resonance range to accurately calculate the absorption reaction rate. Also, note that the total cross section exceeds the background scattering cross section over a range from about 1 eV to 15 eV.

Now consider when the U^{238} is diluted relative to the hydrogen concentration and we have 104 hydrogen atoms for every U^{238} atom. This case is plotted in Fig. 7.19. In this case, the cross section goes up by a factor of a little over 1000, and the flux drops in the resonance range by about the same amount.

It is still important to get a good approximation for the flux in the resonance region. It is also worth noting that the resonance cross section exceeds the asymptotic scattering cross section only over a range from 5 eV to 8 eV. The range over which the resonance cross section is important is about 1/fifth of what it was in Fig. 7.18.

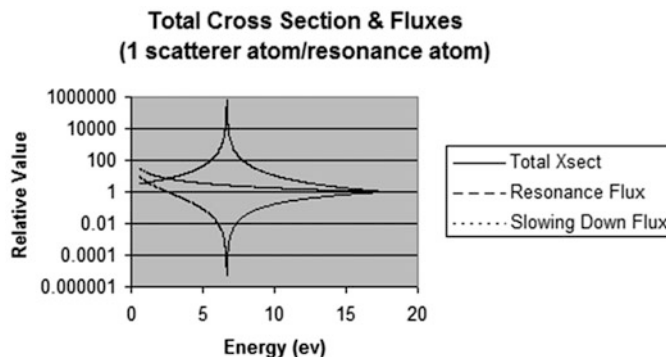


Fig. 7.18 One scatterer atom per absorber atom

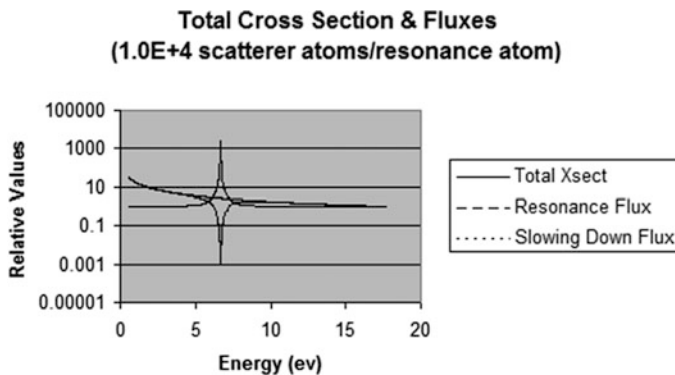


Fig. 7.19 10^4 scatterer atoms per absorber atom

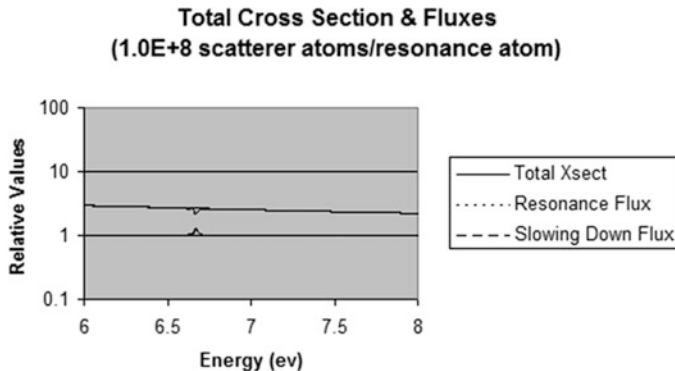


Fig. 7.20 10^8 scatterer atoms per absorber atom

Now consider when there are 10^8 scatterer atoms per absorber atom. This case is described in Fig. 7.20.

Note that in this case, the absorber is a small perturbation on the total cross section, and the change in the flux is a small fraction of the total flux. For this case, an average flux is probably adequate to evaluate the absorption in this resonance. This case is generally referred to as the infinite dilute limit. The cross section is referred to as the infinite dilute cross section.

Therefore, the absorption cross section for a resonance absorber will depend on the amount of background absorber mixed into the material mixture that the absorber is in. Obviously, this complicates the production of multi-group cross sections for resonance absorbers by a significant amount.

There is one other effect, which also affects resonance cross sections. Since the typical width of a resonance in a high of atomic mass A nucleus is on the order of 0.025 eV, the relative velocity between the neutrons and the nuclei in a material will be greatly affected by the thermal velocity of the nuclei. Increases in temperature of the material containing the resonance absorber will greatly affect the absorption in the resonance.

Multi-group cross sections will depend on the amount of background scatterer present and the temperature of the medium.

In order to develop these dependencies, the temperature effects will be treated first. Start with the conservation of reactions equation given by:

$$\begin{aligned}\phi(E)\sigma_\gamma(E) &= nv(E)\sigma_\gamma(E) = \int_0^\infty v_{rel}\sigma_\gamma(E_{rel})np(\bar{V})_{MB}d\bar{V} \\ \sigma_\gamma(E) &= \frac{1}{v(E)} \int_0^\infty v_{rel}\sigma_\gamma(E_{rel})p(\bar{V})_{MB}d\bar{V}\end{aligned}\quad (7.40)$$

where the nuclei of the absorber are assumed to have a Maxwell-Boltzmann distribution and the bar over the V represents a vector velocity. The Maxwell-Boltzmann energy distribution is given by:

$$\begin{aligned}p(\bar{V})_{MB}d\bar{V} &= \left(\frac{M}{2\pi kT}\right)^{3/2} e^{-\frac{MV^2}{2kT}} dV_x dV_y dV_z \\ \int_0^\infty p(\bar{V})_{MB}d\bar{V} &= 1.0\end{aligned}\quad (7.41)$$

Since only the relative velocity is important in evaluating the reaction cross section, it is convenient to define the axis system for evaluating the velocities of the nuclei relative to the direction the neutron is traveling. If the direction of neutron travel is chosen as the z -axis, then the relative energy can be written as:

$$E_{rel} = \frac{1}{2}m(v_n - |\bar{V}|)^2 = \frac{1}{2}m([v_n - V_z]^2 + V_x^2 + V_y^2) \quad (7.42)$$

In addition, the resonance absorption cross section is given by:

$$\begin{aligned}\sigma_\gamma &= \frac{\Gamma_\gamma}{\Gamma} \frac{\sigma_o}{1 + y^2} \\ y &= \frac{2}{\Gamma}(E - E_r)\end{aligned}\quad (7.43)$$

Then:

$$\begin{aligned}\sigma_\gamma(E) &= \sigma_o \frac{\Gamma_\gamma}{\Gamma} \int_0^\infty \frac{v_{rel}}{v(E)} \left(\frac{M}{2\pi kT}\right)^{3/2} \frac{e^{-\frac{M(V_x^2 + V_y^2 + V_z^2)}{ekT}}}{1 + \left(\frac{2}{\Gamma}[E_{rel} - E_r]\right)^2} dV_x dV_y dV_z \\ \frac{\sigma_\gamma(E)}{\sigma_o \frac{\Gamma_\gamma}{\Gamma}} &= \int_0^\infty e^{-\frac{MV_x^2}{2kT}} dV_x \int_0^\infty e^{-\frac{MV_y^2}{2kT}} dV_y \int_0^\infty \left(\frac{M}{2\pi kT}\right)^{3/2} \frac{v_{rel}}{v(E)} \frac{e^{-\frac{MV_z^2}{2kT}}}{1 + y^2} dV_z\end{aligned}\quad (7.44)$$

The integrals over the velocity distributions in the x and y directions can be performed immediately as the relative energy or velocity does not matter. The ratio of v_{rel} to $v(E)$ can be set to 1 as it will not vary significantly over the range that the rest of the integrand varies. The equation then becomes:

$$\frac{\sigma_\gamma(E)}{\sigma_o \frac{\Gamma_\gamma}{\Gamma}} = \int_0^\infty \left(\frac{M}{2\pi kT} \right)^{1/2} \frac{e^{-\frac{MV_z^2}{2kT}}}{1+y^2} dV_z \quad (7.45)$$

Now E_{rel} can be expanded to give:

$$\begin{aligned} E_{rel} &= \frac{1}{2}m(v_n - V_z)^2 = \frac{1}{2}mv_n^2 - mv_n V_z + \frac{1}{2}mV_z^2 \\ &\approx \frac{1}{2}mv_n^2 + mv_n V_z = E - mv_n V_z = E - V_z \sqrt{2mE} \\ V_z &= \frac{E - E_{rel}}{\sqrt{2mE}} \\ dV_z &= -\frac{dE_{rel}}{\sqrt{2mE}} \end{aligned} \quad (7.46)$$

Substituting all of this into the cross-sectional integral and changing the limits from 0 to ∞ to $-\infty$ to $+\infty$ as the peak in the integrand is far above the lower limit give:

$$\begin{aligned} \frac{\sigma_\gamma(E)}{\sigma_o \frac{\Gamma_\gamma}{\Gamma}} &= \left(\frac{M}{2\pi kT} \right)^{1/2} \Gamma^2 \int_{-\infty}^\infty \frac{e^{-\frac{M}{2kT} \frac{(E-E_{rel})^2}{2mE}}}{4(E_{rel} - E_r) + \Gamma^2} \frac{dE_{rel}}{\sqrt{2mE}} \\ \frac{\sigma_\gamma(E)}{\sigma_o \frac{\Gamma_\gamma}{\Gamma}} &= \left(\frac{A}{4kTE} \right)^{1/2} \frac{\Gamma^2}{\sqrt{\pi}} \int_{-\infty}^\infty \frac{e^{-\frac{A}{4kTE} [(E - E_r) - (E_{rel} - E_r)]^2}}{4(E_{rel} - E_r)^2 + \Gamma^2} dE_{rel} \end{aligned} \quad (7.47)$$

Now define:

$$\begin{aligned} x &= \frac{2}{\Gamma}(E_{rel} - E_r) \\ y &= \frac{2}{\Gamma}(E - E_r) \end{aligned} \quad (7.48)$$

and

$$\begin{aligned} \Delta &= \sqrt{\frac{4kTE}{A}} \approx \sqrt{\frac{4kTE_r}{A}} \\ \theta &= \frac{\Gamma}{\Delta} \end{aligned} \quad (7.49)$$

The integral then becomes:

$$\begin{aligned}\frac{\sigma_\gamma(E)}{\sigma_o \frac{\Gamma_\gamma}{\Gamma}} &= \frac{\theta}{2\sqrt{\pi}} \int_{-\infty}^{\infty} \frac{e^{-\frac{\theta^2}{4}(y-x)^2}}{1+x^2} dx = \psi(\theta, y) \\ \sigma_\gamma(E) &= \sigma_o \frac{\Gamma_\gamma}{\Gamma} \psi(\theta, y)\end{aligned}\quad (7.50)$$

Moreover, $\psi(\theta, y)$ is a tabulated function known as the symmetric Voigt profile.

If we were to consider the total cross section including the scattering cross section, we would get an asymmetric term due to the interference part of the scattering cross section, and this would give us the asymmetric Voigt profile. The total cross section could be written as:

$$\sigma_t(E) = \sigma_o \psi(\theta, y) + \left(\sigma_o \sigma_p \frac{\Gamma_n}{\Gamma} \right)^{1/2} \chi(\theta, y) + \sigma_p \quad (7.51)$$

Now remembering that $y = 2(E - E_r)/T$ and $dy = 2dE/\Gamma$, we can integrate the absorption cross section over all energy:

$$\int_0^\infty \sigma_\gamma(E) dE = \frac{\sigma_o \Gamma_\gamma}{2} \int_0^\infty \psi(\theta, y) dy \approx \frac{\sigma_o \Gamma_\gamma}{2} \int_{-\infty}^\infty \psi(\theta, y) dy = \frac{\sigma_o \Gamma_\gamma}{2} \pi \quad (7.52)$$

The most interesting aspect of this result is that it is independent of temperature. That is, if we do simply integrate the cross section over all energy, the final result does not depend on the temperature that the nuclei are at. It would seem that all of this effort has been for naught. However, in the end we must remember that we are trying to conserve reaction rates, and we must consider the product of the flux times the cross section. The result we have just obtained is for a constant flux across the energy range of the resonance. This is seldom the case and only occurs when the resonance does not perturb the flux. For this to be the case, the absorber must not make a significant contribution to the total cross section. Only if the absorber is distributed in the media in very small amounts can this be the case. This condition is called the “infinitely dilute” case.

For the infinitely dilute case, the contribution of the i^{th} resonance to a group absorption cross section can be written as:

$$\sigma_{\gamma i}^g = \frac{\int_{E_{g+1}}^{E_g} \sigma_{\gamma i}(E, T) \phi(E) dE}{\int_{E_{g+1}}^{E_g} \phi(E) dE} \quad (7.53)$$

Assuming that $\phi(E) = \phi_0/E$, the denominator becomes:

$$\int_{E_{g+1}}^{E_g} \frac{\phi_o}{E} dE = \phi_o \int_{E_{g+1}}^{E_g} \frac{dE}{E} = \phi_o \Delta u_g \quad (7.54)$$

Moreover, the contribution from the i^{th} resonance can then be written as:

$$\sigma_{\gamma i}^g = \frac{1}{\Delta u_g} \int_{E_{g+1}}^{E_g} \sigma_{\gamma i}(E, T) \frac{dE}{E} = \frac{1}{\Delta u_g E_{ri}} \int_{E_{g+1}}^{E_g} \sigma_{\lambda i}(E, T) dE = \frac{1}{\Delta u_g E_{ri}} \frac{\sigma_{oi} \Gamma_{\gamma i} \pi}{2} \quad (7.55)$$

where it has been assumed that E_{ri} can be taken out of the integral because it does not vary significantly over the contribution interval. Therefore, this gives for the group absorption cross section:

$$\begin{aligned} \sigma_a^g &= \frac{1}{\Delta u_g} \sum_{i \in g} \frac{\sigma_{oi} \Gamma_{\gamma i} \pi}{E_{ri}} \frac{1}{2} = \frac{1}{\Delta u_g} \sum_{i \in g} I_i^\infty \\ I_i^\infty &= \frac{\sigma_{oi} \Gamma_{\gamma i} \pi}{E_{ri}} \frac{1}{2} = \text{Infinite Dilute Resonance Integrnd} \end{aligned} \quad (7.56)$$

7.9 Homogeneous Narrow Resonance Approximation

In order to estimate the flux in the resonance, we must solve the neutron transport equation in the energy range of the resonance. Fortunately, we can obtain a good approximation by solving the infinite media equation. We will start by considering a homogeneous medium as it is simpler. The infinite medium equation in a homogeneous material is:

$$\sum_i \phi(E) = \int_E^{E/\alpha_A} \frac{\sum_{sA}(E')}{(1 - \alpha_A)E'} \phi(E') dE' + \int_E^{E/\alpha_m} \frac{\sum_{sm}(E')}{(1 - \alpha_m)E'} \phi(E') dE' \quad (7.57)$$

where we have lumped all scatterers into one. We will only treat one absorber at a time. This means that other absorbers in the material are treated as scatterers. We are assuming that the resonances of one absorber do not overlap those of another absorber in energy. It will be obvious why this can be done as we solve for the flux. Since we are interested in approximating the flux in the resonance, we will be interested in the energy range over which the resonance perturbs the cross section by a significant amount. To quantify this, choose the range of interest as that energy

range over which the resonance part of the cross section doubles the scattering cross section outside of the resonance.

We have:

$$\begin{aligned}
 \frac{\Sigma_o}{1+y^2} &= \Sigma_{sm} \\
 \frac{\Sigma_o}{\Sigma_{sm}} &= 1+y^2 = 1 + \left(\frac{2}{\Gamma} [E - E_r] \right)^2 \\
 E - E_r &= \frac{\Gamma}{2} \sqrt{\frac{\Sigma_o}{\Sigma_{sm}} - 1} \\
 \Delta E = 2(E - E_r) &= \Gamma_p = \Gamma \sqrt{\frac{\Sigma_o}{\Sigma_{sm}} - 1} \approx \Gamma \sqrt{\frac{\Sigma_o}{\Sigma_{sm}}} \tag{7.58}
 \end{aligned}$$

where Γ_p is called the practical width. Now the practical width is the region over which the total cross section is perturbed by the resonance. To determine how much this effects the flux in the resonance, we must compare this range with the range over which neutrons can scatter into the resonance. If the range over which neutrons can scatter into the resonance is large compared to the range over which the resonance perturbs the cross section, then we can neglect the effects of the resonance. For the moderator, the range over which neutrons can be scattered by moderator atoms into the resonance is always large compared to the practical width of all resonances. The scatter-in range for the moderator is $(1/\alpha_m - 1)E_r$. Therefore, we will in general have:

$$\Gamma_p \ll (1/\alpha_m - 1)E_r \tag{7.59}$$

for all moderators.

For typical absorbers like the fissile isotopes, whether the in-scatter range is large or small compared to the practical width for the resonance will depend on the mixture parameters. In general, as the resonance energy increases, the in-scatter range increases, so it is likely that the effects of the resonance can be neglected as a perturbation on the in-scatter flux. The narrow resonance approximation refers to the way the in-scatter integral is treated for the absorber if:

$$\Gamma_p \ll (1/\alpha_A - 1)E_r \tag{7.60}$$

We will evaluate the flux in the resonance with the narrow resonance approximation. This means that we can use the asymptotic form for the flux in the in-scatter integrals. This gives:

$$\begin{aligned}
 \Sigma_t(E)\phi(E) &= \int_E^{E/\alpha_A} \frac{\Sigma_{pA}}{(1-\alpha_A)E'} \frac{\phi_o}{E'} dE' + \int_E^{E/\alpha_m} \frac{\Sigma_{sm}}{(1-\alpha_m)E'} \frac{\phi_o}{E'} dE' \\
 \Sigma_t(E)\phi(E) &= \frac{\Sigma_{pA}}{E} \phi_o + \frac{\Sigma_{sm}}{E} \phi_o = \frac{\Sigma_{pA} + \Sigma_{sm}}{E} \phi_o \\
 \phi(E) &= \frac{\Sigma_{pA} + \Sigma_{sm}}{E \Sigma_t(E)} \phi_o \tag{7.61}
 \end{aligned}$$

Then we can use this approximation for the flux in the resonance integral. This becomes:

$$\sigma_{\gamma}^g = \frac{\int_{E_{g+1}}^{E_g} \frac{\sigma_{oA} \frac{\Gamma_{\gamma}}{\Gamma} \psi(\theta, y) (\Sigma_{pA} + \Sigma_{sm})}{\Sigma_{oA} \psi(\theta, y) + N_A (\sigma_{pA} \sigma_o \frac{\Gamma_{\gamma}}{\Gamma})^{1/2} \chi(\theta, y) + \Sigma_{pA} + \Sigma_{sm}} \frac{\phi_o}{E} dE}{\int_{E_{g+1}}^{E_g} \frac{\phi_o}{E} dE} \quad (7.62)$$

Now the denominator can be integrated to get $\phi_0 \Delta u$, and the ϕ_0 will cancel with the one in the numerator. In order to integrate the numerator, we have to neglect the asymmetric term, $\chi(\theta, y)$. The rationale for this is that it is asymmetric, so it adds and subtracts across the resonance, so its effect can be neglected. We will also extend the upper limit to infinity as most groups are a great deal larger than the resonance width. Since the integral is symmetric, we will set the lower limit to zero and double it. We will also pull the E out of the integral and set it equal to E_r . This gives:

$$\begin{aligned} \sigma_{\gamma}^g &= \frac{\sigma_o \Gamma_{\gamma}}{E_r} \frac{1}{\Delta u_g} \int_0^{\infty} \frac{(\Sigma_{pA} + \Sigma_{sm}) \psi(\theta, y)}{\Sigma_{oA} \psi(\theta, y) + \Sigma_{pA} + \Sigma_{sm}} \frac{2dE}{\Gamma} \\ \sigma_{\gamma}^g &= \frac{1}{\Delta u_g} \frac{\sigma_o \Gamma_{\gamma}}{E_r} \beta \int_0^{\infty} \frac{\psi(\theta, y)}{\psi(\theta, y) + \beta} dy \\ \beta &= \frac{\Sigma_{pA} + \Sigma_{sm}}{\Sigma_o} \\ \sigma_{\gamma}^g &= \frac{1}{\Delta u_g} \frac{\sigma_o \Gamma_{\gamma}}{E_r} \beta^* J(\theta, \beta) \end{aligned} \quad (7.63)$$

$J(\theta, \beta)$ is a tabulated function called Dresner's integral. Note that the product $\beta^* J(\theta, \beta)$ must lie between 0 and $\pi/2$.

Then the group absorption cross section with multiple resonances in an energy group is:

$$\sigma_a^g = \frac{1}{\Delta u_g} \sum_{i \in g} \frac{\sigma_{oi} \Gamma_{\gamma i}}{E_{ri}} \beta_i^* J(\theta, \beta_i) \quad (7.64)$$

7.10 Homogeneous Wide Resonance Approximation

Now consider the case when the in-scatter interval for the absorber is smaller than the practical width for the resonance. In this case, we will make the wide resonance approximation or the infinite mass approximation. We have:

$$\Gamma_p >> (1/\alpha_A - 1)E_r \quad (7.65)$$

In this case, we will assume that when the absorber scatters, it remains at the energy of interest. So our infinite medium equation becomes:

$$\begin{aligned} \Sigma_t(E)\phi(E) &= \Sigma_{sA}(E)\phi(E) + \Sigma_{sm}\frac{\phi_o}{E} \\ [\Sigma_t(E) - \Sigma_{sA}(E)]\phi(E) &= \Sigma_{sm}\frac{\phi_o}{E} \\ \phi(E) &= \frac{\Sigma_{sm}}{\Sigma_t(E) - \Sigma_{sA}(E)}\frac{\phi_o}{E} \end{aligned} \quad (7.66)$$

Then the absorption cross section for this resonance becomes:

$$\sigma_\gamma^g = \frac{\int_{E_{g+1}}^{E_g} \frac{\sigma_{oA}\Gamma_\gamma}{\Sigma_{oA}\Gamma}\psi(\theta, y)\Sigma_{sm}}{\int_{E_{g+1}}^{E_g} \frac{\phi_o}{E}dE} \frac{\phi_o}{E}dE \quad (7.67)$$

Once again, the denominator can be integrated to get $\phi_0\Delta u$, and the ϕ_0 will cancel with the one in the numerator. This time we do not have to neglect anything because the asymmetric term has been subtracted out. We will extend the upper limit to infinity, as most groups are a great deal larger than the resonance width. Since the integral is symmetric, we will set the lower limit to zero and double it. We will also pull the E out of the integral and set it equal to E_r . This gives:

$$\sigma_\gamma^g = \frac{\sigma_o\Gamma_\gamma}{E_r} \frac{1}{\Delta u_g} \int_0^\infty \frac{\Sigma_{sm}\psi(\theta, y)}{\Sigma_{oA}\frac{\Gamma_\gamma}{\Gamma}\psi(\theta, y) + \Sigma_{sm}} \frac{2dE}{\Gamma} \quad (7.68)$$

$$\sigma_\gamma^g = \frac{1}{\Delta u_g} \frac{\sigma_o\Gamma_\gamma}{E_r} \beta' \int_0^\infty \frac{\psi(\theta, y)}{\psi(\theta, y) + \beta'} dy \quad (7.69)$$

and

$$\begin{aligned} \beta' &= \frac{\Sigma_{sm}}{\Sigma_o} \frac{\Gamma}{\Gamma_\gamma} \\ \sigma_\gamma^g &= \frac{1}{\Delta u_g} \frac{\sigma_o\Gamma_\gamma}{E_r} \beta'^* J(\theta, \beta') \end{aligned} \quad (7.70)$$

Therefore, we have a result that is of the same form as for the narrow resonance approximation, and it can be evaluated with Dresner's J function once again. In the end the difference is only in how we calculate the two β s. Since Γ/Γ_γ is always greater than 1.0 and $\Sigma_{sm} < \Sigma_{sm} + \Sigma_{pA}$, no general statement can be made about the ratio of the two evaluations.

So what happens if we do not have either $\Gamma_p > > (1/\alpha_A - 1)E_r$ or $\Gamma_p < < (1/\alpha_A - 1)E_r$. There have been methods developed to interpolate between these limits and they work quite well. However, that is beyond the level of this course and they are not widely used. Approximate treatment of resonances has been rendered a thing of the past by the ultrafast computers that can numerically solve the equations to create tables that can be easily interpolated.

Before we get to that however, let us consider the much more useful case of heterogeneous resonances.

7.11 Heterogeneous Narrow Resonance Approximation

So far, we have only considered resonance absorption when the fuel or absorber nuclei are intimately mixed with the scattering or moderator nuclei. This is really only the case in a few reactors like the AGN-201 or Sandia's SPR reactors. In most commercial reactors, the fuel is consolidated into fuel elements and surrounded by moderator. This condition greatly affects the average resonance absorption in the fuel nuclei because the nuclei in the center of the fuel see very few neutrons at resonance energies as most of the neutrons are stopped on the surface of the fuel element.

Start the analysis by considering one fuel element lump in a sea of moderator. At energies far above the resonance, the neutron flux is flat across both media, and a given neutron does not know whether it is in the fuel or the moderator. We will assume that in each of the regions as we approach the resonance energy, the flux in both media can be represented by its average value. (This is probably a weak assumption as we get close to the resonance.) In the resonance energy range, the average flux in the fuel will be depressed relative to its value in the moderator.

Now the total interaction rate in the fuel can be written as:

$$\text{Collision Rate in Fuel} = V_F \Sigma_t^F(E) \phi_{\text{avg}}^F(E) \quad (7.71)$$

where V_F is the volume of the fuel and $\Sigma_t^F(E)$ is the total cross section for the fuel material which may include one or more moderators mixed in with the resonance absorber. Neutrons that collide in the fuel at energy E must have either come from the fuel via a downscatter process and not leak out before interacting or have come from the moderator and leaked into the fuel before interacting. So an approximate infinite medium equation can be written as:

$$\begin{aligned}
V_F \Sigma_t^F(E) \phi^F(E) = & [1 - P_{FO}(E)] V_F \int_E^{E/\alpha_A} \frac{\Sigma_{sA}^F(E') \phi^F(E') dE'}{(1 - \alpha_A) E'} \\
& + [1 - P_{FO}(E)] V_F \int_E^{E/\alpha_{mf}} \frac{\Sigma_{smf}^F(E') \phi^F(E') dE'}{(1 - \alpha_{mf}) E'} \\
& + P_{MO}(E) V_m \int_E^{E/\alpha_M} \frac{\Sigma_{sm}^M(E') \phi^M(E') dE'}{(1 - \alpha_M) E'}
\end{aligned} \quad (7.72)$$

where:

α_A, Σ_{sA}^F are the properties of the absorber in the fuel region.

$\alpha_{mf}, \Sigma_{smf}^F$ are the properties of the moderator in the fuel region (admixed moderator).

α_M, Σ_{sm}^M are the properties of the moderator in the moderator region (outside moderator).

$P_{FO}(E)$ is the probability of traveling from a collision in the fuel lump to a collision in the moderator in one flight.

$P_{MO}(E)$ is the probability of traveling from a collision in the moderator to a collision in the fuel in one flight.

Note that $P_{FO}(E)$ and $P_{MO}(E)$ are averages over both the volume of the fuel and the volume of the moderator in both cases. Then $[1 - P_{FO}(E)]$ is the probability of not escaping the fuel in one flight.

Now by a general theorem known as the reciprocity theorem, the collision rate in the fuel times the fuel escape probability from the fuel to the moderator must be equal to the collision rate in the outside moderator times the escape probability from the outside moderator to the fuel. We have:

$$P_{FO}(E) V_F \Sigma_t^F(E) \phi^F(E) = P_{MO}(E) V_M \Sigma_t^M \phi^M(E) \quad (7.73)$$

at energies above the resonance. This must hold, as, if it did not, the flux would build up in one material or the other. Making use of this relationship and making the narrow resonance approximation for both moderators, the equation for the collision rate in the fuel becomes:

$$\begin{aligned}
V_F \Sigma_t^F(E) \phi^F(E) = & [1 - P_{FO}(E)] V_F \int_E^{E/\alpha_A} \frac{\Sigma_{sA}^F(E') \phi^F(E') dE'}{(1 - \alpha_A) E'} \\
& + [1 - P_{FO}(E)] V_F \frac{\Sigma_{smf} \phi_o}{E} + P_{FO}(E) V_F \frac{\Sigma_t^F(E) \phi_o}{E}
\end{aligned} \quad (7.74)$$

Dividing out V_F gives:

$$\begin{aligned}\Sigma_t^F(E)\phi^F(E) &= [1 - P_{FO}(E)] \int_E^{E/\alpha_A} \frac{\Sigma_{sA}^F(E')\phi^F(E')dE'}{(1 - \alpha_A)E'} + [1 - P_{FO}(E)] \frac{\Sigma_{smf}\phi_o}{E} \\ &\quad + P_{FO}(E) \frac{\Sigma_t^F(\phi_o)}{E}\end{aligned}\tag{7.75}$$

Note that we have eliminated any dependence on the outside moderator at this point. Now it is time to make the narrow resonance approximation for the absorber, as we have done before.

$$\begin{aligned}\Sigma_t^F(E)\phi^F(E) &= [1 - P_{FO}(E)] \frac{\Sigma_{pA}^F\phi_o}{E} + [1 - P_{FO}(E)] \frac{\Sigma_{smf}\phi_o}{E} + P_{FO}(E) \frac{\Sigma_t^F(E)\phi_o}{E} \\ \Sigma_{FP}^F &= \Sigma_{pA}^F + \Sigma_{smf}^F \\ \Sigma_t^F(E)\phi^F(E) &= [1 - P_{FO}(E)] \frac{\Sigma_{pF}^F\phi_o}{E} + P_{FO}(E) \frac{\Sigma_t^F(E)\phi_o}{E}\end{aligned}\tag{7.76}$$

Now define a pseudo-cross section called the “escape” cross section such that:

$$\Sigma_{esc}(E) = \frac{P_{FO}(E)}{1 - P_{FO}(E)} \Sigma_t^F(E)$$

or

$$P_{FO}(E) = \frac{\Sigma_{esc}(E)}{\Sigma_{esc}(E) + \Sigma_t^F(E)}\tag{7.77}$$

Inserting this into the infinite media equation gives:

$$\begin{aligned}\Sigma_t^F(E)\phi^F(E) &= \frac{\Sigma_{esc}(E) + \Sigma_t^F(E) - \Sigma_{esc}(E)}{\Sigma_{esc}(E) + \Sigma_t^F(E)} \frac{\Sigma_{pF}^F\phi_o}{E} + \frac{\Sigma_{esc}(E)}{\Sigma_{esc}(E) + \Sigma_t^F(E)} \frac{\Sigma_t^F(E)\phi_o}{E} \\ \phi_F(E) &= \frac{\Sigma_{pF}^F + \Sigma_{esc}(E)}{\Sigma_{esc}(E) + \Sigma_t^F(E)} \frac{\phi_o}{E}\end{aligned}\tag{7.78}$$

after the total cross section in the fuel has been divided out of both sides.

7.12 Heterogeneous Wide Resonance Approximation

If we make the wide resonance approximation for the absorber, we will obtain:

$$\begin{aligned}\Sigma_t^F(E)\phi^F(E) &= [1 - P_{FO}(E)]\Sigma_{sA}^R(E)\phi^F(E) + [1 - P_{FO}(E)]\frac{\Sigma_{smf}^F\phi_o}{E} \\ &\quad + P_{FO}(E)\frac{\Sigma_t^F(E)\phi_o}{E}\end{aligned}\quad (7.79)$$

Now substituting for $P_{FO}(E)$, dividing out $\Sigma_t^F(E)$, and multiplying by $\Sigma_{esc} + \Sigma_t^F(E)$, this becomes:

$$[\Sigma_{esc}(E) + \Sigma_t^F(E)]\phi^F(E) = \Sigma_{sA}^R(E)\phi^F(E) + \frac{\Sigma_{smf}^F\phi_o}{E} + \frac{\Sigma_{esc}(E)\phi_o}{E} \quad (7.80)$$

Subtracting $\Sigma_{sA}^R(E)\phi^F(E)$ from both sides and solving for $\phi^F(E)$ give:

$$\phi^F(E) = \frac{\Sigma_{smf}^F + \Sigma_{esc}(E)}{\Sigma_{smf}^F + \Sigma_{esc}(E) + \Sigma_{sA}^R(E)} \frac{\phi_o}{E} \quad (7.81)$$

Now remembering that we had for the homogeneous cases:

$$\begin{array}{c|c} \text{Narrow resonance} & \text{Wide resonance} \\ \hline \phi(E) = \frac{\Sigma_{sm} + \Sigma_{pA}}{\Sigma_t(e)} \frac{\phi_0}{E} & \phi(E) = \frac{\Sigma_{sm}}{\Sigma_{sm} + \Sigma_{sA}(E)} \frac{\phi_0}{E} \end{array}$$

We make the following substitutions in going from the homogeneous to the heterogeneous case:

$$\begin{array}{c|c|c} & \text{Homogeneous} & \text{Heterogeneous} \\ \hline \text{Narrow resonance} & \Sigma_{sm} + \Sigma_{pA} & \rightarrow \Sigma_{esc} + \Sigma_{smf}^F + \Sigma_{pA}^F \\ \text{Wide resonance} & \Sigma_{sm} & \rightarrow \Sigma_{esc} + \Sigma_{smf}^F \end{array}$$

and simply use the formulas for the homogeneous approximations. These are known as the *equivalence relations*.

All that remains is to determine a value for Σ_{esc} . The most useful relationship for determining the “escape cross section” is due to Wigner and is called the Wigner rational approximation. Wigner proposed that we approximate $P_{FO}(E)$ by:

$$P_{FO}(E) = \frac{\frac{S_F}{4V_F\Sigma_t^F}}{1 + \frac{S_F}{4V_F\Sigma_t^F(E)}} \quad (7.82)$$

S_F = fuel element surface area

V_F = fuel element volume

He noted that this gives the correct limits as the ratio V_F/S_F goes to 0 and infinity.

$$V_F/S_F \rightarrow 0, \quad P_{FO}(E) \rightarrow 1.0$$

$$V_F/S_F \rightarrow \text{Infinity}, \quad P_{FO}(E) \rightarrow S_F/4V_F\Sigma_t^F(E)$$

The maximum error in this approximation is about 10% over portions of the range between the limits. Then $4V_F/S_F$ can be defined as the average chord length $\langle R \rangle$ in the fuel material. Then we have:

$$P_{FO}(E) = \frac{\frac{1}{\langle R \rangle \Sigma_t^F(E)}}{1 + \frac{1}{\langle R \rangle \Sigma_t^F(E)}} = \frac{\Sigma_{esc}(E)}{\Sigma_{esc}(E) + \Sigma_t^F(E)} = \frac{1}{1 + \langle R \rangle \Sigma_t^F(E)}$$

$$= \frac{\frac{1}{\langle R \rangle}}{\frac{1}{\langle R \rangle} + \Sigma_t^F(E)} \Sigma_{exc} = \frac{1}{\langle R \rangle} \quad (7.83)$$

Note that Σ_{esc} in the rational approximation is not a function of energy. This is particularly convenient computationally and is what makes the rational approximation so useful. It gives quite good answers.

Remember that what we have developed is for a single fuel lump in a sea of moderator. Also, remember that we completely eliminated the dependence of the resonance integral on the outside moderator. When we consider a fuel pin array, these simplifying assumptions are no longer valid. Specifically we have to take into account the fact that a neutron can escape from one fuel element, escape from the outside moderator, and collide in a second fuel element. The correction for this effect is accomplished with the Dancoff factor. We modify our escape cross section to become:

$$\Sigma_{esc} = \frac{1 - c}{\langle R \rangle} \quad (7.84)$$

where c is called the Dancoff factor. There are a number of useful correlations for calculating the Dancoff factor, but the one most widely used appears to be attributed to Sauer. Sauer's approximation is given by:

$$c = \frac{e^{-\tau \Sigma_{sm} \langle l_m \rangle}}{1 + (1 - \tau) \Sigma_{sm} \langle l_m \rangle} \quad (7.85)$$

$$\langle l_m \rangle = \langle R \rangle * (V_M/V_F) = \langle R \rangle VR$$

Σ_{sm} = outside moderator total cross section

$\langle R \rangle$ = average chord length in the fuel

V_M = moderator volume fraction

V_F = fuel volume fraction

VR = Moderator to fuel volume ratio

τ for a square lattice of fuel pins similar to those in light water reactors:

$$\tau_{sq} = \frac{\sqrt{\frac{\pi}{4}(1 + VR)} - 1.0}{VR} - 0.08 \quad (7.86)$$

In addition, for a hex lattice like fast reactors:

$$\tau_{hex} = \frac{\sqrt{\frac{\pi}{\sqrt{12}}(1 + VR)} - 1.0}{VR} - 0.12 \quad (7.87)$$

Therefore, we can use the homogeneous formulas for the heterogeneous integrals if we calculate the β s as:

$$\text{Narrow resonance} \quad \beta = \frac{\frac{1-c}{\langle R \rangle} + \Sigma_{smf} + \Sigma_{pA}}{\Sigma_o} \quad (7.88)$$

$$\text{Wider resonance} \quad \beta = \frac{\frac{1-c}{\langle R \rangle} + \Sigma_{smf}}{\Sigma_o} \frac{\Gamma}{\Gamma_\gamma} \quad (7.89)$$

Problems

Problem 7.1 Explain how the temperature coefficient of reactivity is largely determined by the resonances in U^{238} .

Problem 7.2 Why does a PWR need to be refueled well before all the U^{235} in the fuel rod is used up?

Problem 7.3 The 129 keV gamma ray transitioning in Ir^{191} was used in a Mösbauer experiment in which a line shift equivalent to the full width at half maximum (Γ) was observed for a source speed of 1 cm/s. Estimate the value of Γ and the mean lifetime of the excited state in Ir^{191} .

Problem 7.4 An excited atom of total mass M at rest with respect to a certain inertial system emits a photon, thus going over into a lower state with an energy smaller by Δw . Calculate the frequency of the photon emitted.

Problem 7.5 Calculate the spread in energy of the 661 keV internal conversion line of Cs^{137} due to the thermal motion of the source. Assume that all atoms move with the root mean square velocity for a temperature of 15 °C.

Problem 7.6 Pound and Rebka at Harvard performed an experiment to verify the red shift predicted by general theory of relativity. The experiment consisted of the use of 14 keV γ -ray of Fe^{57} source placed on the top of a tower 22.6 meter high and the absorber at the bottom. The red shift was detected by the Mössbauer technique. What velocity of the absorber foil was required to compensate the red shift, and in which direction?

Problem 7.7 Obtain an expression for the Doppler line width for a spectral line of wavelength λ emitted by an atom of mass m at a temperature T .

Problem 7.8 For the $2\text{P}_{3/2} \rightarrow 2\text{S}_{1/2}$ transition of an alkali atom, sketch the splitting of the energy levels and the resulting Zeeman spectrum for atoms in a weak external magnetic field. (Express your results in terms of the frequency v_0 of the transition, in the absence of an applied magnetic field.)

$$\left\{ \text{The Lande g-factor is given by } g = 1 + \frac{j(j+1) + s(s+1) - l(l+1)}{2j(j+1)} \right\}$$

Problem 7.9 The spacings of adjacent energy levels of increasing energy in a calcium triplet are 30×10^{-4} and 60×10^{-4} eV. What are the quantum numbers of the three levels? Write down the levels using the appropriate spectroscopic notation.

Problem 7.10 An atomic transition line with wavelength 350 nm is observed to be split into three components, in a spectrum of light from a sunspot. Adjacent components are separated by 1.7 pm. Determine the strength of the magnetic field in the sunspot. $\mu_B = 9.17 \times 10^{-24} \text{ J T}^{-1}$.

Problem 7.11 Calculate the energy spacing between the components of the ground-state energy level of hydrogen when split by a magnetic field of 1.0 T. What frequency of electromagnetic radiation could cause a transition between these levels? What is the specific name given to this effect?

Problem 7.12 Consider the transition $2\text{P}_{1/2} \rightarrow 2\text{S}_{1/2}$, for sodium in the magnetic field of 1.0 T, given that the energy splitting $\Delta E = g\mu_B B m_j$, where μ_B is the Bohr magneton. Draw the sketch.

Problem 7.13 Find the Doppler shift in wavelength of H line at $6563 \text{ } ^0\text{A}$ emitted by a star receding with a relative velocity of $3 \times 10^6 \text{ ms}^{-1}$.

Problem 7.14 Show that for slow speeds, the Doppler shift can be approximated as $(\Delta\lambda/\lambda) = (v/c)$ where $\Delta\lambda$ is the change in wavelength.

Problem 7.15 A physicist was arrested for going over the railway level crossing on a motorcycle when the lights were red. When he was produced before the magistrate,

the physicist declared that he was not guilty as red lights ($\lambda = 670$ nm) appeared green ($\lambda = 525$ nm) due to Doppler effect. At what speed was he traveling for the explanation to be valid? Do you think such a speed is feasible?

Problem 7.16 Find the wavelength shift in the Doppler effect for the sodium line 589 nm emitted by a source moving in a circle with a constant speed $0.05 c$ observed by a person fixed at the center of the circle.

Problem 7.17 A π -meson with a kinetic energy of 140 MeV decays in flight into μ -meson and a neutrino. Calculate the maximum energy, which:

- (a) The μ -meson.
- (b) The neutrino may have in the laboratory system.

(Mass of π -meson = 140 MeV/c 2 , mass of μ -meson = 106 MeV/c, mass of neutrino = 0). Assume $T_\mu^* = 4.0$ MeV.

Problem 7.18 A linear accelerator produces a beam of excited carbon atoms of kinetic energy of 120 MeV. Light emitted on de-excitation is viewed at right angles to the beam and has a wavelength λ' . If λ is the wavelength emitted by a stationary atom, what is the value of $(\lambda' - \lambda)/\lambda$? (Take the rest energies of both protons and neutrons to be 10^9 eV.)

Problem 7.19 A certain spectral line of a star has natural frequency of 5×10^{17} c/s. If the star is approaching the earth at 300 km/s, what would be the fractional change of frequency?

Problem 7.20 Show that deuteron energy E has twice the range of proton of energy $E/2$.

Problem 7.21 If the mean range of 10 MeV protons in lead is 0.316 mm, calculate the mean range of 20 MeV deuterons and 40 MeV α -particles.

Problem 7.22 Show that the range of α -particles and protons of energy 1–10 MeV in aluminum is 1/1600 of the range in air at 15 °C, 760 mm of Hg. *Hint:* Apply the Bragg-Kleeman formula from your modern physics book.

Problem 7.23 Show that except for small ranges, the straggling of a beam of He 3 particles is greater than that of a beam of He 4 particles of equal range.

Problem 7.24 The range of a 15 MeV proton is 1100 μm in nuclear emulsions. A second particle whose initial ionization is the same as the initial ionization of proton has a range of 165 μm . What is the mass of the particle? (The rate at which a singly ionized particle loses energy E by ionization along its range is given by $dE/dR = K/(\beta c)^2$ MeV μm where βc is the velocity of the particle and K is a constant depending only on emulsion; the mass of proton is 1837 mass of electron.)

Problem 7.25

- (a) Show that the specific ionization of 480 MeV α -particle is approximately equal to that of 30 MeV proton.

- (b) Show that the rate of change of ionization with distance is different for the two particles, and indicate how this might be used to identify one particle, assuming the identity of the other is known.

Problem 7.26 Calculate the 6.67 eV resonance integral for U^{238} in a typical PWR. Compare the actual resonance integral with its infinite dilute value.

Fuel	Moderator	Resonance
$UO_2 = 3\% \text{ enriched}$	Water	$E_R = 6.67 \text{ eV}$
$N^{UO}_2 = 0.0223 \text{ Mol/barn/cm}$	$N^{H_2O} = 0.0335 \text{ Mol/barn/cm}$	$\sigma_0 = 216,000 \text{ barns}$
$\sigma_s^O = 4.2 \text{ barns/atom}$	$\sigma_s^H = 20.2 \text{ barns/atom}$	$\Gamma_r = 0.0275 \text{ eV}$
$\sigma_p^U = 8.3 \text{ barns/atom}$	Volume fraction = 0.55	$\Gamma_\gamma = 0.026 \text{ eV}$
$\langle R \rangle = 0.94 \text{ cm}$	Square lattice	$\Gamma_n = 0.0015 \text{ eV}$
Volume fraction = 0.45	$T_{\text{fuel}} = 600 \text{ K}$	

References

1. Y. Oka, T. Kiguchi, *Nuclear Reactor Design (An Advanced Course in Nuclear Engineering)*, Springer Publishing Company, June 2014
2. J. Duderstadt, L. Hamilton, *Nuclear Reactor Analysis* (John Wiley Publishing Company, New York, NY, 1976)
3. <http://www.nuclear-power.net/nuclear-power/reactor-physics/nuclear-engineering-fundamentals/neutron-nuclear-reactions/compound-nucleus-reactions/what-is-nuclear-resonance-compound-nucleus/>
4. <http://www.nuclear-power.net/glossary/doppler-broadening/#prettyPhoto>
5. H.A. Bethe, G. Placzek, Resonance effects in nuclear processes. *Phys. Rev.* **51**, 450 (1937)
6. J.R. Lamarsh, *Introduction to Nuclear Reactor Theory* (Addison Wesley Publishing Company, Inc, New York, NY, 1966)
7. A. Alpan, L.C. Leal, A. Courcelle, Effect of Energy Self-Shielding Methods on U^{238} for Criticality Safety, PHYSOR 2004 – The Physics of Fuel Cycles and Advanced Nuclear Systems: Global Developments Chicago, Illinois, April 25–29, 2004, on CD-ROM, American Nuclear Society, Lagrange Park, IL (2004)

Chapter 8

Heterogeneous Reactors and Wigner-Seitz Cells



When deterministic neutron transport methods are applied to lattice or whole-core problems, the multi-group approximation is usually applied to the cross-sectional treatment for the energy domain. Due to the complicated energy behavior of resonance cross sections, the weighting spectrum for collapsing multi-group cross sections is very dependent on energy and space, which becomes a crucial challenge when analyzing a lattice or full-core configuration.

8.1 Homogeneous and Heterogeneous Reactors

So far, all of our analyses are assumed based on homogeneous-type reactors, where fuel and moderator are combined in their design and consequently their structure, yet in real world of commercial reactors, very few reactors are of this type. However, in most reactors, the fuel is speared out in some kind of structural material to form *solid fuel elements*, which are usually in a uniform lattice configuration. At this stage, it is important for us recognize and distinguish these two types of reactors and understand the difference between them.

If a reactor core consists of fuel, moderator, coolant, and structural materials that were assumed to be combined and homogeneously mixed, where the neutron mean free path at *all* energies is large compared with thickness of the fuel element, the reactor is called *quasi-homogeneous* or ultimately *homogeneous reactor*.

On the other hand, if the reactor is structurally constructed to facilitate thermal design such as:

1. Coolant channel, heat transfer surfaces (i.e., thermal hydraulic analysis of reactor design) [1]
2. Integrity of core structure such as fuel fabrication
3. Reactivity control such as control rods, burnable poisons, etc. where also the mean free path of neutrons at *any* energy is comparable to, or less than, the thickness of

a fuel element, then the reactor is said to be *heterogeneous* type. The analysis of this type of reactor is not easy as what have been dealt with so far and rather is a very complicated problem from neutronic analysis point of view.

A typical commercial heterogeneous reactor is pressurized water reactor (PWR) as it is shown in Fig. 8.1 with its fuel assembly depicted in Fig. 8.2. As it can be seen

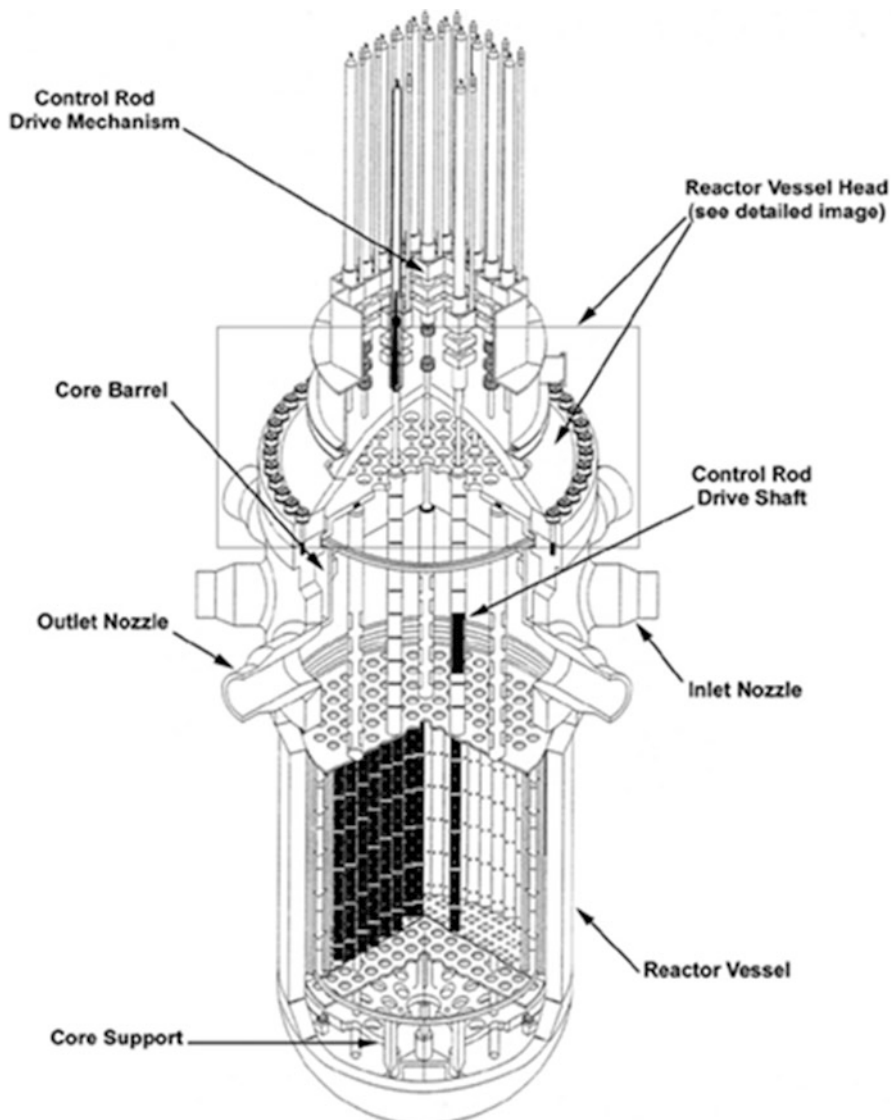


Fig. 8.1 A typical pressurized water reactor. (Courtesy of US Nuclear Regulatory Commission (NRC))

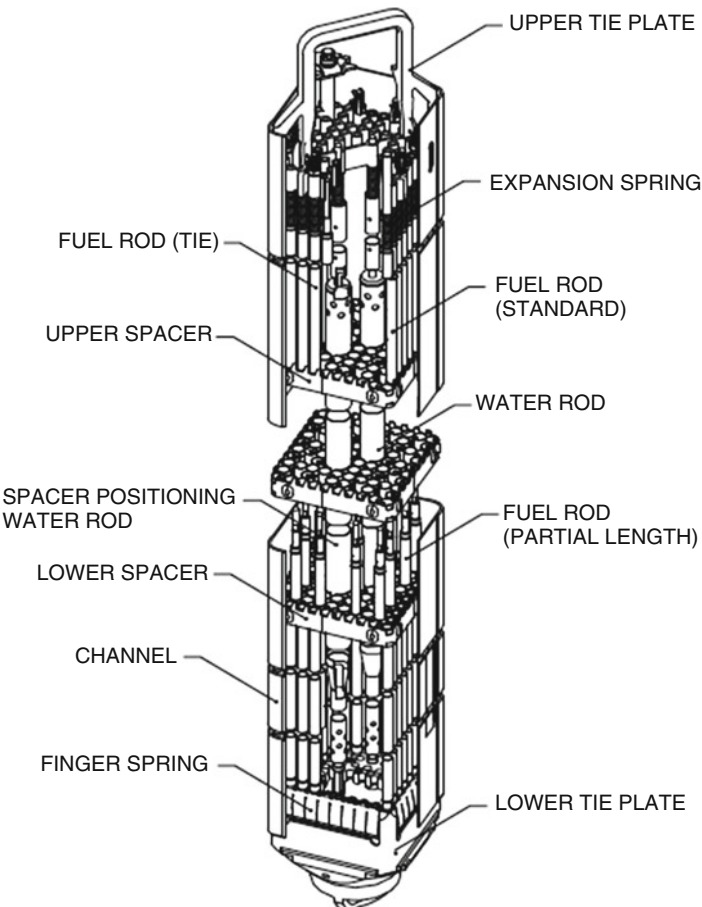


Fig. 8.2 Fuel element and fuel assembly. (Courtesy of US Nuclear Regulatory Commission (NRC))

in these pictures, heterogeneities in the reactor fuel array or *lattice* must be taken into consideration in the design of nuclear fission reactor, because they will cause a local spatial variation in the neutron flux, which may have strong influence for core multiplication. The degree of consideration for core lattice effect in reactor design depends on the characteristic dimension of lattice structure, such as fuel pin diameter or the spacing between fuel elements, which may be compared to the mean free path of neutron in the core that is typically in order of centimeter.

Typically, light water reactor (LWR) designs can be used as an example, where the core lattice dependency of thermal neutrons have centimeter order of mean free path within the core of reactor, compared to the fuel pin diameter. Therefore, the flux distribution in the fuel might be expected to be different from that in the moderator or coolant channel. Hence, the details of heterogeneity analysis may apply, and it is

necessary to find the number of the fuel elements or the concentration of fuel configuration of them for the purpose of criticality versus the fuel concentration in the moderator, as it is for the case of homogeneous reactor design. In books by Duderstadt and Hamilton [2] as well as Lamarsh [3], one can find more details for mathematical analysis approach of such conditions, where we encourage the readers to refer to them.

Now that we have covered the basic differences between these two fission reactors, i.e., homogeneous and heterogeneous, we can continue with our subject of spectrum calculation in heterogeneous-type reactor and move on to the cross-sectional self-shielding as well as Wigner-Seitz cells in the next few sections of this chapter.

8.2 Spectrum Calculation in Heterogeneous Reactors

Before we launch into this subject, “it is convenient to divide the fuel-moderator lattice into *unit cells*, each containing one fuel lump at its center” [3] where two most commonly used lattice and the unit cells are depicted in Fig. 8.3. Note that since all the cells are identical in an infinite uniform lattice, there is no net flow of neutrons from one cell to the next one and due to this argument, *the current density is zero along the boundary of each cell*. Thus, for purpose of the flux calculation within the cell, we need to replace the actual lattice cell by a cell having a more simple geometry, such as fuel lump sum in shape of cylinder. The actual cell then is replaced by a cylindrical cell of the *same volume* as in Fig. 8.3. Since there is no flow of thermal neutrons from one cell to another, the thermal neutron current density may consider being zero on the surface of the equivalent cell from our knowledge of electromagnetic science. This consideration, where we use an equivalent cell with a zero-current boundary condition, is known as the *Wigner-Seitz method*, which is the discussion in the following sections of this chapter.

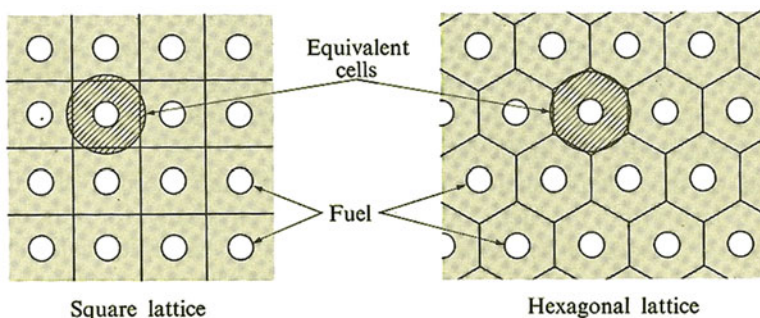


Fig. 8.3 Two typical heterogeneous lattices and equivalent cells for each [2]

So far, for any treatment of spectrum analysis, we have only paid attention on homogeneous-type fission reactors and for all practical purposes; we are encountering fission reactor systems that are containing various levels of heterogeneity. The entire commercial nuclear power fission reactors consist of at least two regions, namely, *core* and *reflector*. For design purposes in terms of power shaping, the core is normally configured either radially or axially, and they are subdivided into different composition regions. Usually a spectrum calculation needs to be done independent of these regions for each reactor. In order to achieve such calculation, we couple these regions using energy-dependent bucklings, obtained from a few group two- or three-dimensional calculations over the complete reactor shape and requires iteration analysis as necessary. For purpose of this iteration approach, one needs to guess the buckling for the first round spectrum calculations, and it can be performed by producing condensed few-group constants for two- or three-dimensional calculations, out of which new energy-dependent buckling are yielding for each region. This process of iteration continues until the desired accuracy is achieved, and then the second level of heterogeneity analysis will take place by the fine structure of the reactor cells [4].

Note that heterogeneity effect in fuel structure cannot be neglected, even for high-temperature reactors (HTRs) that are homogeneous-type fission reactors compared with many other reactors. As we have mentioned above, all reactors consist of regular lattices of cells containing fuel pins, coolant channels, moderator, and absorbers as schematically are shown in Figs. 8.1 and 8.2.

For purpose of spectrum calculations, we need to choose between either a multi-group space-dependent transport treatment or an analysis over a homogenized cell. Today's computer code that commercially available to us and we have examined so far follow the second procedure.

Once the fine structure of the flux within the cell is becoming obvious, then the homogenization can be performed multiplying the cross sections by energy-dependent self-shielding, which is also called disadvantage factors. We can represent this self-shielding as $S_k(E)$ that is defined for each material k in such a way as to yield the same reaction rate in the homogenized calculation as in the real cell. However, as we have learned in neutronic analysis of reactor so far, the homogenized calculation deals only with a reference flux $\phi_R(E)$, yet in real analysis, the reference flux depends on the position within cell and thus can be symbolized as $\phi_R(\vec{r}, E)$.

If we take the reference flux $\phi_R(E)$ at any point of the cell, let us say at its center, or at the boundary of interest, or an average value, then we can write the following relation as:

$$\phi_R(E) = \frac{\int \phi_R(\vec{r}, E) d\vec{r}}{V} \quad (8.1)$$

where V is the cell volume and the integral is taken over the whole cell. The spectrum, which resulted from the flux calculation, depends, of course, on the reference, which has been chosen, although reaction rates and reactivity are independent of this reference.

Now if we define the average concentration of isotope k using symbol of $\bar{N}_k(\vec{r})$, which is space-dependent and written as:

$$\bar{N}_k(\vec{r}) = \frac{\int N_k(\vec{r}) d\vec{r}}{V} \quad (8.2)$$

Then, to obtain the proper reaction rates, the self-shielding $S_k(E)$ must satisfy the following equation:

$$\sigma_k \bar{N}_k(\vec{r}) \phi_R(E) = \frac{1}{V} \int \sigma_k N_k(\vec{r}) \phi_R(\vec{r}, E) d\vec{r} \quad (8.3)$$

where σ_k is the cross section of isotope k .

The self-shielding then has to be defined as follows:

$$S_k = \frac{\int N_k(\vec{r}) \phi_R(\vec{r}, E) d\vec{r}}{V \bar{N}_k(\vec{r}) \phi_R(E)} = \frac{\int N_k(\vec{r}) \phi_R(\vec{r}, E) d\vec{r}}{\phi_R(E) \int N_k(\vec{r}) d\vec{r}} \quad (8.4)$$

The cross section of each material must be multiplied by its self-shielding. In most cases, the average cell flux is used as ϕ_R , which may give rise to some difficulty in imposing boundary conditions, so that sometimes the flux at the outer cell boundary is used as reference. A homogenization by means of self-shieldings as in the case of cell calculation is very possible. In the case of resonance absorption, this gain structure can become very important [4].

8.3 Cross-Sectional Self-Shielding and Wigner-Seitz Cells

The Wigner-Seitz cell, named after Eugene Wigner and Frederick Seitz, is a type of Voronoi cell used in the study of crystalline material in solid-state physics. A Wigner-Seitz cell is an example of another kind of primitive cell. The primitive unit cell (or simply primitive cell) is a special case of unit cell, which has only one lattice point combined and shared by eight other primitive cells. It is the most “primitive” cell one can construct, and it is a parallelepiped. The general unit cell has an integral number of lattice points. The simple cubic lattice is the only primitive unit cell conventionally. The body-centered cubic (BCC) and face-centered cubic (FCC) lattices are simply unit cells, not primitive cells.

Consider a typical PWR core that contains between 51,000 and 57,000 fuel elements or a boiling water reactor (BWR) core that contains around 46,000 fuel elements. In order to calculate the critical size, control rod positions, poison concentration, and fuel burnup, it is important to get the reaction rates correct in each

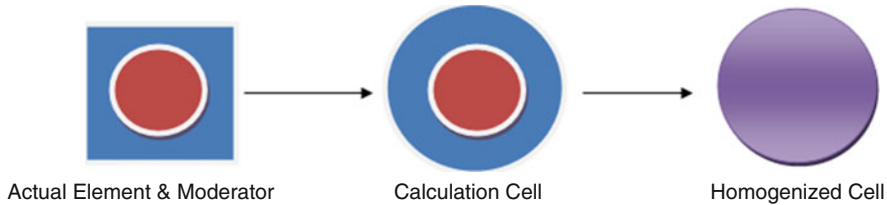


Fig. 8.4 Typical cell sequence

fuel element. It is virtually impossible to run a 3-D calculation that places enough mesh points in each fuel element to get the detailed neutron flux very accurately. So some form of homogenization of fuel elements is required to get average cross sections for fuel assemblies (typical 17×17 elements in a PWR and 8×8 in a BWR). Since most fuel assemblies are repeating arrays, the standard approach is to consider one fuel element and its associated moderator as a cell and calculate average cross sections for the cell. A typical sequence is described below (Fig. 8.4):

The square cell (or hexagonal cell) is converted to a cylindrical cell for a 1-D calculation conserving the volumes of the fuel and moderator regions. It is possible to do a 2-D calculation for the square cell, but the utility of this is negligible for most reactors that have been designed to date. A k-effective (k_{∞}) calculation is performed for the cylindrical cell with enough leakage to get a near critical system. Then the cross sections are homogenized to get values as if all of the materials in the fuel element and moderator were smeared out across the cell. The obvious thing that must be accomplished here is that in the smeared cell, we must have the same number of atoms of each nuclide as we have in the actual element and moderator. The conservation of atoms relationship gives us:

$$\int_{\text{cell}} N_{\text{cell}} \sigma_x^{\text{cell}} dV_{\text{cell}} = \int_{FE} N_{FE} \sigma_x^{FE} dV_{FE} \quad (8.5)$$

In addition, assuming a constant cross section as always, this gives:

$$N_{\text{cell}} = (V_{FE}/V_{\text{cell}}) * N_{FE} \quad (8.6)$$

However, we not only want to conserve atoms, but we want to conserve reaction rates. If we were only conserving atoms, we would not need to do a cell calculation to get the relative fluxes in the cell. So in order to conserve reaction rates, we have:

$$\int_{\text{cell}} N_{\text{cell}} \sigma_x^{\text{cell}} \phi_{\text{cell}}(V) dV_{\text{cell}} = \int_{FE} N_{FE} \sigma_x^{FE} \phi_{FE}(V) dV_{FE} \quad (8.7)$$

Now assuming the number density and cross sections are constant as always, this gives:

$$N_{\text{cell}} \sigma_x^{\text{cell}} \int_{\text{cell}} \phi_{\text{cell}}(V) dV_{\text{cell}} = N_{FE} \sigma_x^{FE} \int_{FE} \phi_{FE}(V) dV_{FE} \quad (8.8)$$

which can be written as:

$$N_{\text{cell}} \sigma_x^{\text{cell}} \bar{\phi}_{\text{cell}} V_{\text{cell}} = N_{\text{FE}} \sigma_x^{\text{FE}} \bar{\phi}_{\text{FE}} V_{\text{FE}} \quad (8.9)$$

Then to conserve atoms, we have:

$$N_{\text{cell}} = (V_{\text{FE}}/V_{\text{cell}}) * N_{\text{FE}} \quad (8.10)$$

So we must have:

$$\sigma_x^{\text{cell}} = (\bar{\phi}_{\text{FE}}/\bar{\phi}_{\text{cell}}) \sigma_x^{\text{FE}} \quad (8.11)$$

in order to conserve reaction rates. Thus when we homogenize the cell, we have to modify the cross sections with what are called *flux disadvantage factors* or *self-shielding factors*. They are the ratio of the average flux in the region the material of interest is in to the average flux for the whole cell.

The term *self-shielding factor* is more appropriate because it is the average flux in the region under consideration divided by the cell average flux. This ratio could be greater or less than 1.0 depending on many things. The term *disadvantage factor* came from the fact that it is usually less than 1.0 for the thermal flux in a thermal reactor. The concept was first applied to only the thermal flux in the fuel element, but as time went on, it became obvious that all cross sections no matter what material they are in could merit from this approach. So typically the moderator cross sections in the thermal region are weighted with a *flux disadvantage factor* that is greater than 1.0. This tends not to be a very big deal because scattering reactions in the moderator do not affect criticality or burnup very significantly. Of course, when a burnable poison is added to the coolant, the situation changes, and *self-shielding factors* must be applied to all materials in all energy ranges. Typically, cell codes used to homogenize cells do this automatically.

It is important to realize that a Wigner-Seitz cell, as they are called, does not have to consist of just fuel and moderator. Any other material that is in the repeating array can be put in the cell and self-shielding factors calculated for its cross sections. However, there are other problems. Some fuel element positions have the fuel element replaced with an instrumentation thimble or a control rod. There are also fuel assembly cans and coolant channels between fuel assemblies that have nuclides in the core, but not in our repeating array cell. We could do a separate cell calculation for these positions, except they do not contain fissile materials so we could not find a k-effective (k_{∞}). Normally what is done is that instrumentation materials, control materials, assembly structure, and inter-assembly materials are added as an outer layer on our cylindrical cell calculation and we calculate self-shielding factors for them in that position. It is also possible that we could take the homogenized cross sections from the fuel element calculation and build another larger cell, nominally two dimensional, which had the additional materials in their correct positions and do a second homogenization calculation. This is normally not worth the effort.

Problems

Problem 8.1 Cadmium has a resonance for neutrons of energy 0.178 eV, and the peak value of the total cross section is about 7000 b. Estimate the contribution of scattering to this resonance.

Problem 8.2 A nucleus has a neutron resonance at 65 eV and no other resonances nearby. For this resonance, $\Gamma_n = 4.2$ eV, $\Gamma_\gamma = 1.3$ eV, and $\Gamma_\alpha = 2.7$ eV, and all other partial widths are negligible. Find the cross section for (n, γ) and (n, α) reactions at 70 eV.

Problem 8.3 Neutrons incident on a heavy nucleus with spin $JN = 0$ show a resonance at an incident energy $E_R = 250$ eV in the total cross section with a peak magnitude of 1300 barns, the observed width of the peak being $\Gamma = 20$ eV. Find the elastic partial width of the resonance.

Problem 8.4 The diffusion length of beryllium metal is determined by measuring the flux distribution in an assembly $100\text{ cm} \times 100\text{ cm} \times 65\text{ cm}$ high, at the base of which is a plane source of thermal neutrons. The corrected saturation activities in counts per minute of foils located at various vertical distances above the base are given in the table below. Similar measurements in a horizontal direction gave a value of 2.5 cm as the extrapolation distance, i.e., the distance from the assembly at which the neutron flux extrapolated to zero. Using the figure below, what would be the diffusion length of thermal neutron in beryllium? (Fig. 8.5)

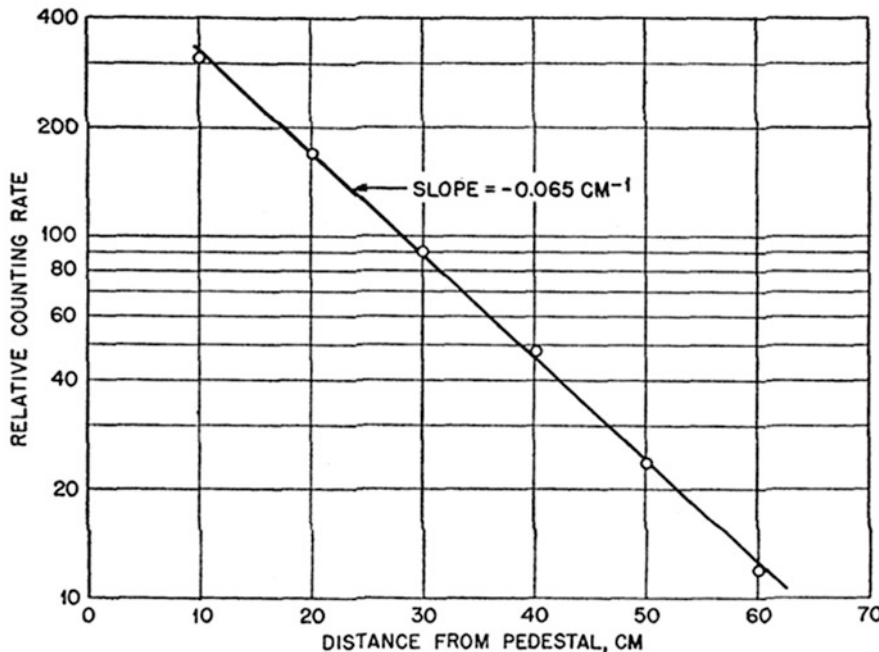


Fig. 8.5 Data for evaluation of diffusion length of beryllium

Vertical distance (z cm)		Saturation activity (c/m)
10	310
20	170
30	90
40	48
50	24
60	12

Problem 8.5 A reactor core contains enriched uranium as fuel and beryllium oxide as moderator ($\Sigma_s = 0.64 \text{ cm}^{-1}$ and $\xi = 0.17$ at a neutron energy of 7 eV). The thermal neutron flux is $2 \times 10^{12} \text{ neutrons}/(\text{cm}^2 \text{ s})$, and Σ_a for these neutrons in the fuel is 0.005 cm^{-1} ; for each thermal neutron absorbed, 1.7 fission neutrons are produced. Neglecting all absorption during slowing down, estimate the epithermal neutron flux at 7 eV per unit *lethargy* interval. Hint: Use Eq. 3.75 that is given in Chap. 3 for *lethargy* or the so-called logarithmic energy decrement as well.

Problem 8.6 An experiment was performed to measure the Fermi age of fission neutrons slowing down to indium resonance in an assembly of beryllium oxide blocks, using a fission plate as the neutron source. The corrected indium foil saturation activities, normalized to 1000 at the source plate, are given in the table below. Using Eq. (a) below for the age of neutron of specified energy in a given medium, determine the neutron age at the indium resonance energy.

Distance from fission plate (r cm)	Relative activity (A_0)	$A_0 r^2$	$A_0 r^4$
0	1000	—	—
4.0	954	1.53×10^4	2.44×10^5
7.9	828	5.16×10^4	5.16×10^5
11.7	660	9.04×10^4	1.24×10^7
19.35	303	1.13×10^5	5.59×10^7
27.15	103	7.59×10^4	4.24×10^7
34.5	29.3	3.55×10^4	4.3×10^7
42.7	7.2	1.31×10^4	2.4×10^7
50.5	1.6	4.08×10^3	1.04×10^7
62.2	0.45	1.74×10^3	6.7×10^6
77.8	0.15	9.08×10^2	5.5×10^6

Problem 8.7 A reactor consists of natural uranium rods of 1 inch diameter, arranged in a square lattice with a pitch of 6 inches in heavy water. If the thermal utilization f is given by the following equation:

$$\frac{1}{f} = 1 + \left(\frac{V_1 \Sigma_{a1}}{V_0 \Sigma_{a0}} \right) F + (E - 1)$$

where F and E for a cylindrical fuel rod are given as follows:

$$F = \frac{\kappa_0 r_0}{2} \cdot \frac{I_0(\kappa_0 r_0)}{I_1(\kappa_0 r_0)}$$

and

$$E = \frac{\kappa_1 (r_1^2 - r_0^2)}{2r_0} \left[\frac{I_0(\kappa_1 r_0)K_1(\kappa_1 r_1) + K_0(\kappa_1 r_0)I_1(\kappa_1 r_1)}{I_1(\kappa_1 r_1)K_1(\kappa_1 r_0) - K_1(\kappa_1 r_1)I_1(\kappa_1 r_0)} \right]$$

I_0 and K_0 are being zero-order modified Bessel functions of first and second kinds, respectively, and I_1 and K_1 are the corresponding first-order function.

Note: The modified Bessel functions may be expanded in series form for cases where the ratio of moderator to fuel is fairly high and absorption in the fuel is weak. When $\kappa_0 r_0$ is less than 1 and $\kappa_1 r_1$ is less than 0.75, the results may be approximated to give the following results [5]:

$$F \approx 1 + \frac{(\kappa_0 r_0)^2}{8} - \frac{(\kappa_0 r_0)^4}{192}$$

and

$$E \approx 1 + \frac{(\kappa_1 r_1)^2}{2} \left[\frac{r_1^2}{r_1^2 - r_0^2} \ln \frac{r_1}{r_0} + \frac{1}{4} \left(\frac{r_0}{r_1} \right)^2 - \frac{3}{4} \right]$$

Then calculate the thermal utilization for this lattice. The diffusion length of thermal neutron in natural uranium metal is 1.55 cm; the effective macroscopic absorption cross section is 0.314 cm^{-1} .

Problem 8.8 Calculate the resonance escape probability for the natural uranium-heavy water lattice in Problem 8.7. Use the following table of data as well (Table 8.1):

Table 8.1 Resonance neutron data for moderators

Moderator	$\kappa_1 \text{ cm}^{-1}$
Water	0.885
Heavy	0.22
Beryllium	0.325
Beryllium oxide	0.19
Graphite	0.145

References

1. B. Zohuri, N. Fathi, *Thermal-Hydraulic Analysis of Nuclear Reactors*, 1st edn. (Springer, New York, 2015)
2. J.J. Duderstadt, L.J. Hamilton, *Nuclear Reactor Analysis* (Wiley, New York, 1976)
3. J.R. Lamarsh, *Introduction to Nuclear Reactor Theory* (Addison-Wesley, Reading, 1966)
4. L. Massimo, *Physics of High-Temperature Reactors*, 1st edn. (Pergamon, Oxford, 2013)
5. A.M. Weinberg, E.P. Wigner, *The Physical Theory of Neutron Chain Reactors* (University of Chicago Press, Chicago, 1958), p. 635

Chapter 9

Thermal Spectra and Thermal Cross Sections



Although accurate determination of the thermal spectrum also requires advanced computational methods, averages over simplified spectra often serve as a reasonable first approximation in performing rudimentary reactor calculations. The main aspect of nuclear reactor analysis, as we have learned so far, is a multi-group diffusion theory. In previous chapters, we developed the general form of multi-group diffusion equations and recommended a strategy for their solution. However, these set of equations contained various parameters known as group constants formally defined as average over the energy-dependent intergroup fluxed which must be determined before these equations play a formal important roles. In this chapter, we introduce the calculation of neutron energy spectrum characterizing fast neutrons, and as result, the calculation of *fast neutron spectra* as well as generation of *fast group constants* will be of concern. At the conclusion, we will deal with the development of the theory of neutron slowing down and resonance absorption.

9.1 Coupling to Higher-Energy Sources

In order to generate group constants for the thermal neutron groups, it is necessary to calculate detailed thermal neutron spectra. However due to the fact that thermal neutron mean free paths are small, the heterogeneities that are present in typical thermal reactor cores are very significant and must be included in any reactor design calculation. Since we have not talked about heterogeneities yet, we will only treat thermal spectra in a very simplified form. Later in the section on generating cell cross sections, we will deal with the problem directly and calculate thermal group constants. The treatment we will apply here only applies to homogeneous thermal reactors like the AGN-201 reactor. Let us begin with the equation in an infinite medium. The P_0 equation for an energy E in the thermal range can be written as:

$$\Sigma_t(E)\phi_0(E) = \int_0^{E_{th}} \Sigma_{s0}(E' \rightarrow E)\phi_0(E')dE' + S(E) \quad (9.1)$$

Equation 9.1 is a significantly reduced version of transport equation that is written in form of an *integral equation* in the single variable E , which will refer to as the *infinite medium spectrum equation*. Note that the abbreviation of th stands for thermal in all equations below.

Note that both downscattering and upscattering must be included. Now if we write

$$\Sigma_a(E)\phi_0(E) + \Sigma_s(E)\phi_0(E) = \int_0^{E_{th}} \Sigma_{s0}(E' \rightarrow E)\phi_0(E')dE' + S(E) \quad (9.2)$$

and integrate the P_0 equation over the thermal energy range, we will have:

$$\begin{aligned} \int_0^{E_{th}} \Sigma_a(E)\phi_0(E)dE + \int_0^{E_{th}} \Sigma_a(E)\phi_0(E)dE &= \int_0^{E_{th}} \int_0^{E_{th}} \Sigma_{s0}(E' \rightarrow E)\phi_0(E')dEdE' \\ &+ \int_0^{E_{th}} S(E)dE \end{aligned} \quad (9.3)$$

But noting that for thermal neutrons, the order of integral can be interchanged, therefore, we can write the following result:

$$\Sigma_s(E') = \int_0^{E_{th}} \Sigma_{s0}(E' \rightarrow E)dE \quad (9.4)$$

The two scattering terms will cancel and we obtain:

$$\int_0^{E_{th}} \Sigma_a(E)\phi(E)dE = \int_0^{E_{th}} S(E)dE \quad (9.5)$$

Or we arrive at the balance equation that:

THERMAL ABSORPTIONS=THERMAL SOURCES

If we now consider a finite homogeneous medium and make the diffusion approximation for the fundamental mode, we have:

$$\begin{aligned} D(E)B^2\phi(E) + \Sigma_a(E)\phi(E) + \Sigma_s(E)\phi(E) &= \int_0^{E_{th}} \Sigma_s(E' \rightarrow E)\phi_0(E')dE' \\ &+ S(E) \end{aligned} \quad (9.6)$$

Integrating this equation over all energy and making the same order of integration change for the scattering integral on the right-hand side, we will have:

$$B^2 \int_0^{E_{th}} D(E) \phi(E) dE + \int_0^{E_{th}} \Sigma_a(E) \phi(E) dE = \int_0^{E_{th}} S(E) dE \quad (9.7)$$

or, we can state that:

**THERMAL LEAKAGE + THERMAL ABSORPTIONS
= THERMAL SOURCES**

Now let us consider how one would determine the source for an infinite medium calculation. We begin by noting that the flux in the slowing down region above thermal has its asymptotic shape:

$$\phi(E) = \frac{Q_0}{E \xi \Sigma_s(E)} \quad (9.8)$$

where we can take the source, Q_0 , equal to 1.0 without loss of generality. Then we can treat the slowing down flux as producing our source by writing the P_0 equation as:

$$\begin{aligned} \{\Sigma_a(E) + \Sigma_s(E)\} \phi(E) &= \int_0^{E_{th}} \Sigma_s(E' \rightarrow E) \phi_0(E') dE' \\ &+ \int_{E_{th}}^{E/\alpha} \frac{\Sigma_s(E')}{(1-\alpha)E'} \frac{1}{E \xi \Sigma_s(E)} dE' \end{aligned} \quad (9.9)$$

or, we have:

$$\begin{aligned} S(E) &= \int_{E_{th}}^{E/\alpha} \frac{\Sigma_s(E')}{(1-\alpha)E'} \frac{1}{E \xi \Sigma_s(E)} dE' \\ &= \frac{1}{\xi} \int_{E_{th}}^{E/\alpha} \frac{dE'}{(1-\alpha)E'^2} \end{aligned} \quad (9.10)$$

This gives:

$$\begin{aligned} S(E) &= \frac{1}{\xi(1-\alpha)} \left\{ \frac{1}{E_{th}} - \frac{\alpha}{E} \right\} & \text{for } E \geq \alpha E_{th} \\ S(E) &= 0 & \text{for } E < \alpha E_{th} \end{aligned} \quad (9.11)$$

The total source to the thermal range is given by:

$$\int_0^{E_{th}} S(E) dE = \frac{1}{\xi(1-\alpha)} \int_0^{E_{th}} \left(\frac{1}{E_{th}} - \frac{\alpha}{E} \right) dE = \frac{1}{\xi(1-\alpha)} [1 - \alpha + \alpha \ln \alpha] \quad (9.12)$$

or, we have:

$$\int_0^{E_m} S(E)dE = \frac{1}{\xi} \left(1 + \frac{\alpha}{1-\alpha} \ln \alpha \right) = 1.0 \quad (9.13)$$

as required to meet the normalization we established when we let $Q_0 = 1.0$.

Note that so far we have not been able to say anything about the energy dependence of the flux in the thermal range. To do this we will begin with a very simplified model and assume the following:

1. Infinite medium – no leakage.
2. No absorption.
3. No sources or slowing down.

Under these assumptions, the principle of detailed balance must hold. This principle states that:

$$\Sigma_s(E' \rightarrow E)\phi(E')dE' = \Sigma_s(E \rightarrow E')\phi(E)dE \quad (9.14)$$

Basically it states that at equilibrium, the number of neutrons scattering from energy (E') to energy E must exactly equal the number scattering from energy E to energy (E') . If this were not true, neutrons would continue to build up at one energy, which must be impossible. Under this restriction, we essentially have two nuclear species in equilibrium with each other. If we treat the neutrons as a high-temperature monatomic gas, the distribution of neutron energies assumes the form of a Maxwell-Boltzmann distribution. This is of the form:

$$\phi(E) = \phi_{MB}(E) = v n_0 M(E) = \frac{2\pi n_0}{(\pi K T)^{3/2}} \left(\frac{2}{m} \right)^{1/2} E e^{-E/KT} \quad (9.15)$$

where:

n_0 is the number of thermal neutrons per cm³.

T is the media temperature in degrees Kelvin.

K is the Maxwell-Boltzmann constant.

m is the mass of the neutron.

E is the neutron energy.

Thus, as our thermal spectrum, we can use the Maxwell-Boltzmann distribution, and temperature T is Kelvin:

$$\phi_{MB}(E) = \frac{2\pi n_0}{(\pi K T)^{3/2}} \left(\frac{2}{m} \right)^{1/2} E e^{-E/KT} \quad (9.16)$$

This distribution is characterized by a:

Most probable energy:

$$\phi_{MB}(E) = KT = \frac{T}{11600} \text{ eV} \quad (9.17)$$

Most probable speed:

$$V_0 = \sqrt{\frac{2KT}{m}} = 1.28 \times 10^4 \sqrt{T} \text{ cm/sec} \quad (9.18)$$

Note also that $T = 293 \text{ K} = 20 \text{ }^{\circ}\text{C}$, $E_T = 0.0253 \text{ eV}$, and $V_T = 2200 \text{ m/s}$. As this temperature is fairly easily obtainable around the world, typical parameters are evaluated at it or referenced to it. In particular, consider the common $1/v$ thermal absorption cross section. It can be expressed in the form:

$$\sigma_a(E) = \frac{\sigma_a(E_0)v_0}{v} \begin{cases} E_0 = 0.0253 \text{ eV} \\ v_0 = 2200 \text{ cm/sec} \end{cases} \quad (9.19)$$

Most tabulation of thermal data lists the value of:

$$\sigma_a(E_0) = \sigma_a(0.0253 \text{ eV}) = \sigma_a(2200 \text{ cm/sec}) \quad (9.20)$$

Now that we have obtained a spectrum for the thermal range, let us evaluate some group constants. In particular, consider the thermal absorption cross section:

$$\sigma_a^{th} = \frac{\int_0^{E_{th}} \sigma_a(E) \phi_{MB}(E) dE}{\int_0^{E_{th}} \phi_{MB}(E) dE} \quad (9.21)$$

For all practical purposes, we can let E_{th} be infinite and obtain for the denominator:

$$\int_0^{\infty} \phi_{MB}(E) dE = \frac{2}{\sqrt{\pi}} v_0 n_0 = 2 \sqrt{\frac{2KT}{\pi m}} v_0 \quad (9.22)$$

where T is the moderator temperature. This can be written as:

$$\phi^{th} = \frac{2}{\sqrt{\pi}} \left(\frac{T}{T_0} \right)^{1/2} \phi_0 \quad (9.23)$$

and $T_0 = 20 \text{ }^{\circ}\text{C}$ and $v_0 = 2200 \text{ meters/sec}$.

The numerator is equal to:

$$\int_0^\infty \frac{\sigma_a(E_0)v_0}{v} \phi_{MB}(E) dE = \int_0^\infty \frac{\sigma_a(E_0)v_0}{v} v M(E) dE = \sigma_a(E_0) \phi^0 \quad (9.24)$$

Therefore, the thermal absorption cross section becomes:

$$\begin{cases} \sigma_a^{th} = \frac{\sigma_a(E_0)\phi_0}{\frac{2}{\sqrt{\pi}}\left(\frac{T}{T_0}\right)^{1/2}\phi_0} = \sqrt{\frac{\pi}{4}}\left(\frac{T_0}{T}\right)^{1/2}(\sigma_a)(E_0) \\ \sigma_a^{th} = 0.886\sqrt{\frac{T_0}{T}}\sigma_a(E_0) \end{cases} \quad (9.25)$$

Note that not all nuclides are strictly $1/v$ absorbers, and therefore this simple relationship does not always hold. However, a relationship of this form can be developed by introducing the so-called g factor to give:

$$\sigma_a^{th} = \sqrt{\frac{\pi}{4}}g(T)g(T)\left(\frac{T_0}{T}\right)^{1/2}\sigma_a(E_0) \quad (9.26)$$

Normally scattering cross sections do not vary significantly in the thermal range if crystal or binding effects are not considered; therefore:

$$\sigma_s^{th} = \sigma_s(E_0) \quad (9.27)$$

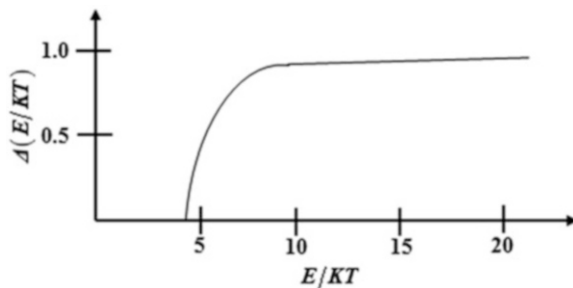
We will deal with binding effects later. Thus, we can define group constants for an infinite medium considering no absorption or sources. When we consider real media, we must consider the effects of these phenomena. In general, the following changes take place. As absorption is introduced, the fundamental spectrum tends to harden as more of the lower energy neutrons are absorbed by the typical $1/v$ absorbers. As leakage takes place, more of the higher-energy neutrons leak out due to the longer mean free paths at these energies. This effect tends to soften the spectrum and is known as "diffusion cooling." As sources are introduced (slowing down sources), the spectrum tends to harden due to the increased number of neutrons at the higher energies.

All three effects can be included by defining an effective temperature neutron and temperature model. We have:

$$T_n = T(1 + A\Gamma) \quad \Gamma = \frac{\sigma_a(E_0)}{\xi\Sigma_s} \quad (9.28)$$

Typical values for atomic number A lie in the range 1.2 to 1.8. T_n is called the neutron temperature and is typically higher than the actual moderator temperature T . It should also be pointed out that the Maxwell-Boltzmann distribution will be in error

Fig. 9.1 Depiction of joining function



at higher neutron energies as it fails to yield the $1/E$ slowing down flux behavior at epithermal energies. This has traditionally been corrected by defining the flux as:

$$\phi(E) = \phi_{MB}(E, T_n) + \lambda \frac{\Delta(E/KT)}{E} \quad (9.29)$$

where:

$$\lambda = \phi_{th} \sqrt{\frac{\pi}{4}} \left\{ \frac{\Gamma}{1 - \Gamma} \right\} \quad (9.30)$$

where $\Delta(E/KT)$ is called a joining function and is given by (Fig. 9.1):

The joining function $\Delta(E/KT)$ is obtained by using one of the numerical techniques described in the text to calculate an actual thermal-epithermal spectrum and then subtracting a Maxwell-Boltzmann distribution at T_n from it. The residual is the joining function. Luckily $\Delta(E/KT)$ does not vary much as a function of the absorption cross section, so it is a very nearly universal function.

9.2 Chemical Binding and Scattering Kernels

Now let us consider the effects of chemical binding on the scattering nucleus. When the scattering nucleus is bound in a crystal or large moderator, this binding effects the size of the thermal neutron cross section. When the energy of the neutron is large relative to the binding energy of the crystal, the atom scatters as an essentially unbound nucleus. When the energy of the neutron is significantly less than the binding energy of the atom in the crystal, the neutron effectively interacts with the whole crystal (or molecule).

In order to calculate this effect, a detailed quantum mechanical analysis must be performed. The results of this analysis simply state that the scattering cross section is given by:

$$\sigma_0 = 4\pi a^2 \quad (9.31)$$

where a is known as the scattering length and is given by:

$$a = \frac{m}{4\pi\hbar^2} \int_{\text{All Space}} V(\vec{r}) d\mathbf{r} \quad (9.32)$$

$V(\vec{r})$ is the nucleus potential for the interaction and m is the reduced mass of the system. We can then write:

$$\sigma_s^{\text{Bound}} = \sigma_s^{\text{Free}} \left(\frac{m_{\text{Bound}}}{m_{\text{Free}}} \right)^2 \quad (9.33)$$

Now for a free atom, we have for the reduced mass:

$$m_{\text{Free}} = \frac{mM}{m+M} = \frac{A}{1+A} \quad (9.34)$$

And for a bound atom, we have:

$$m_{\text{Bound}} = \frac{mM_{\text{eff}}}{m+M_{\text{eff}}} = \frac{A_{\text{eff}}}{1+A_{\text{eff}}} \quad (9.35)$$

Plugging this into the equation for the cross section and comparing bound cross sections with unbound ones, we have:

$$\begin{aligned} \sigma_s^{\text{Bound}} &= \sigma_s^{\text{Free}} \left(\frac{\frac{A_{\text{eff}}}{1+A_{\text{eff}}}}{\frac{A}{1+A}} \right)^2 \\ &= \sigma_s^{\text{Free}} \frac{\left(1 + \frac{1}{A} \right)^2}{\left(1 + \frac{1}{A_{\text{eff}}} \right)^2} \end{aligned} \quad (9.36)$$

If we let A_{eff} become very large, this reduces to:

$$\sigma_s^{\text{Bound}} = \sigma_s^{\text{Free}} \left(1 + \frac{1}{A} \right)^2 \quad (9.37)$$

Thus, the cross section of a bound nucleus will increase in effective size as the neutron slows down to energies of the order of the chemical binding energy. Hydrogen will show the most significant increase as its atomic mass is approximately 1.0. We have:

$$\begin{aligned} \sigma_s^{\text{Bound}} &= \sigma_s^{\text{Free}} & E_M > 1.0 \text{ eV} \\ \sigma_s^{\text{Bound}} &= 4\sigma_s^{\text{Free}} & E_M \approx 0.0 \text{ eV} \end{aligned} \quad (9.38)$$

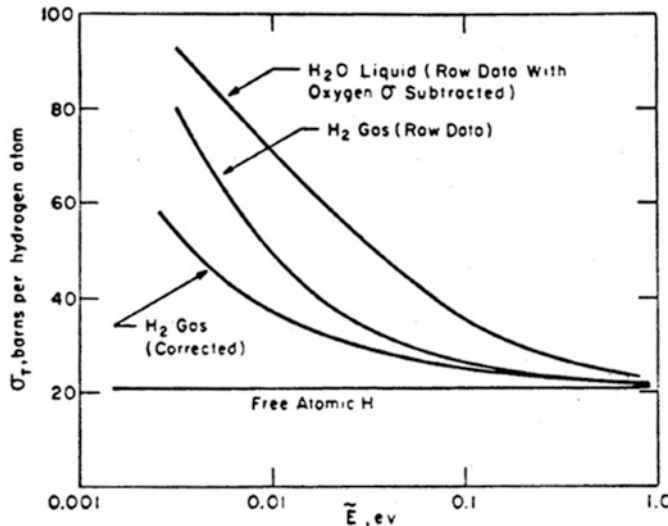


Fig. 9.2 The total slowdown cross section per proton bound in H_2 and in water. (Courtesy after K. H. Beckurts and K. Wirtz [1])

The total slow-neutron cross section per proton bound in H_2 gas and in water is depicted, and plots are shown in Fig. 9.2. Analyzing this figure indicates that the water curve has been corrected by subtracting the oxygen cross-section 3.73 barns atom, but has not been corrected for thermal motion. Both the raw data and the corrected H_2 curves are shown. The scattering cross section of atom hydrogen is 20.4 barns. The absorption cross section is 0.33 at 0.025 eV and varies as $1/\tilde{E}$.

In addition, it is worth noting that the actual increase is dependent on the binding energy of the crystal or molecule and its molecular mass. Consider some examples for hydrogen in terms of $\sigma_s^{\text{Bound}}/\sigma_s^{\text{Free}}$:

$$\mathbf{H = 1.0} \quad \mathbf{H_2 = 1.78} \quad \mathbf{H_2O = 3.31} \quad \mathbf{C_{22}H_{46}(\text{Poly}) = 3.98}$$

9.2.1 Scattering Materials

Polyethylene has a low-energy limit for the hydrogen scattering cross section that is about 80 barns as opposed to the 20 barns recorded for hydrogen in the epithermal region. Typically, the 2200 m/sec cross section for hydrogen is given as 38 barns. This corresponds to hydrogen gas. The 2200 m/sec cross section in water is about 49.4 barns.

Now let us consider the other significant effect of scattering of thermal neutrons, that of inelastic scattering of thermal neutrons by a crystal. Basically, we have considered the atoms of the moderator as a monatomic gas. When we do this, we obtained the monatomic gas scattering transfer function as:

$$\sigma_s(E')f(E' \rightarrow E) = \left\{ \begin{array}{l} e^{\epsilon' - \epsilon} [erf(\eta\sqrt{\epsilon} - \rho\sqrt{\epsilon}) \pm erf(\eta\sqrt{\epsilon'} + \rho\sqrt{\epsilon})] \\ + erf(\eta\sqrt{\epsilon} - \rho\sqrt{\epsilon}) \mp erf(\eta\sqrt{\epsilon} + \rho\sqrt{\epsilon'}) \end{array} \right\} \quad (9.39a)$$

where:

$$\eta = \frac{A+1}{2\sqrt{A}} \quad \rho = \frac{A-1}{2\sqrt{A}} \quad \epsilon = E/KT \quad \epsilon' = E'/KT \quad (9.39b)$$

The upper signs are used for $E > E'$ and the lower signs for $E < E'$.

We considered this scattering function to be totally elastic. That is, energy went from the neutron translational motion to the translational motion of the nuclei with which it interacted. Both energies were capable of varying continuously over their allowed range. However, when the scattering atoms are bound in a crystal, it is possible to raise an atom to a higher vibrational state in the crystal. This process is considered “inelastic” and is known as creating a phonon of vibrational energy. Note that there are discrete levels of vibrational excitation and therefore energies can only be interchanged in discrete packets. In order to calculate the scattering cross section and transfer probabilities for this type of analysis, the interaction of the neutron with the whole crystal or molecule must be considered. See Figs. 9.3 and 9.4 for energy transfer function a in monatomic gas with $A = 1$ and $A = 16$, respectively.

The wavelength of neutrons at low energies is given by:

$$\lambda = \frac{\lambda}{2\pi} = \frac{0.445 \times 10^2 \text{ (cm)}}{\sqrt{\frac{A}{A+1} E \text{ (MeV)}}} = \frac{2.86 \times 10^2 \text{ (cm)}}{\sqrt{E} \text{ (eV)}} \quad (9.40)$$

Fig. 9.3 Energy transfer function in a monatomic gas with $A = 1$. (Courtesy after Beckurts and Wirtz [1])

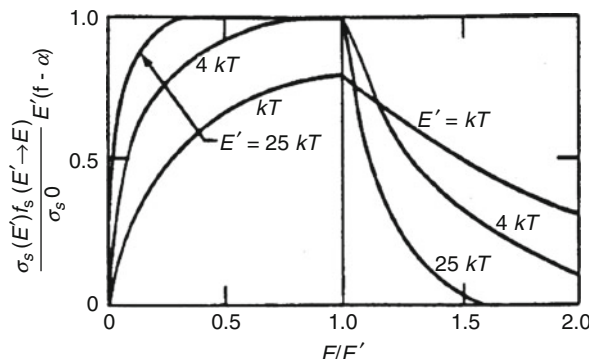
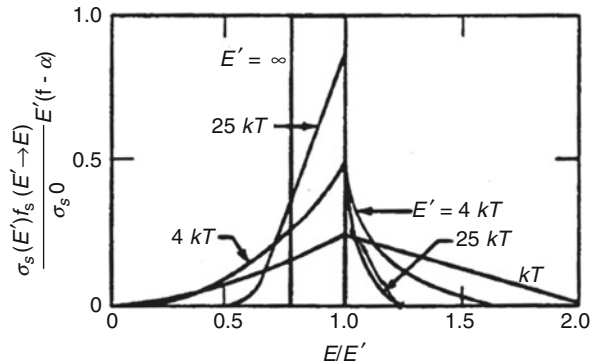


Fig. 9.4 Energy transfer function in a monatomic gas with $A = 16$. (Courtesy after Beckurts and Wirtz [1])



and for neutrons of energies like 0.01 eV, their wavelength is of the order of 3×10^{-8} cm, which is comparable to the atomic spacing in crystals. Therefore, it is possible for a neutron to scatter coherently off of the crystal itself. An additional complication is introduced by the fact that scattering depends on the neutron spin and the nucleus spin and the manner in which they combine. If we write:

$$\sigma_{\text{Coh}} = 4\pi a_{\text{Coh}}^2 \quad (9.41)$$

then a_{Coh} is given by:

$$a_{\text{Coh}} = \frac{I+1}{2I+1} a_+ + \frac{I}{2I+1} a_- \quad (9.42)$$

where:

I is the spin of the nucleus (the neutron spin = 1/2).

a_{Coh} is the coherent scattering length.

a_+ is the scattering amplitude for the $I+1/2$ state.

a_- is the scattering amplitude for the $I - 1/2$ state.

The average scattering cross section is given by:

$$\sigma_{\text{Ave}} = 4\pi \left\{ \frac{I+1}{2I+1} a_+^2 + \frac{I}{2I+1} a_-^2 \right\} \quad (9.43)$$

and the incoherent cross section is given by:

$$\sigma_{\text{Incoh}} = \sigma_{\text{Ave}} - \sigma_{\text{Coh}} = 4\pi \left[\frac{I(I+1)}{(2I+1)^2} \right] (a_+ - a_-)^2 \quad (9.44)$$

The following table gives the interesting result of all of these definitions when applied to the common moderators.

Moderator	Type scattering	Comments	
Hydrogen	Incoherent	$a_{\text{Coh}} = 1.8 \text{ barn}$	$\sigma_{\text{Ave}} = 81.5 \text{ barn}$
Deuterium	Mixed	$a_{\text{Coh}} = 5.4 \text{ barn}$	$\sigma_{\text{Ave}} = 7.6 \text{ barn}$
Beryllium	Coherent		
Carbon	Coherent		
Oxygen	Coherent		

The common assumption that hydrogen scatters incoherently is probably a very good approximation based on the above data.

So far, in above, we have covered the subject of thermal spectrum calculations and thermal group constants to generate multi-group constant characterization for low-energy neutron. Once again the general approach was to develop methods for determining the details of energy dependence or spectrum of such neutrons in those situations in which spatial dependence was ignored. Now we can briefly pay our attention to thermal cross-sectional averages, and for further information, we encourage our readers to refer to a book by Lewis [2].

9.2.2 Thermal Cross Sectional Average

For the purpose of neutron energy spectra, we have learned that the distribution of neutrons in energy is determined largely by the competition between absorption and scattering reactions, and this distribution may be expressed in terms of density distribution [2].

A more quantitative understanding of neutron energy distributions results from writing a balance equation in terms of the neutron flux $\phi(E)$ and total *macroscopic cross section* $\Sigma_t(E)$; thus we can write the balance equation in the following form as:

$$\Sigma_t(E)\phi(E) = \int p(E \rightarrow E')\Sigma_s(E')\phi(E')dE' + \chi(E)S_f \quad (9.45)$$

where the specific form of the probability $p(E \rightarrow E')$ for elastic scattering by a single nuclide where the neutron energy following collision will be between E' and $E' + dE$ will be given by the following equation at energy E :

$$p(E \rightarrow E')dE' = \begin{cases} \frac{1}{(1 - \alpha)E}dE' & \alpha E \leq E' \leq E \\ 0 & \text{otherwise} \end{cases} \quad (9.46)$$

where α is proven to in the following as it was shown in the past section:

$$\alpha = (A - 1)^2 / (A - 1)^2 \quad (9.47)$$

Note that the probability of $p(E \rightarrow E')dE'$ is that of a neutron elastic scattering with initial E will emerge with a new energy E' in the interval E' to $E'+dE'$.

Now, if we let $\Sigma_s(E' \rightarrow E) = p(E \rightarrow E')\Sigma_s(E')$, then Eq. 9.45 shapes to the following form as:

$$\Sigma_t(E)\phi(E) = \int \Sigma_s(E' \rightarrow E)\phi(E')dE' + \chi(E)S_f \quad (9.48)$$

The balance equation is normalized by the fission term, which indicates a rate of S_f fission neutrons produced/s/cm³.

Using Eq. (3.15) to examine idealized situations over three different energy ranges provides some insight into the nature of neutron spectra, particularly of thermal reactors, and these three situations are listed below as: [2]

1. The fast neutrons, whose energies are sufficient that is significant.
2. The slowing down region of the energy spectra, which is intermediate energy range and is often referred to as the resonance.
3. Thermal neutrons with energies less than 1.0 eV, where at the lower energies, thermal motions of the surrounding nuclei play a predominant role in determining the form of the spectrum.

In each of the three energy ranges, general restrictions apply to Eq. 9.48. In the thermal and intermediate ranges, no fission neutrons are born, and thus $\chi(E) = 0$. In the intermediate and fast ranges, there is no upscatter, and therefore, $\Sigma_s(E' \rightarrow E)$ for $E' < E$.

However, about thermal neutron, which is the third case in above, at lower energies, within thermal neutron range, we utilize Eq. 9.48 as our departing point. The fission term on the right vanishes and the source of neutrons then comes from those scattering down from higher energies. We may represent this as a scattering source, and we divide the integral in Eq. 9.48 according to whether energy E is less or greater than the cutoff energy for the thermal neutron range. Typically this range is taken as $E_0 = 1.0$ eV. We then partition the Eq. 9.48 as follows and write:

$$\begin{aligned} \Sigma_t(E)\phi(E) &= \int_0^{E_0} \Sigma_s(E' \rightarrow E)\phi(E')dE' \\ &+ \int_{E_0}^{\infty} \Sigma_s(E' \rightarrow E)\phi(E')dE' \quad \text{for } E < E_0 \end{aligned} \quad (9.49)$$

Or we can reduce Eq. 9.49 to the following form as:

$$\Sigma_t(E)\phi(E) = \int_0^{E_0} \Sigma_s(E' \rightarrow E)\phi(E')dE' + S(E)q_0 \quad \text{for } E < E_0 \quad (9.50)$$

where we have assumed that:

$$S(E)q_0 = \int_{E_0}^{\infty} \Sigma_s(E' \rightarrow E)\phi(E')dE' \quad \text{for } E < E_0 \quad (9.51)$$

which is nothing more than just being the source of thermal neutrons that arises from neutron making a collision at energies $E' > E_0$, but having an energy of $E < E_0$ after the collision. This was explained at the previous section that the source might be shown to be proportional to the slowing down density at E_0 , and if pure scattering and a $1/E$ flux is assumed at energies $E' > E_0$, then a simple expression results for $S(E)$, the energy distribution of the source neutrons. In the thermal range, the scattering distribution is difficult to represent in a straightforward manner, for not only thermal motion but also binding of the target nuclei to molecules or within a crystal lattice must be factored into the analysis [2].

Now all these said, the solution to Eq. 9.49, or for that matter Eq. 9.50, is time dependent, considering an idealized case of pure scattering materials for a situation of no neutron absorption in an infinite medium. In this case the neutron population will grow continuously with time, because each slowed down neutron would go on through scattering process forever. However, if after sometime it collapses, the slowing down density will get equal to zero, and using Maxwell-Boltzmann distribution criteria, an equilibrium distribution will reach out to satisfy the following equation in terms of neutron flux:

$$S(E)q_0 = \int_{E_0}^{\infty} \Sigma_s(E' \rightarrow E) \phi_{MB}(E') dE' \quad (9.52)$$

which is first term on right-hand side (RHS) of integral Eq. 9.49 or Eq. 9.50.

One of the beauties of kinetic theory in any nuclear-related analysis is to prove that for this to be satisfied, the principle of detailed balance should be enforced, and putting this detailed balance states in perspective, the following equation is given as Eq. 9.53, no matter what the law of scattering applies:

$$\Sigma_s(E \rightarrow E') \phi_{MB}(E) = \Sigma_s(E' \rightarrow E) \phi_{MB}(E) \quad (9.53)$$

Now, recall the Maxwell-Boltzmann distribution of Eq. 9.16 and reform it as the following equation:

$$M(E) = \frac{2\pi}{(\pi KT)^{3/2}} E^{1/2} \exp(-E/KT) \quad (9.54)$$

where E is energy in electron volt (eV) range and again Boltzmann's constant is $K = 8.617 \times 10^{-5}$ eV/K and $M(E)$ over the energy range is normalized to one as:

$$\int_0^{\infty} M(E) dE = 1 \quad (9.55)$$

Figure 9.5 shows $M(E)$ along with $\chi(E)$ for fission and thermal neutron energy spectra to indicate the energy range over which neutrons may exist in a nuclear reactor.

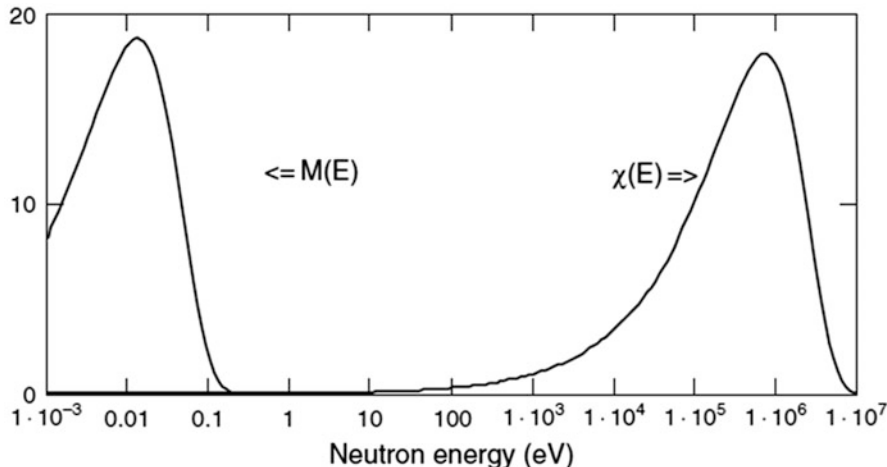


Fig. 9.5 Fission and thermal neutron energy spectra [2]

Now, taking the new form of Maxwell-Boltzmann distribution Eq. 9.54 under consideration, we can do further analysis of we find the following result. We notice that for Eq. 9.53 to be satisfied, it is important that the principle states, where these circumstances exists, the flux that satisfies the condition stated in that Eq. 9.53 is the form found by multiplying the Maxwell-Boltzmann distribution, Eq. 9.54, by the neutron speed, to obtain similar form of mathematical equation analogous to Eq. 9.16 as follows:

$$\phi_{MB}(E) = \frac{1}{(KT)^2} E \exp(-E/KT) \quad (9.56)$$

Following the normalization similar to Eq. 9.55 as new form of the following relation, over all the neutron energy exists in nuclear reactor as:

$$\int_0^\infty \phi_{MB}(E) dE = 1 \quad (9.57)$$

In reality, some absorption is always present. Absorption shifts the thermal neutron spectrum upward in energy from the Maxwell-Boltzmann distribution, since complete equilibrium is never reached before neutron absorption takes place.

Figure 9.6 illustrates the upward shift, called spectral hardening, which increases with the size of the absorption cross section. Nevertheless, Eq. 9.56 provides a rough approximation to a reactor's thermal neutron distribution. A somewhat better fit to hardened spectra, such as those in Fig. 9.6, may be obtained by artificially increasing the temperature T by an amount that is proportional to $\Sigma_a/\xi\Sigma_s$ [2].

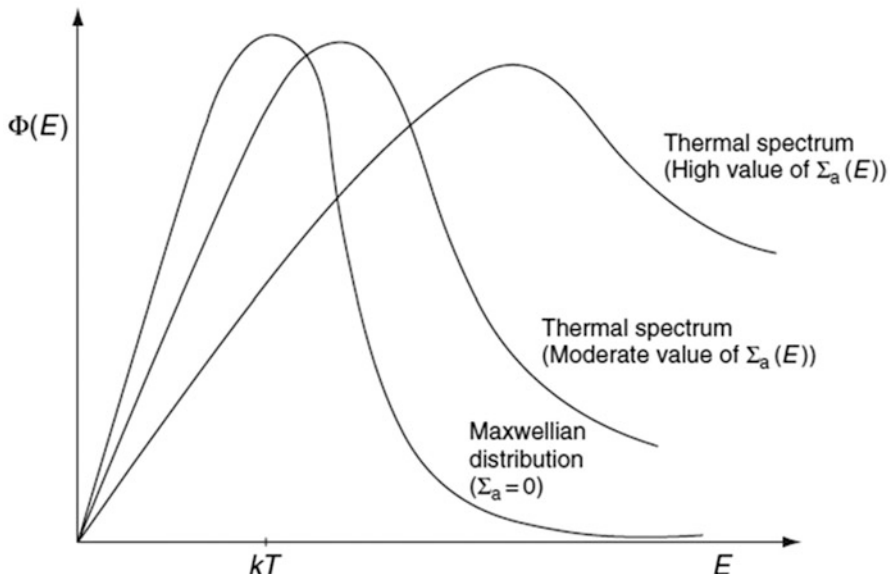


Fig. 9.6 Thermal spectra compared to a Maxwell-Boltzmann distribution. (Courtesy of Henry [3])

9.3 Derivation of the Maxwell-Boltzmann Spectrum

Consider now a closed system of particles consisting of two different types. These particles can be identified as the nuclei in a material and the neutrons that diffuse through the material. The system will be restricted to a fixed number of nuclei and a fixed number of neutrons. Both of these fixed numbers are very large for any real system. The system will also be restricted to a fixed quantity of energy that can be shared between the two types of particles. There are a set number of energy levels to which a particle can be assigned. The neutron energy levels will be identified by E_s and the nuclei levels will be identified by E_r . The width of these energy levels will be identified by dE_s and dE_r . The levels are fixed and do not depend on the relative location of the particles to each other. They could depend on the location of the particles within an external field but that will not be considered here. Energy can be exchanged between any two particles but the total energy is conserved.

The total number of neutrons will be N_n and the total number of nuclei as N_N . We will want to determine the location of the neutrons and nuclei in the allowed energy levels. Now each level can also be degenerated. That is, each level can have different states with the same energy, but the states are identified as different. An example would be several particles with the energy E_s but having different momentum by virtue of traveling in different directions. The number of different states at a particular level will be identified by m_s and m_r .

Now consider the arrangement of the N_n particles among the energy levels available to the neutrons and the arrangement of the N_N particles among the energy levels available to the nuclei. We will attempt to determine the most likely arrangement of the two sets of particles into the allowed energy levels. If n_{n1} particles are selected at energy level E_1 from the N_n total neutrons, the number of ways they can be chosen is given by:

$$P_1 = \frac{N_n!}{(N_n - n_{n1})!n_{n1}!} \quad (9.58)$$

For the second set of energy levels at energy E_2 , the number of ways that n_{n2} particles can be arranged is:

$$P_2 = \frac{(N_n - n_{n1})!}{(N_n - n_{n1} - n_{n2})!n_{n2}!} \quad (9.59)$$

Or the number of ways that n_{n1} particles can be arranged in energy level E_1 and the number of ways that n_{n2} particles can be arranged in energy level E_2 are given by:

$$P_{12} = \frac{N_n!}{n_{n1}!n_{n2}!(N_n - n_{n1} - n_{n2})!} \quad (9.60)$$

For k total energy levels, we have:

$$P_k = \frac{N_n!}{n_{n1}!n_{n2}!n_{n3}!\dots n_{nk}!} \quad (9.61)$$

Or as k becomes very large or approaches infinity:

$$P_\infty = N_n! \prod_{s=1}^{\infty} \frac{1}{n_{ns}!} \quad (9.62)$$

Now let us assume that there are m_s degenerate levels in each level s and then there are $m_s^{n_{ns}}$ ways that the n_{ns} particles may be arranged in the m_s degenerate levels. Then the number of distinct microscopic distributions is:

$$P = N_n! \prod \frac{m_s^{n_{ns}}}{n_{ns}!} \quad (9.63)$$

The same analysis would hold for the nuclei. The number of distinct microscopic distributions for the nuclei is:

$$Q = N_N! \prod \frac{m_r^{n_{Nr}}}{n_{Nr}!} \quad (9.64)$$

Therefore, the total number of microscopic arrangements is:

$$PQ = N_n! N_N! \prod_{s=1}^{\infty} \frac{m_s^{n_{ns}}}{n_{ns}!} \prod_{r=1}^{\infty} \frac{m_r^{n_{Nr}}}{n_{Nr}!} \quad (9.65)$$

Now in order to maximize the number of distinct distributions which is the most likely state to find the system in, with the largest entropy as postulated by Boltzmann, consider the log of PQ . The log of PQ will be maximized when PQ is maximized, but it is easier to perform the analysis with the log of PQ . The following auxiliary conditions must also be met to conserve particles and the system total energy:

$$\sum_{s=1}^{\infty} n_{ns} = N_n \quad (9.66)$$

$$\sum_{r=1}^{\infty} n_{Nr} = N_N \quad (9.67)$$

$$\sum_{s=1}^{\infty} E_s n_{ns} + \sum_{r=1}^{\infty} E_r n_{Nr} = E_{\text{total}} \quad (9.68)$$

The natural log of PQ can be maximized subject to these three constraints by introducing three Lagrange multipliers into the equation for $\ln(PQ)$ and forming the variational equation:

$$\delta \ln PQ - \alpha \delta N_n - \beta \delta N_N - \gamma \delta E_{\text{total}} = 0 \quad (9.69)$$

Expanding $\delta \ln (PQ)$ gives:

$$\delta \ln PQ = \delta \ln P + \delta \ln Q \quad (9.70)$$

$$\ln P = \ln N_n! + \sum_{s=1}^{\infty} [n_{ns} \ln m_s - \ln (n_{ns}!)] \quad (9.71)$$

$$\ln Q = \ln N_N! + \sum_{r=1}^{\infty} [n_{Nr} \ln m_r - \ln (n_{Nr}!)] \quad (9.72)$$

$$\delta \ln P = \sum_{s=1}^{\infty} [\delta n_{ns} \ln m_s - \delta(\ln n_{ns}!)] \quad (9.73)$$

$$\delta \ln Q = \sum_{r=1}^{\infty} [\delta n_{Nr} \ln m_r - \delta(\ln n_{Nr}!)] \quad (9.74)$$

Then using Stirling's approximation for the \ln function for a factorial of a very large number:

$$\ln n! \approx n \ln n - n \approx n \ln n \quad (9.75)$$

$$\delta \ln P + \delta \ln Q = \sum_{s=1}^{\infty} (\ln m_s - \ln n_{ns}) \delta n_{ns} + \sum_{r=1}^{\infty} (\ln m_r - \ln n_{Nr}) \delta n_{Nr} \quad (9.76)$$

Then the whole balance equation becomes:

$$\begin{aligned} & \sum_{s=1}^{\infty} (\ln m_s - \ln n_{ns}) \delta n_{ns} + \sum_{s=1}^{\infty} (\ln m_r - \ln n_{Nr}) \delta n_{Nr} - \alpha \sum_{s=1}^{\infty} \delta n_{ns} - \beta \sum_{r=1}^{\infty} \delta n_{Nr} \\ & - \gamma \sum_{s=1}^{\infty} E_s \delta n_{ns} - \gamma \sum_{r=0}^{\infty} E_r \delta n_{Nr} = 0 \end{aligned} \quad (9.77)$$

Combining sums for δn_{ns} and δn_{Nr} gives:

$$\sum_{s=1}^{\infty} (\ln m_s - \ln n_{ns} - \alpha - \gamma E_s) \delta n_{ns} + \sum_{r=1}^{\infty} (\ln m_r - \ln n_{Nr} - \beta - \gamma E_r) \delta n_{Nr} = 0 \quad (9.78)$$

Now if the changes in n_{ns} and n_{Nr} are chosen as arbitrary, their coefficients in the above equation must be identically zero. This gives the following equation for the neutrons:

$$\ln m_s - \ln n_{ns} - \alpha - \gamma E_s = 0 \quad (9.79)$$

or:

$$n_{ns} = m_s e^{-(\alpha + \gamma E_s)} \quad (9.80)$$

For the nuclei, a similar equation can be derived:

$$n_{Nr} = m_r e^{-(\beta + \gamma E_r)} \quad (9.81)$$

Up to this point, the number of degenerate states at each energy level has not been specified, and the above equations are very general. If only kinetic energy of the neutrons is considered, then the degeneracy at energy E is due to different velocity vectors. Or:

$$m_s = dv_x dv_y dv_z \quad (9.82)$$

If the velocity components are expressed in spherical coordinates, this can be written as:

$$m_s = dv_x dv_y dv_z = v^2 \sin \theta d\theta d\phi dv \quad (9.83)$$

This can be integrated over θ and ϕ to get:

$$m_s = 4\pi v^2 dv$$

Now noting that n_{ns} is equal to $n(E)dE$, we have:

$$n(E)dE = 4\pi v^2 e^{-(\alpha+\gamma E)} dv \quad (9.84)$$

and if γ is set to $1/kT$ and E is substituted for $\frac{1}{2}mv^2$ and $dE = mdv$, this becomes:

$$n(E)dE = \frac{4\pi}{m^{3/2}} 2^{1/2} E^{1/2} e^{-\alpha} e^{-E/kT} dE \quad (9.85)$$

Note this does not depend on the distribution of energy levels for the nuclei and is a quite general result. The Lagrange multiplier α turns out to be normalization constant. The equation can be normalized for one neutron to give:

$$M(E, T) = \frac{2}{\pi^{1/2} (kT)^{3/2}} E^{1/2} e^{-E/kT} \quad (9.86)$$

which is known as a Maxwell-Boltzmann distribution. If this distribution is multiplied by the neutron velocity, to get the flux at energy E , the resulting distribution is:

$$\phi_{MB}(E, T) = v(E)M(E, T) = \frac{2^{3/2}}{(m\pi)^{1/2} (kT)^{3/2}} E e^{-E/kT} \quad (9.87)$$

This represents the energy distribution of the thermal range neutron flux in an infinite medium without absorption, leakage, or sources.

Note that this distribution is unsymmetrical about its peak and skewed to the high-energy side. The peak of the neutron number distribution is given by:

$$E_{M(E, T)}^{\max} = \frac{kT}{2} \quad (9.88)$$

and the average value of the neutron number distribution is given by:

$$E_{M(E, T)}^{ave} = \frac{3kT}{2} \quad (9.89)$$

The peak of the neutron flux distribution is given by:

$$E_{\phi(E,T)}^{\max} = kT \quad (9.90)$$

and the average value for the neutron flux distribution is given by:

$$E_{\phi(E,T)}^{\text{avg}} = 2kT \quad (9.91)$$

The above derivation strictly only applies when the nuclei are the constituents of an ideal gas. However, if the nuclei are bound in the solid matrix such that their motion can be described by a particle trapped in a potential well given by:

$$V(r) = \frac{1}{2}Kr^2 \quad \text{or} \quad \text{Hooke's law in 3 dimensions,} \quad (9.92)$$

then, at high temperatures, the nuclei behave exactly as an ideal gas, and all of the above formulas apply directly.

At low temperatures, two models are used to describe an equivalent temperature, T^* , so that the Maxwellian distributions can be used. For the Einstein model of a solid, the atoms are assumed to vibrate independently with frequencies that are integral multiple of the fundamental frequency ν_E .

For example the hydrogen atoms in zirconium hydride, the moderator used in a TRIGA reactor, the solid nuclei can be represented by this model:

$$T^* = \frac{1}{2}\theta_E \coth\left(\frac{\theta_E}{2T}\right) \quad k\theta_E = h\nu_E = E_{\text{vib}} \quad (9.93)$$

where $E_{\text{vib}} = 0.137$ eV. This gives a θ_E of 1589 K and a T^* of 795 K for a moderator temperature of 300 K.

An alternative model for calculating T^* is given by the Debye model for a solid. In this case the following Table 9.1 gives an estimate of T^* as a function of θ_D , the Debye temperature, and the true temperature.

The following Table 9.2 gives some typical Debye temperatures for various solids.

Table 9.1 T^*/T as a function of T/θ_D

T/θ_D	T^*/T
0.10	3.77
0.25	1.68
0.50	1.19
0.75	1.09
1.0	1.05
2.0	1.01
3.0	1.00

Table 9.2 Debye temperatures for several solids

Solid	θ_D (K)
Graphite	1000
Aluminum	375
Beryllium	1160
Cadmium	165
Iron	355
Hafnium	213
Indium	109
Manganese	410
Molybdenum	360
Sodium	160
Nickel	413
Lead	96
Tin	195
Tantalum	230
Uranium	200
Tungsten	270
Zirconium	265
Uranium dioxide	160

Problems

Problem 9.1 Fission Spectra Calculate the most probable energy and the average energy of a neutron emitted in fission, if the fission spectrum is given by one of the following two formulas (E in MeV):

$$N(E) = 0.453(e^{-1.036E}) \sinh\left\{(2.29*E)^{0.5}\right\} \quad \text{Watt-Cranberg Spectrum}$$

$$N(E) = 0.77*E^{0.5*}e^{-E/1.29} \quad \text{Maxwellian Spectrum}$$

For the one of the above two spectra, what is the probability that a neutron will have an energy in the range 1–2 eV? What is the probability that it will have an energy of 1 eV?

Problem 9.2 Decay from Fission There are two popular equations available for predicting the decay heat from fission after a nuclear reactor is shut down. The oldest and least accurate is given by the power law point kernel:

$$E(t) = 2.66t^{-1/2}\text{MeV/Sec /fission, } \{t \text{ in Second}\}$$

A more current and more accurate kernel is given by the sum of exponentials kernel, as below:

$$E(t) = \sum \alpha_\gamma \exp(-t/\tau_\gamma) + \sum \alpha_\beta \exp(-t/\tau_\beta) \text{ MeV/Sec /fission, } \{t \text{ in Second}\}$$

where the α_γ and τ_γ constants apply to gamma decay energy and the α_β and τ_β apply to beta decay energy. A consistent set of constants for U²³⁵ is given below:

α_γ	τ_γ	α_β	τ_β
2.808×10^{-11}	1.364×10^9	6.169×10^{-11}	1.257×10^9
6.038×10^{-10}	2.307×10^7	2.249×10^{-9}	3.626×10^7
3.227×10^{-8}	5.176×10^6	2.365×10^{-8}	4.803×10^6
4.055×10^{-7}	6.031×10^5	2.194×10^{-7}	5.417×10^5
8.439×10^{-6}	4.658×10^4	1.140×10^{-5}	4.160×10^4
2.421×10^{-4}	4.699×10^3	1.549×10^{-4}	4.279×10^3
1.792×10^{-3}	522.2	1.991×10^{-3}	527.1
2.810×10^{-2}	56.53	3.256×10^{-2}	51.92
0.1516	6.053	0.2227	6.357
0.4162	0.7899	0.5381	0.7911
0.1053	0.1915	0.1282	0.1925

Use one of the above kernels and answer the following questions:

Suppose a reactor operates at 2400 Mw for 1 year and is then shut down. What would be the decay power in megawatts 1 year after shutdown? (*Hint:* Use Simpson's rule integration for integrating over the 1 year of operation. Use only one time interval with three data evaluations, beginning of interval, middle of interval, and end of interval). Suppose, instead, that all the energy released during the 1 year of power operation had been released at the beginning of that period. What would the decay power of the debris be 2 years after the burst?

Problem 9.3 Macroscopic Cross Sections What is the probability per centimeter of travel that a neutron having energy 0.025 eV and moving in pure Pu239, with a density of 19.6 gm/cc, will be captured? The thermal absorption cross section for Pu239 is 1029 barns.

Problem 9.4 Estimate the minimum group spacing that will yield directly coupled equations for the following moderators.

Carbon	($A = 12$)
Deuterium	($A = 2$)
Beryllium	($A = 9$)
Sodium	($A = 22$)
Uranium	($A = 238$)

Express your answer as the ratio of the upper energy bound to the lower energy bound and as the group width in lethargy units.

Problem 9.5 What fraction of neutrons scattering in hydrogen at 1.0 MeV, the lower bound of energy group 1, will jump to group 3, if the groups are set up with a constant lethargy spacing such that the ratio of the upper to lower energy group bounds is 100.

Problem 9.6 For the four-group cross-sectional data given below, calculate an infinite medium spectrum. Assume the groups are directly coupled.

Cross section	Group 1	Group 2	Group 3	Group 4
$\Sigma_{g_{\text{ABSORPTION}}}$	0.001394	0.000315	0.001881	0.03552
$v\Sigma_{g_{\text{FISSION}}}$	0.00287	0.000196	0.001480	0.04970
$\Sigma_{g_{\text{DOWNSCATTER}}}$	0.04148	0.06503	0.04106	0.0
$\Sigma_{g_{\text{TRANSPORT}}}$	0.0789	0.16704	0.3095	1.09223
χ_g	0.5503	0.4348	0.0149	0.0

Problem 9.7 Given the infinite medium spectrum that you calculated for Problem 6, collapse the four-group set to two-group set. Collapse groups 1 and 2 to group I of the two-group set, and collapse groups 3 and 4 to group II of the two-group set.

Problem 9.8 As a reactor heats up, thermal cross sections change due to a shift toward higher energies of the thermal neutron population. The following relationship holds for thermal fission and absorption cross sections:

$$\Sigma_{th} = (\pi/4)^{1/2} (T_0/T_m)^{1/2} \Sigma_{2200}$$

Note: Σ_{th} is the multi-group cross section (i.e., absorption or fission) for the thermal group. The only thing that changes when reactor heats up is T_m , the moderator temperature. Evaluate the derivative at 300 K.

Using the following data for Sandia's ACRR reactor, calculate an isothermal (core all at same temperature) feedback coefficient for this reactor based on zero-dimensional perturbation theory.

Parameter	Fast group	Thermal group
$\Sigma_{g_{\text{ABSORPTION}}}$	0.00364	0.2062
$v\Sigma_{g_{\text{FISSION}}}$	0.00595	0.3959
$\Sigma_{g_{\text{DOWNSCATTER}}}$	0.02935	---
D_g	2.0043	0.2055
$\phi_{g_{\text{VECTOR}}}$	7.124	1.0000
$\phi_{g^*_{\text{VECTOR}}}$	0.528	1.0000
Temperature = 300 K		Core $B^2 = 0.01405$

References

1. K.-H. Beckurts, K. Wirtz, *Neutron Physics* by Karl-Heinrich Beckurts (2013-03-25) Paperback 1656, Published by Springer
2. E.E. Lewis, *Fundamentals of Nuclear Reactor Physics*, Published by Academic Press, January 2008
3. A.F. Henry, *Nuclear Reactor Analysis* (MIT Press, New York, NY, 1975)

Chapter 10

Perturbation Theory for Reactor Neutronics



Perturbation theory in neutronic analysis for nuclear reactor system is often necessary, when we analyze and compute the effect of small changes on the behavior of a reactor. On the other hand, for a uniform occurrence of perturbation throughout the entire reactor or a region of it, then, we use methods that we have so far discussed and presented in previous chapters, although we never encounter uniform perturbation in practice of reactor operations. However, most of the changes, which occur in the operation mode of a reactor, are non-uniform, and there are numerous examples of such non-uniform perturbations.

10.1 Perturbation Theory

From reactor analyses' point of view, the effect of non-uniform perturbations on the performance of a reactor could be observed by performing a multi-group calculation in which perturbations are represented by appropriate space-dependent group constants. However, if we take under consideration any small yet localized perturbation, this procedure is not usually practical.

By the very nature, a localized perturbation requires that a multi-group calculation be performed in at least two-dimensional but more probably in three-dimensional as it was mentioned in previous chapters.

Now let us consider a mathematical technique that has quite general applicability and is particularly useful for calculating the deviations from criticality produced by small changes in a critical system. There are many uses for perturbation theory, and it can be used to calculate changes in the fundamental eigenvalue of a reactor due to changes in any of the parameters that describe that reactor or the numerical approx-

imations that go into modeling it. Consider the eigenvalue equation that shows up in a multi-group diffusion theory:

$$[\mathbf{M}]\{\boldsymbol{\phi}\} = \mathbf{1}/k[\mathbf{F}]\{\boldsymbol{\phi}\} \quad (10.1)$$

Let $\lambda = 1/k$, and then Eq. 4.108 will reduce to the following form as:

$$\{[\mathbf{M}] - \lambda[\mathbf{F}]\}\{\boldsymbol{\phi}\} = \{\mathbf{0}\} \quad (10.2)$$

as the reactor criticality equation. The \mathbf{M} and \mathbf{F} matrices can represent infinite media multi-group parameters, zero-dimensional multi-group parameters, and one-group spatially dependent numerical approximations to differential operators, or they can represent multi-group, multidimensional numerical approximations to partial differential operators. Any reactor criticality problem can be written in this form. In general, for a critical reactor, we have $k = 1.0$ and $\lambda = 1.0$. We can solve this equation for the fundamental eigenfunction.

Frequently we will want to know what happens to k as we change \mathbf{M} and/or \mathbf{F} slightly. We do not necessarily want to recalculate the new flux vector in order to determine the change in k .

10.2 Zero-Dimensional Methods

As perhaps the most straightforward example of this type of problem that exhibits all of the important features of the general problem, consider a zero-dimensional, two-group problem described by the following set of equations:

$$\left\{ \begin{bmatrix} M_{11}^0 & M_{12}^0 \\ M_{21}^0 & M_{22}^0 \end{bmatrix} - \lambda_o \begin{bmatrix} F_{11}^0 & F_{12}^0 \\ F_{21}^0 & F_{22}^0 \end{bmatrix} \right\} \begin{Bmatrix} \phi_0^1 \\ \phi_0^2 \end{Bmatrix} = \begin{Bmatrix} 0 \\ 0 \end{Bmatrix} \quad (10.3)$$

where

$$\begin{aligned} M_{11}^0 &= D^1 B^2 + \Sigma_R^1 & M_{12}^0 &= 0 \\ M_{21}^0 &= -\Sigma_S^{12} & M_{22}^0 &= D^2 B^2 + \Sigma_a^2 \\ F_{11}^0 &= \chi_1 v \Sigma_f^1 & F_{12}^0 &= \chi_1 v \Sigma_f^2 \\ F_{21}^0 &= \chi_2 v \Sigma_f^1 & F_{22}^0 &= \chi_2 v \Sigma_f^2 \end{aligned} \quad (10.4)$$

Now we will represent a perturbation in the system as:

$$\begin{aligned} M_{11} &= M_{11}^0 + m_{11} & F_{11} &= F_{11}^0 + f_{11} \\ \lambda &= \lambda_0 + d\lambda & \phi &= \phi_0 + d\phi \end{aligned} \quad (10.5)$$

If we substitute the perturbed quantities into our equations, we will obtain the following set of equations:

$$\left\{ \begin{bmatrix} M_{11}^0 + m_{11} & M_{12}^0 + m_{12} \\ M_{21}^0 + m_{21} & M_{22}^0 + m_{22} \end{bmatrix} - (\lambda_0 + \delta\lambda) \begin{bmatrix} F_{11}^0 + f_{11} & F_{12}^0 + f_{12} \\ F_{21}^0 + f_{21} & F_{22}^0 + f_{22} \end{bmatrix} \right\} \left\{ \begin{array}{l} \phi_0^1 + \delta\phi^1 \\ \phi_0^2 + \delta\phi^2 \end{array} \right\} = \left\{ \begin{array}{l} 0 \\ 0 \end{array} \right\} \quad (10.6)$$

Note that from the notation point of view and convenience, we are moving all the subscripts for ϕ to superscript position.

We would like to calculate the change in k for the above set of equations without completely resolving them. As we have two equations and three unknowns, the change in k and the perturbations in both fluxes, we must in general combine them in some way to obtain one equation that expresses the change in k as a function of the change in M and F . The easiest way to accomplish this is to multiply each of the equations by a weighting function and then add them. The resulting equation can be solved for the change in k . Of course, we would like to choose the weighting function in some optimal way. Since we do not wish to recalculate ϕ , we would prefer a weighting function that is insensitive to changes in the perturbed flux eigenfunction. We can derive a set of equations for this weighting function by expanding our perturbed equations.

$$\{W_1, W_2\} \left\{ \begin{bmatrix} M_{11}^0 + m_{11} & M_{12}^0 + m_{12} \\ M_{21}^0 + m_{21} & M_{22}^0 + m_{22} \end{bmatrix} - (\lambda_0 + \delta\lambda) \begin{bmatrix} F_{11}^0 + f_{11} & F_{12}^0 + f_{12} \\ F_{21}^0 + f_{21} & F_{22}^0 + f_{22} \end{bmatrix} \right\} \left\{ \begin{array}{l} \phi_0^1 + \delta\phi^1 \\ \phi_0^2 + \delta\phi^2 \end{array} \right\} = \left\{ \begin{array}{l} 0 \\ 0 \end{array} \right\} \quad (10.7)$$

We have:

$$\begin{aligned} \{W_1, W_2\} \left\{ \begin{bmatrix} M_{11}^0 & M_{12}^0 \\ M_{21}^0 & M_{22}^0 \end{bmatrix} - \lambda_0 \begin{bmatrix} F_{11}^0 & F_{12}^0 \\ F_{21}^0 & F_{22}^0 \end{bmatrix} \right\} \left\{ \begin{array}{l} \phi_0^1 \\ \phi_0^2 \end{array} \right\} & \quad [1] \\ + \{W_1, W_2\} \left\{ \begin{bmatrix} M_{11}^0 & M_{12}^0 \\ M_{21}^0 & M_{22}^0 \end{bmatrix} - \lambda_0 \begin{bmatrix} F_{11}^0 & F_{12}^0 \\ F_{21}^0 & F_{22}^0 \end{bmatrix} \right\} \left\{ \begin{array}{l} \delta\phi^1 \\ \delta\phi^2 \end{array} \right\} & \quad [2] \\ + \{W_1, W_2\} \left\{ \begin{bmatrix} m_{11} & m_{12} \\ m_{21} & m_{22} \end{bmatrix} - \lambda_0 \begin{bmatrix} f_{11} & f_{12} \\ f_{21} & f_{22} \end{bmatrix} - \delta\lambda \begin{bmatrix} F_{11}^0 & F_{12}^0 \\ F_{21}^0 & F_{22}^0 \end{bmatrix} \right\} \left\{ \begin{array}{l} \phi_0^1 \\ \phi_0^2 \end{array} \right\} & \quad [3] \\ + \{W_1, W_2\} \left\{ \begin{bmatrix} m_{11} & m_{12} \\ m_{21} & m_{22} \end{bmatrix} - \lambda_0 \begin{bmatrix} f_{11} & f_{12} \\ f_{21} & f_{22} \end{bmatrix} - \delta\lambda \begin{bmatrix} F_{11}^0 & F_{12}^0 \\ F_{21}^0 & F_{22}^0 \end{bmatrix} \right\} \left\{ \begin{array}{l} \delta\phi^1 \\ \delta\phi^2 \end{array} \right\} & \quad [4] \\ + \{W_1, W_2\} \left\{ -\delta\lambda \begin{bmatrix} f_{11} & f_{12} \\ f_{21} & f_{22} \end{bmatrix} \right\} \left\{ \begin{array}{l} \delta\phi^1 \\ \delta\phi^2 \end{array} \right\} = \left\{ \begin{array}{l} 0 \\ 0 \end{array} \right\} & \quad [5] \end{aligned} \quad (10.8)$$

Examining this series of inner products on a term-by-term basis, we find that the first [1] set of terms is identically zero as it represents the solution of the unperturbed problem. The second [2] and third [3] inner products contain terms of the first order in the changes in \mathbf{M} , \mathbf{F} , and \mathbf{k} and the fluxes, and the fourth [4] and fifth [5] inner products contain terms of either second or third order in the system changes. If the system changes are small, then we should be able to neglect the fourth and fifth terms relative to the second and third terms. If we do this, the equations become:

$$\begin{aligned} \{W_1, W_2\} \left\{ \begin{bmatrix} M_{11}^0 & M_{12}^0 \\ M_{21}^0 & M_{22}^0 \end{bmatrix} - \lambda_0 \begin{bmatrix} F_{11}^0 & F_{12}^0 \\ F_{21}^0 & F_{22}^0 \end{bmatrix} \right\} \begin{Bmatrix} \delta\phi^1 \\ \delta\phi^2 \end{Bmatrix} + \\ \{W_1, W_2\} \left\{ \begin{bmatrix} m_{11} & m_{12} \\ m_{21} & m_{22} \end{bmatrix} - \lambda_0 \begin{bmatrix} f_{11} & f_{12} \\ f_{21} & f_{22} \end{bmatrix} - \delta\lambda \begin{bmatrix} F_{11}^0 & F_{12}^0 \\ F_{21}^0 & F_{22}^0 \end{bmatrix} \right\} \begin{Bmatrix} \phi_0^1 \\ \phi_0^2 \end{Bmatrix} = \begin{Bmatrix} 0 \\ 0 \end{Bmatrix} \end{aligned} \quad (10.9)$$

The changes in the flux eigenfunction only show up in the first set of terms above. Therefore, if we choose our weighting function such that this set of terms exactly cancels to zero, irrespective of changes in the eigenfunction, we will be able to neglect first-order changes in the flux. For this to be the case, we must have the coefficient of the flux change exactly equal to 0.0 in each equation. Thus, we must have:

$$\begin{aligned} W_1(M_{11}^0 - \lambda_0 F_{11}^0) + W_2(M_{21}^0 - \lambda_0 F_{21}^0) = 0 \\ W_1(M_{12}^0 - \lambda_0 F_{12}^0) + W_2(M_{22}^0 - \lambda_0 F_{22}^0) = 0 \end{aligned} \quad (10.11)$$

This can be written in a matrix form as:

$$\left\{ \begin{bmatrix} M_{11}^0 & M_{21}^0 \\ M_{12}^0 & M_{22}^0 \end{bmatrix} - \lambda_0 \begin{bmatrix} F_{11}^0 & F_{21}^0 \\ F_{12}^0 & F_{22}^0 \end{bmatrix} \right\} \begin{Bmatrix} W^1 \\ W^2 \end{Bmatrix} = \begin{Bmatrix} 0 \\ 0 \end{Bmatrix} \quad (10.12)$$

Note that the two matrices above that multiply the weighting function vector are simply the transposes of the original two-group diffusion equations. It is a well-known theorem of linear algebra that the eigenvalues of the original problem are also the eigenvalues of the transposed problem, and the solution of the transposed problem is called the adjoint function. Therefore, if we choose our weighting function as the adjoint function, we will not have to compute a new flux eigenfunction to obtain changes in \mathbf{k} due to changes in \mathbf{M} or \mathbf{F} to first order. (Though this demonstration has only dealt with the two-group zero-dimensional equations, this property holds quite generally for an arbitrary number of groups and spatial dimensions.) Then if we choose our weighting function to be the zero-dimensional adjoint function, we will have:

$$(\phi^{1*}, \phi^{2*}) \left\{ \begin{bmatrix} m_{11} & m_{12} \\ m_{21} & m_{22} \end{bmatrix} - \lambda_0 \begin{bmatrix} f_{11} & f_{12} \\ f_{21} & f_{22} \end{bmatrix} - \delta\lambda \begin{bmatrix} F_{11}^0 & F_{12}^0 \\ F_{21}^0 & F_{22}^0 \end{bmatrix} \right\} \begin{Bmatrix} \phi_0^1 \\ \phi_0^2 \end{Bmatrix} = \begin{Bmatrix} 0 \\ 0 \end{Bmatrix} \quad (10.13)$$

where the asterisk will be used to denote the adjoint, and the equation can be rewritten as:

$$\begin{aligned} & [\phi^{1*}(m_{11} - \lambda_0 f_{11}) + \phi^{2*}(m_{21} - \lambda_0 f_{21})] \phi_0^1 \\ & + [\phi^{1*}(m_{21} - \lambda_0 f_{21}) + \phi^{2*}(m_{22} - \lambda_0 f_{22})] \phi_0^2 \\ & = \delta\lambda [(\phi^{1*} F_{11}^0 + \phi^{2*} F_{21}^0) \phi_0^1 + (\phi^{1*} F_{12}^0 + \phi^{2*} F_{22}^0) \phi_0^2] \end{aligned} \quad (10.14)$$

Rearranging terms and solving for the change in the eigenvalue give:

$$\delta\lambda = \frac{[\phi^{1*}(m_{11} - \lambda_0 f_{11}) + \phi^{2*}(m_{21} - \lambda_0 f_{21})] \phi_0^1 + [\phi^{1*}(m_{12} - \lambda_0 f_{12}) + \phi^{2*}(m_{22} - \lambda_0 f_{22})] \phi_0^2}{(\phi^{1*} F_{11}^0 + \phi^{2*} F_{21}^0) \phi_0^1 + (\phi^{1*} F_{12}^0 + \phi^{2*} F_{22}^0) \phi_0^2} \quad (10.15)$$

Now since $\lambda = 1/k$, we have $d\lambda = dk/k$. And since for criticality we have $k = 1$, we then obtain for $dk = \rho$ the following expression:

$$\delta k = \rho = - \frac{[\phi^{1*}(m_{11} - \lambda_0 f_{11}) + \phi^{2*}(m_{21} - \lambda_0 f_{21})] \phi_0^1 + [\phi^{1*}(m_{12} - \lambda_0 f_{12}) + \phi^{2*}(m_{22} - \lambda_0 f_{22})] \phi_0^2}{(\phi^{1*} F_{11}^0 + \phi^{2*} F_{21}^0) \phi_0^1 + (\phi^{1*} F_{12}^0 + \phi^{2*} F_{22}^0) \phi_0^2} \quad (10.16)$$

In order to demonstrate the utility of this last expression, consider a rather straightforward example. Let us assume that our slab (or zero-dimensional) reactor is critical and a small amount of boron is added to the core material of the reactor. The effect of adding the boron can be represented as a perturbation in the thermal absorption cross section of the reactor core. To calculate the change in reactivity of the reactor, we can simply evaluate our perturbation formula. We have:

$$\begin{aligned} m_{11} &= f_{11} = m_{21} = f_{21} = m_{12} = f_{12} = f_{22} = 0 \\ m_{22} &= \delta\Sigma_a^2 \end{aligned} \quad (10.17)$$

As a result:

$$\rho = - \frac{\phi^{2*} \delta\Sigma_a^2 \phi_0^2}{(\phi^{1*} F_{11}^0 + \phi^{2*} F_{21}^0) \phi_0^1 + (\phi^{1*} F_{12}^0 + \phi^{2*} F_{22}^0) \phi_0^2} \quad (10.18a)$$

And

$$\rho = -\frac{\phi^{2*} \delta \Sigma_a^2 \phi_0^2}{\phi^{1*} F_{11}^0 \phi_0^1 + \phi^{2*} F_{21}^0 \phi_0^1 + \phi^{1*} F_{21}^0 \phi_0^2 + \phi^{2*} F_{22}^0 \phi_0^2} \quad (10.18b)$$

If we choose $\phi^{2*} = \phi_0^2 = 1.0, \chi_2 = 0.0$
then:

$$\rho = -\frac{\delta \Sigma_a^2}{\phi^{1*} (v \Sigma_f^1 \phi_0^1 + v \Sigma_f^2)} \quad (10.19)$$

Note that the adjoint equations for the general two-group zero-dimensional model are:

$$\begin{bmatrix} D^1 B^2 + \Sigma_F^1 - \chi^1 v \Sigma_f^1 & -\Sigma_s^{12} - \chi^2 v \Sigma_f^1 \\ -\chi^1 v \Sigma_f^2 & D^2 B^2 + \Sigma_a^2 - \chi^2 v \Sigma_f^2 \end{bmatrix} \begin{Bmatrix} \phi^{1*} \\ \phi^{2*} \end{Bmatrix} = \begin{Bmatrix} 0 \\ 0 \end{Bmatrix} \quad (10.20)$$

Moreover, the determinant equation for criticality is:

$$(D_1 B^2 + \Sigma_R^1 - \chi_1 v \Sigma_f^1)(D B^2 + \Sigma_a^2 - \chi_2 v \Sigma_f^2) - \chi_2 v \Sigma_f^2 (\Sigma_s^{12} + \chi_2 v \Sigma_f^1) = 0 \quad (10.21)$$

which has the same solutions for B^2 as the forward (flux) determinant equation. However, the eigenfunctions are different. We have:

Adjoint eigenvector	Adjoint eigenvector
$(D_2 B^2 + \Sigma_a^2 - \chi_2 v \Sigma_f^2) \phi_0^2 = (\Sigma_s^{12} + \chi_2 v \Sigma_f^1) \phi_0^1$	$(D^2 B^2 + \Sigma_a^2 - \chi^2 v \Sigma_f^2) \phi^{2*} = \chi^1 v \Sigma_f^2 \phi^{1*}$
$\phi_0^1 = \begin{bmatrix} D_2 B^2 + \Sigma_a^2 - \chi_2 v \Sigma_f^2 \\ \Sigma_s^{12} + \chi_2 v \Sigma_f^1 \end{bmatrix}$	$\phi^{1*} = \begin{bmatrix} D_2 B^2 + \Sigma_a^2 - \chi_2 v \Sigma_f^2 \\ \chi_1 v \Sigma_f^2 \end{bmatrix}$
$\phi_0^2 = 1.0$	$\phi^{2*} = 1.0$

Thus, we can evaluate the reactivity change caused by a small homogeneous change in the core composition.

10.2.1 Spatial Method (1 Group)

It is also possible to treat changes in the spatial makeup of the reactor. In order to keep the analysis as simple as possible, consider a one-group model for the homogeneous slab, and introduce a small perturbation that is a function of z in the slab. We have:

$$\begin{aligned}
& -D \frac{d^2 \phi(z)}{dz^2} + \left(\Sigma_{aa} - \frac{1}{k} v \Sigma_f \right) \phi(z) = 0 \\
& D(z) = D_0 + \delta D(z) \\
& \Sigma_a(z) = \Sigma_{a0} + \delta \Sigma_a(z) \\
& v \Sigma_f(z) = v \Sigma_{f0} + \delta v \Sigma_f(z)
\end{aligned} \tag{10.23}$$

Now we want to find the change in k caused by this spatial perturbation. Note that k is an integral parameter for the reactor and not a function of z within the reactor. The differential equation with $\lambda = 1/k$ becomes:

$$\begin{aligned}
& -[D_0 + \delta D(z)] \frac{d^2}{dz^2} [\phi_0(z) + \delta \phi(z)] + [\Sigma_{a0} + \delta \Sigma_a(z) - \{\lambda_0 + \delta \lambda\} \{v \Sigma_{f0} \delta v \Sigma_f(z)\}] \\
& [\phi_0(z) + \delta \phi(z)] = 0
\end{aligned} \tag{10.24}$$

or:

$$\begin{aligned}
& -D_0 \frac{d^2}{dz^2} \phi_0(z) + [\Sigma_{a0} - \lambda_0 v \Sigma_{f0}] \phi_0(z) & [1] \\
& -D_0 \frac{d^2}{dz^2} \delta \phi(z) + [\Sigma_{a0} - \lambda_0 v \Sigma_{f0}] \delta \phi(z) & [2] \\
& -\delta D(z) \frac{d^2}{dz^2} \phi_0(z) + [\delta \Sigma_a(z) - \lambda_0 \delta v \Sigma_f(z) - \delta \lambda v \Sigma_{f0}] \phi_0(z) & [3] \\
& -\delta D(z) \frac{d^2}{dz^2} \delta \phi(z) + [\delta \Sigma_a(z) - \delta \lambda v \Sigma_{f0} - \lambda_0 \delta v \Sigma_f(z)] \phi_0(z) & [4] \\
& -\delta \lambda \delta v \Sigma_f(z) [\delta \phi(z)] = 0 & [5]
\end{aligned} \tag{10.25}$$

Note that line [1] is the original equation and lines [4] and [5] are second order or higher in the small perturbations. Thus, making the small perturbation assumption, we can reduce the equation down to lines [2] and [3]. We have:

$$\begin{aligned}
& -D_0 \frac{d^2}{dz^2} \delta \phi(z) + [\Sigma_{a0} - \lambda_0 v \Sigma_{f0}] \delta \phi(z) - \delta D(z) \frac{d^2}{dz^2} \phi_0(z) \\
& + [\delta \Sigma_a - \lambda_0 \delta v \Sigma_f(z) - \delta \lambda v \Sigma_{f0}] \phi_0(z) = 0
\end{aligned} \tag{10.26}$$

If we want to calculate one $\delta\lambda$ for this differential equation, we must convert it to an algebraic expression of some form. The simplest way to do this is to multiply the equation by some weighting function, $W(z)$, and integrate from 0 to L . When we do this, we have:

$$\begin{aligned} & \int_0^L W(z) \left\{ -D_0 \frac{d^2}{dz^2} \delta\phi(z) + [\Sigma_{a0} - \lambda_0 v \Sigma_{f0}] \delta\phi(z) \right\} dz \\ & + \int_0^L W(z) \left\{ -\delta D(z) \frac{d^2}{dz^2} \phi_0(z) + [\delta \Sigma_a - \lambda_0 \delta v \Sigma_f(z)] \phi_0(z) \right\} dz \\ & - \int_0^L W(z) \delta \lambda v \Sigma_f \phi_0(z) dz = 0 \end{aligned} \quad (10.27)$$

Solving for $\delta\lambda$ gives:

$$\delta\lambda = \frac{\int_0^L W(z) \left[-D_0 \frac{d^2}{dz^2} + \Sigma_{a0} - v \Sigma_{f0} \right] \delta\phi_0(z) dz}{\int_0^L W(z) v \Sigma_{f0} \phi_0(z) dz} \quad (10.28)$$

In order for the solution not to depend on the flux perturbation, we must perform some manipulations. Consider the first term above:

$$\int_0^L W(z) \left[-D_0 \frac{d^2}{dz^2} + \Sigma_{a0} - v \Sigma_{f0} \right] \delta\phi_0(z) dz = 0 \quad (10.29)$$

The second derivative term can be integrated by parts as follows:

$$\begin{aligned} & \int_0^L W(z) \left[-D_0 \frac{d^2}{dz^2} \delta\phi(z) \right] dz = -W(z) D_0 \frac{d\delta\phi_0(z)}{dz} \Big|_0^L + \int_0^L \frac{dW(z)}{dz} D_0 \frac{d\delta\phi(z)}{dz} dz \\ & = -W(z) D_0 \frac{d\delta\phi(z)}{dz} \Big|_0^L + \frac{dW(z)}{dz} D_0 \delta\phi(z) \Big|_0^L - \int_0^L \delta\phi(z) D_0 \frac{d^2W(z)}{dz^2} dz \end{aligned} \quad (10.30)$$

Since the boundary condition on the flux at 0 and L has not changed, the flux perturbation must be zero on the boundary. Therefore:

$$\delta\phi(0) = \delta\phi(L) = 0 \quad (10.31)$$

This will eliminate the first set of boundary terms. The second set of boundary terms can be eliminated by requiring $W(z)$ to be zero at $z = 0$ and $z = L$. This corresponds to applying the “approximate diffusion theory” boundary conditions. If the “consistent diffusion theory” boundary conditions are applied, similar results will be obtained, with the necessary boundary conditions on $W(z)$ involving a derivative term in the same manner that the flux equations do.

Therefore, we have the following equation and boundary conditions on $W(z)$:

$$-D_0 \frac{d^2 W(z)}{dz^2} + [\Sigma_{a0} - v\Sigma_{f0}] W(z) = 0, \quad W(0) = 0, \quad W(L) = 0 \quad (10.32)$$

We can completely eliminate any dependence of $\delta\lambda$ on changes in the flux to first order by this choice of weighting function. This equation and boundary conditions define the spatially dependent adjoint function. Note that for the one-group problem, the adjoint equation is identical with the flux equation. We can say that the one-group problem is self-adjoint. In fact, all multi-group diffusion problems are spatially self-adjoint. The adjoint flux is:

$$\phi^*(z) = \phi_0^* \sin(Bz) \quad (10.33)$$

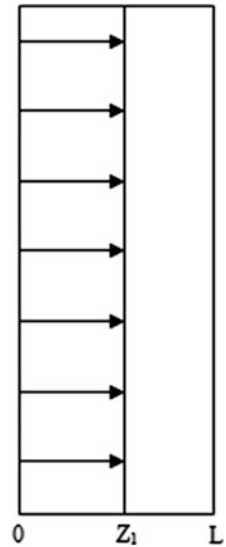
Using this in our perturbation equation, we have:

$$\delta\lambda = \frac{\int_0^L \varphi^*(z) \left[-\delta D(z) \frac{d^2}{dz^2} + \delta \Sigma_a(z) - \delta v \Sigma_f(z) \right] \phi_0(z) dz}{\int_0^L \varphi^*(z) v \Sigma_{f0} \phi_0(z) dz} \quad (10.34)$$

This equation is the equivalent of the reactivity change equation for the zero-dimensional case that was considered earlier. For real perturbations in real reactors, the two forms have to be combined to treat real perturbations as energy and spatially dependent. Once again, the problem of writing the equations down becomes massive. However, the form and process should be fairly easy to combine and it should be obvious how to do it.

Now consider two spatial perturbations. In one case a control poison will be inserted into the slab from the left to a distance z_1 . This could simulate a uniform change in core or moderator absorption. It would be a reasonable approximation to a thermal reactor with banked control rods moving down from the top of the core or up from the bottom of the core. It also is similar to a first approximation for the effects of the change in the boiling level in a boiling water reactor (BWR).

Fig. 10.1 Homogeneous perturbation scenario



A schematic picture is included as shown in Fig. 10.1.
We have:

$$\delta\lambda = \frac{\int_0^{z_1} \varphi^*(z) \delta\Sigma_a(z) \phi_0(z) dz}{\int_0^L \varphi^*(z) v\Sigma_{f0} \phi_0(z) dz} \quad (10.35)$$

$$\delta\lambda = \frac{\delta\Sigma_a}{v\Sigma_{f0}} \frac{\int_0^{z_1} \phi^*(z) \varphi_0(z) dz}{\int_0^L \phi^*(z) \varphi_0(z) dz} \quad (10.36)$$

$$\phi^*(z) = \phi_0^* \sin(Bz), \quad \phi_0(z) = \phi_0 \sin(Bz) \quad (10.37)$$

$$\delta\lambda = \frac{\delta\Sigma_a}{v\Sigma_{f0}} \frac{2}{\pi} \int_0^{z_1} \sin^2(Bz) dz \quad (10.38)$$

$$\delta k = \rho = -\frac{\delta\Sigma_a}{v\Sigma_{f0}} \left[\frac{z_1}{L} - \frac{1}{2\pi} \sin\left(\frac{2\pi z_1}{L}\right) \right] \quad (10.146)$$

Now consider the perturbation introduced by running a plane absorber down through the reactor at a position z_1 in the reactor. We have:

$$\delta\lambda = \frac{\int_0^{z_1} \phi^*(z) \delta\Sigma_a \delta(z - z_1) \phi_0(z) dz}{\int_0^L \phi^*(z) v \Sigma_{f0} \phi_0(z) dz} \quad (10.39a)$$

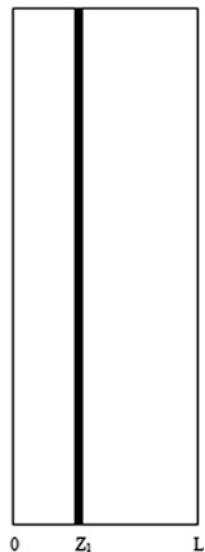
or

$$\delta\lambda = \frac{\delta\Sigma_a \phi^*(z_1) \phi_0(z_1)}{v \Sigma_{f0} \int_0^L \phi^*(z) \phi_0(z) dz} \quad (10.40b)$$

$$\delta k = \rho = -\frac{\delta\Sigma_a}{v \Sigma_{f0}} \frac{2}{\pi} \sin^2(Bz_1) \quad (10.41)$$

This can be seen as Fig. 10.2, which is the representation of a delta function perturbation.

Fig. 10.2 Delta function perturbation



Problems

Problem 10.1 Listed below are a set of typical group constants for a BWR. Calculate the multiplication factor for this reactor if it can be treated as a right circular cylinder of a height of 370 cm and a diameter of 340 cm.

Group constant	Group 1	Group 2
$v\Sigma_{g\text{FISSION}}$	0.001348	0.040783
$\Sigma_{g\text{ABSORPTION}}$	0.001469	0.040249
Σ_g	0.859599	0.142481
$\Sigma_{g\text{REMOVAL}}$	0.044587	0.040249
χ_g	1.0	0.0

Problem 10.2 Using the group constants from the previous problem, calculate:

- (a) The k_∞ .
- (b) The resonance escape probability
- (c) The fast fission factor
- (d) The fast and thermal non-leakage probabilities for this reactor.

Problem 10.3 Calculate the critical radius for an unreflected right circular cylinder reactor characterized by the following group constants. Assume that:

The reactor height = 25 cm		
Group constant	Group 1	Group 2
$v\Sigma_{g\text{FISSION}}$	0.002562	0.15180
$\Sigma_{g\text{ABSORPTION}}$	0.001930	0.09509
$\Sigma_{g\text{TRANSPORT}}$	0.466100	2.95420
$\Sigma_{g\text{DOWNSTREAM}}$	0.055140	–
χ_g	1.0	0.0

Problem 10.4 Calculate the multiplication factor for an unreflected fast reactor with the following cross-sectional data and core size. Assume that:

Core radius = 111 cm and core height 91.44 cm

Group constant	Group 1	Group 2
$v\Sigma_{g\text{FISSION}}$	0.011040	0.005486
$\Sigma_{g\text{ABSORPTION}}$	0.004598	0.004108
$\Sigma_{g\text{DOWNSTREAM}}$	0.023420	–
$\Sigma_{g\text{TRANSPORT}}$	0.028020	0.242200
χ_g	0.55	0.45

Problem 10.5 Calculate the critical height for a fast reactor core that is reflected on top and bottom by a blanket with the cross sections given below. Assume that:

Core radius = 100 cm 1 group cross sections	Core	Blanket
$v\Sigma_{\text{FISSION}}$	0.006017	0.000594
$\Sigma_{\text{ABSORPTION}}$	0.004159	0.001471
$\Sigma_{\text{TRANSPORT}}$	0.22836	0.31325

Problem 10.6 Given the flux solutions below for a two-group calculation in a sphere for a pebble bed reactor, calculate the self-shielding factors for both the fast and thermal groups. The fuel extends from 0.0 to 0.8 cm and the moderator extends from 0.8 to 1.2 cm. Assume linear variation across each of the regions. The plot below gives a picture even though it is not labeled very well

	Flux	
Radius	Thermal	Fast
0.0	0.1	1.0
0.8	0.5	0.95
1.2	1.0	0.30

Chapter 11

Reactor Kinetics and Point Kinetics



The point kinetics model can be obtained directly from the space- and time-dependent transport equations. However, these equations are too complicated to be of any practical application. The diffusion approximation, obtained by keeping only the PI terms of the spherical harmonic expansion in the angular variable of the directional flux, is frequently used in neutronic analysis. This chapter discusses reactor characteristics that change because of changing reactivity. A basic approach using a minimum of mathematics has been followed. Emphasis has been placed on distinguishing between prompt and delayed neutrons and showing relationships among reactor variables, k_{eff} , period, neutron density, and power level.

11.1 Time-Dependent Diffusion Equation

For the analysis of point reactor kinetics, the situation arises where one needs to consider the transient changes resulting from the departure of the reactor condition from the critical state. This results under the following conditions as:

1. Startup.
2. Shutdown.
3. Accidental disturbances in the course of what is intended to be steady-state operation.

The power produced during a reactor transient is one of the most significant factors, which is determining the degree of damage that can happen from an accident within reactor.

The time-dependent power production is related to the effective multiplication factor k_{eff} and the prompt and delayed neutron properties through the reactor kinetics equations. The spatial distribution of the reactor neutron flux can be ignored in lieu of an emphasis on its time behavior. The reactor is viewed as a point; hence, the

terminology of point reactor kinetics arises. In this regard, a distinction must be made between the behaviors of the prompt and delayed neutrons.

Point kinetics is very interesting because of the apparent simplicity of the resulting differential equations. The method is very frequently used, but the underlying difficulties in obtaining the parameters are hidden. In spite of all this, many inherent characteristics of the dynamics of nuclear cores can be deduced from these equations. In addition, these same equations provide a tool for the analysis, the comparison, and the practical implementation of various numerical schemes that may eventually be used in more complex situations. An integration technique that does not pass the test of point kinetics will certainly not be used in space-time kinetics. Point kinetics can thus play the role of an experimental bench before expensive problems are attempted with more advanced methods [1].

The driving factor, behind point kinetics, is to separate the flux into two factors: the first one being a shape function depending both on space and time and a second factor depending only on time in the following fashion:

$$\phi(\vec{r}, t) = S(\vec{r}, t)T(t) \quad (11.1)$$

Note that this equation for the flux does not involve any approximation and that the equality is maintained. However, the shape function $S(\vec{r}, t)$ depends both on space and on time in this approach. We now introduce a column vector of weight functions as:

$$W(\vec{r}) = \begin{bmatrix} W_1(\vec{r}) \\ W_2(\vec{r}) \\ \vdots \\ W_G(\vec{r}) \end{bmatrix} \quad (11.2)$$

whose function will be to give *rise* to general equations. In effect, Eq. 11.1 presents a degree of arbitrariness in the choice of $S(\vec{r}, t)$ and of $T(t)$; only the product of the two variables needs to be specified. We will use $W(\vec{r})$ to introduce normalization constraints, which it will obey at all times during a transient condition. Specifically, we define:

$$T(t) = \left\langle [W]^T [v]^{-1} [\phi] \right\rangle, \quad (11.3)$$

and it *follows* that Eq. 11.1 and the shape function $S(\vec{r}, t)$ must obey the following constraint, by substituting Eq. 11.1 into Eq. 11.3:

$$\left\langle [W]^T [v]^{-1} [S(\vec{r}, t)] \right\rangle = 1 \quad (11.4)$$

where *the* symbol $\langle \rangle$ means spatial integration over the whole domain of the nuclear core.

Note that the factor $T(t)$ in Eq. 11.3 is called the amplitude function and the shape function $S(\vec{r}, t)$ represents in some sense the total number of neutrons in the reactor, but this number depends on the weight function. As the constraint on $S(\vec{r}, t)$ does not depend on time, the shape function may change in time, but its integral is time independent. Thus, $T(t)$ itself represents the neutron population change in the reactor.

We can now seek for a differential equation for the time-dependent variable $T(t)$ by replacing $\phi(\vec{r}, t)$ by the product of $S(\vec{r}, t)T(t)$ in the *space-time kinetics* equations, by *pre-multiplying the resulting equations by $W(\vec{r})^T$* , and by integrating over the whole core volume. Thus using Eq. 11.4, we obtain the following results:

$$\begin{aligned} & \left\langle \left[W(\vec{r}) \right]^T \left\{ \begin{array}{l} \left\langle [W]^T [v]^{-1} [S] \right\rangle \frac{\partial T}{\partial t} \\ \nabla \cdot [D] \vec{\nabla} [S] - [\Sigma][S] \\ + \left((1 - \beta)[\chi^p] + \sum_{i=1}^D \beta_i [\chi_i^d] \right) [v\Sigma_f]^T [S] \end{array} \right\} \right\rangle T(t) \\ & - \left\langle \left[W(\vec{r}) \right]^T \sum_{i=1}^D \beta_i [\chi_i^d] [v\Sigma_f]^T [S] \right\rangle T(t) + \sum_{i=1}^D \lambda_i \left\langle [W]^T [\chi_i^d] C_i \right\rangle \end{aligned} \quad (11.5)$$

where in order to *conform* to certain conventions, we have added and subtracted the term in:

$$\sum_{i=1}^D \beta_i [\chi_i^d] [v\Sigma_f]^T [S] \quad (11.6)$$

Very similar operations are performed on the precursor equations that we pre-multiply by $[W]^T [\chi_i^d]$ before integrating over space to get the following relationship:

$$\frac{\partial}{\partial t} \left\langle [W]^T [\chi_i^d] C_i \right\rangle = \left\langle [W]^T \beta_i [\chi_i^d] [S] \right\rangle T - \lambda_i \left\langle [W]^T [\chi_i^d] C_i \right\rangle \quad (11.7)$$

We now *define* the following quantities as:

$$C_i(t) = \frac{\left\langle [W]^T [\chi_i^d] C_i \right\rangle}{\left\langle [W]^T [v]^{-1} [S] \right\rangle} \quad (11.8)$$

Now, we first define another quantity that is known as the *mean neutron generation time* as $\Lambda(t)$ so we can write:

$$\Lambda(t) = \frac{\left\langle [W]^T [v]^{-1} [S] \right\rangle}{\left\langle [W]^T \left\{ (1 - \beta) [\chi^P] + \sum_{i=1}^D \beta_i [\chi_i^d] \right\} [v\Sigma_f]^T [S] \right\rangle} \quad (11.9)$$

where *again* $\Lambda(t)$ is defined as:

$\Lambda(t) \equiv \frac{1}{k} \equiv$ mean generation time between birth of neutron and subject absorption inducing fission.

Note that if $k \sim 1$, then $\Lambda(t)$ is essentially just the prompt neutron lifetime ℓ .

Now, if we introduce the quantity of $\beta_i(t)$, as the following form:

$$\beta_i(t) = \beta_i \frac{\left\langle [W]^T [\chi_i^d] [v\Sigma_f]^T [S] \right\rangle}{\left\langle [W]^T \left\{ (1 - \beta) [\chi^P] + \sum_{i=1}^D \beta_i [\chi_i^d] \right\} [v\Sigma_f]^T [S] \right\rangle} \quad (11.10)$$

then we can *write*:

$$\beta(t) \approx \sum_{i=1}^D \beta_i(t) \quad (11.11)$$

Now if we define a very important quantity known as the *reactivity* and represented by $\rho(t)$, which essentially measures the deviation of core multiplication from its critical value, where $k = 1$, then we can write the following equation by utilizing what we have shown in Eq. 11.5:

$$\rho(t) = \frac{\left[W(\vec{r}) \right]^T \left\{ \nabla \cdot [D] \vec{\nabla} [S] - [\Sigma][S] + \left((1 - \beta) [\chi^P] + \sum_{i=1}^D \beta_i [\chi_i^d] \right) [v\Sigma_f]^T [S] \right\}}{\left\langle [W]^T \left\{ (1 - \beta) [\chi^P] + \sum_{i=1}^D \beta_i [\chi_i^d] \right\} [v\Sigma_f]^T [S] \right\rangle} \quad (11.12)$$

Another form of reactivity factor $\rho(t)$ is presented by Duderstadt and Hamilton [2] in the following:

$$\rho(t) = \frac{k(t) - 1}{k(t)} = \text{reactivity} \quad (11.13)$$

Note that Eq. 11.13 explicitly indicates criticality factor k as a function of time t ; hence reactivity factor ρ may be a function of time as well.

Now that we have definitions in Eq. 11.10 and Eq. 11.12, the *space-time kinetics equation* becomes:

$$\begin{cases} \frac{dT}{dt} = \frac{[\rho(t) - \beta]}{\Lambda(t)} T + \sum_{i=1}^D \lambda_i C_i \\ \frac{dC_i}{dt} = \frac{\beta_i(t)}{\Lambda(t)} - \lambda_i C_i \quad i = 1, \dots, 6 \end{cases} \quad (11.14)$$

Note that Eq. 11.14 presents a set of seven coupled ordinary differential equations, in time, which describe both the time dependence of the neutron population in the reactor and the decay of the delayed neutron precursor [2].

11.2 Derivation of Exact Point Kinetics Equations (EPKE)

The most accurate description of the neutron behavior in a near critical nuclear reactor is given by the three-dimensional, energy-, angle-, and time-dependent form of the Boltzmann transport equation given by:

$$\begin{aligned} \frac{1}{v(E)} \frac{d\phi(\vec{r}, E, \vec{\Omega}, t)}{dt} + \vec{\Omega} \cdot \nabla \phi(\vec{r}, E, \vec{\Omega}, t) + \Sigma_t(\vec{r}, E, t) \phi(\vec{r}, E, \vec{\Omega}, t) = q(\vec{r}, E, \vec{\Omega}, t) \\ + \int_{E'} \int_{\vec{\Omega}'} \Sigma_s(\vec{r}, E', \vec{\Omega}' \rightarrow E, \vec{\Omega}, t) \phi(\vec{r}, E', \vec{\Omega}', t) dE' d\vec{\Omega}' \\ + \chi(E, t) \int_{E'} \int_{\vec{\Omega}'} \frac{v(E')}{4\pi} \Sigma_f(\vec{r}, E', \vec{\Omega}', t) \phi(\vec{r}, E', \vec{\Omega}', t) dE' d\vec{\Omega}' \end{aligned} \quad (11.15)$$

where fission has been assumed to be isotropic in the laboratory reference frame. In addition, the following quantities are defined:

$\phi(\vec{r}, E, \vec{\Omega}, t)$ is the time-dependent angular flux density (the number of neutrons at position \vec{r} , moving in direction $\vec{\Omega}$ with energy E , at time t)

$v(E)$ is the velocity of neutrons with energy E

$\Sigma_t(\vec{r}, E, t)$ is the macroscopic material total cross section for neutrons of energy E , at position \vec{r} , and time t

$q(\vec{r}, E, \vec{\Omega}, t)$ is the source of neutrons at position \vec{r} , energy E , and moving in direction $\vec{\Omega}$ at time t

$\Sigma_s(\vec{r}, E', \vec{\Omega}' \rightarrow E, \vec{\Omega}, t)$ is the macroscopic material cross section for scattering from direction $\vec{\Omega}'$ and energy E' to direction $\vec{\Omega}$ and energy E at position \vec{r} and time t

$\chi(E, t)$ is the time-dependent yield of fission neutrons at energy E

$v(E')$ is the total yield of neutrons because of fission caused by a neutron of energy E'
 $\Sigma_f(\vec{r}, E', \vec{\Omega}', t)$ is the macroscopic fission cross section for neutrons of energy E' at
 position \vec{r} and time t

Fission has been assumed isotropic in the laboratory reference frame.

Since not all neutrons are produced at the moment of fission, the source term must be broken up into an independent source term and a delayed neutron source term. This can be accomplished as follows. Let:

$$\begin{aligned} \chi(E, t) \int_{E'} \int_{\vec{\Omega}'} \frac{v}{4\pi} \Sigma_f(\vec{r}, E', \vec{\Omega}', t) \phi(\vec{r}, E', \vec{\Omega}', t) dE' d\vec{\Omega}' \\ = \chi_p(E)(1 - \beta) \int_{E'} \int_{\vec{\Omega}'} \frac{v}{4\pi} \Sigma_f(\vec{r}, E', \vec{\Omega}', t) \phi(\vec{r}, E', \vec{\Omega}', t) dE' d\vec{\Omega}' + \sum_{i=1}^M \chi_{id}(E) \lambda_i C_i(\vec{r}, t) \end{aligned} \quad (11.16)$$

where a separate *energy* spectrum has been prescribed for prompt and delayed neutrons and the precursor concentrations have been introduced as $C_i(\vec{r}, t)$.

This equation can theoretically be solved by applying straightforward finite difference methods in all variables (seven for the most general case). However, this is a very large computational task and has never really been accomplished for the most general case. Usually the number of dimensions has been reduced, by taking advantage of symmetry in the spatial dimensions and the lack of a strong angular dependence in the energy-dependent flux. Even so, the energy-dependent diffusion equations in more than one spatial dimension present a formidable computation task. It has been found that this level of effort is not required for a significant number of reactor kinetics problems and a heuristic point kinetics equation approach is very accurate. The objective of the following derivation is to make explicit the approximations inherent in the point kinetics equations and therefore in some way provide an indication of their adequacy in untried circumstances.

With this goal in mind, it is useful to factor the time-dependent angular flux density into two parts:

$$\phi(\vec{r}, E', \vec{\Omega}', t) = \varphi(\vec{r}, E', \vec{\Omega}', t) \cdot P(t) \quad (11.17)$$

where $P(t)$ will *hopefully* contain the major time dependence and φ will not be a strong function of time. In order to unambiguously perform this splitting, or factorization, a rule for sorting out $P(t)$ is required. The most useful rule is:

$$\int_{\vec{r}, E, \vec{\Omega}} W(\vec{r}, E, \vec{\Omega}) \frac{1}{v(E)} \varphi(\vec{r}, E, \vec{\Omega}, t) = 1.0 \quad (11.18)$$

where $W(\vec{r}, E, \vec{\Omega})$ is some *arbitrary* weighting function yet to be selected. Multiplying the transport equation by $W(\vec{r}, E, \vec{\Omega})$ and integrating over all space, energies, and angles, the following equation can be obtained:

$$\frac{d}{dt} \int_{\vec{r}, E, \vec{\Omega}} W(\vec{r}, E, \vec{\Omega}) \frac{1}{v(E)} \varphi(\vec{r}, E, \vec{\Omega}, t) P(t) d\vec{r} dE d\vec{\Omega} \quad (11.19a)$$

$$+ \int_{\vec{r}, E, \vec{\Omega}} W(\vec{r}, E, \vec{\Omega}) \vec{\Omega} \cdot \nabla \varphi(\vec{r}, E, \vec{\Omega}, t) P(t) d\vec{r} dE d\vec{\Omega} \quad (11.19b)$$

$$+ \int_{\vec{r}, E, \vec{\Omega}} W(\vec{r}, E, \vec{\Omega}) \Sigma_t(\vec{r}, E, t) \varphi(\vec{r}, E, \vec{\Omega}, t) P(t) d\vec{r} dE d\vec{\Omega} \quad (11.19c)$$

$$= \int_{\vec{r}, E, \vec{\Omega}} W(\vec{r}, E, \vec{\Omega}) q(\vec{r}, E, \vec{\Omega}, t) d\vec{r} dE d\vec{\Omega} \quad (11.19d)$$

$$+ \int_{\vec{r}, E, \vec{\Omega}} W(\vec{r}, E, \vec{\Omega}) \int_{E', \vec{\Omega}} \Sigma_s(\vec{r}, E', \vec{\Omega}' \rightarrow E, \vec{\Omega}, t) \varphi(\vec{r}, E', \vec{\Omega}', t) P(t) dE' d\vec{\Omega}' d\vec{r} dE d\vec{\Omega} \quad (11.19e)$$

$$+ \int_{\vec{r}, E, \vec{\Omega}} W(\vec{r}, E, \vec{\Omega}) \chi_p(E) (1 - \beta) \int_{E', \vec{\Omega}} \frac{v(E')}{4\pi} \Sigma_f(\vec{r}, E', \vec{\Omega}', t) \varphi(\vec{r}, E', \vec{\Omega}', t) P(t) dE' d\vec{\Omega}' d\vec{r} dE d\vec{\Omega} \quad (11.19f)$$

$$+ \int_{\vec{r}, E, \vec{\Omega}} W(\vec{r}, E, \vec{\Omega}) \sum_{i=1}^M \chi_{id}(E) \lambda_i C_i(\vec{r}, t) d\vec{r} dE d\vec{\Omega} \quad (11.19g)$$

The individual terms in this equation are identified because it will be convenient to reduce them one at a time.

Consider first Eq. 11.19a. Removing $P(t)$ from the phase space integrals gives:

$$\text{Eq. 11.19a} = \begin{cases} \frac{d}{dt} P(t) \int_{\vec{r}, E, \vec{\Omega}} W(\vec{r}, E, \vec{\Omega}) \frac{1}{v(E)} \varphi(\vec{r}, E, \vec{\Omega}, t) d\vec{r} dE d\vec{\Omega} + \\ P(t) \frac{d}{dt} \int_{\vec{r}, E, \vec{\Omega}} W(\vec{r}, E, \vec{\Omega}) \frac{1}{v(E)} \varphi(\vec{r}, E, \vec{\Omega}, t) d\vec{r} dE d\vec{\Omega} \end{cases}$$

Applying the normalization condition reduces this term to:

$$\text{Eq.11.19a} = \frac{d}{dt} P(t) \cdot 1.0 + P(t) \cdot \frac{d}{dt} 1.0 = \frac{d}{dt} P(t)$$

This is the major motivation for choosing the normalization condition in the form it was specified.

The next step is to define the equilibrium fission source term. The equilibrium fission source is composed of the prompt and delayed components. At equilibrium, or the critical condition, the spatial dependence of the delayed spectrum is the same as the prompt spectrum spatial dependence. The difference between the equilibrium spectrum and the conventional spectrum is that the delayed part of the neutron emission has a different energy spectrum. For the equilibrium or critical condition fission source, we have:

$$\begin{aligned} \chi(E) \int_{E, \vec{\Omega}'} \frac{v(E')}{4\pi} \Sigma_f(\vec{r}, E', \vec{\Omega}') \phi(\vec{r}, E', \vec{\Omega}') dE' d\vec{\Omega}' \\ = \chi_p(E)(1 - \beta) \int_{E', \vec{\Omega}'} \frac{v(E')}{4\pi} \Sigma_f(\vec{r}, E', \vec{\Omega}') \phi(\vec{r}, E', \vec{\Omega}') dE' d\vec{\Omega}' \\ + \sum_{i=1}^M \chi_{id}(E) \beta_i \int_{E', \vec{\Omega}'} \frac{v(E')}{4\pi} \Sigma_f(\vec{r}, E', \vec{\Omega}') \phi(\vec{r}, E', \vec{\Omega}') dE' d\vec{\Omega}' \end{aligned} \quad (11.20)$$

Therefore, to incorporate the equilibrium fission source, we must add and subtract the delayed fission source components from the transport equation. When this is done and the terms are added to T6, it becomes:

$$\text{Eq.11.19f} = \begin{cases} \int_{\vec{r}, E, \vec{\Omega}} W(\vec{r}, E, \vec{\Omega}) \{ \chi_p(E)(1 - \beta) \int_{E', \vec{\Omega}'} \frac{v(E')}{4\pi} \Sigma_f(\vec{r}, E', \vec{\Omega}', t) \\ \phi(\vec{r}, E', \vec{\Omega}', t) P(t) dE' d\vec{\Omega}' \\ + \sum_{i=1}^M \chi_{id}(E) \beta_i \int_{E', \vec{\Omega}'} \frac{v(E')}{4\pi} \Sigma_f(\vec{r}, E', \vec{\Omega}', t) \phi(\vec{r}, E', \vec{\Omega}', t) P(t) \\ - \sum_{i=1}^M \chi_{id}(E) \beta_i \int_{E', \vec{\Omega}'} \frac{v(E')}{4\pi} \Sigma_f(\vec{r}, E', \vec{\Omega}', t) \phi(\vec{r}, E', \vec{\Omega}', t) P(t) \} \\ d\vec{r} dE d\vec{\Omega} \end{cases} \quad (11.21)$$

Now define an equilibrium reduced fission source, FS , as:

$$\int_{\vec{r}, E, \vec{\Omega}} W(\vec{r}, E, \vec{\Omega}) \left\{ \chi_p(E)(1 - \beta) + \sum_{i=1}^M \chi_{id}(E) \beta_i \right\} \int_{E', \vec{\Omega}'} \frac{v(E')}{4\pi} \Sigma_f(\vec{r}, E', \vec{\Omega}', t) \varphi(\vec{r}, E', \vec{\Omega}', t) dE' d\vec{\Omega}' d\vec{r} dEd \vec{\Omega} \quad (11.22)$$

And dividing every term by FS will give the following equation:

$$\{ \text{Eq.11.19a} + \text{Eq.11.19b} + \text{Eq.11.19c} \} / FS = \{ \text{Eq.11.19d} + \text{Eq.11.19e} + \text{Eq.11.19f} + \text{Eq.11.19g} \} / FS$$

Identifying $1/FS$ as Λ and rearranging the terms give:

$$\begin{aligned} \Lambda \text{Eq.11.19a} &= \Lambda \{ \text{Eq.11.19e} + \text{Eq.11.19f} - \text{Eq.11.19b} \} - \text{Eq.11.19c} \\ &\quad + \Lambda \text{Eq.11.19d} + \Lambda \text{Eq.11.19g} \end{aligned}$$

Now consider Eq. 11.19d and define a reduced independent source as:

$$Q(t) = \int_{\vec{r}, E, \vec{\Omega}'} W(\vec{r}, E, \vec{\Omega}') q(\vec{r}, E, \vec{\Omega}', t) d\vec{r} dEd d\vec{\Omega}' \quad (11.23)$$

Define $Z_i(t)$ as:

$$Z_i(t) = \int_{\vec{r}, E, \vec{\Omega}} W(\vec{r}, E, \vec{\Omega}) C_i(\vec{r}, t) \chi_{id}(E) d\vec{r} dEd d\vec{\Omega} \quad (11.24)$$

The transport equation can now be written as:

$$\Lambda \frac{dP(t)}{dt} = \Lambda \{ \text{Eq.11.19f} + \text{Eq.11.19e} + -\text{Eq.11.19b} - \text{Eq.11.19c} \} \quad (11.25)$$

Consider Eq. 11.19f again and write it as:

$$\text{Eq. 11.19f} = FS^* P(t) + \text{Eq. 11.19f} \quad (11.26)$$

where:

$$\text{Eq.11.19f} = - \sum_{i=1}^M \beta_i \chi_{id}(E) \int_{E', \vec{\Omega}'} \frac{v(E')}{4\pi} \Sigma_f(\vec{r}, E', \vec{\Omega}', t) \varphi(\vec{r}, E', \vec{\Omega}', t) P(t) dE' d\vec{\Omega}' \quad (11.27)$$

Then, defining:

$$\beta = -\frac{\text{Eq. 11.19f}'\Lambda}{P(t)} \quad (11.28)$$

and:

$$\rho = \frac{\{\text{Eq.11.19e} + FS^*P(t) - \text{Eq.11.19b} - \text{Eq.11.19c}\}\Lambda}{P(t)} \quad (11.29)$$

gives:

$$\Lambda \frac{dP(t)}{dt} = (\rho - \beta)P(t) + \Lambda Q(t) + \Lambda \sum_{i=1}^M \lambda_i Z_i(t) \quad (11.30)$$

or:

$$\frac{dP(t)}{dt} = \frac{\rho - \beta}{\Lambda} P(t) + Q(t) + \sum_{i=1}^M \lambda_i Z_i(t) \quad (11.31)$$

This is essentially the power equation for the point kinetics description of reactor behavior.

Now consider the precursor equations given by:

$$\frac{dC_i(\vec{r}, t)}{dt} = \beta_i \int_{E, \vec{\Omega}} \frac{v(E)}{4\pi} \Sigma_f(\vec{r}, E, \vec{\Omega}, t) \varphi(\vec{r}, E, \vec{\Omega}, t) P(t) dEd \vec{\Omega} - \lambda_i C_i(\vec{r}, t) \quad (11.32)$$

Multiplying these equations by:

$$\int_{\vec{r}, E, \vec{\Omega}} W(\vec{r}, E, \vec{\Omega}) \chi_{id}(E) d\vec{r} dEd \vec{\Omega} \quad (11.33)$$

will give:

$$\begin{aligned} \frac{dZ_i(\vec{r}, t)}{dt} &= \beta_i \int_{\vec{r}, E, \vec{\Omega}} \chi_{id}(E) W(\vec{r}, E, \vec{\Omega}) \int_{E', \vec{\Omega}'} \frac{v(E)}{4\pi} \Sigma_f(\vec{r}, E, \vec{\Omega}, t) \varphi(\vec{r}, E, \vec{\Omega}, t) \\ &\quad P(t) dE' d\vec{\Omega}' d\vec{r} dEd \vec{\Omega} - \lambda_i C_i(\vec{r}, t) \end{aligned} \quad (11.34)$$

Remembering that:

$$\begin{aligned} \beta &= \frac{-\text{Eq.11.19f}'\Lambda}{P(t)} \\ &= \frac{\sum_{i=1}^M \beta_i \int_{\vec{r}, E, \vec{\Omega}} \chi_{id} W \int_{E', \vec{\Omega}'} \frac{v(E')}{4\pi} \Sigma_f \varphi P(t) dE' d\vec{\Omega}' d\vec{r} dEd\vec{\Omega}}{P(t) \int_{\vec{r}, E, \vec{\Omega}} W \left\{ \chi_p(1 - \beta) + \sum_{i=1}^M \chi_{id} \beta_i \right\} \int_{E', \vec{\Omega}'} \frac{v(E')}{4\pi} \Sigma_f \varphi dE' d\vec{\Omega}' d\vec{r} dEd\vec{\Omega}} \end{aligned} \quad (11.35)$$

The precursor equations become:

$$\frac{dZ_i(t)}{dt} = \frac{\beta_i}{\Lambda} P(t) - \lambda_i Z_i(t) \quad (11.36)$$

The “exact” point kinetics equations are then:

$$\frac{dP(t)}{dt} = \frac{\rho - \beta}{\Lambda} P(t) + \sum_{i=1}^M \lambda_i Z_i(t) \quad (11.37)$$

$$\frac{dP(t)}{dt} = \frac{\rho - \beta}{\Lambda} P(t) + \sum_{i=1}^M \lambda_i Z_i(t) \quad (11.38)$$

These equations are exact if all of the parameters in them are computed according to the formulas given above. However, to apply the formulas given above exactly would be as difficult a task as integrating the original transport equation directly. The real advantage of deriving the “exact” equations in this manner is to rigorously prescribe how to compute the quantities used to predict kinetic behavior. When approximations are introduced in computing these quantities, at least there is a standard to compare against in order to understand the impact of the approximations.

Consider the definition of ρ . The complete expression for ρ is given by:

$$\rho = \frac{\{\text{Eq.11.19e} + FS^*P(t) - \text{Eq.11.19b} - \text{Eq.11.19c}\}\Lambda}{P(t)} \quad (11.39)$$

or:

$$\begin{cases} \int_{\vec{r}, E, \vec{\Omega}} W \int_{E', \vec{\Omega}'} \Sigma_s(E', \vec{\Omega}' \rightarrow E, \vec{\Omega}') \varphi dE' d\vec{\Omega}' d\vec{r} dEd\vec{\Omega} + \\ \int_{\vec{r}, E, \vec{\Omega}} W \left\{ \chi_p(1 - \beta) + \sum_{i=1}^M \chi_{id} \beta_i \right\} \int_{E', \vec{\Omega}'} \frac{v}{4\pi} \Sigma_f \varphi dE' d\vec{\Omega}' d\vec{r} dEd\vec{\Omega} \end{cases} \quad (11.40a)$$

or we find ρ to be as follows:

$$\rho = \frac{-\int_{\vec{r}, E, \vec{\Omega}} W \vec{\Omega} \cdot \nabla \varphi d\vec{r} dEd \vec{\Omega} - \int_{E, E, \vec{\Omega}} W \Sigma_t \varphi d\vec{r} dEd \vec{\Omega}}{\int_{\vec{r}, E, \vec{\Omega}} W \left\{ \chi_p (1 - \beta) + \sum_{i=1}^M \chi_{id} \beta_i \right\} \int_{E', \vec{\Omega}} \frac{v}{4\pi} \Sigma_f \varphi dE' d\vec{\Omega}' d\vec{r} dEd \vec{\Omega}} \quad (11.40b)$$

where the functional dependence of the major variables has been suppressed. The notation can be further simplified by defining:

$$F\varphi = \int_{E, \vec{\Omega}} \frac{v(E')}{4\pi} \Sigma_f(\vec{r}, E', \vec{\Omega}', t) \varphi(\vec{r}, E', \vec{\Omega}', t) dE' d\vec{\Omega}' \quad (11.41)$$

$$\chi = \chi_p (1 - \beta) + \sum_{i=1}^M \chi_{id} \beta_i \quad (11.42)$$

and suppressing most of the variable dependence. Then:

$$\rho = \frac{-\int_{\vec{r}, E, \vec{\Omega}} W (\vec{\Omega} \cdot \nabla \varphi + \Sigma_t \varphi - \chi F\varphi - \Sigma_s \varphi)}{\int_{\vec{r}, E, \vec{\Omega}} W \chi F\varphi} \quad \beta = \frac{\sum_{i=1}^M \beta_i \int_{\vec{r}, E, \vec{\Omega}} W \chi_{id} F\varphi}{\int_{\vec{r}, E, \vec{\Omega}} W \chi F\varphi} \quad (11.43)$$

$$\Lambda = \frac{1}{\int_{\vec{r}, E, \vec{\Omega}} W \chi F\varphi} \quad Q(t) = \int_{\vec{r}, E, \vec{\Omega}} W q \quad Z_i(t) = \int_{\vec{r}, E, \vec{\Omega}} W \chi_{id} C_i \quad (11.44)$$

Note that for a critical reactor, the static eigenvalue equation is given by:

$$\vec{\Omega} \cdot \nabla \varphi + \Sigma_t \varphi = \chi F\varphi + \Sigma_s \varphi \quad (11.45)$$

It is also worth noting at this time that φ is not the diffusion flux, but is actually a reduced transport flux and definitely can contain anisotropic components that may be necessary to evaluate in order to correctly calculate the reactivity. However, the analysis that we have gone through will apply to both transport models and diffusion theory models.

11.3 The Point Kinetics Equations

Now that we have derived the point kinetics equations (PKE), we should investigate what they say about nuclear reactor behavior. We begin by noting that form a homogeneous set of ordinary differential equations. As we know the solution to a homogeneous set of equations only exists for certain parameters called eigenvalues. We can write the equations as:

$$\begin{aligned}
 \frac{dP}{dt} &= \frac{\rho - \beta}{\Lambda} P + \lambda_1 z_1 + \lambda_2 z_2 + \lambda_3 z_3 + \lambda_4 z_4 + \lambda_5 z_5 + \lambda_6 z_6 \\
 \frac{dz_1}{dt} &= \frac{\beta_1}{\Lambda} P - \lambda_1 z_1 \\
 \frac{dz_2}{dt} &= \frac{\beta_2}{\Lambda} P - \lambda_2 z_2 \\
 \frac{dz_3}{dt} &= \frac{\beta_3}{\Lambda} P - \lambda_3 z_3 \\
 \frac{dz_4}{dt} &= \frac{\beta_4}{\Lambda} P - \lambda_4 z_4 \\
 \frac{dz_5}{dt} &= \frac{\beta_5}{\Lambda} P - \lambda_5 z_5 \\
 \frac{dz_6}{dt} &= \frac{\beta_6}{\Lambda} P - \lambda_6 z_6
 \end{aligned} \tag{11.46}$$

And if we assume a form for P and each z_i that incorporates an eigenvalue ω such that:

$$P(t) = P_0 e^{\omega t} \quad \frac{dP(t)}{dt} = \omega P(t) \quad Z_i(t) = Z_{i0} e^{\omega t} \quad \frac{dZ_i(t)}{dt} = \omega Z_i(t) \tag{11.47}$$

then each of the $Z_i(t)$ equations can be solved for Z_i to get:

$$(\omega + \lambda_i) z_i(t) = \frac{\beta_i}{\Lambda} P(t) \quad z_i(t) = \frac{\beta_i}{\Lambda(\omega + \lambda_i)} P(t) \tag{11.48}$$

Then:

$$\omega P(t) = \frac{\rho - \beta}{\Lambda} P(t) + P(t) \sum_{i=1}^6 \frac{\lambda_i \beta_i}{\Lambda(\omega + \lambda_i)} \tag{11.49}$$

And dividing out $P(t)$ gives:

$$\left\{ \begin{array}{l} \sum_{i=1}^6 \frac{\lambda_i \beta_i}{\omega + \lambda_i} = \rho - \sum_{i=1}^6 \beta_i \frac{\omega + \lambda_i}{\omega + \lambda_i} + \sum_{i=1}^6 \beta_i \frac{\lambda_i}{\omega + \lambda_i} = \rho - \omega \sum_{i=1}^6 \frac{\beta_i}{\omega + \lambda_i} \\ \rho = \omega \left(\Lambda + \sum_{i=1}^6 \frac{\beta_i}{\omega + \lambda_i} \right) \end{array} \right. \quad (11.50)$$

There are seven roots for w in this inhour equation.

Inhour Equation

The relationship between a step change in reactivity (ρ) and the resulting reactor period (T), allowing for the delayed neutrons, can be derived in the form of an equation such as:

$$\rho = \frac{\ell}{kT} + \sum_{i=1}^6 \frac{\beta_i}{1 + \lambda_i T} \text{ where:}$$

β_i is delayed neutron fraction for group i

λ_i is decay constant of delayed neutron group i (s^{-1}) = $\ln 2/t_{1/2}$

ℓ is prompt neutron lifetime (s)

T is reactor period.

This equation is often called the reactivity equation or the inhour equation, although strictly speaking this is not the inhour equation proper. (The term inhour comes from expressing reactivity in the units of inverse hours. The inhour unit is then that reactivity will make the stable reactor period equal to 1 h.) These are numerous different formulations of the reactivity equation, but this one will suffice for the purposes of this book.

Now consider the One Delay Family model. The inhour equation in this case becomes:

$$\left[\begin{array}{l} \rho = \omega \left(\Lambda + \frac{\beta}{\omega + \lambda} \right) \\ (\omega + \lambda) \rho = \omega \Lambda (\omega + \lambda) + \omega \beta \\ \omega \frac{\rho - \beta}{\Lambda} + \frac{\lambda \rho}{\Lambda} = \omega^2 + \lambda \omega \\ \omega^2 + \left(\lambda - \frac{\rho - \beta}{\Lambda} \right) \omega - \frac{\lambda \rho}{\Lambda} = 0 \end{array} \right. \quad (11.51)$$

Note that for most cases, if $\rho < \beta$, $\lambda \ll (\rho - \beta)/\Lambda$, so λ can be neglected. Then:

$$\omega = \frac{\rho - \beta}{2\Lambda} \pm \sqrt{\left(\frac{\rho - \beta}{2\Lambda}\right)^2 + \frac{\lambda\rho}{\Lambda}} = \frac{\rho - \beta}{2\Lambda} \pm \frac{\rho - \beta}{2\Lambda} \sqrt{1 + \frac{4\lambda\rho}{\Lambda(\frac{\rho - \beta}{\Lambda})^2}} \quad (11.52)$$

And noting that $\sqrt{1+x} = 1 + \frac{x}{2} + \dots$ for small x :

$$\begin{cases} \omega_1 = \frac{\rho - \beta}{\Lambda} + \frac{\rho - \beta}{\Lambda} \frac{\lambda\rho}{\Lambda(\frac{\rho - \beta}{\Lambda})^2} = \frac{\rho - \beta}{\Lambda} + \frac{\lambda\rho}{\rho - \beta} \approx \frac{\rho - \beta}{\Lambda} \\ \omega_2 = -\frac{\lambda\rho}{\rho - \beta} = \frac{\lambda\rho}{\beta - \rho} \end{cases} \quad (11.53)$$

Therefore, the general solution for a step reactivity change is:

$$P(t) = P_{01}e^{\frac{\rho-\beta}{\Lambda}t} + P_{02}e^{\frac{\beta-\rho}{\beta-\rho}t} \quad (11.54)$$

We will find the unknown coefficients P_{01} and P_{02} from the initial conditions. Continuity of the power and the derivative of the power give:

$$P_0 = P_{01} + P_{02} \quad (11.55a)$$

$$\begin{aligned} \frac{dP}{dt}(0) &= \frac{\rho - \beta}{\Lambda} P_0 + \lambda z_0 \\ &= \frac{\rho - \beta}{\Lambda} P_0 + \lambda \frac{\beta}{\lambda\Lambda} P_0 \\ &= P_0 \left(\frac{\rho}{\Lambda} \right) \\ &= \omega_1 P_{01} + \omega_2 P_{02} \end{aligned} \quad (11.55b)$$

$$\begin{aligned} P_0 \left(\frac{\rho}{\Lambda} \right) &= \frac{\rho - \beta}{\Lambda} (P_0 - P_{02}) + \frac{\lambda\rho}{\beta - \rho} P_{02} \\ P_0 \frac{\beta}{\Lambda} &= \left(\frac{\lambda\rho}{\beta - \rho} - \frac{\rho - \beta}{\Lambda} \right) P_{02} \\ P_{02} &\approx \frac{\beta}{\beta - \rho} P_0 \\ P_{01} &= \frac{-\rho}{\beta - \rho} P_0 \end{aligned} \quad (11.55c)$$

This gives the complete solution for a step insertion of reactivity as:

$$P(t) = P_0 \left\{ \frac{\beta}{\beta - \rho} e^{\frac{\lambda\rho}{\beta - \rho} t} - \frac{\rho}{\beta - \rho} e^{\frac{\rho - \beta}{K} t} \right\} \quad (11.56)$$

Now that we are here, next we have dynamic and static reactivity, which is the subject of the next section here.

11.4 Dynamic Versus Static Reactivity

An often discussed concept is the difference between dynamic and static reactivity. There are a large number of ways of computing reactivity which is being used in the field today. The simplest, most straightforward, and least accurate is the eigenvalue difference method. That is, two reactor configurations are mocked up as critical systems. An eigenvalue, K , is found that makes each of them critical, and the difference between these two eigenvalues is assumed to be the same as the reactivity defined above. In the limit of small reactivity, this will be approximately correct; however, as the time-dependent flux shape changes in a reactor, it becomes more and more difficult to evaluate reactivity based on a hypothetical eigenvalue.

A more accurate method would be to use the formalism defined above for the time-dependent case but use a time-independent shape function. This static function usually corresponds to the shape function for an exactly critical reactor, $k = 1.0$. In this case, the weighting function, W , can be chosen to make this approximate reactivity as accurate as possible by letting it equal the ADJOINT function for the exactly critical reactor. If the critical ADJOINT function is used, then the reactivity will be insensitive to first-order changes in the shape function; thus, the static reactivity will be as accurate an approximation to the actual reactivity as is possible.

The most accurate method of computing the reactivity is to use the actual time-dependent shape function in the integral. Of course, this is much more difficult to do, as somehow the time dependence has to be calculated. It is also important to note that for this case, the choice of W is somewhat arbitrary. A constant value of 1.0 could be chosen, but the ADJOINT function for an exactly critical reactor is normally used in hopes of mitigating some of the errors introduced in calculating the time-dependent shape function.

The three definitions are:

1. *Eigenvalue difference reactivity*

$$\rho = \frac{k_1 - k_0}{k_1 k_0} \quad (11.57)$$

2. Static reactivity

$$\rho = \frac{\int_{\vec{r}, E, \vec{\Omega}} \phi^* (\vec{\Omega} \cdot \nabla \varphi + \Sigma_t \varphi - \chi F \varphi - \Sigma_s \varphi) d\vec{r} dEd \vec{\Omega}}{\int_{\vec{r}, E, \vec{\Omega}} \phi^* \chi F \varphi d\vec{r} dEd \vec{\Omega}} \quad (11.58)$$

where the *ADJOINT* function for the critical configuration is used as the weighting function and the fluxes are obtained from a static criticality calculation for the current configuration of the reactor assembly.

3. Dynamic reactivity

$$\rho = \frac{\int_{\vec{r}, E, \vec{\Omega}} \phi^* (\vec{\Omega} \cdot \nabla \varphi + \Sigma_t \varphi - \chi F \varphi - \Sigma_s \varphi) d\vec{r} dEd \vec{\Omega}}{\int_{\vec{r}, E, \vec{\Omega}} \phi^* \chi F \varphi d\vec{r} dEd \vec{\Omega}} \quad (11.59)$$

where the *ADJOINT* function for the critical configuration is used as the weighting function and the fluxes are obtained from a time-dependent calculation for the shape function. The difference between the most accurate approach for static reactivity, *ADJOINT* weighting, and the true dynamic reactivity is the use of the time-dependent shape function in the dynamic reactivity case. So now, consider how to calculate this shape function.

11.5 Calculating the Time-Dependent Shape Function

Given that the dynamic reactivity is the actual quantity required in the point kinetics equations, an integrodifferential equation can be derived for its calculation. This equation can then be approximated in many ways in order to obtain solutions that are useful for particular problems. Substituting the factored flux into the transport equation and dividing by $P(t)$ give:

$$\begin{aligned}
& \frac{1}{v(E)} \left\{ \frac{d\varphi(\vec{r}, E, \vec{\Omega}, t)}{dt} + \varphi(\vec{r}, E, \vec{\Omega}, t) \frac{dP(t)}{dt} / P(t) \right\} \\
& + \vec{\Omega} \cdot \nabla \varphi(\vec{r}, E, \vec{\Omega}, t) + \Sigma_t(\vec{r}, E, t) \varphi(\vec{r}, E, \vec{\Omega}, t) = \\
& \int_{E', \vec{\Omega}'} \Sigma_s(\vec{r}, E', \vec{\Omega}' \rightarrow E, \vec{\Omega}, t) \varphi(\vec{r}, E', \vec{\Omega}', t) dE' d\vec{\Omega}' \\
& + \chi_p(1 - \beta) \int_{E', \vec{\Omega}'} \frac{v(E')}{4\pi} \Sigma_f(\vec{r}, E', \vec{\Omega}', t) \varphi(\vec{r}, E', \vec{\Omega}', t) dE' d\vec{\Omega}' \\
& + \frac{1}{P(t)} \left\{ q(\vec{r}, E, \vec{\Omega}, t) + \sum_{i=1}^M \chi_{id}(E) \beta_i \lambda_i Z_i(\vec{r}, t) \right\}
\end{aligned} \tag{11.60}$$

Of course, this equation is more complicated than the original transport equation. It would be much harder to integrate it directly for any particular problem. However, by performing the factorization and writing the equation in this manner, simplifications are possible depending on the problem.

In shorthand notation this equation can be written as:

$$\frac{1}{v(E)} \frac{d\varphi}{dt} + \frac{1}{v(E)} \varphi \frac{dP}{dt} / P + \vec{\Omega} \cdot \nabla \varphi + \Sigma_t \varphi = \Sigma_s \varphi + \chi_p F \varphi + \frac{1}{P} \left\{ q + \sum_{i=1}^M \chi_{id} \beta_i \lambda_i Z_i \right\} \tag{11.61}$$

Rearranging the terms gives:

$$\frac{1}{v(E)} \frac{d\varphi}{dt} + \vec{\Omega} \cdot \nabla \varphi + \Sigma_t \varphi = \Sigma_s \varphi + \chi_p F \varphi + S / P \tag{11.62}$$

where:

$$S = q + \sum_{i=1}^M \chi_{id} \beta_i \lambda_i Z_i - \frac{1}{v} \varphi \frac{dP}{dt}$$

This looks almost identical to the complete transport equation except for the S/P term. If P is large and S small (fast transients), this term can be neglected, and the shape function equation is essentially the same as the original transport equation. Thus, it would appear that no simplification has been achieved, and for the most general case, this is indeed true. However, in many cases, the time dependence of the shape function is considerably smaller than the time dependence of the angular flux density, and significantly larger time steps can be taken in its integration.

11.6 Point Kinetics Approximations

If the time dependence of the shape function is completely neglected, all quantities can be evaluated for the critical reactor. This is often considered the least accurate of the methods for dealing with the shape function. However, it will be accurate enough for many applications.

11.6.1 *Level of Approximation to the Point Kinetics Equations*

As we have seen, the point kinetics equations (PKE) are approximations to the full spatial and time-dependent behavior of a nuclear reactor. For very many cases of reactor behavior, they are a quite accurate approximation and are a more than adequate approximation to allow complete control of the reactor and characterization of its behavior.

However the PKE are still too complicated to easily explain some behavior and derive physical data about the reactor from observed measurements. Therefore, we are going to look at several levels of approximation the PKE mainly based on how accurately or detailed we treat the delayed neutron phenomena. The following levels of approximation have applications as noted and are frequently used to describe reactor transients.

- No delayed neutron approximation (*NDN*)
- Prompt kinetics (*PK*)
- Constant delayed source (*CDS*)
- Precursor accumulation (*PA*)
- One delay family (*ODF*)
- Prompt jump approximation [zero lifetime] (*PJA* or *ZL*)

11.7 Adiabatic Approximation

If the reactor configuration at any point in time is considered to be static, the problem becomes a homogenous one. This is exactly the problem most design codes are set up to calculate. (However, the eigenvalue K must now be introduced in order to obtain a solution. Note this eigenvalue will also compensate for the fact that the reduced equation is based on $\chi_p(E)$ rather than $\chi(E)$). Note that the eigenfunction obtained may not in this case correspond to any real reactor flux shape. And even if the critical ADJOINT solution is used, the accuracy of this technique can be questioned. In addition, since this method requires the computation of an eigenvalue-eigenfunction solution every time it is desired to update the shape function, it can be computationally expensive.

11.8 Adiabatic Approximation with Pre-computed Shape Functions

One method that has been proposed for overcoming this computation obstacle is the use of pre-computed shape functions and their mixing as time goes on to approximate the actual shape function. This is one of those tricks, which will usually work if you know the answer to your problem before you try to solve it, but for “extrapolation” cases, “let the analyst beware.” In general, it is not recommended, and accuracy limits cannot be specified.

11.9 Quasi-Static Approximation

In this approximation the shape function is integrated on a much longer time interval than the power function, $P(t)$. The “inhomogeneous” source term S/P can be included or not included. The form used will depend on which terms are relevant for a particular problem and part of the transient is being evaluated. Normally a less than second-order implicit scheme will be used for this integration.

That means either an Euler’s backward method or a trapezoidal rule integration method. The Euler’s backward method is much faster to compute and therefore has generally been the method of choice.

For the no source (S/P) case, this would be written as:

$$\left\{ \frac{1}{v(E)\Delta t} + \vec{\Omega} \cdot \nabla + \Sigma_t - \Sigma_s - \chi_p F \right\} \varphi_2 = \frac{1}{v(E)\Delta t} \varphi_1 \quad (11.63)$$

and the flux shape at the start of the time interval becomes the source for the shape at the end of the time interval. If parts of the S/P source are to be included, they are time differenced and added to the equation on the right- and left-hand sides as appropriate.

11.10 Zero-Dimensional Reactors

Now consider a diffusion theory model of a zero-dimensional reactor. We will base this on an infinite slab, but the analysis is the same for any zero-dimensional model. The flux and adjoint solutions are:

$$\begin{aligned}\phi(E, z) &= \sum_{g=1}^{NOG} \varphi^g \cos Bz \\ \phi^*(E, z) &= \sum_{g=1}^{NOG} \varphi^{*g} \cos Bz\end{aligned}\quad (11.64)$$

Now consider evaluating some of the terms in the point kinetics equations. Start with the generation time:

$$\Lambda = \frac{1}{\int_{-H/2}^{H/2} \left[\sum_{g=1}^{NOG} \varphi^g \cos Bz \left\{ \chi_p^g (1 - \beta) + \sum_{i=1}^M \beta_i \chi_{id}^g \right\} \sum_{g=1}^{NOG} v \sum_f^g \varphi^g \cos Bz \right] dz} \quad (11.65)$$

There are a couple of items to note about this definition. First of all this is the only term where the absolute normalization of φ^{*g} is important. In all other terms, there will be a φ^{*g} on the bottom and on the top of the parameter definition, so only the relative values will be important. In order to get the absolute normalization, we must go back to the definition of the factorization:

$$\begin{aligned}\int_{\vec{r}, E, \vec{\Omega}} W(\vec{r}, E, \vec{\Omega}) \frac{1}{v(E)} \varphi(\vec{r}, E, \vec{\Omega}, t) = 1.0 &= \sum_{g=1}^{NOG} \frac{\varphi^{*g} \varphi^g}{v^g} \int_{-H/2}^{H/2} \cos^2 Bz dz \\ &= \frac{\pi}{2} \sum_{g=1}^{NOG} \frac{\varphi^{*g} \varphi^g}{v^g} = 1.0\end{aligned}\quad (11.66)$$

This will give us the absolute normalization of the weighting function or adjoint function. The weighting function can be written as some constant W_0 times the normalized adjoint function. The inner product of the normalized adjoint and flux divided by the group velocity can then be computed, and the normalizing constant becomes 1 over the inner product:

$$\begin{aligned}W(E, z) &= W_0 \sum_{g=1}^{NOG} \varphi^{*g} \cos Bz \\ W_0 &= \frac{1}{\frac{\pi}{2} \sum_{g=1}^{NOG} \frac{\varphi^{*g} \varphi^g}{v^g}}\end{aligned}\quad (11.67)$$

Then we can define a χ^g as:

$$\chi^g = \chi_p^g(1 - \beta) + \sum_{i=1}^M \beta_i \chi_{id}^g \quad (11.68)$$

Also note that the second summation in the denominator is completed before it is multiplied by the first two terms, so we can sum the fission source once and for all and use it in evaluating all of the other integrals.

Thus, we can write a simplified generation time computation as:

$$\begin{aligned} \Lambda &= \frac{1}{W_0 \frac{\pi}{2} \left(\sum_{g=1}^{NOG} \varphi^{*g} \chi^g \right) (FS)} \\ &= \frac{1}{W_0 \frac{\pi}{2} \left(\sum_{g=1}^{NOG} \varphi^{*g} \chi^g \right) \left(\sum_{g=1}^{NOG} v \Sigma_f^g \varphi^g \right)} \end{aligned} \quad (11.69)$$

Now we can calculate $\beta_{\text{effective}}$ as:

$$\beta = \frac{\sum_{i=1}^M \beta_i \int_{-H/2}^{H/2} \sum_{g=1}^{NOG} W_0 \varphi^{*g} \cos Bz \chi_{id}^g \sum_{g=1}^{NOG} v \Sigma_f^g \varphi^g \cos Bz dz}{W_0 \frac{\pi}{2} \left(\sum_{g=1}^{NOG} \varphi^{*g} \chi^g \right) \left(\sum_{g=1}^{NOG} v \Sigma_f^g \varphi^g \right)} \quad (11.70)$$

Note that in this case, the W_0 divides out on the top and bottom as does the $\pi/2$ factor and the total fission source. The formula becomes:

$$\beta = \frac{\sum_{i=1}^M \beta_i \sum_{g=1}^{NOG} \varphi^{*g} \chi_{id}^g}{\sum_{g=1}^{NOG} \varphi^{*g} \chi^g} \quad (11.71)$$

Finally, it is worth making some comments about the reactivity term. We have for the diffusion model:

$$\left\{ \begin{array}{l} \rho = - \frac{\int_{\vec{r}, E\vec{\Omega}} W(\vec{\Omega} \cdot \nabla \varphi + \Sigma_t \varphi - \chi F \varphi - \Sigma_s \varphi)}{\int_{\vec{r}, E\vec{\Omega}} W \chi F \varphi} \\ \rho = - \frac{\int_{-H/2}^{H/2} \sum_{g'=1}^{NOG} W_0 \varphi^{*g} \left(D^g B^2 \varphi^g + \Sigma_\gamma^g \varphi^g - \chi^g \sum_{g'=1}^{NOG} v \Sigma_f^{g'} \varphi^{g'} - \sum_{g'=g-1}^1 \Sigma_s^{g' \rightarrow g} \varphi^{g'} \right) \cos^2 B z dz}{W_0 \frac{\pi}{2} \left(\sum_{g=1}^{NOG} \varphi^{*g} \chi^g \right) \left(\sum_{g=1}^{NOG} v \Sigma_f^g \varphi^g \right)} \\ \rho = - \frac{\sum_{g'=1}^{NOG} \varphi^{*g} \left(D^g B^2 \varphi^g + \Sigma_\gamma^g \varphi^g - \chi^g \sum_{g'=1}^{NOG} v \Sigma_f^{g'} \phi^{g'} - \sum_{g'=g-1}^1 \Sigma_s^{g' \rightarrow g} \varphi^{g'} \right)}{\left(\sum_{g=1}^{NOG} \varphi^{*g} \chi^g \right) \left(\sum_{g=1}^{NOG} v \Sigma_f^g \varphi^g \right)} \end{array} \right. \quad (11.72)$$

Note that the numerator contains the exact material properties and flux shape functions. If we make the linear perturbation approximation, this can be rewritten as:

$$\rho = - \frac{\sum_{g'=1}^{NOG} \varphi_0^{*g} \left(\delta D^g B^2 \varphi_0^g + \delta \Sigma_\gamma^g \varphi_0^g - \chi^g \sum_{g'=1}^{NOG} \delta v \Sigma_f^{g'} \varphi_0^{g'} - \sum_{g'=g-1}^1 \delta \Sigma_s^{g' \rightarrow g} \varphi_0^{g'} \right)}{\left(\sum_{g=1}^{NOG} \varphi^{*g} \chi^g \right) \left(\sum_{g=1}^{NOG} v \Sigma_f^g \varphi^g \right)} \quad (11.73)$$

where basically we have subtracted off the critical equation and said that the product of two small changes is negligible compared to a single small change.

Problems

Problem 11.1 Thermal Reactor Example

Consider a thermal reactor example. The following results were obtained for a six-group model of the Advanced Reactivity Measurement Facility reactor: a small 93% enriched aluminum, slab core reactor. The model is based on a bare core version of this reactor shaped into a cube with a 51.09 cm side dimension. This gave a buckling of $B^2 = 0.011344/\text{cm}^2$. Note that this is a fairly small reactor.

Consider the following results:

Group	Upper energy	Velocity	$v\Sigma_f$	Flux	Adjoint	χ_p	χ_d	χ
1	17.33 MeV	4.24 (+9) cm/s	0.000643	0.03691	0.122862	0.05258	1.27(-6)	0.05221
2	4.97. MeV	2.24 (+9) cm/s	0.000492	1.00383	0.531294	0.52040	0.050525	0.51711
3	1.35 MeV	8.66 (+8) cm/s	0.000433	2.03885	0.695888	0.41086	0.803196	0.41361
4	111.0 keV	1.93 (+8) cm/s	0.000854	0.59341	0.849079	0.01608	0.145344	0.01699
5	3.35 keV	5.95 (+6) cm/s	0.01863	1.89784	0.875391	8.0(-5)	0.000933	8.6(-5)
6	0.100 eV	2.20 (+5) cm/s	0.18219	1.00000	1.000000	0.0	0.0	0.0

Calculate the normalization factor.

Calculate $\beta_{\text{effective}}$ and β_{physical} for this problem.

Problem 11.2 The thermal absorption cross section for Xe-135 at 2200 meters is $2.7\text{E}+6$ barns. Based on the bounds developed in class, what is the maximum absorption cross section that could be expected at 0.0253 eV for this nuclide? Estimate the total cross section at 2.0 MeV also.

Problem 11.3 Determine the thermal lifetime or diffusion time of neutron in the bare critical reactor where $L^2 = 57.3$ and $B^2 = 0.0051 \text{ cm}^{-2}$ and consisting of beryllium and uranium-235 in the atomic ratio of 10^4 to 1.

Problem 11.4 The reactivity in a steady-state reactor, in which the neutron generation time is 10^{-3} s, is suddenly made 0.0022 positive; assuming one group of delayed neutrons, determine the subsequent change of neutron flux with time. Compare the stable period with that which would result had no delayed neutrons. Use the following equation for variation of the neutron density with time:

$$n \approx n_0 \left[\frac{\beta}{\beta - \rho} e^{\frac{\beta \rho t}{\beta - \rho}} - \frac{\rho}{\beta - \rho} e^{-\frac{(\beta - \rho)t}{t^*}} \right] \quad (11.74a)$$

In addition, for the stable reactor period, assuming one (average) group of delayed neutron is given by:

$$T_p \approx \frac{\beta - \rho}{\lambda \rho} \quad (11.75b)$$

Assume on average, for one group of delayed neutron, λ is 0.08 s^{-1} ; ρ is given as 0.0022 and neutron generation time Λ as 10^{-3} s ; β for uranium-235 is 0.0065.

Problem 11.5 The prompt neutron lifetime in a reactor moderated by heavy water is $5.7 \times 10^{-4} \text{ s}$. For a reactivity of 0.00065, express the reactor period (a) in second, (b) in hours (lh), using the relationship between reactor period T_p , and in hours (lh) as $T_p \approx 3600/\Lambda$. What is the reactivity in dollar units? Assume for very long periods and very small reactivity the following equation applies and $(\beta/\lambda) = 0.084$:

$$T_p \approx \frac{\beta}{\lambda\rho} \quad (11.76a)$$

where:

T_p is reactor period

β is total fraction of delayed neutrons = 0.0065

λ is radioactive decay constant

ρ is reactivity

In addition, the unit that is called “the dollar,” is defined by:

$$\text{Reactivity in dollars} \equiv \frac{\rho}{\beta}$$

Problem 11.6 As part of one-group point kinetics equation, if we assume a case for when only one group of delayed neutron is assumed, the results of solution provide a polynomial in the denominator as part of general solution, when we assume source term is constant and equal to S_0 with two roots of s_1 and s_2 of the following mathematical notation:

$$s_{1,2} = \frac{-(\frac{\beta}{\Lambda} - \frac{\rho_0}{\Lambda} + \lambda) \pm \sqrt{(\frac{\beta}{\Lambda} - \frac{\rho_0}{\Lambda} + \lambda)^2 + 4\frac{\lambda\rho_0}{\Lambda}}}{2} \quad (11.77a)$$

where:

β is fractional yield of the delayed neutrons

Λ is average neutron generation time

ρ_0 is reactivity for constant source S_0

λ is decay constant.

Then the neutron flux can be obtained as:

$$\begin{aligned} n(t) &= n_e x(t) + n_e \\ &= n_e \left\{ 1 + \left(\frac{\rho_0}{\Lambda} + \frac{S_0}{n_e} \right) \left[\frac{\lambda}{s_1 s_2} + \frac{s_1 + \lambda}{s_1(s_1 + s_2)} e^{s_1 t} + \frac{s_2 + \lambda}{s_2(s_2 - s_1)} e^{s_2 t} \right] \right\} \end{aligned} \quad (11.78b)$$

where:

$n(t)$ is neutron density as function of time t

n_e is neutron density at equilibrium

Assuming one group of delayed neutrons, determine the subsequent change of neutron flux with time. Additionally, the reactivity is taking place in a steady-state thermal reactor with no external neutron source, in which the neutron generation time $\Lambda = 10^{-3}$ s is suddenly made 0.0022 positive and the following data applies: $\lambda = 0.08 \text{ s}^{-1}$ and $\beta = 6.5 \times 10^{-3}$.

Problem 11.7 A critical reactor operated during a long period of time with the mean weighted number of neutrons equal to $n_e = 10^6$. Suddenly a source of neutrons with mean weighted yield equal to $S_0 = 10^6 \text{ s}^{-1}$ was introduced into the reactor. Find the number of neutrons as a function of time, $n(t)$. In calculations assume one group of delayed neutrons with $\lambda = 0.1 \text{ s}^{-1}$ and $\beta = 6.4 \times 10^{-3}$ and the mean generation time $\Lambda = 10^{-3}$ s.

Problem 11.8 An under-critical reactor operated during a long period of time with the reactivity equal to $\rho_0 = -9\beta$. A source of neutrons with a mean weighted yield equal to $S_0 = 10^6 \text{ s}^{-1}$ was present in the reactor. Suddenly the source of neutrons was removed from the reactor. Find the number of neutrons as a function of time, $n(t)$. In calculations assume one group of delayed neutrons with $\lambda = 0.1 \text{ s}^{-1}$ and $\beta = 6.5 \times 10^{-3}$ and the mean generation time $\Lambda = 10^{-3}$ s. Note that the equilibrium number of neutrons before the removal of the source is given by $n_e = -S_0\Lambda/\rho_0$.

References

1. J. Koclas, *Neutronic Analysis of Reactor*, Nuclear Engineering Department at Ecole Polytechnique de Montreal, February 1998
2. J. Duderstadt, L. Hamilton, *Nuclear Reactor Analysis* (John Wiley Publishing Company, 1976)

Chapter 12

Reactor Dynamics



In order for nuclear fission power to operate at a constant power level, the rate of neutron production via fission reactions must be exactly balanced by neutron loss via absorption and leakage. If we deviate from this simple balancing role, it would cause time dependence of neutron population and therefore the power level of the reactor. Such situation may take place, for a number of reasons, such as reactor operator may have a requirement to change the reactor power level by temporarily altering the control fuel rod so it will change the core or source multiplication or there may be long-term changes in core multiplication due to fuel depletion and isotopic buildup. Other examples may also be encountered that require attention and adjustment to day-to-day operation of reactor, such as unforeseen accident or failure of primary coolant pump system, etc. The topic of *nuclear kinetic reactor* as we have learned in the previous chapter is handling this situation by allowing us to predict the time behavior of the neutron population in a reactor core driven by changes in reactor multiplication, which are not circumstances that are totally controlled by the operator of power plant and reactor core. Furthermore, variables such as indirect accessibility to control such as the fuel temperature or coolant density distribution throughout reactor do have impact to the situation. However, these variables depend on the reactor power level and hence the neutron fluxes itself. Additionally, study of the time dependence of the related process, which is involved in determining the core multiplication as a function of power level of the reactor multiplication, is subject of our study in this chapter, and it is called *nuclear reactor dynamics*. This usually involves detailed modeling of the entire nuclear steam supply system, which is part of *feedback* system as well.

12.1 Background on Nuclear Reactor

As we know from our basic knowledge of nuclear reactor, their main task is to produce and control the release of energy from splitting the atoms of certain elements, via carrying out the chain reaction in a controlled way and then using the resultant heat to produce steam that turns a generator to produce electricity for our day-to-day consumption. See Fig. 12.1, which shows a typical modern pressurized water reactor (PWR) with its primary and secondary loops.

For a nuclear power plant to achieve the task of producing electricity driven by split of atom of certain elements in a controlled chain reaction way, there exist three fundamental ways, and they are listed below:

1. Thermal MW_t, which depends on the design of the actual nuclear reactor itself and relates to the quantity and quality of the steam it produces.
2. Gross electrical MW_e, which indicates the power produced by the attached steam turbine and generator and takes into account the ambient temperature for the condenser circuit (cooler means more electric power, warmer means less) as well. Rated gross power assumes certain conditions with both.
3. Net electrical MW_e, which is the power available to be sent out from the plant to the grid, after deducting the electrical power needed to run the reactor (cooling and feedwater pumps, etc.) and the rest of the plant [2].

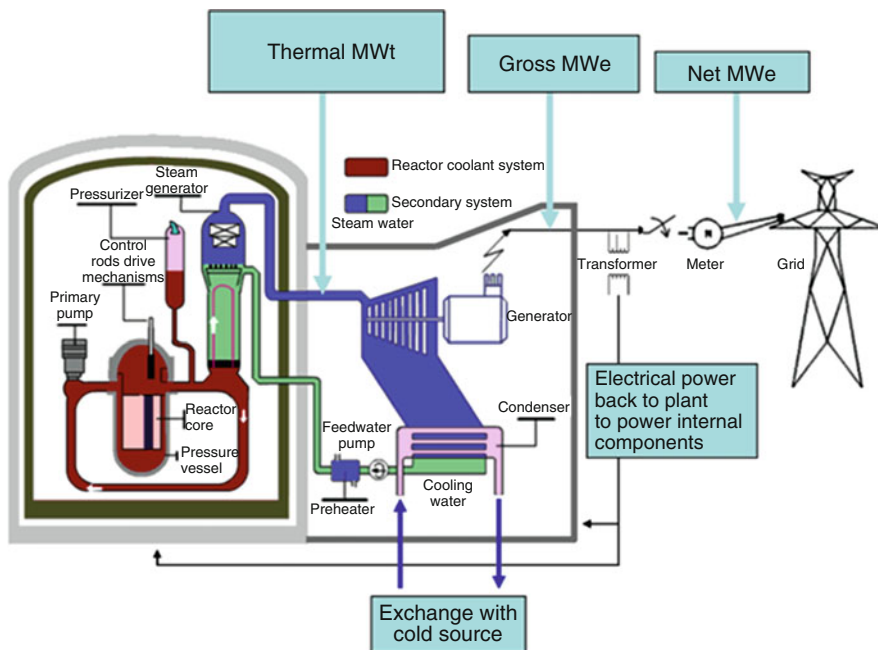


Fig. 12.1 Typical schematic of pressurized water reactor producing electricity. (Courtesy of the US National Nuclear Regulatory Commission)

The relationship between those three fundamental ways is expressed in two ways:

- Thermal efficiency %, the ratio of gross MWe to thermal MW. This relates to the difference in temperature between the steam from the reactor and the cooling water. It is often 33–37%.
- Net efficiency %, the ratio of net MWe achieved to thermal MW. This is a little lower and allows for plant usage.

Pressurized water reactor (PWR) as it is shown in Fig. 12.2 is the most common type, with estimated over 230 in use for power generation and several hundred more employed for naval propulsion. The design of PWRs originated as a submarine power plant. PWRs use ordinary water as both coolant and moderator. The design is distinguished by having a primary cooling circuit, which flows through the core of the reactor under very high pressure, and a secondary circuit in which steam is generated to drive the turbine. In Russia, these are known as VVER types – water-moderated and water-cooled.

A PWR has fuel assemblies of 200–300 rods each, arranged vertically in the core, and a large reactor would have about 150–250 fuel assemblies with 80–100 tons of uranium.

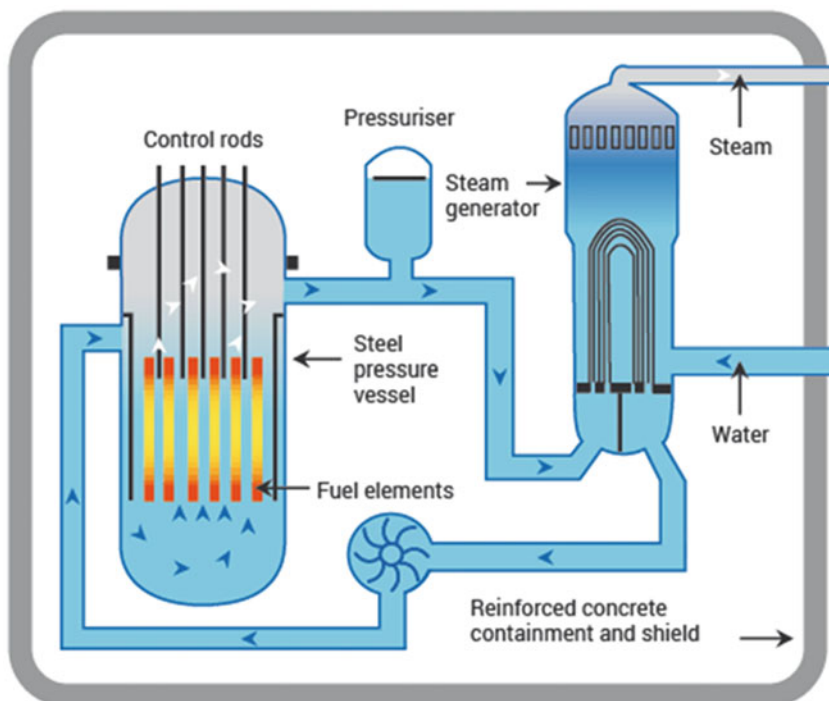


Fig. 12.2 Core of a pressurized water reactor (PWR). (Courtesy of the US National Nuclear Regulatory Commission)

Water in the reactor core reaches about 325 °C; hence, it must be kept under about 150 times atmospheric pressure to prevent it from boiling. Pressure is maintained by steam in a pressurizer (see diagram). In the primary cooling circuit, the water is also the moderator, and if any of it turned to steam, the fission reaction would slow down. This negative feedback effect is one of the safety features of this type. The secondary shutdown system involves adding boron to the primary circuit.

The secondary circuit is under less pressure, and the water here boils in the heat exchangers, which are thus steam generators. The steam drives the turbine to produce electricity and is then condensed and will be returned to the heat exchangers in contact with the primary circuit.

12.2 Neutron Multiplication

It is important for reactor operator to know how to handle starting of a reactor for the first time. For instance, either first time start-up of a new reactor coming on line, after refueling, the critical level of the control fuel rods is not known; therefore, the control rod withdrawal must be done cautiously in order to avoid supercriticality and an unexpected power. The level of control rod criticality could be determined by monitoring the neutron flux in the core while withdrawing the control rods, which is a common practice as part of safety procedure and always should be performed at first start-up of any nuclear fission-powered reactors.

Having the basic consideration of the above, we introduce a source of neutrons, represented by symbol of S into a subcritical reactor with multiplication factor k . In that case, there will be $S \cdot k$ neutrons after the first fission generation, $S \cdot k^2$ neutrons after the second generation, and so on, so that the total number of neutrons per source neutrons after many generations approaches a geometrical series as:

$$M = \frac{(1 + k + k^2 + \dots)S}{S} = \frac{1}{1 - k} \quad (12.1)$$

In Eq. 12.1, M is called the *core or source multiplication*, describing the ratio of the fission source to the external source, and gives consequently the total number of neutrons appearing in the fissionable materials per source neutron.

The multiplication factor k is defined as:

$$k \equiv \text{Multiplication Factor} \equiv \frac{\text{Number of neutrons in one generation}}{\text{Number of neutrons in preceding generation}}$$

However, since the number of fission neutrons v in any generation is proportional to the number of fission events spawning that generation, by knowing the fact that each fission reaction releases, on the average, v fission neutrons, then we could

justify to easily define multiplication factor k using the number of fission events in each generation as well.

Additionally, note that since the expression is valid for a subcritical system, where multiplication factor $k < 1$. It can also be seen that both the reciprocal source multiplication factor, $1/M$, and $1 - k$ decrease when approaching criticality, so we can write:

$$\frac{1}{M} = 1 - k \quad (12.2)$$

This relationship is often employed in bringing a reactor system to criticality, by extrapolating to the critical condition. If, for example, the operator starts withdrawing control rods, the multiplication constant, and thus the source multiplication factor M , increases with increasing rod withdrawal. When the reactor reaches critical condition, the source multiplication factor becomes infinite. This “approach to criticality” is monitored by placing a neutron source in the reactor and measuring the neutron flux for various rod positions. The neutron count rate is proportional to M . A plot of the inverse counting rate or $1/M$ as a function of rod position becomes equal to zero at the critical condition. If we extrapolate a curve to the zero value, then we can predetermine the control rod position at which the critical condition will be reached.

This discussion is valid under the assumptions that the reactor is reasonably close to critical and that the neutron population is in equilibrium. If the reactor is far below critical, then Eq. 12.2 is not valid. Eq. 12.2 only applies to the multiplication of neutrons in the *eigenstate*. Eigenstate in this sense refers to neutrons such that their energy spectrum and spatial distribution are characteristic of the reactor, i.e., asymptotic spectrum, so-called fundamental mode distribution, and with an effective multiplication factor k_{eff} . Source neutrons, in general, do not have these properties and multiply differently compared to eigenstate neutrons. In that case, we cannot formulate a simple geometric series, based on a single k -value. In close-to-critical conditions, this effect has negligible influence since source neutrons are small in number in comparison to the total neutron population. The neutron flux is characterized by the eigenstate at criticality.

Although the measurement of source multiplication is a static technique, there are time-dependent effects that can be important in the interpretation of results. The multiplication following a reactivity change (e.g., change in control rod position) in a subcritical system is observed only after all delayed neutrons have attained equilibrium concentration. During a sequence of stepwise addition of reactivity, as in the following “ $1/M$ ” approach to criticality, the total asymptotic multiplication will clearly be observed at each step if one waits sufficiently long after each reactivity addition. Nevertheless, if reactivity is added too rapidly – either stepwise or continuously – the observed multiplication will lag the asymptotic multiplication, thus giving an underestimate of the instantaneous multiplication of the system. The physical reason for this transient effect is clear. The equilibrium condition is

identified by a self-sustained constant power level only when all delayed neutron precursors are in equilibrium, meaning that the formation rate of delayed neutron precursors equals the decay rate.

Under very weak source conditions, the neutron level during the early stages of start-up is so low that statistical fluctuations tend to dominate and the kinetic equations are not applicable. At later stages, the power level becomes sufficiently high and statistical fluctuations are no longer important. In general, distorting effects become relatively small near criticality, and extrapolated critical points become progressively more reliable as the critical condition is approached.

12.3 Simple Feedbacks

The feedback system plays an important role in the study of nuclear reactor dynamics, where the detailed modeling of steam supply system is involved. The feedback mechanisms consist of determining core multiplication and mainly concentrate in the prediction of the time behavior of the neutron flux in the reactor for a given change in multiplication, basically transient analysis that we need to study and model.

The main task of such application is an analysis that not only deals with the study of operating transients in reactor but also the predication of the consequences of accidents involving changes in core multiplication and the interpretation of experimental techniques measuring reactor parameters by inducing time-dependent changes in neutron flux [1].

We started our discussion about nuclear reactor dynamics, which concerns with analysis of the time-dependent behavior of the nuclear reactor both under normal operation status and during accident encounters as well. In addition, this concern deals with the interpretation of most reactor physics, experiments that are involving with reactivity $\rho(t)$ changes requires by analysis of core dynamics, which is time dependent and transient form.

Again talking about nuclear reactor kinetics, which generally indication of time-dependency of the neutron population. On the contrary, the dynamics of nuclear reactor also, includes all the aspect of reactor kinetics and additionally is involved in the temperature T and feedback of control system. Kinetics of nuclear reactor could be described as a set of equations connecting the variables describing the state of the system; and variables involved in these are the neutron flux $\phi(\vec{r}, t)$ and the temperatures of the various reactor components. This together with the parameters, which can drive quantities such as poison concentrations, cross sections, coolant mass flow, etc. of the system as well as data describing the causes of the transients, is part of nuclear reactor kinetic studies [3].

Part of the task assigned to study nuclear reactor kinetics involves a parameter known as *kinetic equation*, which is the equation connecting the neutron flux to the other system variables such as temperatures at each component level. Further

analysis of kinetic equation indicates that its coefficients are usually temperature dependent and the equation cannot be solved without taking the reactor heat transfer equations under consideration. This includes the point reactor kinetic modeling and the involvement of delayed neutron β in reactor kinetic analysis. Therefore, understanding of time-dependent behaviors of nuclear reactors and the methods of their control is essential to the operation and safety of nuclear power plants.

As we did learn from previous chapters for a simple bare slab reactor analysis, we found that the neutron flux $\phi(\vec{r}, t)$ in such a system as a superposition of spatial modes in terms of eigenfunctions which represents the characteristic of the reactor geometry, and each weighing with an exponentially varying time-dependence presented in the following equation as: [1]

$$\phi(\vec{r}, t) = \sum_n A_n \exp(-\lambda_n t) \psi_n(\vec{r}) \quad (12.3)$$

Equation 12.3 is the solution of the eigenvalue problem of the following problem as:

$$\nabla^2 \psi_n(\vec{r}) + B_n^2 \psi_n(\vec{r}) = 0 \quad \psi_n(\vec{r}_s) = 0 \quad (12.4)$$

While the time eigenvalues λ_n were given by:

$$\lambda_n = vDB_n^2 + v \sum_a + vv \sum_f \quad (12.5)$$

where v is neutron velocity corresponding to energy E , and it is the distance traveled by the neutron in unit time, with that velocity, while v is the average number of fission neutron emitted per fission at the energy E as well.

Note that Eq. 12.3 is a form of Helmholtz equation, where $\psi_1(\vec{r})$ is the fundamental mode or eigenfunction of this equation.

These eigenvalues are ordered as $-\lambda_1 > -\lambda_2 > \dots$. Hence, for long times, the flux approaches an asymptotic form:

$$\phi(\vec{r}, t) \approx A_1 \exp(-\lambda_1 t) \psi_1(\vec{r}) A_1 \exp\left[\left(\frac{k-1}{l}\right)\right] \equiv \text{Mean lifetime of neutron in reactor} \quad (12.6)$$

$$k \equiv \frac{v\Sigma_f/\Sigma_a}{1 + L^2 B_g^2} \equiv \text{Multiplication factor} \quad (12.7)$$

However, the concern is how long it takes for this asymptotic behavior to settle. This matter can be answered simply by assuming that reactor is operating in a critical state such that $\lambda_1 = 0$ and then estimate λ_n . The estimation of λ_n also can be done by

recalling that for a slab $B_n^2 = n^2(\pi/\bar{a})^2$, and for a typical reactor, where $\bar{a} \sim 300$ cm, $v \sim 3 \times 10^{15}$ cm/s, and $D \sim 1$, then we have:

$$\begin{cases} \lambda_n = -vD(B_n^2 + B_m^2) \\ = -vD(B_n^2 + B_g^2) \\ = -vD(n^2 - 1)\left(\frac{\pi}{\bar{a}}\right)^2 \end{cases} \quad (12.8)$$

Alternatively, plugging the given values for thermal reactor, we obtain:

$$\begin{cases} \lambda_n = -3 \times 10^5 \text{ (cm/sec)} \cdot (1) \cdot (n^2 - 1) \cdot \left(\frac{3.14}{300 \text{ cm}}\right)^2 \\ \lambda_n \approx 3.28(n^2 - 1) \end{cases} \quad (12.9)$$

Hence, it shows that the higher order of λ_n is of the order of $100\text{--}1000 \text{ s}^{-1}$, which implies that the higher-order spatial modes die out very rapidly indeed [1].

Now that we briefly have discussed a nuclear power reactor and we have better understanding of reactor kinetics, we pay attention to the subject in hand and that is reactor dynamics. Reactor dynamic starts with handling a simple reactivity feedback for the reactivity $\rho(t)$ that was appearing in the study of point kinetic equation in Chap. 11 of the book, and it is given as function of time t . In reality, the reactivity $\rho(t)$ is dependent on the neutron flux which presents power level in any nuclear reactors. This dependency is due to the fact that reactivity depends on macroscopic cross sections, which themselves are depending on the atomic number density $N(\vec{r}, t)$ of materials in the core as it is shown mathematically here:

$$\sum(\vec{r}, t) = N(\vec{r}, t)\sigma(\vec{r}, t) \quad (12.10)$$

Further, analysis of Eq. 12.10 reveals why the atomic number density $N(\vec{r}, t)$ can depend on the nuclear reactor power level, and the reasons are summarized here as follows [1]:

- (a) Material densities have dependency on the temperature T , which itself depends on the power distribution and hence the flux.
- (b) The concentrations of certain nuclei are constantly changing due to neutron interactions such as buildup of poison or burnup of fuel.

However, we should note that so far we have treated the microscopic cross section as explicit function of spatial position \vec{r} and time t . This can be achieved because the cross sections which appear in one-speed diffusion model of neutronic analysis are actually averages of the true energy-dependent microscopic cross sections over an energy $\chi(E)$ spectrum characterizing the neutrons in the nuclear reactor core. Additionally, this neutron energy spectrum will itself depend on the temperature distribution T in the core and hence the reactor power level.

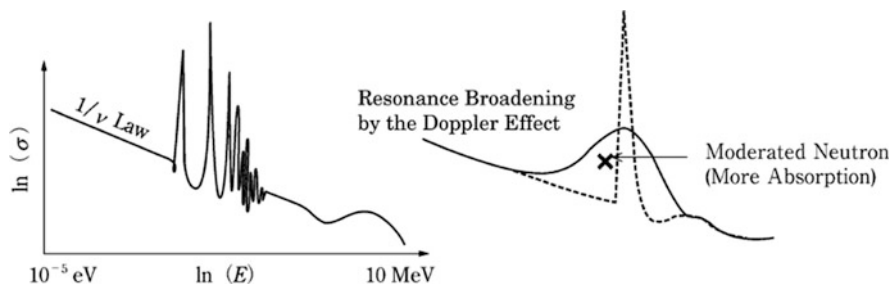


Fig. 12.3 Resonance absorption cross section and Doppler effect [4]

As we talked and learned from Chap. 7 so far, the elastic scattering cross section is mostly constant in all the energies except for the MeV region. Meanwhile, in inelastic scattering, the incident neutron should have sufficient kinetic energy to place the target nucleus in its excited state. Hence, the inelastic scattering cross section is zero up to some threshold energy of several MeV. Fast neutrons can be moderated by inelastic scattering with heavy nuclides but by elastic scattering with light nuclides below threshold energies of the heavy nuclides [4].

In Chap. 7, we discussed that most absorption cross sections including the fission cross section appear as a straight line with a slope of $-1/2$ on a log-log scale. This means that the absorption cross sections are inversely proportional to the neutron speed ($1/v$) law as we discussed before and therefore increase as the neutron energy decreases. Using such large fission cross sections at low neutron energies and thermal neutrons in the Maxwellian distribution makes it possible that natural or low-enrichment uranium-fueled reactors reach a critical state. The current thermal reactors, represented by LWRs, use the characteristics of the cross section [4].

For heavy nuclides such as fuel materials, many resonances are observed in elastic scattering and absorption cross section as shown in Fig. 12.3. The widths of the resonances broaden as fuel temperature increases. And also, we learned from Chap. 7 that this was called Doppler effect and the width broadening facilitates resonance absorption of neutrons under moderation [4].

Most low-enrichment uranium fuel is composed of fertile U^{238} , and thermal neutrons escaping from the resonance of capture reaction induce fissions for the next generation.

Hence, a rise in fuel temperature leads to a decrease in resonance escape probability of moderated neutrons, and then fission events in the reactor decrease with thermal neutrons. Such a mechanism is called *negative temperature feedback*. The temperature dependence T is not described in the Boltzmann Eq. 3.1 but is, however, reflected in the cross sections of the equation [4].

One more phenomenon that is worth mentioning in the analysis of nuclear reactor dynamics and its characterizing behavior is the presence of the delayed neutrons. The β -decay of a fission product leads in some cases to a highly excited similar product, which can then emit a neutron. These fission products as we have said are commonly called delayed neutron precursors.

Note that in nuclear reactor dynamics, for reactivity ρ much larger than neutron decay β , i.e., $\rho \gg \beta$, we can ignore the delayed neutron, and as a result the precursor equation in point kinetic equation (PKE) goes away. In that case, we are left with the power distribution $P(t)$ with no precursor term as below, which is the same equation as what was mentioned in Chap. 11, and it was written in form of Eqs. 11.31, 11.37, and 11.38:

$$\frac{d}{dt}P(t) = \frac{\rho(t) - \beta}{\Lambda}P(t) + \sum_i \lambda_i C_i(t) \approx \frac{\rho(t) - \beta}{\Lambda}P(t) \quad (12.11)$$

The historical reason behind ignorance of the delayed neutron for $\rho \gg \beta$ assumption goes to the nuclear weapon design, where the model was developed and used, hence $\rho \gg \beta$ and rapid transient. We also use $P(t)$ instead of $T(t)$ that was used in Chap. 11 to represent the amplitude function, to avoid the confusion with temperature T that we are using repeatedly in this section. The ignorance assumption can be explained by Fuchs-Nordheim for no precursors in Eq. 12.8, which is the subject of the next section of this chapter and can be observed in Fig. 12.4:

Analysis of Fig. 12.4 reveals that we can see that the power with precursor is small enough that the Fuchs-Nordheim (F-N) model provides a good approximation;

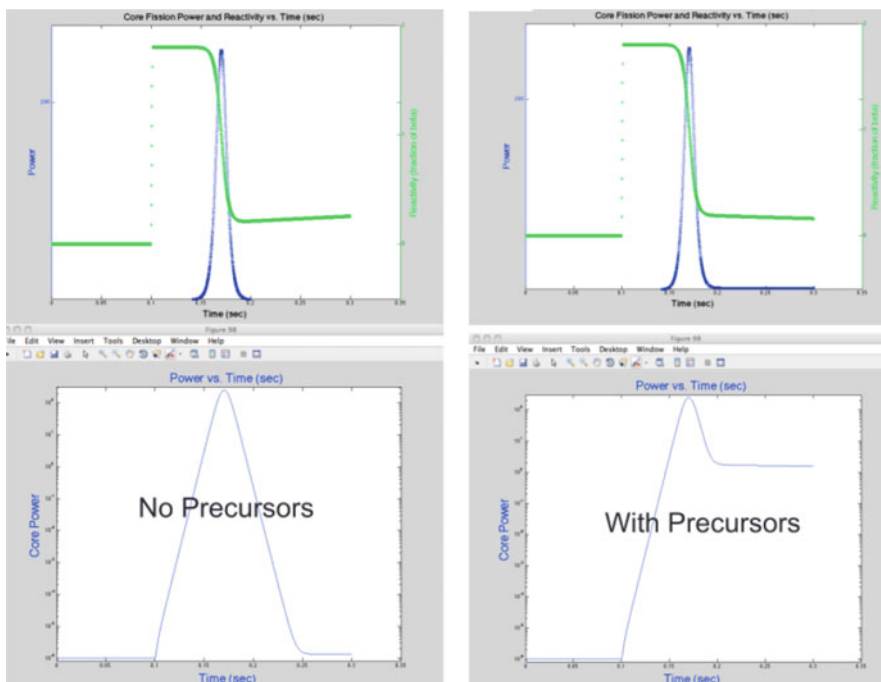


Fig. 12.4 Assumption in Fuchs-Nordheim, no precursors

the bottom row images are plotted on a log-log scale to show the small difference made by the precursors.

Back to mainstream of our subject of feedback phenomena and nuclear reactor dynamic analysis, we mention that the neutron emission follows, almost immediately within roughly 10^{-14} s, the β radiation, and the delay of the delay of the neutron is determined by the β -decay constants of the parent nuclide, which ranges from milliseconds to minutes. The delayed neutrons are usually grouped to more or less six groups according to the β -decay of the parent nuclides. Table 12.1 shows the six groups as an example of experimental data collected for delayed neutron β_i data for thermal fission in U^{235} along with decay constant λ_i and other related parameters. Here, β -decay related to β_i by the following relationship:

$$\sum_{i=1}^m \beta_i = \beta \quad i = 1, 2, \dots, m \quad (12.12)$$

Equation 12.12 is defining β_i as the yield of group i of delayed neutrons, and β_i and β are for various fissionable isotopes. These are given in Table 12.1 and Table 12.2, together with the decay constant of the delayed neutron precursors.

G. R. Keepin [5] provides more complicated version of Table 12.1, and we are presenting a partial version of it here in Table 12.2.

The time variation of the reactor state is the result of various phenomena, which include:

- Fuel burnup.
- Fission product buildup and decay.
- Temperature variations.
- Reactivity changes due to movement of absorber rod or other geometrical and material changes within reactor.

Each of these phenomena is characterized by a different time constant. The result of reactivity changes $\rho(t)$ is usually rapid transients, which as we mentioned in above has historical weapon design applications. However, in our case, the time constant is determined by the lifetime of the prompt and delayed neutrons.

Table 12.1 Delayed neutron data for thermal fission U^{235}

Group	Half-life ¹ , $t_{1/2}$ [s]	Decay constant, λ_i [s^{-1}]	Mean energy [keV]	Yield, ν_i [n/fissions $\times 100$]	Fraction, β_i [pcm]
1	54.6 ± 0.9	0.0127 ± 0.0002	250 ± 20	0.060 ± 0.005	21.5
2	21.9 ± 0.6	0.0317 ± 0.0008	460 ± 10	0.364 ± 0.0013	142.4
3	6.0 ± 0.2	0.115 ± 0.003	405 ± 20	0.349 ± 0.024	127.4
4	2.23 ± 0.06	0.311 ± 0.008	450 ± 20	0.628 ± 0.015	256.8
5	0.50 ± 0.03	1.40 ± 0.081	-	0.179 ± 0.014	74.8
6	0.18 ± 0.02	3.87 ± 0.37	-	0.070 ± 0.005	27.3

¹The values are calculated from the decay constants, which are true experimental values, through the relation $t_{1/2} = \ln(2)/\lambda_i$

Table 12.2 Delayed neutron, half-lives, decay constants, and yield [5]

Group index, i	Half-life, sec	Decay constant λ_i , sec $^{-1}$	Relative abundance $\alpha_i \equiv \beta_i/\beta$
^{235}U (99.9% 235)			
1	54.51 \pm 0.94	0.0127 \pm 0.0002	0.038 \pm 0.003
2	21.84 \pm 0.54	0.0317 \pm 0.0008	0.213 \pm 0.005
3	6.00 \pm 0.17	0.115 \pm 0.003	0.188 \pm 0.016
4	2.23 \pm 0.06	0.311 \pm 0.008	0.407 \pm 0.007
5	0.496 \pm 0.029	1.40 \pm 0.081	0.128 \pm 0.008
6	0.179 \pm 0.017	3.87 \pm 0.369	0.026 \pm 0.003
^{238}U (99.98% 238)			
1	52.38 \pm 1.29	0.0132 \pm 0.0003	0.013 \pm 0.001
2	21.58 \pm 0.39	0.0321 \pm 0.0006	0.137 \pm 0.002
3	5.00 \pm 0.19	0.139 \pm 0.005	0.162 \pm 0.020
4	1.93 \pm 0.07	0.358 \pm 0.014	0.388 \pm 0.012
5	0.490 \pm 0.023	1.41 \pm 0.067	0.225 \pm 0.013
6	0.172 \pm 0.009	4.02 \pm 0.214	0.075 \pm 0.005
^{233}U (100% 233)			
1	55.11 \pm 1.86	0.0126 \pm 0.0004	0.086 \pm 0.003
2	20.74 \pm 0.86	0.0334 \pm 0.0014	0.274 \pm 0.005
3	5.30 \pm 0.19	0.131 \pm 0.005	0.227 \pm 0.035
4	2.29 \pm 0.18	0.302 \pm 0.024	0.317 \pm 0.011
5	0.546 \pm 0.108	1.27 \pm 0.266	0.073 \pm 0.014
6	0.221 \pm 0.042	3.13 \pm 0.675	0.023 \pm 0.007
^{239}Pu (99.8% 239)			
1	53.75 \pm 0.95	0.0129 \pm 0.0002	0.086 \pm 0.003
2	22.29 \pm 0.36	0.0311 \pm 0.0005	0.274 \pm 0.005
3	5.19 \pm 0.12	0.134 \pm 0.003	0.216 \pm 0.018
4	2.09 \pm 0.08	0.331 \pm 0.012	0.328 \pm 0.010
5	0.549 \pm 0.049	1.26 \pm 0.115	0.103 \pm 0.009
6	0.216 \pm 0.017	3.21 \pm 0.255	0.035 \pm 0.005
^{240}Pu (81.5% 240)			
1	53.56 \pm 1.21	0.0129 \pm 0.0004	0.028 \pm 0.003
2	22.14 \pm 0.38	0.0313 \pm 0.0005	0.273 \pm 0.004
3	5.14 \pm 0.42	0.135 \pm 0.011	0.192 \pm 0.053
4	2.08 \pm 0.19	0.333 \pm 0.031	0.350 \pm 0.020
5	0.511 \pm 0.077	1.36 \pm 0.205	0.128 \pm 0.018
6	0.172 \pm 0.033	4.04 \pm 0.782	0.029 \pm 0.006
^{232}Th (100% 232)			
1	56.03 \pm 0.95	0.0124 \pm 0.0002	0.034 \pm 0.002
2	20.75 \pm 0.66	0.0334 \pm 0.0011	0.150 \pm 0.005
3	5.74 \pm 0.24	0.121 \pm 0.005	0.155 \pm 0.021
4	2.16 \pm 0.08	0.321 \pm 0.011	0.446 \pm 0.015
5	0.571 \pm 0.042	1.21 \pm 0.090	0.172 \pm 0.013
6	0.211 \pm 0.019	3.29 \pm 0.297	0.043 \pm 0.006

12.4 Multiple Time Constant Feedbacks

We also need to know that temperature feedbacks have time constants determined by the heat capacity and conductivity of the fuel as well as moderator. Fission product build, fission product decay, and fuel burn-up are usually characterized by very long-time constants. Most short-lived fission products do not have a need to be treated explicitly, with exception of element Xe^{135} , because of its huge high thermal absorption cross section [3].

The stable nuclide Sm^{149} element gives rise to transients with short time constant because it has a high cross section and a short-lived parent element. For Xe^{135} and Sm^{149} transients, the time constants vary between 9 and 48 h.

Each of these phenomena could be mathematically expressed in terms of sets of differential equations, and as a general rule it is possible to treat independently transients with widely differing time constants. Readers should refer themselves to the book by Massimo [3] to seek solution procedures for these differential equations.

As we have already mentioned, the feedback of the control system on the reactor acts through two quantities, and they are as follows:

1. The control of fuel rod position
2. The coolant mass flow

For reactor accident analysis, where we deal with short-time dynamics, it is not usually necessary to involve the complicated system of equations describing the core dynamic behavior in order to describe the control system. However, it is sufficient to assume that when given quantities such as neutron flux, coolant outlet temperature, etc. exceed a previously determined designed, threshold value, a scram will take place. This induced that a negative reactivity Δk_c given by the control fuel rods and a reduction of the coolant mass flow are introduced as given functions of time [3].

Analysis of long-time dynamics, in the nuclear reactor operation and stability studies for the control system, has to be simulated in the dynamic equations. It is also usually required in this case that power $P_r(t)$ released by the reactor follows a given power diagram $P(t)$ while a given gas outlet temperature T must be maintained. Various methods of regulation can be implemented and a general regulation of the thermal power through the coolant mass flow \dot{m} in the reactor, and it is presented by [3]:

$$\dot{m} = K_p[P(t) - P_r(t)] + K_I \int [P(t) - P_r(t)]dt + K_D \frac{d}{dt}[P(t) - P_r(t)] \quad (12.14)$$

where K_p , K_I , and K_D are the coefficients of the proportional, integral, and differential member respectively, and

$$P_r(t) = c_p \dot{m} (T_{c2} - T_{c1}) \quad (12.15)$$

where:

T_{c1} is coolant inlet temperature
 T_{c2} is coolant outlet temperature
 c_p is specific heat at constant pressure

A regulation of the gas outlet temperature through the control rod reactivity Δk_c would be given by the following equation:

$$\Delta k_c = K_P(T_{c2} - T_{c1}) + K_I \int [P(t) - P_r(t)] dt + K_D \frac{d}{dt}(T_{c2} - T_{c1}) \quad (12.16)$$

12.5 Fuchs-Nordheim Model

Before we jump on this subject, we remind the readers again about the effect of temperature on reactivity ρ , and as a general consideration we look at if the power of a nuclear reactor stays constant during the multiplication factor $k_{eff} = 1$.

At constant power, the cooling system of the reactor removes all the heat that is generated. If the multiplication factor is increased by $\Delta k_{eff} = k_{eff} - 1 > 0$, the power of the reactor starts to grow at a rate determined by the magnitude of Δk_{eff} . The cooling system cannot at least immediately absorb all the thermal energy released in fission. However, part of it will raise the temperature of the reactor core. In the absence of any limiting factors, the temperature would rise indefinitely, and finally the core would melt. In cases like this, the temperature dependence of the reactivity $\rho = \Delta k_{eff}/k_{eff}$ and the feedback caused by it usually constitute a limiting factor.

The dependence of the reactivity on temperature is described by the temperature coefficient of the reactivity. For that matter, we have to assume that the whole reactor core can be characterized by one single temperature T . The temperature coefficient α is defined as a derivative:

$$\alpha = \frac{d\rho}{dT} \quad (12.17)$$

If we assume that when reactivity ρ is expanded into a series of $(T - T_0)$, then the series can be truncated after the first-degree term for a linear relationship. Here T_0 is some suitable reference temperature and α has unit of $1/^\circ\text{C}$.

If the temperature coefficient α is negative, i.e., the reactivity ρ decreases as the temperature T increases, the reactor will behave stably. When the multiplication factor k for some reason or other undergoes a positive change the neutron flux and thus the power start to rise. Since all the heat generated is not removed from the reactor, the core temperature will raise. This reduces the reactivity and slows down the increase in power. Finally, the temperature reaches a level where it is sufficient to

compensate the completely original reactivity insertion. The power will stop increasing and with still rising temperature will start decreasing [6].

Finally, the system will stabilize at a new power level between the original level and the power peak. Such a behavior is of course highly desirable for safety reasons. It is easy to accomplish reactor designs, which lead to increased reactivity with rising temperature and, consequently, are inherently unstable. Chernobyl accident is an example of such situation [6].

However, merely a negative temperature coefficient is not a sufficient guarantee for safe operation. Often there is a delay in the feedback between power increase and reduced reactivity. This delay is usually caused by the time needed for heat transfer or, e.g., for expelling the excess water volume created by thermal expansion from the core. If a reactor achieves strong prompt criticality, the power increase will be extremely fast. The heat transfer from the fuel elements to the coolant and moderator is then far too slow to have an influence on phenomena whose time behavior is determined by the neutron lifetime in the core [6].

The phenomena associated with the expulsion of matter from the core also require a time, which is of the same order as the reactor dimensions divided by the speed of sound. For a reactor to be safe even in a prompt critical state, one must therefore require that the temperature coefficient of reactivity be not only negative but also be fast. By fast, we here mean a time, which is short compared to the neutron lifetime [6].

Now that we have established our simple ground rules, we can continue to study the kinetic behavior of the reactor, by stating that the time-dependent neutron flux in a reactor can be described by the point kinetic equation (PKE), which was defined in Chap. 11 as follows without source $S(t)$:

$$\begin{cases} \frac{dP(t)}{dt} = \frac{k_{eff}(1 - \beta_{eff})^{-1}}{l} P(t) + \sum_{i=1}^6 \lambda_i C_i(t) \\ \frac{dC_i(t)}{dt} = -\lambda_i C_i(t) + \frac{\beta_i k_{eff}}{l} P(t) \quad \text{for } i = 1, 2, \dots, 6 \end{cases} \quad (12.18)$$

Equation 12.18 has been reduced to the form that is shown based on utilizing the following parameters:

$$\begin{cases} \rho = \frac{k_{eff} - 1}{k_{eff}} \\ k_{eff} = \frac{l}{\Lambda} \end{cases} \quad (12.19)$$

where:

$P(t)$ is the reactor power.

l is the prompt neutron lifetime.

Λ is the neutron generation or reproduction time.

k_{eff} is the effective multiplication factor.

$C_i(t)$ is the concentration of delayed neutron precursor of group i .

λ_i is the decay constant for delayed neutron precursors of group i .

β_i is the fraction of the total number of fission neutrons emitted as delayed neutrons of group i

Equation 12.18 along with parameters in Eq. 12.19 is considered as one group space-independent kinetic equation analysis and most frequently used form of point kinetic equation (PKE)). Eq. 12.18 can be derived easily via the kinetic equation, the neutron energy, and the space dependence to be eliminated by averaging over all energies that is known as one-group approximation. This also requires assumptions that the neutron flux $\phi(\vec{r}, t)$, neutron source $S(\vec{r}, t)$, and delayed neutron precursor concentration $C_i(\vec{r}, t)$ of group i are separable in space and time. See Problem 12.1.

For Eq. 12.19, the effective multiplication factor k_{eff} could be written in the following form:

$$k_{eff} = 1 + \Delta k_{eff} + \alpha(T - T_0) \simeq 1 + \rho + \alpha\Delta T \quad (12.20)$$

where $\Delta T = (T - T_0)$ is the value of the temperature T with the reactor running at constant power P_0 . The temperature coefficient α has been assumed negative in Eq. 12.20.

In addition, the cooling system of the reactor must be modeled in some way. In the following treatment, the reactor core is assumed to consist only of fuel. It is assumed that during the time interval under consideration, the cooling system removes heat from the fuel elements with a power $\gamma(T - T_c)$ proportional to the difference between the core temperature and an external temperature T_c , which is assumed to remain constant. T_c mainly describes the temperature of the cooling system, and the proportionality factor γ , which is assumed constant, is then the heat transfer coefficient between the core and the cooling system. Since at constant power the cooling system removes all the heat generated in the core, we have:

$$\gamma = \frac{P_0}{T_0 - T_c} \quad (12.21)$$

Here, we have also assumed the heat capacity of the core C also sometimes designated as the heat capacity of the reactor fuel elements is also constant.

Under the above assumptions, we obtain the following equation for the temperature change:

$$\frac{d\Delta T}{dt} = \frac{P - \gamma(T - T_c)}{C} = \frac{(P - P_0) - \gamma\Delta T}{C} \quad (12.22)$$

When the reactivity injection is large enough to make the reactor prompt critical, the so-called Fuchs-Nordheim models can be applied.

However, in all practical purpose of importance, for many cases, the heat capacity, C , of the reactor fuel elements may be assumed to vary linearly with temperature, T , and is written as:

$$C = C_0 + \gamma T \quad (12.23)$$

where C_0 and γ are constants. Eq. 12.23 is again the definition of Fuchs-Nordheim model, which yields for the equations of motion of the reactor:

$$\frac{dP(t)}{dt} = \frac{\delta k_p - \alpha T(t)}{l} P(t) \quad (12.24a)$$

and

$$C \frac{dT(t)}{dt} = P(t) \quad (12.24b)$$

In both Eq. 12.24a and 12.24b, the power reactor at time t is designated as $P(t)$, and δk_p is the prompt reactivity insert, α is the magnitude of the prompt reactivity temperature that is assumed constant, and finally l is the prompt neutron lifetime.

For reactors with narrow pulses, such as TRIGA reactor, delayed neutron and heat transfer effects in Eq. 12.24a and 12.24b could be neglected.

12.6 Fuchs-Hansen Model

Large power excursions in reactor and neutronic analysis for nuclear reactor, where these large power excursions are a matter of interest, bring to a treatment that is known as Fuchs-Hansen model.

This model comes to play when a system is brought rapidly to a state above prompt critical, so that the neutron population then begins to multiply at rapid rate. The normal cooling cannot remove the heat being generated, and so the temperature rises until some compensation sets in that reduces the reactivity to zero, thereby terminating the excursion [7].

In practice, the manner in which the reactivity is reduced may depend in detail on the reactor design and on the rate at which the neutron population (and power) increases. Hence, for computing the reactivity reduction, a point-reactor model may not be adequate. Nevertheless, some useful conclusions can be drawn from such a model of the excursion in which the reactivity reduction is included as a simple feedback parameter. This treatment then is called Fuchs-Hansen Model, and it is subject of this section.

Let us assume that, all of sudden, the reactivity is increased, i.e., step function-type scenario; thus it is bringing the value of reactivity $\rho'(t)$ as function of time t to above the prompt critical, which is shown as $\rho'(t) = \rho(t) - \beta$ where $\rho(t)$ is actual

reactivity as function of time t . The assumption is now made that the feedback reactivity is proportional to the energy generated.

Now, assume in general that the power reactor that consists of the source and precursor terms is described as:

$$\frac{dP(t)}{dt} = \frac{\rho(t) - \beta(t)}{\Lambda(t)} P(t) + \sum_j \lambda_j C_j(t) + Q(t) \quad j = 1, 2, \dots, 6 \quad (12.25)$$

where.

$P(t)$ is reactor power density as function of time t

$\rho(t)$ is actual reactivity as function of time t

$\beta(t)$ is total fraction of delayed neutron as function of time t

$\Lambda(t)$ is average neutron generation time as function of time t

λ_j is decay constant

$C_j(t)$ is precursor nuclei of i th kind as function of time t

$Q(t)$ is volumetric heat source strength (rate of heat release per unit volume) as function of time t

However, under the Fuchs-Hansen model treatment, since the response to the sudden increase in reactivity is fast, it is justifiable to neglect the delayed neutrons while the transient is under way; hence Eq. 12.25 will reduce to the following form:

$$\frac{dP(t)}{dt} = \frac{\rho(t) - \beta(t)}{\Lambda(t)} P(t) \quad (12.26)$$

The reactivity at time t is given by:

$$\rho(t) - \beta(t) = \rho'(t) - \gamma E(t) = \rho'(t) - \gamma \int_0^t P(t') dt' \quad (12.27)$$

where γ represents the energy feedback coefficient and $E(t)$ is the total energy generated between time zero and time t . Upon combining Eq. 12.26 and Eq. 12.27, the result is:

$$\frac{dP(t)}{dt} = P(t) \left[\frac{\rho'(t)}{\Lambda(t)} - \frac{\gamma}{\Lambda(t)} \int_0^t P(t') dt' \right] \quad (12.28)$$

Now if we define constant α_0 as the initial multiplication rate and set it to be as $\alpha_0 = \rho'/\Lambda$ and constant b as $b = \gamma/\Lambda$ at time $t = 0$ and $(dP(t)/dt) = \alpha_0 P(t)$, then we can write compact version of Eq. 12.28 as:

$$\frac{dP(t)}{dt} = P(t) \left[\alpha_0 - b \int_0^t P(t') dt' \right] \quad (12.29)$$

Equation 12.29 can be solved in closed form (see homework Problem 12.8 for the solution); it is found that:

$$E(t) = \frac{\alpha_0 + c}{b} \left[\frac{1 - e^{-ct}}{Ae^{-ct} + 1} \right] \quad (12.30)$$

and

$$P(t) = \frac{2c^2 A e^{-ct}}{b(A e^{-ct} + 1)^2} \quad (12.31)$$

where

$$c \equiv \sqrt{\alpha_0^2 + 2bP_0} \quad (12.32)$$

and

$$A \equiv \frac{c + \alpha_0}{c - \alpha_0} \quad (12.33)$$

A number of interesting results can be derived from these solutions, and we refer the readers to the classical textbook by Bell and Glasstone [7].

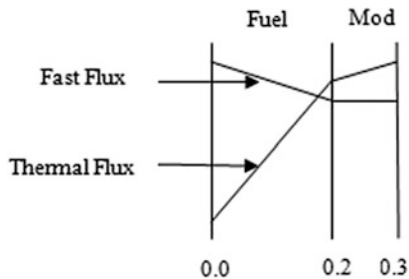
Problems

Problem 12.1 The AGN-201 is operating at 5 watts. It is then placed on a positive transient by inserting a reactivity of 0.00375. After 30 s, the reactor scrams automatically. At what power level is the scram point set? Use a One Delay Family model for the reactor's behavior. The following data apply.

$$\beta_{\text{effective}} = 0.0075 \quad \Lambda = 0.00015 \text{ s} \quad \lambda - \text{bar} - \text{inv} = 0.07675/\text{s}$$

Problem 12.2 Given the following solution for half of a cell in slab geometry, calculate the fast and thermal self-shielding factors for the cross sections in this cell.

Z Dimension	0.0	Fuel	0.2	Moderator	0.3
Fast Flux	1.0		0.85		0.85
Thermal Flux	0.15		0.9		1.0

Fig. 12.5 Problem 12.2

Problem 12.3 Consider a hypothetical reactor in which all of the materials have the same volumetric coefficient of thermal expansion. Thus, all of the nuclide densities decrease according to the same ratio: $\dot{N}/N = \text{constant} < 1$. Additionally, consider that relationship between leakage effects and infinite medium is given by the following equation:

$$\frac{dk}{k} = \frac{dk_\infty}{k_\infty} - \frac{M^2 B^2}{k_\infty} \left(\frac{dM^2}{M^2} + \frac{dB^2}{B^2} \right) \quad (12.34)$$

Moreover, since the leakage probability P_L for large power reactors usually is quite small, so we can write:

$$P_L = \frac{M^2 B^2}{1 + M^2 B^2} \ll 1 \quad (12.35)$$

In addition, the effective multiplication k_∞ can be expressed as Eq. (12.35) below, using energy-averaged cross section. This is based on examination of neutron spectra, assuming that all the constituents of a reactor core are exposed to the same energy-dependent flux $\phi(E)$:

$$k_\infty = \frac{\int_0^\infty v \Sigma_f(E) \phi(E) dE}{\int_0^\infty \Sigma_a(E) \phi(E) dE} \quad (12.36)$$

- (a) Show that the expansion with increased temperature has no effect on k_∞ .
- (b) Using the facts that the core mass, NV , remains constant and that $M \propto N^{-1}$, show from Eq. (9.4) that the reactivity change from expansion is negative, with a value of $\frac{dk}{k} = -\frac{4}{3} P_L \frac{dV}{V}$.

Problem 12.4 Heat transmission in system with internal sources.

If the heat transfer balance for steady state is defined as below for a thin slab of thickness dx at x :

$$\begin{aligned} & \text{Heat Conducted out of } Adx - \text{Heat Conducted into } Adx \\ & = \text{Heat Generated in } Adx \end{aligned}$$

where A is the heat conduction area and Adx is the volume of the section A normal to the direction of x , then (a) define the flow of heat by conduction, and describe your parameters in the equation defining the heat flow. This is what we know as Fourier law. (b) Expand the Fourier law to a volumetric thermal source that is expressed by $Q(x)$, which is heat generated per unit time per unit volume at x with dimension of $\text{Btu}/(\text{hr})(\text{ft}^2)$ in British system.

Problem 12.5 Using the part (b) of solution for Problem 12.4:

Part (a): Provide the appropriate differential equation for a situation, where we have heat transmission in shields and pressure vessels, i.e., slab with exponential heat source $Q(x) = Q_0 e^{-\mu x}$, where again $Q(x)$ is volumetric heat source strength rate of heat release per unit volume, Q_0 is constant for heat source, and μ is the linear attenuation coefficient or macroscopic cross section of the radiations.

Part (b): Solve the differential equation of Part (a), by firstly finding the general solution and secondly giving the boundary condition as $T(x)|_{x=0} = T_1$ and $T(x)|_{x=L} = T_2$, and find the particular solution of the general solution in the first part. Thirdly draw the depiction of heat transmission in slab with exponential source and the given boundary conditions.

Part (c): Under certain condition, one can find the maximum for the particular solution in second step of part (b) and then find that maximum expression.

Problem 12.6 A water-cooled and water-moderated power reactor is contained within a thick-walled pressure vessel. This vessel is protected from excessive irradiation and thus excessive thermal stress by a series of steel thermal shields between the reactor core and the pressure vessel. One of these shields, 2 in. thick, whose surfaces are both maintained at 500 °F, receives a gamma-ray energy flux of $10^{14} \text{ MeV}/(\text{cm}^2)(\text{s})$. Calculate the location and magnitude of the maximum temperature in this shield. The linear attenuation coefficient of the radiation in the steel may be taken to be 0.27–1 cm and the thermal conductivity as 23 $\text{Btu}/(\text{hr})(\text{ft}^2)(^0\text{F}/\text{ft})$. Hint: Use the results of solution that you found in Part (c) of Problem 15.5 and Figure in Part (b). Additionally, assume that for steel $Q_0 = \phi E \mu_e$, where μ_e is energy absorption coefficient, which is 0.164 for steel, and ϕE is gamma-ray energy flux of gamma-ray energy E .

Problem 12.7 The Fuchs-Nordheim model predicts the shape and magnitude of the transient. We do not really solve analytical solution of the model but instead some characteristic from it. If we write the first part of Eq. 12.18 as the following form for point kinetic equation (PKE), we have to:

- (a) Argue under what assumption Eq. 12.18 (i.e., first part) reduces to Eq. 12.25 and why historically this assumption was made by Manhattan Project weapon designers.
- (b) Assume that if transient is so rapid that no heat is transferred from the fuel (i.e., The time constant for heat to be removed from UO_2 fuel is about 5 min) with heat capacity, C_p is given by the following relation:

$$T_{fuel}(t) = T_{fuel}^0 + \frac{1}{C_p} \int P(t) dt \quad (12.37)$$

In addition, assume a Doppler feedback coefficient independent of temperature (recall that we calculate that PWRs have a Doppler coefficient which is about -3 pcm/K), and we can write:

$$\rho(t) = \rho_{rod} - \alpha \left(T_{fuel} - T_{fuel}^0 \right) \quad (12.38)$$

Then calculate the peak temperature characteristics for power distribution $P(t)$.

- (c) Calculate asymptotic characteristics for power distribution $P(t)$.
- (d) Finally, yet importantly, show that asymptotic temperature is independent of the reactivity insertion rate.

Problem 12.8 Solve Eq. 12.29.

References

1. J. Duderstadt, L. Hamilton, Nuclear reactor analysis, in *John Wiley Publishing Company*, (1976)
2. Net electrical MWe and gross MWe vary slightly from summer to winter, so normally the lower summer figure, or an average figure, is used. If the summer figure is quoted plants may show a capacity factor greater than 100% in cooler times. Watts Bar PWR in Tennessee is, reported to run at about 1125 MWe in summer and about 1165 MWe net in winter, due to different condenser cooling water temperatures. Some design options, such as powering the main large feed-water pumps with electric motors (as in Evolutionary Power Reactor (EPR)) rather than steam turbines (taking steam before it gets to the main turbine-generator), explains some gross to net differences between different reactor types. The EPR has a relatively large drop from gross to net MWe for this reason.
3. L. Massimo, *Physics of the High Temperature Reactors* (Pergamon Press, 1976)
4. Y. Oka, T. Kiguchi, *Nuclear Reactor Design (An Advanced Course in Nuclear Engineering)* (Springer Publishing Company, 2014)

5. G.R. Keepin, *Physics of Nuclear Kinetic* (Addison-Wesley Publishing Co. Inc, 1965)
6. J. Ala-Heikkila, T. Seren, Calle Persson, *Student Reactor Exercises at VTT*, KTH Engineering Science, Center of Finland and Royal Institute of Technology (KTH) 2008
7. G.I. Bell, S. Glasstone, *Nuclear Reactor Theory*, Published Under Auspices of the Davison of Technical Information, United Sates Atomic Energy Commission, Van Nostrand Reinhold Company, 1970

Chapter 13

Reactor Stability



Understanding time-dependent behaviors of nuclear reactors and the methods of their control is essential to the operation and safety of nuclear power plants. This chapter provides researchers and engineers in nuclear engineering very general yet comprehensive information on the fundamental theory of nuclear reactor kinetics and control and the state-of-the-art practice in actual plants, as well as the idea of how to bridge the two. The dynamics and stability of engineering equipment affect their economical and operation from safety and reliable operation point of view. In this chapter, we will talk about the existing knowledge that is today practiced for the design of reactor power plants and their stabilities as well as available techniques to designers. Although, stable power processes are never guaranteed. An assortment of unstable behaviors wrecks power apparatus, including mechanical vibration, malfunctioning control apparatus, unstable fluid flow, unstable boiling of liquids, or combinations thereof. Failures and weaknesses of safety management and safety management systems are the underlying causes of most accidents.

13.1 Frequency Response

The engineers and designers of today's nuclear power reactors are doing their best to provide us commercially safe reactors, using inherent reactor kinetics and dynamics characteristic to limit undesirable/unwanted rise in reactor power. A necessary condition for stable reactor power stable is that the reactor perturbation or distortion, accompanying a temperature rise decreases the reactivity, thus slowing any further rise in power. For instance, the reactor distortion caused by a temperature rise could allow more neutrons to be wasted by leakage, thus decreasing the reactivity. Overly simple equations for reactor power dynamics indicate that this idea should work, and sometimes it does.

The supposition that satisfying the above condition guarantees power stability is based on a false assumption that the reactor distortion occurs simultaneously with

the temperature rise, which caused it. The distortion lags behind the temperature change by a time determined by the mechanical dynamics of the reactor system. Therefore, the change in reactivity also lags behind the temperature change, raising the possibility of unstable power oscillations. This conclusion is supported by actual experience with seriously unstable reactors such as the inoperable Ft. St. Vrain power reactor [1].

As part of failure analysis, utilization of *Frequency Response* allows to take a quantitative measure of the output spectrum of a system such as overall nuclear power plant or device at the components level, in response to a stimulus of design process. This process used to characterize the dynamics of the system, and it measures magnitude and *phase* of the output as a function of *frequency*, in comparison to the input.

As an example of such circumstances, we look at a sine wave condition. If a sine wave is injected into a system at a given frequency, a linear system will respond at that same frequency with a certain magnitude and a certain phase angle relative to the input. However, if a linear time-invariant (LTI) theory applies for a linear system, doubling the amplitude of the input will double the amplitude of the output. In addition, if the system is time-invariant or LTI, then the frequency response also will not vary with time. Thus, for LTI systems, the frequency response can be seen as applying the system's transfer function to a purely imaginary number argument representing the frequency of the sinusoidal excitation.

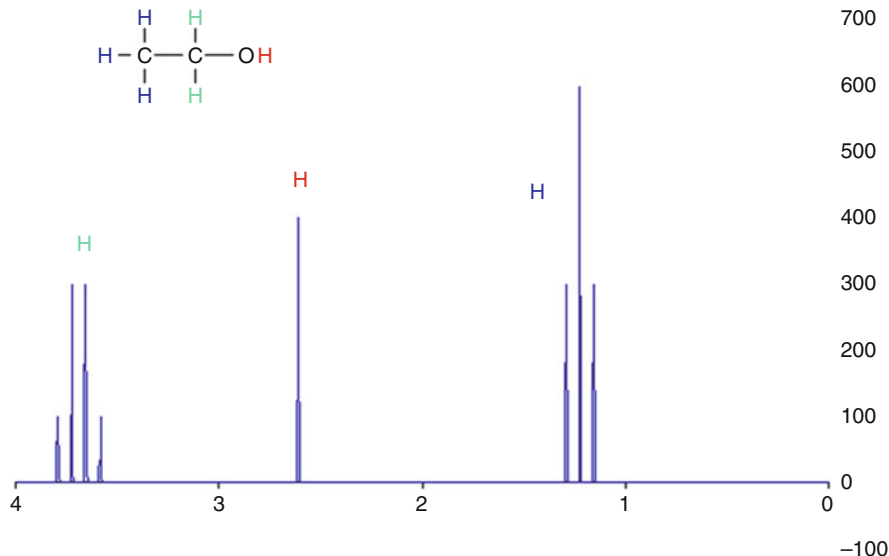
Note that linear time-invariant theory, commonly known as LTI system theory, comes from applied mathematics and has direct applications in nuclear magnetic resonance (NMR) spectroscopy, seismology, circuits, signal processing, control theory, and other technical areas. It investigates the response of a linear and time-invariant system to an arbitrary input signal. Trajectories of these systems are commonly measured and tracked as they move through time (e.g., an acoustic waveform), but in applications like image processing and field theory, the LTI systems also have trajectories in spatial dimensions. Thus, these systems are also called linear translation-invariant to give the theory the most general reach. In the case of generic discrete-time (i.e., sampled) systems, linear shift-invariant is the corresponding term. A good example of LTI systems is electrical circuits that can be made up of resistors, capacitors, and inductors.

In addition, *nuclear magnetic resonance* (NMR) spectroscopy, commonly known as NMR spectroscopy, is a research technique that exploits the magnetic properties of certain atomic nuclei. It determines the physical and chemical properties of atoms or the molecules in which they are contained.

Figure 13.1 is the presentation of H^1 NMR spectrum, one-dimensional of ethanol, which is plotted as signal intensity versus chemical shift. As it can be seen in this figure, the hydrogen H on the -OH group is not coupling with the other H atoms and appears as a singlet, but the CH^3 - and the $-CH^2-$ hydrogen are coupling with each other, resulting in a triplet and quartet, respectively.

Overall view of property definitions of LTI system is *linearity* and *time invariance*, and they fall into the two following categories:

Ethanol

Fig. 13.1 H^1 nuclear magnetic resonance spectrum

13.2 Linearity

This means that the relationship between the input and the output of the system is a linear map and mathematically could be presented as a linear input process, and in response, it produces a linear output. If input $x_1(t)$ produces response $y_1(t)$, and input $x_2(t)$ produces response $y_2(t)$, then the *scaled* and *summed* input $a_1x_1(t)+a_2x_2(t)$ produces the scaled and summed response $a_1y_1(t)+a_2y_2(t)$, where a_1 and a_2 are real scalars. It follows that this can be extended to an arbitrary number of terms and thus for real numbers c_1, c_2, \dots, c_k , and we can write the following relations in mathematical notation as:

$$\text{Input } \sum_k c_k x_k(t) \text{ produces output as } \sum_k c_k y_k(t) \quad (13.1)$$

In particular, we can write:

$$\text{Input } \int_{-\infty}^{+\infty} c_\omega x_\omega(t) d\omega \text{ produces output as } \int_{-\infty}^{+\infty} c_\omega y_\omega(t) d\omega \quad (13.2)$$

where c_ω and x_ω are scalars and inputs that vary over a continuum index by ω . Thus, if an input function can be represented by a continuum of input functions, combined “linearly,” as shown, then the corresponding output function can be represented by the corresponding continuum of output functions, *scaled* and *summed* in the same way.

13.3 Time Invariance

This means that whether we apply an input to the system now or T seconds from now, the output will be identical except for a time delay of T seconds. That is, if the output due to input $x(t)$ is $y(t)$, then the output due to input $x(t - T)$ is $y(t - T)$. Hence, the system is time-invariant because the output does not depend on the particular time the input is applied.

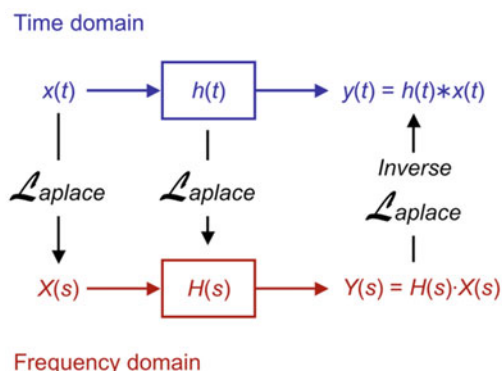
A single function known as system's impulse response can characterize the fundamental result in linear time-invariant (LTI) system theory. The output of the system is simply the convolution of the input to the system with the system's impulse response. This method of analysis is often called the time domain point of view. The same result is true of discrete-time linear shift-invariant systems in which signals are discrete-time samples, and convolution is defined on sequences.

Equivalently, any LTI system can be characterized in the frequency domain by the system's transfer function, which is the Laplace transform of the system's impulse response (or Z transform in the case of discrete-time systems). Because of the properties of these transforms, the output of the system in the frequency domain is the product of the transfer function and the transform of the input. In other words, convolution in the time domain is equivalent to multiplication in the frequency domain. Figure 13.2 is depicting such situation, where the relationship between the time domain and the frequency domain is shown.

For all LTI systems, the eigenfunctions and the basic functions of the transforms are complex exponentials. This is, if the input to a system is the complex waveform Ae^{st} for some complex amplitude A and complex frequency s , then the output will be some complex constant times the input, let say Be^{st} for some new complex amplitude B . However, the ratio B/A is the transfer function at frequency s .

Since sinusoids are a sum of complex exponentials with complex-conjugate frequencies, if the input to the system is a sinusoid, then the output of the system will also be a sinusoid, perhaps with a different amplitude and a different phase but always with the same frequency upon reaching steady state. Linear time-variance (LTI) systems cannot produce frequency components that are not in the input.

Fig. 13.2 Relationship between the time domain and the frequency domain



LTI system theory is good at describing many important systems. Most LTI systems are considered “easy” to analyze, at least compared to the time-varying and/or nonlinear case. Any system that can be modeled as a linear homogeneous differential equation with constant coefficients is an LTI system. Examples of such systems are electrical circuits made up of resistors, inductors, and capacitors (RLC circuits). Ideal spring-mass-damper systems are also LTI systems and are mathematically equivalent to RLC circuits [2].

Most LTI system concepts are similar between the continuous-time and discrete-time (linear shift-invariant) cases. In image processing, the time variable is replaced with two space variables, and the notion of time invariance is replaced by two-dimensional shift invariance. When analyzing filter banks and multiple input and multiple output (MIMO) systems, it is often useful to consider vectors of signals.

A linear system that is not time-invariant can be solved using other approaches such as the Green’s function method. The same method must be used when the initial conditions of the problem are not null. Estimating the frequency response for a physical system generally involves exciting the system with an input signal, measuring both input and output time histories, and comparing the two through a process such as the fast Fourier transform (FFT). One thing to keep in mind for the analysis is that the frequency content of the input signal must cover the frequency range of interest or the results will not be valid for the portion of the frequency range not covered. Figure 13.3 is presenting frequency response of a low-pass filter with 6 dB (decibel) per octave or 20 dB per decade.

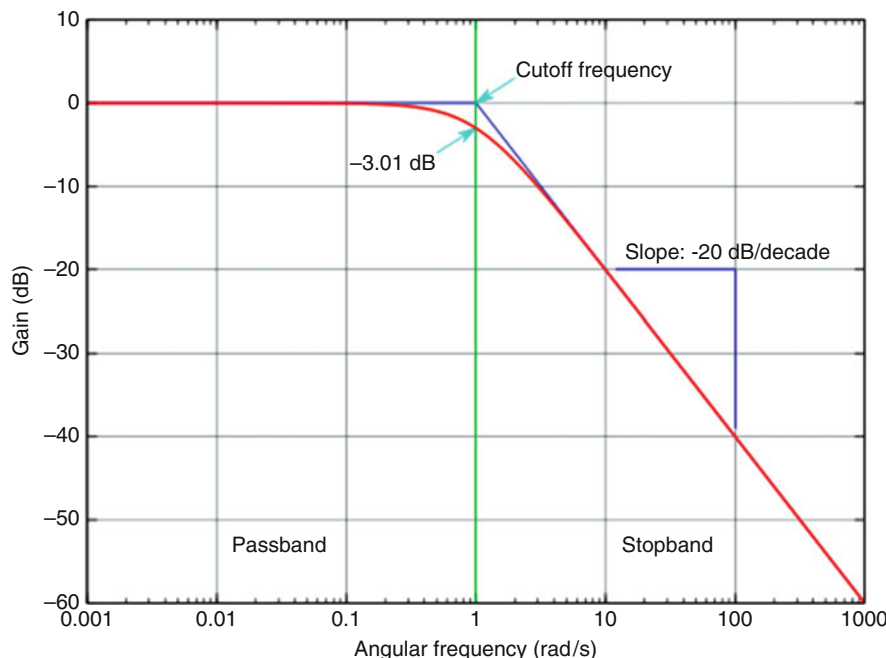


Fig. 13.3 Frequency response of a low-pass filter with 6 dB per octave or 20 dB per decade

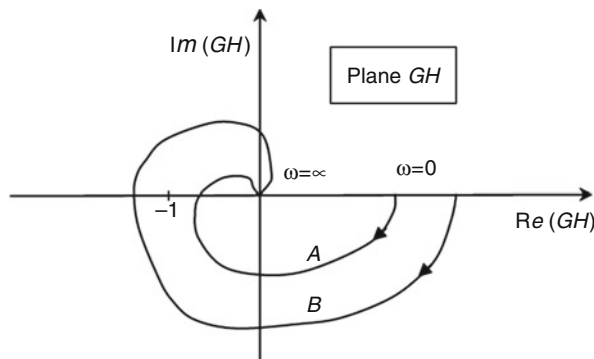
In summary, the two applications of frequency response, namely, phase and frequency analyses, are related but have different objectives. For an audio system, the objective may be to reproduce the input signal with no distortion. That would require a uniform (flat) magnitude of response up to the bandwidth limitation of the system, with the signal delayed by precisely the same amount of time at all frequencies. That amount of time could be seconds or weeks or months in the case of recorded media. In contrast, for a feedback apparatus used to control a dynamic system, the objective is to give the closed-loop system improved response as compared to the uncompensated system. The feedback generally needs to respond to system dynamics within a very small number of cycles of oscillation (usually less than one full cycle) and with a definite phase angle relative to the commanded control input. For feedback of sufficient amplification, getting the phase angle wrong can lead to instability for an open-loop stable system or failure to stabilize a system that is open-loop unstable. Digital filters may be used for both audio systems and feedback control systems, but since the objectives are different, generally, the phase characteristics of the filters will be significantly different for the two applications [3].

13.4 Nyquist Plots

The Nyquist stability criterion is used to investigate the stability of any open or closed system using its frequency characteristics. Usually, the criterion is used for closed systems, though. A useful but not the most general formulation of the Nyquist criterion is as follows: if the mapping of the transfer function of an open system $G(s) * H(s)$ on the plane GH encircles point $(-1, 0)$, then the system is unstable if it is closed. The criterion is illustrated in Fig. 13.4, where Nyquist plots of a stable and unstable closed system. Curve A does not encircle point $(-1, 0)$, and then the system is stable. On the other hand, curve B encircles point $(-1, 0)$, and the system therefore is called to be unstable.

The Nyquist criterion can be easily proved, which requires basic knowledge of mathematics of complex variables, and we assume the readers have such

Fig. 13.4 Nyquist plots



background. With assumption of such knowledge, we let $f(s)$ be meromorphic throughout the bounded region inside and continuous on a closed contour C on which $f(s) \neq 0$. Let Z be the number of zeros and P be the number of poles of $f(s)$ inside C , respectively, where a zero or pole of order m is counted m times. Then, using knowledge of our complex variables, we can write the following relation:

$$\frac{1}{2\pi i} \oint_C \frac{f'(\xi)}{f(\xi)} d\xi = Z - P \quad (13.3)$$

For $P = 0$, we can obtain the principle of the argument as:

$$N = \frac{\Delta_c \vartheta}{2\pi} \quad (13.4)$$

where $\Delta_c \vartheta$ is the variation of the argument ϑ of $f(s)$ around the contour C . This equation means that $f(s)$ maps a moving point s describing the contour C once into a moving point $f(s)$ which encircles the f plane origin $N = 1, 2, \dots$ times, if $f(s)$ has, respectively, $0, 1, 2, \dots$ zeros inside the contour C in the s plane. The above criterion is used for locating zeros and poles of $f(s)$ and is known as the Nyquist criterion.

As an example, consider a function $f(s)$ that has two zeros as $s = z_1$ and $s = z_2$ as well as one pole $s = p_1$. The function can be given as [4]:

$$f(s) = \frac{(s - z_1)(s - z_2)}{(s - p_1)} \quad (13.5)$$

The locations of the zeros and the pole are depicted in Fig. 13.5.

Assume that point s is moving along the contour and encircles it. The argument of the number $(s - z_1)$ will increase by 2π . It means that with a single encirclement of the contour C by point s , the argument of function $f(s)$ will increase by 2π for each zero, which is inside of the contour. In a similar way, it is obtained that the argument

Fig. 13.5 Location of zeros and poles on s plane

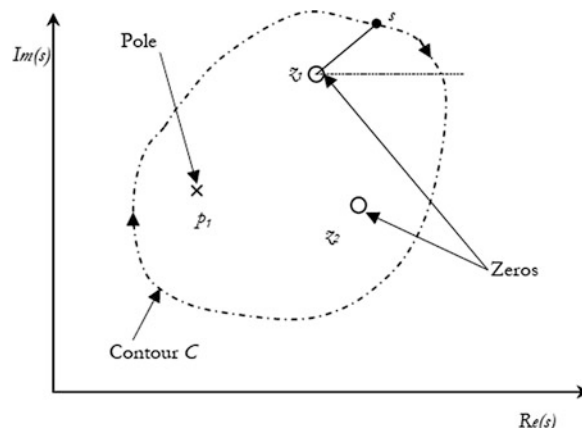
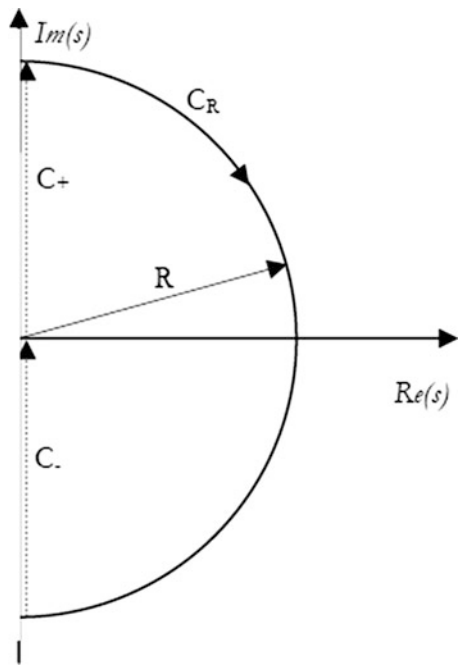


Fig. 13.6 Contour in the s plane that covers the whole right-hand side half plane when $R \rightarrow \infty$



of function $f(s)$ decreases with 2π for each pole located inside of the contour C . As a consequence, the mapping of $f(s)$ on plane f will encircle the plane origin the corresponding number of times. In the considered case, $f(s)$ will encircle the origin only once, since its argument will increase with $(2 - 1)$ multiplied by 2π .

The Nyquist criterion is very useful in the theory of stability. To evaluate the stability of any system, it is necessary to find the locations of zeros of the characteristic function of the system. If any of the zeros is located on the right-hand side of the s plane, then the system is unstable. The contour on the s plane is shown in Fig. 13.6.

An example of the corresponding mapping of function $f(s)$ on the f plane is shown in Fig. 13.7 as below, where it shows the mapping function $f(s)$ for encircling the right half plane as shown in Fig. 13.6.

As we have stated, the frequency domain method can be used for linear systems only and is an approach similar to the Laplace transformation. If the system under consideration is nonlinear, then it should be first linearized around a certain operational point for the frequency domain approach to work. A frequency response of any system is the behavior of the system that should be subjected to a sinusoidal-type forcing function or input signal, and such forcing function is described here as:

$$u(t) = u_0 \sin(\omega t) \quad (13.5)$$

Fig. 13.7 Mapping of function $f(s)$ for s encircling the right half plane

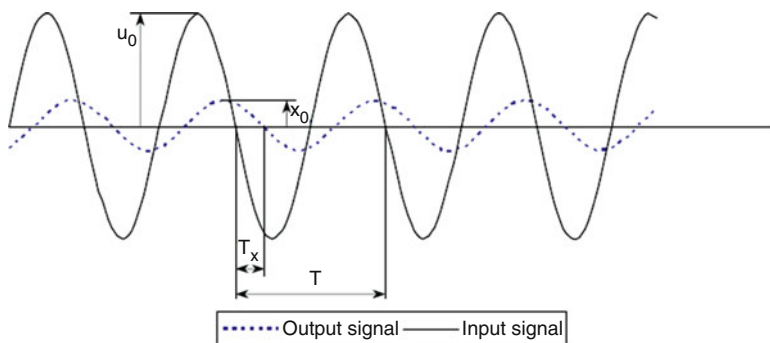
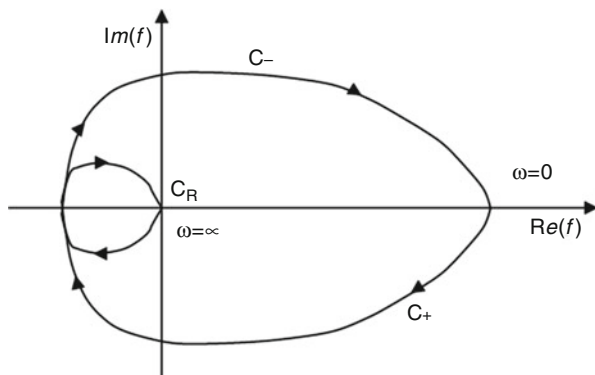


Fig. 13.8 A linear system response to a sinusoidal forcing function at steady state. The system introducing a lag to the signal and reduce its amplitude [4]

where u_0 is the amplitude of the input signal and ω is the signal frequency expressed in radian per second.

When a linear system is subject to a sinusoidal signal at input, the system response will also be a signal of the same shape and frequency. However, the output signal will have different amplitude and phase. Thus, the output signal can be written as:

$$x(t) = x_0 \sin(\omega t + \theta) \quad (13.6)$$

Graphically, the input or forcing function and its output signal for a linear system can be depicted in Fig. 13.8 [4].

However, the system amplification can be expressed in terms of the transfer function $G(s)$; the amplification is as follows [4]:

$$L = 20 \lg \frac{|G(j\omega)|}{|G(0)|} \text{ dB (decibels)} \quad (13.7)$$

while the phase shift θ is given as:

$$\theta = \arg G(j\omega) \quad (13.8)$$

The frequency approach can give an answer whether the system is stable or not without specifically finding the poles of the transfer function. For that purpose, the Nyquist plot is used, in which the imaginary part of $G(j\omega)$ is plotted against the real part of $G(j\omega)$.

For the first-order system expressed by the following differential equation along its initial condition as:

$$u(t) = \frac{dx(t)}{dt} + \omega_0 x(t) \quad \text{Initial condition } x(0) = 0 \quad (13.9)$$

The transfer function could be obtained by utilizing the Laplace transformation of Eq. 13.9 over variable t on both sides of equation, as it is shown below:

$$\begin{aligned} \mathfrak{L}\{u(t)\} &= \mathfrak{L}\left\{\frac{dx(t)}{dt}\right\} + \omega_0 \mathfrak{L}\{x(t)\} \\ u(s) &= sx(s) + x(0) + \omega_0 x(s) \end{aligned} \quad (13.10)$$

Here, we have assumed $\mathfrak{L}\{x(t)\} = x(s)$ and Eq. 13.10 will be reduced to the following form:

$$G(s) = \frac{x(s)}{u(s)} = \frac{1}{s + \omega_0} \quad (13.11)$$

The real and the imaginary parts of $G(j\omega)$ are readily obtained as:

$$G(j\omega) = \frac{1}{j\omega + \omega_0} = \frac{(-j\omega + \omega_0)}{(j\omega + \omega_0)(-j\omega + \omega_0)} = \frac{\omega_0}{\omega^2 + \omega_0^2} - j \frac{\omega}{\omega^2 + \omega_0^2} \quad (13.12)$$

Thus,

$$\begin{aligned} \text{Re}[G(j\omega)] &= \frac{\omega_0}{\omega^2 + \omega_0^2} \\ \text{Im}[G(j\omega)] &= -\frac{\omega}{\omega^2 + \omega_0^2} \end{aligned} \quad (13.13)$$

The module and argument of $G(j\omega)$ are now found as:

$$\begin{aligned} |G(j\omega)| &= \sqrt{\text{Re}^2[G(j\omega)] + \text{Im}^2[G(j\omega)]} \\ &= \sqrt{\left(\frac{\omega_0}{\omega^2 + \omega_0^2}\right)^2 + \left(\frac{\omega}{\omega^2 + \omega_0^2}\right)^2} \\ &= \frac{1}{\sqrt{\omega^2 + \omega_0^2}} \end{aligned} \quad (13.14)$$

Now, from Eq. 13.7, the system amplification is found as:

$$L = 20\lg \frac{|G(j\omega)|}{|G(0)|} = 20\log \left\{ \frac{\left| \frac{1}{j\omega + \omega_0} \right|}{\left| \frac{1}{\omega_0} \right|} \right\} = 20\lg \left(\frac{1}{\sqrt{1 + \beta^2}} \right) \quad (13.13)$$

where $\beta = \omega/\omega_0$. Similarly, from Eq. 13.8, the phase shift is found to be:

$$\theta = \arg G(j\omega) = \arctan \left(\frac{\text{Im}G(j\omega)}{\text{Re}G(j\omega)} \right) = \arctan(-\beta) \quad (13.14)$$

As it can be seen, identical expressions have been obtained for L and θ as previously derived in the time domain analysis.

The Bode plots for the first-order system have been already shown in Fig. 13.8. The Nyquist plot can be obtained in an analytical form by expressing the imaginary part of $G(j\omega)$ with its real part. This can be achieved as follows:

$$\text{Im}[G(j\omega)] = -\frac{\omega}{\omega^2 + \omega_0^2} = -\frac{\omega}{\omega^2 + \omega_0^2} \frac{\omega}{\omega_0} = -\text{Re}[G(j\omega)] \frac{\omega}{\omega_0} \quad (13.15)$$

Thus,

$$\omega = -\frac{\text{Im}[G(j\omega)]}{\text{Re}[G(j\omega)]} \omega_0 \quad (13.16)$$

The imaginary part can be now expressed as:

$$\text{Im}[G(j\omega)] = -\frac{\frac{\text{Im}[G(j\omega)]}{\text{Re}[G(j\omega)]} \omega_0}{\omega_0^2 + \left(\frac{\text{Im}[G(j\omega)]}{\text{Re}[G(j\omega)]} \omega_0 \right)^2} = -\frac{-\frac{\text{Im}[G(j\omega)]}{\text{Re}[G(j\omega)]}}{1 + \left(\frac{\text{Im}[G(j\omega)]}{\text{Re}[G(j\omega)]} \right)^2} \frac{1}{\omega_0} \quad (13.17)$$

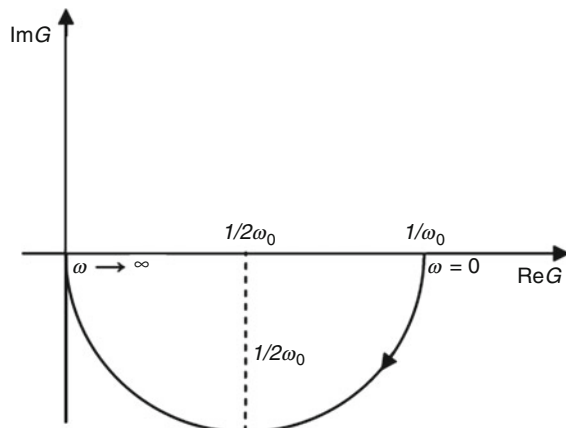
or

$$\text{Re}^2[G(j\omega)] + \text{Im}^2[G(j\omega)] = \frac{\text{Re}[G(j\omega)]}{\omega_0} \quad (13.18)$$

This equation represents a half circle on the $G(j\omega)$ plane, which can be readily seen from the following form of the equation:

$$\left(\text{Re}[G(j\omega)] - \frac{1}{2\omega_0} \right)^2 + \text{Im}^2[G(j\omega)] = \left(\frac{1}{2\omega_0} \right)^2 \quad (13.19)$$

Fig. 13.9 Nyquist plot for the first-order system



The Nyquist plot for the first-order system is shown in Fig. 13.9.

The Bode and Nyquist characteristics can be plotted with dedicated Scilab functions.

Nyquist and Bode. See Problem 13.1.

13.5 Nonlinear Stability

In the design, construction, and operation of nuclear reactors, an attempt is made to maintain steady operation at any desired power level from fission of the nuclear fuels, uranium or plutonium. This attempt can fail sometimes catastrophically. A nuclear power plant is a nuclear system and a mechanical system. It is also a heat transfer system, tied in with controls, boilers, turbines, human operators, and a multiplicity of other complicating factors. The possibilities for instability are myriad. This fiercely complicated set of systems is such as to preclude any possibility of the formation of adequate analytical equations and their solution to guarantee the stability of power. An experimental program sufficient to eliminate the possibilities of power instability in reactors would be expected to be ruinous of both the economy and the environment. Our program covers only a small part of the complicated possibilities and demonstrates only one type of power instability.

Changes in reactor temperature also affect the density. A decrease in the density of reactor parts tends to increase the leakage of neutrons, which in turn decreases the reactivity. This adds the complications of mechanical dynamics to the analysis of reactor stability. Fast density changes in a reactor structure may cause it to vibrate, and reactor power may oscillate as a result. Accounting for this effect requires adding to the temperature coefficient described above a “density coefficient of reactivity.” The density coefficient couples mechanical and nuclear power oscillations. As previously mentioned, inclusion of mechanical effects requires solution of

a fourth-order differential equation of reactor kinetics, as opposed to the second-order nuclear equation. Prediction of power stability becomes more precarious [1].

Nonlinearity or perturbation to reactor power can be studied by calculating the power dynamics of a reactor, based on (Thompson and Thompson) [5, 6] paper, where they present some necessary conditions for power stability provided by nuclear physics, as analyzed by Weinberg and (Weinberg and Wigner) [7].

Their analysis generated a second-order differential equation whose solution is always stable if the coefficients in the equation are all positive. Then we consider mechanical characteristics of reactors, which render the nuclear analysis insufficient to assure stability. This results in a fourth-order differential equation whose stability requires not only that all coefficients be positive but also that a relationship among the coefficients be satisfied (Routh's criterion). It turns out that for power stability, motion of any reactor parts, which affect reactivity, must be sufficiently damped by mechanical friction in the moving parts.

Routh's Criterion

In control system theory, the Routh–Hurwitz stability criterion is a mathematical test that is a necessary and sufficient condition for the stability of a linear time- invariant (LTI) control system. The Routh test is an efficient recursive algorithm, that English mathematician Edward John Routh proposed in 1876 to determine whether all the roots of the characteristic polynomial of a linear system have negative real parts.

German mathematician Adolf Hurwitz independently, proposed in 1895 to arrange the coefficients of the polynomial into a square matrix. This is called the Hurwitz matrix, and showed that the polynomial is stable if and only if the sequence of determinants of its principal sub-matrices is are all positive. The two procedures are equivalent, with the Routh test providing a more efficient way to compute the Hurwitz determinants than computing them directly. A polynomial satisfying the Routh–Hurwitz criterion is, called a Hurwitz polynomial.

Reactivity and stability are unavoidably affected by the depletion of reactor fuels and the accumulation of “poisons” during operation. Other destabilizing effects not considered here, or anywhere else, are so numerous and so complicated in their interrelationships as to thwart human efforts to guarantee reactor stability.

Thompson and Thompson [5] in their paper are demonstrating that mechanical friction in a reactor core structure, like the shock absorber in an automobile, is necessary to limit oscillations of reactor power. Without adequate internal friction, a nuclear power-driven mechanical oscillation increases toward destruction of the reactor core. Design engineers in many fields have found to their sorrow that any given level of mechanical friction is difficult to guarantee. Some of the computer-generated examples later in this section show the changing core temperature and reactor power for a reactor without adequate friction to provide stability. A small

perturbation in power causes an initially small oscillation, which either builds rapidly to destruction, blowup, or meltdown. Their approach is based on a computer program, which they had developed together. Their program solves by finite difference mathematics a nonlinear, fourth-order differential equation involving nuclear, mechanical, and thermal characteristics of reactors. Our paper, “A Model of Reactor Kinetics” demonstrates a mechanism for catastrophic instability [1].

In the design, construction, and operation of nuclear reactors, an attempt is made to maintain steady operation at any desired power level from fission of the nuclear fuels, uranium or plutonium. This attempt can fail sometimes catastrophically. A nuclear power plant is a nuclear system and a mechanical system. It is also a heat transfer system, tied in with controls, boilers, turbines, human operators, and a multiplicity of other complicating factors. The possibilities for instability are myriad. This fiercely complicated set of systems is such as to preclude any possibility of the formation of adequate analytical equations and their solution to guarantee the stability of power. An experimental program sufficient to eliminate the possibilities of power instability in reactors would be expected to be ruinous of both the economy and the environment. Their program covers only a small part of the complicated possibilities and demonstrates only one type of power instability [1].

Problems

Problem 13.1 Perform the Nyquist and Bode plots for first-order system using Scilab functions.

Problem 13.2 *The Stability of Dynamic System*

The equations which describe the dynamic behavior of a reactor are complicated and, in particular, are essentially nonlinear for the diffusion equation:

$$l \frac{\partial P(\vec{r}, t)}{\partial t} = M^2 \nabla^2 P(\vec{r}, t) + (k_\infty - 1)P(\vec{r}, t) \quad (1)$$

where

l is prompt neutron life time (s)

P is reactor power density (W/cm^2)

M is migration length (cm)

k is multiplication factor

Equation (1) necessarily involves the product $k_\infty P(\vec{r}, t)$. Since k_∞ is itself a function of the reactor temperature, Xenon concentration, and so on, this term is essentially nonlinear as well. Consequently, it is not in general possible to solve the dynamic equation (1) in analytic terms, and extensive numerical integrations are normally necessary. Such calculations are carried out, for example, in the

investigation of fault conditions. In stability studies, however, a number of simplifications are possible.¹ Assume that Eq. (1) reduces to form of Eq. (2) below, by setting up a mesh of points in three dimensions covering the reactor and defining each variable –power density, fuel temperature, xenon concentration, and so on – at each point of mesh. Terms in the equations like $\partial^2 p(x)/\partial x^2$ can now be represented approximately as:

$$\frac{\partial^2 p(x)}{\partial x^2} = \frac{1}{h^2} \{p(x - h, y, z) - 2p(x, y, z) + p(x + h, y, z)\} \quad (2)$$

and so on. This can be made accurate as one wishes by taking a fine enough mesh, provided one is not concerned with quantities that vary arbitrarily steeply in space. From physical considerations, however, such variations are of no interest in a stability study, for the stabilizing effect of neutron leakage must dominate all other effects in a highly localized disturbance. Thus, such a representation is legitimate. Then, Eq. (2) now takes the following form:

$$\frac{dx_i}{dt} = \sum_{j=1}^n a_{ij} x_j \quad i = 1, 2, \dots, n \quad (3)$$

where x_i is the various representations of reactor temperature, power densities, and so on, at the different mesh points. The a_{ij} is independent of t . Equation (3) is a very simple set of differential equations, and they can, in principle, be solved easily. Find the general solution of this equation.

References

1. A.S. Thompson, Unstable nuclear power. <http://www.ratical.org/radiation/CoNP/3instability.html>
2. https://en.wikipedia.org/wiki/LTI_system_theory
3. https://en.wikipedia.org/wiki/Frequency_response
4. H. Anglart, *Nuclear Reactor Dynamics and Stability* (KTH Engineering Science, Center of Finland and Royal Institute of Technology (KTH)), New York, NY, p. 2011
5. A.S. Thompson, R. Bruce, A. Thompson, Model of reactor kinetics. *Nucl. Sci. Eng.* **100**, 83 (1988)
6. A.S. Thompson, O.E. Rodgers, *Thermal Power from Nuclear Reactors* (Wiley, New York, 1956)
7. A.M. Weinberg, E.P. Wigner, *The Physical Theory of Neutron Chain Reactors* (The University of Chicago Press, Chicago, 1958), pp. 603–609

¹See for details in the book by A. Hitchcock, “Nuclear Reactor Stability,” Published by Temple Press, 1960.

Chapter 14

Numerical Modeling for Time-Dependent Problems



The possibility of a plutonium-fueled nuclear-powered reactor, such as a fast-breeder reactor that could produce more fuel than it consumed, was first raised during World War II in the United States by scientists involved in Manhattan Project and the US Atomic Bomb Program. In the past two decades, the Soviet Union, the United Kingdom, France, Germany, Japan, and India followed the United States in developing a nationalized plutonium-breeder reactor programs, while Belgium, Italy, and the Netherlands collaborated with the French and German programs. In all of these programs, the main driver of this effort was the hope of solving the long-term energy supply problem using the large-scale deployment of fissional nuclear energy for electric power. Breeder reactors, such as plutonium-fueled breeder reactors, appeared to offer a way to avoid a potential shortage of the low-cost uranium required to support such an ambitious vision using other kinds of reactors, including today's new generation of power reactors known as GEN-IV.

14.1 Fast-Breeder Reactor History and Status

The International Panel on Fissile Materials (IPFM) was founded in January 2006. It is an independent group of arm-control and nonproliferation experts from 17 countries, including both nuclear weapon and nonnuclear weapon states [1].

The mission of the IPFM is to analyze the technical basis for practical and achievable policy initiatives to secure, consolidate, and reduce stockpiles of highly enriched uranium and plutonium. These fissile materials are the key ingredients in nuclear weapons, and their control is critical to nuclear disarmament, halting the proliferation of nuclear weapons and ensuring that terrorists do not acquire nuclear weapons [1].

Both military and civilian stocks of fissile materials have to be addressed. The nuclear weapon states still have enough fissile materials in their weapon stockpiles for tens of thousands of nuclear weapons. On the civilian side, enough

plutonium has been separated to make a similarly large number of weapons. Highly enriched uranium is used in civilian reactor fuel in more than 100 locations. The total amount used for this purpose is sufficient to make about 1000

Hiroshima-type bombs, a design potentially within the capabilities of terrorist groups [1].

Uranium proved to be much more abundant than originally imagined, and, after a fast start, nuclear power growth slowed dramatically in the late 1980s, and global nuclear capacity is today about one tenth the level that had been projected in the early 1970s. The urgency of deploying fast-neutron reactors for plutonium breeding therefore abated – at least in the western Organization for Economic Co-operation and Development (OECD) countries. In India and Russia, however, concerns about potential near-term uranium shortages persist, and new demonstration breeder reactors are being built. China, which currently is building up its nuclear capacity at an enormous rate, is considering the possibility of building two Russian-designed breeder reactors. Because of the high costs and reliability and safety issues, no commercial breeder reactors have been deployed, at least not in the United States [1].

Interest in fast-neutron (energetic neutron) reactors persists in the OECD countries for a new reason, political difficulties with storing or disposing of spent fuel. “Reprocessing” spent fuel does not eliminate the problem of siting a geological repository, but a reprocessing plant does provide an interim destination that has proved a path forward with regard to the spent fuel problem in a number of nations.

Spent fuel reprocessing was originally launched in countries that planned to deploy breeder reactors. They wanted separated plutonium for manufacturing startup fuel for their first breeder reactors. Standard light water reactor spent fuel contains about 1% plutonium. In the absence of breeder reactors, the separated plutonium has become a disposal problem, and some countries have decided to recycle it into fuel for the same reactors that produced it. Slow-neutron reactors are relatively ineffective, however, in fissioning some of the plutonium isotopes, which therefore build up in recycled fuel.

Fast-neutron reactor advocates argue that, if the plutonium and other long-lived transuramics in spent fuel could be fissioned almost entirely, the political problem of finding a geological disposal site for radioactive waste consisting of mostly shorter-lived fission products would become much easier. Fast-neutron reactors would be more effective in fissioning all the transuranic isotopes. Fast-neutron breeder reactors could be converted into transuranic “burner” reactors by removing the plutonium-breeding uranium blankets around their cores and flattening the cores into more of a “pancake” shape so that more neutrons would leak out of them.

Cochran et al. [1] look at the experience and status of breeder reactor programs in France, India, Japan, the Soviet Union/Russia, the United Kingdom, and the United States. The major breeder reactors built in these countries are listed in Table 14.1. Germany also built two breeder reactors. All were sodium cooled.

In the United States and around the world, countries that are capable of having technology of fission reactor power plant are looking for energy production by fast-breeding reactors, especially the main goal of the liquid-metal fast-breeder reactor (LMFBR) remains in order to ensure a sustainable long-term fissile fuel supply. In

Table 14.1 Major experimental, pilot, and demonstration fast-breeder reactors [2]

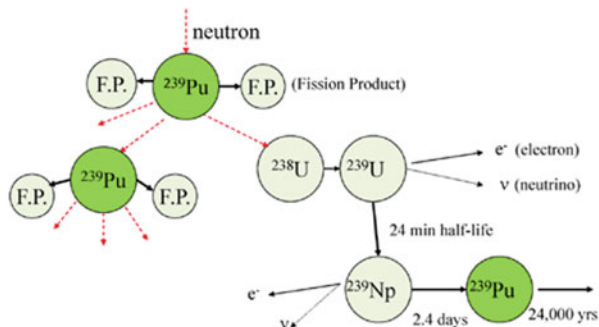
	MWe	MWt	Operation
<i>France</i>			
Rapsodie		40	1967–1983
Phénix	250		1973–2009
Superphénix	1240		1985–1998
<i>India</i>			
FBTR		40	1985–
PFBR	500		2010?
<i>Japan</i>			
Joyo		140	1977–
Monju	280		1994–1995, 2010?
<i>USSR/Russia</i>			
BR-5		5	1959–2004
B0R-60	12		1969–
BN-350 (Kazakhstan)	350		1972–1999
BN-600	600		1980–
BN-800	800		2014?
<i>United Kingdom</i>			
DFR	15		1959–1977
PFR	250		1974–1994
<i>United States</i>			
EBR-I	0.2		1951–1963
EBR-II	20		1963–1994
Fermi 1	66		1963–1972
SEFOR		20	1969–1972
Fast Flux Test Facility		400	1980–1993

addition, the use of LMFBRs allows the recycling of the minor actinide content of nuclear waste by burning them to produce energy and reduce the amounts of disposed waste. Another advantage of the LMFBR is its higher efficiency compared with water-cooled reactors, which makes it a good candidate among other commercial reactors for the purpose of thermal efficiency output driven by a combined cycle [3–12].

The basic operational concept, behind the fast-neutron breeder reactors, lies behind the nature of fissile isotopes which are the essential nuclear materials in both nuclear reactors and nuclear weapons. They undergo fission when they absorb neutrons and, on average, release more neutrons than they absorb. This makes a sustained chain reaction possible in a “supercritical mass.” This supercritical mass must contain a significant concentration of fissile isotopes and must be large enough so that only a small fraction of the neutrons escape without interacting.

The most important fissile materials are uranium-235 and plutonium-239. Uranium-235 is found in nature, constituting 0.7% of natural uranium. Plutonium-239 is created when uranium-238 (99.3% of natural uranium) absorbs a neutron as depicted in Fig. 14.1. Observation in Fig. 14.1 is showing that a plutonium-breeder reactor

Fig. 14.1 Plutonium-breeding process [1]



produces more plutonium than it consumes by using its extra fission neutrons to convert uranium-238 to uranium-239, which changes by radioactive decays involving electron and neutrino emission into neptunium-239 and then plutonium-239.

The sustainable, environmentally clean long-term use of nuclear power can be achieved with fast reactors, since thermal reactors are capable of burning less than 1% of the uranium fuel.

The plutonium-239 breeder reactor is commonly called a fast-breeder reactor, and the cooling and a liquid metal do heat transfer. The metals, which can accomplish this, are sodium and lithium, with sodium being the most abundant and most commonly used. The construction of the fast breeder requires a higher enrichment of U^{235} than a light water reactor, typically 15–30%. The reactor fuel is surrounded by a “blanket” of nonfissionable U^{238} . No moderator is used in the breeder reactor since fast neutrons are more efficient in transmuting U^{238} to Pu^{239} . At this concentration of U^{235} , the cross section for fission with fast neutrons is sufficient to sustain the chain reaction. Using water as coolant would slow down the neutrons, but the use of liquid sodium avoids that moderation and provides a very efficient heat-transfer medium. Figure 14.2 is typical schematic and layout of a liquid-metal fast-breeder reactor.

The Superphenix was the first large-scale breeder reactor. It was put into service in France in 1984. It ceased operation as a commercial power plant in 1997. Such a reactor can produce about 20% more fuel than it consumes by the breeding reaction. Enough excess fuel is produced over about 20 years to fuel another such reactor. Optimum breeding allows about 75% of the energy of the natural uranium to be used compared to 1% in the standard light water reactor. The commercialized LMFBR, namely, Superphenix, in France is depicted in Fig. 14.3.

The reactor core, the primary coolant pump, and the intermediate heat exchanger are contained in the main reactor tank in the pool design. The liquid sodium metal is contained in a simple double-walled tank as shown in Fig. 14.4, without penetrations below the sodium surface level and operating at atmospheric pressure. The loss of primary coolant becomes as unlikely as to be incredible.

The primary sodium has such a large thermal heat capacity that it can survive the loss of decay heat cooling after the reactor has been shut down for about 10 h. There

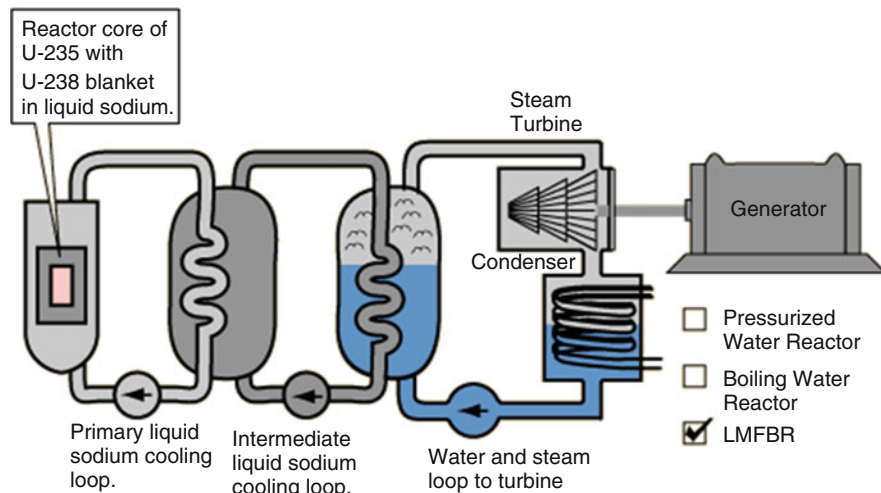


Fig. 14.2 A typical layout of liquid-metal fast-breeder reactor



Fig. 14.3 Superphenix fast reactor in France

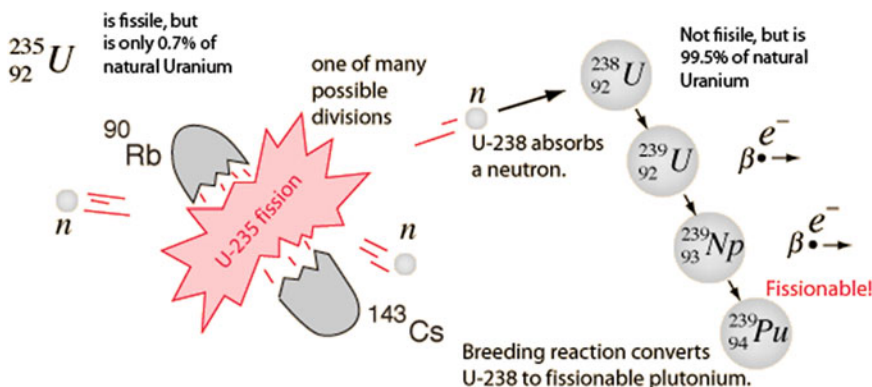
exist a substantial margin between normal operating temperatures and the coolant boiling temperature.

Under appropriate operating conditions, the neutrons given off by fission reactions can “breed” more fuel from otherwise nonfissionable isotopes. The most common *breeding reaction* is that of plutonium-239 from nonfissile uranium-238.

Fig. 14.4 This is a photo of a model of the containment vessel of the Superphenix. It is displayed at the National Museum of Nuclear Science and Technology in Albuquerque, NM

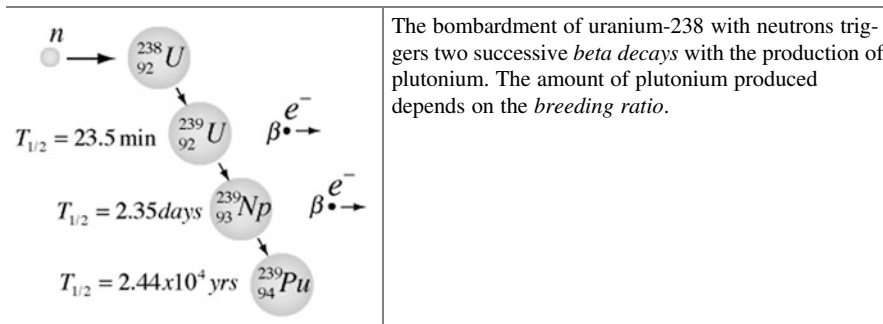


The term “fast breeder” refers to the types of configurations, which can actually produce more fissionable fuel than they use, such as the LMFBR. This scenario is possible because the nonfissile uranium-238 is 140 times more abundant than the fissile U^{235} and can be efficiently converted into Pu^{239} by the neutrons from a fission chain reaction.

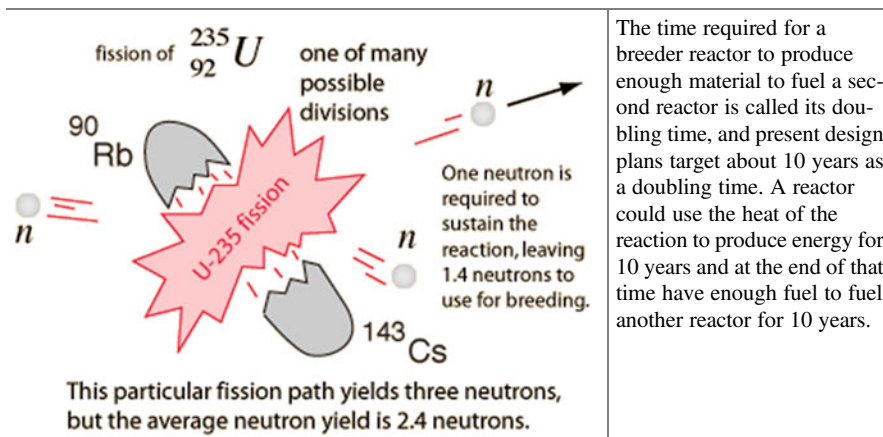


France has made the largest implementation of breeder reactors with its large Superphenix reactor (today is not in production line) and an intermediate Russian scale reactor (BN-600) on the Caspian Sea for electric power and desalination [13].

Breeding plutonium-239 can be accomplished from nonfissile uranium-238 by the reaction illustrated.



The concept of breeding ratio of plutonium-239 can be defined in following: in the breeding of plutonium fuel in breeder reactors, an important concept is the breeding ratio, the amount of fissile plutonium-239 produced compared to the amount of fissile fuel (like U^{235}) used to produce it. In the liquid-metal fast-breeder reactor (LMFBR), the target breeding ratio is 1.4, but the results achieved have been about 1.2. This is based on 2.4 neutrons produced per U^{235} fission, with 1 neutron used to sustain the reaction.



Liquid sodium is used as the coolant and heat-transfer medium in the LMFBR. That immediately raised the question of safety since sodium metal is an extremely reactive chemical and burns on contact with air or water (sometimes explosively on contact with water). It is true that the liquid sodium must be protected from contact with air or water at all times and kept in a sealed system. However, it has been found

that the safety issues are not significantly greater than those with high-pressure water and steam in the light water reactors.

Sodium is a solid at room temperature but liquefies at 98 °C. It has a wide working temperature since it does not boil until 892 °C. That brackets the range of operating temperatures for the reactor so that it does not need to be pressurized, as does a water-steam coolant system. It has a large *specific heat* so that it is an efficient heat-transfer fluid.

In practice, those reactors, which have used liquid-metal coolants, have been fast-neutron reactors. The liquid-metal coolant has a major advantage there because water as a coolant also moderates or slows down the neutrons. Such fast-neutron reactors require a higher degree of enrichment of the uranium fuel than do the water-moderated reactors.

14.2 The Concept of Stiffness

Scientists and engineers often are in need of solving mathematical models that are defined by means of partial differential equations (PDEs). The solution of such PDEs using the Concept of Stiffness Method are achieved by integrating the equations in the time domain, with special regard for the constraints prescribed by the fact that the time-dependent Ordinary Differential Equations (ODEs) in space and time. Aiken [14] in his published paper under the title of *Stiff Computation* shows cases that are studied in solving these PDEs through this concept via time-dependent ODEs. As part of his case studies in particular, we can mention:

1. When a partial differential equation (PDE) is discretized in the spatial domain by using a finite-difference, finite-element, or global-collection method, where the resulting equations in time are stiff and the degree of stiffness can more often be estimated.
2. When integration schemes that work well for large error tolerance are valuable.
3. Schemes and packages must be applicable to combined ODEs and algebraic equation, since these often occur in practice.
4. For large time-dependent problems in two and three spatial dimensions, extensive codes have already been developed using schemes that may not be the best for stiff problems.

Case studies can be applied to chemical reactors in the form of packed beds for kinetic behavior that traditionally are stiff, and the reactor of this type can become stiffer due to sharp changes in temperature. These type reactors provide a useful and require more testing ground for stiff integrators. The other studies are observed for flow within porous media, where the problem is extremely stiff and good numerical solutions are not easy to find given the conditions of the problem in hand. In this particular case, the spatial variation of the solution plays a role both in defining the stiffness and in limiting certain advantages of stiff integration codes. The other examples of stiffness concept are in the convective diffusion equations, where

these equations have similar difficulties to the equation for flow through porous media, but they are linear-type PDEs or ODEs. However, in two-dimensional time-dependent simulations, the most sophisticated techniques are in demand [14].

For a chemical reactor with packed bed model, the following partial differential equations including the appropriate boundary and initial conditions do apply:

$$\frac{\partial c}{\partial r} = \frac{\alpha}{r} \frac{\partial}{\partial r} \left(r \frac{\partial c}{\partial r} \right) + \beta r(c, T) \quad (14.1)$$

$$\frac{\partial T}{\partial t} = \frac{\alpha'}{r} \frac{\partial}{\partial r} \left(r \frac{\partial T}{\partial r} \right) + \beta' R(c, T) \quad (14.2)$$

$$\frac{\partial c}{\partial r} = \frac{\partial T}{\partial r} = 0 \quad \rightarrow \quad \text{at} \quad r = 0 \quad (14.3)$$

$$c = c_0 \quad T = T_0 \quad \rightarrow \quad \text{at} \quad t = 0 \quad (14.4)$$

$$\frac{\partial c}{\partial r} = 0 \quad - \frac{\partial T}{\partial r} = Bi_w(T - T_w) \quad \rightarrow \quad \text{at} \quad r = 1 \quad (14.5)$$

One method to solve these equations numerically is the utilization of a finite-difference method in order to illustrate the spatial variation of the solution and then use some other methods such as the Runge-Kutta method for the solution in time, given the Crank-Nicolson strategy [14].

Other method worth mentioning here, in order to solve these types of PDEs, is to illustrate the spatial variation of the solution with a polynomial defined over the entire domain, $0 \leq r \leq 1$, where the collocation is applied at the Gaussian quadrature points, given the orthogonal collocation method.

In case of neutronic analysis for nuclear reactor systems, one can use an original methodology based on the Padé and Chebyshev rational approximations for the solution of the nonlinear point kinetics equations with temperature reactivity feedback. In this type approach, one can make an assumption of piecewise constant approximations of the reactivity and source function, where the applied technique is enhancing the case by explicitly accounting for the feedback and the reactivity variations within a time step through an iterative cycle [15].

In approach like the above, Chebyshev rational method can be employed, and an important feature of such rational method is that good numerical approximations to the solutions of the stiff coupled kinetics differential equation can be obtained, using a single time step, as opposed to several time steps required for the conventional methods. As part of Chebyshev rational method, we can point out the following as:

- The stiffness of the kinetic systems is resolved by piecewise approximation.
- The Chebyshev rational approximations are one-step approach and not alpha stable.
- The results confirm the theoretical analysis and indicate the range of applicability.

- The Chebyshev exhibits a significant computational advantage by reducing the CPU time.
- The great advantage is that the method remains valid for full space-time kinetics.

Aboanber's [15] study indicates that the cases of approximations which combined with its $A(\alpha)$ -stability lead to a better reduction of the errors when intermediate and large times are reached after series of small time steps if the inserted reactivity is positive and sufficiently large. Numerical studies are presented for different benchmark problems of various reactivity insertions, time-varying reactivity, and temperature feedback reactivity. The results confirm the theoretical analysis and indicate the range of applicability of the methods presented. The computational results indicate that the method is efficient and accurate.

14.3 The Quasi-Static Method

The study of the dynamic behavior of the present generation, namely, generation three (GEN-III), and next-generation (GEN-IV) nuclear reactors is a fundamental aspect for safety and reliability assessments. Despite the growing performances of modern computers, the full solution of the neutron Boltzmann equation in the time domain is still an impracticable task; thus, several approximate dynamic models have been proposed for the simulation of nuclear reactor transients; the quasi-static method represents the standard tool currently adopted for the space-time solution of neutron transport problems. All the practical applications of this method that have been proposed contain a major limit, consisting in the use of isotropic quantities, such as scalar fluxes and isotropic external neutron sources, being the only data structures available in most deterministic transport codes. The loss of the angular information produces both inaccuracies in the solution of the kinetic model and the inconsistency of the quasi-static method itself [16].

The innovative features introduced by next-generation nuclear reactors require as much innovation in the analysis of their performances and safety aspects. The safety assessment of such reactors, in particular, requires the accurate simulation of the behavior of the reactor core during typical operational and accidental conditions, with the need for the solution of the neutron transport equation. Being the full time-inversion of the neutron Boltzmann equation an impracticable task, the study of the dynamics of a reactor has to rely on the definition of approximate mathematical models. Hence, several approaches have been proposed during the years; as a result of such efforts, the quasi-static method has become a reference procedure to address reactor dynamics, and several implementations of the method can be found in the literature, both in diffusion and in transport [13, 16–23].

Generally speaking, the quasi-static method is a standard tool for the space-time solution of neutron transport problems in multiplying media. Its basic principle lies in a factorization of the angular flux into the product of two functions, "amplitude" and "shape," where the amplitude depends only on time (and contains the major part

of the time dependence), while the shape function depends on all variables, time included. The shape equation is solved on a long time scale, while the amplitude is determined on a short time scale. The factorization is made unique by proper normalization conditions for the shape function. Most implementations replace the basic equation (transport or diffusion) by the set of coupled amplitude and shape equations derived from the factorization, the so-called improved quasi-static method (IQM). An alternate approach already known for some time is what we have called “predictor-corrector quasi-static method” (PCQM). We discuss its efficiency for both solid and liquid fuel system dynamics [24].

14.4 Bethe-Tait Models

It has been calculated that the core of a fast-breeder reactor could explode with an explosion intensity equivalent to that of up to 3000 tons of TNT. This greatly exceeds the explosive energy needed to destroy the containment and release the vaporized plutonium fuel and fission products into the atmosphere.

In an accident in which no significant explosion occurred, the molten fuel may collect at the bottom of the reactor vessel and melt through it. Sodium fires may become fierce enough to breach the containment, releasing radioactivity into the atmosphere, even way beyond safety level. The interaction of sodium with some materials produces hydrogen, which is also inflammable or can accumulate to a concentration, which is explosive. In most safety analyses that are done, for fast-breeder reactors (FBRs), even the basic information needed to make a rough judgment is not within public domain.

The amount of energy release (i.e., the size of the explosion) which would challenge the containment for most of these breeder reactors around the world is not publicly known.

Due to the nature of FBRs and the fuel that they use, there is a very real risk that an explosion at some breeder reactor is equivalent to a 3 kiloton nuclear weapon. In fact, in terms of radiation hazard, an FBR nuclear explosion would lead to greater contamination.

The amount of the radioactive fission products in the core of an FBR will eventually build up to possibly about 300 million curies. This is equivalent to the amount of radioactivity initially released by the explosion of a nuclear weapon with the explosive power equivalent to that of the explosion of about 3000 tons of TNT (3 Kt). The explosive power of the nuclear weapon, which destroyed Hiroshima, was about 12.5 Kt.

Although the radioactivity produced in a reactor is of the same origin as that produced by a nuclear weapon (i.e., nuclear fission), its composition is very different. The main difference is that in a nuclear weapon only the primary fission fragments are present at the moment of explosion. These are mostly short-lived radioisotopes, which subsequently decay into longer-lived ones. In a reactor, these

longer-lived radioisotopes are continuously produced by the decay of the shorter-lived ones. The longer-lived radioisotopes, therefore, steadily accumulate.

This means that in a nuclear reactor the proportion of longer-lived radioisotopes is much greater than in a nuclear weapon. The decay of the radioactivity from a reactor is, therefore, much slower than that from a nuclear weapon. Thus, after 1 week, the radioactivity of the fission products from a nuclear weapon will have decayed to only 0.5% of the initial amount, whereas the radioactivity from the fission products of a nuclear reactor will have decayed to one third of the initial amount.

It takes nearly 3 months before the radioactivity from the fission products of a nuclear reactor to decay to a tenth of the initial amount. Therefore, the radiation doses resulting from a release of fission products from a nuclear reactor would remain at unacceptably high levels for a great deal longer than those from a nuclear weapon, which initially produced the same amount of radioactivity.

The nuclear accident at the Chernobyl reactor released about 50 million curies of radioactivity, some 5% of the total in the core. If a very serious accident at any FBR was releasing about 17% of the maximum amount of radioactivity in the core, it would release about the same amount as did the Chernobyl accident. In addition, a large amount of plutonium could be released into the environment.

Dealing with situation like described in above from nuclear power accidental point of view, is called Core Disruptive Accidents (CDA) and that is the event resulting in significant damage to a reactor core. In an FBR, a CDA could be the melting of part of the reactor core, a meltdown of the core, or an energetic explosion.

CDAs are sometimes called hypothetical (or unthinkable) core-disruptive accidents. This is usually done by those not wishing to acknowledge that such accidents are credible and could happen.

An energetic CDA is sometimes called a Bethe-Tait event [25].

Beth and Tait [25] devised a method of providing a rough estimate of the energy released in an energetic CDA, founding an approach widely used to find an upper limit for the containment of an FBR (Bethe and Tait 1956) [25].

Events that can lead to a core-disruptive accident (CDA) in a fast-breeder reactor (FBR) are as follows:

1. A loss of flow of the sodium together with a failure to automatically insert the control or safety rods to shut down the fission chain reaction (i.e., a failure to scram)
2. The introduction of too much reactivity into the core of the reactor, which in this scenario will cause a rapid increase in power (called an overpower transient) together with a failure to scram

In short, a serious accident can occur with an FBR either from losing cooling capacity without reducing the power level or from increasing the power without increasing the cooling capacity (Cochran 1991) [3].

A scram has to be automated because a human being cannot generally react quickly enough to control a reactor in an emergency. For example, there is less than a

millisecond to control a reactor, which has gone prompt critical, whereas the reaction of a human is typically about 200 milliseconds.

The Fermi 1 reactor accident was an example of a loss of flow of sodium, caused by a blockage of the coolant, causing the fuel to melt. The melting point of the fuel is about 2800 degrees centigrade.

There may also be a major fracture in a pipe carrying coolant. A loss of power to the main pumps circulating the coolant and a failure of the diesel emergency generators to restart these pumps, or any stand-by pumps, in time, could lead to a CDA.

Because of the large mass of sodium in a pool-type FBR, it takes a few hours for the temperature to fall to the temperatures at which the cladding fails if the emergency cooling system does not work and no decay heat can be removed from the primary circuit. If there is a total loss of power to the pumps, the sodium will circulate naturally and cool the reactor core sufficiently to maintain its integrity. This will make few hours available to provide emergency cooling. An accident will, of course, be avoided only if the reactor is scrammed immediately after the power to the pumps is lost.

An earthquake could destroy the pumps and the control and safety rods and result to inevitable damage to the core of the reactor. An earthquake could also produce an overpower transient (a rapid increase in power due to the addition of reactivity), which could also be produced from the misuse or malfunction of the control and safety systems. As described earlier, unexplained positive reactivity fluctuations occurred in the Phenix FBR, which is still shutdown.

Note that Westinghouse Electric Corporation, which was known as the Clinch River Project around the 1980s, originally designed a prototype of Phenix reactor, a liquid-metal fast-breeder reactor (LMFBR). This author was involved with the analysis of fully inherent shutdown heat removal system for fast-breeder reactors [26] as well as designing the mercury heat pipe [27, 28] for cooling systems as part of the secondary loop.

A serious loss of flow of the sodium coolant or a fluctuation in positive reactivity could cause the fuel elements to melt. This may cause an explosion in the core of the reactor. Cochran describes how such an explosion could be produced after a loss of flow of the coolant.

The accident begins when power is lost to the pumps and the redundant safety and control systems fail to shut down (scram) the reactor. Sodium begins to boil near the center of the core of the reactor (the hottest part of the core). Bubbles are formed in the coolant when the sodium boils, reducing the moderating effect on the neutrons and causing the average energy of the neutrons to increase. The fission cross section for plutonium increases with increasing neutron energies. The rate of fission, therefore, increases. In other words, the loss of coolant leads to a positive reactivity coefficient in the reactor core and an increase in the power level.

The increase in power causes the sodium to boil more vigorously, which adds more reactivity, and so on. Webb [29] calls this process “autocatalytic reactivity” increases. The fact that an LMFBR is its own catalyst for generating power excursions is an inherent safety problem in the reactor (Webb 1976) [29].

In Cochran's accident scenario [3], almost immediately after the sodium begins to boil, the cladding on the fuel elements begins to melt. The molten cladding flows up the channels between the fuel assemblies (bundles of fuel rods). Immediately after the cladding melts, the fuel itself melts, and molten fuel flows up the channel. When the cladding and fuel flow into a part of the core, which is colder, they refreeze and clog up the flow of sodium in the fuel assemblies. Chunks of cladding and fuel fall to the bottom of the core, clogging it.

Fuel at the top of the reactor core could fall to the bottom of the core under gravity. If enough falls, re-criticality could occur. The extent of the accident would, of course, depend on how much mechanical energy was released. If enough energy is released (i.e., a powerful explosion occurs), the seal between the reactor head and the reactor vessel could be breached, and the total energy released may be more than the reactor containment can withstand (Cochran 1991) [3].

If, in an accident, molten cladding or molten fuel comes into contact with liquid sodium, a sodium vapor explosion might take place, damaging the rest of the core of the reactor. This is analogous to a steam explosion, like the first explosion in the Chernobyl reactor, which can take place when water is mixed suddenly with some molten metal, due to the rapid transfer of the heat from the metal to the water.

A CDA which does not cause an explosion, but in which the core melts and collects on the floor of the reactor vessel, is likely to result in a melt through of the reactor vessel. This could lead to a sodium fire, which could eventually breach the secondary containment.

In recent decade, a lot of research and calculations by scientists and engineers around Bethe-Tait method have taken place. One study that is done by Sha and Walter [25] that is around a two-dimensional ($r - z$) integral model for characterizing fast reactor excursions from accident inception through core disassembly was presented.

For predisassembly calculations, they have taken into account, an Eulerian geometric model is used and multichannel heat-transfer computations were, performed. Reactivity feedback due to Doppler broadening, coolant density change and voiding, and fuel movement were, taken into account. A Lagrangian coordinate system was used in the disassembly phase, wherein the neutronic balance consists of Doppler broadening and material motion. A unique feature of the model is the ability to accommodate a point-wise energy density-dependent equation of state according to the local sodium inventory that actually exists at the time of disassembly. By providing a consistent basis for establishing the effective reactivity ramp rate, Doppler coefficient, appropriate equation of state, and temperature distribution at the start of core disassembly, much of the arbitrariness normally associated with large accident analyses can be removed. For most accident analyses, this model predicts a significantly lower energy yield during a super-prompt critical nuclear excursion than would be computed by using the conventional modified Bethe-Tait analysis [30].

The original Bethe-Tait analysis [1] was intended only as an order of magnitude estimate of potential energy release from a worst-case disassembly accident. For the purpose of these analyses, many approximations were made by Bethe-Tait for their

model to allow them a back-of-the-envelope calculation solution. Their principle assumptions included the following topics:

1. Taking the advantage of the point kinetics formulation analyses.
2. Use of perturbation theory.
3. Eliminating consideration for delayed neutrons.
4. No Doppler feedback.
5. Assumption for a threshold equation of state.
6. Considering spherical shape for reactor core geometry.
7. Reactor was assumed to be completely homogeneous core.
8. Constant fuel density.

The third assumption above was very well justified for the Bethe-Tait model [25] by core dynamic response analyses, only during the prompt critical condition, and Doppler feedback was ignored, because of the core designs in the United States. Their assumption was also based on these early reactor cores that were metal fueled; hence, little Doppler effects and spherical geometry were chosen for the simplicity of finding an analytical solution without any access to a large-scale computing platform, as it is available to us today.

In the Bethe-Tait model [25], reactivity could be added at a constant ramp rate until a threshold energy density is reached, and beyond this time, internal pressures quickly rise and disassembly occurs. In this case, the neutronic transient terminates when the magnitude of the negative disassembly reactivity equals the input reactivity in excess of prompt critical.

References

1. T.B. Cochran, H.A. Feiveson, W. Patterson, G. Pshakin, M.V. Raman, M. Schneider, T. Suzuki, F. von Hippel, *Fast Breeder Reactor Programs: History and Status*. Research Report 8, International Panel on Fissile Materials, February 2010. Released by www.fissilematerials.org
2. H. Kouts, The development of breeder reactors in the United States. *Annu. Rev. Energy* **8**, 383 (1983)
3. T.B. Cochran, The plutonium burner, in *Proceeding of the International Conference on Plutonium*, Omiya, Japan, November 2–4, 1991, pp. 119–151
4. B. Zohuri, *Combined Cycle Driven Efficiency for Next Generation Nuclear Power Plants: An Innovative Design Approach* (Springer, New York, 2015)
5. B. Zohuri, *Application of Compact Heat Exchangers for Combined Cycle Driven Efficiency in Next Generation Nuclear Power Plants: A Novel Approach* (Springer, Cham, 2015)
6. B. Zohuri, P.J. McDaniel, C.R. De Olivera, Advanced nuclear open air-Brayton cycles for highly efficient power conversion. *Nucl. Technol.* **192**(1), 48–60 (2015)
7. C. Forsberg, P.J. McDaniel, B. Zohuri, Variable electricity and steam from salt, helium, and sodium cooled base-load reactors with gas turbines and heat storage, in *Proceedings of ICAPP 2015*, May 03–06, 2015 – Nice (France) Paper 15115

8. B. Zohuri, P. McDaniel, Cassiano R. R. De Oliveira, A comparison of a recuperated open cycle (air) Brayton power conversion system with the traditional steam Rankine cycle for the next generation nuclear power plant. *Nucl. Technol.* **192**(1), 48–60 (2015) <https://doi.org/10.13182/NT14-42>
9. B. Zohuri, *Innovative Open Air Brayton Combined Cycle Systems for the next Generation Nuclear Power Plants* (University of New Mexico Publications, Albuquerque, 2014)
10. P.J. McDaniel, B. Zohuri, C.R.E. de Oliveira, A combined cycle power conversion system for small modular LMFBRs, in *ANS Transactions*, September 2014
11. B. Zohuri, P. McDaniel, C.R.E. de Oliveira, A comparison of a recuperated open cycle (air) Brayton power conversion system with the traditional steam Rankine cycle for the next generation nuclear power plant. *Trans. Am. Nucl. Soc.* **110**, 391 (2014)
12. P.J. McDaniel, C.R.E. de Oliveira, B. Zohuri, J. Cole, A combined cycle power conversion system for the next generation nuclear power plant. *Trans. Am. Nucl. Soc.* **107**, 858 (2012)
13. F. Alcaro, S. Dulla, G. Marleau, E.H. Mund, P. Ravetto, Development of dynamic models for neutron transport calculations. II *Nuovo Cimento C* **33**, 13–20 (2010)
14. R.C. Aiken, *Stiff Computation* (Oxford University Press, New York, Oxford, 1985)
15. A. Aboanber, Tanta University stiffness treatment of differential equations for the point reactor dynamic systems. *Prog. Nucl. Energy* **71**, 248–257 (2014)
16. F. Alcaro, S. Dulla, P. Ravetto, R. Le Tellier, C. Suteau, Implementation of the quasi-static method for neutron transport, in *International Conference on Mathematics and Computational Methods Applied to Nuclear Science and Engineering (M&C 2011)* Rio de Janeiro, RJ, Brazil, May 8–12, 2011, on CD-ROM, Latin American Section (LAS)/American Nuclear Society (ANS) ISBN 978-85-63688-00-2
17. K.O. Ott, D.A. Meneley, Accuracy of the quasistatic treatment of spatial reactor kinetics. *Nucl. Sci. Eng.* **36**, 402–411 (1969)
18. J. Devogaught, Quasistatic solutions of reactor kinetics. *Ann. Nucl. Energy* **7**, 47–58 (1980)
19. J. Devogaught, E.H. Mund, Generalized quasistatic method for space-time kinetics. *Nucl. Sci. Eng.* **76**, 10–17 (1980)
20. S. Dulla, E.H. Mund, P. Ravetto, The quasi-static method revisited. *Prog. Nucl. Energy* **50**, 908–920 (2008)
21. P. Picca, S. Dulla, E.H. Mund, P. Ravetto, G. Marleau, Quasi-static time-dependent computational tool using the DRAGON transport code, in *PHYSOR2008*, Interlaken, September 14–19, 2008
22. S. Goluoglu, H.L. Dodds, A time-dependent, three-dimensional neutron transport methodology. *Nucl. Sci. Eng.* **139**, 248–261 (2001)
23. S. Yun, J.W. Kim, N.Z. Cho, Monte Carlo space-time reactor kinetics method and its verification with time-dependent SN method, in *PHYSOR 2008*, Interlaken, September 14–19, 2008
24. S. Dulla, E.H. Mund, The quasi-static method revisited. *Prog. Nucl. Energy* **50**(8), 908–920 (2008)
25. H.A. Bethe, J.H. Tait, An estimate of the order of magnitude of the explosion when the core of a fast reactor collapses. UKAEA-RHM, 1956
26. B. Zohuri, Applied Technology Publication on inherent shutdown heat removal system for fast breeder reactors for Division of Reactor Research and Technology, U.S. Department of Energy
27. B. Zohuri, *Heat Pipe Design and Technology: Modern Applications for Practical Thermal Management*, 2nd edn. (Springer, Switzerland, 2016)
28. B. Zohuri, *Heat Pipe Design and Technology: A Practical Approach* (CRC and Francis Taylor Publishing Company, CRC Press, Boca Raton, FL, 2012)
29. R. Webb, Catastrophic nuclear accident hazards – a warning for Europe, Hinkley Point C Inquiry document S1982, p. 83
30. W.T. Sha, A.E. Walter, An integrated model for analyzing disruptive accident in fast reactors. *Nucl. Sci. Eng.* **44**(2), 135–156 (1971)

Chapter 15

Fission Product Buildup and Decay

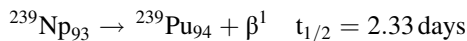
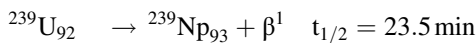
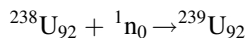
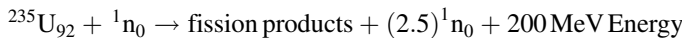


Nuclear fission products are the atomic fragments left after a large atomic nucleus undergoes nuclear fission. Typically, a nucleus that has a large atomic mass like uranium could fission by splitting into two smaller nuclei, along with a few neutrons. This process results in release of heat energy such as kinetic energy of the nuclei and gamma rays. The fission products themselves are often unstable and radioactive, due to being relatively neutron-rich for their high atomic number, and many of them quickly undergo beta decay. This releases additional energy in the form of beta particles, antineutrinos, and gamma rays. Thus, fission events normally result in beta radiation and antineutrinos, even though these particles are not produced directly by the fission event itself.

15.1 Background Introduction

Early in World War II, the scientific community in the United States, including those Europeans now calling the United States their safe home, pursued the idea that uranium fission and the production of excess neutrons could be the source of extraordinary new weapons. They knew Lisa Meitner's interpretation, in Sweden, of Hahn's experiments would likely be known in Germany. Clearly, there might now be a race commencing for the development and production of a new, super weapon based on the fission of $^{235}\text{U}_{92}$ or $^{239}\text{Pu}_{94}$.

By early 1942, it was known that the two naturally occurring isotopes of uranium reacted with neutrons as follows:



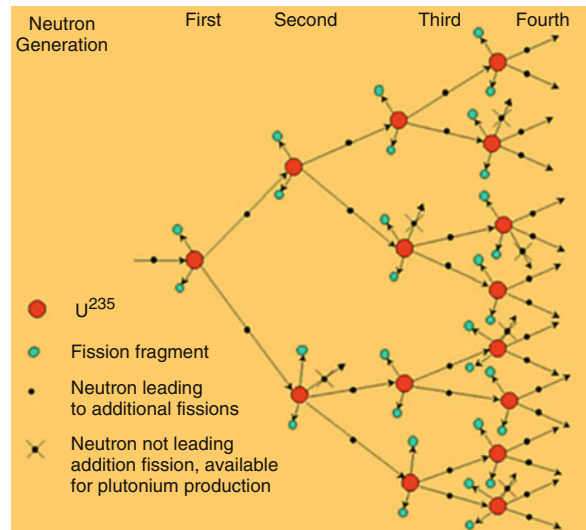
Each U^{235} that undergoes fission produces an average of 2.5 neutrons. In contrast, some U^{238} nuclei capture neutrons become U^{239} and subsequently emit two beta particles to produce Pu-239. The plutonium is a fissile element also, and it would produce energy by the same mechanism as the uranium. A flow sheet for uranium fission is shown in Fig. 15.1 below [1].

The answers to two questions were critical to the production of plutonium for atomic bombs:

1. Is it possible, using natural uranium (99.3% U^{238} and 0.7% U^{235}), to achieve a controlled chain reaction on a large scale? If so, some of the excess neutrons produced by the fission of U^{235} would be absorbed by U^{238} and produce fissionable Pu-239.
2. How can we separate in a reasonable time period the relatively small quantities of Pu-239 from the unreacted uranium and the highly radioactive fission-product elements?

Although fission had been observed on a small scale in many laboratories, no one had carried out a controlled chain reaction that would provide continuous production of plutonium for isolation.

Fig. 15.1 The first generations of a nuclear chain reaction [1]



The fission products themselves are often unstable and radioactive, due to being relatively neutron-rich for their high atomic number, and many of them quickly undergo beta decay. This releases additional energy in the form of beta particles, antineutrinos, and gamma rays. Thus, fission events normally result in beta radiation and antineutrinos, even though these particles are not produced directly by the fission event itself.

Many of these nuclides have a very short half-life and therefore are very radioactive. For instance, strontium-90, strontium-89, and strontium-94 are all fission products; they are produced in similar quantities, and each nucleus decays by shooting off one beta particle (electron) [1].

Enrico Fermi thought that he could achieve a controlled chain reaction using natural uranium. He had started this work with Leo Szilard at Columbia University but moved to the University of Chicago in early 1942.

The first nuclear reactor, called a pile, was a daring and sophisticated experiment that required nearly 50 tons of machined and shaped uranium and uranium oxide pellets along with 385 tons – the equivalent of four railroad coal hoppers – of graphite blocks machined on site. See Fig. 15.2.

The pile itself was assembled in a squash court under the football field at the University of Chicago from the layered graphite blocks, uranium, and uranium oxide lumps (Fermi's term) arranged roughly in a sphere with an anticipated 13-foot radius. Neutron-absorbing, cadmium-coated control rods were inserted in the pile. By slowly withdrawing the rods, neutron activity within the pile was expected to increase, and at some point, Fermi predicted there would be one neutron produced for each neutron absorbed in either producing fission or by the control rods [1].

On December 2, 1942, with 57 of the anticipated 75 layers in place, Fermi began the first controlled nuclear chain reaction occurred. At around 3:20 p.m. the reactor went critical; that is, it produced one neutron for every neutron absorbed by the uranium nuclei. Fermi allowed the reaction to continue for the next 27 min before inserting the neutron-absorbing control rods. The energy-releasing nuclear chain reaction stopped as Fermi predicted it would. See Fig. 15.3.

Fig. 15.2 CP-1 – Graphite blocks with 3 in. diameter uranium cylinders inserted – part of a layer of CP-1, the first nuclear reactor. A layer of graphite blocks without inserted uranium is seen covering the active layer [1]

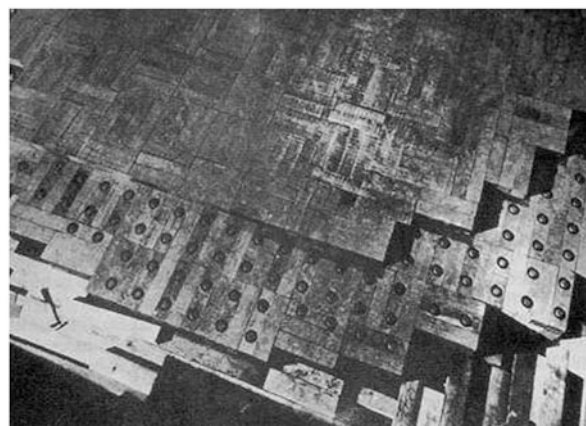
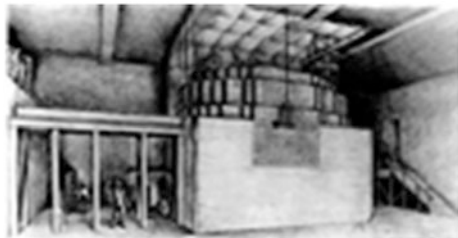


Fig. 15.3 The first controlled chain reaction, Stagg Field, Chicago, Dec. 2, 1942. (Courtesy of the Argonne National Laboratory)



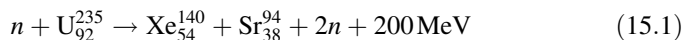
In addition to excess neutrons and energy, the pile also produced a small amount of Pu-239, the other known fissionable material.

The achievement of the first sustained nuclear reaction was the beginning of a new age in nuclear physics and the study of the atom. Humankind could now use the tremendous potential energy contained in the nucleus of the atom. However, while a controlled chain reaction was achieved with natural uranium and could produce plutonium, it would be necessary to separate U^{235} from U^{238} to build a uranium bomb [1].

15.2 Nuclear Fission and the Fission Process

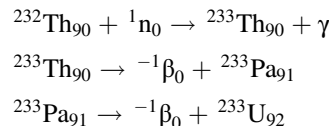
As we have learned so far, the fission occurs with certain nuclei of high atomic or mass number and the large value of Z^2 , and hence the repulsive force within the nucleus is an important contributory factor. When fission takes place, the excited compound nucleus formed after absorption of a neutron breaks up into two lighter nuclei, and this is called *fission fragments*.

During this process, if the neutron is one of low kinetic energy, which is known as *slow neutron*, then generally speaking, the two fragment nuclei have unequal masses. This states that symmetrical fission by slow neutrons is rare and in the majority of slow neutron fissions, the mass ratio of the fragments is approximately 2–3. Anyhow, in most fission process cases, one fission fragment has a substantially heavier mass than the other one. For example, a typical fission reaction is:



Note that we have mixed out our chemical notations for fission process, so our reader get use to all kind of them presented in different books and literatures as well. Bear in your mind that fission fragments are unstable because they have neutron to proton ratios that are too large and only three nuclides that are having sufficient stability to permit storage for a long time. They are, namely, uranium-233, uranium-235, and plutonium-239, fissionable by neutrons of all energies, from thermal values

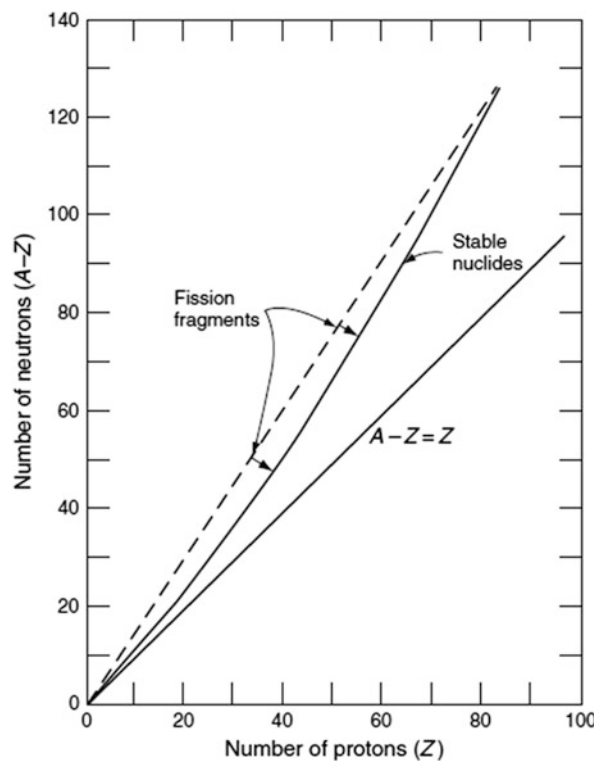
or less to millions of electron volts. U^{235} is the only one, which occurs in nature, and the other two are produced artificially from U^{238} and thorium-232, respectively, and this can be seen as below steps.



where ${}^{233}\text{Pa}$ is the symbol for protactinium-233.

Figure 15.4, which is depicting, plot of neutrons versus protons, and it is indicating an upward curvature in the line of stable nuclei. This also is indicating that the ratio of neutrons to protons increases above 1:1 as the atomic number becomes larger (e.g., the prominent isotopes of carbon and oxygen are ${}^{12}\text{C}_6$ and ${}^{16}\text{O}_8$, but for lead and thorium, they are ${}^{207}\text{Pb}_{82}$ and ${}^{232}\text{Th}_{90}$). Dashed line in Fig. 15.4 is the indication of the ratio of neutron to protons staying the same for nucleus fissions, where it is not for the 2–3 neutrons that are giving off promptly at the time of fission.

Fig. 15.4 Fission fragment instability. (Adopted from Glasstone and Sesonske [2])

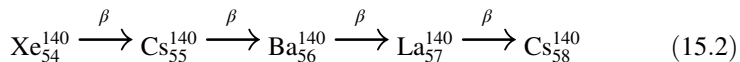


Even though the fission fragments lie above the curve of stable nuclei, less than 1% of these fragments go through decay process by virtue of the delayed emission of neutrons. This is due to the predomination of decay mode by the beta emission, accompanied by one or more gamma rays.

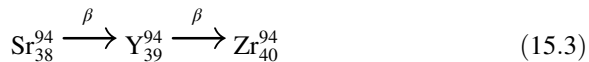
This decay process moves the resulting nuclide toward the line of stable nuclei as the arrows indicating in Fig. 15.4.

However, more than one, decay is normally required to get into the range of stable nuclei.

Given the fission fragments process in Eq. 15.1, we can have the following chemical process as:



and



Each of these decays in Eqs. 15.2 and 15.3 is showing characteristics of half-life, and notably some exceptions are that the half-lives earlier in the decay chain tend to be shorter than those taking place later on in chain reaction process. The fission fragments taken together with their decay products are classified as fission products.

The detailed study of the slow neutrons fission product of uranium-235 reveals that the compound nucleus splits up in more than 40 different ways, yielding over 80 primary fission products or fission fragments. However, the ranges of mass numbers of the fission products are within anywhere, from 72 for possible zinc isotope with (atomic number of 30) to 160 which maybe an isotope of terbium with (atomic number 65) [2].

Figure 15.4 is indicating that the mass numbers of the products of thermal fission of uranium-235 and of the fast-neutron fission of uranium-238 plot against the corresponding *fission yields*. Note that the fission yield can be defined as the proportion or percentage of the total nuclear fissions that form products of a given mass number.

As we can observe, the Fig. 15.5 is plotted in semilogarithmic scale, and this is because fission yields range from 10^{-5} to over 6%. It should be noted that, as two nuclei result from each fission process, the total yield for all mass numbers adds up to 200%.

It should also be noted that the reason why mass numbers are considered over the atomic numbers is that most fission fragments are radioactive, decaying by the loss of a negative beta particles as it was shown in above. Due to this fact, the atomic numbers, consequently, change with time, but the mass numbers are unaffected by such beta decay. We will elaborate on this matter in next section here.

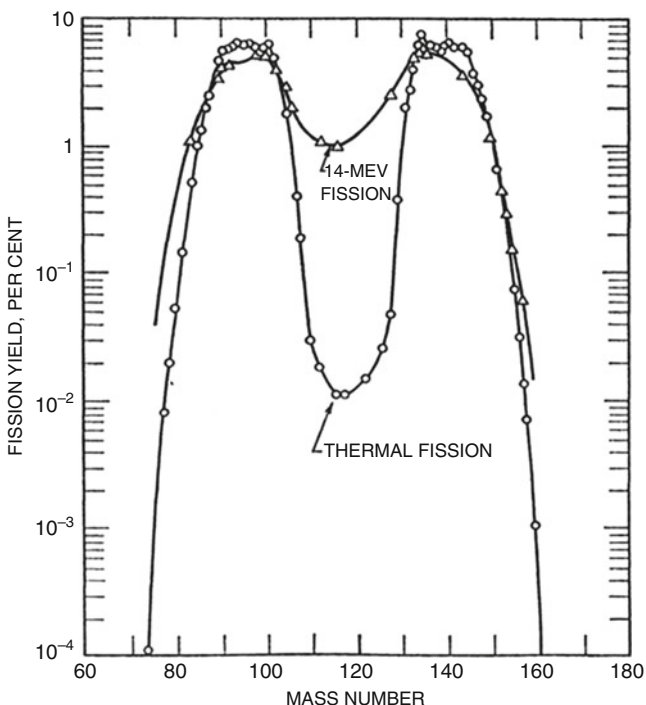


Fig. 15.5 Fission product yield as function of mass number for U^{235} . (Adopted from Glasstone and Sesonske [2])

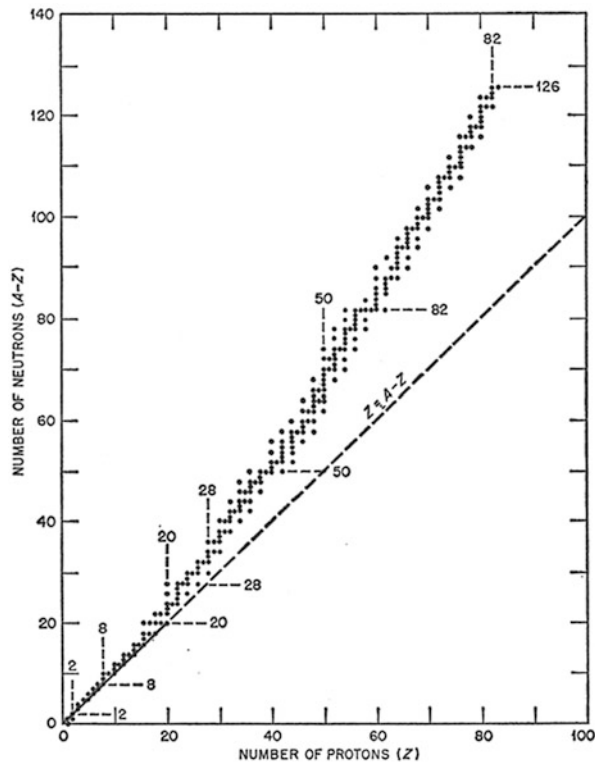
15.3 Radioactivity and Decay of Fission Product

As we mentioned in previous section, nearly all, if not all, fission fragments are negative beta emitter, simply because they have neutron/proton ratios that are above the stability range. Figure 15.4 shows the relationship between the fission fragments and the stability curve for nuclei (see Fig. 15.6 as well). Note that, in Fig. 15.6, the short dashed lines indicate magic number of neutrons and protons, and this number is defined because certain nuclei exhibit exponential stability.

The immediate decay products are also usually radioactive, and, although some decay chains are longer, while some are shorter, each fragment on the average is following three stages of decay prior to any stable species found. Since there are some 80 different radioisotopes produced in fission and each is, on the average, the precursor of two others, there are over 200 radioactive species present among the fission products after a short time [2].

In addition to beta particles, a large proportion of the radioactive fission products emit gamma rays, and these are representing what is so-called delayed fission gamma radiation. Most of the photons are of moderate energy, less than about 2 MeV, but a few of the fission products expel photons of higher energy. The latter

Fig. 15.6 Numbers of neutron and protons in stable nuclei. (Adopted from Glasstone and Sesonske [2])



are of interest for some shielding problems and for reactor control. The total of energy of the delayed gamma radiation amounts to approximately 7 MeV per fission [2].

Also it should be noted that roughly 8% of the 200 MeV of energy produced from fission process is attributable to the beta decay of fission products the gamma rays associated with it. Therefore, even following shutdown of a chain reaction, radioactive decay will continue to produce significant amounts of heat. Figure 15.7 shows the decay heat for a reactor that has operated at a power P for a long time.

The heat is approximated by the Wigner-Way formula as follows:

$$P_d(t) = 0.0622P_0 \left[t^{-0.2} - (t_0 + t)^{-0.2} \right] \quad (15.4)$$

where

$P_d(t)$ = Power generation due to beta and gamma rays

P_0 = Power before shutdown

t = Time, in seconds, of power operation before shutdown

t_0 = Time, in seconds, elapsed since shutdown.

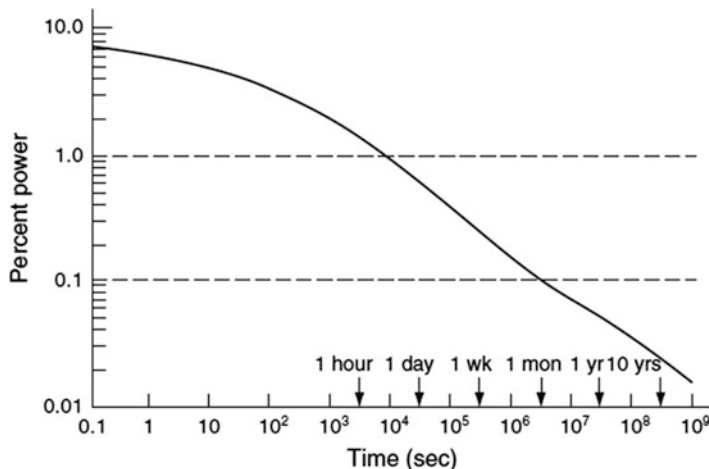


Fig. 15.7 Heat produced by decay of fission products [3]

Because of decay heat, cooling must be provided to prevent overheating of reactor fuel for a substantial period of time following power plant shutdown [3].

The law that is governing the decay of a nucleus will allow us to better understand number of other phenomena associated with reactor physics. This law states that the rate of decay is proportional to the number of nuclei present. Physics of decay for each radioisotope, that is, an isotope that undergoes radioactive decay, allows us to write the following mathematical notation for a simple ordinary differential equation.

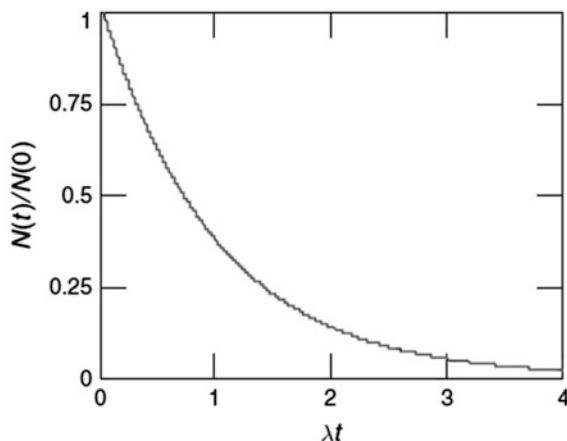
$$\frac{d}{dt}N(t) = -\lambda N(t) \quad (15.5)$$

This differential equation indicates that decay has a characteristic decay constant λ . Thus, if the number of nuclei present at time t is $N(t)$, and the rate at which they decay is governed by Eq. 15.5 that is behavior of radioactive decay.

Solution of this differential equation (i.e., Eq. 15.5) is a simple one and is derived as below:

$$\left\{ \begin{array}{l} \frac{dN(t)}{N(t)} = -\lambda dt \\ \int_{N(0)}^{N(t)} \frac{dN(t)}{N(t)} = -\lambda \int_0^t dt \\ \ln [N(t)/N(0)] = -\lambda t \\ N(t) = N(0)\exp(-\lambda t) \end{array} \right. \quad (15.6a)$$

Fig. 15.8 Exponential decay of a radionuclide [3]



Therefore, Eq. 15.6a, which indicates the final solution of Eq. 15.5, is a characteristic exponential rate of decay, which is written as:

$$N(t) = N(0)\exp(-\lambda t) \quad (15.6b)$$

where $N(0)$ is the initial number of nuclei and graphical presentation of Eq. 15.6b is depicted in Fig. 15.8, which is nothing more than illustration of an exponential decay of radioactive materials.

The half-life, $t_{1/2}$, is a more intuitive measure of the times over which unstable nuclei decay. As defined earlier in Chap. 1, $t_{1/2}$ is the length of time required for one half of the nuclei to decay. Thus it may be obtained by substituting $N(t_{1/2}) = N(0)/2$ into Eq. 15.6b to yield $\ln(1/2) = -0.693 = -\lambda t_{1/2}$ or simply

$$t_{1/2} = 0.693/\lambda \quad (15.7)$$

A second, less-used measure of decay time is the mean time to decay, defined by

$$\bar{t} = \int_0^{\infty} tN(t)dt / \int_0^{\infty} N(t)dt = 1/\lambda \quad (15.8)$$

To calculate the number of nuclei present, we first note that Avogadro's number, $N(0) = 6.023 \times 10^{24}$, is the number of atoms in one gram molecular weight, and thus the total number of atoms is just mN_0/A where m is the mass in grams and A is the atomic mass of the isotope. The concentration in atoms/cm³ is then $\rho N_0/A$, where ρ is the density in grams/cm³.

For us to be able to describe the behavior of fission products and their rates of conversion of fertile to fissile materials and number of other phenomena in reactor physics, the basic understanding of above information is in order.

15.4 Poisons Produced by Fission

So far, we have learned that two fission fragments are produced virtually in every fission. Some of these nuclei and their progeny have substantial absorption cross sections, and their appearance in a nuclear reactor tends to reduce the multiplication factor k . For this given reason, these nuclei are known as *fission-produced poisons*. These play an important role in thermal reactors, because the absorption cross sections decrease rapidly with increasing neutron energy. Control poisons are neutron absorbers that are deliberately included in a reactor core. They may take the form of control rods, of soluble poisons dissolved in liquid coolants, or of so-called burnable poisons permanently embedded in the fuel or other core constituents. Poisons serve a number of purposes [3].

Control rods are inserted or withdrawn in order to control the value of criticality factor k as it is needed for start-up, shutdown, and changes in power level. They may also be used to keep the reactor critical at a constant power by compensating for fuel depletion, fission product buildup, temperature changes, or other phenomena that affect the multiplication. Control poisons affect both the multiplication and the flux distribution of a core; thus, we must consider both. Now for the purpose of this study, if we focus our attention to reactor of infinite homogeneous type, then we can analyze a good approximation, the only effect of fission product poisons. The impact of this affection on multiplication factor k is on the thermal utilization factor f ; therefore, the reactivity equivalent ρ of poisons in a previously critical reactor can be written as:

$$\rho = \frac{k'_\infty - k_\infty}{k'_\infty} = \frac{f' - f}{f'} \quad (15.9)$$

where the primed parameters, k'_∞ and f' , are referring to the poisoned reactor, and in the absence of poison, thermal utilization factor f can be written as:

$$f = \frac{\sum_{aF}}{\sum_{aF} + \sum_{aM}} \quad (15.10)$$

where \sum_{aF} and \sum_{aM} are the macroscopic thermal absorption cross sections of the fuel and everything else, except the fuel, respectively. With presence of poisons in reactor thermal utilization factor $f \rightarrow f'$ and Eq. 15.10 becomes:

$$f' = \frac{\sum_{aF}}{\sum_{aF} + \sum_{aM} + \sum_{aP}} \quad (15.11)$$

where \sum_{aP} is the macroscopic cross section of the poison in the reactor. From Eq. 15.9, the reactivity ρ due to the poison then becomes:

$$\rho \frac{f' - f}{f'} = \frac{\sum_{aP}}{\sum_{aF} + \sum_{aM}} \quad (15.12)$$

Equation 15.13 can be converted to more convenient form by writing the multiplication factor of the unpoisoned reactor as:

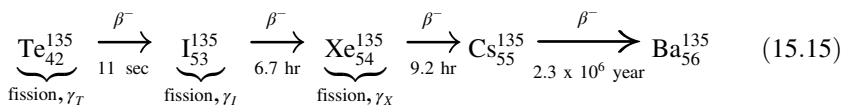
$$\begin{aligned} k_\infty &= 1 = \eta T f p \epsilon \\ &= (\eta T p \epsilon) \left[\frac{\sum_{aF}}{\sum_{aF} + \sum_{aP}} \right] \\ &= \frac{\eta T p \epsilon \sum_{aF}}{(\sum_{aF} + \sum_{aP})} = \frac{p \epsilon v \sum_f}{(\sum_{aF} + \sum_{aP})} \end{aligned} \quad (15.13)$$

where \sum_f is the macroscopic fission cross section. Solving Eq. 15.13 for $(\sum_{aF} + \sum_{aP})$ and inserting this into Eq. 15.12, we get the following relationship:

$$\rho = - \frac{\sum_{aP} / \sum_f}{p \epsilon v} \quad (15.14)$$

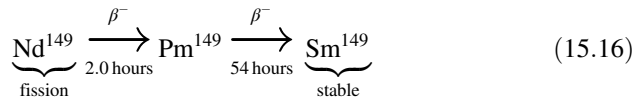
Equation 15.14 is most suitable form of reactivity ρ for calculation of fission-product poisoning.

However, in large reactor operating at a high thermal-neutron flux and at constant power, the phenomenon called *Xenon Instability* can take place, which is the most important fission product poison and is designated by chemical symbol of Xe^{135} . Its thermal (2200 m/s) absorption cross section is 2.7×10^6 barns. This isotope is formed as the result of the decay of I^{135} and is produced directly in the fission of U^{235} as well. The I^{135} is not formed in fission but appears as the result of the decay of tellurium-135 or Te^{135} . These process and their half-lives are summarized below:



In view of the fact that Te^{135} decays so rapidly to I^{135} , it is possible to assume that the I^{135} is produced directly in fission [4].

Next to Xe^{135} (xenon-135), the most important fission product poison, as it can be seen in below chemical chain reaction, is Sm^{149} (samarium-149). This is a stable isotope with a capture cross section of 5×104 barns for thermal neutrons. Sm^{149} is not formed directly in fission product but appears as the result of the decay of Nd^{149} (neodymium-149), and it is the end product of the decay chain reaction as follows:



Since the Nd^{149} decays comparatively rapidly to Pm^{149} (promethium-149), the Pm^{149} may be assumed to be produced directly in fission with yield Pm^{149} .

Although xenon makes the major contribution to fission-product poisoning of a nuclear reactor operating at a flux of 10^{13} neutrons/(cm³)(s) or more, there are many other nuclides which accumulate during reactor operation and cause a decrease in the reactivity ρ . The method for determining the poisoning of each nuclide is the same, but it's beyond the scope of this book; therefore we recommend that our reader for further information should refer to list of references at the end of this chapter.

Problems

Problem 15.1 A thermal reactor using uranium-235 as fissile materials has been operating for some time (about 6.7 h) at an average flux $\phi = 2 \times 10^{14}$ neutron/(cm²)(s): How long after shutdown will the xenon poisoning reach a maximum, and what is the poisoning at this time?

Assume that the time to attain the maximum concentration of xenon (Xe) after shutdown is t_{\max} , and it is given by:

$$t_{\max} = \frac{1}{\lambda_X - \lambda_I} \ln \frac{\lambda_X}{\lambda_I} \left(1 - \frac{\lambda_X - \lambda_I}{\lambda_I} \cdot \frac{X_0}{I_0} \right) \quad (a)$$

where

λ_I = Decay constant of iodine-135

λ_X = Decay constant of xenon-135

X_0 = Xenon concentration at equilibrium

I_0 = Iodine concentration at equilibrium

In addition, the *poisoning* $\psi(t)$ in general of a reactor is defined as the ratio of the number of thermal neutrons absorbed by the poison to those absorbed in fuel, hence we can write:

$$\psi(t_s) = \frac{X(t_s)\sigma_X}{\sum_u} \quad (b)$$

where

$X(t_s)$ = Xenon concentration at time t_s after shutdown

σ_X = Absorption cross section of xenon-135

\sum_u = Fuel macroscopic absorption cross section

Additionally, the equilibrium concentration, I_0 , attained after reactor has been operating for some time, is obtained by:

$$I_0 = \frac{\gamma_I \Sigma_f \phi}{\lambda_I + \sigma_I \phi} \approx \frac{\gamma_I \Sigma_f \phi}{\lambda_I} \quad (c)$$

where

Σ_f = Macroscopic fission cross section

γ_I = Fission yield for iodine-135

ϕ = Neutron flux

σ = Absorption cross section of iodine-135

And, similarly, the equilibrium concentration, X_0 , of xenon is obtained from the following equation as well:

$$X_0 = \frac{\lambda_I I_0 + \gamma_X \Sigma_f \phi}{\lambda_X^*} = \frac{\lambda_I \left(\frac{\gamma_I \Sigma_f \phi}{\lambda_I} \right) + \gamma_X \Sigma_f \phi}{\lambda_X^*} = \frac{(\gamma_I + \gamma_X) \Sigma_f \phi}{\lambda_X^*} \quad (d)$$

where $\lambda_X^* = \lambda_X + \sigma_X \phi$; because the absorption cross section of xenon-135 is so high, λ_X^* is appreciably greater than λ_X and γ_X is fission yield for xenon-135.

We can also write the xenon-135 concentration $X(t_s)$ at time t_s after shutdown as:

$$X(t_s) = \frac{\lambda_I}{\lambda_X - \lambda_I} I_0 (e^{-\lambda_I t_s} - e^{-\lambda_X t_s}) X_0 e^{-\lambda_X t_s} \quad (e)$$

Problem 15.2 Let I and X denote the concentrations of the iodine and xenon isotopes. We then have

$$\frac{d}{dt} I(t) = \gamma_I \Sigma_f \phi - \lambda_I I(t) \quad (a)$$

and

$$\frac{d}{dt}X(t) = \gamma_X \Sigma_f \phi - \lambda_I I(t) - \lambda_X X(t) - \sigma_{aX} X(t) \phi \quad (\text{b})$$

Note that no neutron absorption term, $\sigma_{aI} I(t) \phi$, in the Eq. (a) here, since even at high flux levels, iodine absorption is insignificant compared to its decay.

Considering now, following reactor start-up, both iodine and xenon concentrations build from zero to equilibrium values over a period of several half-lives. Since the half-lives are in hours, after a few days equilibrium is achieved. Find the final form of both Eqs. (a) and (b) for $t \rightarrow \infty$. Variables definitions are as what are given in Problem 15.1.

Problem 15.3 Let I_0 and X_0 be the concentrations of the iodine and xenon at the time of reactor shutdown. If the reactor is put on a large negative period, to first approximation, we may assume that the shutdown is instantaneous compared to the time spans of hours over which the iodine and xenon concentration evolves. Find the solution of Eqs. (a) and (b) that are given by Problem 15.2. Variables definitions are as what are given in Problem 15.1.

Problem 15.4

Prove that the following relation is valid, if the reactor has been running for several days – long enough for iodine and xenon in order to reach equilibrium.

$$X(t) = \Sigma_f \phi \left[\frac{(\gamma_I + \gamma_X)}{\lambda_X - \sigma_{aX} \phi} e^{-\lambda_X t} + \frac{\gamma_I}{\lambda_I - \lambda_X} (e^{-\lambda_X t} - e^{-\lambda_I t}) \right] \quad (\text{a})$$

Variables definitions are as what are given in Problem 15.1. *Hint:* Use the results that are given by solution of Problems 15.2 and 15.3.

Problem 15.5 Prove that for a reactor operating at a very high flux level, the maximum xenon-135 concentration takes place at approximately 11.3 h following shutdown.

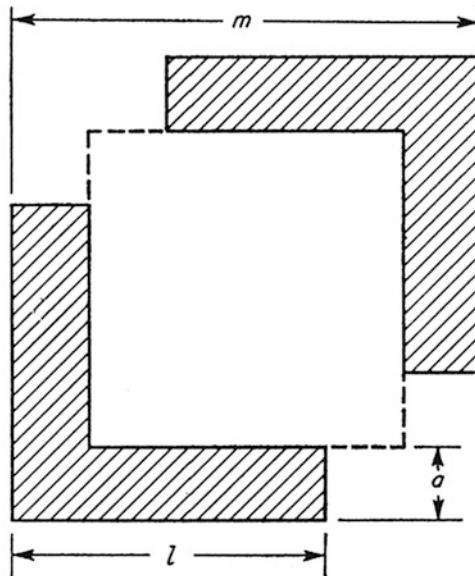
Variables definitions are as what are given in Problem 15.1. *Hint:* Use result of solution for Problem 15.4.

Problem 15.6 Make a logarithmic plot of the effective half-life of xenon-135 over the flux range of $10^{10} \leq \phi \leq 10^{15}$ n = cm² = s. Use the relation of $\lambda' = \lambda + \sigma_a \phi$, where σ_a is absorption cross section, λ radioactive decay constant, and neutron flux ϕ . Note that the effective half-life xenon is given by $t_{1/2} = 0.693/\lambda$. Hint: Use the result of solution of Problem 15.2 for xenon. Note also that uranium-235 has date of $\gamma_I = 0.0639$ and $\gamma_X = 0.00237$ and $\sigma_f^{25} = 2.65 \times 10^6$ barns.

Problem 15.7 A thermal reactor fueled with uranium has been operating at constant power for several days. Make a plot of the ratio of concentration of xenon-135 to uranium-235 atoms in the reactor versus its average flux. Determine the maximum value in this ratio. Note that the effective half-life xenon is given by $t_{1/2} = 0.693/\lambda$. *Hint:* Use the result of solution of Problem 15.2 for xenon. Note also that uranium-235 has date of $\gamma_I = 0.0639$ and $\gamma_X = 0.00237$ and $\sigma_f^{25} = 2.65 \times 10^6$ barns.

Problem 15.8 If the rate of formation of neutron designated by q and is taken to be constant outside the rod and zero inside, then the fraction of neutrons absorbed in single rod δk , which may be taken as the total worth of all the rods as it can be seen in figure below, and it may be written as following equation (Fig. 15.9):

Fig. 15.9 Poison cell for control rod calculation



$$\delta k = \frac{(\text{Exposed perimeter of rod}) D \nabla^2 \phi \text{ (at rod surface)}}{q \text{ (Area of source region)}} \approx \frac{4l}{(m-2a)^2} \cdot \frac{1}{h\Sigma_a + \frac{1}{L} \coth\left(\frac{m-2a}{2L}\right)} \quad (\text{a})$$

where

h = Linear extrapolation distance

m = Poison cell dimension

a = Half-thickness of cruciform control rod

l = Half-length of arm of cruciform rod

L = Diffusion length

Σ_a = Macroscopic absorption cross section

Now consider that in a water-moderated reactor, in which 32 cruciform control rods are distributed evenly throughout the core, the following dimensions are applicable: $l = 10.0$ cm, $a = 0.336$ cm, and $m = 19.5$ cm. The thermal-neutron diffusion length in the core is 1.8 cm, and $\Sigma_a = 0.114 \text{ cm}^{-1}$. Estimate the total worth of the system of control rods.

References

1. https://en.wikipedia.org/wiki/Nuclear_fission_product
2. S. Glasstone, A. Sesonske, *Nuclear Reactor Engineering* (D Van Nostrand Company, Inc, Princeton, 1967)
3. E.E. Lewis, *Fundamentals of Nuclear Reactor Physics* (Academic Press, Amsterdam/Boston, 2008)
4. J.R. Lamarsh, *Introduction to Nuclear Reactor Theory* (Addison Wesley Publishing Company, Inc, Reading, 1966)

Chapter 16

Fuel Burnup and Fuel Management



Nuclear fuel is removed from a reactor every few years when it can no longer economically keep a chain reaction going. This “spent” fuel remains radioactive and must be managed. At first, it goes into a pool onsite for cooling and storage. Some utilities are moving their spent fuel after several years in the pool into US Nuclear Regulatory Commission (NRC)-certified dry storage casks. These casks are specially designed to contain the radioactivity and allow hot spent fuel to cool further. In contrast to fossil fuel, the fuel in nuclear reactors cannot be converted since the fuel undergoes changes during its use in the reactor, which require the fuel elements to be exchanged.

16.1 The World’s Energy Resources

For the past half century, fossil fuels, namely, coal, oil, and natural gas, have supplied the major portion of the world’s energy requirements. It has long been realized, however, that in the not-too-distant future, these sources of energy will be largely exhausted. At the present time, the total energy consumption, for all countries, is about 1×10^{17} Btu per year. Since the world’s population is steadily growing and the power use per capita is increasing as well, the rate of energy utilization by the year 2020 could well be five to ten times the current value. According to one estimate, the known coal, oil, gas, and oil shale, which can be extracted at no more than twice the present cost, would be equivalent to roughly 4×10^{19} Btu¹⁰. This means, about 100 years, the world’s economically useful reserves of fossil fuels may approach exhaustion [1].

16.2 Today's Global Energy Market

Today's global energy market places many demands on power generation technology including high thermal efficiency, low cost, rapid installation, reliability, environmental compliance, and operation flexibility. The conclusion above, even considering some margin error in it, is inevitable that new sources of power must be found during the next 50 years or so if the earth is to support the growing population with some increase in living standards. Some consideration has been given to few such sources, for example, solar and wind energies as well as nuclear energy. Although solar and wind energies are very attractive, developing large-scale processes along with large farm of such systems is still some years away; on the other hand, nuclear energy has been made available and advanced in fission of heaviest elements or at stage of still research using fusion of very light nuclei. Technology of fusion process in commercial use with controlled release of such energies using either magnetic confinement of laser drive pellet of deuterium and tritium, the two isotopes of hydrogen, is too far in advanced. Nuclear fission, on the other hand, has already been established as a practical means for the production of energy and is getting to the point where it is economically very competitive with the energy produced from fossil fuels in the very near future.

The total amount of basic raw materials as source of fuel for fission power plant, such as uranium and thorium, in the earth's crust, to a depth of 3 miles, is very large, possibly something like 10^{12} tons. However, much of this is present in minerals containing such a small proportion of the desired element that extraction would be very expensive and not very cost-effective. This is in particular for high-grade ore reserves that are believed to be in other of 2×10^6 tons; therefore we need to reduce the cost of recovery from moderately low-grade ores to at least \$100 or less per pound of metal with advancing technology in this matter.

Development of plant layout and modularization concepts requires an understanding of both primary and secondary systems.

General Electric's **S**Team **A**nd **G**as (STAG) combined-cycle power generation equipment has met these demands and surpassed them, taking power plant performance to unprecedented levels.

The development of steam and gas turbine combined cycles has paralleled gas turbine development, resulting in reliable combined-cycle plants. Those incorporating GE's advanced gas turbine technology have achieved efficiency levels approaching 58%, due primarily to the higher firing temperatures of advanced technology gas turbines. The MS9001H gas turbine will achieve 60% efficiency in combined-cycle application when it goes into full operation.

In addition to advances in gas turbine technology, steam turbine performance also has evolved. GE's STAG combined-cycle power generation product line includes steam cycle options that satisfy a wide range of economic considerations including fuel flexibility, fuel cost, duty cycle, and space limitations.

Heat exchangers, filters, turbines, and other components in integrated coal gasification combined-cycle system must withstand demanding conditions of high

temperatures and pressure differentials. Under the highly sulfiding conditions of the high-temperature coal gas, the performance of components degrades significantly with time unless expensive high alloy materials are used. Deposition of a suitable coating on a low-cost alloy may improve its resistance to such sulfidation attack and decrease capital and operating costs. A review of the literature indicates that the corrosion reaction is the competition between oxidation and sulfidation reactions. The Fe- and Ni-based high-temperature alloys are susceptible to sulfidation attack unless they are fortified with high levels of Cr, Al, and Si. To impart corrosion resistance, these elements need not be in the bulk of the alloy and need only be present at the surface layers [1].

16.3 Fuel Utilization and Fuel Burnup

The fuel, which has not been spent, and the generated plutonium may be recovered by *reprocessing* the removed fuel elements. Light water reactors have a burnup of 45,000 to 50,000 Megawatt-days per metric ton (MWd/t) of uranium. This means that about 45 to 50 kg of fissionable material per ton of nuclear fuel used have been fissioned and 360 to 400 million kilowatt hours (kWh) of electricity have been generated at a nuclear power plant efficiency of 34% [2].

Reprocessing is applied to nuclear fuel reprocessing procedures, where the chemical treatment of nuclear fuel after its use in a reactor is to remove the fission products and to recover the unused uranium and the new fissile material plutonium generated during the fission.

In general sense, the concept of nuclear fuel utilization should be in contrast with nuclear reactor design, and its relation to the concept of reactor design should be considered as part of the process.

In the present Generation III (GEN-III) of nuclear reactors, there exist systems ranging from “burners” of highly enriched uranium, in which there is essentially no conversion of U^{238} to Pu^{239} , to breeders, which produce more fissile nuclei than are consumed. Therefore, if any attempt is to be made to use the nuclear energy available from natural uranium and thorium, a certain amount of breeding of fissile material will be necessary. These days, breeder reactor shows better output efficiency than highly developed reactors that use nuclear fuel less effectively [2].

In summary, to understand “burnup,” it helps to know more about the uranium that fuels a reactor. Before it is made into fuel, uranium is processed to increase the concentration of atoms that can split in a controlled chain reaction in the reactor. The atoms release energy as they split. This energy produces the heat that is turned into electricity. In general, the higher the concentration of those atoms, the longer the fuel can sustain a chain reaction. In addition, the longer the fuel remains in the reactor, the higher the burnup [2].

In other words, burnup is a way to measure how much uranium is burned in the reactor. It is the amount of energy produced by the uranium. Burnup is expressed in gigawatt-days per metric ton of uranium (GWd/MTU). Average burnup, around

35 GWd/MTU two decades ago, is over 45 GWd/MTU today. Utilities now are able to get more power out of their fuel before replacing it. This means they can operate longer between refueling outages. It also means they use less fuel.

The burnup level affects the fuel's temperature, radioactivity, and physical makeup. It is important to the NRC's review of spent fuel cask designs because each system has limits on temperature and radioactivity. How hot and how radioactive spent fuel is depends on burnup, as well as the fuel's initial makeup and conditions in the core. All these factors must be taken into account in designing and approving dry storage and transport systems for spent fuel [2].

Nuclear fuel is encased in metal cladding. In the reactor, this cladding reacts with cooling water. The reaction forms oxide on the outside (similar to rust) and releases hydrogen. These processes begin slowly and then start to accelerate as the fuel reaches burnup of 45 GWd/MTU. Anything higher is considered high burnup. However, in reality, there is no sharp line between low and high burnup. It is a continuum. That means the difference between fuel burned to 45 GWd/MTU and 46 or 47 GWd/MTU can be very small [2].

When spent fuel is placed in a dry storage system and the water is removed, the temperature of the fuel increases, and the makeup of the cladding can change. This change can result in the fuel cladding becoming less "ductile," or pliable, as it cools. It was also once thought that cladding of higher burnup fuel could become brittle enough to create a safety concern. Research now shows that while it may become less ductile, safety of the public will not be impacted for the systems the NRC has approved [2].

16.4 Fuel Reprocessing

A key, nearly unique, characteristic of nuclear energy is that used fuel may be reprocessed to recover fissile and fertile materials in order to provide fresh fuel for existing and future nuclear power plants. Several European countries, such as Russia and Japan, have had a policy to reprocess used nuclear fuel, although government policies in many other countries have not yet come around to seeing used fuel as a resource rather than as a waste.

Application of chemical processes to separate the valuable substances – the still existing uranium and the newly generated fissile material plutonium – from the fission products, the radioactive waste in the spent nuclear fuel after its use in the reactor. The PUREX process for reprocessing underwent several years of large-scale trial. A spent fuel element has, apart from the structural material, approximately the following composition: 96% uranium, 3% fission products (waste), 1% plutonium, and small amount of transuranium elements. The recovered uranium and the plutonium can be reused as fuel in a nuclear power plant following appropriate further chemical treatment. The nuclear fuel recoverable in a reprocessing plant with an annual throughput of 350 t corresponds, in the case of use in modern light water reactors, to an energy quantity of approximately ten million *t* hard coal. In the

reprocessing, the high active waste (fission products) is separated and by verification brought into a form suitable for safe ultimate disposal [3].

Details for the overall reprocessing are depicted below, which are adopted from the European Nuclear Society [3] (Figs. 16.1 and 16.2).

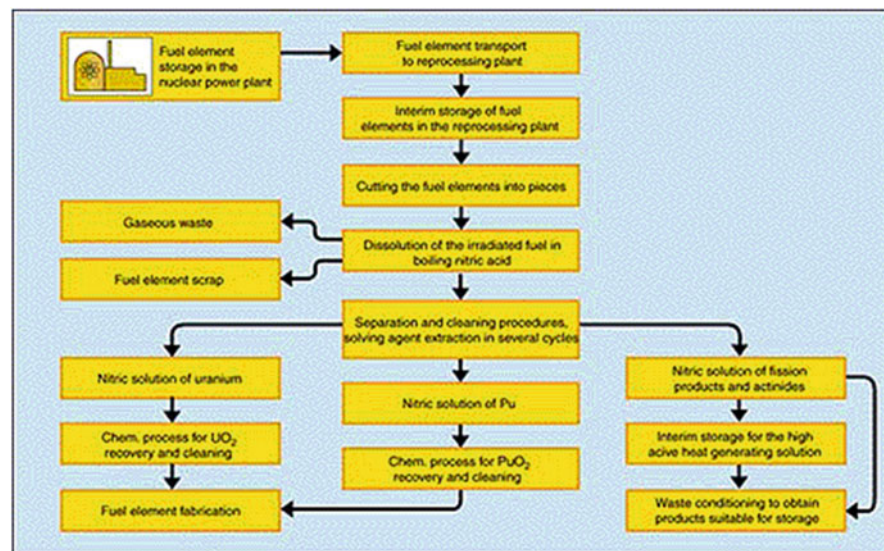


Fig. 16.1 Scheme of the reprocessing of irradiated fuel elements [3]

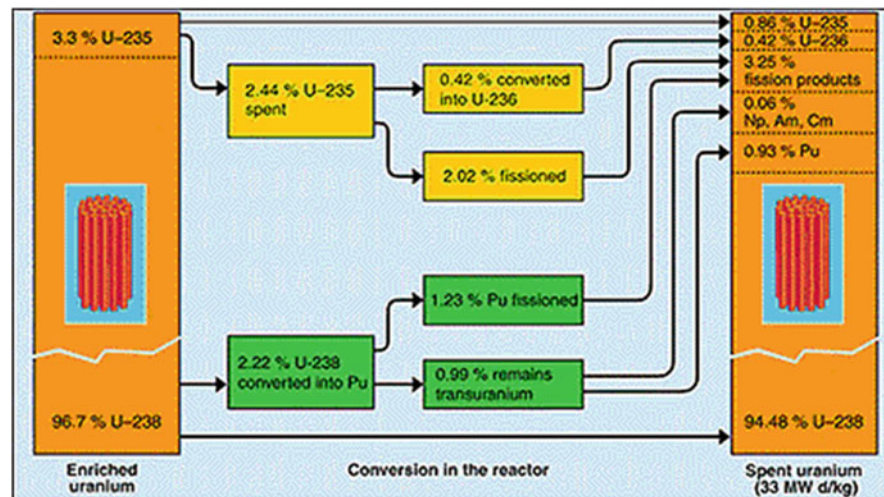


Fig. 16.2 Composition of nuclear fuel for light water reactors prior and after the use in a reactor [3]

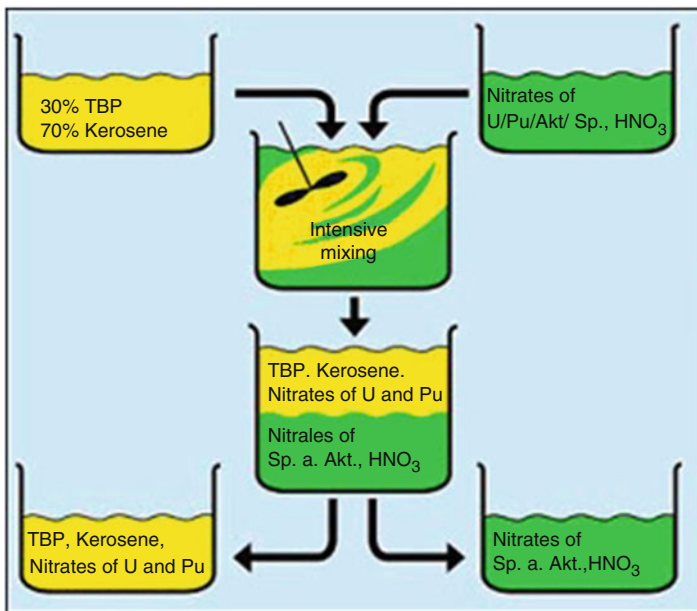


Fig. 16.3 Principle of the PUREX process for the separation of uranium and plutonium from fission products [3]

16.4.1 *PUREX Process*

PUREX process is the process for the reprocessing of spent nuclear fuel to separate uranium and plutonium from the fission products and from one another. Following the dissolution of the irradiated fuel in aqueous nitric acid, uranium and plutonium are transferred to an organic phase by intensive mixing with an organic solvent extraction – 30% tributyl phosphate (TBP) in kerosene is used as organic solvent – while the fission products remain in the aqueous nitric phase. Further process steps enable the subsequent separation of uranium and plutonium from one another [3] (Fig. 16.3).

16.4.2 *Transuranium Elements*

Transuranium is a chemical element in the classification of elements, the atomic number of which is greater than 92, that of uranium. Except for the plutonium isotopes Pu^{244} (half-life about 80 million years) and Pu^{239} (continuous reformation in uranium by neutron capture in U^{238} by neutrons from the spontaneous fission of U^{238}) detected in very small quantities, all transuranium elements must be produced artificially (see Table 16.1 below) [3].

Table 16.1 Transuranium elements

Element name	Symbol	Atomic number
Neptunium	Np	93
Plutonium	Pu	94
Americium	Am	95
Curium	Cm	96
Berkelium	Bk	97
Californium	Cf	98
Einsteinium	Es	99
Fermium	Fm	100
Mendelevium	Md	101
Nobelium	No	102
Lawrencium	Lw	103
Rutherfordium	Rf	104
Dubnium	Db	105
Seaborgium	Sb	106
Bohrium	Bh	107
Hassium	Hs	108
Meitnerium	Mt	109
Darmstadtium	Ds	110
Roentgenium	Rg	111
Copernicium	Cn	112
Still without name		113
Flerovium	Fl	114
Still without name		115
Livermorium	Lv	116
Still without name		117
Still without name		118

16.4.3 Vitrification

The highly active fission product solutions arising in reprocessing must be transferred to a product suitable for ultimate disposal. Vitrification has proven to be a suitable method for this purpose. In the French AVM process, the liquid high active waste solution is heated to high temperatures that causes the liquid to evaporate and the resulting granulate is molten at 1100 °C to glass adding glass frit. This process is used in the French large-scale reprocessing plant La Hague. In the process developed by the Karlsruhe Research Centre, liquid high active waste solution is added directly to the molten glass mass at 1150 °C. The liquid evaporates, and the radioactive solids are homogeneously embedded in the molten glass mass. In both processes, the molten glass mass is filled into 1.3-m-high 150 steel containers holding about 400 kg glass products. The heat production due to the radioactive decay of the ingredients of such a container amounts to 1.5–2 kW [3].

16.5 Fuel Management for Nuclear Reactors

The heart of a nuclear power plant (NPP) is the reactor core producing power from the fissioning of uranium or plutonium fuel. In reality, a nuclear reactor is composed of individual fuel assemblies having a heterogeneous design. A fuel assembly (FA) consists of discrete components such as fuel rods, spacer grids, control rod channels, etc. Figure 16.4 shows typical fuel assemblies of pressurized water reactors (PWR) and boiling water reactors (BWR), respectively.

A PWR fuel assembly comprises a bottom nozzle into which rods are fixed through the lattice, and to finish the whole assembly, a top nozzle ends it. There are spacing grids between these nozzles. These grids ensure an exact guiding of the fuel rods. The bottom and top nozzles are heavily constructed as they provide much of the mechanical support for the fuel assembly structure.

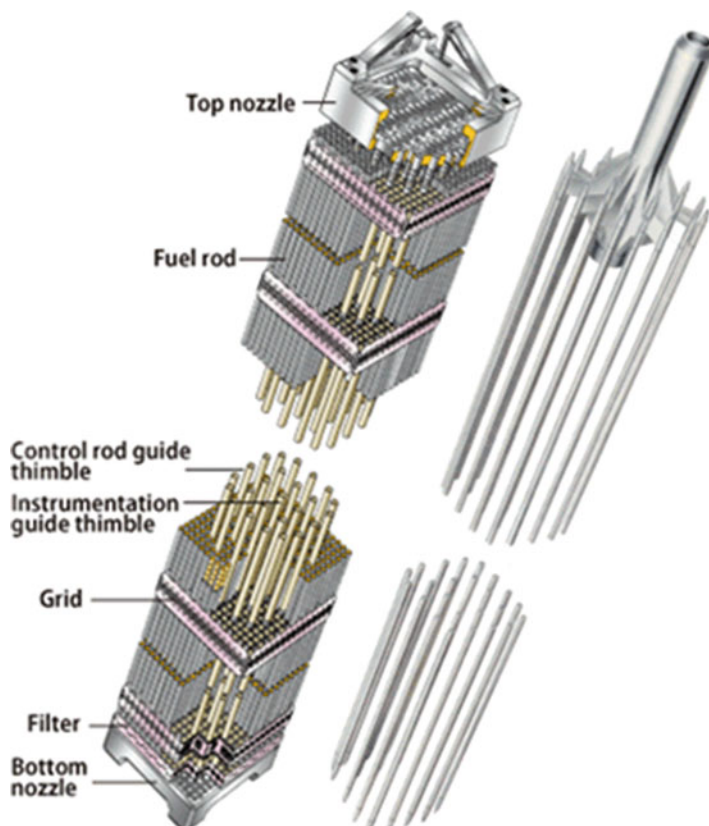


Fig. 16.4 Cutaway of typical rod cluster control assembly for a PWR. (Source: www.world-nuclear.org)

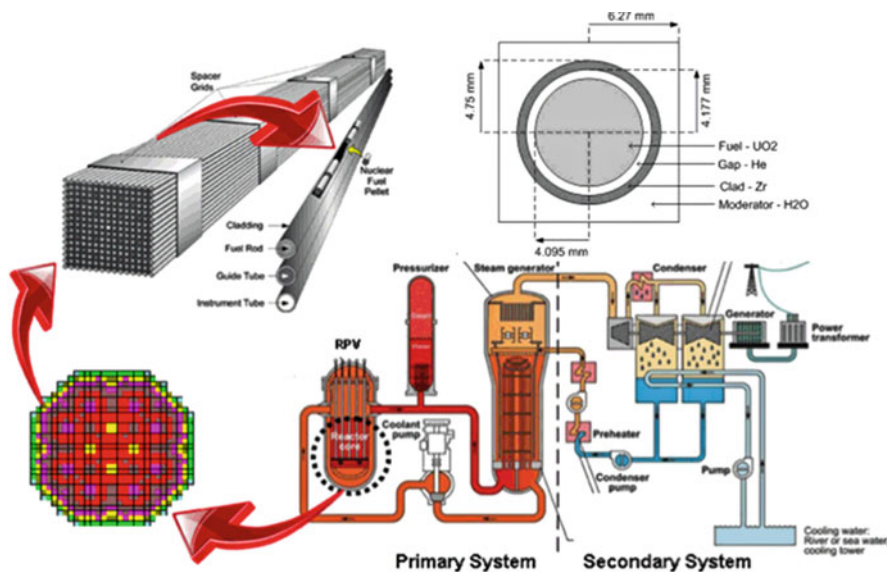


Fig. 16.5 Nuclear reactor, reactor core, fuel loading pattern, fuel assembly, fuel rod, fuel pellet. (Source: www.world-nuclear.org)

Typical PWR fuel assembly consists of the following subsystem and is depicted in Fig. 16.5:

- *Fuel rods*: Fuel rods contain the fuel and burnable poisons.
- *Top nozzle*: Provides the mechanical support for the fuel assembly structure.
- *Bottom nozzle*: Provides the mechanical support for the fuel assembly structure.
- *Spacing grid*: Ensures an exact guiding of the fuel rods.
- *Guide thimble tube*: Vacant tube for control rods or in-core instrumentation.

A 1100 MWe (3300 MWth) nuclear core may contain 157 fuel assemblies composed of over 45,000 fuel rods and some 15 million fuel pellets. Generally, a common fuel assembly contains energy for approximately 4 years of operation at full power. Once loaded, fuel stays in the core for 4 years depending on the design of the operating cycle. During these 4 years, the reactor core has to be refueled.

During refueling, every 12–18 months, some of the fuel – usually one third or one quarter of the core – is removed to spent fuel pool, while the remainder is rearranged to a location in the core better suited to its remaining level of enrichment. The removed fuel (one third or one quarter of the core, i.e., 40 assemblies) has to be replaced by fresh fuel assemblies.

Figure 16.6 shows the top view of a reactor core, where the fuel assemblies are arranged in a cylindrical type configuration.

The typical neutron spectrum for light water reactors (LWR) is shown in Fig. 16.7.

BWR Fuel Bundle Geometry

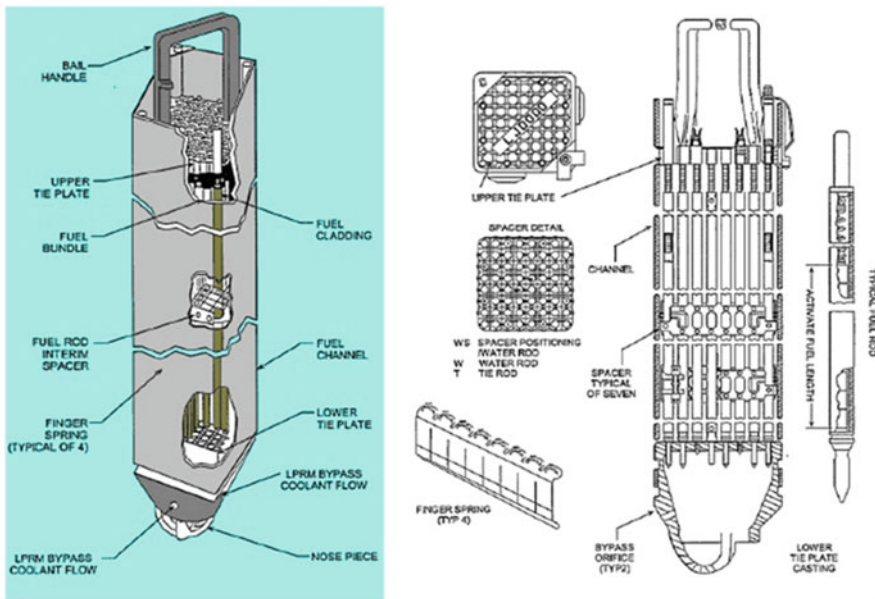


Fig. 16.6 Fuel assembly for a BWR

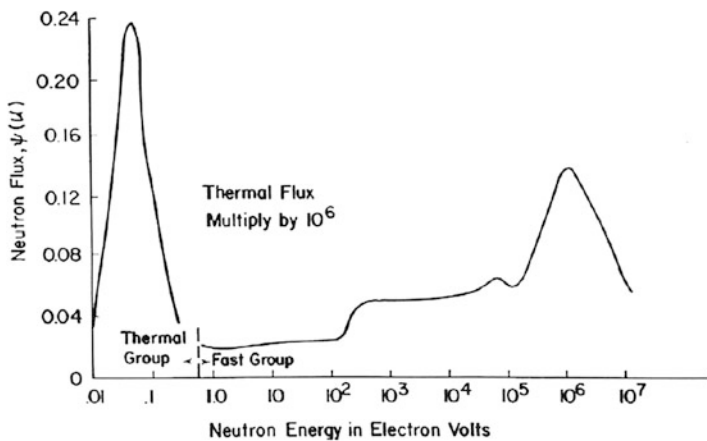


Fig. 16.7 Typical neutron spectrum for a LWR

Now that we have a little history of nuclear reactor core assembly and their types, we can pay our attention to the subject of fuel management and then talk about nuclear fuel cycle as well.

For fuel of a given enrichment, the burnup can be extended by suitable fuel loading schedules, generally referred to as “fuel management.” A number of such procedures, with their advantages and disadvantages, can be described and will be found in various books and open literatures [4].

Some of these conditions as above require changing the location of the fuel elements within core according to predetermined schedule. Although these schemes may increase the burnup and the expenditure of fuel, they may add to the cost of the reactor operation, especially if shutdown is necessary for rearranging the fuel [4].

16.6 Nuclear Fuel Cycle

The nuclear fuel cycle includes all activities involved in obtaining and irradiating fuel in nuclear reactors, as well as spent fuel processing and disposing of the fission product wastes produced during irradiation of these reactors. The many activities involved in the fuel cycle may be divided into three categories:

1. The first category involves activities that take place prior to fuel irradiation, when fuel radioactivity levels are relatively low. These activities include milling, conversion to uranium hexafluoride, enrichment in the fissile isotope U^{235} (in the case of all but natural uranium fueled reactors), and fabrication into fuel elements and assemblies. These activities are designed as head-end fuel management.
2. The second category of activities involves fuel cycle design and irradiation of the fuel assemblies in the reactor. These activities include evaluation of reactivity and control requirements, programming of fuel assemblies in the reactor, power distribution analysis, and core capability evaluation. This category is primarily the responsibility of the nuclear engineer and will be covered in depth in later chapters of the book. It will be referred to as *in-core fuel management*.
3. The third category of fuel management activities includes those activities that involve operations on the highly radioactive spent fuel storage and shipping, reprocessing of the spent fuel to remove fission products and separate transuranium elements, and waste disposal. It will be designed as tail-end fuel management.

There are several features of nuclear fuel that are considerably different from fossil fuel. A unit mass of fissile material fissioned yields nearly four million times as much energy as a unit mass of coal burned. Nuclear fuel is therefore quite valuable. A second feature of nuclear fuel and the nuclear fuel cycle is the presence of radioactivity. Although activity levels in the head end of the fuel cycle are relatively low, they are not insignificant, and care must be taken to prevent the release of radioactivity to the environment. Once any fissioning has taken place in the fuel, activity levels resulting from both fission products and neutron capture products are extremely high, and the release of even a small fraction of this activity to the environment would cause acceptable radioactivity levels to be exceeded.

Another feature of nuclear fuel that differentiates it from other energy sources is that the material produced for use in some types of reactors, and some of the by-products of the reactor operation, could be used to produce crude nuclear explosive. For this reason, access to many phases of the fuel cycle must be carefully controlled and the probability of diversion of such material reduced to a very low value.

A final feature of nuclear fuel management, as opposed to the management of fossil fuel, is the long time required between mining the ore, irradiation of the fuel in the reactor, and removal of fission product wastes. This process requires a minimum of 2 years and could extend to many decades if spent fuel is stored for an indefinite period prior to the separation of fuel material from fission products, if this separation is performed at all.

Although the nuclear engineer may not be directly involved with the technical details of these activities, he or she should be familiar with how the major fuel processing steps are affected when changes are made in fuel design or reactor operation, as well as how these interactions affect fuel cycle economics.

A cycle is a period of time in which certain events are repeated in the same order and at the same intervals. This is the case with nuclear fuel cycle. Not all fuel cycles are the same, however, and there are a number of different types of fuel cycles that are of interest to us. The differences arise both because of differences in resource availability and differences in the state of technology or national policy objectives in various parts of the world.

As part of fuel management, the integrated used fuel management is part of the procedure. Used nuclear fuel consists of small uranium fuel pellets stacked inside alloy fuel rods. All the used nuclear fuel produced by the nuclear energy industry in nearly 50 years – if stacked end to end – would cover an area the size of a football field to a depth of less than 10 yards.



Under a sustainable, integrated approach for managing the back end of the fuel cycle, used fuel storage at nuclear energy facilities will continue in the near term. One or more consolidated storage facilities, to be built in willing host communities, will help move used fuel from shutdown and operating reactors and reduce the mounting federal liability for delays in the repository program. Eventually, the government will remove it and place the unusable end product in a deep geologic repository. Before a repository is established, research into used fuel recycling can potentially reduce the quantity, heat, and toxicity of radioactive waste by-products needing repository disposal.

The nuclear energy industry supports completion of the Yucca Mountain project. The industry also supports legislation to create a sustainable, integrated program for federal management of high-level radioactive waste and used nuclear fuel. The industry supports an integrated used nuclear fuel management strategy, consisting of ten basic elements which may be found in the reference section [5].

16.7 Store and Transport High Burnup Fuel

The questions for this section are that: [2]

1. *Is it safe to store and transport high burnup fuel?*

To be certified by the NRC, dry cask designs must meet the NRC requirements. For transportation, these are found in 10 CFR Part 71 and for storage in 10 CFR Part 72. The NRC approves designs only after a full safety review.

Based on these reviews, the NRC has certified cask designs for storage and transportation of high burnup spent fuel. Because low burnup spent fuel has been around longer and there is more of it, there are more casks for low than for high burnup spent fuel. There is also a great deal of data on low burnup fuel. Still, there is enough data on high burnup fuel that the NRC has certified high burnup spent fuel storage casks for an initial term of 20 or 40 years. Some systems have also been approved for transporting high burnup spent fuel. Operating experience since dry storage began in 1986 and short-term tests show both low and high burnup spent fuel can be stored and transported safely.

2. *How does the NRC make sure it remains safe?*

The NRC assures safety by requiring many layers of protection. Cask designs provide several layers, and the fuel cladding itself provides added protection. The regulations are designed to ensure the health and safety of the public is maintained during storage or in a transportation accident. The NRC's regulations ensure the system will remain safe even if the cladding did break. The NRC carefully reviews each cask application to see if it meets the requirements. As part of this review, the NRC does its own analysis to confirm information in the application.

3. *What confirmatory research is being done?*

The primary focus of research today is to get more data to support the continued certification of storage systems beyond the initial 20- to 40-year license term. Additional research is ongoing to confirm that high burnup fuel will remain safe during transport after extended storage. This research is designed to ensure that the existing data on high burnup spent fuel is accurate and can be reproduced.

Cask designers are also involved in research that will assist them in designing casks for higher burnups and additional fuel types. As more data becomes available, the NRC expects to be able to certify more casks. Testing has provided

a lot of information on how different types of cladding on spent fuel will behave, and this work continues.

The NRC is conducting tests at the Oak Ridge National Laboratory on high burnup fuel samples under stresses greater than the loads expected during normal transport. These tests have already shown that high burnup fuel is very strong. This information further confirms that long-term storage and eventual transportation of high burnup fuel are safe.

In addition, planning is underway for an important new study, run jointly by the nuclear industry and the Department of Energy, with regulatory oversight by the NRC. In this study, high burnup spent fuel will be loaded into a cask fitted with instruments to provide temperature readings and allow sampling of the gas inside. Those readings, combined with tests on the fuel assemblies and inspection of the cask's interior after years of dry storage, will provide more data. The test is expected to confirm the current understanding of what happens to high burnup spent fuel in a storage cask as it cools over time.

All this work will help cask designers, users, and regulators have better understanding how to ensure high burnup spent fuel will remain safe in dry storage over the long term and during transportation to a centralized storage or disposal facility.

16.8 Nuclear Reactors for Power Production

In the United States, most reactor design and development for the generation of electrical power was branched from the early nuclear navy research, when it was realized that a compact nuclear power plant would have great advantages for submarine-driven nuclear propulsion system. To have such power plant on board would make possible long voyages cross the oceans at high speeds without the necessity for resurfacing at frequent intervals, and Argonne National Laboratory was assigned with such task of designing such reactor. Therefore, the first generation of pressurized water reactor (PWR) was born, where the use of highly enriched uranium as the fuel and water under pressure as the moderator as well as coolant allowed small version of this type of high-power reactor. Consequently, the first prototype of such reactor, namely, STR Mark 1, starts operation at Arco, Idaho, in March 1953, and production version of it was installed on USS Nautilus, the first nuclear power submarine after May 31, 1953.

As a result of experience gained in successful operation of the submarine reactors, the first commercial version of PWR was designed in Pennsylvania shipping port and went into operation in December 2, 1957. The design was based on the water pressure of 13.8 MPa, i.e., 2000 psi, and steam produced in the heat exchanger with a temperature of about 254 °C (490 °F) and pressure close to 4.14 MPa (600 psi). In order to make such reactor cost-effective and reduce the cost of the power produced, only a small number of the fuel elements are highly enriched in uranium-235 (U^{235}) as an alloy with zirconium, the remainder being of normal uranium as the dioxide.

The change in core design required bigger real estate for footprint of commercialized version PWR that was not an issue for a land-based facility. The output power of this reactor was about 60 MW electrical equivalents to 230 MW thermal, and further enhancement in core design increased the power out to 150 MW electrical and 505 thermal. Pressurized water reactors, using slightly 2–4% enriched uranium dioxide as the fuel, are now commonly used in the United States and other countries around the globe for commercial power generation. The most recent plants have electrical capacities in the neighborhood of 1000 MW (3000 MW thermal) which is due to a modification of the pressurized water concept where steam is produced directly by utilizing fission heat to boil water within the reactor core, rather than in an external heat exchanger [1].

Later on, other reactor designs based on different fuel materials, moderators, and coolants with various electrical and thermal power outputs were born, and examples are thermal reactors such as:

- Boiling water reactor (**BWR**) initiated in 1953.
- Water-cooled graphite moderated in 1954.
- High-temperature, gas-cooled reactor (**HTGR**).
- Liquid-metal fast-breeder reactors (**LMFBR**).

All commercial reactor power plants of present interest are systems for generating steam utilizing the heat of nuclear fission to boil water and produce steam for turbine, and they are often referred to as “Nuclear Steam Supply Systems” or **NSSS**. The steam is expanded in a turbine which drives a generator to produce electricity in the conventional manner. The exhaust steam from the turbine passes on to a condenser where it is converted into liquid water and this is returned as feed water to the steam generator of **NSSS**.

The proportion of the heat supplied in a power plant that is actually converted into electrical energy is called the *thermal efficiency* of the system; thus, in a nuclear installation:

$$\text{Thermal Efficiency} = \frac{\text{Electrical Energy Generated}}{\text{Heat Produced in the Reactor}} \quad (16.1)$$

The maximum possible value of the thermal efficiency is the *ideal thermodynamic efficiency*, which is given by the following relationship:

$$\text{Ideal Thermodynamic Efficiency} = \frac{T_2 - T_1}{T_2} \quad (16.2)$$

where:

T_1 is the absolute temperature of the steam entering the turbine (^0K Kelvin).
 T_2 is the temperature at which heat is rejected to the condenser (^0K Kelvin).

The ideal thermodynamic efficiency can be increased by having T_2 as high as possible and T_1 as low as possible. In practice, T_1 is more or less fixed by the ambient

temperature; the thermal efficiency of a steam electric plant is then largely determined by the steam temperature, which should be as high as feasible.

Conditions in PWRs and BWRs are such that the steam temperature is lower than in modern fossil fuel power plants, in which the heat is produced by burning coal, oil, or gas. Here, the thermal efficiencies of these reactor plants are only about 33%, compared with 40% for the best fossil fuel facilities. With the HTGRs and fast breeder reactors, however, the thermal efficiencies should equal to those of the best fossil fuel plants, i.e., about 40% [1].

16.9 Future Nuclear Power Plant Systems

In response to the difficulties in achieving suitability, a sufficiently high degree of safety, and a competitive economical basis for nuclear power, the US Department of Energy initiated the Generation IV program in 1999. Generation IV refers to the broad division of nuclear designs into four categories as follows:

1. Early prototype reactor (generation I).
2. The large central station nuclear power plants of today (generation II).
3. The advanced light water reactors and other systems with inherent safety features that have been designed in recent years (generation III).
4. The next-generation system to be designed and built two decades from now (generation IV).

By 2000, international interest in the Generation IV project had resulted in a nine-country coalition that includes:

- (i) Argentina
- (ii) Brazil
- (iii) Canada
- (iv) France
- (v) Japan
- (vi) South Africa
- (vii) South Korea
- (viii) The United Kingdom
- (ix) The United States

Participating countries are mapping out and collaborating on the research and development of future nuclear energy systems.

Although the Generation IV program is exploring a wide variety of new systems, a few examples serve to illustrate the broad approaches reactor designs are developing to meet their objectives.

The next-generation systems are based on three general classes of reactors:

1. Gas-cooled.
2. Water-cooled.
3. Fast-spectrum.

All these categories and their brief designs are discussed in next sections.

16.10 Next Generation of Nuclear Power Reactors for Power Production

Experts are projecting worldwide electricity consumption will increase substantially in the coming decades, especially in the development world, accompanying economic growth and social progress that have direct impact on rising electricity prices which have focused fresh attention on nuclear power plants. New, safer, and more economical nuclear reactors could not only satisfy many of our future energy needs but could combat global warming as well. Today's existing nuclear power plants on line in the United States provide fifth of the nation's total electrical output (see Fig. 16.8).

Taking into account the expected increase in energy demand worldwide and the growing awareness about global warming, climate change issues, and sustainable development, nuclear energy will be needed to meet future global energy demand.

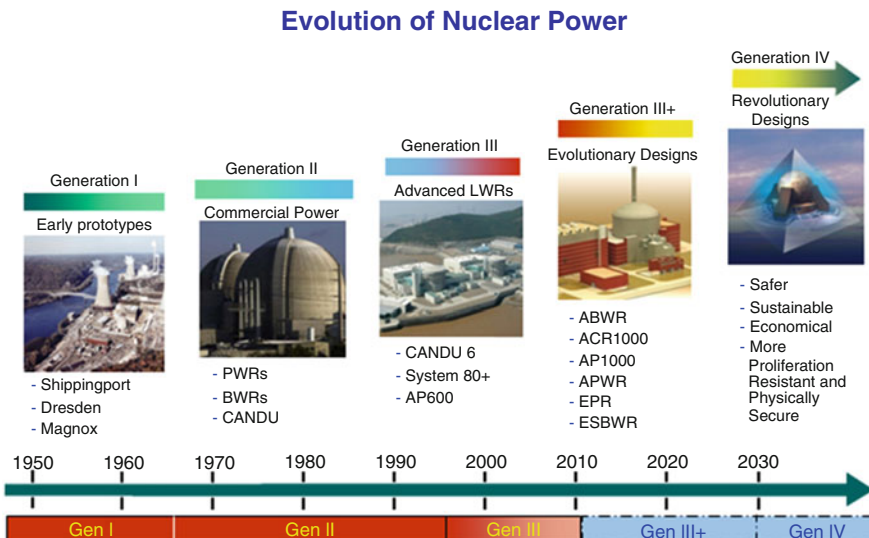


Fig. 16.8 Evolution of nuclear power plants

Nuclear power plant technology has evolved as distinct design generations as we mentioned in the previous section and briefly summarized here again as follows:

- First generation: Prototypes and first realizations (~1950–1970).
- Second generation: Current operating plants (~1970–2030).
- Third generation: Deployable improvements to current reactors (~2000 and on).
- Fourth generation: Advanced and new reactor systems (2030 and beyond).

The **Generation IV International Forum**, or **GIF**, was chartered in July 2001 to lead the collaborative efforts of the world's leading nuclear technology nations to develop next-generation nuclear energy systems to meet the world's future energy needs.

Eight technology goals have been defined for Generation IV systems in four broad areas:

1. Sustainability.
2. Economics.
3. Safety and reliability.
4. Proliferation resistance and physical protection.

A large number of countries share these ambitious goals as they aim at responding to economic, environmental, and social requirements of the twenty-first century. They establish a framework and identify concrete targets for focusing GIF R&D efforts.

The next generation (“Generation IV”) of nuclear energy systems is intended to meet the goals, listed in Table 16.2, while being at least as effective as the “third” generation in terms of economics.

In principle, the Generation IV systems should be marketable or deployable from 2030 onward. The systems should also offer a true potential for new applications compatible with an expanded use of nuclear energy, in particular, in the fields of hydrogen or synthetic hydrocarbon production, seawater desalination, and process heat production.

It has been recognized that these objectives, widely and officially shared by a large number of countries, should be at the basis of an internationally shared R&D program, which allows keeping open and consolidating the technical options and avoiding any early or premature down selection.

In fact, because the next-generation nuclear energy systems will address needed areas of improvement and offer great potential, many countries share a common interest in advanced R&D that will support their development. The international research community should explore such development benefits from the identification of promising research areas and collaborative efforts. The collaboration on R&D by many nations on the development of advanced next-generation nuclear energy systems will in principle aid the progress toward the realization of such systems, by leveraging resources, providing synergistic opportunities, avoiding unnecessary duplication, and enhancing collaboration.

Table 16.2 The intended goal of Generation IV nuclear energy system

Sustainability – 1	Generation IV nuclear energy systems will provide sustainable energy generation that meets clean air objectives and provides long-term availability of systems and effective fuel utilization for worldwide energy production
Sustainability – 2	Generation IV nuclear energy systems will minimize and manage their nuclear waste and notably reduce the long-term stewardship burden, thereby improving protection for the public health and the environment
Economics – 1	Generation IV nuclear energy systems will have a clear lifecycle cost advantage over other energy sources
Economics – 2	Generation IV nuclear energy systems will have a level of financial risk comparable to other energy projects
Safety and reliability – 1	Generation IV nuclear energy systems operations will excel in safety and reliability
Safety and reliability – 2	Generation IV nuclear systems will have a very low likelihood and degree of reactor core damage
Safety and reliability – 3	Generation IV nuclear energy systems will eliminate the need for offsite emergency response
Proliferation resistance and physical protection	Generation IV nuclear energy systems will increase the assurance that they are very unattractive and the least desirable route for diversion or theft of weapons usable materials and provide increased physical protection against acts of terrorism

Problems

Problem 16.1 Which weapons material is easier to handle and to create a weapon or improvised nuclear device (IND)?

Problem 16.2 List the effects from a nuclear weapon (NW) blast, and identify them in terms of energy release from the device. Which have short-term and which have long-term effects?

Problem 16.3 A 1-megaton device explodes at a height of 5000 feet. The equivalent burst height for a 1 kT (kiloton) device is 500 feet, and its equivalent time of arrival is 4 seconds. What would be the time of arrival of the blast wave from the 1 MT (megaton) devices at a distance of 10 miles from ground zero?

Problem 16.4 The Acheson-Lilienthal report and the Baruch Plan have what element in common?

Problem 16.5 Was the nuclear weapon (NW) proliferation threat around the time of Atoms for Peace based on a national or subnational effort?

Problem 16.6 Match the elements of the NPT to the keywords in the right hand column.

- Article 1 (a) NW (nuclear weapon)-free zones
- Article 2 (b) NWS obligations
- Article 3 (c) Carrot
- Article 4 (d) Stick
- Article 5 (e) NNWS (non-nuclear weapon states) obligations
- Article 6 (f) Nuclear disarmament

Problem 16.7 List three levels covered by nuclear safeguards, and indicate the entity responsible for their enforcement.

Problem 16.8 Which of the following countries are under International Atomic Energy Agency (IAEA) safeguards: Russia, Chile, Japan, Australia, United States, Egypt, Iran, and India?

Problem 16.9 List the two main objectives of International Atomic Energy Agency (IAEA) safeguards.

Problem 16.10 List three agreements included in the Information Circular (INCIRC/under 153).

Problem 16.11 List three measures granted to the International Atomic Energy Agency (IAEA) under the Additional Protocol (AP).

Problem 16.12 List three activities by a state under the International Atomic Energy Agency (IAEA) Additional Protocol (AP) that could put the state into noncompliance.

Problem 16.13 List the six key elements of the International Atomic Energy Agency (IAEA) safeguard approaches.

Problem 16.14 True or false. U^{233} is defined as an indirect-use material by the International Atomic Energy Agency (IAEA).

Problem 16.15 List the significant quantity (SQ) amounts for the following: HEU, U^{233} , Th, depleted U, Pu^{239}

Problem 16.16 List the critical mass and critical mass reflected by depleted uranium for U^{233} , Pu^{239} , and HEU.

Problem 16.17 Calculate the expected neutron flux from 1 kg of discharged for light water reactor (LWR) fuel (30,000 MWd/t burnup). What is the main neutron contributor? Could Pu^{239} be detected by measuring neutrons alone?

Problem 16.18 Nuclear material accountancy should satisfy what requirement regarding MUF (Material Unaccounted For)?

Problem 16.19 Match IAEA assumptions of conversion time with the materials below:

- Pu²³⁹ metal weeks
- HEU in irradiated fuel days (7–10)
- U containing <20% U235 months
- Pu in MOX weeks
- U²³⁵O²
- Th containing <20%U²³³

Problem 16.20 Provide International Atomic Energy Agency (IAEA) detection timeliness goals for:

1. Unirradiated direct-use material
2. Irradiated direct-use material

Problem 16.21 Provide four scenarios for cheating International Atomic Energy Agency (IAEA) safeguards.

Problem 16.22 List the elements that go into determination of MUF.

Problem 16.23 List three general categories of nondestructive assay (NDA) measurements. NDA is a measurement of the nuclear material content.

Problem 16.24 Suppose a nuclear plant were built above ground, but at reduced cost, by using inferior materials and shoddy construction. Would that be a violation of the Non-Proliferation Treaty?

Problem 16.25 Suppose a nuclear plant were built underground, completely hidden from view. Would that be a violation of the Non-Proliferation Treaty?

References

1. B. Zohuri, Combined Cycle Driven Efficiency for Next Generation Nuclear Power Plants: An Innovative Design Approach 2015th Edition
2. United Sates Nuclear Regulatory Commission, www.nrc.gov, High Burnup Spent Fuel, September 2015
3. <https://www.euronuclear.org/info/encyclopedia/p/purex-process.htm>
4. S. Glasstone, A. Sesonske, *Nuclear Reactor Engineering*, Published by D. Van Nostrand Company, Inc. 1967
5. <http://www.nei.org/Issues-Policy/Nuclear-Waste-Management/Integrated-Used-Fuel-Management>

Chapter 17

Why Nuclear Power Plant Energy



The major growth in the electricity production industry in the last 30 years has centered on the expansion of natural gas power plants based on gas turbine cycles. The most popular extension of the simple Brayton gas turbine has been the combined cycle power plant with the Air Brayton cycle serving as the topping cycle and the steam Rankine cycle serving as the bottoming cycle for new generation of nuclear power plants that are known as GEN-IV. The Air Brayton cycle is an open-air cycle and the steam Rankine cycle is a closed cycle. The Air Brayton cycle for a natural gas-driven power plant must be an open cycle, where the air is drawn in from the environment and exhausted with the products of combustion to the environment. This technique is suggested as an innovative approach to GEN-IV nuclear power plants in form and type of Small Modular Reactors (SMRs). The hot exhaust from the Air Brayton cycle passes through a Heat Recovery Steam Generator (HRSG) prior to exhausting to the environment in a combined cycle. The HRSG serves the same purpose as a boiler for the conventional steam Rankine cycle [1, 2].

17.1 Introduction

With the aftermath of the major accidents at Three Mile Island in 1979 and Chernobyl in 1986 and then recent devastated Japan's Fukushima nuclear power plant failure in Japan in March of 2011, we can state that before society can make the decision to shift its source of electric power from its present overwhelming dependence on fossil fuels to a future dependence on nuclear fuels, some very important questions must be answered [3–5]:

1. How will the cost of electricity be affected, both from short-term and long-term point of view?
2. What impacts will nuclear energy have on the environment?
3. How should its development and site installation be financed and managed?

4. What is the Total cost of ownership (TOC) and return on investment (ROI) for the owner of these power plants to produce electricity by being in the grid?
5. Are nuclear power plants safe, particularly with advancement of small modular reactors' (SMRs') perspective?
6. What sorts of surveillance are necessary to satisfy both aspects of proliferation and nonproliferation requirements and who should be responsible for them?
7. How are we going to manage our spent fuel and high-level waste from these nuclear power plants? And how our fuel cycle should be dealt with?
8. What is society and public's attitude toward nuclear power plants, and what are their understanding of this fast-moving technology with generation IV coming on line in a very near future?
9. How we are going to implement these power plants (i.e., advanced SMRs) to help decarbonization of environment by enhancing our green and clean air requirements?
10. How will these power plants be used as a source of new energy and help us with additional source of renewable source of energy to match our demand and supply for electricity?

We try our best to address some of these questions in the following sections of this chapter as much as possible, within scope of this book, yet readers can refer to reference such as "The Future of Nuclear Power, An Interdisciplinary MIT Study, 2003" [19].

Our national investment in the United States for generation energy from nuclear power will be hundreds of billions of dollars before the end of this century, which means everyone in our society has a personal stake of thousands of dollars as tax payers in the answers to these questions.

Before they can be answered intelligently, we have to make sure and it is necessary for everyone in our society regardless of their education to some general knowledge and understanding of how the nuclear power plant is working to produce energy in some details.

While we are referring this knowledge and understanding of the working of nuclear energy system in later section of this chapter (i.e., Sect. 17.14), we will elaborate this detail to some degree at introduction section of this chapter here.

Nuclear power plant systems now coming into operation presently drive their energy from *Fission* but not from *fusion* reactions in order for them to function and produce enough heat energy to be used to produce steam for steam turbine to drive electrical generator. It is necessary to arrange for fission reactions to occur continuously in a controlled chain reaction mode and at a high rate fashion without requiring much input energy to breakeven. This behavior takes place in today's fission reactors that are in production line, supply electricity into the grid for consumption, and are used in other different industry such as nuclear drive navy vessels.

Furthermore, futuristic nuclear fusion reactor designs are supposed to work in a very similar fashion to generate heat energy from a fusion reaction rather than fission reactor to drive steam for steam turbine, and the very mechanical energy of the steam

Table 17.1 Cross sections for thermal neutrons (in units of 10^{-24} cm^2)

H^1 – 0.33	Fe^{56} – 2.7
H^2 (deuterium) – 0.0006	Cd^{113} – 20,000
Li^6 – 940 ^a	Xe^{135} – 2,700,000
B^{10} – 3840 ^a	Xe^{136} – 0.15
C^{12} – 0.0037	U^{235} – 590 ^a
O^{16} – 0.0002	U^{238} – 2.7

^aFor Li^6 and B^{10} , these are cross sections for (n, α) , and for U^{235} it is for fission

In all other cases they are for (n, γ)

turbine shaft will ultimately get converted to energy of electricity; however at present technology stage, we are far away from actual breakeven at continues pace [20–22].

Basic concept of fission reactor is driven by the fact that a neutron striking a U^{235} nucleus induces a nuclear reaction leading to fission, where in the fission process, an average of 2.5 neutrons are released. If an average of at least 1.0 of the neutrons, 40 percent, induces another fission by striking another U^{235} nucleus, the original neutron is replaced, so the processes will continue indefinitely in a chain reaction scenario, so one fission reaction leading to another similar reaction in an endless chain, which we call *self-sustaining chain reaction* mode. A system in which a chain reaction as such takes place is called a *nuclear reactor* that we know today [14].

The simplest design of nuclear power reactor infrastructure would be a ball of U^{235} . The requirement that at least 40 per cent of the neutrons released in a fission induce another fission means that the ball must have some minimum size, the *critical mass*, for if it is too small, too many neutrons will escape out the surface. For nearly pure U^{235} this critical mass is about 44 pounds, making it about 5 inches in diameter, the size of a cantaloupe.

However, there is an inherent inefficiency in making a reactor in this way – the neutrons released in fission come out with an energy of about 1 MeV, and at such a high energy, the cross section, which determines the probability of the reaction occurring, is small, about two in the units of Table 17.1.

From that Table 17.1, we see that it would be better to slow the neutrons down to take advantage of the very much larger cross sections for *thermal reactors* – nearly all currently operating reactors are of this type – and the material inserted in a thermal reactor to slow down the neutrons is called a *moderator*, since it moderates their speed within core of the reactor.

In billiards' game table, a rapidly moving cue (i.e., white ball) ball entering a nest of other balls that is set up to start game is quickly slowed down by collisions.

Its energy of motion is transferred to the balls as they recoil from these collisions, assuming the energy conserved per our understanding classical mechanics on a frictionless billiard's surface table, so we do not lose any energy due to friction and natural heat.

The moderator in a reactor works in much the same way:

Neutrons are slowed down by collisions with the nuclei of which the moderator is composed because the struck nuclei recoil away, taking up some of the energy.

However, the question is that, what material makes a good moderator?

If the cue ball passes through a net of solid steel balls, it bounces off without being slowed down appreciatively because the steel balls are too heavy to recoil much due to conservation of momentum. A cue ball is more effectively slowed down by passing through a nest of balls not much more massive than itself, such as other billiard balls, since these absorb more energy in recoiling from a collision due to both conservation of energy and momentum.

Carrying this conclusion over to our analogy with neutrons being slowed down by a moderator, it determines the first requirement for a good moderator that must consist of nuclei not much more massive than a neutron, which means nuclei with very few nucleons. A second requirement for a moderator is that it has a small neutron cross section, since neutrons absorbed by the moderator are not available to induced fissions.

Now we should be looking for the best materials which will be satisfying these two above basic requirements that are:

1. A good moderator that consists of nuclei not much more massive than a neutron.
2. A good moderator that has a small neutron cross section, so neutrons that we need for continuous chain fission reaction will be there to induce fission reactions.

Thus, the best moderator for the first requirement would be ordinary hydrogen (H^1), since its nucleus, a proton, has the same mass as a neutron. From Table 17.1, we see that its rating on the second requirement is only a so-so situation, but it is still a reasonably good moderator as a possibility. The fact that hydrogen is a gas makes the use of water (H^2O) a more practical alternative. The additional oxygen in the water does not have any adverse effect, due to the fact that its cross section is very small.

However, the next best moderator for the first requirement above is H^2 or D for deuterium, and from Table 17.1, we see that it also passes the second requirement with flying colors. “Heavy water,” D^2O , is therefore the best moderator. But deuterium occurs in nature as only 0.015 percent of ordinary hydrogen as it can be seen in Fig. 17.1 here with the remaining 99.985 percent being H^1 , and it costs \$55 per pound of D^2O to separate it – the best moderator is very expensive [14].

As we consider other elements with few nucleons, the next attractive choice is carbon. This element is 12 times massive than neutron; thus it is heavier than we would like, but its cross section is very small, and it is an inexpensive element in terms of graphite, the material of lead pencil. The three most practical moderators are therefore “light water” H^2O , “heavy water” D^2O , and “graphite” C.

Now, we can start to see what moderators can do and what goal they achieve inside the code of a reactor of our intention here. The most desirable thing to consider would be if they could allow us the use of natural uranium, which consists of 99.3% U^{238} and 0.7% U^{235} as a reactor fuel. In the early stage and days of nuclear energy, separation of uranium isotope technologies was not available to us, and even

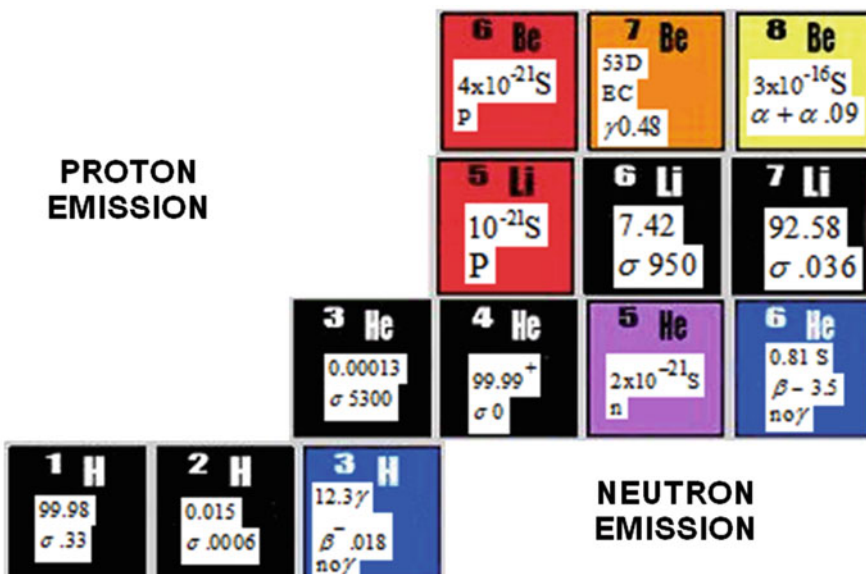


Fig. 17.1 Explanations of sample data

today this separation is difficult and expensive, so it would be quite advantageous if we could use uranium as it occurs in nature.

Furthermore, it turns out that with ordinary water as a moderator, a natural uranium reactor is *not* possible – the neutron cross section of H1 and U238, though not large per Table 17.1, is still sufficient to prevent criticality in any size or configuration [14].

However, in order to use water as the moderator, the uranium must be enriched up to a few percent U²³⁵, and in fact, that is how most present reactors are made today, i.e., Generation III and III⁺. In case of Generation IV, some of the Small Modular Reactors (SMRs) fall in this category such as the one designed by NuScale company out of Oregon in cooperation with Oregon State University (OSU); however, the drawback of such approach is that thermal efficient of this reactor is trapped under Vapor Dome of saturated steam [1, 2, 23].

The best moderator, heavy water D₂O, can easily make a natural uranium reactor critical such as the modern power reactor in Canada, namely, CANDU, which is made that way, but large amounts of deuterium were not available in the 1940s and are still very expensive.

Our third moderator, carbon, can also be used to make a natural uranium reactor critical provided the carbon is very pure and the reactor size is very large. Since this avoids the necessity of isotope separation, the first reactor and nearly all of the early reactors were made in this way.

The next concern in running a reactor in way of practical to control the rate of at which fissions take place certainly needs to be addressed as well. This is done by

inserting *control rods* made of a material with a *large* neutron cross section such as boron as indicated in Table 17.1. When they are inserted *into the reactor*, they *absorb neutrons, greatly reducing the number available to cause fissions, thereby stopping the chain reaction. As they are withdrawn, the point of criticality is reached and passed slightly. At this point of criticality is reached and passed slightly.*

At this point the fission rate – referred to as the *reactor power*, since the rate of energy release is proportional to the rate at which fission reactions occur – begins to increase. Let us consider how fast this happens. Suppose the fuel, the moderator, and the size of the reactor are such that an average of 1.005 neutrons released in a fission make another fission, if we recall that this number must be at least 1.000 for the reactor to go critical.

However, the time required for a neutron emitted in a fission to be thermalized causing another fission is about 10^{-4} s. In analogy with biological reproduction, this is called the time for one *generation* of neutrons, and in each succeeding generation, the number of neutrons increased by an additional factor of 1.005.

After 500 generations ($500 \times 10^{-4} = 0.05$), 1/20 of second, it has increased by $(1.0005)^{500} = 10.6$, so the reactor power, and hence the heat generated, increased by more than a factor of 10. Since it is not easy to move a control rod in 1/20 of a second, this seems like a very serious situation that could easily lead to mass destruction by melting [14].

The situation is mitigated by the phenomenon of delayed neutron induction. In the fission of U235, about 0.6% of the neutrons are not emitted until a half-second or more after the fission; thus the $1.005 - 0.006 = 0.999$ neutrons that are emitted promptly cannot even sustain a chain reaction let alone cause its rate to increase. Criticality now depends on the reactor power which increases by a factor of even 1.005. This situation greatly eases the control problem, but if the control rods are withdrawn to the point where 1.007 or more neutrons from each fission cause another fission, the reactor is critical on prompt neutrons alone, and the reactor power increases very rapidly. This can be a dangerous situation, and great care must be taken not to reach it.

There are some other problems before we reach to a feasible reactor, and those are cooling and shielding; however, there are other books that the reader can find to help them with details of these two problems, details that are beyond scope of this chapter. However the cooling has been detailed out throughout in a book by Zohuri [24], and for shielding readers can refer to a book by Chilton et al. [25]

This is a very basic approach to a very basic reactor and its concept, so it provides some general idea what is involved with a reactor design and of course is more complex than what it was described here.

17.2 Innovative Approach

In 2007 gas turbine combined cycle plants had a total capacity of 800 GW and represented 20% of the installed capacity worldwide. They have far exceeded the installed capacity of nuclear plants; though in the late 1990s, they had less than 5% of the installed capacity worldwide. There are number of reasons for this. First natural gas is abundant and cheap. Second combined cycle plants achieve the greatest efficiency of any thermal plant. And third, they require the least amount of waste heat cooling water of any thermal plant.

A typical gas turbine plant consists of a compressor, combustion chamber, turbine, and an electrical generator. A combined cycle plant takes the exhaust from the turbine and runs it through a heat recovery steam generator (HRSG) before exhausting to the local environment. The HRSG serves the function of the boiler for a typical closed cycle steam plant. The steam plant consists of a steam turbine, a condenser, a water pump, an evaporator (boiler), and an electrical generator. In a combined cycle plant, the gas turbine and steam turbine can be on the same shaft to eliminate the need for one of the electrical generators. However, the two shafts and two generator systems provide a great deal more flexibility at a slightly higher cost. In addition to the closed loop for the steam, an open loop circulating water system is required to extract the waste heat from the condenser. The waste heat extracted by this “circulating” water system is significantly less per megawatt for a combined cycle system as the open Brayton cycle exhausts its waste heat directly to the air.

The layout for the components of a typical combined cycle power plant is given below in Fig. 17.2.

GE currently markets a system that will produce 61% efficiency at design power and better than 60% efficiency down to 87% of design power [6] for gas turbine combined cycle plants.

An approximate efficiency can be calculated for a combined cycle power plant by the following simple argument [7].

$$\text{Brayton cycle efficiency} = \frac{W_B}{Q_{in}} = \eta_B$$

$$\text{Heat to Rankine cycle} = Q_R = (1 - \eta_B)Q_{in}$$

$$\text{Rankine cycle efficiency} = \frac{W_R}{Q_R} = \eta_R$$

$$\begin{aligned} \text{Overall efficiency} &= \frac{W_B + W_R}{Q_{in}} = \eta_T = \frac{\eta_B Q_{in} + \eta_R Q_R}{Q_{in}} \\ &= \frac{\eta_B Q_{in} + \eta_R (1 - \eta_B) Q_{in}}{Q_{in}} = \eta_B + \eta_R - \eta_B \eta_R \end{aligned}$$

$$\eta_T = \eta_B + \eta_R - \eta_B \eta_R$$

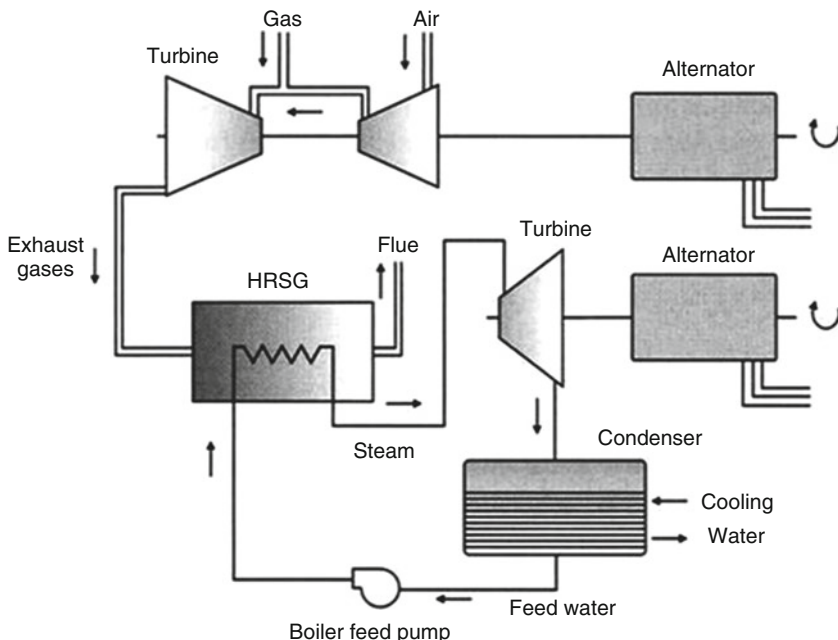


Fig. 17.2 Typical gas turbine combined cycle power plant

This efficiency must be corrected for pressure losses and assumes that all the heat in the Brayton exhaust is used in the heat recovery steam generator (HRSG). For a combustion gas turbine, this is not usually possible if condensation of the water in the exhaust products is to be avoided. The detailed models developed in this effort give a more accurate answer.

For the nuclear reactor system, the heat transfer is in the opposite direction. All reactor components and fluids in the primary and secondary loops must be at a higher temperature than the peak temperature of the gas exiting the heat exchanger. This severely restricts the peak temperature that can be achieved for the air entering the turbine. However, all is not lost.

In a typical combustion system, there are pressure losses approaching 5% of the total pressure to complete the combustion process [8]. Heat exchangers can be built with significantly lower pressure drops than 5% approaching 1% [8]. Therefore, the most straightforward method to overcome this severe temperature limitation is to borrow a technique from steam power plants and implement multiple reheat cycles. That is the first heat exchanger heats the air to its peak temperature. Then the air is expanded through the first turbine. The air is then reheated to the same peak temperature and expanded through the second turbine. Based on the relative pressure losses that appear possible, up to five turbines might be considered. All five turbines will be driving the same compressor. Multiple compressors on concentric shafts driven by different sets of turbines might be possible, but that has not been considered here.

For a nuclear system to take advantage of combined cycle technology, there are many numbers of changes to the plant components that must be made. The most significant of course is that the combustion chamber must be replaced by a heat exchanger in which the working fluid from the nuclear reactor secondary loop is used to heat the air. The normal Brayton cycle is an internal combustion one where the working fluid is heated by the combustion of the fuel with the air in the combustion chamber. The walls of the combustion chamber can be cooled and peak temperatures in the working fluid can be significantly above the temperature that the walls of the chamber can tolerate for any length of time.

17.3 Methodology of Combined Cycle

The approach taken in the combined cycle (CC) code developed for this effort is to model the thermodynamics of the components making up the power conversion systems as real components with non-ideal efficiencies. Pressure drops are included for every component except the connected piping. The compressor design is modeled with a small stage polytropic efficiency to take into account state-of-the-art designs. The gas turbines are likewise modeled with a polytropic efficiency. The steam turbines are modeled with a simple overall thermal efficiency. Pressure drops in each of the heat exchangers are included. The input files specify the pressure drops, and the heat exchangers are designed to meet these specifications if possible [9].

Some scientists are calling the nuclear power plants' source of energy as 100 percent renewable energy, and of course environmentalists arguably are saying that it is a wrong approach, just because in the core of these plants, there exists uranium or plutonium as fuel when we are talking about fission-type nuclear power plants that they exist in grid today and producing electricity to the net. However, on the other side of spectrum, researchers and scientist at national laboratories and universities around the globe that are working toward fusion program to achieve a breakeven passionately argue that nuclear power plants of fusion type are totally clean so long as the source of energy come in form of two hydrogen isotopes such as deuterium (D) and tritium (T) as source of fusion reaction and driving energy from it.

This is a dream that is too far away from reality of today's need and demand for electricity yet is not out of scope of near future. Physics of Plasma for driving energy via Inertial Confinement Fusion (ICF) [10] or Magnetic Confinement Fusion (MCF) [11] is in agreement with such innovative approaches.

17.4 Why We Still Need Nuclear Power

Nuclear power's track record of providing clean and reliable electricity compares favorably with other energy sources. Low natural gas prices, mostly the result of newly accessible shale gas, have brightened the prospects that efficient gas-burning power plants could cut emissions of carbon dioxide and other pollutants relatively quickly by displacing old, inefficient coal plants, but the historical volatility of natural gas prices has made utility companies wary of putting all their eggs in that basket. Besides, in the long run, burning natural gas would still release too much carbon dioxide. Wind and solar power are becoming increasingly widespread, but their intermittent and variable supply make them poorly suited for large-scale use in the absence of an affordable way to store electricity. Hydropower, meanwhile, has very limited prospects for expansion in the United States because of environmental concerns and the small number of potential sites.

The United States must take a number of decisions to maintain and advance the option of nuclear energy. The NRC's initial reaction to the safety lessons of Fukushima must be translated into action; the public needs to be convinced that nuclear power is safe. Washington should stick to its plan of offering limited assistance for building several new nuclear reactors in this decade, sharing the lessons learned across the industry. It should step up its support for new technology, such as SMRs and advanced computer-modeling tools. And when it comes to waste management, the government needs to overhaul the current system and get serious about long-term storage. Local concerns about nuclear waste facilities are not going to magically disappear; they need to be addressed with a more adaptive, collaborative, and transparent waste program.

These are not easy steps, and none of them will happen overnight. But each is needed to reduce uncertainty for the public, the energy companies, and the investors. A more productive approach to developing nuclear power – and confronting the mounting risks of climate change – is long overdue. Further delay will only raise the stakes.

17.5 Is Nuclear Energy Renewable Source of Energy

Assuming for time being we are taking fission reaction as foundation for present (GEN-III) and future (GEN-IV) nuclear power reactors, as source nuclear energy source to somewhat degree, we can argue it is a clean source of energy.

Although nuclear energy is considered clean energy, its inclusion in the renewable energy list is a subject of major debate. To understand the debate, we need to understand the definition of renewable energy and nuclear energy first. However, until we manage through future technology of these fission reactors to manage to bring down the price electricity per kilowatt hours driven by fusion energy down to the point of those by gas or fossil fuels, there is no chance to push these reactors beyond GEN-III.

However, efforts toward reduction price of electricity driven by nuclear fission power plants, especially using some innovative design of GEN-IV plants with high temperature baseline in conjunction with some thermodynamics cycles such as Brayton and Rankine, are on the way by so many universities and national laboratory such as Idaho National Laboratory and Universities such as MIT, UC Berkeley, and University of New Mexico as well as this author.

Renewable energy is defined as an energy source/fuel type that can regenerate and can replenish itself indefinitely. The five renewable sources used most often are biomass, wind, solar, hydro-, and geothermal.

Nuclear energy on the other hand is a result of heat generated through the fission process of atoms. All power plants convert heat into electricity using steam. At nuclear power plants, the heat to make the steam is created when atoms split apart – called fission. The fission releases energy in the form of heat and neutrons. The released neutrons then go on to hit other neutrons and repeat the process, hence generating more heat. In most cases the fuel used for nuclear fission is uranium.

One question we can raise here in order to further understand whether or not we need to present nuclear technology as a source of energy is that:

What is the difference between clean energy and renewable energy? Put another way, why is nuclear power in the doghouse when it comes to revamping the nation's energy mix?

The issue has come to the forefront the time during the debate over the Waxman-Markey energy and climate bill and its provisions for a national renewable energy mandate.

To simply put it, Republicans have tried and failed several times to pass amendments that would christen nuclear power as a “low-emissions” power source eligible for all the same government incentives and mandates as wind power and solar power.

Many environmental groups are fundamentally opposed to the notion that nuclear power is a renewable form of energy – on the grounds that it produces harmful waste by-products and relies on extractive industries to procure fuel like uranium.

Even so, the nuclear industry and pronuclear officials from countries including France have been trying to brand the technology as renewable, on the grounds that it produces little or no greenhouse gases. Branding nuclear as renewable could also enable nuclear operators to benefit from some of the same subsidies and friendly policies offered to clean energies like wind, solar, and biomass.

So far, however, efforts to categorize nuclear as a renewable source of power are making little headway.

The latest setback came in around August of 2009, when the head of the International Renewable Energy Agency (IRENA) – an intergovernmental group known as IRENA that advises about 140-member countries on making the transition to clean energy – dismissed the notion of including nuclear power among its favored technologies.

“IRENA will not support nuclear energy programs because it’s a long, complicated process, it produces waste and is relatively risky,” Hélène Pelosse, its interim director general, told in general.

Energy sources like solar power, Ms. Pelosse said, are better alternatives – and less expensive ones – “especially with countries blessed with so much sun for solar plants,” she said it in 2009.

17.6 Argument for Nuclear Power as Renewable Energy Source

Most supporters of nuclear energy point out the low carbon emission aspect of nuclear energy as its major characteristic to be defined as renewable energy. According to nuclear power opponents, if the goal to build a renewable energy infrastructure is to lower carbon emission, then there is no reason for not including nuclear energy in that list [12].

But one of the most interesting arguments for including nuclear energy in the renewable energy portfolio came from Bernard L Cohen, former professor at University of Pittsburgh. Professor Cohen defined the term “indefinite” (time span required for an energy source to be sustainable enough to be called renewable energy) in numbers by using the expected relationship between the sun (source of solar energy) and the earth. According to Professor Cohen, if the uranium deposit could be proved to last as long as the relationship between the earth and sun is supposed to last (5 billion years), then nuclear energy should be included in the renewable energy portfolio [13].

In his paper Professor Cohen claims that using breeder reactors (nuclear reactor able to generate more fissile material than it consumes), it is possible to fuel the earth with nuclear energy indefinitely. Although the amount of uranium deposit available could only supply nuclear energy for about 1000 years, Professor Cohen believes that the actual amount of uranium deposit available is way more than what is considered extractable right now. In his arguments he includes uranium that could be extracted at a higher cost, uranium from the sea water, and also uranium from eroding earth crust by river water. All of those possible uranium resources if used in a breeder reactor would be enough to fuel the earth for another 5 billion years and hence renders nuclear energy as renewable energy.

17.7 Argument Against Nuclear Power as a Renewable Energy Source

One of the biggest arguments against including nuclear energy in the list of renewables is the fact that uranium deposit on earth is finite, unlike solar and wind. To be counted as renewable, the energy source (fuel) should be sustainable for an indefinite period of time according to the definition of renewable energy.

Another major argument proposed by the opponents of including nuclear energy as renewable energy is the harmful nuclear waste from nuclear power reactors. The nuclear waste is considered as a radioactive pollutant that goes against the notion of a renewable energy source. Yucca Mountain is one of the examples used quite often to prove this point. Most of the opponents in the United States also point at the fact that while most renewable energy source could render the US energy independent, uranium would still keep the country energy dependent as the United States would still have to import uranium.

In conclusion, experts disagree about the future of nuclear power.

- *Proponents of Nuclear Power.*
 - Fund more research and development.
 - Pilot plant testing of potentially cheaper and safer reactors.
 - Test breeder fission and nuclear fusion.
- *Opponents of Nuclear Power.*
 - Fund rapid development of energy efficient and renewable energy resources.

In general, the above bolt points are what we consider as *advantages* and *disadvantages* of nuclear energy.

17.8 Safety

With the aftermath of the major accidents at Three Mile Island in 1979 and Chernobyl in 1986 and then recent devastated Japan's Fukushima nuclear power plant frailer in Japan in March of 2011, pretty much nuclear power fell out of favor, and some countries applied the brakes to their nuclear programs. Concerns about climate change and air pollution, as well as growing demand for electricity, led many governments to reconsider their aversion to nuclear power, which emits little carbon dioxide and had built up an impressive safety and reliability record. Some countries reversed their phaseouts of nuclear power, some extended the lifetimes of existing reactors, and many developed plans for new ones.

Despite all these given concerns and issues in respect to the nuclear energy, still we are facing the fact of why we still need nuclear power as clean source of energy, particularly when we deal with renewable source of energy arguments [5].

Today, roughly 60 nuclear plants are under construction worldwide, which will add about 60,000 megawatts of generating capacity – equivalent to a sixth of the world's current nuclear power capacity – however, this movement has been lost after March of 2001 and Japan's Fukushima nuclear power episode.

Nuclear power's track record of providing clean and reliable electricity compares favorably with other energy sources. Low natural gas prices, mostly the result of newly accessible shale gas, have brightened the prospects that efficient gas-burning power plants could cut emissions of carbon dioxide and other pollutants relatively quickly by displacing old, inefficient coal plants but the historical volatility of

natural gas prices has made utility companies wary of putting all their eggs in that basket. Besides, in the long run, burning natural gas would still release too much carbon dioxide. Wind and solar power are becoming increasingly widespread, but their intermittent and variable supply make them poorly suited for large-scale use in the absence of an affordable way to store electricity.

Hydropower, meanwhile, has very limited prospects for expansion in the United States because of environmental concerns and the small number of potential sites [15].

Part of any nuclear power plant safety that one should consider as part of design and operation of such source of energy is the reactor stability. Understanding time-dependent behaviors of nuclear reactors and the methods of their control is essential to the operation and safety of nuclear power plants. Zohuri [13] provides researchers and engineers in nuclear engineering very general yet comprehensive information on the fundamental theory of nuclear reactor kinetics and control and the state-of-the-art practice in actual plants, as well as the idea of how to bridge the two. The dynamics and stability of engineering equipment that affects their economical and operation from safety and reliable operation point of view. In Chap. 13 of this book, we will talk about the existing knowledge that is today's practice for design of reactor power plants and their stabilities as well as available techniques to designers. Although, stable power processes are never guaranteed. An assortment of unstable behaviors wrecks power apparatus, including mechanical vibration, malfunctioning control apparatus, unstable fluid flow, unstable boiling of liquids, or combinations thereof. Failures and weaknesses of safety management systems are the underlying causes of most accidents [16].

The safety and capital cost challenges involved with traditional nuclear power plants may be considerable, but a new class of reactors in the development stage holds promise for addressing them. These reactors, called small modular reactors (SMRs), produce anywhere from 10 to 300 megawatts, rather than the 1000 megawatts produced by a typical reactor. An entire reactor, or at least most of it, can be built in a factory and shipped to a site for assembly, where several reactors can be installed together to compose a larger nuclear power station. SMRs have attractive safety features, too. Their design often incorporates natural cooling features that can continue to function in the absence of external power and the underground placement of the reactors and the spent fuel storage pools is more secure.

Since Small Modular Reactors (SMRs) are smaller than conventional nuclear plants, the construction costs for individual projects are more manageable, and thus the financing terms may be more favorable. And because they are factory assembled, the on-site construction time is shorter. The utility company can build up its nuclear power capacity step by step, adding additional reactors as needed, which means that it can generate revenue from electricity sales sooner. This helps not only the plant owner but also customers, who are increasingly being asked to pay higher rates today to fund tomorrow's plants [17, 18].

With the US federal budget under tremendous pressure, it is hard to imagine taxpayers funding demonstrations of a new nuclear technology. But if the United States takes a hiatus from creating new clean-energy options – be it SMRs,

renewable energy, advanced batteries, or carbon capture and sequestration – Americans will look back in 10 years with regret. There will be fewer economically viable options for meeting the United States' energy and environmental needs, and the country will be less competitive in the global technology market.

Today, nationwide there are about 100 nuclear power plants are operational in United States and just about 400 worldwide that, they all, altogether using mostly Light Water Reactor technologies. With the benefit of experience and improved plan toward more advanced design that are getting ready to go into operation as part of Gen-III+, the performance has improved over time to provide better efficiency as well as unit *capacity factor* of 90% and higher at least in the United States.

Bear in mind that capacity factor is the ratio of actual annual plant electrical production and maximum annual production capability, while worldwide capacity factors are around 75% which are lower than those recently achieved in the United States; a similar trend of improved capacity factors is observed outside of the United States as well.

Thus, as part of safe operations of the entire nuclear fuel cycle are a parameter of concern and this section we touched upon some of them in above, which should be included the continuation of training personnel for nuclear operations, the threat of terrorist attack as part of nonproliferation and proliferation nuclear plant coming on line or exiting one is concern, as well as nuclear fuel cycle safety, including nuclear fuel reprocessing of these plants [19].

As part of nuclear power installation safety concerns, we need to take under consideration the infiltration of domestic or international terrorist attack into these facilities and installation. On the one hand, experts have concluded that civil works and security provisions make nuclear plants hard targets. On the other hand, the hazards are on a scale previously considered to be extremely rare in evaluation of severe reactor accidents. The question is: What new security measures, if any, are appropriate? We believe there is no simple, one-size-fits-all answer. It depends on many factors including threat evaluation, plant location, facility design, and government security resources and practices. Thus, nuclear plant safety is a good starting point for the evaluation of security risk [19].

Nuclear plant safety has considered natural external events, such as earthquakes, tornadoes, floods, and hurricanes. Terrorist attack by fire or explosion is analogous to external natural events in its implication for damage and release of radioactivity. The strength of containment buildings and structures presents a major obstacle and hardened target for attack.

The Electric Power Research Institute (EPRI) [26] carried out an evaluation of aircraft crash and Nuclear Power Plant (NPP) structural strength, concluding that US containments would not be breached.

The US NRC is performing its own evaluation, including structural testing at Sandia National Laboratory (SNL), not yet complete. A broad survey and evaluation of hazards and protective actions are in order to make decisions on adequate protection. Such a survey must begin by identifying possible modes of attack and vulnerabilities associated with designs and locations. It must also identify the cost-effectiveness of a range of security options for new designs, old plants near decommissioning, and plants in mid-life. There is also a need for sharing

information with governments of countries and supporting institutions that will undertake nuclear power programs in order to provide effective intelligence and security.

17.9 Fuel Cycle

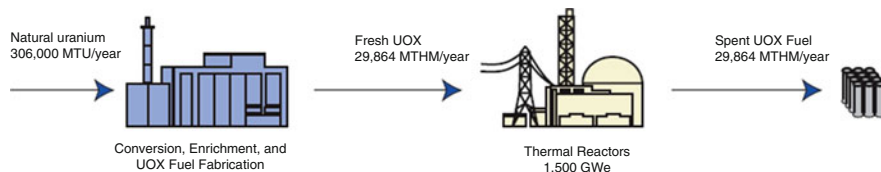
The description of a possible global growth scenario for nuclear power with 1000 or so GWe deployed worldwide must begin with some specification of the nuclear fuel cycles that will be in operation. The nuclear fuel cycle refers to all activities that occur in the production of nuclear energy.

Realization of the global growth scenario entails construction and operation of many fuel cycle facilities around the world. It is important to emphasize that producing nuclear energy requires more than a nuclear reactor steam supply system and the associated turbine generator equipment required to produce electricity from the heat created by nuclear fission. The process includes ore mining, enrichment, fuel fabrication, waste management and disposal, and finally decontamination and decommissioning of facilities. All steps in the process must be specified, because each involves different technical, economic, safety, and environmental consequences. A vast number of different fuel cycles appear in the literature [27], and many have been utilized to one degree or another.

We can find two types of classes to the approach to *separation analysis of fuel cycle*, namely, “open,” demonstrated in Fig. 17.3, and “closed,” demonstrated in Fig. 17.4, and each one is described below.

In open class fuel cycle or once-through fuel cycle, the spent fuel discharged from the reactor is treated as waste (see Fig. 17.3).

Current Burnup: 50 GWD/MTIHM:



High Burnup: 100 GWD/MTIHM:

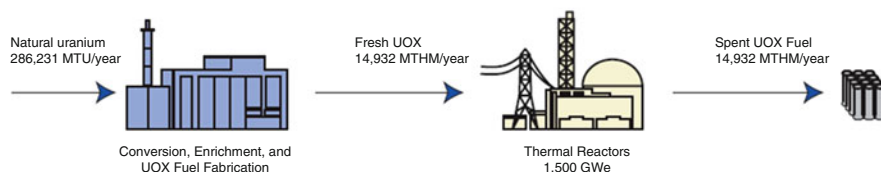


Fig. 17.3 Open fuel cycle: Once-through fuel (projected to 2050 [19])

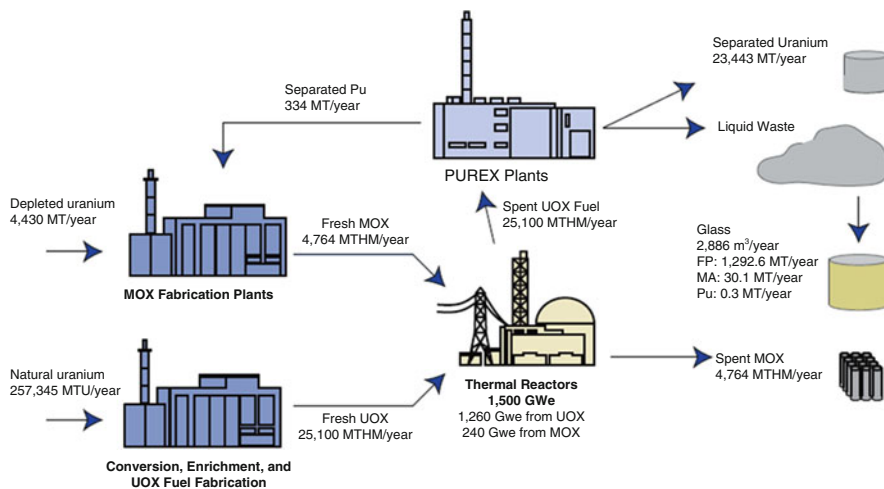


Fig. 17.4 Closed fuel cycle: plutonium recycle (MOX option – one recycle) (projected to 2050 [19])

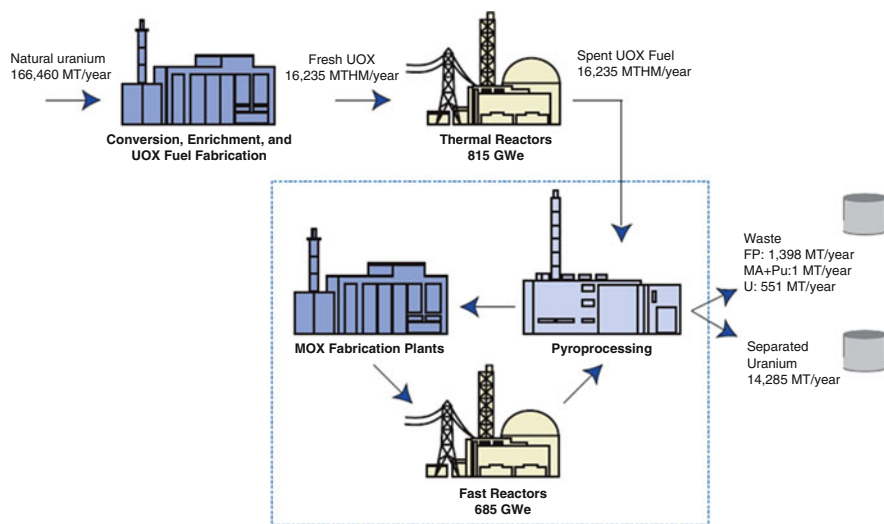


Fig. 17.5 Closed fuel cycle: full actinide recycle (projected to 2050 [19])

In the closed class fuel cycle today, the spent fuel discharged from the reactor is *reprocessed*, and the products are partitioned into uranium (U) and plutonium (Pu) suitable for fabrication into oxide fuel or mixed oxide (MOX) fuel for recycle back into a reactor as illustrated in Fig. 17.4.

The rest of the spent fuel is treated as high-level waste (HLW). In the future, closed fuel cycles could include use of a dedicated reactor that would be used to transmute selected isotopes that have been separated from spent fuel (see Fig. 17.5).

The dedicated reactor also may be used as a breeder to produce new fissile fuel by neutron absorption at a rate that exceeds the consumption of fissile fuel by the neutron chain reaction. Several countries have explored breeder reactors, notably the United States, France, Russia, Japan, and India.

In a situation depicted in Fig. 17.5, a fuel cycle, the waste stream will contain less actinides (i.e., minor actinides are americium (Am), neptunium (Np), and curium (Cm)), which will significantly reduce the long-term radioactivity of the nuclear waste. There are still other options, such as using an accelerator to produce neutrons in subcritical assembly.

However, in general comparing these two classes of fuel cycle open and closed, each one has its own pros and cons, and in summary they can be described here.

We expect the once-through fuel cycle to have an advantage in terms of cost and proliferation resistance (since there is no reprocessing and separation of actinides), compared to the closed cycle. Closed cycles have an advantage over the once-through cycle in terms of resource utilization (since the recycled actinides reduce the requirement for enriched uranium), which in the limit of very high ore prices would be more economical. Some argue that closed cycles also have an advantage for long-term waste disposal, since long-lived actinides can be separated from the fission products and transmuted in a reactor. Our analysis below is focused on these key comparisons.

Both once-through and closed cycles can operate on uranium or Th fuel and can involve different reactor types, e.g., light water reactors (LWRs), heavy water reactors (HWRs), supercritical water reactors (SCWRs), high-temperature and very high-temperature gas-cooled reactors (HTGRs), liquid-metal fast-breeder reactors (LMFRs) and gas fast reactors (GFRs), or molten salt reactors (MSR) of various sizes.

Today, almost all deployed reactors are of the LWR type. The introduction of new reactors or fuel cycles will require considerable development resources and some period of operating experience before initial deployment. Reference [19] at the end of this chapter provides more details, in worldwide current characteristic for fuel cycle with deployed nuclear power plant and reader should refer to this reference.

In summary, the nuclear fuel cycle is summarized here as:

- The nuclear fuel cycle is the series of industrial processes which involve the production of electricity from uranium in nuclear power reactors.
- Uranium is a relatively common element that is found throughout the world. It is mined in a number of countries and must be processed before it can be used as fuel for a nuclear reactor.
- Fuel removed from a reactor, after it has reached the end of its useful life, can be reprocessed so that most is recycled for new fuel.

The various activities associated with the production of electricity from nuclear reactions are referred to collectively as the nuclear fuel cycle. The nuclear fuel cycle starts with the mining of uranium and ends with the disposal of nuclear waste. With the reprocessing of used fuel as an option for nuclear energy, the stages form a true cycle.

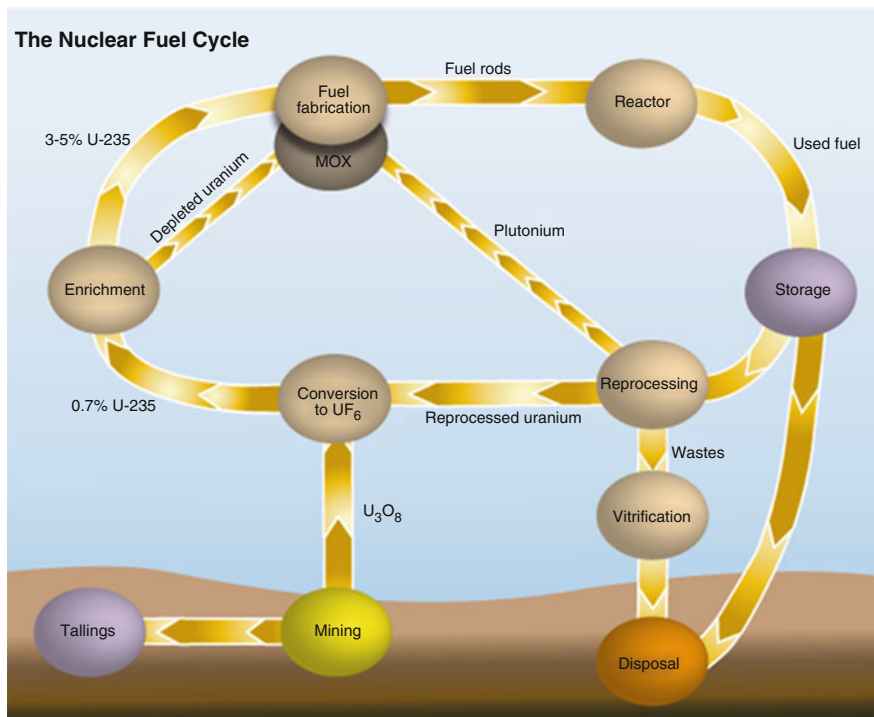


Fig. 17.6 The nuclear fuel cycle. (Courtesy of World Nuclear Association)

To prepare uranium for use in a nuclear reactor, it undergoes the steps of mining and milling, conversion, enrichment, and fuel fabrication. These steps make up the “front end” of the nuclear fuel cycle.

After uranium has spent about 3 years in a reactor to produce electricity, the used fuel may undergo a further series of steps including temporary storage, reprocessing, and recycling before wastes are disposed. Collectively these steps are known as the “back end” of the fuel cycle (see Fig. 17.6).

Figure 17.6 demonstration is based on the following assumptions: enrichment to 4.5% U^{235} with 0.22% tails assay, hence 182,000 SWU (separative work units) of enrichment needed (one SWU requires about 50 kWh of electricity at an enrichment plant); refueling so that 24.3 tU/yr. is replaced annually (or 36.5 tU every 18 months) for core load 73 tU; operation, 45,000 MWday/t (45 GWd/t) burnup; and 33% thermal efficiency.

In fact, a nuclear power reactor cannot be expected to run at 100% load factor – 90% is more typical for good performance – so an output of around 7.9 TWh/yr. is more realistic, but this simply means scaling back the inputs accordingly, e.g., to 190 tU/yr. or 147 tU/yr., for the modern unit.

With the higher (5%) enrichment and burnup in the second (AP1000 or EPR) set of figures, enrichment input rises to 198,000 SWU. In the used fuel, transuranic and fission product numbers will be slightly lower due to high thermal efficiency.

Canadian figures for tU/GWe/yr. suggest slightly lower uranium requirements and utilization for PHWRs than for light water reactors. An International Atomic Energy Agency technical report [1] gives 157 tU at typical 7.5 GWd/t burnup and 31% thermal efficiency, or 142 tU at 90% capacity factor, hence 80% of the input compared with a typical LWR above. This is 17.9 tU/TWh.

Considering just how much of the original uranium is actually used, 0.7% fissile U^{235} is in natural U (Unat), on above “typical” figures: 0.49% of Unat goes into fuel as the fissile part, 0.394% is actually fissioned, and in addition about half that much U^{238} turned into Pu^{239} is fissioned, giving about a 0.6% utilization of the original Unat.

With the EPR figures: 0.538% of Unat goes into fuel as the fissile part, 0.452% of that is actually fissioned, and in addition about half that much U^{238} turned into Pu^{239} is fissioned, giving about a 0.67% utilization of the original Unat.

In conclusion, Nuclear power has unresolved challenges in long-term management of radioactive wastes. A critical factor for the future of an expanded nuclear power industry is the choice of the fuel cycle – what type of fuel is used and what types of reactors “burn” the fuel – and the method of disposal of spent fuel.

17.10 Nuclear Power Economics

Developments in the US economy that will affect the nuclear power industry in the coming years include the emergence of new nuclear technologies, waste disposal issues, proliferation concerns, the streamlining of nuclear regulation, a possible transition to a hydrogen economy, policies toward national energy security, and environmental policy. These developments will affect both the competitiveness of nuclear power and appropriate nuclear energy policies, and particularly, countries like Germany has totally shutting down their nuclear power generating electricity while moving toward coal power plant to subsidize for their need for electricity. Poor economics has been another driving factor and forces behind this move away from nuclear power [28].

Investments in commercial nuclear generating facilities will only be forthcoming if investors expect the cost of producing electricity using nuclear power will be lower than the risk-adjusted costs associated with alternative electric generation technologies. Since nuclear power plants have relatively high capital costs and very low marginal operating costs, nuclear energy will compete with alternative electricity generation sources for “baseload” (high load factor) operation. We recognize that over the next 50 years, some significant but uncertain fraction of incremental electricity supplies will come from renewable energy sources (e.g., wind) either because these sources are less costly than alternatives or because government policies (e.g., production tax credits, high mandated purchase prices, and renewable energy portfolio standards) or consumer choices favor renewable energy investments. Despite the efforts to promote renewable energy options, however, it is likely that a large fraction of the incremental and replacement investments in electric

generating capacity needed to balance supply and demand over the next 50 years will, in the absence of a nuclear generation option, rely on fossil fuels – primarily natural gas or coal. This is particularly likely in developing countries experiencing rapid growth in income and electricity consumption. Accordingly, we focus on the costs of nuclear power compared to these fossil fuel generating alternatives in baseload applications [19].

Any analysis of the costs of nuclear power must take into account a number of important considerations. First, all of the nuclear power plants operating today were developed by state-owned or state-regulated investor-owned vertically integrated utility monopolies. Although, in the United States and the United Kingdom, some nuclear plants were subsequently sold or transferred to merchant generating electricity companies, many developed countries and an increasing number of developing countries are in the process of moving away from an electric industry structure built upon vertically integrated regulated monopolies to an industry structure that relies primarily on competitive generation power plant investors.

We assume that in the future, nuclear power will have to compete with alternative generating technologies in competitive wholesale markets – as merchant plants – where these plants sell their output under short-, medium-, and longer-term supply contracts negotiated competitively with distribution companies, wholesale and retail market. The power plant developers take on permitting development, construction cost, and operating performance risks but may transfer some or all risks associated with market price volatility to buyers for a price through the terms of their contracts.

These changes in the structure of the electric power sector have important implications for investment in generating capacity. Under traditional industry and regulatory arrangements, many of the risks associated with construction costs, operating performance, fuel price changes, and other factors were borne by consumers rather than suppliers. It is often assumed that regulated monopolies were subject to “cost-plus” regulation which insulated utilities from all of these risks. This is an extreme and inaccurate characterization of the regulatory process, at least in the United States. Several US utilities were faced with significant cost disallowances associated with nuclear power plants; they completed or abandoned a result inconsistent with pure cost-plus regulation. Nevertheless, it is clear that a large fraction of these cost and market risks were shifted to consumers from investors when the industry was governed by regulated monopolies.

The insulation of investors from many of these risks necessarily had significant effects on the cost of capital they used to evaluate alternative generation options and on whether and how they took extreme contingencies into account. Specifically, the process reduced the cost of capital and led investors to give less weight to regulatory (e.g., construction and operating licenses) and construction cost uncertainty, operating performance uncertainties and uncertainties associated with future oil, gas, and coal prices than if they had to bear these cost and performance risks.

The commercial/civilian nuclear industry has been in operation for over 50 years so far. During such a long period of time, it would be a usual and natural normal process for technological improvement cycle and experience to result in learning and subsequently to enhancement in economic efficiency, when it comes to deal with

new generation of these power plants known as Generation IV. However, the nuclear industry has not followed this pattern except in past few years that we start seeing some innovative approaches suggested by some experts in this field in particular, in Advanced Modular Reactors (AMRs), including these authors [29, 30].

With these considerations in mind, we now proceed to examine the relative costs of new nuclear power plants, pulverized coal plants, and Combined Cycle Gas Turbine (CCGT) plants in baseload operations in the United States. The combined open-air Brayton cycle has been suggested by this authors and colleagues as an innovative solution to nuclear power plants of SMRs as well [29, 30].

Note that also, we are not considering competition between new nuclear plants and existing coal and gas plants, whose construction costs are now sunk costs. We recognize that there may be economical opportunities to increase the capacity of some existing nuclear plants and to extend their commercial lives. We do not consider these opportunities here.

The analysis is not designed to produce precise estimates either, but rather a “reasonable” range of estimates under a number of different assumptions reflecting uncertainties about future construction and operating costs. Similar analysis for Europe and especially Japan and Korea would be somewhat more favorable to nuclear power plants since gas and coal costs are typically higher than in the United States.

Elements associated as variables that are driving the function of nuclear power economics are listed below and they are as follows.

1. Rising Construction Costs

Country after country are encountering that the nuclear construction programs are getting to be over the budget considerably, in the United States, an assessment of 75 of the country’s reactors predicting costs to be as high as \$45 billion; however, the real costs were almost over tripled, and they got to be around \$145 billion, and in some countries such as India, the cost of completion for 10 reactors was averaged at least 300% over budget. Figure 17.7 Is an illustration of history of timeline cost overruns.

2. Rising Construction Time

The average construction time for nuclear power plants has also increased from 66 months for end-to-end completions in at least mid-1970s to almost 116 months, roughly speaking equivalent of 10 years’ time period for similar in completions projects between 1995 and 2000.

3. Falling Construction Demand

Presently, there 50 nuclear reactors worldwide are under construction and out of that 2 of them are in the United States. Figure 17.8, Statistically, shows the number of under construction nuclear reactors worldwide as of February 2018, by country. There were 18 nuclear reactors under construction in China, compared to the two reactors in the United States that are currently being built.

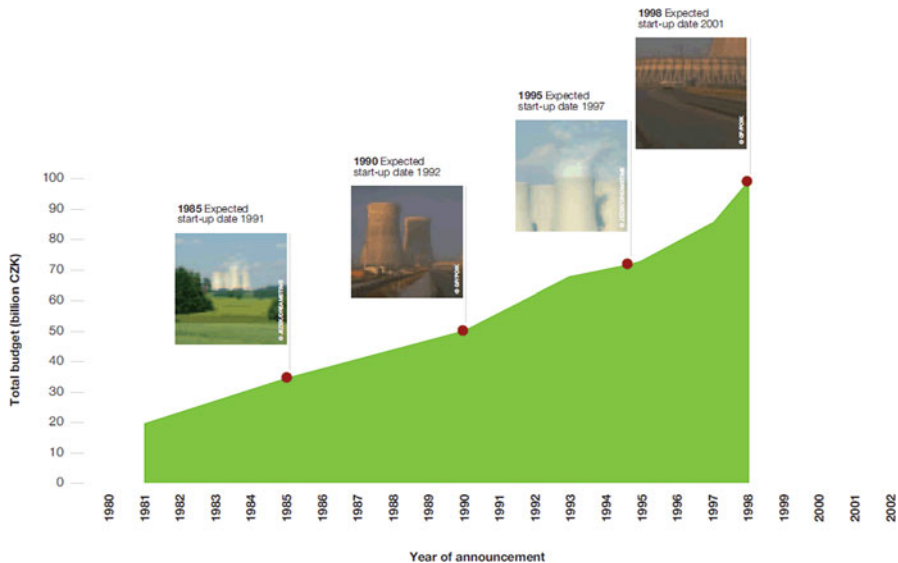


Fig. 17.7 History of timeline cost overrun

Construction started on five of the reactors over 20 years ago, and consequently the likelihood of the reactors being built to their current timetable is open to question.

There are a further 14 reactors on which construction has started but is currently suspended, 10 of which are in central and Eastern Europe. This low level of nuclear construction provides little relevant experience on which to build confidence in cost forecasts [28].

4. Untested Technology

The nuclear industry is promoting a new generation of reactors (Generation III and III+) and hoping that a wave of orders will be placed for them in the next few years. Also at least, at design stage, some nuclear manufacturers are looking at six different and major types of generation IV, which are briefly listed in Table 17.2 here as well.

Generation III+ Reactors: No Generation III+ plant has yet been completed and only one is under construction. The most widely promoted of these latest designs are the new generation of Pressurized Water Reactors (PWRs) and in particular Areva's European Pressurized Water Reactor (EPR) and the Westinghouse AP1000.

Among them are considered as Advance Small Modular Reactors (ASMRs), and they are the focus of this book as well, namely:

- (a) Molten salt reactor (MSR) system.
- (b) Sodium-cooled fast reactor (SFR) system.
- (c) Very high temperature reactor (VHTR) system.

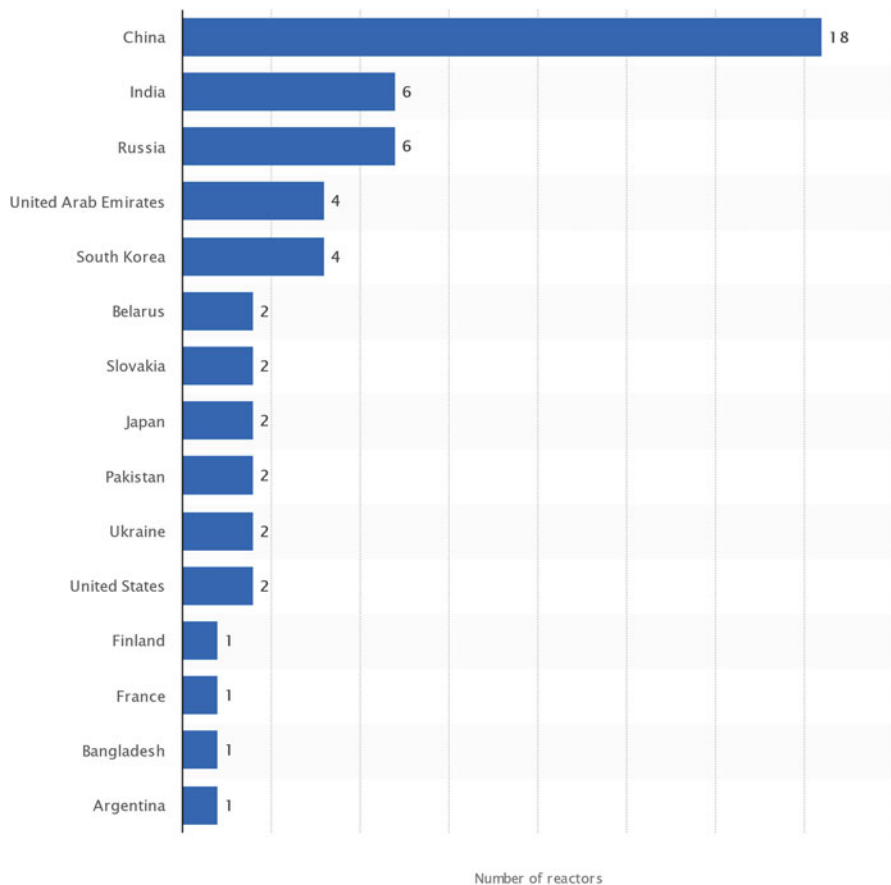


Fig. 17.8 Number of under construction nuclear reactors worldwide as of February 2018, by country

The nuclear present technology is up on Generation III and going forward with built up of Generation III+ reactors, and each are described here as follows:

Generation III reactors: The only generation III reactors currently in operation are the advanced boiling water reactors (ABWR) developed in Japan. By the end of 2006, four ABWR were in service and two under construction in Taiwan. Total construction costs for the first two units were well above the forecast range.

Generation IV reactors: Even more speculative are the “paper” designs for Generation IV plutonium-fueled reactors. While several designs are being produced, technical difficulties make it unlikely that they will be deployed for at least two decades, if at all, while the economics of fuel reprocessing also remains unproven.

Table 17.2 Six major designs of the Generation IV international program

GFR – Gas-cooled fast reactor system: The GFR system is a helium-cooled reactor with fast-neutron spectrum and closed fuel cycle. It uses helium as coolant, due to extreme temperatures (850 °C outlet; compared to 300 °C for PWRs and 500 °C for FBRs). Consequently, “high temperatures and extreme radiation conditions are difficult challenges for fuels and materials.” it will use plutonium and burn actinides

LFR – Lead-cooled fast reactor system: LFR systems are reactors cooled by liquid metal (lead or lead/bismuth) with a fast-neutron spectrum and closed fuel cycle system. A full actinide recycle fuel cycle with central or regional facilities is envisaged. A wide range of unit sizes is planned, from “batteries” of 50–150 MWe, and modular units of 300–400 MWe, to large single plants of 1200 MWe. The LFR battery option is a small factory-built turnkey plant with very long core life (10–30 years). It is designed for small grids and for developing countries that may not wish to deploy a fuel cycle infrastructure. Among the LFR concepts, this battery option is regarded as the best, concerning fulfilment of Generation IV goals. However, it also has the largest research needs and longest development time

MSR – Molten salt reactor system: The MSR system is based on a thermal neutron spectrum and a closed fuel cycle. The uranium fuel is dissolved in the sodium fluoride salt coolant that circulates through graphite core channels. The heat, directly generated in the molten salt, is transferred to a secondary coolant system and then through a tertiary heat exchanger to the power conversion system. It is primarily envisioned for electricity production and waste burn-down. The reference plant has a power level of 1000 MWe. Coolant temperature is 700 °C at very low pressure. Of all six reactor systems, MSR requires the highest costs for development (\$1bn)

SCWR – Supercritical-water-cooled reactor system: The SCWRs are high-temperature, high-pressure water-cooled reactors that operate above the thermodynamic critical point of water (i.e., at pressures and temperatures at which there is no difference between liquid and vapor phase). The reference plant has a 1700 MWe power level, an operating pressure of 25 MPa, and a reactor outlet temperature of 550 °C. Fuel is uranium oxide

SFR – Sodium-cooled fast reactor system: The SFR system consists of a fast-neutron reactor and a closed fuel cycle system. There are two major options: One is a medium size (150–500 MWe) reactor with metal alloy fuel, supported by a fuel cycle based on pyrometallurgical reprocessing in collocated facilities. The second is a medium to large (500–1500 MWe) reactor with MOX fuel, supported by a fuel cycle based upon advanced aqueous reprocessing at a centralized location serving a number of reactors. According to GIF, the SFR has the broadest development base of all the Generation IV concepts.

VHTR – Very high temperature reactor system: The VHTR system uses a thermal neutron spectrum and a once-through uranium fuel cycle. The reference reactor concept has a 600 MWth graphite-moderated helium-cooled core based on either the prismatic block fuel of the GT-MHR or the pebble bed of the PBMR

5. *Unfavorable Market Place*

The economics of nuclear power have always been questionable. The fact that consumers or governments have traditionally borne the risk of investment in nuclear power plants meant that utilities were insulated from these risks and were able to borrow money at rates reflecting the reduced risk to investors and lenders.

However, following the introduction of competitive electricity markets in many countries, the risk that the plant would cost more than the forecast price was transferred to the power plant developers, which are constrained by the views of financial organizations such as banks, shareholders, and credit rating agencies. Such

organizations view investment in any type of power plant as risky, raising the cost of capital to levels at which nuclear is less likely to compete.

The logic of this transfer to competitive electricity markets was that plant developers possessed better information and had direct control over management and so had the means as well as the incentive to control costs. Builders of nonnuclear power plants were willing to take these risks, as were vendors of energy efficiency services. Consequently, when consumers no longer bore the economic risk of new plant construction, nuclear power, which combines uncompetitively high prices with poor reliability and serious risks of cost overruns, had no chance in countries that moved to competitive power procurement.

However, this issue is no longer a concerned risk, going forward with small modular reactors of Generation IV, due to modularization construction and installation each individual module as first element of power plant facility and when demand for electricity is ascending so as number of modules installation accordingly.

6. Unreliable Forecasts

In recent years there have been numerous studies of the economics of nuclear power. The values of the key parameters used to generate the forecast cost of nuclear power vary significantly from one study to another. For example, the assumed cost of construction ranges from \$856 to \$3600/kW, while the assumed construction time varies from 60 to 120 months. The resultant price of electricity consequently also varies significantly, producing a range of between \$21 and \$76/MWh.

7. Subsidies Needed

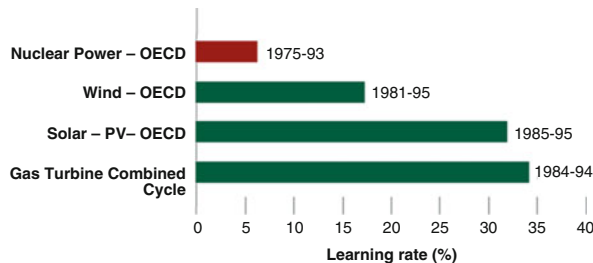
It is now 29 years since the last order for a new nuclear power plant in the United States and 34 years since the last order for a plant that was actually completed. Utilities suffered heavy losses in the 1980s as economic regulators became increasingly unwilling to pass huge cost overruns from nuclear projects on to consumers, forcing utilities to bear the extra costs. The introduction of power markets has meant that plant owners are now fully exposed not just to the risk of cost overruns but also to plant unreliability. The nuclear provisions of the US energy policy act of 2005 (EPACT 2005) are an effort to reverse these changes and protect investors from that large economic risk.

The most important nuclear provisions of EPACT 2005 offer three types of support:

- A limited number of new nuclear power plants can receive an \$18/MWh (€13.7) production tax credit for up to \$125 m per 1000 MW (or about 80% of what the plant could earn if it ran 100% of the time).
- A provision for federal loan guarantees covering up to 80% of project costs.
- Up to \$500 m in risk insurance for the first two units and \$250 m for units 3–6. This insurance is to be paid if delays that are not the fault of the licensee slow the licensing of the plant.

These subsidies are said to be worth between \$2 and \$20/MWh. Without these subsidies, it is unlikely that any US company would be considering investing in a new nuclear plant. Government financial or contractual guarantees would effectively

Fig. 17.9 Learning rates of selected energy technologies. (Courtesy of McDonald, A. and Schratzenholzer, L.)



take nuclear power out of the market so that it is paid for, as in the past, by electricity consumers and taxpayers. If nuclear power is to be subsidized in this way, there needs to be clear and compelling evidence that this is a cost-effective and worthwhile way to use taxpayers' and electricity consumers' money.

Part of prospects and status of technology for nuclear power cost is *the cost of energy production and use from all technologies which are falling systematically with innovation and scale economies in manufacturing and use, apart from nuclear power since the 1970s*.

Various reasons have been put forward for the relatively low learning rate of nuclear power, including the relatively small post-1970s reactor ordering rate, the interface between the complexity of nuclear power plants and the regulatory and political processes, and the variety of designs deployed. While some of these factors may be overcome in the future, for example, the UK Government's Performance and Innovation Unit, it also highlighted a number of areas in which future nuclear power plants may not exhibit comparable learning rates to other technologies, including:

- Nuclear power is a relatively mature technology, and therefore dramatic "technological stretch" is less likely than in other technologies.
- The relatively long lead times for construction and commissioning mean that improvements derived by feeding back information from operating and designing experiences on the first units are necessarily slow.
- The scope for economies of scale is less in the nuclear case than for renewables, due to the latter's smaller initial scale and wider potential application.

Figure 17.9 is depiction of such learning rates of selected energy technologies as indicated.

For further details, readers should refer to Reference [28] at the end of this chapter.

17.11 A Nuclear Revival or Decline

The current list of plants under construction (see Fig. 17.10) is a short one. Sixteen of the 22 units are being supplied by vendors from China, Russia, and India. It seems unlikely that any of these vendors would be considered in Western Europe or North

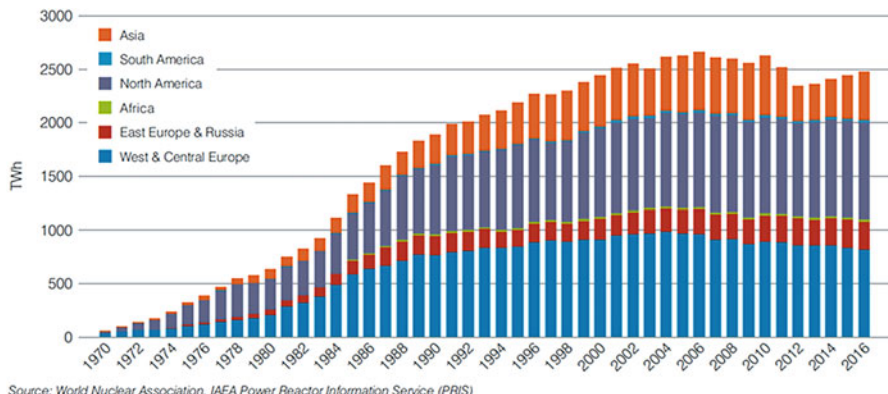
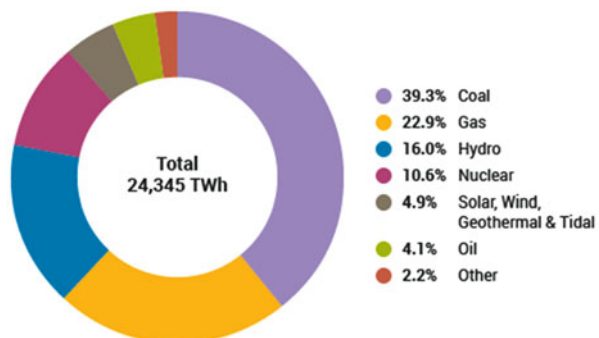


Fig. 17.10 Installation of new nuclear capacity onto grid

Fig. 17.11 2017 World electricity production by source



Source: IEA Electricity Information 2017

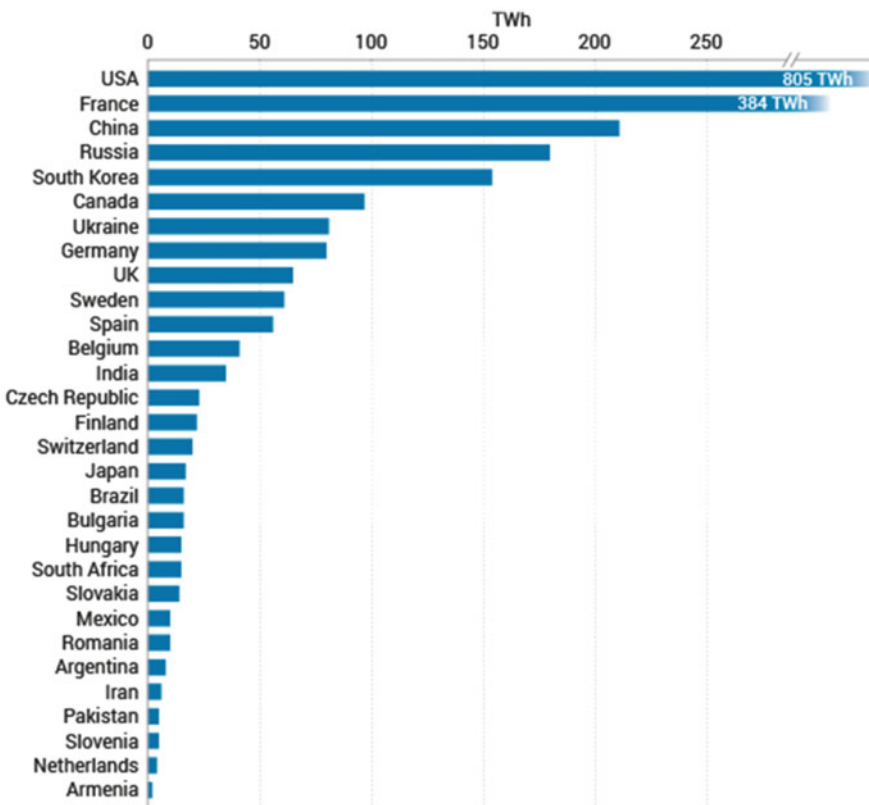
America; the markets that would need new orders if a global nuclear revival were to take place. Most of India's plants are largely based on a Canadian design from the 1960s, long since superseded in Canada. China's plants are also closely modelled on old Western designs – Prior to the AP1000 order – Albeit not so out of date as the Indian plants. China will probably continue to supply mainly its home market, with one or two exports to Pakistan.

As it can be seen from Fig. 17.10, around 11% of the world's electricity is generated by about 450 nuclear power reactors. About 60 more reactors are under construction, equivalent to 16% of existing capacity, while an additional 150–160 are planned, equivalent to nearly half of existing capacity.

In 2016 nuclear plants supplied 2477 TWh of electricity, up from 2441 TWh in 2015. This is the fourth consecutive year that global nuclear generation has risen, with output 130 TWh higher than in 2012.

Figure 17.11 is indication of world electricity production by source in 2017.

Sixteen countries depend on nuclear power for at least one-quarter of their electricity. France gets around three-quarters of its electricity from nuclear energy;



Source: IAEA PRIS Database

Fig. 17.12 2016 Nuclear power generation by countries

Hungary, Slovakia, and Ukraine get more than half from nuclear, while Belgium, the Czech Republic, Finland, Sweden, Switzerland, and Slovenia get one-third or more. South Korea and Bulgaria normally get more than 30% of their electricity from nuclear, while in the United States, United Kingdom, Spain, Romania, and Russia, about one-fifth of electricity is from nuclear. Japan is used to relying on nuclear power for more than one-quarter of its electricity and is expected to return to somewhere near that level (Fig. 17.12).

17.12 Spent Fuel and High-Level Waste Management

In this section we focus on spent fuel and reprocessed high-level waste, since these waste types contain most of the radioactivity generated in the nuclear power fuel cycle and pose the greatest technical and political challenges for final disposal. We

Fig. 17.13 Transuranic waste package



also include in the discussion so-called transuranic (TRU) waste – non-high-level waste contaminated with significant quantities of long-lived transuranic radionuclides – which because of its longevity will likely be disposed of in the same facilities as high-level waste. Other types of nuclear waste, including low-level waste and uranium mill tailings, are generated in larger volumes in the nuclear fuel cycle but pose fewer technical challenges for disposal, although localized opposition to disposal facilities for these materials has sometimes been intense.

Transuranic waste consists of waste that is contaminated with man-made radioactive elements which are heavier than uranium (meaning the elements have higher atomic numbers than uranium on the periodic table of the elements). Because they come after uranium on the periodic table, they are referred to as “transuranic.” The concentration of these transuranic elements in the waste determines whether it is transuranic (TRU) waste or low-level waste (see Fig. 17.13).

Furthermore, materials contaminated with transuranic elements – artificially made, radioactive elements, such as neptunium, plutonium, americium, and others – have atomic numbers higher than uranium in the periodic table of elements. Transuranic waste is primarily produced from recycling spent fuel or using plutonium to fabricate nuclear weapons.

Defined by the Waste Isolation Pilot Plant (WIPP) Land Withdrawal Act as “waste containing more than 100 nanocuries of alpha-emitting transuranic isotopes per gram of waste with half-lives greater than 20 years, except for.

- (A) High-level radioactive waste,
- (B) Waste that the secretary of energy has determined, with concurrence of the administrator of the Environmental Protection Agency, does not need the degree of isolation required by the disposal regulations, or.
- (C) Waste that the nuclear regulatory commission has approved for disposal on a case-by-case basis in accordance with part 61 of title 10 code of Federal Regulations (CFR)."



Fig. 17.14 Storage facility. (Courtesy of DOE Hanford Site)

More than 70,000 containers of this waste (sometimes referred to as suspect TRU waste) were stored under a layer of dirt in the 1970s and 1980s, in the 200 area low-level burial grounds of the Hanford Site. The intention was to retrieve the waste (which is why sometimes it is also referred to as retrievably stored waste) at a later date when a national repository was established to accept transuranic waste.

The management and disposal of radioactive waste from the nuclear fuel cycle is one of the most difficult problems currently facing the nuclear power industry. Today, more than 40 years after the first commercial nuclear power plant entered service, no country has yet succeeded in disposing of high-level nuclear waste – the longest-lived, most highly radioactive, and most technologically challenging of the waste streams generated by the nuclear industry.

With the 1999 opening of the Waste Isolation Pilot Plant (WIPP) outside of Carlsbad, New Mexico, TRU waste from Hanford is now being retrieved, packaged to meet WIPP's acceptance criteria, and shipped to WIPP for permanent disposal (see Fig. 17.14).

The waste was stored in boxes and 55-gallon and 85-gallon drums. The waste consists of tools, clothing, laboratory equipment, and other materials needed during the plutonium production mission at Hanford. As the waste was expected to be dug up when it was originally stored in the 70s and 80s, a typical TRU waste trench consists of several levels of drums stacked on asphalt pads, separated with plywood, draped with tarps, and then covered with dirt.

During retrieval, crews unearth the drums and boxes, check for the stability of the container holding the waste, and determine the level of radioactivity within the container. If the container is damaged or corroded, it must be carefully placed into a second container called an overpack, so that the materials don't spill onto the ground during removal from trenches to allow for future characterization for disposal. The stability of the containers holding the waste varies. In some trenches, most of the containers are in good shape and can be safely removed without the need for an overpack. In other trenches, most containers are damaged or corroded requiring an overpack.

Most transuranic elements emit alpha particles, which are the least penetrating form of radiation and can be blocked (shielded) using a sheet of paper or the outer layer of skin. However, because alpha particles present an internal hazard, damaged



Fig. 17.15 Aerial photo of Chihuahuan Desert, outside Carlsbad, NM

or corroded TRU waste drums require special handling to prevent workers from inhaling the particles. Because of this, crews often work in protective clothing and breathing equipment before they can put such containers into overpacks for safe removal from the trench.

Because the definition of transuranic waste (based on the concentration of transuranic elements) has changed over time, only about half of the retrievably stored waste is considered TRU waste. The other half is low-level waste. The TRU waste is shipped to WIPP for disposal. The low-level waste is treated as necessary and disposed at Hanford.

The Waste Isolation Pilot Plant (WIPP) is a deep geologic repository for the permanent disposal of radioactive waste. WIPP safely disposes of the nation's defense-related transuranic waste (TRU waste). Located in the Chihuahuan Desert, outside Carlsbad, NM, WIPP began disposal operations in March 1999. WIPP is managed by the Carlsbad Field Office (see Fig. 17.15).

It is noteworthy to say that international cooperation in the field of high-level waste management and disposal is presently underdeveloped. Stronger international coordination of standards and regulations for waste transportation, storage, and disposal will be necessary in order to strengthen public confidence in the safety of these activities. There is also considerable potential for international sharing of waste storage and disposal facilities. This might not only reduce proliferation risks from the fuel cycle but could also yield significant economic and safety benefits, although formidable political obstacles will have to be overcome first.

17.13 Proliferation and Nonproliferation

Given geopolitical circumstances that globally exist today between the countries with nuclear power plant technologies and capabilities of developing nations that with the possibility wishing to acquire or enhance their nuclear weapons capability will use commercial nuclear power as a source of technological know-how or nuclear weapons usable material, notably plutonium (i.e., Pu²³⁹) at enriched weapon grade.

Although this has not proved to be the preferred pathway to nuclear weapons capability, the possession of a complete nuclear fuel cycle, including enrichment, fuel fabrication, reactor operation, and reprocessing, certainly moves any nation closer to obtaining such a capability. The key step for achieving nuclear weapons' capability is acquisition of sufficient weapons-usable fissionable material, either high-enriched uranium or plutonium [19].

Unfortunately, reprocessing of spent fuel for the fuel cycle operation in Europe, Russia, and Japan has led to the accumulation of about 200 tons of separated plutonium. The associated risks have been viewed with increased alarm since the 9/11 events that demonstrated the reach of international terrorism. Radiation exposure from spent fuel that is not reprocessed is a strong, but not certain, barrier to theft and misuse.

Nuclear weapon proliferation has been prominent in discussions about nuclear power since its earliest days. The birth of nuclear technology that began with production of the first weapon-usable fissionable material – plutonium production in nuclear reactors and high-enriched uranium (HEU) by isotope enrichment – assured that this would be so. *Today, the objective is to minimize the proliferation risks of nuclear fuel cycle operation.* We must prevent the acquisition of weapons-usable material, either by diversion in the case of plutonium or by misuse of fuel cycle facilities including related facilities, such as research reactors or hot cells and control, to the extent possible, the know-how about how to produce and process either HEU (enrichment technology) or plutonium [19].

This proliferation concern has led, over the last half century, to an elaborate set of international institutions and agreements, none of which have proved entirely satisfactory. The Nuclear Nonproliferation Treaty (NPT) is the foundation of the control regime, since it embodies the renunciation of nuclear weapons by all signatories except for the declared nuclear weapon states – the P-5 (the United States, Russia, the United Kingdom, France, China) – and a commitment to collaborate on developing peaceful uses of nuclear energy. However, non-signatories India and Pakistan tested nuclear weapons in 1998, and signatories, such as South Africa and North Korea, have admitted to making nuclear weapons [19].

The International Atomic Energy Agency (IAEA) has responsibility for verifying NPT compliance with respect to fuel cycle facilities through its negotiated safeguard agreements with NPT signatories. The IAEA's safeguard efforts, however, are seriously constrained by the scope of their authorities (as evidenced in Iraq, Iran,

and North Korea during the last decade), by their allocation of resources, and by the growing divergence between responsibilities and funding.

For further information, please refer to MIT report [19] or IAEA web site please.

17.14 Society Attitude and Public Understanding of Nuclear Power

Nuclear energy is a controversial and sensitive subject among the public because it strongly relates public health and safety. Due to this mass media is handling this subject in a diverse manner; thereby it creates a strong impact among the people. Public's acceptance and support to the nuclear energy is also preoccupied. Monitoring the effectiveness of campaigns to change public attitudes to nuclear power required a tracking study based on a high-quality, representative national sample with high-sensitivity indicators.

We need to have a means and indicator to study and assess the level of public knowledge of nuclear energy that will explore public understanding of the arguments for and against the construction of new nuclear power plant nationwide and worldwide as well and the fact that how much the news media helps the ordinary people have knowledge and desire to understand the new generation of the nuclear power energy regardless of negative impacts recent accidents have such as the one as recent as 2012 in Fukushima Daiichi in Japan, which was based on over 20 years ago technology of plant (see Fig. 17.16).

One strategy that could be implemented to help such indicator of study is a methodology to allow not only the monitoring of attitudes toward nuclear power but also the formulation of an effective communications strategy. The success of the study relied on the quality of the sample and its representativeness of the entire population, both nationwide and worldwide among the countries with nuclear power plant technology and idea of going forward with such clean and renewable source of energy based on new advanced technology in particular with dawn of Generation IV of these plants and small modular reactors (SMRs).

The sample data collection of such methodology should be structured on the formulation of an effective communications strategy and not just only the monitoring toward the nuclear power as well as participation of government of each nation with such technology to back up such methodology and strategy in short and long term as well. This is an effort that certain agencies of each government involved in licensing in cooperation and collaboration with industries designing the new generation of nuclear energy power plants.

One of the key indicators for public awareness about nuclear technology benefits from it as that as stakeholder; we should create an awareness for all the benefits that *Nuclear Technology Brings to Mankind*. We should put our standing point with the fact that "The public are often unaware of the extent to which aspects of their



Fig. 17.16 Arial picture of Fukushima Daiichi in Japan

everyday life involve products and processes originated from the application of nuclear technology via the nuclear industry.”

With the fifth anniversary of Fukushima having just passed last month and the 30th anniversary of Chernobyl this month, we have a steady reminder of the issues that never seem to go away for the nuclear industry. It is our nature. However, the key question of why is it that the safest source of large-scale electricity generation we have ever come up with is considered so dangerous by enough people that in several countries there is an effort to stop using nuclear energy?

But for those who may not get there quickly enough, here is a summary of the benefits that nuclear technology brings to society each and every day. As stated at the beginning of this chapter, “Nuclear technology is vital for more than just providing reliable, low-carbon energy. It also has life-saving medical application; improves manufacturing, mining, transport and agriculture; and help us discover more about the planet we live on and how we can sustainably live with it.”

So, for example, did you know that:

- Nuclear technology saves lives through use of radioisotopes for screening, diagnosis, and therapy of various medical conditions. According to the WNA, over 10,000 hospitals worldwide use radioisotopes. Radioisotopes are used in therapy to control and damage cancerous growths. Iodine-131 is used to treat thyroid cancer and phosphorus-32 to treat leukemia. Nuclear techniques are used for neonatal screening for sickle cell disease, hypothyroidism, and cystic fibrosis, as well as childhood cancers.
- Radiation is used to preserve seeds and food products and breed disease-resistant plants. In plant breeding, some 1800 new crop varieties have been developed through mutation induced by ionizing radiation.
- Irradiation technology is increasingly being used to preserve food – spices, grains, fruit, vegetables, and meat. It avoids the use of potentially harmful chemical fumigants and insecticides.
- Use of the IAEA’s Sterile Insect Technique irradiates the eggs of these insects to sterilize them before hatching. The IAEA estimates that, by suppressing insect pest populations with SIT, pesticide use worldwide has been reduced by 600,000 liters annually.
- In industrial radiography, nuclear substances are used for the nondestructive examination and testing of new materials. Radiation from the substances passes through the material and allows defects in welds or constituency to be recorded on film or a digital imager.

This list does not do justice to the report itself which I strongly suggest you read. It’s time to stop being on the defensive and make sure that we no longer have to write reports that start with “The public are often unaware of the extent to which aspects of their everyday life involve products and processes originated from the application of nuclear technology via the nuclear industry.” It is time to celebrate our successes and not just talk about where we need to improve. We are proud to be part of the nuclear industry, and we are confident that we are making a difference that helps to make the world a better place [31].

17.15 Conclusion

It seems like at the heart of debate lies the confusion over the exact definition of renewable energy and the requirements that needs to be met in order to be one. The recent statement by Helene Pelosi, the interim director General of International

Renewable Energy Agency (IRENA), saying IRENA will not support nuclear energy programs because it is a long, complicated process and it produces waste and is relatively risky, proves that their decision has nothing to do with having a sustainable supply of fuel [15]. However, if that is the case, then nuclear proponents would have to figure out a way to deal with the nuclear waste management issue and other political implications of nuclear power before they can ask IRENA to reconsider including nuclear energy in the renewable energy list [18].

One more strong argument against fission nuclear power plants as source of renewable energy comes from Dr. James Singmaster in August 3, 2009, and has been republished here as follows:

The basic problem of the climate crisis is the ever-expanding overload of heat energy in the closed biosphere of earth. Temperatures going up indicate the increasing heat energy overload. Everyone reading this should check out Dr. E. Chaisson's article titled "Long-Term Global Warming from Energy Usage" in EOS, Trans. Amer. Geophys. Union, V. 89, No. 28, Pgs. 253-4(2008) to learn that nuclear energy, be it fission or fusion, being developed should be dropped with money put into it being put to developing renewable energy supplies using the sun, wind and hydrogen.

The hydrogen needs to be generated from splitting water using sunlight with the best one or two of seven catalysts reported in the last 2 years. Or with excess solar or wind collection generating electricity, that could be used to generate hydrogen by electrolysis of water.

There is no way that nuclear power can avoid releasing trapped energy to increase the energy overload, so it should be forgotten.

To remove some of the energy as well as some of the carbon overload in the biosphere, we need to turn to pyrolysis of massive ever-expanding organic waste streams to remake charcoal that will be removing some of both overloads. It will require using renewable energy and the pyrolysis process expels about 50% of the carbon as small organic chemicals that can be collected, refined and used for fuel that is a renewable one. For more about using pyrolysis, search my name on GreenInc blog or google it for other blog comments on pyrolysis. (Dr. j. Singmaster).

References

1. B. Zohuri, *Combined Cycle Driven Efficiency for Next Generation Nuclear Power Plants: An Innovative Design Approach*, 1st edn, Mar 15, 2015, Springer Publishing Company
2. B. Zohuri, P. McDaniel, *Combined Cycle Driven Efficiency for Next Generation Nuclear Power Plants: An Innovative Design Approach*, 2nd edn, December 15, 2017, Springer Publishing Company
3. B. Zohuri, *Small Modular Reactors as Renewable Energy Sources*, Aug 7, 2018, Springer Publishing Company
4. B. Zohuri, *Hydrogen Energy: Challenges and Solutions for a Cleaner Future*, Aug 20, 2018, Springer Publishing Company

5. B. Zohuri, *Hybrid Energy Systems: Driving Reliable Renewable Sources of Energy Storage*, Nov 26, 2017, Springer Publishing Company
6. GE Energy Flex Efficiency 50 Combined Cycle Power Plant, e-Brochure, 2012
7. J.H. Horlock, *Cogeneration-Combined Heat and Power (CHP)* (Krieger Publishing Company, Malabar), p. 1997
8. J.D. Mattingly, *Elements of Gas Turbine Propulsion* (McGraw-Hill, Inc., New York, 1996)
9. B. Zohuri, P. McDaniel, C. De Oliveira, Advanced nuclear open-air-Brayton cycles for highly efficient power conversion. *Nucl. Technol. J.* **192**(1), 48–60 (2015)
10. B. Zohuri, *Inertial Confinement Fusion Driven Thermonuclear Energy*, Jan 29, 2017, Springer Publishing Company
11. B. Zohuri, *Plasma Physics and Controlled Thermonuclear Reactions Driven Fusion Energy*, Nov 17, 2016, Springer Publishing Company
12. K. Johnson, Is nuclear power renewable energy. *Wall Street J.*, 21 May 2009
13. B.L. Cohen, Breeder reactors: a renewable energy source. *Am. J. Phys.* **51**, 75 (1983)
14. B.L. Cohen, *Nuclear Science and Society* (Anchor Books Publishing, Garden City, New York, 1974)
15. E. Moniz., <http://energy.mit.edu/news/why-we-still-need-nuclear-power/>
16. B. Zohuri, *Neutronic Analysis for Nuclear Reactor Systems*, 1st edn, Nov 3, 2016, Springer Publishing Company
17. J. Kanter, Is nuclear power renewable, *New York Times*, 3 Aug 2009
18. D. Chowdhury, *Is Nuclear Energy Renewable Energy*. Stanford Physics Department, March 22, 2012
19. The Future of Nuclear Power, an Interdisciplinary MIT Study, 2003
20. B. Zohuri, *Plasma Physics and Controlled Thermonuclear Reactions Driven Fusion Energy*, Nov 17, 2016, Springer Publishing Company
21. B. Zohuri, *Inertial Confinement Fusion Driven Thermonuclear Energy*, Feb 16, 2016, Springer Publishing Company
22. B. Zohuri, *Magnetic Confinement Fusion Driven Thermonuclear Energy*, Feb 27, 2017, Springer Publishing Company
23. B. Zohuri, P. McDaniel, *Thermodynamics in Nuclear Power Plant Systems*, Apr 21, 2015, Springer Publisher Company
24. B. Zohuri, *Thermal-Hydraulic Analysis of Nuclear Reactors*, 2nd edn, May 25, 2017, Springer Publishing Company
25. A.B. Chilton, J. Kenneth Shults, R.E. Faw, *Principle of Radiation Shielding*, 1st edn, Prentice Hall; September 1, New York, NY, 1983
26. www.nei.org, December 2002, Deterring Terrorism – Aircraft Crash Impact Analyses Demonstrate Nuclear Power Plant’s Structure Strength; EPRI Study
27. OECD Nuclear Energy Agency, Trends in the Nuclear Fuel Cycle ISBN 92-64-19664-1 (2001) and Nuclear Science Committee “Summary of the workshop on advanced reactors with innovative fuel”, October 1998, NEA/NSC/DOC (99) 2
28. S. Thomas, P. Bradford, A. Froggatt, D. Milborrow, *The Economics of Nuclear Power*, Research Report 2007. [Reenpeace.org](http://www.reenpeace.org)
29. B. Zohuri, P. McDaniel, *Combined Cycle Driven Efficiency for Next Generation Nuclear Power Plants: An Innovative Design Approach*, Dec 8, 2017, Published by Springer Publishing Company
30. B. Zohuri, *Small Modular Reactors as Renewable Energy Sources*, Aug 7, 2018, Published by Springer Publishing Company
31. <http://www.theenergycollective.com/mzconsulting/2376894/lets-create-awareness-for-all-the-benefits-that-nuclear-technology-brings-to-mankind>

Chapter 18

Small Modular Reactors and Innovative Efficient Enhancement Design



The smaller-sized nuclear reactors were becoming instrumental during the pioneering days of commercial nuclear power to facilitate the development and demonstration of early reactor technologies and to establish operational experience for the fledgling nuclear power industry starting with the first powered US Navy nuclear submarine. As part of innovative approach in design of small modular reactors (SMRs) in the new era of nuclear power energy to meet the demand for electricity due to growth of population, researchers are in quest of a more efficient electrical outpower by these types of reactors known as advanced small modular reactors (AdvSMRs) suggested as the air Brayton cycle is an open-air cycle and the steam Rankine cycle is a closed cycle. The air Brayton cycle for a natural gas-driven power plant must be an open cycle, where the air is drawn in from the environment and exhausted with the products of combustion to the environment.

18.1 Introduction

As we have learned so far, nuclear technology is one of the main baseload electricity-generating sources available in the world today, producing around 11.2% of the global power production. According to the International Atomic Energy Agency (IAEA), the use of nuclear energy for electricity generation is expected to grow around the world, particularly in Asia and the Pacific Rim, as demand for electricity increases in that region as foreseen. It is also expected that the types of nuclear power reactors to be used in the future in several countries will not be as large as today, more than 1000 MW of capacity, opening the possibility to the introduction of small modular reactors (SMRs) with a maximum capacity of 300 Me, which could be built in factories and transported to the different sites, by truck, train, or ship.

According to the IAEA designation of plant sizes, 139 of the 442 commercial power reactors that are currently in operation worldwide are SMRs. However, most of these are merely scaled-down versions of large plant designs and are not the focus

of this review. Instead, the current excitement in smaller-sized reactors is for reactor designs that are deliberately small, i.e., designs that do not scale to large sizes but rather capitalize on their smallness to achieve specific performance characteristics. An integral primary system reactor is an example of a deliberately small reactor (DSR) and will be described later in this paper. These DSRs may be appropriate for baseload electricity generation, especially in regions with smaller electricity grids, but are especially well suited for more specialized non-electrical energy applications.

Smaller-sized nuclear reactors were instrumental during the pioneering days of commercial nuclear power to facilitate the development and demonstration of early reactor technologies and to establish operational experience for the fledgling nuclear power industry. As the US embarks on its “second nuclear era,” the question becomes: will smaller-sized plants have a significant role in meeting the nation’s needs for electricity and other energy demands?

The major growth in the electricity production industry in the last 30 years has centered on the expansion of natural gas power plants based on gas turbine cycles. The most popular extension of the simple Brayton gas turbine has been the combined cycle power plant with the air Brayton cycle serving as the topping cycle and the steam Rankine cycle serving as the bottoming cycle for new generation of nuclear power plants that are known as GEN-IV. The air Brayton cycle is an open-air cycle and the steam Rankine cycle is a closed cycle. The air Brayton cycle for a natural gas-driven power plant must be an open cycle, where the air is drawn in from the environment and exhausted with the products of combustion to the environment. This technique is suggested as an innovative approach to GEN-IV nuclear power plants in form and type of small modular reactors (SMRs). The hot exhaust from the air Brayton cycle passes through a heat recovery steam generator (HRSG) prior to exhausting to the environment in a combined cycle. The HRSG serves the same purpose as a boiler for the conventional steam Rankine cycle [1–3].

Nuclear energy can play a very significant long-term role for meeting the world’s increasing energy demands, while simultaneously addressing challenges associated with global climate and environmental impact. Many nations of the world, particularly the Asia/Pacific Rim countries, are actively engaged in a major expansion of their nuclear energy complex. The degree to which nuclear energy can address long-term energy needs, either globally or regionally, will be dictated by the pace and adequacy of technical and policy solutions for waste, safety, security, and nonproliferation issues, as well as the capital cost of construction. Small modular reactors (SMRs) could successfully address several of these issues. SMRs offer simpler, standardized, and safer modular design by being factory built, requiring smaller initial capital investment and having shorter construction times. The SMRs could be small enough to be transportable, could be used in isolated locations without advanced infrastructure and without power grid, or could be clustered in a single site to provide a multi-module, large capacity power plant.

Uniqueness of the subject and benefits of GEN-IV power plants and argument to defend why we need the nuclear power plant for source of renewable energy, efficiency, cost-effectiveness, as well as safety-related issues are discussed in this book with every detail oriented both from an experimental and technical point of

view. This book also goes over different types of GEN-IV nuclear power plants by giving general configurations and specifications of each modular reactor that are considered as part of the new generation of these nuclear plants that fall into the small modular reactors category.

As part of this chapter, we envision a world where almost every country has one affordable type of GEN-IV power plant, such as molten salt reactors burning thorium, uranium, and spent fuel actinides, producing electricity, hydrogen, and desalinated water without any serious accidents.

Small modular reactors (SMRs) are highlighted as a viable alternative to the nuclear power plants (NPPs) that have been used as desalination plant energy sources for the following reasons:

SMRs have lower investment costs.

Almost all SMR concepts appear to show increased availability (\$90%).

Because of inherent safety features, most SMRs have good potential for location near population centers, hence lowering the transport costs.

This chapter also discusses some angles of nuclear energy generated by small modular reactors (SMRs) specifically and why we need nuclear power plants from SMRs' point of view that are the new generation and design for nuclear plants.

In addition, this chapter shows the uniqueness of these small modular reactors (SMRs) and presents innovative approaches to the implementation of these reactors as part of GEN-IV technologies, and it summarizes some of the basic features of SMRs for early deployment and several advanced small modular reactor (AdvSMR) concepts and points out the benefits and challenges in regulatory, economical, safety, and security issues.

18.2 Generation IV Drive New Nuclear Reactor Concepts

Concerns over energy resource availability, climate change, air quality, and energy security suggest an important role for nuclear power in future energy supplies. While the current Generation II and III nuclear power plant designs provide a secure and low-cost electricity supply in many markets, further advances in nuclear energy system design can broaden the opportunities for the use of nuclear energy. To explore these opportunities, the US Department of Energy's Office of Nuclear Energy has engaged governments, industry, and the research community worldwide in a wide-ranging discussion on the development of next-generation nuclear energy systems known as "Generation IV" (see Fig. 18.1).

The goal of the GEN-IV Nuclear Energy Systems is to address the fundamental research and development (R&D) issues necessary to establish the viability of next-generation nuclear energy system concepts to meet tomorrow's needs for clean and reliable electricity and nontraditional applications of nuclear energy. Successfully addressing the fundamental research and development (R&D) issues will allow GEN-IV concepts that excel in safety, sustainability, cost-effectiveness, and

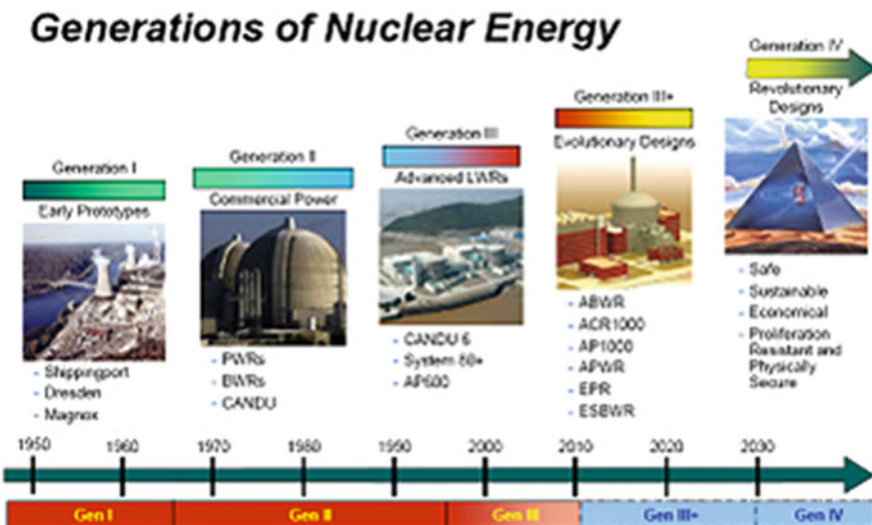


Fig. 18.1 The evolution of nuclear power

proliferation risk reduction to be considered for future commercial development and deployment by the private sector.

GEN-IV reactor concepts are being developed to use advanced fuels, fashioned from recycled reactor fuel and capable of high burnups. The corresponding fuel cycle strategies allow for efficient utilization of domestic uranium resources while minimizing waste. Reduction of proliferation risk and improvements in physical protection are being designed into GEN-IV concepts to help thwart those who would target nuclear power plants for terrorist acts or use them improperly to develop materials for nuclear weapons. GEN-IV concepts will feature advances in safety and reliability to improve public confidence in nuclear energy while providing enhanced investment protection for plant owners. Competitive life-cycle costs and acceptable financial risk are being factored into GEN-IV concepts with high-efficiency electricity generation systems, modular construction, and shortened development schedules before plant start-up [4].

GEN-IV is also an active participant in the International Project on Innovative Nuclear Reactors and Fuel Cycles (INPRO). INPRO was established in 2001 in response to a resolution by the IAEA General Conference to help to ensure that nuclear energy is available to contribute, in a sustainable manner, to meeting the energy needs of the twenty-first century and to bring together technology holders and users so that they can consider jointly the international and national actions required for achieving desired innovations in nuclear reactors and fuel cycles. INPRO provides a forum for discussion for experts and policy makers from industrialized and developing countries on all aspects of nuclear energy planning as well as on the

Table 18.1 Areas of improvement for Generation IV

Sustainability – 1	Generation IV nuclear energy systems will provide sustainable energy generation that meets clean air objectives and provides long-term availability of systems and effective fuel utilization for worldwide energy production
Sustainability – 2	Generation IV nuclear energy systems will minimize and manage their nuclear waste and notably reduce the long-term stewardship burden, thereby improving protection for the public health and the environment
Economics – 1	Generation IV nuclear energy systems will have a clear life-cycle cost advantage over other energy sources
Economics – 2	Generation IV nuclear energy systems will have a level of financial risk comparable to other energy projects
Safety and reliability – 1	Generation IV nuclear energy systems operations will excel in safety and reliability
Safety and reliability – 2	Generation IV nuclear systems will have a very low likelihood and degree of reactor core damage
Safety and reliability – 3	Generation IV nuclear energy systems will eliminate the need for off-site emergency response
Proliferation resistance and physical protection	Generation IV nuclear energy systems will increase the assurance that they are very unattractive and the least desirable route for diversion or theft of weapons-usable materials and provide increased physical protection against acts of terrorism

development and deployment of innovative nuclear energy systems in the twenty-first century.

The Generation IV International Forum (GIF) was chartered in May 2001, to lead the collaborative efforts of the world's leading nuclear technology nations to develop the next generation of nuclear energy systems. The initial efforts of GIF resulted in the identification of the six most promising reactor concepts to be investigated by this international research community and are documented in the Generation IV technology roadmap. Thirteen members have signed the GIF charter: Argentina, Brazil, Canada, People's Republic of China, Euratom, France, Japan, Republic of Korea, the Russian Federation, Republic of South Africa, Switzerland, the United Kingdom, and the United States. This unique international effort reached a major milestone on February 28, 2005, as five of the forum's member countries (Canada, France, Japan, United Kingdom, and United States) signed the world's first multi-lateral agreement aimed at the international development of advanced nuclear energy systems – the Framework Agreement for International Collaboration on Research and Development of Generation IV Nuclear Energy Systems. Subsequent signatories to the Framework Agreement included the People's Republic of China, Euratom, Republic of Korea, Republic of South Africa, and Switzerland. The United Kingdom is a signatory of the framework but is currently a non-active member. Argentina and Brazil have not ratified the Framework Agreement and are therefore considered non-active. The Russian Federation is working on the necessary approvals for its accession to the Framework [4] (see Fig. 18.2).



Fig. 18.2 Map of member countries

As detailed in its charter and subsequent GIF policy statements, GIF is led by the Policy Group (PG), which is responsible for the overall coordination of GIF's research and development (R&D) collaboration, and policy formation and for interactions with other organizations. France currently chairs the Policy Group with vice chairs from the United States and Japan. An Experts Group and the Senior Industry Advisory Panel advises the Policy Group on (R&D) strategy, priorities, and methodology and on evaluating research plans for each Generation IV system. The Framework Agreement establishes two levels of implementing arrangements in order to conduct the joint (R&D). The first level consists of a system arrangement for each Generation IV reactor concept directed by a System Steering Committee (SSC). Under each SSC, project arrangements are established with project management boards to manage and implement the joint (R&D).

18.3 Technological State- of- the-Art and Anticipated Developments

It has been demonstrated that Generation II plants can be safely and economically operated for up to 60 years through the development of improved harmonized plant-life management technologies and plant license extension practices (PLIM/PLEX)

and that developments in fuel technologies can still lead to improvements in reactor performance [5]. The first Generation III reactors, which are an evolution of thermal reactors with even further improved safety characteristics and economy, are now being built. In the coming decades, nuclear electricity generation should increase or at least maintain its current level by a combination of lifetime extension and power upgrades of Generation II reactors and new build of Generation III reactors. Two 1.6 GWe Generation III reactors are presently under construction in Finland and France, targeted for connection to the grid in 2012.

The Finnish reactor was a first of a kind (FOAK) and the construction has suffered delays with the overnight cost increasing from 2000 to 3100 €/kWe, whereas the overnight cost for the second reactor in France is now 2400 €/kWe. In series production, the industry expects the cost to be 2000 ± 500 €/GWe, which is in line with recent international studies. An additional capacity of 100 GWe of Generation III reactors over the next 25 years is a reasonable estimate, which would require an investment in the range of 200–280 billion Euros. The capital costs represent typically 60–70% of the leveled cost for nuclear electricity, operation and maintenance 20–25%, and fuel 10–15%. The front-loaded cost profile means that the leveled cost is very sensitive to construction time and the financial schemes for the investment. Estimates in 2007 for United Kingdom resulted in range of 31–44 £/MWh (37–53 €/MWh).

Though uranium is relatively abundant in the Earth's crust and oceans, estimates of natural reserves are always related to the cost of mineral extraction. As the price of uranium increases on world markets, the number of economically exploitable deposits also increases. The most recent estimates [6] identified 5.5 million tons of uranium (MtU) that could be exploited below 130 \$/kg. The total amount of undiscovered resources (reasonably assured and speculative) available at an extraction cost below 130 \$/kgU is estimated at 10.5 MtU. Unconventional resources, from which uranium is extracted as a by-product only, e.g., in phosphate production, lie between 7 and 22 MtU, and reserves in seawater are estimated to be 4000 MtU. Japanese studies suggest that uranium from seawater can be extracted at 300 €/kg [7]. At a conservative estimate, 25,000 tons of the uranium are required to produce the fuel to generate 1000 TWhe in an open fuel cycle. The global electricity supplied by nuclear is 2600 TWhe, which means that the conventional resources below 130 \$/kgU at the current rate of consumption would last for at least 85 years with the already identified resources (5.5 MtU) and 246 years, if the undiscovered are also included (5.5 + 10.5 MtU). In addition to uranium, it is also possible to use thorium, which is three times more abundant in the Earth's crust, though would require different reactors and fuel cycles. Nonetheless, natural resources are plentiful and do not pose an immediate limiting factor for the development of nuclear energy.

However, in a scenario with a large expansion of nuclear energy, resources will become an issue much earlier, especially since new plants have at least a 60-year lifetime and utilities will need assurances when ordering new build that uranium supply can be maintained for the full period of operation. Eventually, known conventional reserves will all be earmarked for current plants or those under construction, and this could happen by the middle of this century. This underlines

the need to develop the technology for a new generation, the so-called Generation IV, of reactors and fuel cycles that are more sustainable. In particular, fast-neutron breeder reactors could produce up to 100 times more energy from the same quantity of uranium than current designs and may significantly reduce the amount of ultimate radioactive waste for disposal.

Fast reactors convert non-fissile material (U^{238}) in the fuel into fissile material (Pu^{239}) during reactor operation so that the net amount of fissile material increases (breeding). After reprocessing of the spent fuel, the extracted fissile materials are then recycled as new fuels. Reduction of the radiotoxicity and heat load of the waste is achieved by separating some long-lived radionuclides, the minor actinides, which could then be “burned” in fast reactors or alternatively in accelerator-driven systems (ADS), through transmutation. The fast reactor concept has been demonstrated in research programs and national prototypes in the past, but further R&D is needed to make it commercially viable and to develop the designs in compliance with true Generation IV criteria. Major issues involve new materials that can withstand higher temperatures, higher burnups and neutron doses, and corrosive coolants, reactor designs that eliminate severe accidents, and development of fuel cycles for waste minimization and elimination of proliferation risks. Fast reactors are expected to be commercially available from 2040.

So far nuclear power has primarily been used to produce electricity, but it can also be used for process heat applications [7, 8]. Currently, LWRs are already being used to a limited extent for some lower-temperature applications ($200\text{ }^{\circ}\text{C}$), such as district heating and desalination of seawater. Existing designs of high-temperature reactors (HTR) that can reach $800\text{ }^{\circ}\text{C}$ can be deployed in the coming decades, and very high-temperature reactors (VHTR) that can reach gas coolant temperatures beyond $1000\text{ }^{\circ}\text{C}$ are being studied as a Generation IV concept for later deployment. Process heat applications include petroleum refinery applications ($400\text{ }^{\circ}\text{C}$), recovery of oil from tar sands ($600\text{--}700\text{ }^{\circ}\text{C}$), synthetic fuel from CO^2 and hydrogen ($600\text{--}1000\text{ }^{\circ}\text{C}$), hydrogen production ($600\text{--}1000\text{ }^{\circ}\text{C}$), and coal gasification ($900\text{--}1200\text{ }^{\circ}\text{C}$). Small reactors that can be inherently safe and used to support specific high-energy applications and often in remote areas are another very interesting application that is receiving more attention, in particular in the IAEA INPRO Initiative.

The management of radioactive waste, as either spent fuel or ultimate waste, depending on the national strategy, is a key issue for public acceptance of nuclear energy. There is scientific consensus that geological disposal is the only safe long-term solution for the management of ultimate waste. After a long period of intensive research and development coupled with in-depth political and social engagement, the world’s first deep geological repositories for nuclear waste will be in operation in Sweden and Finland by 2020, with France following a few years later, demonstrating that practical solutions exist for the safe long-term management of hazardous waste from the operation of nuclear power plants. Though there will also be ultimate waste from Generation IV fast reactor fuel cycles after reprocessing, the volumes and heat loads will be greatly reduced, thereby facilitating disposal operations and optimizing use of space in available geological repositories.

18.4 Next Generation Nuclear Plant (NGNP)

The Next Generation Nuclear Plant (NGNP) demonstration project forms the basis for an entirely new generation of advanced nuclear plants capable of meeting the nation's emerging need for greenhouse-gas-free process heat and electricity. The NGNP is based on the very high-temperature gas-cooled reactor (VHTR) technology, which was determined to be the most promising for the United States in the medium term. The determination is documented as part of the Generation IV implementation strategy in a report submitted to Congress in 2013 following an extensive international technical evaluation effort. The VHTR technology incorporates substantive safety and operational enhancements over existing nuclear technologies. As required by the Energy Policy Act (EPAct) of 2005, the NGNP will be a prototype nuclear power plant, built at the Idaho National Laboratory (INL). Future commercial versions of the NGNP will meet or exceed the reliability, safety, proliferation resistance, and economy of existing commercial nuclear plants [9].

It is envisioned that these advanced nuclear plants would be able to supply cost-competitive process heat that can be used to power a variety of energy-intensive industries, such as the generation of electricity, hydrogen, enhanced oil recovery, refineries, coal-to-liquids and coal-to-gas plants, chemical plants, and fertilizer plants [9].

The US Nuclear Regulatory Commission (NRC) is responsible for licensing and regulating the construction and operation of the NGNP. The EPAct authorizes the US Department of Energy (DOE) to build the NGNP at the Idaho National Laboratory and charges INL with responsibility for leading the project development. The project's completion depends on the collaborative efforts of DOE and its national laboratories, commercial industry participants, US universities, and international government agencies as well as successful licensing by the NRC. At present and pending further evaluation as the NGNP proceeds through Phase 1 in cost-shared collaboration with industry as required by the EPAct, DOE has not made a final determination on whether the license applicant will be DOE or one or more entities that reflect a partnership between DOE and private sector firms [9].

Under the provisions of Section 644 of the EPAct, the Secretary of Energy and the Chairman of the Nuclear Regulatory Commission are to jointly submit to Congress a licensing strategy for the New Generation Nuclear Power (NGNP) within 3 years of the enactment of the Act on August 8, 2005. This report addresses the requirement by outlining a NGNP licensing strategy jointly developed by the NRC and DOE. The scope of the document includes all four elements of the NGNP licensing strategy described in Section 644 (b) of the EPAct:

1. A description of the ways in which current NRC light water reactor (LWR) licensing requirements need to be adapted for the types of reactors considered for the project
2. A description of the analytical tools that the NRC will need to develop in order to independently verify the NGNP design and its safety performance

3. A description of other research or development activities that the NRC will need to conduct for the review of an NGNP license application
4. A budget estimate associated with the licensing strategy

DOE has determined that the NGNP nuclear reactor will be a very high-temperature gas-cooled reactor (VHTR) for the production of electricity, process heat, and hydrogen. The VHTR can provide high-temperature process heat (up to 950 °C) that can be used as a substitute for the burning of fossil fuels for a wide range of commercial applications. Since the VHTR is a new and unproven reactor design, the NRC will need to adapt its licensing requirements and process, which have historically evolved around light water reactor (LWR) designs, for licensing the NGNP nuclear reactor. Thus, Section 644 of the EPAct recognized the need for an alternative licensing strategy. This report provides the recommended NGNP licensing strategy, jointly developed by the NRC and DOE. As the technology matures, the government/industry partnership evolves, and input is provided by the general public, revisions to the strategy may be necessary and appropriate [9].

The report addresses the four elements of the licensing strategy set forth in Section 644(b) of the EPAct. These elements are summarized above [9].

18.5 Generation IV Systems

The world's population is expected to expand from 6.7 billion people today to over 9 billion people by the year 2050, all striving for a better quality of life. As the earth's population grows, so does the demand for energy and the benefits that it brings: improved standards of living, better health and longer life expectancy, improved literacy and opportunity, and many others. Simply expanding the use of energy along the same mix of today's production options, however, does not satisfactorily address concerns over climate change and depletion of fossil resources. For the earth to support its population while ensuring the sustainability of humanity's development, we must increase the use of energy supplies that are clean, safe, and cost-effective and which could serve for both basic electricity production and other primary energy needs. Prominent among these supplies is nuclear energy.

There is currently 370 GWe of nuclear power capacity in operation around the world, producing 3000 TWh each year – 15% of the world's electricity – the largest share provided by any non-greenhouse-gas-emitting source. This reduces significantly the environmental impact of today's electricity generation and affords a greater diversity of electricity generation that enhances energy security.

For more than a decade, Generation IV International Forum (GIF) has led international collaborative efforts to develop next-generation nuclear energy systems that can help meet the world's future energy needs. Generation IV designs will use fuel more efficiently, reduce waste production, be economically competitive, and meet stringent standards of safety and proliferation resistance.

As we said the Generation IV International Forum (GIF) was initiated in May 2001 and formally chartered in mid-2001. It is an international collective representing government of 13 countries where nuclear energy is significant now and also seen as vital for the future. Most are committed to joint development of the next generation of nuclear technology. Led by the United States, Argentina, Brazil, Canada, China, France, Japan, Russia, South Korea, South Africa, Switzerland, and the United Kingdom are charter members of the GIF, along with the EU (Euratom). Most of these are party to the Framework Agreement (FA), which formally commits them to participate in the development of one or more Generation IV systems selected by GIF for further R&D. Argentina and Brazil did not sign the FA, and the United Kingdom withdrew from it; accordingly, within the GIF, these three are designated as “inactive members.” Russia formalized its accession to the FA in August 2009 as its tenth member, with Rosatom as implementing agent. In 2011 the 13 members decided to modify and extend the GIF charter indefinitely.

With these goals in mind, some 100 experts evaluated 130 reactor concepts before GIF selected six reactor technologies for further research and development.

These include:

1. Very High-Temperature Reactor (*VHTR*)
2. The Molten Salt Reactor (*MSR*)
3. The Sodium-cooled Fast Reactor (*SFR*)
4. The Super Critical Water-cooled Reactor (*SCWR*)
5. The Gas-cooled Fast Reactor (*GFR*)
6. The Lead-cooled Fast Reactor (*LCFR*)

Figure 18.3 below is illustration of the six types of reactors that are considered as part of Generation IV power plant. More details of each of these reactors are provided in later sections.

18.5.1 Very High-Temperature Reactor (*VHTR*)

Among the six candidates of the GEN-IV nuclear systems in the technical roadmap of GEN-IV International Forum (GIF), the very high-temperature reactor (VHTR) is primarily dedicated to the cogeneration of electricity and hydrogen, the latter being extracted from water by using thermochemical, electrochemical, or hybrid processes. Its high outlet temperature makes it attractive also for the chemical, oil, and iron industries (Fig. 18.4). Original target of outlet temperature of 1000 °C from VHTR can support the efficient production of hydrogen by thermochemical processes. The technical basis for VHTR is the tristructural-isotropic (TRISO)-coated particle fuel, the graphite as the core structure, helium coolant, as well as the dedicated core layout and lower power density to removal decay heat in a natural way. The VHTR has potential for inherent safety, high thermal efficiency, process heat application capability, low operation and maintenance costs, and modular construction.

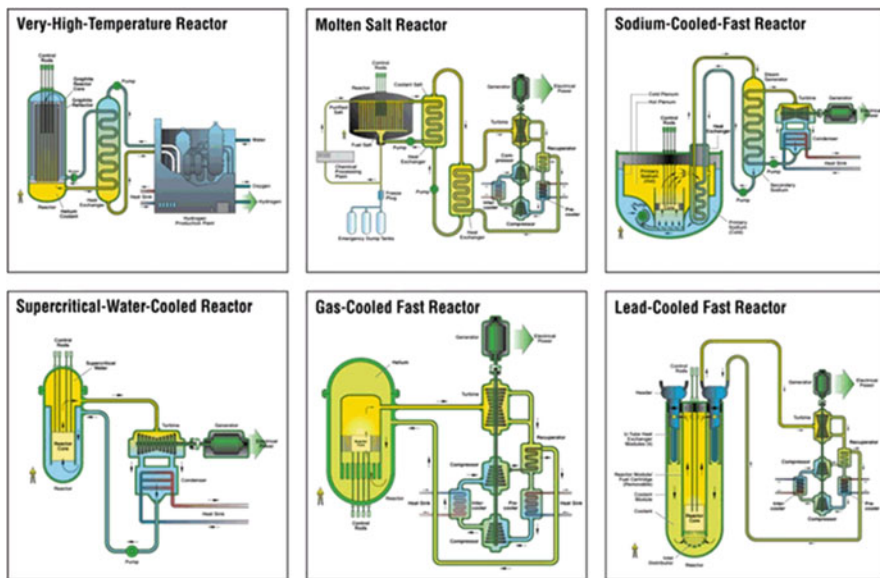


Fig. 18.3 Six reactor technologies of Generation IV. (Courtesy of the Generation IV International Forum)

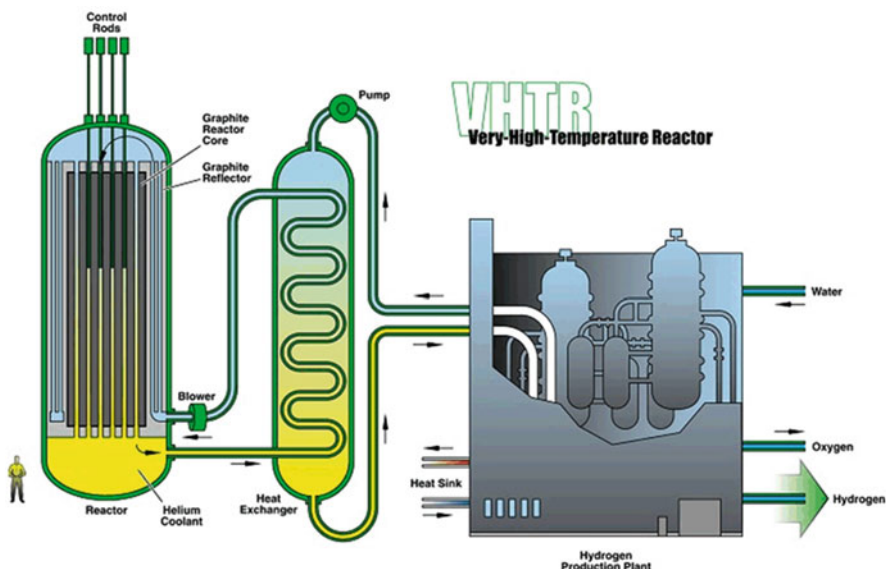


Fig. 18.4 Very high-temperature reactor. (Courtesy of the Generation IV International Forum)

The VHTR is a next step in the evolutionary development of high-temperature gas-cooled reactors. It is a graphite-moderated, helium-cooled reactor with thermal neutron spectrum. It can supply nuclear heat and electricity over a range of core outlet temperatures between 700 and 950 °C or more than 1000 °C in the future. The reactor core type of the VHTR can be a prismatic block core such as the Japanese HTTR or a pebble-bed core such as the Chinese HTR-10. For electricity generation, a helium gas turbine system can be directly set in the primary coolant loop, which is called a direct cycle or at the lower end of the outlet temperature range, a steam generator can be used with a conventional Rankine cycle. For nuclear heat applications such as process heat for refineries, petrochemistry, metallurgy, and hydrogen production, the heat application process is generally coupled with the reactor through an intermediate heat exchanger (IHX), the so-called indirect cycle. The VHTR can produce hydrogen from only heat and water by using thermochemical processes (such as the sulfur-iodine (S-I) process or the hybrid sulfur process) and high-temperature steam electrolysis (HTSE) or from heat, water, and natural gas by applying the steam reformer technology.

While the original approach for VHTR at the start of the Generation IV program focused on very high outlet temperatures and hydrogen production, current market assessments have indicated that electricity production and industrial processes based on high-temperature steam that require modest outlet temperatures (700–850 °C) have the greatest potential for application in the next decade. This also reduces technical risk associated with higher outlet temperatures. As a result, over the past decade, the focus has moved from higher outlet temperature designs such as GT-MHR and PBMR to lower outlet temperature designs such as HTR-PM in China and the NGNP in the United States.

The VHTR has two typical reactor configurations, namely:

- I. The pebble-bed type
- II. The prismatic block types

Although the shape of the fuel element for two configurations is different, the technical basis for both configurations is the same, such as the TRISO-coated particle fuel in the graphite matrix, full ceramic (graphite) core structure, helium coolant, and low power density.

This will allow achieving high outlet temperature and the retention of fission production inside the coated particle under normal operation condition and accident condition. The VHTR can support alternative fuel cycles such as U-Pu, Pu, MOX, and U-Th.

18.5.2 Molten Salt Reactor (MSR)

The MSR is distinguished by its core in, which the fuel is dissolved in molten fluoride salt. The technology was first studied more than 50 years ago. Modern interest is on fast reactor concepts as a long-term alternative to solid-fueled fast-

neutron reactors. The on-site fuel-reprocessing unit using pyrochemistry allows breeding plutonium or uranium-233 from thorium. R&D progresses toward resolving feasibility issues and assessing safety and performance of the design concepts. Key feasibility issues focus on a dedicated safety approach and the development of salt redox potential measurement and control tools in order to limit corrosion rate of structural materials. Further work on the batchwise online salt processing is required. Much work is needed on molten salt technology and related equipment (see Fig. 18.5).

Molten salt reactor (MSR) technology was partly developed, including two demonstration reactors, in the 1950s and 1960s in the United States (Oak Ridge National Laboratory). The demonstration MSRs were thermal-neutron-spectrum graphite-moderated concepts. Since 2005, R&D has focused on the development of fast-spectrum MSR concepts (MSFR) combining the generic assets of fast-neutron reactors (extended resource utilization, waste minimization) with those relating to molten salt fluorides as fluid fuel and coolant (low pressure and high boiling temperature, optical transparency).

In contrast to most other molten salt reactors previously studied, the MSFR does not include any solid moderator (usually graphite) in the core. This design choice is motivated by the study of parameters such as feedback coefficient, breeding ratio, graphite life-span, and ^{233}U initial inventory. MSFR exhibit large negative temperature and void reactivity coefficients, a unique safety characteristic not found in solid-fuel fast reactors.

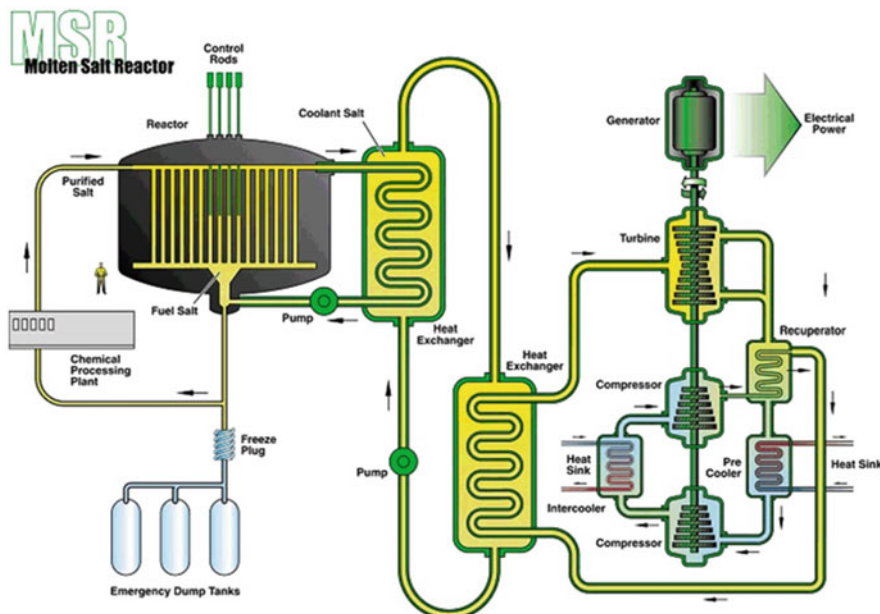


Fig. 18.5 Molten salt reactor. (Courtesy of the Generation IV International Forum)

Compared with solid-fuel reactors, MSFR systems have lower fissile inventories, no radiation damage constraint on attainable fuel burnup, no requirement to fabricate and handle solid fuel, and a homogeneous isotopic composition of fuel in the reactor. These and other characteristics give MSFRs potentially unique capabilities for actinide burning and extending fuel resources.

MSR developments in Russia on the Molten Salt Actinide Recycler and Transmuter (MOSART) aim to be used as efficient burners of transuranic (TRU) waste from spent UOX and MOX light water reactor (LWR) fuel without any uranium and thorium support and also with it. Other advanced reactor concepts are being studied, which use the liquid salt technology, as a primary coolant for fluoride salt-cooled high-temperature reactors (FHRs), and coated particle fuels similar to high-temperature gas-cooled reactors.

More generally, there has been a significant renewal of interest in the use of liquid salt as a coolant for nuclear and nonnuclear applications. These salts could facilitate heat transfer for nuclear hydrogen production concepts, concentrated solar electricity generation, oil refineries, and shale oil processing facilities among other applications.

18.5.3 Sodium-Cooled Fast Reactor (SFR)

The sodium-cooled fast reactor (SFR) uses liquid sodium as the reactor coolant, allowing high power density with low coolant volume fraction and operation at low pressure. While the oxygen-free environment prevents corrosion, sodium reacts chemically with air and water and requires a sealed coolant system (see Fig. 18.6).

Plant size options under considerations are ranging from small, 50 to 300 MWe, modular reactors to larger plants up to 1500 MWe. The outlet temperature is 500–550 °C for the options, which allows the use of the materials developed and proven in prior fast reactor programs.

The SFR closed fuel cycle enables regeneration of fissile fuel and facilitates management of minor actinides. However, this requires that recycle fuels be developed and qualified for use. Important safety features of the Generation IV system include a long thermal response time, a reasonable margin to coolant boiling, a primary system that operates near atmospheric pressure, and an intermediate sodium system between the radioactive sodium in the primary system and the power conversion system. Water/steam, supercritical carbon dioxide, or nitrogen can be considered as working fluids for the power conversion system to achieve high performance in terms of thermal efficiency, safety, and reliability. With innovations to reduce capital cost, the SFR is aimed to be economically competitive in future electricity markets. In addition, the fast-neutron spectrum greatly extends the uranium resources compared to thermal reactors. The SFR is considered to be the nearest-term deployable system for actinide management.

Much of the basic technology for the SFR has been established in former fast reactor programs and is being confirmed by the Phenix end-of-life tests in France,

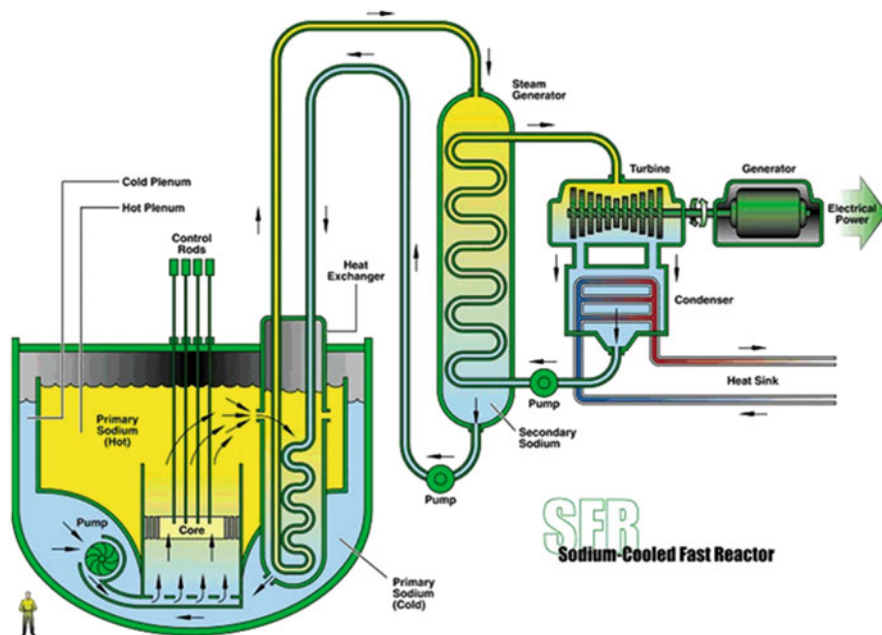


Fig. 18.6 Sodium-cooled fast reactor. (Courtesy of the Generation IV International Forum)

the restart of Monju in Japan, and the lifetime extension of BN-600 in Russia. New programs involving SFR technology include the Chinese experimental fast reactor (CEFR) which was connected to the grid in July 2011 and India's prototype fast breeder reactor (PFBR) which is currently planned to go critical in 2013.

The SFR is an attractive energy source for nations that desire to make the best use of limited nuclear fuel resources and manage nuclear waste by closing the fuel cycle.

Fast reactors hold a unique role in the actinide management mission because they operate with high-energy neutrons that are more effective at fissioning actinides. The main characteristics of the SFR for actinide management mission are:

- Consumption of transuranic in a closed fuel cycle, thus reducing the radiotoxicity and heat load, which facilitates waste disposal and geologic isolation
- Enhanced utilization of uranium resources through efficient management of fissile materials and multi-recycle

High level of safety achieved through inherent and passive means also allows accommodation of transients and bounding events with significant safety margins.

The reactor unit can be arranged in a pool layout or a compact loop layout. Three options are considered:

- A large size (600–1500 MWe) loop-type reactor with mixed uranium-plutonium oxide fuel and potentially minor actinides, supported by a fuel cycle based upon advanced aqueous processing at a central location serving a number of reactors
 - An intermediate-to-large size (300–1500 MWe) pool-type reactor with oxide or metal fuel
- A small size (50–150 MWe) modular-type reactor with uranium-plutonium-minor-actinide-zirconium metal alloy fuel, supported by a fuel cycle based on pyrometallurgical processing in facilities integrated with the reactor.

18.5.4 Supercritical Water-Cooled Reactor (SCWR)

The supercritical water-cooled reactors (SCWRs) are high-temperature, high-pressure, light water-cooled reactors that operate above the thermodynamic critical point of water (374 °C, 22.1 MPa) (see Fig. 18.7).

The reactor core may have a thermal or a fast-neutron spectrum, depending on the core design. The concept may be based on current pressure vessel or on pressure-tube reactors and thus use light water or heavy water as moderator. Unlike current water-cooled reactors, the coolant will experience a significantly higher enthalpy rise in the core, which reduces the core mass flow for a given thermal power and increases the core outlet enthalpy to superheated conditions. For both pressure vessel and pressure-tube designs, a once-through steam cycle has been envisaged, omitting any coolant recirculation inside the reactor. As in a boiling water reactor, the superheated steam will be supplied directly to the high-pressure steam turbine, and the feed water from the steam cycle will be supplied back to the core. Thus, the SCWR concepts combine the design and operation experiences gained from hundreds of water-cooled reactors with those experiences from hundreds of fossil-fired power plants operated with supercritical water (SCW). In contrast to some of the other Generation IV nuclear systems, the SCWR can be developed incrementally step-by-step from current water-cooled reactors.

A. Advantage and Challenges

Such SCWR designs have unique features that offer many advantages compared to state-of the-art water-cooled reactors:

- SCWRs offer increases in thermal efficiency relative to current-generation water-cooled reactors. The efficiency of a SCWR can approach 44% or more, compared to 34–36% for current reactors.
- Reactor coolant pumps are not required. The only pumps driving the coolant under normal operating conditions are the feedwater pumps and the condensate extraction pumps.
- The steam generators used in pressurized water reactors and the steam separators and dryers used in boiling water reactors can be omitted since the coolant is superheated in the core.

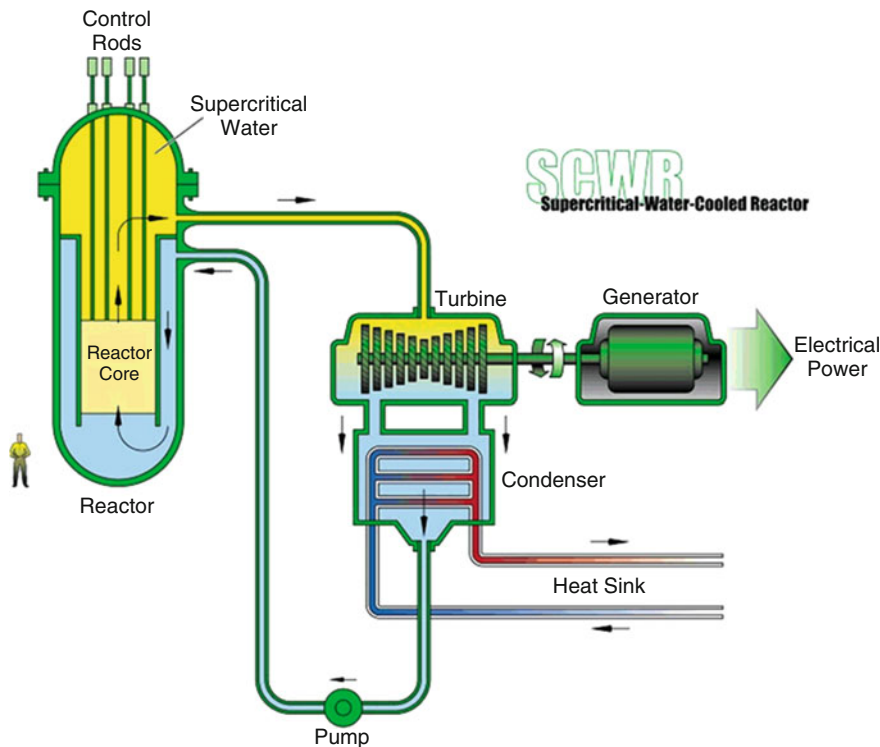


Fig. 18.7 Supercritical water-cooled reactor. (Courtesy of the Generation IV International Forum)

- Containment, designed with pressure suppression pools and with emergency cooling and residual heat removal systems, can be significantly smaller than those of current water-cooled reactors can.
- The higher steam enthalpy allows to decrease the size of the turbine system and thus to lower the capital costs of the conventional island.

These general features offer the potential of lower capital costs for a given electric power of the plant and of better fuel utilization and thus a clear economic advantage compared with current light water reactors.

However, there are several technological challenges associated with the development of the SCWR and particularly the need to validate transient heat transfer models (for describing the depressurization from supercritical to sub-critical conditions), qualification of materials (viz., advanced steels for cladding), and demonstration of the passive safety systems.

B. *GIF Progress up to 2012*

Pre-conceptual core design studies for a core outlet temperature of more than 500 °C have been performed in Japan, assuming either a thermal neutron spectrum or a fast-neutron spectrum. Both options are based on a coolant heat-

up in two steps with intermediate mixing underneath the core. Additional moderator for a thermal neutron spectrum is provided by feed water inside water rods. The fast-spectrum option uses zirconium hydride (ZrH_2) layers to minimize hardening of the neutron spectrum in case of core voiding. A pre-conceptual design of safety systems for both options has been studied with transient analyses.

A pre-conceptual plant design with 1700 MW net electric power based on a pressure-vessel-type reactor has been studied by Yamada et al. and has been assessed with respect to efficiency, safety, and cost. The study confirms the target net efficiency of 44% and estimates a cost reduction potential of 30% compared with current pressurized water reactors. Safety features are expected to be similar to advanced boiling water reactors.

A pre-conceptual design of a pressure-vessel-type reactor with a 500 °C core outlet temperature and 1000 MW electric power has been developed in Europe, as summarized by Schulenberg and Starflinger. The core design is based on coolant heat-up in three steps. Additional moderator for the thermal neutron spectrum is provided in water rods and in gaps between assembly boxes. The design of the nuclear island and of the balance of the plant confirms results obtained in Japan, namely, an efficiency improvement up to 43.5% and a cost reduction potential of 20–30% compared with latest boiling water reactors. Safety features as defined by the stringent European utility requirements are expected to be met.

Canada is developing a pressure-tube-type SCWR concept with a 625 °C core outlet temperature at the pressure of 25 MPa. The concept is designed to generate 1200 MW electric power (a 300 MW concept is also being considered). It has a modular fuel channel configuration with separate coolant and moderator. A high-efficiency fuel channel is incorporated to house the fuel assembly. The heavy-water moderator directly contacts the pressure tube and is contained inside a low-pressure calandria vessel. In addition to providing moderation during normal operation, it is designed to remove decay heat from the high-efficiency fuel channel during long-term cooling using a passive moderator cooling system. A mixture of thorium oxide and plutonium is introduced as the reference fuel, which aligns with the GIF position paper on thorium fuel. The safety system design of the Canadian SCWR is similar to that of the ESBWR. However, the introduction of the passive moderator cooling system coupled with the high-efficiency channel could reduce significantly the core damage frequency during postulated severe accidents such as large-break loss-of-coolant or station blackout events.

Pre-conceptual designs of three variants of pressure vessel supercritical reactors with thermal, mixed, and fast-neutron spectrum have been developed in Russia, which joined the SCWR System Arrangement in 2011.

Outside of the GIF framework, two conceptual SCWR designs with thermal and mixed neutron spectrum cores have been established by some research institutes in China. This is done, under framework of the Chinese national R&D projects from 2007 to 2012, covering some basic research projects on

materials and thermohydraulics, the core/fuel design, main system design (including the conventional part), safety systems design, reactor structure design, and fuel assembly structure design. The related feasibility studies have also been completed and show that the design concept has promising prospects in terms of the overall performance, integration of design, component structure feasibility, and manufacturability.

Prediction of heat transfer in SCW can be based on data from fossil-fired power plants as discussed by Pioro et al. Computational tools for more complex geometries like fuel assemblies are available but still need to be validated with bundle experiments. System codes for transient safety analyses have been upgraded to include SCW, including depressurization transients to subcritical conditions. Flow stability in the core has been studied numerically. As in boiling water reactors, flow stability can be ensured using suitable inlet orifices in fuel assemblies.

A number of candidate cladding materials have been tested in capsules, autoclaves, and recirculating loops up to 700 °C at a pressure of 25 MPa. Stainless steels with more than 20% chromium (Cr) are expected to have the required corrosion resistance up to a peak cladding temperature of 650 °C. More work is needed to develop alloys suitable for use at the design peak cladding temperatures of 850 °C for the Canadian SCWR concept. Further work is also needed to better identify the coolant conditions that lead to stress corrosion cracking. It has been shown that the creep resistance of existing alloys can be improved by adding small amounts of elements, such as zirconium (Zr), as reported by Kaneda et al. In the longer term, the steel experimental oxide dispersion-strengthened (ODS) alloys offer an even higher potential, whereas nickel-based alloys are being considered for use in ultra-supercritical fossil-fired plants which are less favorable for use in SCWRs due to their high neutron absorption and associated swelling and embrittlement.

Key water chemistry issues have been identified by Guzonas et al.; predicting and controlling water radiolysis and corrosion product transport (including fission products) remain the major R&D areas. In this regard, the operating experience using nuclear steam reheat at the Beloyarsk nuclear power plant in Russia is extremely valuable.

18.5.5 **Gas-Cooled Fast Reactor (GFR)**

The gas-cooled reactor (GFR) system is a high-temperature helium-cooled fast-spectrum reactor with a closed fuel cycle. It combines the advantages of fast-spectrum systems for long-term sustainability of uranium resources and waste minimization (through fuel multiple reprocessing and fission of long-lived actinides) with those of high-temperature systems (e.g., high thermal cycle efficiency and industrial use of the generated heat, for hydrogen production) (see Fig. 18.8).

The GFR uses the same fuel recycling processes as the SFR and the same reactor technology as the VHTR. Therefore, its development approach is to rely, in so far as feasible, on technologies developed for the VHTR for structures, materials, components, and power conversion system. Nevertheless, it calls for specific R&D beyond the current and foreseen work on the VHTR system, mainly on core design and safety approach.

The reference design for GFR is based around a 2400 MWth reactor core contained within a steel pressure vessel. The core consists of an assembly of hexagonal fuel elements, each consisting of ceramic-clad, mixed-carbide-fueled pins contained within a ceramic hex tube. The favored material at the moment for the pin clad and hex tubes is silicon carbide fiber-reinforced silicon carbide. The figure below shows the reactor core located within its fabricated steel pressure vessel surrounded by main heat exchangers and decay heat removal loops. The whole of the primary circuit is contained within a secondary pressure boundary, the guard containment.

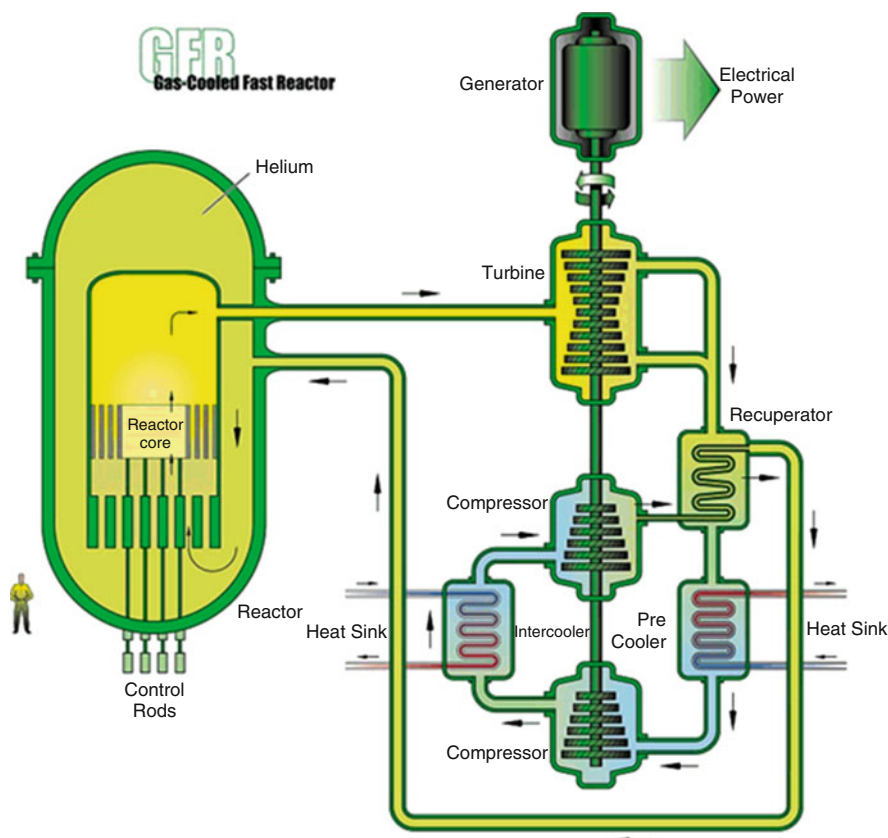


Fig. 18.8 Gas-cooled fast reactor. (Courtesy of the Generation IV International Forum)

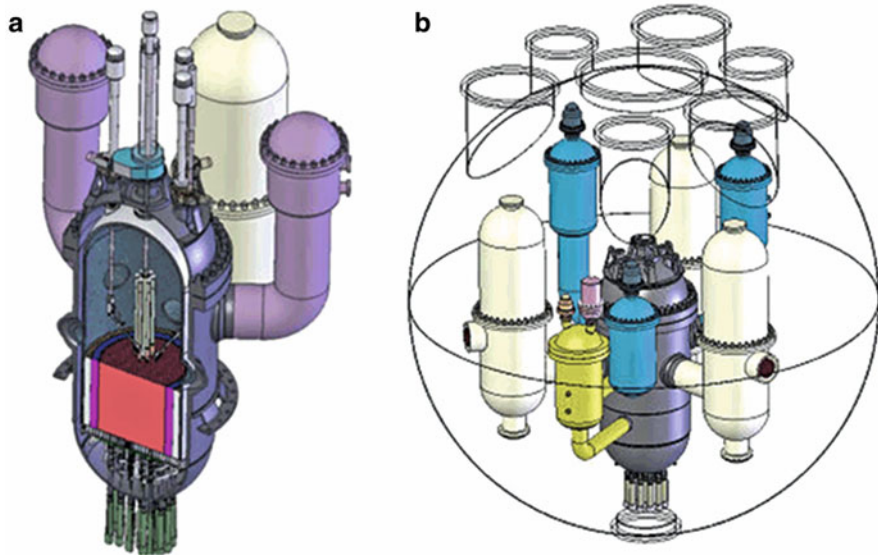


Fig. 18.9 (a) GFR reactor, decay heat loops, main heat exchangers, and fuel handling equipment. (b) GFR spherical guard vessel. (Courtesy of the Generation IV International Forum)

As it is illustrated in Fig. 18.9, the coolant is helium and the core outlet temperature will be of the order of 850 °C. A heat exchanger transfers the heat from the primary helium coolant to a secondary gas cycle containing a helium-nitrogen mixture, which, in turn drives a closed cycle gas turbine. The waste heat from the gas turbine exhaust is used to raise steam in a steam generator, which is then used to drive a steam turbine. Such a combined cycle is common practice in natural gas-fired power plant so it represents an established technology, with the only difference in the GFR case being the use of a closed cycle gas turbine.

18.5.6 Lead-Cooled Fast Reactor (LFR)

The lead-cooled fast reactor (LFR) features a fast-neutron spectrum, high-temperature operation, and cooling by molten lead or lead-bismuth eutectic (LBE), low-pressure, chemically inert liquids with very good thermodynamic properties. It would have multiple applications including production of electricity, hydrogen, and process heat. System concepts represented in plans of the Generation IV International Forum (GIF) System Research Plan (SRP) are based on Europe's ELFR lead-cooled system, Russia's BREST-OD-300, and the SSTAR system concept designed in the United States (see Fig. 18.10).

The LFR has excellent materials management capabilities since it operates in the fast-neutron spectrum and uses a closed fuel cycle for efficient conversion of fertile

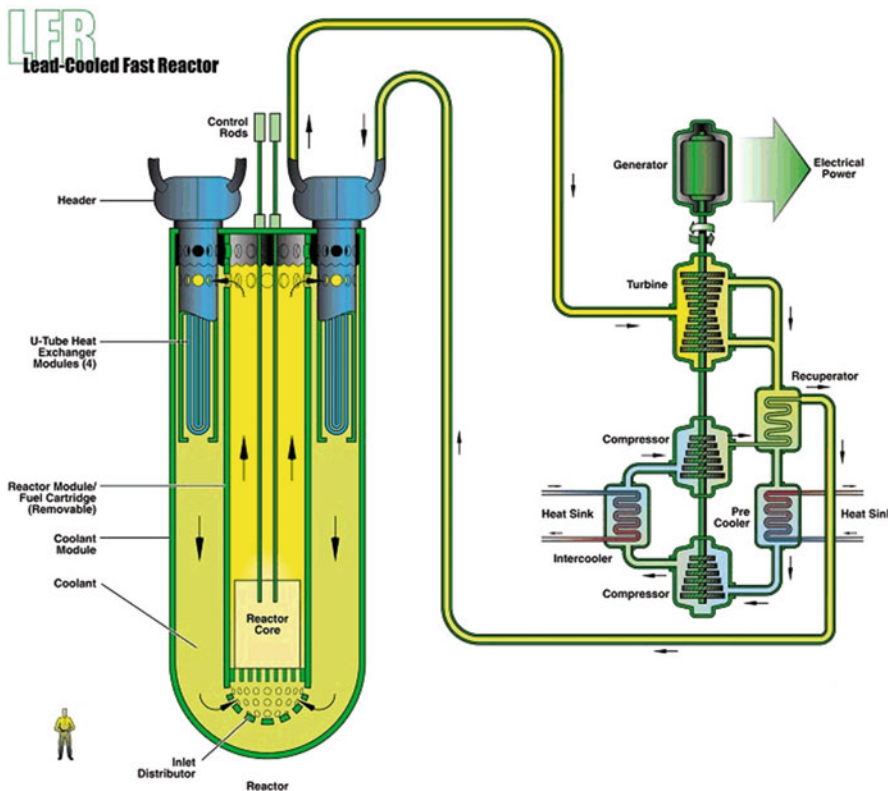


Fig. 18.10 Lead-cooled fast reactor. (Courtesy of the Generation IV International Forum)

uranium. It can also be used as a burner to consume actinides from spent LWR fuel and as a burner/breeder with thorium matrices. An important feature of the LFR is the enhanced safety that results from the choice of molten lead as a chemically inert and low-pressure coolant. In terms of sustainability, lead is abundant and hence available, even in case of deployment of a large number of reactors. More importantly, as with other fast systems, fuel sustainability is greatly enhanced by the conversion capabilities of the LFR fuel cycle. Because they incorporate a liquid coolant with a very high margin to boiling and benign interaction with air or water, LFR concepts offer substantial potential in terms of safety, design simplification, proliferation resistance, and the resulting economic performance. An important factor is the potential for benign end state to severe accidents.

The LFR has development needs in the areas of fuels, materials performance, and corrosion control. During the next 5 years, progress is expected on materials, system design, and operating parameters. Significant test and demonstration activities are underway and planned during this period.

18.6 Next Generation of Nuclear Power Reactors for Power Production

Experts are projecting worldwide electricity consumption will increase substantially in the coming decades, especially in the development world, accompanying economic growth and social progress that has direct impact on rising electricity prices have focused fresh attention on nuclear power plants. New, safer, and more economical nuclear reactors could not only satisfy many of our future energy needs but could combat global warming as well. Today's existing nuclear power plants on line in the United States provide fifth of the nation's total electrical output.

Taking into account the expected increase in energy demand worldwide and the growing awareness about global warming, climate change issues, and sustainable development, nuclear energy will be needed to meet future global energy demand.

Nuclear power plant technology has evolved as distinct design generations as we mentioned in the previous section and briefly summarized here again as follows:

- First generation: prototypes and first realizations (~1950–1970)
- Second generation: current operating plants (~1970–2030)
- Third generation: deployable improvements to current reactors (~2000 and on)
- Fourth generation: advanced and new reactor systems (2030 and beyond)

The Generation IV International Forum, or *GIF*, was chartered in July 2001 to lead the collaborative efforts of the world's leading nuclear technology nations to develop next-generation nuclear energy systems to meet the world's future energy needs.

Eight technology goals have been defined for Generation IV systems in four broad areas:

1. Sustainability
2. Economics
3. Safety and reliability
4. Proliferation resistance and physical protection

A large number of countries share these ambitious goals as they aim at responding to economic, environmental, and social requirements of the twenty-first century. They establish a framework and identify concrete targets for focusing *GIF* R&D efforts.

18.7 Goals for Generation IV Nuclear Energy Systems

The next generation ("Generation IV") of nuclear energy systems is intended to meet the below goals (while being at least as effective as the "third" generation in terms of economic competitiveness, safety, and reliability) in order to provide a sustainable development of nuclear energy.

In principle, the Generation IV systems should be marketable or deployable from 2030 onward. The systems should also offer a true potential for new applications compatible with an expanded use of nuclear energy, in particular in the fields of hydrogen or synthetic hydrocarbon production, seawater desalination, and process heat production.

It has been recognized that these objectives, widely and officially shared by a large number of countries, should be at the basis of an internationally shared R&D program, which allows keeping open and consolidating the technical options and avoiding any early or premature down selection.

In fact, because the next-generation nuclear energy systems will address needed areas of improvement and offer great potential, many countries share a common interest in advanced R&D that will support their development. The international research community should explore such development benefits from the identification of promising research areas and collaborative efforts that. The collaboration on R&D by many nations on the development of advanced next-generation nuclear energy systems will in principle aid the progress toward the realization of such systems, by leveraging resources, providing synergistic opportunities, avoiding unnecessary duplication, and enhancing collaboration.

As it is illustrated in Fig. 18.1, we are able to see the evolution of nuclear power plant life cycles

In 2009, the Experts Group published an outlook on Generation IV R&D, to provide a view of what GIF members hope to achieve collectively in the period 2010–2014. All Generation IV systems have features aiming at performance improvement, new applications of nuclear energy, and/or more sustainable approaches to the management of nuclear materials. High-temperature systems offer the possibility of efficient process heat applications and eventually hydrogen production. Enhanced sustainability is achieved primarily through adoption of a closed fuel cycle with reprocessing and recycling of plutonium, uranium, and minor actinides using fast reactors; this approach provides significant reduction in waste generation and uranium resource requirements.

18.8 Why We Need to Consider the Future Role of Nuclear Power Now

The following reasonings are some arguments that show why we need to consider the future role in the design of new nuclear power plant:

1. Nuclear power has been part of the global energy need mix for the past five decades. Currently it provides about 18% of the electricity we use in our homes and workplaces. For example, in the United Kingdom, about one third of our emissions of carbon dioxide come from electricity generation [10]. The vast majority of those emissions come from coal and gas power plants.

2. Energy companies will need to invest in around 30–35 GW of new electricity-generating capacity – as coal and nuclear plants retire – over the next two decades, with around two thirds needed by 2020. This is equivalent to about one third of our existing capacity. The world needs a clear and stable regulatory framework to reduce uncertainty for business to help ensure sufficient and timely investment in technologies that contribute to our energy goals.
3. Of the capacity that is likely to close over the two decades, two thirds is from carbon intensive fossil fuel generation and about 10 GW is nuclear and therefore low carbon. So companies' decisions on the type of power stations they invest in to replace this capacity will have significant implications for the level of carbon emissions. As an illustration, if our existing nuclear power stations were all replaced with fossil fuel-fired power stations, our emissions would be between 8 and 16 MtC (million tons of carbon) a year higher as a result (depending on the mix of gas and coal-fired power stations). This would be equivalent to about 30–60% of the total carbon savings we project to achieve under our central scenario from all the measures we are bringing forward in the reference that is known as Energy White Paper [11]. Our gas demand would also be higher, at a time when we are becoming more dependent on imported sources of fossil fuels.
4. Electricity demand in the United States is expected to grow significantly in the future. Over the past decade, Americans used 17% more electricity, but domestic capacity rose only 2.3% (National Energy Policy, May 2001). Unless the United States significantly increases its generating capacity, the country will face an energy shortage that is projected to adversely affect our economy, our standard of living, and our national security. Coupled with this challenge is the need to improve our environment.
5. New nuclear power stations have long lead times. This time is necessary to secure the relevant regulatory and development consents, which must be obtained before construction can begin, and there is also a long construction period compared to other generating technologies. Our conservative assumption is that for the first new nuclear plant the pre-construction period would last around 8 years (to secure the necessary consents) and the construction period would last around 5 years. For subsequent plants, this is assumed to be 5 and 5 years, respectively. New nuclear power stations are therefore unlikely to make a significant contribution to the need for new capacity before 2020.
6. Even with our expectations that the share of renewable will grow, it is likely that fossil fuel generation will meet some of this need. However, beyond that date there are still significant amounts of new capacity needed; for example, in 2023 one third or 3 GW of our nuclear capacity will still be operational, based on published lifetimes. Given the likely increase in fossil fuel generation before this date, it is important that much of this capacity is replaced with low-carbon technologies. New nuclear power stations could make an important contribution, as outlined in this consultation document, to meeting our needs for low-carbon electricity generation and energy security in this period and beyond to 2050. Because of the lead times, without clarity now we will foreclose the opportunity for nuclear power.

7. The existing approach on new nuclear build was set out in 2003: “Nuclear power is currently an important source of carbon-free electricity. However, its current economics make it an unattractive option for new, carbon-free generating capacity and there are also important issues of nuclear waste to be resolved. These issues include our legacy waste and continued waste arising from other sources. This white paper does not contain specific proposals for building new nuclear power stations. However, we do not rule out the possibility that at some point in the future new nuclear build might be necessary if we are to meet our carbon targets. Before any decision to proceed with the building of new nuclear power stations, there will need to be the fullest public consultation and the publication of a further white paper setting out our proposals.”
8. Since 2003 there have been a number of developments, which have led the government to consider afresh the potential contribution of new nuclear power stations. Firstly, there has been significant progress in tackling the legacy waste issue:
 - We have technical solutions for waste disposal that scientific consensus and experience from abroad suggest it could accommodate all types of wastes from existing and new nuclear power stations
 - There is now an implementing body (the Nuclear Decommissioning Authority), with expertise in this area, and the government is reconstituting the Committee on Radioactive Waste Management (CoRWM) in order to provide continued independent scrutiny and advice
 - A framework for implementing long-term waste disposal in a geological repository will be consulted on in the coming months.
9. The government has also made progress in considering the issue of waste management in relation to potential new nuclear power stations:
 - This consultation provides the opportunity to discuss the ethical, intergenerational, and public acceptability issues associated with a decision to allow the private sector to invest in new nuclear power stations and generate new nuclear waste.
 - The government is developing specific proposals to protect the taxpayer. Under these proposals, private sector developers would meet the full decommissioning costs and full share of waste management costs. The proposals would be implemented in the event that we conclude that energy companies should be allowed to invest in new nuclear power stations. They would need to be in place before proposals for new power stations could go ahead.
10. Secondly, the high-level economic analysis of nuclear power, prepared for the Energy Review, concluded that under likely scenarios for gas and carbon prices and taking prudent estimates of nuclear costs, nuclear power would offer general economic benefit to the United Kingdom in terms of reduced carbon emissions and security of supply benefits²⁵. Therefore, the government believes that it has a potential contribution to make, alongside other low-carbon-generating technologies.

11. Thirdly, some energy companies have expressed a strong interest in investing in new nuclear power stations. They assess that new nuclear power stations could be an economically attractive low-carbon investment, which could help diversify their generation portfolios. Their renewed interest reflects assessments that with carbon being priced to reflect its impacts and gas prices likely to be higher than previously expected, the economics of new nuclear power stations are becoming more favorable.
12. Nuclear power stations have long lead times. If they are to be an option to replace the capacity closing over the next two decades, and in particular after 2020, a decision on whether allowing energy companies the option of investing in new nuclear power stations would be in the public interest needs to be taken now. Energy companies would need to begin their initial preparations in the near future in order to have a reasonable prospect of building new generation in this period. Not taking the public interest decision now would foreclose the option of new nuclear being one of our options for tackling climate change and achieving energy security.

18.9 The Generation IV Roadmap Project

As the Generation IV goals were being finalized, preparations were made to develop the Generation IV technology roadmap. The organization of the roadmap is shown in the Fig. 18.11 below. The Roadmap Integration Team (RIT) is the executive group. Groups of international experts were organized to undertake identification and evaluation of candidate systems and to define R&D to support them [12].

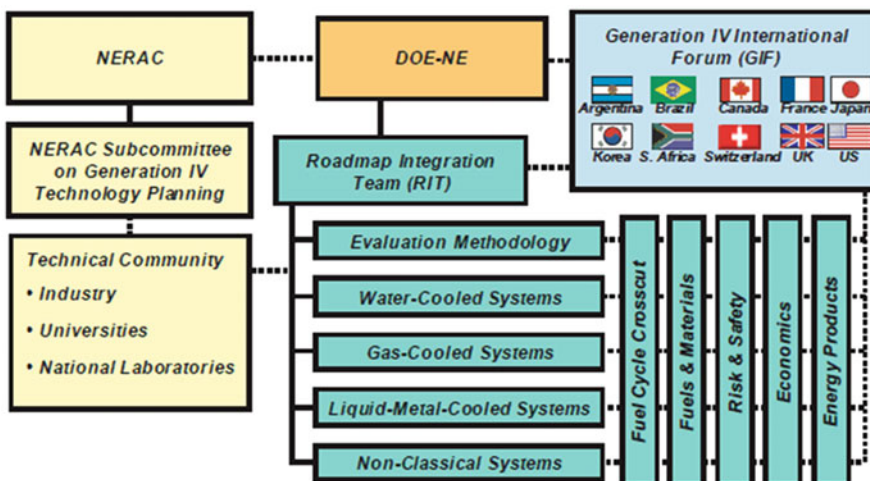


Fig. 18.11 The roadmap organization

In a first step, an Evaluation Methodology Group was formed to develop a process to systematically evaluate the potential of proposed Generation IV nuclear energy systems to meet the Generation IV goals. A discussion of the Evaluation Methodology Group's evaluation methodology is included in this report. At the same time, a solicitation was issued worldwide, requesting that concept proponents submit information on nuclear energy systems that they believe could meet some or all of the Generation IV goals. Nearly 100 concepts and ideas were received from researchers in a dozen countries [12].

Technical Working Groups (TWGs) were formed – covering nuclear energy systems employing water-cooled, gas-cooled, liquid-metal-cooled, and nonclassical reactor concepts – to review the proposed systems and evaluate their potential using the tools developed by the Evaluation Methodology Group. Because of the large number of system concepts submitted, the TWGs collected their concepts into sets of concepts with similar attributes. The TWGs conducted an initial screening, *termed screening for potential*, to eliminate those concepts or concept sets that did not have reasonable potential for advancing the goals or were too distant or technically infeasible [12].

A Fuel Cycle Crosscut Group (FCCG) was also formed at a very early stage to explore the impact of the choice of fuel cycle on major elements of sustainability – especially waste management and fuel utilization. Their members were equally drawn from the working groups, allowing them to compare their insights and findings directly. Later, other crosscut groups were formed covering economics, risk and safety, fuels and materials, and energy products. The crosscut groups reviewed the TWG reports for consistency in the technical evaluations and subject treatment and continued to make recommendations regarding the scope and priority for crosscutting R&D in their subject areas. Finally, the TWGs and crosscut groups worked together to report on the R&D needs and priorities of the most promising concepts [12].

The international experts that contributed to this roadmap represented all ten GIF countries, the Organization for Economic Cooperation and Development Nuclear Energy Agency, the European Commission, and the International Atomic Energy Agency [12].

At least in the United States under the Department of Energy (DOE), with Idaho SMRs project, with a roadmap, federal agencies may wish to follow, when making power purchase decisions that may involve a small modular reactor, the key steps in the decision process which may be summarized in Fig. 18.12. SMRs are designed to provide valuable resilience services as a secure, reliable, and flexible source of primary and backup power. SMRs, coupled with transmission hardening, could provide highly reliable, non-intermittent, clean, and carbon-free power. SMRs can also easily store 2 years' worth of fuel on-site. Certain SMR designs allow for output to be varied over days, hours, or minutes, thereby enabling the SMR to adjust to be in line with changing load demands.

However, implementing SMR projects around the country is difficult due to the FOAK technology, construction challenges, and licensing requirements. SMRs introduce significant expenses and risks that may be challenging for a project to

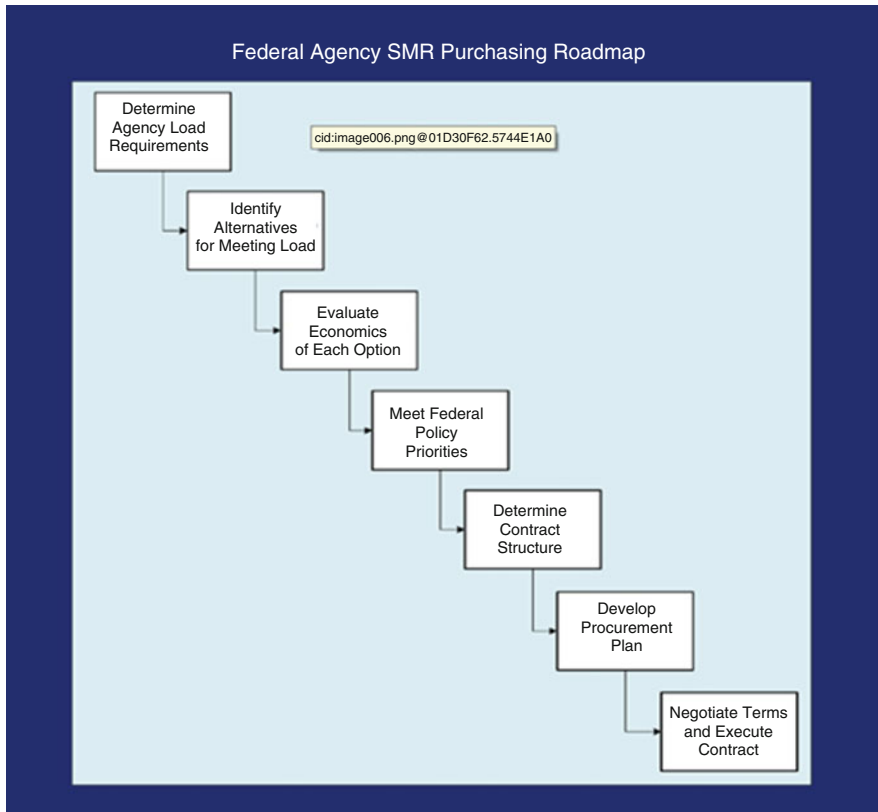


Fig. 18.12 Federal agency SMR purchasing roadmap

bear without any financial support from the intended end user. The recommendations offered in this chapter, along with the potential solutions described elsewhere in this report, may be considered to assist with overcoming these challenges and advance the deployment of SMRs in the United States while improving grid resiliency at the Oak Ridge Reservation.

More specifically, this chapter identifies how the federal government can assist with making the financing and development of SMRs easier – both in its role as a customer and as a governing body, which permits federal agencies to enter into agreements for a term of up to 30 years to purchase power produced by small modular reactors.

The Congress may wish to consider enacting legislation which would permit federal agencies to share in the risks associated with the construction of SMRs. Leveraging the federal government's strong credit standing as a purchaser of the power and its continual need for baseload power is important in the development of SMRs. Federal agency purchasers can help to set the market and offer more certainty to other initial buyers. While there are a range of legal authorities, federal agencies

may use to purchase power, most often GSA's 40 U.S.C. § 501 is used, limiting PPA terms to 10 years. This 10-year limitation impacts a party's ability to take advantage of government purchasing for financing.

Federal agencies should be able to purchase power produced by an SMR for a term of up to 30 years. Currently, only DOD (pursuant to 10 U.S.C. § 2922a) has the authority to purchase power for a term of up to 30 years in limited circumstances. By creating an authority that permits federal agencies to purchase power for up to 30 years, SMR developers will be able to use traditional financing to repay a financed project or a long-term bond over an up to 30-year term, making the financing more affordable. Depending upon the size of the federal agency's offtake, as compared to the size of the power source being funded, this discrepancy may make it difficult for financing.

18.10 Licensing Strategy Components

A DOE and NRC working group was formed to develop the licensing strategy. This group conducted an in-depth analysis of LWR licensing process and technical requirement options, which was performed by the experienced senior staff of the two agencies. The methodology used in formulating the NGNP licensing strategy alternatives also included development of a Phenomena Identification and Ranking Table (PIRT) for a prototypical NGNP by subject matter experts in the nuclear field. The PIRT results assisted in the identification of key R&D needs. Based on the detailed analysis of these alternatives and balancing schedule considerations with licensing risk and other pertinent factors, the Secretary of Energy and the Commission concluded that the following NGNP licensing strategy provides the best opportunity for meeting the 2021 date for initial operation of a prototype NGNP, which details of such analysis can be found in NGNP report to Congress [13].

NGNP reactor technology will differ from that of commercial LWRs currently used for electric power generation. LWRs have a well-established framework of regulatory requirements, a technical basis for these requirements, and supporting regulatory guidance on acceptable approaches an applicant can take to show that NRC requirements are met. The NRC uses a standard review plan to review licensing applications for these reactor designs. Additionally, the NRC has a well-established set of validated analytical codes and methods and a well-established infrastructure for conducting safety research needed to support its independent safety review of an LWR plant design and the technical adequacy of a licensing application.

New nuclear power plants can be licensed under either of two existing regulatory approaches. The first approach is the traditional "two-step" process described in Title 10, Part 50, "Domestic Licensing of Production and Utilization Facilities," of the *Code of Federal Regulations* (10 CFR Part 50), which requires both a construction permit (CP) and a separate operating license (OL). The second approach is the new "one-step" licensing process described in 10 CFR Part 52, "Licenses, Certifications,

and Approvals for Nuclear Power Plants,” which incorporates a combined construction and operating license (COL). Both of these processes allow a deterministic or risk-informed performance-based approach to technical requirements.

Many of the regulatory requirements and supporting review guidance for LWRs are technology-neutral; that is, they are applicable to non-LWR designs as well as LWR designs. However, certain LWR requirements may not apply to the unique aspects of a VHTR design. Accordingly, in developing the NGNP licensing strategy, the NRC and DOE considered the various options available to the NRC staff for adapting current NRC LWR licensing requirements for the NGNP VHTR. These options related to legal, process, technical, research, and regulatory infrastructure matters and included an examination of historical licensing activities. These considerations led to selection of a licensing strategy that would comply best with the considerations identified in the EPAct.

The licensing strategy outlined in this report is composed of two distinct aspects. The first aspect is a recommended approach for how the NRC will adapt the current LWR technical requirements to apply to a VHTR. The second aspect is a recommended licensing process alternative that identifies which of the procedural alternatives in the NRC regulations would be best for licensing the NGNP. To arrive at these recommendations, NRC and DOE evaluated a number of options and alternatives.

18.11 Market and Industry Status and Potentials

Europe plays a leading role in the development of nuclear energy and has 35% of the globally installed capacity. The reactors in Europe have been in operation for 27 years on average. Current plans in most EU member countries are to extend their lifetime on a case-by-case basis beyond 40 years and even beyond 60 years in some cases, in combination with power upgrades. The first two Generation III reactors, European pressurized water reactor (EPR), are currently being constructed.

The global growth of the nuclear energy can be measured by the increasing number of reactors [9, 10] (3 more in 2005 and 2006, 7 in 2007, and 10 in 2008), but with a strong concentration in Asia. Nevertheless, a number of these reactors are of European design. There are presently four reactors under construction in Europe: the EPRs in Finland and France and two smaller reactors of Generation II type (VVER 440) in Slovakia and with plans to build new reactors in France, Romania, Bulgaria, and Lithuania. Perhaps more importantly the United Kingdom has taken concrete steps toward new build with bidding beginning in 2009 from leading utilities, and Italy has declared that it intends to start a nuclear program with a target to produce 25% of the electricity by 2030. The estimated maximum potential installed capacities of nuclear fission power for the EU-27 (150 GWe by 2020 and 200 GWe by 2030) appear more realistic than the baseline (115 GWe in 2020 and 100 GWe in 2030).

Programs to build fast reactor and high-temperature reactor demonstrators are being implemented in Russia and several Asian countries. Although these are not Generation IV designs, transfer of knowledge and experience from operation will contribute significantly to future Generation IV development. In Europe, a concerted effort is proposed in the form of a European Industrial Initiative in sustainable nuclear fission as part of the community's SET Plan. The EII has singled out the sodium fast reactor (SFR) as its primary system with the basic design selected by 2012 and construction of a prototype of 250–600 MWe that is connected to the grid and operational by 2020.

In parallel, a gas- or lead-cooled fast reactor (GFR/LFR) will also be investigated. The selection of the alternative fast reactor technology is scheduled for 2012 on the basis of a current program of pre-conceptual design research. The reactor will be a 50–100 MWth demonstrator reactor that should also be in operation by 2020. The SFR prototype and LFR/GFR demonstrator will be complemented by a fuel fabrication workshop that should serve both systems and by a range of new or refurbished supporting experimental facilities for qualification of safety systems, components, materials, and codes. A commercial deployment for a SFR reactor is expected from 2040 and for the alternative design a decade later.

High-temperature reactors dedicated to cogeneration of process heat for the production of synthetic fuels or industrial energy products could be available to meet market needs by 2025, which would trigger requirements to construct "first-of-a-kind" demonstrators in the next few years. Indeed, such programs are currently being set up in some countries (United States, Japan, South Africa, and China). The key aspect is the demonstration of the coupling with the conventional industrial plant. Supercritical water reactors and molten salt reactors, as well as accelerator-driven subcritical systems dedicated to transmutation of nuclear waste, are currently being assessed in terms of feasibility and performance, though possible industrial applications have yet to be clearly identified.

18.12 Barriers

The high capital cost of nuclear energy in combination with uncertain long-term conditions constitutes a financial risk for utilities and investors. The lack of widespread support in the EU member states may undermine the strength of EU industry for the development of new technologies. Harmonized regulations, codes, and standards at the EU level would strengthen the competitiveness of Europe's nuclear sector and promote deployment of Generation III technology in the near term. The industry, infrastructures, and services that support nuclear power have shrunk significantly during the last decades. This situation in Europe is not unique but it may pose a bottleneck for the deployment of reactors in the relatively near future. One example is large forgings needed for pressure vessel heads. World capacity is limited and even at the present new build construction rate there is a waiting list for delivery of these components.

Public acceptance remains an important issue, but even though opinion is not very favorable in a number of member states, there are signs that the mood is changing. Nevertheless, concerted efforts are still required, based on objective and open dialogue among all stakeholders. International cooperation currently exists at the level of research, and this is being facilitated in the area of Generation IV systems by the Generation IV International Forum (GIF). However, EU industry is facing stiff competition, especially in Asia where strong corporate support for R&D is putting industry in a better position to gain leadership in the near future. Another significant potential barrier for nuclear fission is the shortage of qualified engineers and scientists as a result of the lack of interest in nuclear careers during the 1990s and the reduced availability of specialist courses at universities. Preservation of nuclear knowledge remains a major issue, especially since most of the current generations of nuclear experts are nearing retirement.

18.13 Needs

The high initial capital investments and sensitive nature of the technology involved mean that renewed deployment of currently available nuclear technology can only take place in a stable (or, at least, predictable) regulatory, economic, and political environment. In June 2009, the EU established a common binding framework on nuclear safety with the adoption of the Council Directive establishing a community framework for the safety of nuclear installations [14, 15]. This is the first binding EU legislation in this field.

In order to retain its leading position and to overcome bottlenecks in the supply chain, Europe also needs to reinvigorate the industrial supply chains supporting the nuclear sector. Apart from this overriding requirement for a clear European strategy on nuclear energy, a new research and innovation system is needed that can assure additional funding, especially for the development of Generation IV technology. In this context the Sustainable Nuclear Energy Technology Platform [11] plays a key role. The time scales involved, and the fact that key political and strategic decisions are yet to be taken regarding this technology, mean that a significant part of this additional funding must be public. The launch of the European Sustainable Nuclear Industrial Initiative under the community's SET Plan bringing together key industrial and R&D organizations would be a very significant step toward the construction and operation of the necessary demonstrators and prototypes.

High-temperature reactors based on existing technology can also be deployed in the near future with the aim of demonstrating the cogeneration of process heat and the coupling with industrial processes. This would need to be built and funded through a European or international consortium, which should also include the process heat end-user industries. In the meantime, an enhanced research effort is needed to ensure Europe's leadership in sustainable nuclear energy technologies that include continuous innovation in LWRs, qualification and development of materials,

closed fuel cycle with U-Pu multi-recycling, and (very) high-temperature reactors and related fuel technology.

Breakthroughs are especially sought in the fields of materials to enhance safety, nuclear fuels, and fuel cycle processes. Additionally, there is a need for harmonization of European standards and a strategic planning of national and European research infrastructures for use by the European research community. The implementation of geological disposal of high-level waste is also being pursued as part of national waste management programs, though some countries are not as advanced as others. The new Implementing Geological Disposal of Radioactive Waste Technology Platform, launched in November 2009, is coordinating the remaining necessary applied research in Europe leading up to the start of operation of the first geological repositories for high-level and long-lived waste around 2020 and will facilitate progress in and technology transfer with other national programs.

More effort is needed to inform and interact with the public and other stakeholders, and the education and training of a new generation of nuclear scientists and engineers and transfer of knowledge from the generation that designed and built reactors in the 1970s and 1980s need urgent attention. The European Nuclear Energy Forum (ENEF) provides a unique platform for a broad open discussion on the role nuclear power plays today and could play in the low-carbon economy of the future. ENEF analyzes and discusses the opportunities (competitiveness, financing, grid, etc.) and risks (safety, waste) and need for education and training associated with the use of nuclear power and proposes effective ways to foster communication with and participation of the public.

18.14 Synergies with Other Sectors

Nuclear energy provides a very stable baseload electricity supply and can therefore work in synergy with renewable energies that are more intermittent. Nuclear energy should also contribute significantly to a low-carbon transport sector as high-temperature application can provide synthetic fuel and hydrogen, while generated electricity could provide a large share of the energy for electrical cars. Interactions are anticipated with activities in “hydrogen energy and fuel cells” through the potential of nuclear hydrogen production and with “grids” from the characteristics of nuclear electricity generation. With respect to basic materials research, there should be synergies with other applications, such as “biofuels” and “clean coal,” where materials are subjected to extreme environments. In addition, the opportunities for important common research with the fusion program, especially in the area of materials, need to be fully exploited. The European Energy Research Alliance under the SET Plan is also expected to provide opportunities for synergies and collaborative work in the area of nuclear materials. In general, crosscutting research would benefit from more clearly defined channels of interaction, responsibilities, and increased flexibility regarding funding and programming.

18.15 Combined Cycles for Efficiency of New Generation Nuclear Power Plants

In Chap. 17, Sect. 17.1 of this book, we briefly explained an innovative design approach to combined cycles driven efficiency for next generation of nuclear power plants as part of Generation IV, which includes all six types of small modular reactors (SMRs) as well as references by this author [1–3].

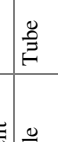
Out of the six chosen reactor design of Generation IV systems that are described in Sect. 18.4 and with more details of each of these reactors are given in its subsections, while they are summarized in Table 18.2, three to four of them perfectly fit into combined cycles of open-air Brayton cycle due to the nature of their high-temperature design requirements, namely, very high-temperature gas reactor (VHTR), sodium-cooled fast reactor (SFR), gas-cooled fast reactor (GFR), and molten salt reactor (MSR), where their temperature design ranges anywhere from 550 °C to 900 °C, and that is the type of temperature range which is required by innovative open-air Brayton combined cycle, where the steady-state thermal analysis computer code is developed by this author and his collaborator [1–3].

For this combined cycle to work in a more efficient way, we pay our attention and are more interested in a very high-temperature reactor (VHTR) within this generation (i.e., GEN-IV) for open-air Brayton cycle implementation as part of a new innovative design. Historically, speaking the development of high-temperature gas-cooled reactor (HTGR), also known as very high-temperature gas-cooled reactor (VHTR) for its Generation IV designs, has continued for over half a century. Several reactors have been built or being constructed. These are identified in Table 18.3. Still others are being developed at various stages, including more units of high-

Table 18.2 Summary of the main characteristics of the six Generation IV systems

System	Neutron spectrum	Coolant	Temp. °C	Fuel cycle	Size (MWe)
<i>VHTR</i> (Very high-temperature gas reactor)	Thermal	Helium	900 to 1000	Open	250–300
<i>SFR</i> (Sodium-cooled fast reactor)	Fast	Sodium	550	Closed	30–150, 300–1500 1000–2000
<i>SCWR</i> (Supercritical water-cooled reactor)	Thermal/fast	Water	510–625	Open/ closed	300–700 1000–2000
<i>GFR</i> (Gas-cooled fast reactor)	Fast	Helium	850	Closed	1200
<i>LFR</i> (Lead-cooled fast reactor)	Fast	Lead	480–800	Closed	20–180 300–200 600–1000
<i>MSR</i> (Molten salt reactor)	Epithermal	Fluoride salt	700–800	Closed	1000

Table 18.3 High-temperature gas-cooled reactor built worldwide

Test HTGRs				Prototype HTGRs			
							
Country	AVR	HTGR	HTR-10	Peach bottom	FSV	THTR-300	HTR-PM
Period of operation	UK (OECD)	Germany	Japan	China	USA	Germany	China
Reactor core type	Tube	Pebble bed	Prismatic	Pebble bed	Tube	Prismatic	Pebble bed
Thermal power, MW _{th}	21.5	46	30	10	115	842	750
Coolant outlet temperature, °C	750	950	700	725	775	750	750
Coolant pressure, MPa	2	1.1	4.0	3.0	2.25	4.8	3.9
Electrical output, MW _e	—	13	—	2.5	40	330	211
Process heat output, MW _{th}	—	—	10	—	—	—	—
Process heat temperature, °C	—	—	863	—	—	—	—
Core power density, W/cm ³	14	2.6	2.5	2	8.3	6.3	6.0
Fuel design	UO ₂ TRISO	(Th/U, U)O ₂ , C ₂ BISO	UO ₂ TRISO	ThC ₂ BISO	(Th/U)C ₂ TRISO	(Th/U)O ₂ BISO	UO ₂ TRISO

Courtesy of X.L. Yan, Japan Atomic Agency, Oarai-Machi, Ibaraki-ken, Japan
BISO Bi-isotropic coating of fuel particle

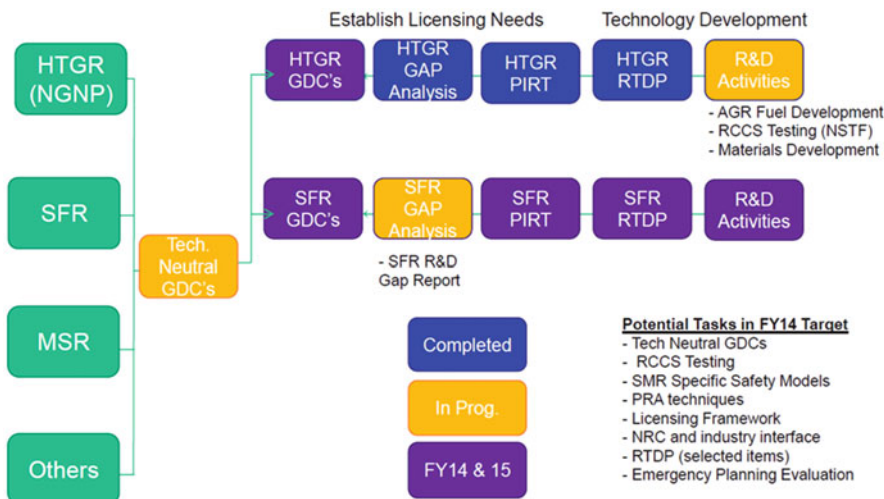


Fig. 18.13 Overview of advanced small modular reactor safety and licensing progress. (Courtesy of Idaho National Laboratory)

temperature reactor-pebble-bed module (HTR-PM) power reactor in China, multipurpose GTHTR300C in Japan, NuH² for nuclear hydrogen and process heat in Korea, Next Generation Nuclear Plant (NGNP) cogenerating reactor in the United States, and an experimental power reactor in Indonesia.

Dragon, the first reactor built, pioneered the use of tri-isotropic (TRISO)-coated particle fuel, still the standard fuel form today. The Arbeitsgemeinschaft Versuchsreaktor (AVR) tested additional fuel designs and accumulated extensive performance data. The prototypical Fort St. Vrain (FSV) validated the prismatic core physics design with high burnup (90 GWd/t) on thorium fuel and demonstrated steam turbine power generation at 39% thermal efficiency and easy load following.

As part of advanced small modular reactor (AdvSMR) safety and licensing progress is concerned an overview of this roadmap demonstrated in Fig. 18.13

Yet the component failures, such as with the primary coolant circulator, forced excess outage and undermined its economics. The thorium high-temperature reactor-300 (THTR-300) of a pebble-bed core design encountered technical problems after only a brief period of operation, and their scrutiny led to protracted shutdown. The FSV and THTR- 300 were prematurely decommissioned largely as business decision [16].

Asia then became home to the latest builds. The high-temperature engineering test reactor (HTTR) in Japan and the high-temperature test reactor (HTR-10) in China were constructed and started up around the turn of the millennium. Both remain operational today. The 30-MWth HTTR demonstrated operation of 950 °C reactor outlet coolant and export of 863 °C process heat. Such high-temperature capability would raise reactor thermal efficiency and support advanced applications as reported by the plant design of GTHTR300 by the Japan Atomic Energy Agency

(JAEA) (Sato et al. [17]; Yan et al. [18]). The Generation IV system employs a 600-MWth reactor with outlet coolant temperature of 950 °C to power a gas turbine for electricity generation and a thermochemical process for hydrogen production, yielding thermal efficiency of 50% or higher [16].

Based on the experience of HTR-10 and extensive engineering development of the reactor components, China is constructing the world's first prototype modular reactor plant HTR-PM in the northeastern Shandong province (Fu et al. 2014) [19]. Although not a VHTR by coolant temperature, the twin-unit (2 × 250 MWth) power plant with reactor coolant temperature of 750 °C shares some of the design approaches of VHTR, including passive safety features and high-temperature heat application potential. The construction began in December 2012 and the operation is expected in 2017.

Note that any small modular reactor of VHTR type is an excellent candidate for innovative design approach for open-air Brayton combined cycle [1–3]. These types of reactors are considered as advance small modular reactor (AdvSMR), which is part of family Generation IV nuclear power reactors.

In 2001, the Generation IV International Forum (GIF) endorsed six nuclear system concepts, which will deliver affordable energy products while satisfactorily addressing the issues of nuclear safety, waste, and proliferation (Petti, 2014) [20]. Recognizing the VHTR to be nearest-term deployable and exceptionally suitable, not only for electricity generation but also for hydrogen production and other industrial applications, the US Department of Energy (DOE) has placed the Generation IV priority on the VHTR. The Energy Policy Act of 2005 formally established the NGNP as a DOE project to demonstrate commercial high-efficiency generation of electricity and hydrogen (the US Energy Policy Act of 2005). At present, the advanced gas reactor (AGR) fuel development and qualification program at the US Idaho National Laboratory is qualifying uranium oxide/uranium carbide (UCO) TRISO fuel (Petti 2014) [20]. And the NGNP Industry Alliance, a consortium of HTGR designers, utility plant owner/operators, suppliers, and end users, is promoting the reactor commercialization and industrial applications (ngnpalliance). In 2012, the Alliance selected AREVA's prismatic SC-HTGR of 625 MWth that provides steam and electricity cogeneration as its primary choice of reactor design for prototype implementation in the mid-2020s (Shahrokh et al. 2014) [21].

For further information, reader should refer to reference written by Yan [16].

18.16 Advanced Modular Reactors (AdvSMRs)

Based on what we have seen in recent studies of pronuclear industry, it seems that small modular reactors (SMRs) are nuclear's future, particularly with more advanced version and types of SMRs given suggested combined drive efficiency as an innovative approach to raise their thermal and electrical out more efficient as well as a new renewable source of energy [3].

Small modular reactor (SMR) start is a new organization of potential customers and vendors investing in the development of advanced small modular reactors (AdvSMRs), which provided a hope for new source of energy when the demands on electricity are growing at almost 17% per year due to growth in population and industry globally. The new generation of SMRs is also a very promising generation of nuclear power plant when it comes to idea of decarbonizing the world environment by being a new renewable source of energy as well as driving hydrogen production [22] while offering better total cost of ownership (TCO) and return on investment (ROI) for the customers and vendors of this newly formed organization.

This newly established organization was formed with one main goal in mind, and that was to get SMRs over the initial market humps that plague all new technologies by using proven public/private partnerships that have succeeded with other technologies like renewable energies. Because of their small size of 300 MW or less, SMRs are economic, factory built, and shippable, flexible enough to desalinate, refine oil, load follow wind, produce hydrogen, and provide something we have all been waiting for – a reactor that cannot melt down and the most important aspect of these AdvSMRs by utilizing the open-air Brayton combined cycles that have no need for water as source of cooling down, while they are not constraint under *steam dome* as the light water reactors (LWRs) are [1–3].

Note that some even newly chosen design of SMRs such as the design approach taken by NuScale is following LWR technology; therefore they are limited to the steam dome constraint.

SMR start's goal is to ensure that SMRs are a cost-competitive option in the future, with the first units operating by the mid-2020s.

There is increasing interest in small modular reactors (SMRs) and their applications. SMRs are newer-generation reactors designed to generate electric power up to 300 MW, whose components and systems can be shop-fabricated and then transported as modules to the sites for installation as demand arises. Most of the SMR designs adopt advanced or even inherent safety features and are deployable either as a single or multi-module plant. SMRs are under development for all principal reactor lines: water-cooled reactors; high-temperature gas-cooled reactors; liquid-metal-, sodium-, and gas-cooled reactors with fast-neutron spectrum; and molten salt reactors. The key driving forces of SMR development are fulfilling the need for flexible power generation for a wider range of users and applications, replacing aging fossil-fired units, enhancing safety performance, and offering better economic affordability.

Many SMRs are envisioned for niche electricity or energy markets where large reactors would not be viable. SMRs could fulfil the need of flexible power generation for a wider range of users and applications, including replacing aging fossil power plants; providing cogeneration for developing countries with small electricity grids, remote, and off-grid areas; and enabling hybrid nuclear/renewable energy systems. Through modularization technology, SMRs target the economics of serial production with shorter construction time. Near-term deployable SMRs will have safety performance comparable or better to that of evolutionary reactor designs.

Furthermore, *small-* and *medium-*sized reactors include a large variety of designs and technologies and, in general, consist of:

- Advanced SMRs, including modular reactors and integrated PWRs
- Innovative SMRs, including small-sized GEN-IV reactors with non-water coolant/moderator
- Converted or modified SMRs, including barge-mounted floating NPP and seabed-based reactors
- Conventional SMRs, those of GEN-II technologies and still being deployed

Advanced SMRs having an equivalent electric power of less than 700 MW(e) or even less than 300 MW(e) are part of a new generation of nuclear power plant designs being developed to provide a flexible, cost-effective energy for various applications. Advanced SMR designs include water-cooled reactors, high-temperature gas-cooled reactors, as well as liquid-metal-cooled reactors with fast-neutron spectrum. The trend of development has been toward design certification of small modular reactors, which are defined as advanced reactors that produce equivalent electric power less than 300 MW(e) designed to be built in factories and shipped to utilities for installation as demand arises. The SMR systems adopt modularization, by which the structures, systems, and components are shop-fabricated and then shipped and assembled on-site, thus the construction time for SMRs can be substantially reduced. Some of the SMRs are to be deployed as multiple-module power plants allowing utilities to add additional reactor and power conversion modules as demand for local power increases.

Advanced SMRs will use different approaches from large reactors for achieving a high level of safety and reliability in their systems, structures, and components, and that will be the result of a complex interaction between design, operation, material, and human factors. Interest in SMRs continues to grow as an option for future power generation and energy security. However, the first phase of advanced SMR deployments will have to ultimately demonstrate high levels of plant safety and reliability and prove their economics in order for further commercialization to be feasible. This situation is an issue for the technology developers since building the first plants will be relatively expensive and the “nth of a kind” costs can only be confirmed after the first demonstration plants are deployed. As a result, new private-public partnership arrangements may be needed to support the first phase of advanced SMR deployments. These plants would have greater automation but will still rely on human interaction for supervision, system management, and operational decisions because operators are still regarded as the last line of defense if failures in automated protective measures occur.

18.17 Advantages of Small Modular Reactors (SMRs)

Associated with smaller modular reactors (SMRs), there exist certain benefits, which these SMRs offer, and to start with is their cost-effectiveness from investment and total cost of ownership (TCO), thus the return on investment (ROI) point of view.

Small modular reactors offer a lower initial capital investment, greater scalability, and siting flexibility for locations unable to accommodate more traditional larger reactors. They also have the potential for enhanced safety and security compared to earlier designs. Deployment of advanced SMRs can help drive economic growth. These low initial costs are coming with certain associated benefits that are listed here, and they are:

1. *Modularity*

The term “modular” in the context of SMRs refers to the ability to fabricate major components of the nuclear steam supply system in a factory environment and ship to the point of use. Even though current large nuclear power plants incorporate factory-fabricated components (or modules) into their designs, a substantial amount of fieldwork is still required to assemble components into an operational power plant. SMRs are envisioned to require limited on-site preparation and substantially reduce the lengthy construction times that are typical of the larger units. SMRs provide simplicity of design, enhanced safety features, the economics and quality afforded by factory production, and more flexibility (financing, siting, sizing, and end-use applications) compared to larger nuclear power plants. Additional modules can be added incrementally as demand for energy increases.

2. *Lower Capital Investment*

SMRs can reduce a nuclear plant owner’s capital investment due to the lower plant capital cost. Modular components and factory fabrication can reduce construction costs and duration.

3. *Siting Flexibility*

SMRs can provide power for applications where large plants are not needed or sites lack the infrastructure to support a large unit. This would include smaller electrical markets, isolated areas, smaller grids, sites with limited water and acreage, or unique industrial applications. SMRs are expected to be attractive options for the replacement or repowering of aging/retiring fossil plants or to provide an option for complementing existing industrial processes or power plants with an energy source that does not emit greenhouse gases.

4. *Greater Efficiency*

SMRs can be coupled with other energy sources, including renewables and fossil energy, to leverage resources and produce higher efficiencies and multiple energy end products while increasing grid stability and security. Some advanced SMR designs can produce a higher temperature process heat for either electricity generation or industrial applications.

5. Safeguards and Security/Nonproliferation

SMR designs have the distinct advantage of factoring in current safeguards and security requirements. Facility protection systems, including barriers that can withstand design basis aircraft crash scenarios and other specific threats, are part of the engineering process being applied to new SMR design. SMRs also provide safety and potential nonproliferation benefits to the United States and the wider international community. Most SMRs will be built below grade for safety and security enhancements, addressing vulnerabilities to both sabotage and natural phenomena hazard scenarios. Some SMRs will be designed to operate for extended periods without refueling. These SMRs could be fabricated and fueled in a factory, sealed and transported to sites for power generation or process heat, and then returned to the factory for defueling at the end of the life cycle. This approach could help to minimize the transportation and handling of nuclear material. Light water-based SMRs are expected to be fueled with low enriched uranium, i.e., approximately 5% U ²³⁵, which is similar to existing large nuclear power plants. The “security by design” concepts being applied to these technologies are expected to increase SMR resistance to theft and diversion of nuclear material. Also, reactor cores for these light water SMRs can be designed to burn plutonium as a mixed oxide (MOX) fuel. Further, SMRs based on non-light water reactor coolants could be more effective at dispositioning plutonium while minimizing the wastes requiring disposal.

6. US Industry, Manufacturing, and Job Growth

The case for SMR economic competitiveness is rooted in the concept that mass manufacture of modular parts and components will reduce the cost per kilowatt of electricity on par with current generating sources. There is both a domestic and international market for SMRs, and the US industry is well positioned to compete for these markets. DOE hopes that the development of standardized SMR designs will also result in an increased presence of US companies in the global energy market. If a sufficient number of SMR units were ordered, it would provide the necessary incentive to develop the appropriate factory capacity to further grow domestic and international sales of SMR power plants.

7. Economic Development

SMR deployment to replace retiring electricity generation assets and meet growing generating needs would result in significant growth in domestic manufacturing, tax base, and high-paying factory, construction, and operating jobs. A 2010 [7] study on economic and employment impacts of SMR deployment estimated that a prototypical 100 MWe SMR costing \$500 million to manufacture and install would create nearly 7000 jobs and generate \$1.3 billion in sales, \$404 million in earnings (payroll), and \$35 million in indirect business taxes. The report examines these impacts for multiple SMR deployment rates, i.e., low (1–2 units/year), moderate (30 units/year), high (40 units/year), and disruptive (85 units/year). The study indicates significant economic impact would be realized by developing an SMR manufacturing enterprise at even moderate deployment levels.

If we consider these above benefits that are coming from SMR-type nuclear power plants, we do see their cost-effectiveness and initial capital investment, in comparison to today's analysis of cost of electricity from nuclear power plants.

1. *Cost of electricity from nuclear power*

The newest estimates for the cost of nuclear power in the United States are (costs indicated are per delivered kWh):

11.2 US cents per kWh nuclear power (MIT 2003)

14.1 US cents per kWh nuclear power (keystone June 2007)

18.4 US cents per kWh nuclear power (keystone midrange estimate)

In the United Kingdom, the cost of nuclear electricity was estimated to be 8.2 US cents per kWh (for an interest rate of 10%) and US cents 11.5 per kWh (for an interest rate of 15%). Here transmission and distribution of the electricity (usually about 3 US cents per kWh) have to be added (source: Thomas, Bradford, Froggatt, Milborrow, 2007) [9]. So, in the United Kingdom, the costs of nuclear energy is estimated to be in the same range as indicated above.

In comparison with other technologies, e.g., large wind power farms, 7 US cents per kWh are delivered.

Of course most of environmentalists are arguing over wind and solar energy as a cheap way of producing electricity and call them as an alternative renewable source of energy, are getting less expensive almost daily while nuclear power is getting more and more expensive. Isn't this alone a very strong indication that nuclear power is a technology from the past?

However, one needs to bear in mind that wind does not blow 24×7 nor sun will shine all the time during day and night, providing during cloudy day, we may have this issue, while at night there is no sun out.

2. *Cost of nuclear technology is too high*

The reactor types you are describing are not available. A lot of research and development would be needed to develop this technology for productive applications. We probably talk about a time frame of 30–50 years, if not even longer. But we need a solution now! It is urgent.

The costs for the development are very difficult to estimate and therefore the costs indicated above might be (and probably are) wrong. In the history of nuclear power, the cost of development has always been tremendously underestimated.

We should put full effort into developing sustainable energy technologies further and phase out nuclear technology. This will open many opportunities and have many positive side effects. It is time for change!

In addition, we will inevitably have to change our behavior: We should only use as much energy as we are able to produce with sustainable technologies. Demand of energy has to follow available supply of sustainable energy. This will have many positive side effects, too.

18.18 Conclusions

Small modular reactor communities advocate for public/private partnerships – similar to those that provide support for the introduction of other new energy technologies such as solar and wind – to help ensure the successful commercialization of SMRs. Public/private partnerships stimulate the private investments required to ensure that the technology continues to advance and is capable of competing in domestic and overseas markets without additional direct support once the technology matures.

Today's energy markets are characterized by low natural gas prices, heavily subsidized renewable generation, and low growth in electricity demand. American vendors also compete in the international markets for the deployment of SMRs and other advanced nuclear designs. Unfortunately, most countries like Russia and China directly subsidize their nation's nuclear technologies in order to penetrate global markets.

The new waves of SMR designs have been supported in many recent DOE and NRC initiatives, and a final SMR design is necessary for the first power plant to begin construction and to take advantage of factory fabrication. But even after an SMR design certification application has been submitted to the US Nuclear Regulatory Commission (NRC), there are still significant cost and uncertainty involved in the design certification approval process, as well as work to finalize the design. A cost-sharing program for design finalization activities would help reduce the risk for first reactor design companies and would increase the probability that a final SMR design is produced for factory fabrication.

The low price of natural gas poses a challenge to low-carbon technology deployment, and a production tax credit (PTC) would help to value the carbon-free benefits of SMRs and close this price gap as it has for renewables. Power purchase agreements (PPAs) would help to create demand for new, low-carbon technologies in an era of slower electrical demand growth.

PPAs between SMR operators and federal facilities would align with the directive to support low-carbon technologies codified in Executive Order 13693, as well as promote national security.

Note that: Traditionally, a *power purchase agreement*, or PPA, is a contract between a government agency and a private utilities company. The private company agrees to produce electricity, or some other power source, for the government agency over a long period of time.

Investments in advanced manufacturing will reduce cost and construction time for SMRs and create manufacturing jobs for components that currently have to be made outside the United States for the large traditional nuclear reactors.

New reactor designs are pretty advanced and ready to be rolled out. In January, NuScale Power out of Oregon announced their submission to the Nuclear Regulatory Commission of the first design certification application for any SMR in the United States. It is expected to be built in the early 2020s.



Fig. 18.14 Terrestrial Energy's IMSR small modular reactors general depiction

Terrestrial Energy (Fig. 18.14), another innovative small modular reactor company, has notified the Nuclear Regulatory Commission of its intentions to license their Integral Molten Salt Reactor (IMSR). They have plans to submit its licensing application in 2019.

IMSR® technology can be brought to market quickly. IMSR® power plants can be built in 4 years and produce electricity or industrial heat at prices competitive with fossil fuels while emitting no greenhouse gases.

The first IMSR® power plants are expected to come online in the 2020s. IMSR® technology is today's clean energy game changer. Learn more about the IMSR® and how Terrestrial Energy is leading the way to a bright energy future [13].

But what really matters to the public is safety. The small size and large surface area-to-volume ratio of SMRs, like NuScale Power, that sits below ground in a super seismic-resistant heat sink, allows natural processes to cool it indefinitely in the case of a complete power blackout, with no humans needed to intervene, no AC or DC power, no pumps, and no additional water for cooling.

References

1. B. Zohuri, *Combined Cycle Driven Efficiency for Next Generation Nuclear Power Plants: An Innovative Design Approach*, 1st edn. (Springer Publishing Company, Cham, 2015)
2. B. Zohuri, P. McDaniel, *Combined Cycle Driven Efficiency for Next Generation Nuclear Power Plants: An Innovative Design Approach*, 2nd edn. (Springer Publishing Company, Cham, 2017)
3. B. Zohuri, *Small Modular Reactors as Renewable Energy Sources* (Springer Publishing Company, Cham, 2018)
4. <http://www.ne.doe.gov/geniv/neGenIV1.html>
5. Sustainable Nuclear Energy Technology Platform, Strategic Research Agenda, 2009, www.SNETP.eu
6. Uranium 2007: Resources, Production and Demand. OECD Nuclear Energy Agency and the International Atomic Energy Agency, OECD 2008 NEA N, p. 6345
7. 2009 Update of the MIT 2003 Future of Nuclear Power, An Interdisciplinary MIT Study, 2003, Massachusetts Institute of Technology, Cambridge USA, May 2009, <http://web.mit.edu/nuclearpower/pdf/nuclearpower-update2009.pdf>
8. Nuclear Energy Outlook, *OECD/NEA Report No. 6348, 2008* (Nuclear Energy Agency, Paris, 2008)
9. http://www.ne.doe.gov/pdfFiles/NGNP_reporttoCongress.pdf
10. Updated Emissions Projections, July 2006, DTI. <http://www.dti.gov.uk/files/file31861.pdf>

11. DTI: Energy White Paper, Meeting the Energy Challenge, <http://www.dti.gov.uk/energy/whitepaper>
12. http://www.ne.doe.gov/geniv/documents/gen_iv_roadmap.pdf
13. <https://www.terrestrialenergy.com/technology/>
14. Proposal for a COUNCIL DIRECTIVE (EURATOM), setting up a Community framework for nuclear safety COM(2008) 790/3, November 2008
15. COUNCIL OF THE EUROPEAN UNION, Legislative Acts and Other Instruments 10667/09, June 2009
16. X.L. Yan, Japan Atomic Agency, Oarai-Machi, Ibaraki-ken, Japan
17. H. Sato, X.L. Yan, Y. Tachibana, K. Kunitomi, GTHT300dA nuclear power plant design with 50% generating efficiency. Nucl. Eng. Des. **275**, 190e196 (2014)
18. X. Yan, H. Sato, Y. Kamiji, Y. Imai, A. Terada, Y. Tachibana, K. Kunitomi, GTHT300 cost reduction through design upgrade and cogeneration. Paper HTR2014-21436, in *Proceedings of the HTR 2014*, Weihai, China, 27–31 October 2014
19. J. Fu, Y. Jiang, H. Cheng, W. Cheng, Overview and progress of high temperature reactor pebble-bed module demonstration project (HTR-PM), HTR2014-11125, in *Proceedings of the HTR 2014*, Weihai, China, 27–31 October 2014
20. D. Petti, Implications of results from the advanced gas reactor fuel development and qualification program on licensing of modular HTGRs. Paper HTR2014-31252, in *Proceedings of the HTR 2014*, Weihai, China, 27–31 October 2014
21. F. Shahrokhi, L. Lommers, J. Mayer III, F. Southworth, US HTGR deployment challenges and strategies. Paper HTR2014-11309, in *Proceedings of the HTR 2014*, Weihai, China, 27–31 October 2014
22. B. Zohuri, *Hydrogen Energy: Challenges and Solutions for a Cleaner Future*, 1st edn. (Published by Springer Publishing Company, Cham, 2018)

Chapter 19

Design and Analysis of Core Design for Small Modular Reactors



The pronuclear energy advocates are lobbying that the sustainable development of the world's energy sector cannot be achieved without extensive use of nuclear energy and the advantages of nuclear-related technologies, including upcoming new generation of the small modular reactors in the near future horizon. The dawn of these SMRs requires new design and analysis no matter if they are falling into light water reactor (LWR), pressurized water reactor (PWR), or even multi-application small light water reactor (MASLWR) categories, depending on the vendor involved with these new technologies and consequently safety standards and their nonproliferation requirements as well. This chapter visits these standards for core design and generally elaborated on them with understanding that readers need to refer just beyond this book and this chapter for more details.

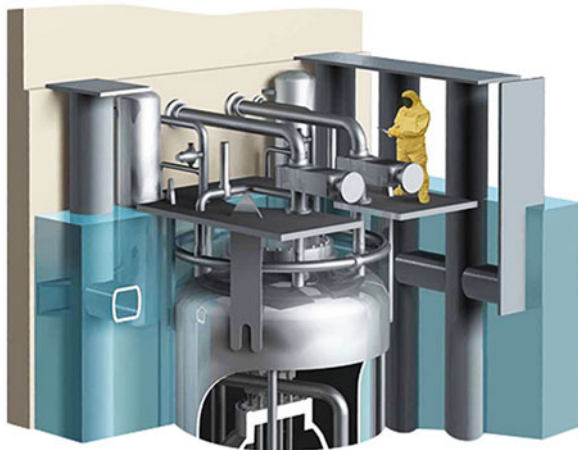
19.1 Introduction

In order to meet national and international requirements to achieve maximum safety and efficiency levels, and address worldwide proliferation concerns, a variety of innovative new technologies implemented into the new generation of nuclear reactors will need to be developed.

There are manufacture vendors such as NuScale that is looking into the design and development of small modular reactor (SMR), using the existing light water reactor (LWR) for their NuScale Power Module as illustrated in Fig. 19.1, while companies like Holtec International with their SMR-160 use similar technologies that exist around pressurized water reactor (PWR) and their scaling down that is used in nuclear vessels such as submarine as it is illustrated in Fig. 19.2.

Then, off course there are other nuclear industrial vendors such as mPower as part of Babcock & Wilcox (B&W) that in 2009 announced its mPower reactor as it is depicted in Fig. 19.3, a 500 Mew integral PWR designed to be factory-made and railed to site. It was a deliberately conservative design, to more readily gain

Fig. 19.1 NuScale Power Module



acceptance and licensing. In November 2012 the US Department of Energy (DOE) announced that it would support accelerated development of the design for early deployment, with up to \$226 million, and it paid \$111 million of this.

On the other hand, universities such as Oregon State University (OSU) are involved with design study of the multi-application small light water reactor (MASLWR) as illustrated in Fig. 19.4 with the following requirements in mind such as the passive safety systems, natural circulation, long core lifetime, and off-site refueling capability, while the use of standard equipment is the basic design features of this reactor design.

Then, globally, the country with the most advanced small modular reactor (SMR) project is China, where Chinergy is starting to build the 210 MWe high-temperature gas-cooled reactor pebble-bed module (HTR-PM), which consists of twin 250 MWe high-temperature gas-cooled reactors (HTRs) which build on the experience of several innovative reactors in the 1960s–1980s, as illustrated in Fig. 19.5.

The HTR-PM reactor uses helium as a coolant instead of water, where after the helium is heated to 750 °C (1,382 °F), it is sent to a steam generator where it heats water until it becomes high-temperature steam and that steam then flows into a steam turbine to generate electricity. The process uses a graphite-moderated nuclear reactor and a once-through uranium fuel cycle.

SNPTC's project as part of China Advanced HTGR Technology consists of two 250 Mwt high-temperature reactor pebble-bed modules as illustrated in Fig. 19.5 and is located in Shandong province. Tests at the project are expected to end in April 2018, at which the time the reactor will go into commercial operation as part of new generation of advanced small modular reactor (AdvSMR) series.

The success of this project will establish a milestone for the nuclear industry and its advocates to push this industry as an option for renewable source of energy, where the SMRs are going to be utilized while helping decarbonization of our environment and pave the way to meet the demand on electricity due to global population growth and related industries to meet this growth.

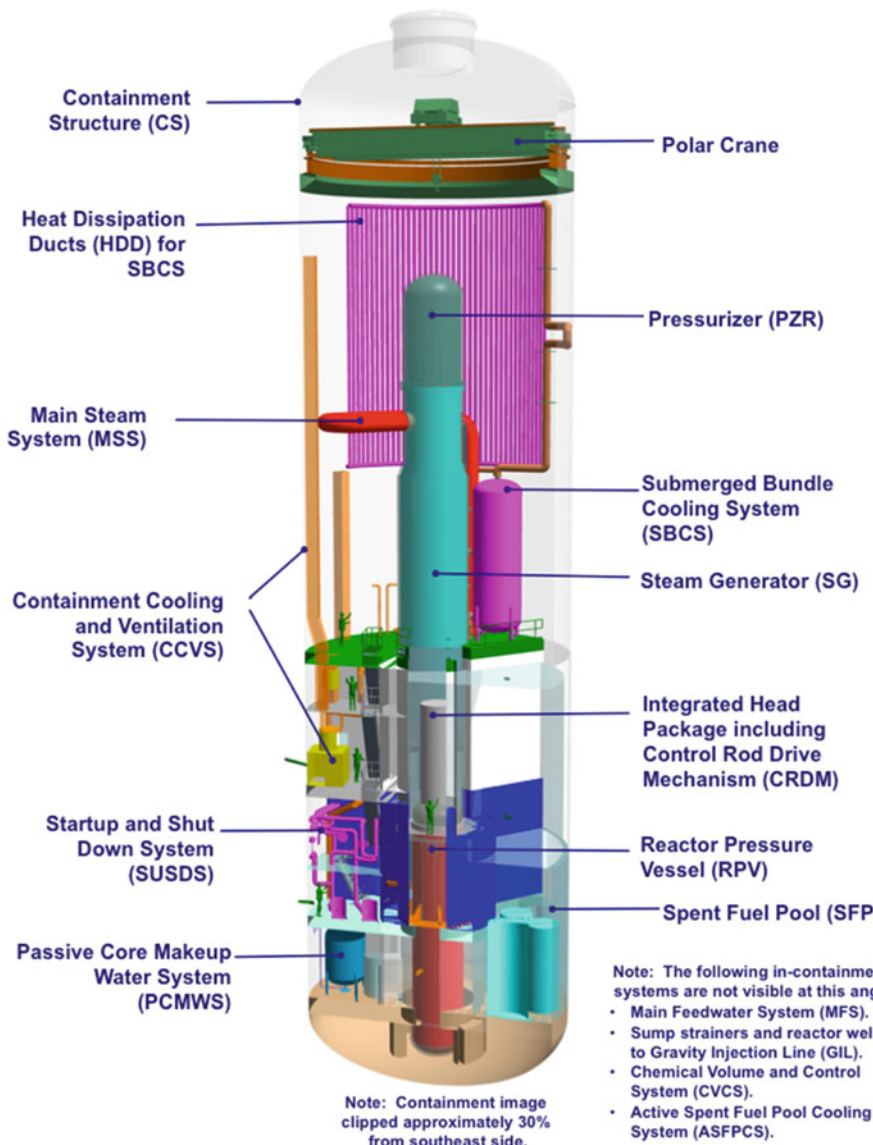


Fig. 19.2 Holtec International SMR-160

Others such as Russian design KLT-40S (Fig. 19.6) from OKBM (full name for OAO I. I. Afrikantov OKB Mechanical Engineering. The company was founded in 1945. In 1998, it was named after its former chief designer and director I. I. Afrikantov) Afrikantov are derived from the KLT-40 reactor well in icebreakers and now – with low-enriched fuel – proposed for wider use in desalination and, on barges, for remote area power supply. Here a 150 MWt unit produces 35 MWe

Fig. 19.3 mPower nuclear reactor depiction

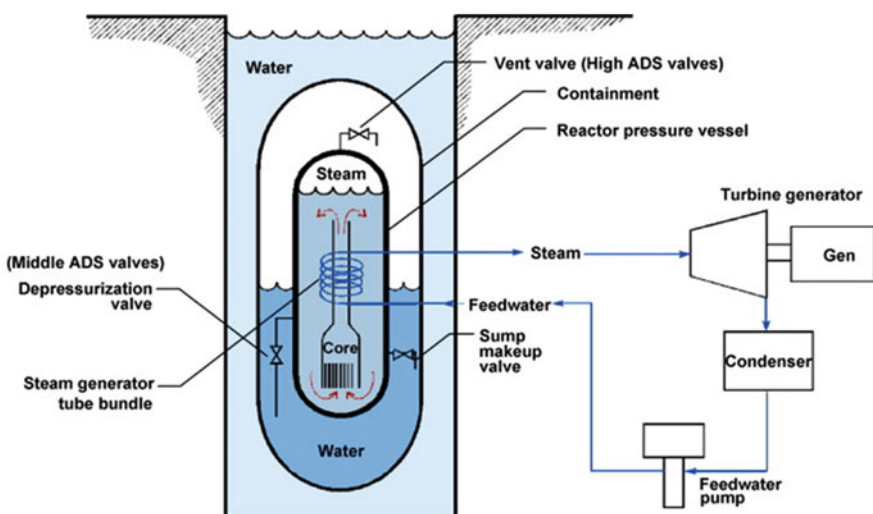
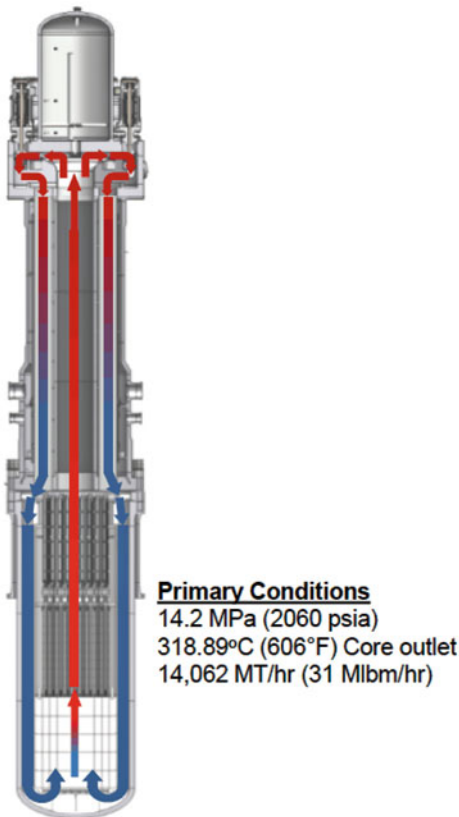


Fig. 19.4 Overview of multi-application small light water reactor

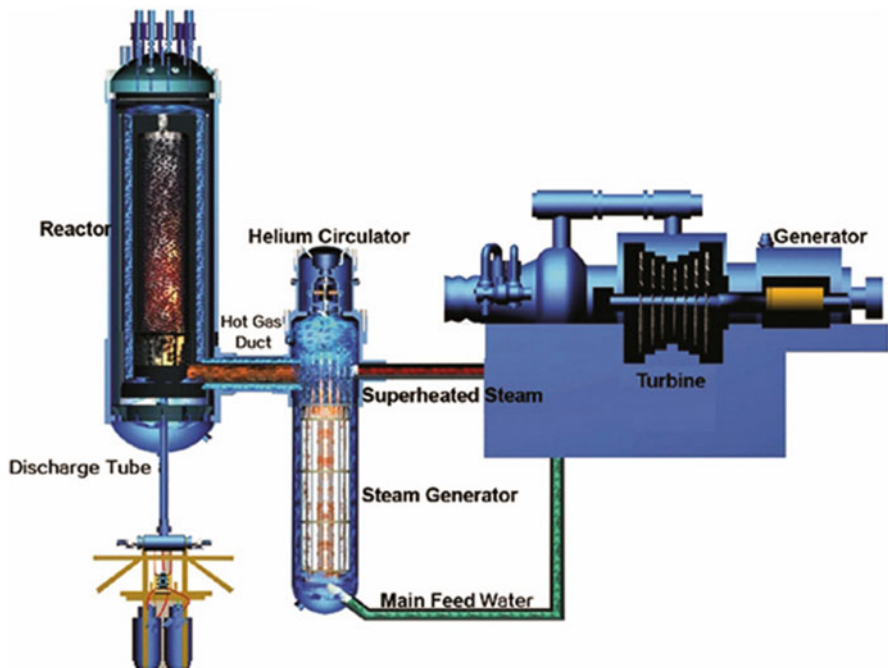
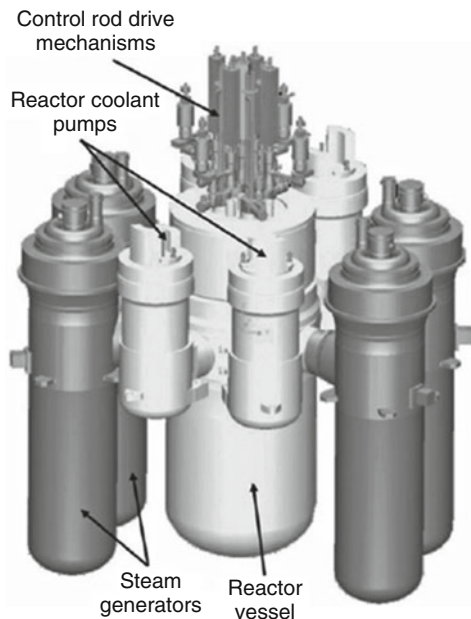


Fig. 19.5 250 Mwt HTGR-PM China's state nuclear power overview

Fig. 19.6 KLT-40S,
Afrikantov OKBM
depiction



(gross) as well as up to 35 MW of heat for desalination or district heating (or 38.5 MWe gross if power only). Burnup is 45 GWd/t. Units are designed to run 3–4 years between refueling with onboard refueling capability and used fuel storage. All fuel assemblies are replaced in each such refueling. At the end of a 12-year operating cycle, the whole plant is taken to a central facility for overhaul and storage of used fuel. Operating plant lifetime is 40 years. Two units will be mounted on a 20,000 ton barge to allow for outages (70% capacity factor). It may also be used in Kaliningrad.

Although the reactor core is normally cooled by forced circulation (four-loop), the design relies on convection for emergency cooling. Fuel is uranium aluminum silicide with enrichment levels of up to 20%, giving up to 4-year refueling intervals. A variant of this is the KLT-20, specifically designed for floating nuclear plants. It is a two-loop version with the same enrichment but with a 10-year refueling interval.

The first floating nuclear power plant, the *Akademik Lomonosov*, commenced construction in 2007. Due to insolvency of the shipyard, the plant is now expected to be completed in late 2018 and operational in 2019.

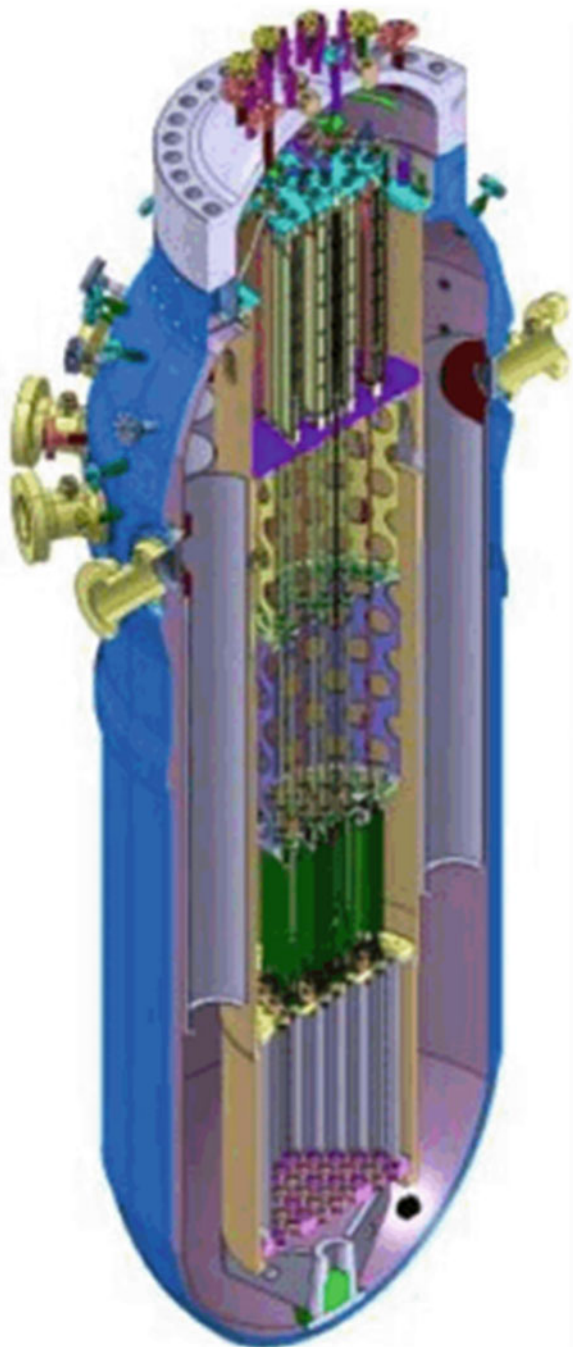
The Argentina's National Atomic Energy Commission (CNEA) is also involved with small modular reactor and prototyping the CAREM-25 reactor, with considerable input from INVAP, which is an older design modular 100 MWe (27 MWe gross) integral pressurized water reactor, first announced in 1984. It has 12 steam generators within the pressure vessel and is designed to be used for electricity generation or as a research reactor or for water desalination (with 8 MWe in cogeneration configuration). CAREM has its entire primary coolant system within the reactor pressure vessel (11 m high, 3.5 m diameter), self-pressurized and relying entirely on convection (for modules less than 150 MWe). The final full-sized export version will be 100 MWe or more, with axial coolant pumps driven electrically. Fuel is standard 3.1% or 3.4% enriched PWR fuel in hexagonal fuel assemblies, with burnable poison, and is refueled annually.

The 25 MWe prototype unit is being built next to Atucha, on the Parana River in Lima, 110 km northwest of Buenos Aires, and the first larger version (probably 100 MWe) is planned in the northern Formosa province, 500 km north of Buenos Aires, once the design is proven. Some 70% of CAREM-25 components will be local manufacture. The pressure vessel is being manufactured by Industrias Metalurgicas Pescarmona SA (IMPSA) (see Fig. 19.7).

The CAREM-25 is an integral type PWR to produce 27 MWe developed by CNEA, and the reactor is adopting advanced features that include an integral primary cooling system using natural circulation, in-vessel hydraulic control rod drive mechanisms, and passive safety systems. Neither air conditioning (AC) power nor operator actions are required to mitigate postulated design events during grace period.

By adopting the integrated primary cooling system, the possibility of typical PWR postulated design basis accident, such as large loss of coolant accidents and shutdown systems, is designated with diversity and redundancy that meet regulatory requirements. The CAREM-25 reactor is currently under construction in Argentina as a prototype to validate the adopted innovative features for future commercial

Fig. 19.7 Argentina CAREM-25 small modular reactor image



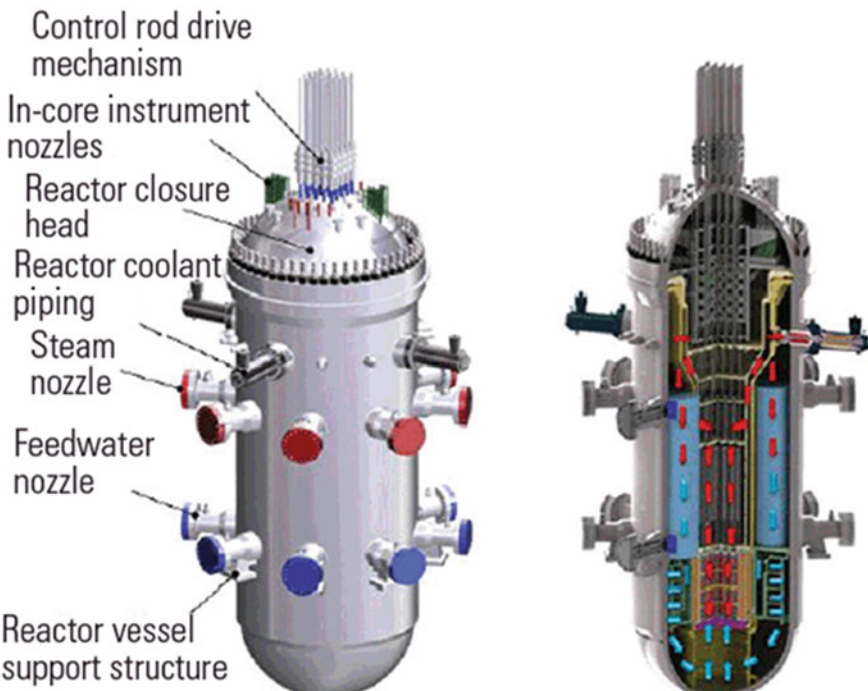


Fig. 19.8 SMART reactor depiction by South Korea

version of CAREM that will generate up to 300 Mwe output power and as the prototype plant is targeting start-up commissioning in 2018, which is one of many advanced small modular reactors built by other forging countries.

South Korea's SMART approach to small modular reactor in beginning of the conceptual design is another AdvSMR with its System-Integrated Modular Advanced Reactor as illustrated in Fig. 19.8.

SMART reactor is a 300 MWt small modular reactor design that was firmed up and was developed and components tested over the next decade with the Korea Atomic Energy Research Institute (KAERI) spending some \$300 million and 1500 person-years on the project, which won approval from the Korea Institute of Nuclear Safety.

According to the World Nuclear Organization, SMART's design life is 60 years, fuel enrichment is 4.8%, and the design features a 3-year refueling cycle. As in many SMRs, the residual heat removal is passive. According to KAERI, the passive heat recovery design gives the plant a “20 days grace period against Fukushima-type accidents.”

In the design, all fuel is submerged in water, and the containment building can withstand a crash from a Boeing 767. The containment also includes a passive hydrogen removal system to prevent hydrogen explosions.

Many of today's SMR plans have their roots in naval reactor technology, as did Shippingport. Its technology was based on Westinghouse reactors that powered the first US nuclear submarines. Argentina's CAREM-25 reactor design came from the Argentine navy. The country unveiled the design at a 1984 IAEA conference. The project then got shelved but was revived in 2006 as Argentina moved to revitalize its nuclear power program in the face of limited supplies and high prices for imported natural gas. Argentina has few easily accessible indigenous energy resources.

Russia's floating nukes also rely on maritime technology, reactors developed for its successful fleet of nuclear icebreakers, dating back well into the days of the Soviet Union. The nation's first nuclear icebreaker, the NS Lenin, was launched in 1957, the same year that Shippingport went into commercial service.

In the United States, two of the major SMR industrial developers, Babcock & Wilcox and Westinghouse, both have extensive experience with naval reactors. But that technology advantage has not provided commercial leverage, as both companies have scaled back their SMR programs in the face of a lack of demand for their product (see "What Went Wrong with SMRs?" in the September 2014 issue).

The Japan Atomic Energy Research Institute (JAERI) designed the MRX, a small (50–300 MWt) integral PWR reactor for marine propulsion or local energy supply (30 MWe). The entire plant would be factory built. It has conventional 4.3% enriched PWR uranium oxide fuel with a 3.5-year refueling interval and has a water-filled containment to enhance safety. Little has been heard of it since the start of the Millennium.

In summary, what accounts for the inability of the United States (and European, for that matter) market to embrace SMR technology, when less developed and less financially muscular countries and utilities are moving ahead?

Giorgio Locatelli of the UK's University of Lincoln, who published a recent paper on the economics of SMRs, "Small Modular Reactors: A Comprehensive Overview of Their Economics and Strategic Aspects," argues that the smaller reactors make sense in developing countries, where "it can be very tricky to get equity to make the investments. But with a small modular reactor, you build the first one, which comes cheaper, and then when you've raised more money you create the second, and then you start to sell electricity with the first and the second, and by selling electricity you can finance the construction of the third and then the fourth."

19.2 Heat Pipe Micro Reactor

It is worth mentioning here that there exists another distinct form of reactor that is different than other small reactor designs, namely, heat pipe reactor that is known as eVinci by Westinghouse.

Distinct from other small reactor designs, the eVinci is a heat pipe reactor, using a fluid in numerous sealed horizontal steel heat pipes to conduct heat from the hot fuel (where the fluid vaporizes) to the external condenser (where the fluid releases latent

heat of vaporization) with heat exchanger. No pumps are needed to effect continuous isothermal vapor/liquid internal flow at low pressure. The principle is well established on a small scale, but here a liquid metal is used as the fluid, and reactor sizes up to several megawatts are envisaged. Experimental work on heat pipe reactors for space has been with much smaller units (about 100 kWe), using sodium as the fluid. They have been developed since 1994 as a robust and low technical risk system for space exploration with an emphasis on high reliability and safety.

The eVinci reactors would be fully factory built and fueled. As well as power generation, process heat to 600 °C would be available. Units would have 5- to 10-year operational lifetime, with walkaway safety due to inherent feedback diminishing the nuclear reaction with excess heat, also affecting load following. Although, eVinci is not considered as an advanced small modular reactor (AdvSMR), due to its small-scale size, it is a good candidate for space-based source of energy as it is mentioned in above and falls into category of micro reactor for lack of better classification choice. As it is illustrated in Fig. 19.9, the eVinci micro reactor's innovative design is a combination of nuclear fission, space reactor technologies, and 50 + years of commercial nuclear systems design, engineering, and innovation. The eVinci micro reactor aims to create affordable and sustainable power with improved reliability and minimal maintenance, particularly for energy consumers in remote locations. The small size of the generator allows for easier transportation and rapid, on-site installation in contrast to large, centralized stations. The reactor core is designed to run for more than 10 years, eliminating the need for frequent refueling.

The key benefits of the eVinci micro reactor are attributed to its solid core and advanced heat pipes. The core encapsulates fuel to significantly reduce proliferation risk and enhances the overall safety for the user. The heat pipes enable passive core

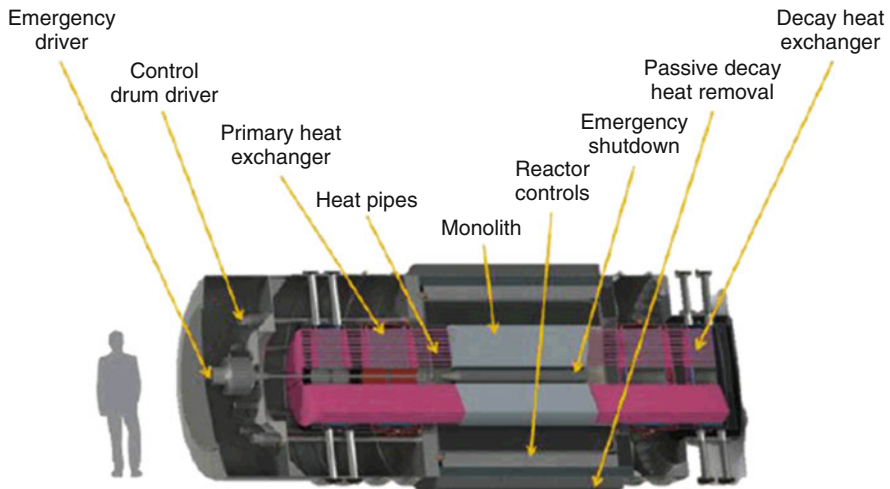


Fig. 19.9 Westinghouse eVinci heat pipe reactor

heat extraction and inherent power regulation, allowing autonomous operation and inherent load following capabilities. These advanced technologies together make the eVinci micro reactor a pseudo “solid-state” reactor with minimal moving parts.

The Key Attributes of eVinci Micro Reactor is:

- Transportable energy generator
- Fully factory built, fueled, and assembled
- Combined heat and power – 200 kWe to 25 MWe
- Up to 600 °C process heat
- 5- to 10-year life with walkaway inherent safety
- Target less than 30 days on-site installation
- Autonomous load management capability
- Unparalleled proliferation resistance
- High reliability and minimal moving parts
- Green field decommissioning and remediation

As part of the feature of eVinci as a micro reactor design, it could represent itself as an ultimate energy solution for the off-grid customer as depicted in Fig. 19.10.

The use of the heat pipes in a reactor system addresses some of the most difficult reactor safety issues and reliability concerns present in the current Generation II and III and, to some extent, Generation IV concepts commercial nuclear reactors – in particular, loss of primary coolant. Heat pipes operate in a passive mode at relatively low pressures, less than an atmosphere. Each individual heat pipe contains only a small amount of working fluid, which is fully encapsulated in a sealed steel pipe. There is no primary cooling loop, hence no mechanical pumps, valves, or large-diameter primary loop piping typically found in all commercial reactors today. Heat



Fig. 19.10 Various application of eVinci in off-grid mode

pipes simply transport heat from the in-core evaporator section to the ex-core condenser in continuous isothermal vapor/liquid internal flow. Heat pipes offer a new and unique means to remove heat from a reactor core.

19.3 High-Temperature Gas-Cooled Reactors/Advanced Small Modular Reactor

The high-temperature gas-cooled reactors (HTGRs) as illustrated in Fig. 19.11 design feature and operational temperature requirements are considered as family of an advanced small modular reactor (AdvSMR), which fit them into category where the innovative open-air Brayton or closed- CO_2 combined Brayton cycle takes advantages of the high temperature into account in order to boost thermal efficiency of these HTGRs to its maximum possible [1–3].

These types of advanced small modular reactors use graphite as moderator unless they are fast neutron-type AdvSMRs and either helium, carbon dioxide, or nitrogen

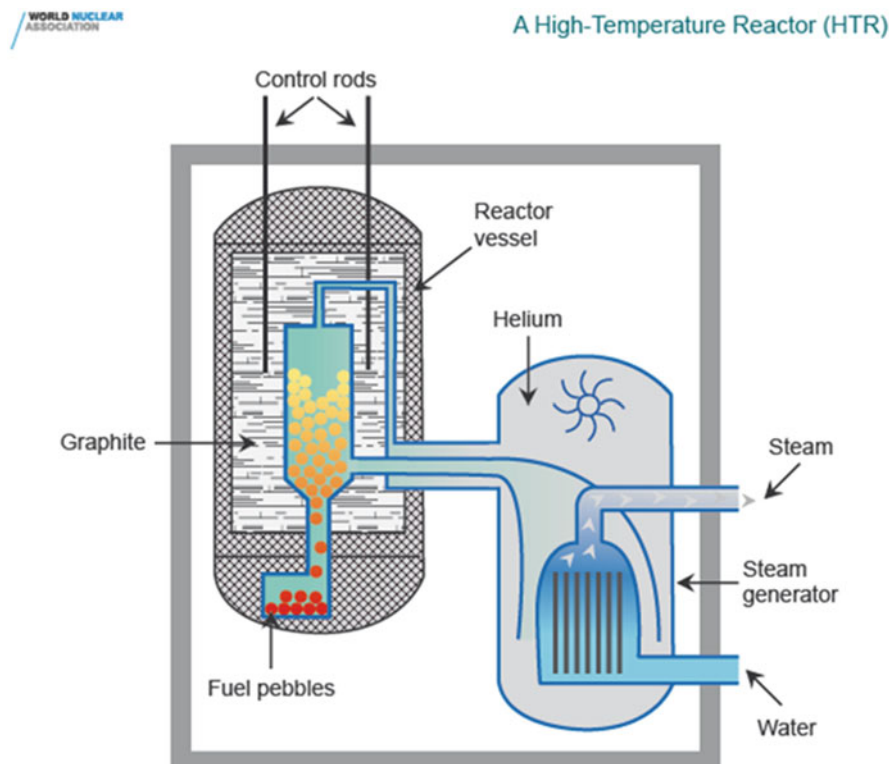


Fig. 19.11 A high-temperature reactor overview picture. (Courtesy of World Nuclear Association)

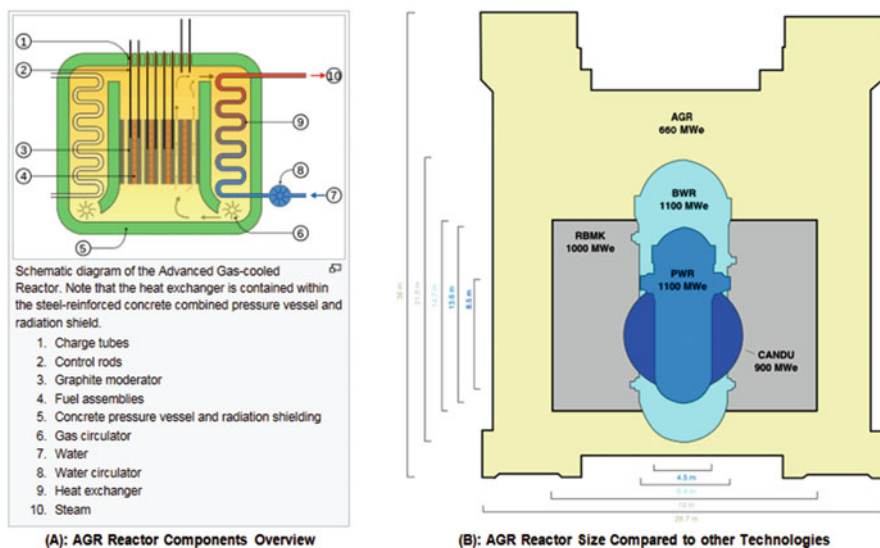


Fig. 19.12 Advanced gas-cooled reactor (AGR). (a) AGR reactor components overview. (b) AGR reactor size compared to other technologies

as primary coolant. The experience of several innovative reactors built in the 1960s and 1970s, notably those in Germany, has been analyzed, especially in the light of US plans for its Next Generation Nuclear Plant (NGNP) and China's launching its High-Temperature Reactor-Pebble Module (HTR-PM) project in 2011. Lessons learned and documented for NGNP include the use of TRISO fuel, use of a reactor pressure vessel, and use of helium cooling (UK advanced gas-cooled reactors (AGR)s) are the only high-temperature reactors (HTRs) to use CO_2 as primary coolant) (see Fig. 19.12a, b). However, US government funding for Next Generation Nuclear Plant (NGNP) has now virtually ceased, and the technology lead has passed to China these days.

New high-temperature gas-cooled reactors (HTRs) are being developed which will be capable of delivering high-temperature ($700\text{--}950\text{ }^\circ\text{C}$ and eventually up to about $1000\text{ }^\circ\text{C}$) helium either for industrial application via a heat exchanger or to make steam conventionally in a secondary circuit via a steam generator or directly to drive a Brayton cycle gas turbine for electricity with almost 50% thermal efficiency possible (efficiency increases around 1.5% with each $50\text{ }^\circ\text{C}$ increment) [1–4]. One design uses the helium to drive an air compressor to supercharge a combined cycle gas turbine (CCGT) unit. Improved metallurgy and technology developed in the last decade makes HTRs more practical than in the past, though the direct cycle means that there must be high integrity of fuel and reactor components [4]. All but one of those described below have neutron moderation by graphite, and one is a fast neutron reactor.

Note that there is little interest in pursuing the direct Brayton cycle for helium at present due to higher technological risk. Attrition of fuel tends to give rise to graphite dust with radioactivity in the coolant circuit

Fuel for these reactors is in the form of TRISO (tristructural-isotropic) particles less than a millimeter in diameter. Each has a kernel (ca. 0.5 mm) of uranium oxycarbide (or uranium dioxide), with the uranium enriched up to 20% U²³⁵, though normally less. This is surrounded by layers of carbon and silicon carbide, giving a containment for fission products which is stable to over 1600 °C.

There are two ways in which these particles are arranged: in blocks – hexagonal “prisms” of graphite or in billiard ball-sized pebbles of graphite, each with about 15,000 fuel particles and 9 g uranium. There is a greater volume of used fuel (20 times) than from the same capacity in a light water reactor, due to the fact that the fuel pebbles are mainly graphite – less than 1% is uranium. However, the used fuel is overall less radiotoxic and produces less decay heat due to higher burnup. The HTR moderator is graphite.

HTRs can potentially use thorium-based fuels, such as high-enriched or low-enriched uranium with Th, U²³³ with Th, and Pu with Th. Most of the experience with thorium fuels has been in HTRs

With negative temperature coefficient of reactivity (the fission reaction slows as temperature increases) and passive decay heat removal, the reactors are inherently safe. HTRs therefore are put forward as not requiring any containment building for safety. They are sufficiently small to allow factory fabrication and will usually be installed below ground level.

Three HTR designs in particular – Pebble-Bed Modular Reactor (PBMR) Fig. 19.13a, b, Gas Turbine-Modular Helium Reactor (GT-MHR) Figs. 19.14 and 19.15, and Areva’s Steam Cycle High-Temperature Gas Reactor (SC-HTGR) Fig. 19.16a, b – were contenders for the Next Generation Nuclear Plant (NGNP) project in the USA. In 2012 Areva’s HTR was chosen. However, the only HTR project currently proceeding is the Chinese HTR-PM

Hybrid Power Technologies have a hybrid-nuclear small modular reactor (SMR) coupled to a fossil fuel-powered gas turbine.

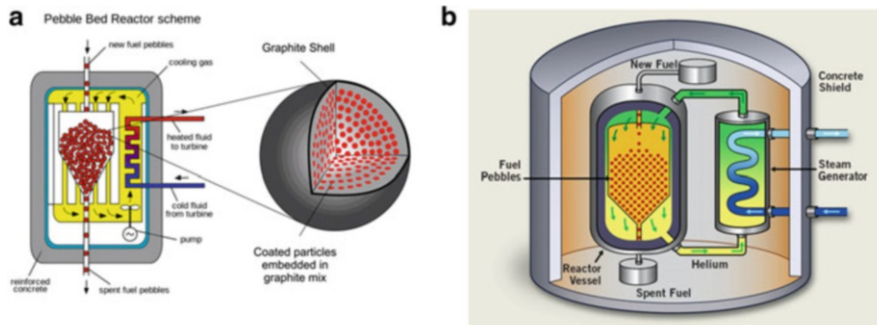
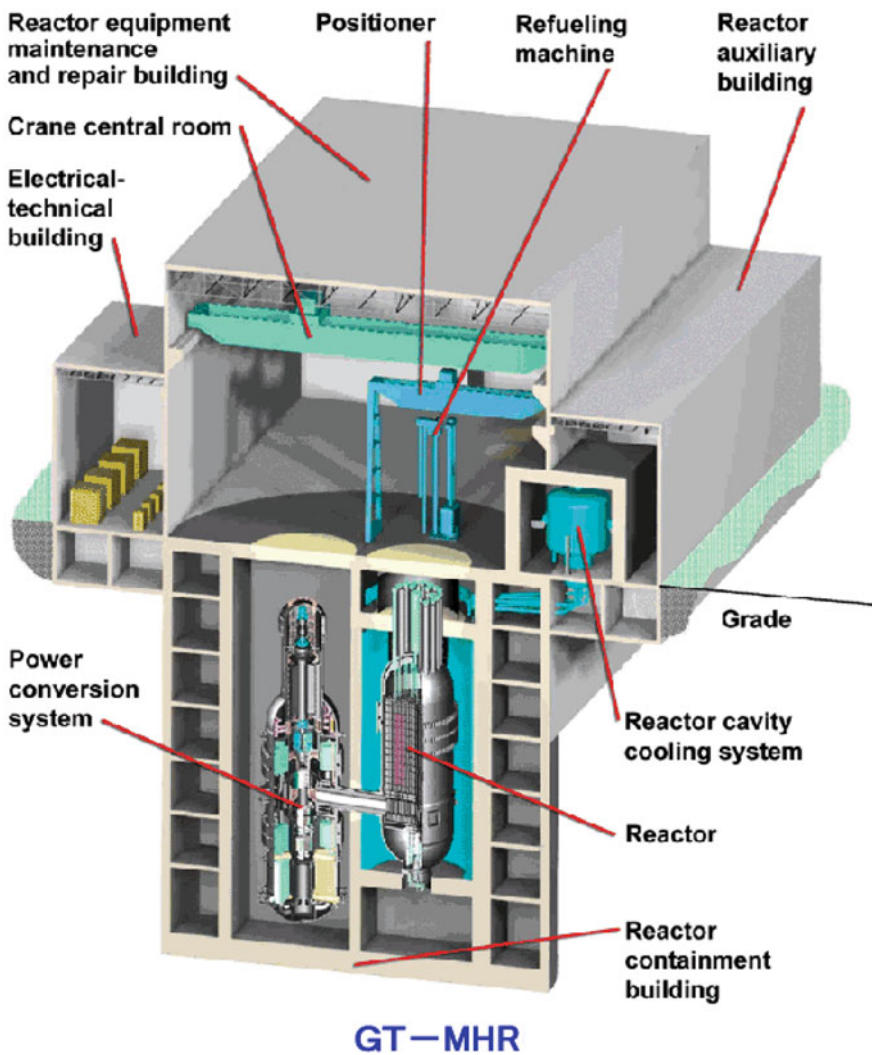


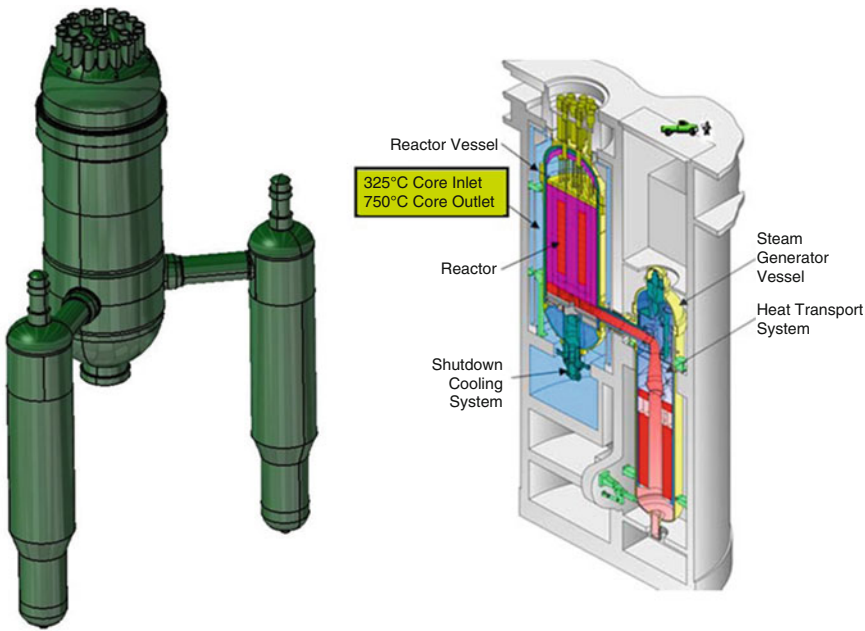
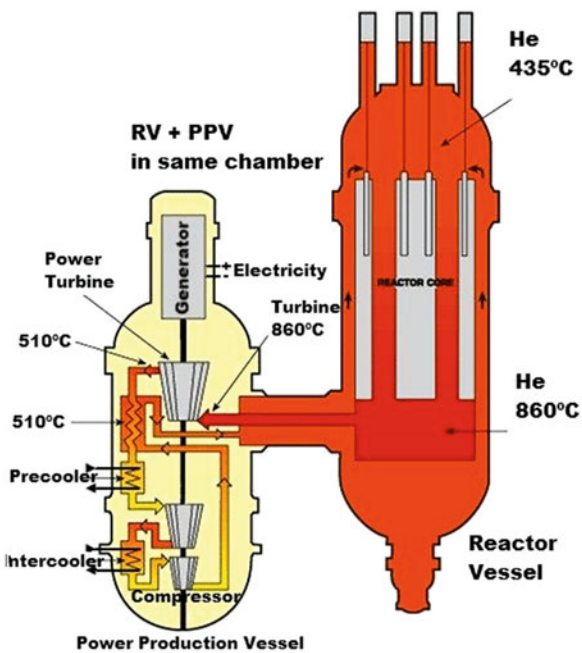
Fig. 19.13 Pebble-bed reactor schema



M.P.LaBar, A.S.Shenoy, W.A.Simon and E.M.Campbel, "Status of the GT-MHR for Electricity Production", World Nuclear Association Annual Symposium 2003, <http://www.world-nuclear.org/sym/2003/fig-htm/labf2-h.htm>

Fig. 19.14 Schematic of GT-MHR overview

Fig. 19.15 GT-MHR Layout



(A): Design Certificate Boundaries

(B): Reactor and Steam Generator General Arrangement

Fig. 19.16 AREVA's design layout of SC-HTGR. **(a)** Design certificate boundaries. **(b)** Reactor and steam generator general arrangement

19.4 Core Design and Analysis

As we stated at the opening of this chapter, one of the major challenges of the reintroduction of nuclear energy into the world energy mix is the development of a nuclear power plant that is competitive with other energy alternatives, such as natural gas, oil, or coal. The environmental imperative of nuclear energy is obvious. There are no greenhouse gases emitted, small amounts of fuel required, and small quantities of waste to be disposed of. Unfortunately, the capital costs of new nuclear plants are quite large relative to the fossil alternatives. Despite the fact that nuclear energy's operating costs in terms of operations and maintenance and, most importantly, fuel are much lower than fossil alternatives, the barrier of high initial investment is a significant one for utilities around the world.

In order to deal with this challenge, we need proper and suitable reactor core design configuration that will fit with these complex requirements stated at the beginning of this chapter, given the new technology that goes along with these small modular reactors (SMRs).

Despite the use of standard equipment such as standard fuel geometry, in-core internals, the combination of features listed at the beginning of this chapter will require fuel characteristics for these SMRs and AdvSMRs that are different from traditional light water reactor (LWR) fuel assemblies. The design of small, natural circulation LWR cores requires an understanding of the reactor physics, thermal hydraulic [5], neutronic analysis for nuclear reactor (i.e., this book), and an accurate and efficient set of computational tools and software and a well-developed design methodology.

The purpose of this section along with this chapter as a whole is to evaluate the effects of increased enrichment, burnup rates, increased leakage, and burnable poison distribution on reactor performance and to design in general a prototype core for use in a small light water reactor from top-level point of view; however readers can find more detailed oriented information in a book by A. E. Walter [6].

However, if we use the state-of-the-art tools based on modeling of traditional light water reactors as, for example, vendors, such as NuScale, using their design approach to small modular reactors technologies could be helpful for obtaining licensing operational process. Codes like RELAP which is used by the Nuclear Regulatory Commission (NRC) for validation and verification of such design have been developed around traditional LWRs and easily can be applied toward these types of SMRs, when it comes to safety analyses and shows that the core will remain covered during the entire transient procedure of design basis from loss of coolant accidents' point of view. It is important to notice that LWRs are confined under Vapor Dome as it is pointed out by Zohuri and McDaniel [1, 2].

Furthermore the above design approach and data generated through these simulations cover a new range of fuel enrichments, temperatures, pressure, power, and flow rates that are very important for an improved core design of new generation of nuclear power plants of GEN-IV from top point of view. An evaluation of the reactor control system options can also be performed in order to meet the stringent design criteria of these types of light water reactors (LWRs).

In such situation, one can concentrate on the increased enrichment fuel and analysis of phenomena related with the use of this fuel rate at a specific operational conditions from top point of view, where, for example, multi-application small light water reactor (MASLWR) may be considered. A part of the first-level analysis can be done via neutron transport burnup code such as CASMO-4 or COSMO-5 for a fuel assembly with reflected boundary conditions. This analysis is able to evaluate characteristics of the MASLWR fuel and compare them with characteristics of conventional pressurized water reactors (PWRs) fuel, and results are shown by Soldatov [7].

Note that Light Water Reactor Core Simulations using CASMO codes are able to do the following analyses:

- Lattice physics codes (e.g., CASMO) are used to prepare problem-dependent few group cross sections based on a smaller region (e.g., fuel assembly) for input to a whole-core program (e.g., SIMULATE).
- The CASMO few group cross sections are curve fitted to functions of important variables such as burnup, moderator temperature and void content, fuel temperature, and soluble poison concentration.
- These workhorse codes (CASMO) are all deterministic. There is also a growing use of stochastic “Monte Carlo” programs for these applications (MCNP will be introduced in later lab sessions), but code running times are still excessive for many purposes.

The results of such above simulations will be the effects of the increased fuel enrichment and operational conditions onto:

1. Infinite lattice multiplication factor
2. The fuel isotopic content
3. Neutron energy spectrum
4. Reactor kinetic parameters
5. Reactivity feedbacks
6. Worth of the control rods and soluble boron

In addition the series of COSMO computer code modules will have the following abilities as well, and they are:

- *Transport-burnup codes*
 - Infinite lattice, fuel cell, or assembly
 - Many energy groups
 - Region average cross-section data
 - Time (burnup) dependent
 - Operation condition dependent (T_f , T_m , Power, Xe, Boron concentrations)
- *Nodal Diffusion Codes*
 - 3D core power distribution
 - Two energy groups
 - Account for thermal feedback

Furthermore, former analyses mentioned in above by use of the increased enrichment fuel in a reactor such as MASLWR core leads to the high reserve of the reactivity for a fuel burnup. This reactivity reserve is compensating with a Gadolinium burnable absorbers.

The self-shielding of the gadolinia in a MASLWR fuel, fuel shadowing, and control rod shadowing effects were evaluated for such type of reactor fuel and discussed by Soldatov [7].

Taking under consideration the core design of small modular reactors, the small reactor core has a high neutron leakage based on traditional LWR core design approach. The evaluation of such neutron leakage on the multiplication factor and fuel utilization and discussion of the core reflector issues are also discussed in the reference by Soldatov [7].

In this case, the neutron leakage, use of the burnable absorbs, and coupled neutronic and thermal hydraulic analysis (i.e., Zohuri) [5] should also be taken into account during a core design as it was mentioned before.

Additionally, reactor theory uses will reveal the following technical points as well, and they are:

- *Slowing down*
 - Energy spectrum calculation
 - Homogenization of heterogeneous regions
- *Transport*
 - Spatial power distribution where diffusion does not work
 - Preparation of region averaged cross sections
- *Diffusion*
 - Nodal methods for 3D core power distribution
- *Burnup*
 - Evolution of nuclide concentrations with time

All these technical features possibly could be handled with computer codes such as CASMO code family.

Current computer code sets used for light water reactor reload analysis are presented in Table 19.1.

However, bear in your mind that several applications in nuclear reactor physics and dynamics require three-dimensional modeling of the core neutronics. Such calculations are presently carried out using few group nodal diffusion codes. Thus, the geometry in the diffusion calculation should be consisted of homogenized material regions or nodes. The input data for the calculation may include spectrum-averaged cross sections, kinetic parameters, and other group constants, which are generated in such a way that the integral reaction rate balance is preserved within each node [8].

Table 19.1 Current code sets used for LWR reload analysis

Code supplier	Code set ^a	Users		
		Vendor	Licensee	Consultant
ABB-CE	PHOENIX/POLKA	✓	✓	
B&W/Framatome	CASMO ^b /NEMO	✓	✓	
General electric	TGEBLA/PANACEA	✓	✓	
Siemens	CASMO ^b /MICROBURN	✓	✓	
Westinghouse	PHOENIX/ANC	✓	✓	
EPRI	CPM-2/NODE-P		✓	✓
EPRI	CPM-2/SIMULATE-E		✓	✓
EPRI	CPM-3/CORETRAN			✓
Studsvik	CASMO ^b /SIMULATE-3 ^b		✓	✓
Scandpower ^c	HELIOS/RAMONA		✓	

^aMany different versions of these codes are in use today

^bCodes developed by Studsvik of America

^cScandpower has merged with Studsvik

In summary, CASMO-5 is the latest code version in the Studsvik Scandpower series of lattice physics codes for general LWR analysis and has capabilities, features, and numerical models not previously available in CASMO-4. Among the new capabilities of CASMO-5 are a “quadratic gadolinium depletion model” and the ability to perform 2D transport calculations in hundreds of energy groups. The description of CASMO-5 capabilities and the role of CASMO-5 in generating cross section and discontinuity factor data for SIMULATE-4 can be found in the website of the vendor of the code, where also it describes the new CASMO-5 data libraries (586 group neutron and 18 group gamma) and interested readers should be refereeing themselves to that site.

19.5 Small Modular Reactors General Concepts

The driving forces in the development of small modular reactors (SMRs) are their specific characteristics. They can be deployed incrementally to closely match the increasing energy demand resulting in a moderate financial commitment for countries or regions with smaller electricity grids. SMRs show the promise of significant cost reduction through modularization and factory construction which should further improve the construction schedule and reduce costs. In the area of wider applicability, SMR designs and sizes are better suited for partial or dedicated use in non-electrical applications such as providing heat for industrial processes, hydrogen production, or seawater desalination. Process heat or cogeneration results in significantly improved thermal efficiencies leading to a better return on investment. Some SMR designs may also serve niche markets, for example to burn nuclear waste.

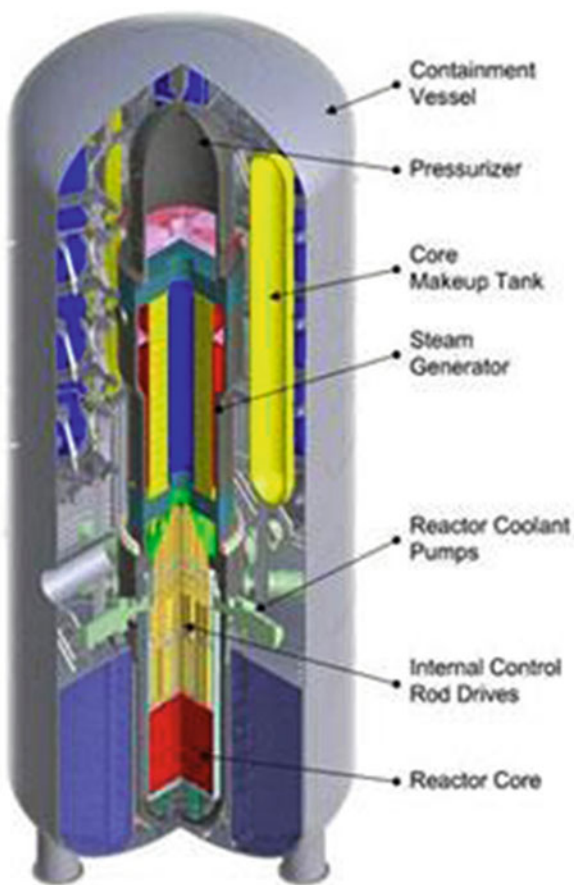
As it was stated in the former few sections of this chapter, small modular reactors (SMRs) are designed with a potential of providing clean and cost-effective energy.

As per the International Atomic Energy Association (IAEA) classification, SMRs are defined as reactors which produce power output of less than or equal to 300 MWe; but in general any reactor with an electrical output less than 700 MW is considered as a SMR. Based on the characteristics, they are further categorized into three types, and they listed as:

1. Light water reactors (LWRs)
2. High-temperature gas-cooled reactors (HTGCs)
3. Liquid-metal (i.e., sodium-cooled fast reactors (SFRs) and gas-cooled reactors (GCRs)).

As shown in Fig. 19.17, the scalability, modularity, robust design, and enhanced safety features of the SMR offer great advantages over large commercial reactors' modularity and flexibility: In contrast to large reactors, SMRs can be fabricated and assembled in a factory environment and then transported to the nuclear power site. This will help limit the on-site preparation and also reduce the lengthy construction

Fig. 19.17 Isometric section of small modular reactor. (Courtesy of Nuclear Regulatory Commission)



duration further reducing the construction cost and making the SMRs 20–30% less expensive [9]. In addition, the scalability and flexibility features of SMR also make it more suitable for small isolated areas with low-energy demands, limited infrastructure, and smaller and less established grid system.

19.5.1 *Modularity and Flexibility*

In contrast to large reactors, SMRs can be fabricated and assembled in a factory environment and then transported to the nuclear power site. This will help limit the on-site preparation and also reduce the lengthy construction duration further reducing the construction cost and making the SMRs 20–30% less expensive [9]. In addition, the scalability and flexibility features of SMR also make it more suitable for small isolated areas with low-energy demands, limited infrastructure, and smaller and less established grid system.

19.6 Safety Features and Licensing of Small Modular Reactors (SMRs)

Nuclear energy can play a very significant long-term role for meeting the world's increasing energy demands while simultaneously addressing challenges associated with global climate and environmental impact. Many nations of the world, particularly the Asia/Pacific Rim countries, are actively engaged in a major expansion of their nuclear energy complex. The degree to which nuclear energy can address long-term energy needs, either globally or regionally, will be dictated by the pace and adequacy of technical and policy solutions for waste, safety, security, and nonproliferation issues, as well as the capital cost of construction. Small modular reactors (SMRs) could successfully address several of these issues. SMRs offer simpler, standardized, and safer modular design by being factory built, requiring smaller initial capital investment, and having shorter construction times. The SMRs could be small enough to be transportable, could be used in isolated locations without advanced infrastructure and without power grid, or could be clustered in a single site to provide a multi-module, large capacity power plant.

The both topics of safety and licensing, in general, are described below and divided in two general summaries as:

19.6.1 Safety Features of Small Modular Reactors

The safety aspects of SMRs have been intensively reviewed in several recent publications, mostly originating from the International Atomic Energy Agency (IAEA), and they all can be found in IAEA website, which are summarized below. However, one should keep in mind that the safety features of SMRs will be reanalyzed following the Fukushima Daiichi accident in order to take into account the lessons learned from it.

The major findings regarding small modular reactor safety are the following:

- The design manufacturers of advanced small modular reactors (AdvSMRs) aim to implement safety design options with maximum use of inherent and passive safety feature, which is also referred to as “by design” safety features.
- On their own, the “by design” safety features used in SMRs are in most cases not size-dependent and could be applied in the reactors of large capacity. However, SMRs offer broader possibilities to incorporate such features with higher efficiency.
- In the case of some technologies such as high-temperature gas reactors, the incorporation of passive safety features limits the reactor capacity.
- All of the SMRs designs are considered with an aim to meet international safety norms and standard set by the IAEA, such as those formulated in the IAEA Safety Standard NS-R-1 Safety of the Nuclear Power Plants, which includes design requirements, regarding implementation of the defense-in-depth strategy and provision of redundant and diverse, *active and passive safety systems*.
- The available information on safety features of advanced SMRs for plant protection against the impacts of natural and human-induced events is generally sparser compared to that on internal events.
- The core damage frequencies (CDFs) indicated by the designers of advanced SMRs are comparable to or even lower than the ones indicated for the state-of-the-art, large water-cooled reactors (LWCRs).

Note that in case of *Passive Safety System*, the integral design of small modular reactor makes it safer in case of any sever accidents preventing any radiation leak into the environment. The passive safety system is another important safety feature in the SMRs. In case of loss of coolant accident, this system shuts down the reactor and cools it without any human intervention or air conditioning (AC) power for a period of 7 days. The safety system incorporates an on-site water inventory, which operates on natural forces (i.e., natural circulation or gravity or compressed gas) [10].

19.6.2 Licensing of Small Modular Reactors

The licensing of SMRs will be affected by the Fukushima accident in the same way as for the large reactors that are in place today. Regarding licensing status and regulatory issues relevant to SMRs, the analysis of recent publications leads to the following observations as listed here:

- According to the vendors and designers of the advanced small modular reactors (AdvSMRs) listed here in Table 19.2, they have been designed or are being designed in compliance with their current national (i.e., imposed by NRC) and international (i.e., imposed by IAEA) regulations.
- The SMRs available for deployment, which are the CANDU-6, the PHWR, the QP-300, the CNNP-600, and the KLT-40S, have already completed the licensing procedures in the countries of origin. The CANDU-6 and the QP-300 have also been licensed and deployed in countries other than the country of origin.
- For advanced SMR designs, three of them are in a formal licensing process in Argentina, China, and the Republic of Korea (i.e., South Korea), and several others are in prelicensing negotiations in the United States and India as indicated in Table 19.2

However, government support for licensing of selected advanced SMRs (AdvSMRs) could help overcome the corresponding delays.

Another important set of regulatory requirements concerns the ability of SMRs to resist nuclear proliferation. All advanced light water PWR SMRs use conventional low-enriched uranium (LEU) fuel, and most of the PWR SMR designs use the *same* fuel as large PWRs. However, particular attention should be paid to the nonproliferation potential of some heavy-water or liquid-metal cooled designs, especially if they are intended to be deployed in politically unstable areas. The IAEA has an ongoing activity on the options of incorporation of intrinsic proliferation resistance features in nuclear power plants (NPPs) with innovative small modular reactors (SMRs).

19.6.3 Nonproliferation Resistant and Security

The SMR is a sealed unit built below grade, thus making it safer against any terrorist activities or aircraft impact or any vulnerabilities due to natural phenomenon. They are also designed to operate for longer periods without refueling (i.e., approximately 18–24 months); and the reactor can be refueled in a factory environment and then transported back to site, thus securing it against any proliferation issues.

Table 19.2 Design status and potential timeframes for deployment of advanced SMRs

SMR	Technology family	Electric output, MWe	Plant configuration	Design status	Licensing status/completion (application) date	Targeted deployment date
KLT-40S, Russia	PWR	2 × 35	Twin-unit barge-mounted plant	Detailed design completed	Licensed/under construction	2013
VBER-300, Kazakhstan, Russia	PWR	302	Single module or twin-unit, land-based or barge-mounted plant	Detailed design nearly completed	n/a	>2020
ABV, Russia	PWR	2 × 7.9	Twin-unit barge-mounted or land-based plant	<i>Barge-mounted plant:</i> detailed design completed <i>Land-based plant:</i> detailed design for plant modification in progress	Part of design licensed	2014–2015
CAREM-25, Argentina	PWR	27	Single module land-based plant	Detailed design being finalized	Licensing in progress/ 2011	Prototype: 2015
SMART, Republic of Korea	PWR	90	Single module land-based plant	Detailed design in progress	Licensing in progress/ 2011	~2015
NuScale, USA	PWR	12 × 45	Twelve-module land-based plant	Detailed design being finalized	Licensing pre-application/ (Application: 2011)	FOAK in 2018
mPower, USA	PWR	×125	Multi-module land-based plant	Detailed design in progress	Licensing pre-application/ (Application: 2011)	~2018
IRIS ^a , USA	PWR	335	Single module or twin-unit land-based plant	Basic design completed and is under review by the vendor		
Westinghouse SMR	PWR	>225				

(continued)

Table 19.2 (continued)

SMR	Technology family	Electric output, MWe	Plant configuration	Design status	Licensing status/ completion (application) date	Targeted deployment date
HTR-PM, China	HTGR	2 × 105	Two-module land-based plant	Detailed design completed	Licensing in progress/ 2010 or 2011	FOAK in 2013
AHWR, India	Advanced heavy water reactor	300	Single module land-based plant	Detailed design being finalized	Licensing pre-application/ (Application: 2011)	~2018
SVBR-100, Russia	Pb-Bi cooled fast reactor	×101.5	Single module or multi-module land-based or barge-mounted plant	Detailed design in progress	n/a /Prototypes have operated in Russian submarines	Prototype: 2017
New Hyperion power module, USA	Pb-Bi cooled fast reactor	×25	Single module or multi-module land-based plant	n/a	Licensing pre-application/ (application: not known)	FOAK by 2018
4S, Japan	Na cooled fast reactor	10	Single module land-based plant	Detailed design in progress	Licensing pre-application/ (Application: 2012)	FOAK after 2014

^aLate in 2010, the Westinghouse Electric Company stopped the development of the IRIS project and announced it would go with an alternative integral design PWR of a 200 Mwe class. Very few technical details of this new SMR were available as of 2011

19.7 Small Reactor Designs in Market

Carbon emission concerns and volatility in fossil fuel resources have renewed worldwide interest in nuclear energy as a solution to growing energy demands. Several large nuclear reactors are currently under construction in the United States, representing the first new construction in over 30 years. Small modular reactors (SMRs) have been in design for many years and offer potential technical and economic advantages compared with traditionally larger reactors. Current SMR capital and operational expenses have a wide range of uncertainty.

According to the Organization for Economic Cooperation and Development/Nuclear Energy Agency (OECD/NEA) estimates, nuclear power plants (NPPs) whether with a large reactor or with small modular reactors (SMRs), with electric output of less than 300 MWe, using light water technology, are competitive with many other electricity generation technologies in the large majority of cases, the exceptions being natural gas in the United States with the current level of prices and large hydro.

However, SMRs, including multi-module plants, may have higher values of levelized cost of electricity (LCOE) than NPPs with large reactors. The LCOE for an SMR should decrease with large-scale serial production, which is the key element for proving the competitiveness of SMRs. However, large initial orders of SMRs are needed to launch the serial production process, and it is important to know who could be the first customers and how many SMR designs will really be deployed in the near future.

Today, the world's major reactor vendors have targeted markets in developed countries and currently offer designs that have large power outputs (1000–1700 MWe) [11]. However, these large reactors are unsuitable for many developing countries for several reasons [12].

As with large reactors, the market for SMRs is difficult to estimate. However, using the commonly accepted assumption that SMRs could be competitive with many nonnuclear technologies for generating electricity, in the cases when NPPs with large reactors are, for whatever reason, unable to compete, one can try to identify the key market opportunities.

However, many developing countries have limited electric grid capacity that cannot accommodate a single power plant with output approaching or exceeding 1000 MWe. Also, the grid in some countries is localized in a few isolated population centers with minimal interconnections. This situation favors the use of smaller power plants sited at geographically separated locations.

As we know about the nuclear power industry so far, nuclear power plants traditionally have a large capital cost relative to fossil power plants, which creates an additional barrier to choosing nuclear power. By virtue of their reduced size and complexity, smaller-sized nuclear plants will have a lower capital cost per plant and shorter construction time. Thus the initial power unit can be generating revenue before the second and third units are constructed, reducing the maximum capital outlay for the combined generating capacity. This is especially important for developing economies, which typically have limited availability of capital funds.

Because of the lower power levels of small- or medium-sized nuclear plants, countries have more flexibility to install generating capacity in smaller increments that better match their rate of power demand and economic growth. The reduced power levels allow greater use of passive safety systems and plant simplifications, such as natural circulation of the primary coolant. These features enhance the safety and reliability of the nuclear power facility, which is especially advantageous in countries that have limited nuclear experience and trained workforces.

Current, worldwide nuclear energy is based on medium and high capacity level reactors [13] (IAEA classification of capacity levels 300–900 MWe and 900–1600 MWe, respectively [14]). The primary technology for operational nuclear reactors worldwide is light water reactor (LWR) technology [14–16]. The world “technology” here does not specifically refer to the nuclear power plant design but also the LWR-oriented fuel cycle facilities and comprehensive supply chain. LWR technology is well studied and well reflected in regulatory practice [17–21]. This makes LWR technology most attractive for innovative reactor design in the short-term and midterm time frames.

Several countries are currently working on the design of innovative nuclear power plants in the low-power range (10–300 MWe). There are a variety of design concepts being considered worldwide (such as high-temperature gas-cooled reactors and liquid-metal fast breeder reactors) [14, 22–24]. However, LWRs are considered the most economically feasible and deployable technology for innovative reactors in the near future [25].

In order to design a competitive reactor and successfully promote it into international markets, the overview of close competitors is necessary. In order to perform this analysis, first of all, it is necessary to recognize and list all major reactor design concepts (projects, designs) being proposed during the last decade, identify major advantages and disadvantages of the proposed designs, identify designs which have similarities with multi-application small light water reactor (MASLWR), and try to understand the ideas and motivation behind these designs. Learning the difficulties and unsuccessful designs of small reactors (particularly LWRs) is also important in order to avoid the repetition of the other mistakes and potential challenges in the early design stage. The general overview of the competing designs is given for large-scale innovative LWRS [26–30] and for different designs of small reactors [25] including innovative LWR. Detailed discussions of the innovative reactor designs are given in the sources [31–37].

19.8 Conclusions

A principle conclusion of this chapter is that small modular reactors (SMRs) have a significant potential to expand the peaceful applications of nuclear power by catering to the energy needs of those market segments that cannot be served by conventional nuclear power plants (NPPs) with large reactors. Such segments could be:

- Niche applications in remote or isolated areas, where large generating capacities are not needed, where the electrical grids are poorly developed or absent, and where the non-electrical products such as heat or desalinated water are as important as the electricity
- Replacement for the decommissioned small- and medium-sized fossil fuel plants, as well as an alternative to newly planned such plants, in the cases, when certain siting restrictions exist, such as limited free capacity of the grid, limited spinning reserve, and/or limited supply of water for cooling towers of a power plant
- Replacement for those decommissioned fossil-fueled combined heat and power plants, where the SMR power range seems to better fit the requirements of the currently existing heat distribution infrastructure
- Power plants in liberalized energy markets or those owned by private investors or utilities for whom small upfront capital investments, short on-site construction time with the accordingly reduced cost of financing, and flexibility in plant configuration and applications matter more than the levelized unit electricity cost

It should be noted, however, that none of the smaller reactors have yet been licensed for these applications and there remain both development challenges to overcome and regulatory approvals to obtain before deployment, especially in light of the recent accident at Fukushima.

These observations in this chapter have found no situations, where NPPs with SMRs could compete with the NPPs with state-of-the-art large reactors, on low-enriched uranium (LUE) basis. However, it is also found that *SMRs could be competitive with many nonnuclear technologies in the cases, when NPPs with large reactors are, for whatever reason, unable to compete.*

References

1. B. Zohuri, *Combined Cycle Driven Efficiency for Next Generation Nuclear Power Plants: An Innovative Design Approach*, 1st edn. (Springer Publishing Company, Cham, 2015)
2. B. Zohuri, P. McDaniel, *Combined Cycle Driven Efficiency for Next Generation Nuclear Power Plants: An Innovative Design Approach*, 2nd edn. (Springer Publishing Company, Cham, 2017)
3. B. Zohuri, *Small Modular Reactors as Renewable Energy Sources* (Springer Publishing Company, Cham, 2018)
4. B. Zohuri, P. McDaniel, C. De Oliveira, Advanced nuclear open-air-Brayton cycles for highly efficient power conversion. *Nucl. Technol.* **J** *192*, 48–60 (2015)
5. B. Zohuri, *Thermal-Hydraulic Analysis of Nuclear Reactors*, 2nd edn. (Springer Publishing Company, Cham, 2017)
6. A.E. Walter, *Fast Breeder Reactors* (Pergamon Press, New York, 1981)
7. A. Soldatov, Design and Analysis of a Nuclear Reactor Core for Innovative Small Light Water Reactors, A Dissertation Submitted to Oregon State University, 2009
8. J. Leppänen, NEW ASSEMBLY-LEVEL MONTE CARLO NEUTRON TRANSPORT CODE FOR REACTOR PHYSICS CALCULATIONS, Mathematics and Computation, Supercomputing, Reactor Physics and Nuclear and Biological Applications Palais des Papes, Avignon, France, September 12–15, 2005, on CD-ROM, American Nuclear Society, LaGrange Park, IL (2005), Jaakko.Leppanen@vtt.fi

9. Nuclear Energy Association (NEA), June 2011. Current Status, Technical Feasibility and Economics of Small Modular Reactors
10. T. Kozlowski, T.J. Downar, December 2003. OECD/NEA AND U.S. NRC PWR MOX/UO₂ Core Transient Benchmark
11. International Atomic Energy Agency, IAEA-TECDOC-1117, Evolutionary water-cooled reactors: Strategic issues, Technologies and Economic Viability, in *Proceedings of a Symposium held in Seoul*, 30th November – 4th December 1998, IAEA, Vienna, 1999. (ISSN 1011-4289)
12. D.T. Ingersoll, W.P. Poore, III, Reactor technology options study for near-term deployment of GNEP grid-appropriate reactors, ORNL/TM-2007/157, ORNL, Oak Ridge, TN, 26 Sept 2007
13. 2005 World Nuclear Industry Handbook, Nuclear Engineering International, 2005
14. IAEA CSP-14 (Parts 1–5), Small and Medium Sized Reactors: Status and Prospects, in *Proceeding of International Seminar held in Cairo*, Egypt, 27–31 May 2001, IAEA, Vienna, 2002
15. IAEA PUB 1280, *Operating Experience with Nuclear Power Stations in Member States in 2005* (IAEA, Vienna, 2006)
16. Nuclear Energy Today, Nuclear Development, NEA/OECD 2003
17. European Utility Requirements for LWR Nuclear Power Plants, Volume 1 *Main Policies and Objectives* Revision C, EUR-Club, 2001. Chapters 1–6 with list of acronyms and definitions section
18. European Utility Requirements for LWR Nuclear Power Plants, Volume 2 *Generic Nuclear Island Requirements* Revision C, EUR-Club, 2001. Chapters 0–19 with list of acronyms and definitions section annexes
19. European Utility Requirements for LWR Nuclear Power Plants, Volume 3 *Application of EUR to the Specific Projects* Revision C, EUR-Club, 2001. Chapters 0–19 with list of acronyms and definitions section, annexes
20. European Utility Requirements for LWR Nuclear Power Plants, Volume 4 *Generic Conventional Island Requirements* Revision B, EUR-Club, 2000. Chapters 0–19 with list of acronyms and definitions section annexes
21. 10 CFR Part 52, *Domestic Licenses, Certifications, and Approvals for Nuclear Power Plants*, US Nuclear Regulatory Commission, Electronic Publication, <http://www.nrc.gov/reading-rm/doc-collections/cft/part052/>
22. International Atomic Energy Agency, IAEA-TECDOC-1485, Status of innovative small and medium sized reactor designs 2005, Reactors with conventional refueling schemes IAEA, Vienna, 2006. (ISSN 1011-4289)
23. IAEA, Progress in Design and Technology Development for Innovative Small and Medium Sized Reactors, in *Proceeding of IAEA 51st General Conference* 17 September 2007, IAEA, Vienna 2007
24. IAEA, Current Trends in Nuclear Fuel for Power Reactors, in *Proceeding of IAEA 51st General Conference* 17 September 2007, IAEA, Vienna 2007
25. International Atomic Energy Agency, IAEA-TECDOC-1391, *Status of Advanced Light Water Reactor Designs 2004* (IAEA, Vienna, 2004)
26. International Atomic Energy Agency, IAEA-TECDOC-1290, *Improving Economics and Safety of Water-Cooled Reactors: Proven Means and New Approaches* (IAEA, Vienna, 2002). (ISSN 1011-4289)
27. J. Kupitz, Y. Bussurin, P. Gowin, Considerations Related To Specific Concepts: Water- Cooled Reactors, Gas-Cooled Reactors, Metal- Cooled Reactors, Non-Conventional Reactors, <http://www.mi.infn.it/~landnet/Doc/Reactors/kupitz.pdf>
28. IAEA, *Overview of Global Development of Advanced Nuclear Power Plants Annex 1* (IAEA, Vienna, 2003), pp. 1094–1110
29. IAEA, *IAEA Overview of Global Development of Advanced Nuclear Power Plants Information NPTDS Brochure* (IAEA, Vienna, 2006)
30. B. Guerrini, S. Paci, *Lessons on Nuclear Plants Part IIB: Advanced Reactors Training materials*, RL (811) 99, (University of Pisa, 1998)

31. J.E. Fisher, S.M. Modro, K.D. Weaver, J.N. Reyes Jr, J.T. Groome, P. Bapka, *Performance and safety studies for Multi-Application, Small, Light Water Reactor (MASLWR)*, in Proceedings of RELAP5 International Users Seminar was held in Sun Valley, Idaho, 5–7 Sept 2001
32. J.E. Fisher, S.M. Modro, K.D. Weaver, J.N. Reyes Jr, J.T. Groome, P. Bapka, *Performance and safety studies for Multi-Application, Small, Light Water Reactor (MASLWR)*, in Proceedings of RELAP5 International Users Seminar was held in Park City, Utah, 4–6 Sept 2002
33. S.M. Modro, J.E. Fisher, K.D. Weaver, J.N. Reyes, Jr., J.T. Groome, P. Bapka, G. Wilson, *Generation-IV Multi-Application Small Light Water Reactor (MASLWR)*, in 10th International Conference on Nuclear Energy, INEEL/CON-02-00017, 14 Apr 2002
34. S.M. Modro, J.E. Fisher, K.D. Weaver, J.N. Reyes, Jr., J.T. Groome, P. Bapka, T.M. Carlson, *Multi-Application Small Light Water Reactor Final Report*, INEEL/EXT-04-01626, December 2003, p. 105. J.N. Reyes, J. Groome, B.G. Woods, E. Young, K. Abel, Y. Yao, Y.J. Yoo, Testing of the multi-application small light water reactor (MASLWR) passive safety systems, *Nucl. Eng. Des.* **237**, 1999–2005, (2007)
35. B.G. Woods, J.N. Reyes, Q. Wu, *Flow Stability Testing under Natural Circulation Conditions in Integral Type Reactors*, in Presentation at IAEA Natural Circulation Research Coordination Meeting Corvallis, OR, USA, 1 Sept 2005
36. A. Soldatov, W. Marcum, J. Magedanz, K. Nelson, J. Dahl, *Advanced Thermal Accessible Reactor Final Report* Course NE 574 – Design Project Report, OSU, March, 2007
37. A. Soldatov, J. Magedanz, J. Dahl, *MASLWR Extended Core Live Design and Preliminary Instrumentation*, Course NE 575 – Design Project Report, OSU, June, 2007, p. 109. M. Galvin A. Soldatov, *Multi-Application Small Light Water Reactor (MASLWR), Global Viability*, Course ECE599 – design project report, OSU, March, 2007

Appendix A

Laplace Transforms

To the young engineering student, Laplace transforms seem to be almost a mathematical curiosity. They were developed by Laplace (1749–1827) and Cauchy (1789–1857) as mathematical transforms for mathematicians. Hence, they gave mathematicians a logical reason for studying the complex plane and complex variable theory. However, when it was recognized that they actually provided a mathematical basis for Heaviside's (1850–1925) operational calculus, they became useful to engineers and could be applied to solve real-world problems. Heaviside was an English engineer that suggested solving differential equations by replacing the derivative function by a large D symbol and then treating this “D operator” as if it were similar to an algebraic operator. His operational calculus based on this concept enabled him to simplify systems of differential equations that modeled physical systems and made the prediction of their behavior much more easily understood. Analysis of coupled systems of differential equations,

Particularly those that contain control loops or feedback operators are much easier to understand when transformed to the “s” or complex plane. Asymptotic behaviors can be understood without completely solving the time-dependent equations. Unfortunately, the Laplace transform method can only be applied to linear systems, but these have always been the easiest for the human mind to formulate and adequately describe the behavior of the majority of engineered systems.

Definition of Laplace Transform

The Laplace transform is defined by the following integral equation. If $f(t)$ is a time-dependent function that is piecewise continuous and of exponential order, then its transform $F(s)$ is given by:

$$F(s) = \int_0^{\infty} e^{-st} f(t) dt = \mathcal{L}\{f(t)\} \quad (\text{A.1})$$

Piecewise continuous simply means that over the t interval of interest, there are only a finite number of discontinuities, and *exponential order* simply means that the function can be bounded by an exponential function with an exponent that increases no faster than the first power in the variable “ t .” Most physically realizable functions satisfy these two criteria. Of course, we really do not know how $f(t)$ behaves when we transform its differential equation. Normally we will simply apply the transform, and if we get a solution that does not satisfy these criteria, we will conclude the method does not work.

Note that the Laplace of first and second derivatives of a function $f(t)$ demonstrated by $f'(t)$ and $f''(t)$, respectively, are given by the following relationships:

$$\begin{cases} \mathcal{L}\{f'(t)\} = sf(s) - F(0) \\ \mathcal{L}\{f''(t)\} = s^2f(s) - sF(0) - F'(0) \end{cases} \quad (\text{A.2})$$

Having defined the Laplace transform, it now seems logical that we would define the inverse Laplace transform. Unfortunately, this requires complex variable math and is probably way beyond the realistic math requirements for this course. Therefore, we will simply try to invert the $F(s)$ functions by inspection. That is, we hopefully recognize the form of $F(s)$ as something we have obtained as a transform of a known function $f(t)$. We can then conclude that the transform process and its inversion are unique. If we know that a particular $F(s)$ is the transform of a known $f(t)$, then $f(t)$ must be the inverse transform of $F(s)$. This leads us to the concept of “transform pairs.” Laplace transforms are traditionally used based on having a table of transforms and their inverses in a table, so that when a $F(s)$ is obtained for a system of equations, its inverse can simply be looked up in a table of “transform pairs.” We will not even become this sophisticated in this course. We will find a few transforms that will cover the vast majority of cases, and then we will simply use these and combinations of these. In fact, the real power of Laplace transforms lies in the ability of the engineer to apply some analytical tools to the transform function in the s (complex) variable and determine the answers to all reasonable questions about the generic time-dependent behavior of the system.

Basic Transforms

Some basic transforms that we will use are as follows:

1. Constant function

Consider a function that is simply a constant for all time. Since we are dealing with time-dependent functions, this is sometimes given the symbol $KU(t)$, where

K is a real number and $U(t)$ is the function that has a zero value for all $t < 0$ and is equal to 1.0 for all $t > 0$.

The Laplace transform is given by:

$$\mathfrak{L}\{KU(t)\} = \int_0^\infty Ke^{-st}dt = \frac{K}{s} \int_0^\infty e^{-st}sdt = \frac{K}{s} \int_0^\infty e^{-x}dx = \frac{K}{s} \quad (\text{A.3})$$

2. Ramp function

Consider now a linear function of t . Let $f(t) = Kt$, then its Laplace transform is given by:

$$\begin{aligned} \mathfrak{L}\{Kt\} &= \int_0^\infty Kte^{-st}dt = \frac{K}{s^2} \int_0^\infty ste^{-st}sdt = \frac{K}{s^2} \int_0^\infty xe^{-x}dx \\ &= \frac{K}{s^2} \left\{ -xe^{-x} \Big|_0^\infty + \int_0^\infty e^{-x}dx \right\} = \frac{K}{s^2} \end{aligned} \quad (\text{A.4})$$

3. Power of t function

Now consider an arbitrary power of t given by t^α then, its Laplace transform is given by, $f(t) = Kt^\alpha$ as follow:

$$\mathfrak{L}\{Kt^\alpha\} = \int_0^\infty Kt^\alpha e^{-st}dt = \frac{K}{s^{\alpha+1}} \int_0^\infty (st)^\alpha e^{-st}sdt = \frac{K}{s^{\alpha+1}} \int_0^\infty \alpha x^{\alpha-1} e^{-x}dx = \frac{K}{s^{\alpha+1}} \alpha! \quad (\text{A.5})$$

4. Exponential function

The exponential function, $f(t) = e^{\alpha t}$, has the transform:

$$\mathfrak{L}\{e^{\alpha t}\} = \int_0^\infty e^{\alpha t} e^{-st}dt = \frac{1}{s - \alpha} \int_0^\infty e^{-(s-\alpha)t}sdt = \frac{1}{s - \alpha} \int_0^\infty e^{-x}dx = \frac{1}{s - \alpha} \quad (\text{A.6})$$

5. Sinusoid function

Consider $f(t) = \cos(\omega t)$, then its Laplace transform is given as:

$$\begin{aligned} \mathfrak{L}\{\cos(\omega t)\} &= \int_0^\infty \frac{e^{i\omega t} + e^{-i\omega t}}{2} e^{-st}dt = \frac{1}{2} \int_0^\infty \left(e^{-(s-i\omega)t} + e^{-(s+i\omega)t} \right) dt \\ &= \frac{1}{2} \left\{ \frac{1}{s - i\omega} + \frac{1}{s + i\omega} \right\} = \frac{s}{s^2 + \omega^2} \end{aligned} \quad (\text{A.7})$$

Note also that $\mathfrak{L}\{\sin(\omega t)\} = \frac{\omega}{s^2 + \omega^2}$

Fundamental Properties

1. Linearity

$$\mathfrak{L}\{af(t)\} = \int_0^\infty af(t)e^{-st}dt = a \int_0^\infty f(t)e^{-st}dt = aF(s) \quad (\text{A.8})$$

2. Superposition

$$\mathfrak{L}\{f(t) + g(t)\} = \int_0^\infty f(t)e^{-st}dt + \int_0^\infty g(t)e^{-st}dt = F(s) + G(s) \quad (\text{A.9})$$

3. Time translation

$$\mathfrak{L}\{f(t-a)\} = \int_0^\infty f(t-a)e^{-st}dt = e^{-as} \int_0^\infty e^{-s(t-a)}d(t-a) = e^{-as}F(s) \quad (\text{A.10})$$

4. Complex differentiation

$$\mathfrak{L}\{tf(t)\} = \int_0^\infty rf(t)e^{-st}dt = -\frac{dF(s)}{ds} \quad (\text{A.11})$$

5. Translation in the s variable

$$\mathfrak{L}\{e^{at}f(t)\} = \int_0^\infty e^{at}f(t)e^{-st}dt = F(s-a) \quad (\text{A.12})$$

6. Real differentiation

$$\mathfrak{L}\left\{\frac{df(t)}{dt}\right\} = \int_0^\infty \frac{df(t)}{dt}e^{-st}dt = sF(s) - f(0) \quad (\text{A.13})$$

7. Final value theorem

$$\lim_{s \rightarrow 0} sF(s) = \lim_{t \rightarrow \infty} f(t) \quad (\text{A.14})$$

8. Initial value theorem

$$\lim_{s \rightarrow \infty} sF(s) = \lim_{t \rightarrow 0} f(t) \quad (\text{A.15})$$

Inversion by Complex Variable Residue Theorem

The general inversion formula is given by the following form:

If

$$F(s) = \frac{N(s)}{\prod_{i=1}^n (s - p_i)^{m_i}} \quad (\text{A.16})$$

Then

$$f(t) = \sum_{i=1}^n \lim_{s \rightarrow p_i} \frac{\partial^{m_i-1}}{\partial s^{m_i-1}} (s - p_i)^{m_i} F(s) e^{st} \quad (\text{A.17})$$

Examples Simple pole ($n = 1, m = 1$)

$$f(t) = \lim_{s \rightarrow p} (s - p) F(s) e^{st} \quad (\text{A.18})$$

$$\text{Let } p = 5, f(t) = \lim_{s \rightarrow p} (s - 5) F(s) e^{st} = \lim_{s \rightarrow 5} \frac{(s-5)N(s)e^{st}}{(s-5)} = n(5)e^{5t}$$

Higher-order pole ($n = 1, m_i = 2$):

$$f(t) = \lim_{s \rightarrow p} \frac{\partial}{\partial s} (s - p)^2 F(s) e^{st} = \lim_{s \rightarrow p} \frac{\partial (N(s)e^{st})}{\partial s} = \frac{\partial n(p)}{\partial p} e^{pt} + t n(p) e^{pt}$$

Multiple poles with a zero ($n = 2, m_1 = 1, m_2 = 1$)

Let $F(s) = \frac{s + \alpha}{(a + \beta)(s + \gamma)}$ then,

$$\begin{aligned} f(t) &= \lim_{s \rightarrow -\beta} (s + \beta) \frac{s + \alpha}{(s + \beta)(s + \gamma)} e^{st} + \lim_{s \rightarrow -\gamma} (s + \gamma) \frac{s + \alpha}{(s + \beta)(s + \gamma)} e^{st} \\ &= \frac{\alpha - \beta}{\gamma - \beta} e^{-\beta t} + \frac{\alpha - \gamma}{\beta - \gamma} e^{-\gamma t} \end{aligned} \quad (\text{A.19})$$

Appendix B

Transfer Functions and Bode Plots

Bode plots are a very useful way to represent the gain and phase of a system as a function of frequency. This is referred to as the frequency domain behavior of a system. The concept of transfer function representation of nuclear power plants has proved a very fruitful tool both from the point of view of dynamic analysis and from the interpretation of experimental data. Much of the analysis of reactor kinetics and control can be in the form of systems of ordinary differential equations and their boundary conditions by suitable definitions.

Transfer Functions

As we have seen in Appendix A, the Laplace transformation is a technique that replaces the operation of integration with its general solution and subsequent fitting of boundary conditions with an operation of algebraic manipulation, which, in return, requires at least one boundary and one initial condition to find a solution of an ordinary differential equation for dependent variable $x_i \rightarrow i = 1, 2, \dots$ in space on the independent variable time t .

The one-sided Laplace transform $\mathcal{L}\{f(t)\}$ of a function of time is defined via an integral over all time which has the effect of replacing time dependence with dependence on a new or transform variable s as it was shown in Appendix A, and it was presented as a relationship of following form:

$$\mathcal{L}\{f(t)\} = F(s) = \int_0^{\infty} e^{-st} f(t) dt \quad (B.1)$$

As it can be seen, the exponential weighting will make this integral converging even for function of $f(t)$ increasing with variable t . Now we can suppose that s to be a real number and s_0 sufficiently large as to dominate any exponential behavior in $f(t)$,

then the advantage of the Laplace transform in the case of constant coefficient is evident since $\mathcal{L}\{ax(t)\} = aX(s)$. The application to differential equations comes by considering the transform of the differential via an integration by parts:

$$\int_0^\infty \frac{dx}{dt} e^{-st} dt = [xe^{-st}]_0^\infty + \int_0^\infty sxe^{-st} dt = sX(s) - s_0 \quad (\text{B.2})$$

for all reasonable $x(t)$. Thus, the system of linear equations with constant coefficient reduces to an algebraic system:

$$sX_i - \sum_{i'=1}^n a_{ii'}X_{i'} = S_i + x_{i0} \quad (\text{B.3})$$

With the transformed source separated from the summation. We can expect to find the algebraic matrix inverse, and they are able to write the following form as:

$$X_i = \sum_{i'=1}^n G_{ii'}(s)[S_{i'} + x_{i'0}] \quad (\text{B.4})$$

or $X = G(s)[S + x_0]$ in matrix form.

The right-hand side divides into two noticeable different parts as follows:

1. A driving term due to the source and initial conditions, normally called the excitation function.
2. The term $G_{ii}(s)$ that gives the system behavior modifying the excitation function to yield the system output or response X_i .

However, we expect that if a system is going to be *stable*, the inherent response with zero driving terms by itself must display a stable nature and not lead to increasing values of $x(t)$. $G_{ii}(s)$ relates to the *transfer* function for the i th output variable in terms of the i th input.

Sample Transforms

Simple functions of time lead to Laplace transforms that can be found in any books of Laplace transform subject. Utilizing the definition of Dirac delta distribution, we note that $1/s$ is strictly a step function transform, where the time-dependent function rises to 1 at time zero having been zero beforehand. However, this is not strictly a function – defined as being zero everywhere except around $t = 0$ and of such a magnitude that the integral over $\delta(t)$ is normalized to unity. Its transform is readily obtained directly from such a definition with the following notation in mind:

Table B.1 Short table of Laplace and Fourier transforms

$f(t); \lambda \equiv 1/\tau$	$F(s)$	$F(j\omega); j^2 = -1$
$\delta(t)$	1	1
$h(t)$ step function	$\frac{1}{s}$	$\frac{1}{j\omega} = -\frac{j}{\omega}$
$e^{-\lambda t}$ or $e^{-t/\tau}$	$\frac{1}{\lambda + s}$	$\frac{\tau}{1 + j\omega\tau}$
$te^{-\lambda t}$	$\frac{1}{(\lambda + s)^2}$	$\left(\frac{\tau}{1 + j\omega\tau}\right)^2$
$\sin at$	$\frac{a}{a^2 + s^2}$	$\frac{a}{a^2 - \omega^2}$
$\cos at$	$\frac{s}{a^2 + s^2}$	$\frac{j\omega}{a^2 + \omega^2}$
$e^{-\lambda t}f(t)$ $f(t - \tau)$	$f(s + \lambda)$ $e^{s\tau}F(s)$	$F(j\omega + \lambda)$ $e^{-j\omega\tau}F(j\omega)$
$\lim_{t \rightarrow 0^+} f(t)$	$\lim_{s \rightarrow \infty} sF(s)$	For well-behaved
$\lim_{t \rightarrow \infty} f(t)$	$\lim_{s \rightarrow 0} sF(s)$	$sF(s)$

$$\int_{-\infty}^{+\infty} f(t)\delta(t)dt = f(0) \quad (\text{B.5})$$

With the help of this distribution, initial conditions can be stated as equivalent sources. In particular, consider the response of the system for one output x to an impulse source as describable via the Dirac distribution and no other initial condition. However, we have $X(s) = G(s)S(s) \rightarrow G(s)$, where $G(s)$ is the *system* function as opposed to $S(s)$ and the initial condition providing a driving term or excitation function. We have the important result that $G(s)$ is the response to an impulse source.

Note as well that the general “shifting” relations of any table of Laplace transform with the limiting value relationships are useful for steady-state displacement, etc. See Table B.1.

If we are in a situation that the system of equations leads, as it often does, to rational polynomial fractions $g(s)/f(s)$, where both $g(s)$ and $f(s)$ are polynomial functions in respect to variable s , then the inverse transform can generally be found via the method of *partial fractions*. Let $f(s) = 0$; then this leads to roots s_i for $i = 1, 2, \dots$ such that we can write $f(s) = [s - s_1][s - s_2] \cdots [s - s_i] \cdots [s - s_n]$. Three useful results arise from this situation as follows:

(a) If all the roots s_i are distinct, consider the residues R_i where.

$$R_i(s) = \frac{g(s)}{f(s)} [s - s_i] \quad (\text{B.5})$$

Then

$$F(s) = \frac{g(s)}{f(s)} = \sum_{i=1}^n \frac{R_i}{s - s_i} \quad (\text{B.6})$$

where the $R_i(s)$ is evaluated at $s = s_i$. The results will be distinguished as the sum of a number of time-dependent exponential terms and their coefficients:

$$f(t) = \sum_i^n R_i e^{s_i t} \quad (\text{B.7})$$

Note that for the same situation of distinct roots, $R_i(s_i) = g(s_i)/f'(s_i)$, where the derivative of $f(s)$ is take with respect to variable s before substituting $s = s_i$. These results lead to the well-known “cover-up” rule for finding partial fractions, for example:

$$\frac{1}{[s - 2][s + 3]} = \frac{1}{5} \frac{1}{s - 2} - \frac{1}{5} \frac{1}{s + 3} \rightarrow \frac{1}{5} [e^{2t} - e^{-3t}] \quad (\text{B.8})$$

- (b) If the roots are repeated, let say one root repeated once, the expansion in partial fractions is of second order of the form:

$$\frac{A_i}{s + s_i} + \frac{B_i}{[s + s_i]^2} + \sum_{i' \neq i} \frac{C_{i'}}{s + s_{i'}} \quad (\text{B.9})$$

While formula for residues are available, it is probably easier to use a direct equation of this form with the original to determine the expansion coefficients A , B , etc.

- (c) If the coefficients of the original equations are real, then any complex roots must occur in conjugate pairs of the form:

$$p_i = r_i \pm j\omega_i \text{ with } j = \sqrt{-1} \text{ or in the polar form } A_i e^{\pm j\theta_i}$$

Those complex pairs then lead to real trigonometrically functions. It is often convenient to note the implication of a *shift* of the Laplace transform variables as being equivalent to the transform of the unshifted function exponential of the time shift, e.g.:

$$\frac{s}{s^2 + 4s + 5} = \frac{s}{(s + 2)^2 + 1} = \frac{s + 2 - 2}{(s + 2)^2 + 1} \rightarrow e^{-2t} [\cos t - 2 \sin t] \quad (\text{B.10})$$

Fourier Transforms

Now, we need to consider another mathematical transformation, known as Fourier transforms. So far we talked about Laplace transform parameter s as a real number chosen to dominate the real exponentials of the function $f(t)$. More generally, it can

be considered a complex number, $s = s_0 + j\omega$, where s is chosen to meet this necessity. If the time dependence of $f(t)$ is such that it does not grow exponentially but remains constant or falls, the s_0 may be put to zero. The Laplace transform with $s = j\omega$ is called the Fourier transform of $f(t)$, and its existence is subject to this restriction on the behavior of $f(t)$.

Suppose a function is to be represented over an interval $-\frac{1}{2}T$ to $\frac{1}{2}T$ and is assumed periodic outside this range. We may try to represent it in a set of periodic trigonometric functions, $\sin n\omega t$ and $\cos n\omega t$ with $\omega = 2\pi/T$. Thus, we can write:

$$f(t) \simeq a_0 + \sum_{n=1}^{\infty} [a_n \cos(n\omega t) + b_n \sin(n\omega t)] \quad (\text{B.11})$$

The expansion coefficients will be determined by using the orthogonality properties of the trigonometric functions over the range T , i.e., multiply by one of the expansion functions and integrate over the range; all other functions on the right-hand side when integrated are *zero*.

Thus

$$a_0 = \frac{1}{T} \int_{-\frac{1}{2}T}^{+\frac{1}{2}T} f(T) dt \quad \text{Mean value} \quad (\text{B.12})$$

and

$$a_n = \frac{2}{T} \int_{-\frac{1}{2}T}^{+\frac{1}{2}T} \cos n\omega t f(t) dt \quad \text{Symmetric} \quad (\text{B.13})$$

Last but not least

$$b_n = \frac{2}{T} \int_{-\frac{1}{2}T}^{+\frac{1}{2}T} \sin n\omega t f(t) dt \quad \text{Anti-Symmetric} \quad (\text{B.14})$$

Having these coefficients available to us, the function is represented in the “best” way. If the initial function is continuous, this representation is indeed exact, an equality. If discontinuous, it is best in the sense of minimizing the integral of the square error over the range. Of course it may call for the infinite terms as $n \rightarrow \infty$ to achieve these properties.

A more compact representation comes from using the imaginary exponential forms of the trigonometric functions, $e^{j\omega t} = \cos n\omega t + j \sin n\omega t$. Noting the symmetry involved, we write:

$$f(t) \simeq \sum_{n=1}^{\infty} F(n\omega) e^{j\omega t} \quad (\text{B.15})$$

where the complex expansion coefficients $F(n\omega)$ are given by the following mathematical relationship as:

$$F(n\omega) = \frac{1}{T} \int_{-\frac{1}{2}T}^{+\frac{1}{2}T} f(t) e^{-in\omega t} dt \quad (B.16)$$

To pass to a continuous representation, the Fourier transform, over an infinite period $T = (2\pi/\omega) \rightarrow \infty$, we let $n\omega$ be the continuous variable ω to obtain

$$F(\omega) = \int_{-\infty}^{+\infty} e^{-i\omega t} f(t) dt \quad \text{and} \quad f(t) = \frac{1}{2\pi} \int_{-\infty}^{+\infty} e^{i\omega t} F(\omega) d\omega \quad (B.17)$$

Equation B.17 shows a formal *inversion* for the Fourier transfer. There is an analogous integral inversion, which is known as Bromwich integral, for the Laplace transform though we will not use it for now. Some folks will change the normalization of Eq. B.17 so that the term $\sqrt{2\pi}$ appears symmetrically in both forms. Note that the Fourier transform of a continuous spectrum would have Dirac delta distribution as we described before, added to represent discrete frequency components.

Transfer Functions

Keeping in mind that initial conditions can be written with the source terms of given equation interest to us via the Dirac delta distribution, or original problem of Eq. B.1 in the Laplace transform, space can be represented as:

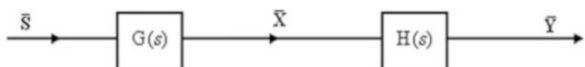
$$\bar{\mathbf{X}}(s) = \mathbf{G}(s) \bar{\mathbf{S}}(s) \quad (B.18)$$

The circumstances are depicted in Fig. B.1 graphically. In this figure, the as it shown, the output of one of the system may well supply the input for the next element of the system and so on.

Given a linear system with constant coefficients, we have an important simplification when we use Laplace or for that matter Fourier transforms in such chains of systems. The transform of the overall system is simply the product of the transforms of the individual elements and in particular can be set as the following form:

$$\bar{\mathbf{Y}}(s) = \mathbf{G}(s) \mathbf{H}(s) \bar{\mathbf{S}}(s) \quad (B.19)$$

Fig. B.1 Block transfer functions



This result is also known as convolution or folding theorem, and it is developed as follows for a single variable system. If we have compound systems, where the response of one element becomes the input of the next, how may these be expressed in terms of $G(s)$ or $G(i\omega)$ can be discussed in following matter.

First of all we consider the time-dependent solution to an impulse source $g(t)$ called Green's function, and then due to linearity, the response to any source can be obtained by adding integration all the elementary solutions in the form:

$$f(t) = \int_0^t g(t-\tau)s(\tau)d\tau \quad (t \geq 0) \quad (\text{B.20})$$

where the integral is take up to t , the latest time that a source can affect the responses. If we are in quest of taking the Laplace transform, it is convenient to extend this upper limit to ∞ which we may do artificially by introducing a step function $h(t)$, which is zero before $t = 0$ and unity for $t > 0$. Thus, we can write:

$$\begin{aligned} L\{f(t)\} &= \int_0^\infty e^{-st} \left[\int_0^\infty h(t-\tau)g(t-\tau)s(\tau)d\tau \right] dt \\ &= \int_0^\infty s(\tau)e^{-st} \left[\int_\tau^\infty e^{-s(t-\tau)}g(t-\tau)dt \right] d\tau G(s) \int_0^\infty e^{-s\tau}S(\tau)d\tau = G(s)S(s) \end{aligned} \quad (\text{B.21})$$

where a change in the order of integration, valid for well-behaved functions g and s , enables the Laplace transform of the convolution integral to be expressed as the product of Laplace transforms. This is in agreement with the results we presented in Eq. B.4, but more generally this is significant as showing that where we have a sequence of elements, the overall transfer function can be obtained simply as the product of the elements in series. However, the transforms equations mathematical manipulation when there is an impulse Dirac Delta Distribution source leads to expressions of the form $F(s) = G(s)$, where $G(s)$ may be called the system transfer function. The more general case will involve arbitrary initial conditions and driving functions, i.e., sources.

In the above situation, the more general case of $G(s)$ is the system response to an impulse source, and we can see that $G(i\omega)$ is the system response to a sinusoidal excitation of unit amplitude at frequency ω , an observation that causes to determine $G(i\omega)$ via experimental process. By letting the value of $s \rightarrow i\omega$, then we loosely allow the transform $G(s)$ to be interchangeable with the transform function $G(i\omega)$. In particular, when we deal with “linearization” of the model is involved and we also deal with small departures of the output f as a result of small departures of the input s around the steady state. We can also write the transfer function as $G(s) = \delta F(s)/\delta S(s)$. When more than one input variable is present, a partial differential or thermodynamic notation may be used such as:

$$G_1(s) = \left(\frac{\partial f}{\partial s_1} \right)_{s_2, s_3, \dots} \quad (\text{B.22})$$

showing the remaining input variables s_2, s_3, \dots kept constant in the above equation.

Feedback and Control

Many systems have an *inherent feedback* term in their response. Therefore, the equation $\dot{f} = \lambda f + s$ leads to a Laplace transform of simple lag form as:

$$\frac{F}{S} = G(s) = \frac{1}{s - \lambda} \quad (\text{B.23})$$

where we are ignoring the initial conditions. But this itself could be graphed or split up as it is demonstrated in Fig. B.2.

Note that the elementary arguments that λ must be negative for stability which an example of such situation we can mention the dying away of radioactive decay. We may also like to follow a positive feedback convention of the type shown in the figure to represent inherent feedback.

More often the output of a system in response to different loads or excitation function is not satisfactory, and the concepts of automatic control are bound up with the idea of modifying the system output. This takes place, by providing, a feedback term, a correction excitation signal that depends on the output or rather on the departure of the output from some desired level.

Thus, we distinguish between open-loop control and closed-loop control. A good example of open-loop control that we can observe in our day-to-day life is a toaster whose time can be set in advance but which does not respond automatically to the degree of browning of the toast [1].

As part of closed loop, we could use the example of a household heating system which is normally supplied with a feedback controller device such as thermostat so that the actual temperature of the rooms or their departure from some desired temperature varies the fuel supply of the furnace.

Fig. B.2 Simple inherent feedback

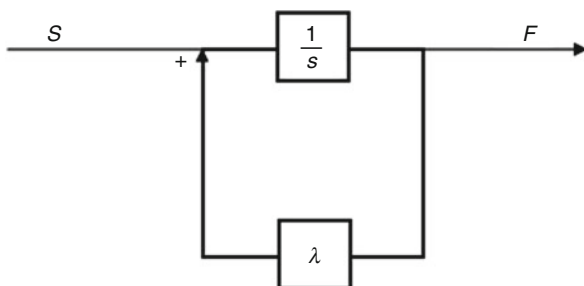
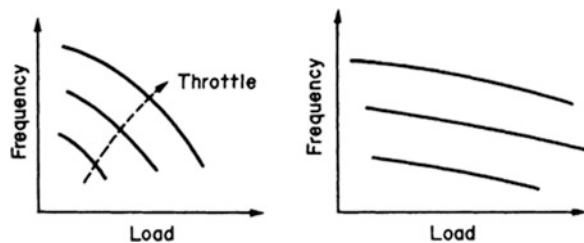


Fig. B.3 Turbine generator droop characteristics and control [1]



Other examples of such matter can be seen in turbine industry where the response of a turbine generator to different electrical loads is shown as per Fig. B.3. In this type of example, we have a noticeable droop in the speed at fixed throttle and higher loads without control action and hence an unacceptable drop in electrical frequency as the load varies.

If there is a control for feedback to vary the throttle opening with change of speed, then through a simple proportional controller, we may anticipate to flatten out this undesirable droop. To flatten it still further, using just proportional control, would demand for bigger control action or gain for a given speed discrepancy. In that case, we are in right track to anticipate that there will be a limit to the efficiency of such a simple system. This system can be brought about by the onset of dynamic instability in which a small fluctuation in the response of the system is magnified by means of resonance via too high a gain, to the point of producing even larger swings in the response. For further discussion, refer to Lewins book [1].

Knowing that the combination of successive forward transfer functions require the *addition* of phases but the *product* of amplitudes, it becomes useful to plot the amplitudes on a logarithmic scale so that they may be added graphically for this purpose. It is convenient, therefore, to plot the amplitude in decibels as $A(\omega)$ in $db = 20\log_{10}|G(i\omega)|$.

Graphical Representation (Bode and Nyquist Diagram)

By now we have seen how to build up system transfer function from the basic and elementary transfer function, either by manipulating $G(s)H(s)$, etc., for open response or, as in Eq. B.24, for a positive feedback:

$$F(i\omega)S = \frac{G(s)}{1 - KH(s)G(s)}S(i\omega) \quad (B.24)$$

where K is a scalar or gain coefficient and $F(i\omega)$ is defining an equivalent closed-loop transfer function.

Transfer functions or Fourier transform may be represented graphically and also conveniently combined graphically as shown in Fig. B.4 to present two system functions. There exist two representations that are known as Bode diagram (i.e., Fig. B.4) and Nyquist diagram (i.e., Fig. B.5).

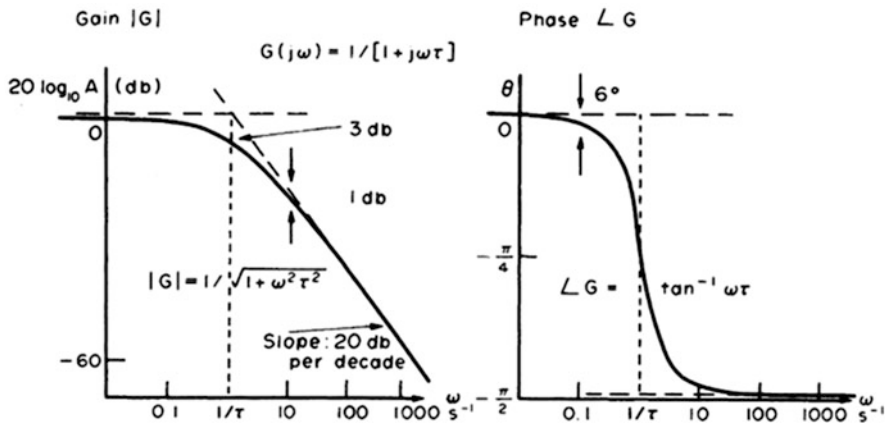
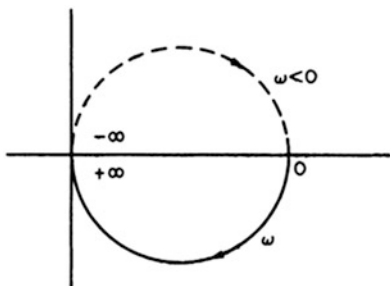


Fig. B.4 The simple Lag as Bode diagram with break frequency construction

Fig. B.5 Nyquist diagram for simple lag [1]



In the Bode diagram, the transfer function $G(i\omega)$ is represented in polar format through its amplitude or gain A and phase θ as a complex number $Ae^{i\theta}$. Normally gain and phase are plotted against the frequency in either radians/sec or hertz (cycle/sec) on a logarithmic scale. Generally speaking, the angular frequency presented by ω is in radians/sec, of course 2π greater than the cycles in hertz (Hz).

Figure B-4 shows the simple lag plotted as a Bode diagram. It also shows the important approximate construction technique of the “break frequency” method in which asymptotes of G are established for large and small ω .

These asymptotes intercept at the frequency $\omega_c \equiv 1/\tau$ that is again known as break frequency, and Fig. B.4 shows the departure of the exact result from the asymptote around the break frequency in the example we presented.

Bode diagram is a convenient approach for the compounding of successive transfer functions, and we can find out that the approximation of 6 db corresponds to a factor of 2. On the other hand, the Nyquist diagram is an alternative representation in which $G(i\omega)$ is plotted as an A grand diagram in radial coordinates. Sometimes, a polar plot of $\log A$ is being more useful; the same simple lag is given as Nyquist diagram in Fig. B.5. Note that for negative ω the diagram is completed as a mirror image. For further information please refer to book by Lewins [1].

Root Locus Construction Rules

1. The poles of the transfer function are the poles of the open-loop transfer function, $G(s)H(s)$, when the gain constant K goes to 0.
2. The poles of the transfer function are the zeros of the open-loop transfer function, $G(s)^*H(s)$, when the gain constant K goes to infinity. For realizable physical systems, there will always be fewer zeros for the open-loop transfer function than there will be poles. The remaining zeros (hypothetical) are located at infinity.
3. For a positive gain constant, $K > 0$, the real axis to the left of an odd number of poles and zeros contains the locus for the poles of the closed-loop transfer function. For a negative gain constant, $K < 0$, the real axis to the left of an even number of poles and zeros contains the locus for the poles of the closed-loop transfer function.
4. As K grows large, the poles moving toward the zeros at infinity do so along asymptotes given by the following angles with the real axis.

For $K > 0$, the angles are given by:

$$\theta = \frac{(2n + 1)\pi}{N_p - N_z} \quad N_p = \text{Number of Poles}, N_z = \text{Number of zeros} \quad (\text{B.25})$$

For $K < 0$, the angles are given by:

$$\theta = \frac{2n\pi}{N_p - N_z} \quad (\text{B.26})$$

5. The point at which the asymptotes intercept the real axis is given by the following formula:

$$B = \frac{\text{Sum of Pole Real Parts} - \text{Sum of Zero Real Parts}}{N_p - N_z} \quad (\text{B.27})$$

6. The actual breakaway points for the locus can be calculated by realizing that the breakaway point must correspond to a double root.

Reference

1. J. Lewins, *Nuclear Reactor Kinetics and Control*, 1st edn. (Pergamon, New York, 2013)

Index

A

Absorption hardening, 105
Accelerator driven systems (ADS), 568
ADJOINT function, 416
Advanced boiling water reactors (ABWR), 546
Advanced gas-cooled reactor (AGRs), 621
Advanced modular reactors (ASMRs), 544, 620
Advanced small modular reactors (AdvSMRs), 563, 599, 610, 632
Air conditioning (AC), 614, 631
Amplitude function, 186, 403, 436
Arbeitsgemeinschaft Versuchsreaktor (AVR), 598
Argentina, 565
Argentina National Atomic Energy Commission (CNEA), 614
Average logarithmic energy decrement, 56, 57

B

Bessel equation, 180
Bessel functions, 155, 157, 181
Bethe-Tait event, 478
Black rods, 106, 110
Bode diagram, 655
Body-centered cubic (BCC), 354
Boiling water reactors (BWRs), 110, 354
Boltzmann constant, 105
Boltzmann equation, 476
Boltzmann transport equation, 59, 103, 112, 119, 229, 239, 254, 305, 435
Bondarenko method, 320
Boundary conditions (BCs), 160
Boundary value problem (BVP), 160, 161
Brazil, 565
Break frequency, 656

Breit and Wigner formula, 20, 25, 307, 316

Bromwich integral, 652
By design, 631

C

Cartesian coordinates, 154
Center of mass coordinate system (CMCS), 129
CENTRM method, 321
Chebyshev rational method, 475
Code of Federal Regulations (CFR), 552
Combined cycle gas turbine (CCGT), 621
Concept of stiffness method, 474
Construction and operating license (COL), 592
Construction permit (CP), 591
Control rod worth, 108
Conversion, 45
Core damage frequencies (CDFs), 631
Core disruptive accidents (CDA), 478
Core multiplication, 430
Crank-Nicolson strategy, 475
Cross Section Evaluation Working Group, 20

D

Dancoff factor, 344
de Broglie wavelength, 25
Deliberately small reactor (DSR), 562
de Moivre identities, 155
Department of energy (DOE), 569, 599, 610
Differential control rod worth, 109
Diffusion approximation, 121
Diffusion cooling, 366
Diffusion length, 142
Dilution cross-section, 322, 329

Dirac delta function, 127, 147, 648, 649, 652
 Doppler broadening, 311, 315, 318, 320
 Doppler effect, 87, 305, 311, 314, 319, 435
 Doppler width of the resonance, 317, 318
 Downscattering, 105
 Dresner's integral, 338

E

Effective multiplication factor, 89
 Eigenfunctions, 160
 Eigenvalues, 160
 Elastic scattering, 105
 Electric power research institute (EPRI), 537
 Endothermic, 7
 Energy Policy Act (EPAct), 569
 Energy release, 54
 Euler's backward method, 420
 Euler's constant, 157
 Euratom, 565
 European nuclear energy forum (ENEF), 595
 European pressurized water reactor (EPR), 592
 European sustainable nuclear industrial initiative, 594
 Evaluated Nuclear Data Formats B (ENDF/B), 18, 20
 Evaluation methodology group, 589
 Exothermic, 7
 External source, 118
 Extrapolation distance, 139
 Extrapolation length, 139

F

Face-centered cubic (FCC), 354
 Fast breeder reactors (FBRs), 477
 Fast fission factor, 85, 86, 88, 94, 97, 218
 Fast Fourier transform (FFT), 455
 Fast utilization factor, 218
 Fertile, 43
 Fertile materials, 45
 Fick's law, 117, 121, 124, 134, 151, 152
 First of a kind (FOAK), 567
 Fission fragments, 486
 Fission-produced poisons, 493
 Fission products, 488
 Fission spectrum, 103
 Fission yields, 488
 Fluoride salt-cooled high-temperature reactors (FHR), 575
 Flux calculator method, 320
 Fort St. Vrain (FSV), 598
 Four-factor, 184

Four-factor formula, 79, 86, 88, 94, 96, 97
 France, 565
 Free surface, 140
 Frequency domain, 454
 Frequency response, 452
 Fuchs-Hansen model, 443
 Fuel cycle crosscut group (FCCG), 589
 Fuel elements, 503
 Fuel fusion cross section, 136
 Fuel management, 510
 Full width at half-maximum (FWHM), 307

G

Galerkin procedure, 259
 Gas-cooled fast reactor, 596
 Gas-cooled reactor, 580
 Gas fast reactors (GFRs), 540
 Gas Turbine-Modular Helium Reactor (GT-MHR), 622
 Gaussian quadrature points, 475
 Gauss-Seidel (SOR), 79
 Generation II, 563
 Generation III, 563
 Generation IV, 563, 565, 566, 569, 588, 589
 Generation IV International Forum (GIF), 565, 570, 599
 Generation nuclear plant (NGNP), 569
 Green's function, 158, 159, 455
 Grey rods, 106, 110

H

Heat pipe reactor, 617
 Heat recovery steam generator (HRSG), 529, 562
 Heavy water, 526
 Heavy water reactors (HWRs), 540
 Helmholtz scalar-type, 138
 Heterogeneous reactor, 350
 High-enriched uranium (HEU), 555
 High-level waste (HLW), 539
 High-temperature and very high temperature gas-cooled reactors, 540
 The high-temperature engineering test, 598
 High temperature gas-cooled reactor pebble-bed module (HTGR-PM), 610
 High temperature gas-cooled reactors (HTGRs), 596, 610, 620, 621
 High temperature reactor-pebble bed module (HTR-PM), 596, 621
 High temperature reactors (HTRs), 353, 568, 621
 High temperature steam electrolysis (HTSE), 573

Homogeneous boundary value problem (HBVP), 161, 165
Homogeneous equilibrium mixture (HEM), 170
Homogeneous reactor, 349
Hydrogen energy and fuel cells, 595

I

Idaho National Laboratory (INL), 569
Industrias Metalurgicas Pescarmona SA (IMPSA), 614
Infinite dilute cross section, 323, 332
Infinite medium multiplication factor, 85, 88
Inhour equation, 414
Initial value problems (IVPs), 160, 161
Innovative nuclear reactors and fuel cycles (INPRO), 564
Integral control rod worth, 108
Integral molten salt reactor (IMSR), 606
Intermediate heat exchanger (IHX), 573
International Atomic Energy Agency (IAEA), 555, 561, 629
Isotropic, 121

J

Japan, 565
Japan Atomic Energy Agency (JAEA), 598
Japan Atomic Energy Research Institute (JAERI), 617
Joining function, 367

K

Kinetics of chain reactions, 80
Korea Atomic Energy Research Institute (KAERI), 616

L

Laboratory coordinate system (LCS), 121, 144, 152
Large water cooled reactors (LWCRs), 631
Lead-bismuth eutectic (LBE), 582
Lead-cooled fast reactor (LFR), 582
Legendre polynomial, 150, 151, 194, 231, 232, 253, 255
Levelized cost of electricity (LCOE), 635
Life cycle, 80
Light water, 526
Light water reactors (LWRs), 77, 104, 351, 540, 569, 609, 625
Linear time-invariant (LTI), 452, 454

Liquid metal fast-breeder reactors (LMFBRs), 468, 470, 479, 540
Logarithmic boundary condition, 139
Long-time dynamics, 439
Low enriched uranium (LEU), 632, 637

M

Macroscopic absorption cross section, 82
Macroscopic slowing down power (MSDP), 58
Mass defect, 3
Maxwell-Boltzmann distribution, 364
Maxwellian distribution, 304, 305, 435
Maxwellian distribution function, 105
Mean free path (MFP), 30, 113
Mean life of the radioactive species, 9
Million tons of uranium (MtU), 567
Mixed oxide (MOX), 539
Moderating ratio, 58
Molten salt reactors (MSR), 540, 574, 596
Multi-application small light water reactor (MASLWR), 610, 626, 636
Multi-group diffusion equation (MGDE), 213, 218
Multiplication factor, 79, 80, 94, 430, 493

N

Negative temperature feedback, 435
Neumann's function, 156, 181
Neutron balance, 80
Neutron energy spectrum, 105
Neutron flux, 117, 118
Neutron line width, 307
Neutron scattering, 121
Neutron spectrum, 104
Neutron transport analysis, 53
Next generation nuclear plant (NGNP), 569, 598, 621
NJOY of MacFarlane, 1978, 19
Nodal expansion method (NEM), 170
Nonhomogeneous boundary value problem (NHBVP), 161
Non-leakage probability, 88
Non-reentrant surface, 139
Nuclear fission, 13
Nuclear fuel cycle, 510
Nuclear magnetic resonance (NMR), 452
Nuclear nonproliferation treaty (NPT), 555
Nuclear power plants (NPPs), 537, 564, 568, 591, 636
Nuclear Regulatory Commission (NRC), 569, 605

Nuclear steam supply system (NSSS), 170
 Nyquist criterion, 457, 458
 Nyquist diagram, 655, 656

O

Ordinary differential equations (ODEs), 158, 474
 Organization for Economic Co-operation and Development (OECD), 468
 Oxide dispersion strengthened (ODS), 580

P

Partial differential equation (PDE), 138
 Partial fractions, 649
 Pebble-Bed Modular Reactor (PBMR), 622
 People's Republic of China, 565
 Phenomena identification and ranking table (PIRT), 591
 Piecewise continuous, 642
 Placzek functions, 296
 Planck's constant, 2
 Plant-life management technologies and plant license extension practices (PLIM/PLEX), 566
 Point kinetic equation (PKE), 413, 436, 441, 442
 Point reactor, 129
 Point reactor kinetics, 13
 Policy Group (PG), 566
 Power purchase agreements (PPAs), 605
 Pressurized water reactors (PWRs), 110, 350, 545
 Probability for absorption, 82, 83
 Production tax credit (PTC), 605

Q

Q -value, 7

R

Radiative capture reaction, 28, 136
 Reactivity factor, 404
 Reactivity-initiated accidents (RIA), 315
 Reactor period, 82
 Reciprocal logarithm derivative, 139
 Reentrant surface, 139
 Relaxation length, 18
 Reprocessing, 503
 Reproduction factor, 84
 Research and Development (R&D), 563
 Resonance absorption of neutrons, 435
 Resonance escape probability, 87
 Resonance integrals (RI), 325
 Return on investment (ROI), 524, 600
 Roadmap integration team (RIT), 588

Rod followers, 106
 Runge-Kutta method, 475
 Russian Federation, 565

S

Sagan's equation, 37
 Sandia National Laboratory (SNL), 537
 Scattering source, 103
 Schrödinger equation, 135, 144, 150
 Short-time dynamics, 439
 Six-factor formula, 88, 218
 Slow neutron, 486
 Small modular reactors (SMRs), 524, 536, 556, 609, 622, 628, 636
 Sodium-cooled fast reactor (SFR), 575, 593, 596
 Solid fuel elements, 349
 Source distribution function, 136
 Source multiplication, 430
 South Africa, 565
 Space-time kinetics equation, 405
 Spherical coordinate, 154
 Standardized Computer Analyses for Licensing Evaluation (SCALE), 20
 Steam Cycle High Temperature Gas reactor (SC-HTGR), 622
 Supercritical water (SCW), 577
 Supercritical water reactors (SCWRs), 540, 577
 Switzerland, 565
 System research plan (SRP), 582
 System Steering Committee (SSC), 566

T

Technical working group (TWG), 589
 Thermal neutrons, 83
 Thermal utilization factor, 83, 97, 98, 493
 Thorium high-temperature reactor-300 (THTR-300), 598
 Time domain, 454
 Total cost of ownership (TCO), 524, 600
 Transfer function, 454
 Transform pairs, 642
 Transmutation, 45
 Transport mean free path, 140
 Transuranic (TRU) waste, 552
 Transuranium elements, 504, 506, 511
 Tristructural-isotropic (TRISO), 571

U

Uncertainty Principle of Heisenberg, 24
 Uniform composition, 83
 United Kingdom (UK), 565, 621
 United States (US), 565

Update Deck (UPD), 22

Upscattering, 105

Uranium oxide/uranium carbide (UCO), 599

V

Very-high temperature reactors (VHTR), 568,
570, 571, 573, 596

Voigt profile, 335

W

Waste Isolation Pilot Plant (WIPP), 552

Wigner-Seitz method, 352

X

Xenon instability, 494